

**From crystal to crust:
the Proterozoic crustal evolution
of southwest Norway**

Thesis submitted for the degree of
Doctor of Philosophy
at the University of Leicester

Nicholas Michael William Roberts

Department of Geology
University of Leicester

October 2010

From crystal to crust: the Proterozoic crustal evolution of southwest Norway

Nicholas Michael William Roberts

Abstract

The geology of the Suldal Sector, southwest Norway, comprises exposures from three orogenic periods; the Telemarkian, Sveconorwegian and Caledonian. Telemarkian (~1500 Ma) basement rocks are interpreted to be the oldest crust in the region; these are intruded by Sveconorwegian granitoid intrusions (~1070-930 Ma). Crystalline nappe units overlie the Mesoproterozoic basement, and from reconnaissance U-Pb dating and zircon hafnium isotopes, are believed to comprise slices of the Mesoproterozoic Norwegian continental margin.

The Telemarkian basement comprises meta-plutonic/volcanic lithologies that represent the deformed upper crustal section of a continental arc - the Suldal Arc; U-Pb dating suggests this arc was active from ~1520 to 1475 Ma. Whole-rock geochemistry and hafnium and oxygen isotopes measured in zircon, suggest that arc magmatism recycled older continental crust (20-50% contribution) that had been mixed with mantle-derived material in the lower crust; the older crustal component comprised late-Palaeoproterozoic sedimentary material derived from the Fennoscandian continent. During the arc's evolution, dehydration of mafic source magma induced by heat from magmatic underplating, and subsequent melting of dehydrated crust enhanced by asthenospheric upwelling, allowed for the intrusion of iron-enriched tholeiitic magmas. The Suldal arc and by extension, the Telemarkia terrane, represent the last stages of continental crust formation within a retreating accretionary orogen that was active since ~1.8 Ga.

Based on whole-rock geochemistry, U-Pb, hafnium and oxygen isotopes in zircon, Sveconorwegian granite suites formed between 1.07 and 0.92 Ga, and are largely derived from ~1.5 Ga mafic lower crust with a limited contribution of juvenile mantle-derived material. The geodynamic setting of granitic magmatism evolved from supra-subduction, to overthickened crust, to thinned crust with possible lithospheric delamination. The varying geochemistry of the granite suites (I- to A-type) is controlled not by geodynamic setting, but dominantly by water content in the magma source. Sveconorwegian deformation in the Suldal Sector is bracketed between ~1069 and ~1047 Ma by intrusions of the Storlivatnet plutonic complex.

Acknowledgements

First and foremost I'd like to acknowledge the person that started the ball-rolling, the late Prof. Tim Brewer. Tim's involvement in this project was unfortunately short-lived, however, his rigorous and comprehensive approach to Precambrian geology, applied with his consistently high level of enthusiasm and wit, have given me a want to succeed and excel and have provided motivation for this project that still continues today.

By agreeing to my supervision, Prof. Randy Parrish probably took on a lot more than expected, but has continued to provide a wealth of knowledge, assistance, constructive criticism as well as praise, and without his input this thesis would be an order of magnitude thinner. Dr. Mike Norry also found himself supervising this project, and continues to be a geochemical 'rock' that one can always bounce ideas off; perhaps more important though is the holistic ideology that influenced me under Norry's tutelage whilst I was as an undergraduate at Leicester.

If during this project Randy and Norry play the role of espoused fathers, then I would liken Steve Noble to an uncle: taking a background role, but always providing unrestrained praise and encouragement, and willing to drop anything to help. Matt Horstwood and Dan Condon have also played key roles in this project, having made sure that I actually had some data to write about. Also at NIGL I would like to thank John Cottle, Jenny Bearcock, Vanessa Pashley, Laura Howell and Adrian Wood for providing technical and analytical assistance. In Edinburgh I owe tremendous thanks to John Craven for enabling me to walk away from the Ionprobe with some useable data, having arrived with the worst prepared samples he'd ever let on the machine!

Mogens Marker and Trond Slagstad at the Norwegian Geological Survey provided indispensable support in my first field season, and have since provided useful discussion, as well as complete access to their samples and data which have been a great benefit to this project. Rich Walker, Rhys Langford and Chris McDonald are also thanked for their assistance in the field.

At the University of Leicester I would like to thank members of the analytical staff, Nick Marsh, Colin Cunningham, Rob Kelly and Rob Wilson, and also all of the academic, technical and administrative staff; everyone at Leicester has made life pretty easy going... it does rather discourage one from 'getting a real job'.

I would like to thank the attendees of the Sveconorwegian fieldtrip that formed part of the International Geological Congress in 2008. The trip provided a great insight into the quirks, unresolved debates, and pros and cons of Precambrian geology and geochronology of Scandinavia; there are too many people to list, but I would like to mention Bernard Bingen for many useful discussions, manuscripts and data. Thanks also to Quentin Crowley, Mike Flowerdew and the guys from BAS for making a long stay in Oslo more enjoyable through a fair amount of (expensive) beer-drinking.

I am grateful to my office mates at Leicester (Pete, Becky and Alex) for keeping the insanity to acceptably low-levels, with a distinctive lack of talking-shop, a passion for sharing gossip, and a keenness to whinge about... well anything that needed whinging about. During my 8 years at Leicester there have been too many other postgrads to name, who have provided support pastorally, academically, and most importantly at the bar. I thank you all.

Outside of geology, many friends have provided support, whether it be a jest about 'going time-travelling', the odd 'so aren't you finished yet?', or just taking my mind off (which was surprisingly hard) very old non-mineralised non-oil bearing non-distinctive grey rocks in Norway. Many friends and family still ask when I'm going to get a job, but if academia isn't classed as a real job, then hopefully the answer will continue to be never.

I owe a great deal to my parents, who have provided unchecked loving support, whether it be motivationally or financially (especially during the days when I believed I still didn't own enough climbing gear, or when my car needed fixing!). And finally I have to thank Abi, who has always given me the most encouragement and support, and for always being there.

Thank you

Nick Roberts

May 2010

1	Introduction.....	13
1.1	Background and rationale.....	13
1.1.1	Topical aspects.....	13
1.1.2	Regional aspects.....	16
1.2	Aims.....	16
1.3	Outline.....	17
1.4	Presentations.....	18
1.5	Data Sources.....	19
2	The geology of the Suldal Sector, southwest Norway.....	20
2.1	Regional Geology.....	20
2.2	Geology of the Suldal Sector.....	24
2.2.1	Description of units.....	24
2.2.2	Structure.....	33
2.2.3	Metamorphism (summary).....	34
2.3	Conclusions.....	34
3	A chemical abrasion LA-MC-ICP-MS and ID-TIMS U-Pb study of Mesoproterozoic magmatism in the Suldal Sector: constraints on Telemarkian and Sveconorwegian crustal evolution.....	36
3.1	Introduction.....	36
3.2	Geological Framework.....	37
3.3	Methodology.....	37
3.4	Sample Descriptions.....	41
3.4.1	SA3-02 tonalite dyke.....	41
3.4.2	SA8-45 banded felsic gneiss.....	41
3.4.3	SA7-04 rhyodacitic gneiss.....	41
3.4.4	SA7-86 metagabbro.....	42
3.4.5	SA7-58 biotite porphyritic granite.....	42
3.4.6	SA7-130 banded rhyodacitic gneiss.....	42
3.4.7	SA7-91 biotite granite.....	42
3.4.8	SA3-60 banded rhyolitic gneiss.....	44
3.4.9	SA3-04 granodiorite gneiss.....	44
3.4.10	SA3-01 biotite-hornblende porphyritic granite.....	44
3.4.11	SA8-69 porphyritic granodiorite.....	44
3.5	Results.....	45
3.5.1	SA3-02 tonalite dyke.....	45
3.5.2	SA8-45 banded felsic gneiss.....	45
3.5.3	SA7-04 rhyodacitic gneiss.....	46
3.5.4	SA7-86 metagabbro.....	46
3.5.5	SA7-58 biotite porphyritic granite.....	51
3.5.6	SA7-130 banded rhyodacitic gneiss.....	52
3.5.7	SA7-91 biotite granite.....	52
3.5.8	SA3-60 banded rhyolitic gneiss.....	52
3.5.9	SA3-04 granodiorite gneiss.....	52
3.5.10	SA3-01 biotite-hornblende porphyritic granite.....	53
3.5.11	SA8-69 porphyritic granodiorite.....	53
3.6	Discussion.....	53
3.6.1	Chemical abrasion for laser ablation studies.....	53

3.6.2	1.5 Ga Telemarkian crustal growth	57
3.6.3	Sveconorwegian events	58
3.7	Conclusions	61
4	The petrogenesis of 1.5 Ga magmatism in the Suldal Sector	64
4.1	Introduction	64
4.2	Geological Framework.....	64
4.3	Geochemistry	65
4.3.1	Analytical techniques	65
4.3.2	Element mobility	65
4.3.3	Sauda Grey Gneiss Association	66
4.3.4	Zinc Mine Banded Gneiss	73
4.3.5	Amphibolites	73
4.3.6	Granitoids.....	74
4.4	Petrogenesis	74
4.4.1	Grey Gneiss.....	74
4.4.2	Amphibolites	77
4.5	Discussion.....	86
4.5.1	Origin of A-type granites	86
4.6	Conclusions	87
5	Continental recycling in arc magmas: Hf-O isotope constraints on Telemarkian (1.52-1.48 Ga) magmatism	88
5.1	Introduction	88
5.2	Geological setting	89
5.3	Analytical methods.....	93
5.3.1	Zircon U-Pb isotopes.....	93
5.3.2	Zircon Hf isotopes.....	93
5.3.3	Zircon O isotopes	95
5.4	Results	96
5.4.1	Zircon Hf isotopes.....	96
5.4.2	Zircon oxygen isotopes	97
5.5	Discussion.....	98
5.5.1	Previous isotopic constraints	98
5.5.2	Zircon inheritance	100
5.5.3	Geochemical indicator of sources	101
5.5.4	Nature of crustal and mantle components	102
5.5.5	Processes of continental recycling	104
5.6	Conclusions	106
6	Geochemical and Hf-O constraints on the petrogenesis of early- to late-Sveconorwegian magmatism in S. Norway	108
6.1	Introduction	108
6.2	Previous studies	109
6.3	Analytical methods.....	113
6.4	Petrography and geochemistry	113
6.4.1	The HBG suite.....	113
6.4.2	The Feda suite	113
6.4.3	Leucogranites	117
6.4.4	Zircon saturation temperature	118
6.5	Results – Hf isotopes	119

6.6	Results – Oxygen isotopes.....	119
6.7	Discussion.....	120
6.7.1	Hf-O constraints on magma source.....	120
6.7.2	Formation of silica melts – magma mixing versus fractional crystallisation....	121
6.7.3	Geochemical constraints on magma source	123
6.7.4	Leucogranite formation.....	126
6.7.5	Continental recycling during Sveconorwegian magmatism.....	127
6.7.6	Reconciling the Hf-O and geochemical constraints.....	129
6.7.7	Geodynamic setting.....	130
6.7.8	Continental growth during Sveconorwegian magmatism	130
6.8	Conclusions	131
7	The 1.24 Ga Gross�-Totak suite, a new age confirms an old correlation in the Telemark supracrustals, southern Norway	132
7.1	Introduction.....	132
7.2	Geological setting	133
7.3	Sample description and results	135
7.4	Discussion.....	136
7.5	Conclusions	138
8	In-situ U-Pb and Hf isotopes constrain the age & provenance of the Hardangervidda-Ryfylke Nappe Complex, SW Norwegian Caledonides	140
8.1	Introduction.....	140
8.2	Geological Setting.....	140
8.2.1	Holmasj� unit (Lower Allochthon).....	142
8.2.2	Storhei unit (Middle Allochthon).....	143
8.2.3	Dyrskard unit (Middle Allochthon).....	143
8.2.4	Kvitenut unit (Middle Allochthon)	144
8.2.5	Revsegg unit (Middle Allochthon).....	144
8.3	Rationale for isotope work	145
8.4	Sample Description	147
8.4.1	SA8-32 Holmasj� unit (fine-grained intermediate grey gneiss)	147
8.4.2	SA8-19 Storhei unit (coarse-grained granitic gneiss)	147
8.4.3	SA8-23 Dyrskard unit (fine-grained felsic gneiss).....	147
8.4.4	SA8-26 Kvitenut unit (mylonitic banded gneiss).....	148
8.4.5	SA8-27 Revsegg unit (garnet-mica gneiss).....	148
8.5	Analytical methods.....	149
8.6	Results – U-Pb	149
8.6.1	SA8-32 Holmasj� unit (fine-grained intermediate grey gneiss)	149
8.6.2	SA8-19 Storhei unit (coarse-grained granitic gneiss)	149
8.6.3	SA8-23 Dyrskard unit (fine-grained felsic gneiss).....	149
8.6.4	SA8-26 Kvitenut unit (mylonitic banded gneiss).....	151
8.6.5	SA8-27 Revsegg unit (garnet-mica gneiss).....	151
8.7	Results – Hf.....	152
8.8	Discussion.....	153
8.8.1	Origin of the nappe units.....	153
8.8.2	Gothian-Telemarkian continental growth	157
8.8.3	Sveconorwegian orogeny in SW Norway	158
8.9	Conclusions	159
9	Discussion.....	161

9.1	Crustal evolution in the Telemarkian (1.52-1.48 Ga) period	161
9.1.1	‘Indigenous’ or ‘Exotic’ Telemarkia.....	162
9.1.2	A retreating accretionary orogenic model.....	165
9.2	Crustal evolution in the Sveconorwegian (1.06-0.92 Ga) period.....	166
9.3	The ‘interorogenic’ period	167
9.3.1	The Hallandian-Danopolonian event	168
9.4	A tectonic synthesis	169
9.5	Reading the isotope barcode	172
9.5.1	Source versus time	173
9.5.2	Comparison with other evidence.....	174
9.5.3	Zircon inheritance	177
9.6	Supercontinents and global correlations.....	177
9.6.1	A global accretionary orogen?	177
9.6.2	Proterozoic supercontinents	181
9.7	Continental growth – a final comment.....	183
9.7.1	A final comment on the final comment – continental versus crustal growth....	184
10	Appendix.....	187
10.1	XRF methodology and precision.....	187
10.2	Sample details.....	188
10.3	Whole-rock geochemical data	201
10.4	U-Pb data	221
10.5	Hafnium isotope data.....	232
10.6	Oxygen isotope data – chapter 5.....	246
10.6	Oxygen isotope data – chapter 6.....	248
10.6	U-Pb TIMS dataBibliography.....	254
10.6	Bibliography	255

List of figures

Fig. 1.1 Compilation of global mineral ages, ages of juvenile crust and U-Pb ages of detrital zircons, compared with periods of supercontinent formation.	14
Fig. 2.1 Map of the East European Craton, Precambrian domains in Fennoscandia and terranes in SW Fennoscandia.	20
Fig. 2.2 Geological map of SW Fennoscandia.	22
Fig. 2.3 Field photographs of Sauda Grey Gneiss outcrops.	26
Fig. 2.4 Field photographs of amphibolite outcrops.	27
Fig. 2.5 Field photographs of Grey Gneiss structures, Zinc Mine Banded Gneiss and the Nesflaten Suite.	28
Fig. 2.6 Field photographs of the Storlivatnet plutonic complex.	29
Fig. 2.7 to 2.12 Thin section photomicrographs of Grey Gneiss and amphibolites.	30
Fig. 2.13 to 2.18 Thin section photomicrographs of Grey Gneiss and amphibolites.	31
Fig. 2.19 to 2.22 Thin section photomicrographs of Grey Gneiss and granitoids.	32
Fig. 2.23 Map of the study area with stereonet for various transects.	33
Fig. 3.1 Map of the study area with new and published U-Pb ages.	38
Fig. 3.2 U-Pb data on standards run during the LA-ICP-MS sessions.	40
Fig. 3.3 Field photographs of samples localities.	43
Fig. 3.4 Field photographs of samples localities.	44
Fig. 3.5 U-Pb concordia for SA3-02 and SA8-45.	47
Fig. 3.6 U-Pb concordia for SA7-04 and SA7-86.	48
Fig. 3.7 U-Pb concordia for SA7-58, SA7-130 and SA7-91.	49
Fig. 3.8 U-Pb concordia for SA3-60, SA3-04 and SA3-01.	50
Fig. 3.9 U-Pb concordia for SA8-69.	51
Fig. 3.10 Effect of reverse discordance and lead-loss on U-Pb systematics.	56
Fig. 3.11 Compilation of new and published ages for the Suldal Sector.	57
Fig. 4.1 Map of the study area showing the sample localities.	64
Fig. 4.2 Geochemical classification of magmatic suites using QAP, Sr/Y vs. Y, Fe* vs. SiO ₂ , MALI vs. 66 SiO ₂ , ASI vs. SiO ₂ and Na+K vs. SiO ₂ .	
Fig. 4.3 Major element oxides vs. SiO ₂ for magmatic suites in the Suldal Sector.	67
Fig. 4.4 Trace elements vs. SiO ₂ for magmatic suites in the Suldal Sector.	68
Fig. 4.5 Trace and rare-earth-elements vs. SiO ₂ for magmatic suites in the Suldal Sector.	69

Fig. 4.6 Primitive mantle normalised spider plots for magmatic suites in the Suldal Sector.	70
Fig. 4.7 Chondrite normalised spider plots for magmatic suites in the Suldal Sector.	71
Fig. 4.8 Rayleigh fractional crystallisation modelling of REE contents in the Grey Gneiss.	76
Fig. 4.9 SiO ₂ vs. FeO ^t /MgO for selected continental arc and continental rifts compared with the Sauda Grey Gneiss.	79
Fig. 4.10 SiO ₂ vs. Fe* for the Sauda Grey Gneiss and Amphibolite suites compared with natural and experimental data.	81
Fig. 4.11 Tectonic/petrogenetic model for ~1.5 Ga magmatism in the Suldal Sector, along with comparison of basalt geochemistry in different suites.	84
Fig. 5.1 Map of the study area showing sample localities with Hf-O results.	90
Fig. 5.2 CL images of selected zircons analysed for Hf-O.	91
Fig. 5.3 Compilation of secondary standard Hf isotope data.	94
Fig. 5.4 Compilation of primary standard oxygen isotope data.	95
Fig. 5.5 Results of in-situ Hf isotope analyses.	97
Fig. 5.6 Results of in-situ oxygen isotope analyses.	98
Fig. 5.7 Time corrected Hf isotope data for new and published data from 1.5 Ga and older units within SW Fennoscandia.	99
Fig. 5.8 Hf vs. O bulk-mixing modelling.	103
Fig. 6.1 Map of southern Norway showing the various Sveconorwegian granitoid suites.	109
Fig. 6.2 Map showing the sample localities.	112
Fig. 6.3 Geochemical classification plots for granitoid suites, using QAP, SiO ₂ vs. ASI, SiO ₂ vs. Fe* and SiO ₂ vs. MALI.	114
Fig. 6.4 Major element oxides vs. SiO ₂ for granitoid suites.	115
Fig. 6.5 Trace elements vs. SiO ₂ for granitoid suites.	116
Fig. 6.6 Trace and rare-earth-elements vs. SiO ₂ for granitoid suites.	117
Fig. 6.7 Primitive mantle normalised spider plots for granitoid suites.	118
Fig. 6.8 M vs. Zr with zircon saturation temperature isotherms for granitoid suites.	118
Fig. 6.9 Results of in-situ Hf isotope analyses.	119
Fig. 6.10 Results of in-situ oxygen isotope analyses.	120
Fig. 6.11 Time corrected Hf isotope data for new and published data from Sveconorwegian units within SW Fennoscandia.	121
Fig. 6.12 SiO ₂ vs. Zr for plutons within southwest Norway, highlighting fractional crystallisation vs. magma mixing models.	122

Fig. 6.13 Petrogenetic model for formation of various Sveconorwegian granitoid suites.	126
Fig. 6.14 Hf vs. O bulk-mixing modelling.	128
Fig. 7.1 Map of SW Fennoscandia showing ‘interorogenic’ units.	134
Fig. 7.2 Map of the Telemark supracrustals showing the sample locality.	135
Fig. 7.3 Stratigraphy of supracrustal belts within Telemarkia.	135
Fig. 7.4 U-Pb concordia for the Fjellhovdane rhyolite.	136
Fig. 7.5 Primitive mantle normalised spider plot comparing the Fjellhovdane and Trossovdal rhyolites with basement gneisses in the Suldal Sector.	137
Fig. 8.1 Geological map of the southern Norwegian Caledonides and the sample localities in the Hardangervidda-Ryfylke Nappe Complex.	141
Fig. 8.2 Tectonostratigraphy of the Hardangervidda-Ryfylke Nappe Complex.	142
Fig. 8.3 Field photographs of sample localities.	145
Fig. 8.4 Thin section photomicrographs of sampled units.	146
Fig. 8.5 Results of U-Pb dating with selected zircon images.	150
Fig. 8.6 Time corrected Hf isotope data compared with fields for autochthonous basement units.	152
Fig. 8.7 Primitive mantle normalised spider plot comparing the Dyrskard unit with the 1260 Ma Trossovdal rhyolite and with Sveconorwegian Feda suite granitoids.	154
Fig. 8.8 Cumulative probability plots for the Kvitenut and Revsegg units compared with a compilation of ages from the autochthonous basement, and a compilation of ages from other nappe complexes within the Scandinavian Caledonides.	157
Fig. 8.9 Postulated provenance of the Middle Allochthon units	158
Fig. 9.1 Strike-slip terrane displacement model for SW Fennoscandia.	163
Fig. 9.2 Compilation of detrital U-Pb zircon data for SW Fennoscandia.	164
Fig. 9.3 Retreating accretionary orogen model.	166
Fig. 9.4 Tectonic model for the Palaeo- to Mesoproterozoic evolution of Fennoscandia.	170
Fig. 9.5 Tectonic model for the Sveconorwegian evolution of SW Fennoscandia.	171
Fig. 9.6 Compilation of Hf data for SW Fennoscandia with interpreted phases of compression and extension, and compilation of U-Pb data to compare inheritance in different domains.	176
Fig. 9.7 1.8-1.0 Ga crustal provinces in Laurentia and Fennoscandia.	178
Fig. 9.8 Postulated reconstruction of the ~1.8 Ga Nuna supercontinent.	182

List of tables

3.1 – Summary of results from U-Pb dating	62
4.1 – Results of fractional crystallisation modelling	87
5.1 – Summary sample descriptions	92
8.1 - Compilation of ages for figure 8.8	159
10.1 – Precision and LLD for XRF (University of Leicester)	187
10.2 – Sample details	188
10.3 – Whole-rock geochemistry	201
10.4 – LA-ICP-MS U-Pb data	221
10.5 – Hafnium isotope data	232
10.6 - Oxygen isotope data – chapter 5	246
10.7 - Oxygen isotope data – chapter 6	248
10.8 – U-Pb (TIMS) data for chapter 3	254

Introduction

1.1 Background and rationale

This thesis is essentially a regional geological study, and one that aims to determine the geological evolution of the continental crust that forms southwest Norway. However, a number of ‘themes’ form subtle undertones throughout this work; in their broadest context these are: how, when and where was the continental crust formed? More specifically, it is the relative amount of new continental addition versus recycling of previously formed crust, that forms the strongest theme within this thesis. Particularly focussed on is crustal growth versus recycling within accretionary orogens; crustal growth in this particular setting has been well-studied in modern examples, but has not until recently been applied to the whole Earth history (Cawood et al. 2009).

1.1.1 Topical aspects

How and when the continental crust form and the rate of its production over time are fundamental questions in Earth Science. Answering these questions however has proved difficult, for example the last four decades have seen continued debate over whether the volume of continental crust has remained essentially unchanged since the early Archaean (e.g. Armstrong 1968, 1981), or whether the volume of crust has grown through time (e.g. Moorbath 1978; O’Nions et al. 1979). A key feature in this debate, is the apparent episodicity of crust formation (or juvenile mantle addition to the crust); such episodicity was recognised some 50 years ago (Gastil 1960), but the origin of apparent rapid continental growth periods is still debated today (e.g. Belousova et al. 2009; Condie et al. 2009; Iizuka et al. 2010).

Proxies for the continental growth record such as U-Pb crystallisation ages of juvenile granitoids, and Hf model ages derived from detrital zircons, all feature a certain element of episodicity, with peaks in individual datasets often overlapping (Figure 1.1); these global peaks in crustal production have been used to constrain models of supercontinent and superplume formation, and the link between these two planetary processes (Condie 2002; Li & Zhong 2009). However, it is poorly understood as to how much the peaks in the continental growth record result from actual increases in the production of continental crust, or result from preservational bias (Hawkesworth et al. 2009; Bahlburg et al. 2009).

Recent estimates on growth and recycling at modern plate margins suggest that the global rates of removal of continental crust are similar to the rates of its generation at magmatic arcs (Scholl & von Huene 2007, 2009; Clift et al. 2009). This leads to the inference that the current volume of continental crust may have existed since 2 to 3 Ga (Hawkesworth et al. 2010). To establish the role

of preservational bias in producing the apparent peaks in crustal growth, it is useful to determine a record of when and where continental crust was added and recycled for each continent, and then compare these to obtain a global record. The timing and extent of continental growth within Fennoscandia will be discussed within this thesis.

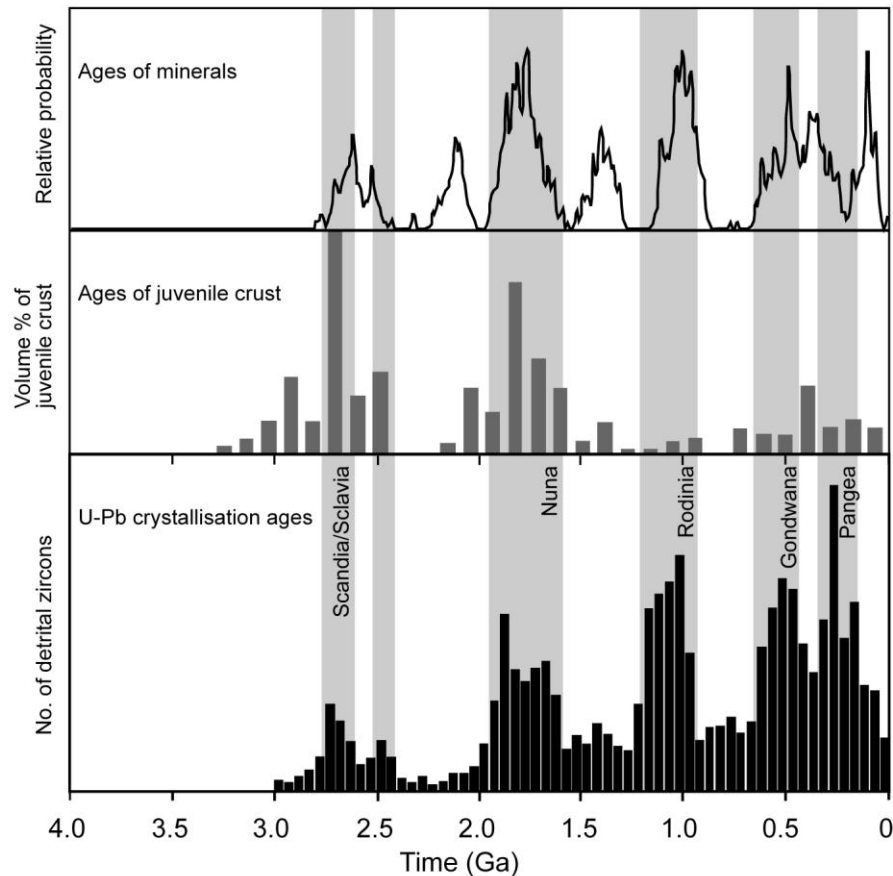


Figure 1.1. Compilation of mineral ages (Gastil 1960), compared with ages of juvenile crust (based on Condie 2005), compared with a compilation of U-Pb ages of detrital zircons (based on Campbell & Allen 2008). Grey bars show the timing of supercontinent formation. Note the episodicity of all three compilations, and the correlation with supercontinent formation. Modified after Hawkesworth et al. (2009).

Convergent margins are complex systems, with various parameters such as the thickness of crust, rate of convergence, angle of convergence, and the width of subduction zone, (e.g. Schellart 2008; Schellart et al. 2008), all impacting on the relative amount of continental growth (i.e. mantle addition) versus continental recycling (i.e. subduction erosion, sediment subduction). Although determining such parameters for ancient subduction zones is fairly unfeasible, general geodynamic settings can be postulated using geochronological and geochemical data. The geodynamic setting of studied magmatic suites is thus discussed in this thesis, with the aim of both constraining the tectonic evolution of the region, and determining the tectonic settings which favour continental growth over continental recycling.

1.1.2 Regional aspects

Proterozoic terranes are exposed over large areas of the continents; crystallisation age compilations of these terranes show peaks at 1.9 and 1.2 Ga (Condie 1998), and the average age of the upper crust determined from Sm-Nd is 2.0 Ga (Miller et al. 1986). Therefore, the Proterozoic is an important time period to study crustal growth. The good correlation of palaeotectonics between the Baltic Shield and other continents, e.g. Laurentia and Amazonia (Karlstrom et al. 2001; Johansson 2009), makes it an ideal location to study Proterozoic crustal growth.

The Fennoscandian Shield (referred to here as Fennoscandia and often referred to as Baltica by previous authors) is thought to involve southwesterly growth and accretion of continental crust, with an Archaean core in the northeast and Mesoproterozoic terranes in the southwest (e.g. Gaál & Gorbatshev 1987). This study focuses on the furthest southwest and what was traditionally thought of as the youngest terrane within the shield, known previously as the Rogaland Vest-Agder sector (Berthelsen 1980), and more recently informally termed the Hardangervidda, Suldal and Rogaland Sectors of the Telemarkia terrane (Bingen et al. 2005b).

Parts of the Rogaland Sector have been relatively well studied as the area is host to the Rogaland Igneous Complex, which comprises a large anorthosite-mangerite-charnockite (AMC) suite. The Suldal and Hardangervidda sectors are relatively poorly studied however, with the oldest gneissic basement not having a known age until recently (Bingen et al. 2005b).

The idea that Fennoscandia grew by sequential accretion of terranes to the west and southwest has been argued against based on data that suggest older crust may exist in the Telemarkia terrane (e.g. Ragnhildsvet et al. 1994). Also, the existence of possible crustal sutures within SW Fennoscandia (Cornell & Austin Hegardt 2004), has lead others to infer that Telemarkia is an exotic addition to Fennoscandia that wasn't accreted till the Sveconorwegian orogen. These arguments formed the initial reason to conduct this study into the poorly known parts of southwest Norway, and they form a topic which is repeatedly discussed within this thesis.

1.2 Aims

Following on from the topical and regional aspects outlined above, the general aims of this study are outlined here:

Using U-Pb geochronology to constrain the timing of tectonothermal events in the Suldal Sector, SW Norway.

Using petrography and whole-rock geochemistry to determine the petrogenesis and tectonic setting of igneous basement rocks in the Suldal Sector.

Using in-situ isotope geochemistry to determine the contribution of mantle material to magmatic events.

Using U-Pb geochronology, isotope and whole-rock geochemistry, assess whether crystalline rocks within Caledonian nappe units correlate with exposed basement that they overlie, and/or with Caledonian nappes elsewhere in Scandinavia.

Using the results collectively, test and develop tectonic models for the Proterozoic geological evolution of southwest Scandinavia.

1.3 Outline

Chapters 2 to 8 form separate entities, each with their own introduction and conclusions; repetition of methods and geological background is kept to a minimum. The reader should refer to Chapter 2 for a regional geological context and background information on the study area. Chapter 9 presents a synthesis of previous findings, as well as new data and ideas on relevant topics.

Chapter 2 presents the geological setting for further chapters, with a brief introduction to the regional geology, and a description of the study area's geology; the latter includes a summary of the field-based and petrographical findings.

Chapter 3 presents a U-Pb geochronological study of basement rocks within the Suldal Sector, using both LA-ICP-MS and TIMS methods. The use of a chemical abrasion method combined with laser-ablation geochronology to produce precise Precambrian U-Pb ages is investigated.

Chapter 4 presents whole-rock geochemistry of the Telemarkian (~1500 Ma) basement rocks in the Suldal Sector, and discusses the petrogeneses of magmatic suites of this age.

Chapter 5 presents hafnium and oxygen isotope analyses measured in-situ in zircons from Telemarkian age gneisses. The data are used to further elucidate the petrogenesis these rocks, and discuss their tectono-magmatic setting in relation to the evolution of the Fennoscandian continent.

Chapter 6 presents whole-rock geochemistry and in-situ hafnium and oxygen isotopes for Sveconorwegian (~1.07-0.93 Ga) rocks from the Suldal Sector; the data are used to constrain the petrogeneses and geodynamic setting of the different granitoid suites.

Chapter 7 presents a LA-ICP-MS U-Pb age for a metarhyolite from a supracrustal belt in the Telemark Sector that has not been previously dated. The origin of this supracrustal belt (Grossæ-Totak) and other 'interorogenic' (~1.45-1.15 Ga) units within SW Fennoscandia is discussed.

Chapter 8 presents a study of the age and provenance of the Caledonian nappe units found within the Suldal Sector (known as the Hardangervidda-Ryfylke Nappe Complex), using LA-ICP-MS U-Pb geochronology and in-situ hafnium isotope analyses.

Chapter 9 presents a synthesis of the conclusions determined in all of the previous chapters. An overview of the tectonic history of the Fennoscandian Shield is presented which combines previous models with the new findings discussed in this thesis. A discussion of continental growth is presented, and is centred around the model of a retreating accretionary orogen. The growth of SW Fennoscandia is also discussed in relation to global tectonics and continental evolution.

1.4 Presentations

Parts of this thesis have been presented as the following presentations:

'SW Fennoscandia in the formation and break-up of Rodinia (1): 1.8 - 1.0 Ga crustal growth and Sveconorwegian reworking.' (Poster), *N. M. W. Roberts, T. Slagstad, M. Marker*, Rodinia Fermor Metting 2009, Edinburgh.

'SW Fennoscandia in the formation and break-up of Rodinia (2): insights from the Hardangervidda-Ryfylke Nappe System.' (Poster), *N. M. W. Roberts*, Rodinia Fermor Metting 2009, Edinburgh.

'Proterozoic crustal growth in SW Fennoscandia' (Poster), *Nick M W Roberts*, Goldschmidt 2009, Davos.

'Proterozoic crustal growth in SW Fennoscandia' (Talk), *Nick M W Roberts*, Crustal Evolution Janet Watson Meeting 2009, London.

'Mesoproterozoic crustal evolution of southwest Norway; 1.5 Ga arc magmatism in Telemarkia.' (Talk), *Nick Roberts, Tim Brewer (decd.)*, 33rd IGC 2008, Oslo.

'Mesoproterozoic crustal evolution of southwest Norway' (Poster), *Nick Roberts, Tim Brewer (decd.)*, Geochemistry Group AGM 2008, London.

U-Pb data that is cited in chapters 5 and 6 was presented as:

‘Mesoproterozoic growth, rifting, drifting and continental collision in Rogaland, SW Sveconorwegian province’ (Poster), *Slagstad, T., Marker, M. and Skår, Ø.*, 33rd IGC 2008, Oslo.

1.5 Data sources

All data was collected by the author, except for a proportion of the whole-rock geochemistry in chapters 3 and 6, which was acquired by Trond Slagstad and Mogens Marker for the Norwegian Geological Survey (NGU), and some of the U-Pb data used in chapters 5 and 6, which was acquired by Trond Slagstad and Mogens Marker on the Nordsim instrument at Stockholm. Also, some samples were collected by Tim Brewer, these have been re-analysed by the author. Some of the hafnium and oxygen isotope data was acquired on zircons already dated by Trond Slagstad and Mogens Marker. The interpretation of geochemical data obtained from NGU, and the interpretation of hafnium and oxygen isotope data obtained on zircons not belonging to the author, are entirely those of the author. Each chapter in this thesis is the work of the author, including all interpretations and conclusions. Supervisors and collaborators did provide some general discussion on data quality, preliminary data interpretation, and the form and presentation of the thesis.

The geology of the Suldal Sector, southwest Norway

2.1 Regional Geology

Fennoscandia is the northwest part of the East European Craton, and comprises an Archaean craton in the northeast, mantled by successively younging geological domains to the southwest (Gaál & Gorbatshev 1987). Southern Norway and southwestern Sweden comprise the Southwest Scandinavian Domain (SSD), which was reworked during the Sveconorwegian orogeny (1.15-0.9 Ga). Crustal growth of this domain has been attributed to Gothian (1.75-1.55 Ga; Gaál & Gorbatshev 1987) and Telemarkian (1.52-1.48 Ga; Bingen et al. 2005b, 2008a) events. During the Sveconorwegian orogeny, lithospheric-scale shear zones are inferred to have displaced crustal domains (Park et al. 1991; Romer 1996; Stephens et al. 1996; Bingen et al. 2001b, Andersen et al. 2002b) so that the pre-Sveconorwegian configuration of the continent is enigmatic.

The SSD is bound by the Transcandinavian Igneous Belt to the east, and by Caledonian nappes to the north, and has been split into lithotectonic domains which young from east to west. The Transcandinavian Igneous Belt (TIB) is a composite belt of igneous rocks that trends NNW-SSE through southern Sweden to the NW Norwegian coast. The belt is dominated by coarse-grained porphyritic granitoids. TIB magmatism is split into two episodes, TIB 1 (1.81-1.77 Ga) and TIB 2/3 (1.72-1.66 Ga; Åhäll & Larson 2000), with TIB 1 intruding Svecofennian crust and TIB 2/3 intruding TIB 1 crust (Åhäll & Connelly 2008). The tectonic setting of the belt has been debated but is generally considered to be related to subduction converging in a NE/E direction (see Högdahl et al. 2004). Andersen et al. (2009a) propose that the voluminous granitoids were produced by anatectic melting of juvenile Svecofennian crust, with voluminous deep crustal mafic intrusions acting as a heat source.

The Eastern Segment (or Kläralven-Aträn terrane) lies to the west of the TIB belt, but is considered to be an extension of the younger TIB 2/3 magmatic belt that has been reworked prior to and during the Sveconorwegian orogeny (Connelly et al. 1996; Söderlund et al. 1999). The Protogine Zone marks the boundary between reworked and relatively undeformed TIB crust, and is a zone of both Gothian and Sveconorwegian deformation (Larson et al. 1990).

The Idefjorden domain lies to the west of the Eastern Segment. The domain comprises gneisses and granitoids of Gothian and Sveconorwegian age, as well as units not found in other terranes within the SSD, e.g. 1.38-1.30 Ga granitoids (Åhäll et al. 1997; Austin Hegardt et al. 2007). Growth of the Idefjorden crust occurred in the Gothian by continental arc magmatism and accretion of island and back-arcs (Brewer et al. 1998; Åhäll & Connelly 2008). The arc-crust of the Idefjorden domain may have formed proximal to the Fennoscandian continent along the same subduction margin that formed the TIB 2/3 crust (e.g. Åhäll & Connelly 2008), or may represent an allochthonous crustal

domain that was accreted to the Fennoscandian craton during the Sveconorwegian (Cornell & Austin Hegardt 2004). The Mylonite Zone that divides the Idefjorden and Eastern Segment is a zone of Sveconorwegian deformation, related to early thrusting of the Idefjorden domain over the Eastern Segment, and later exhumation of the Eastern Segment via east-west extension (Söderlund 1999).

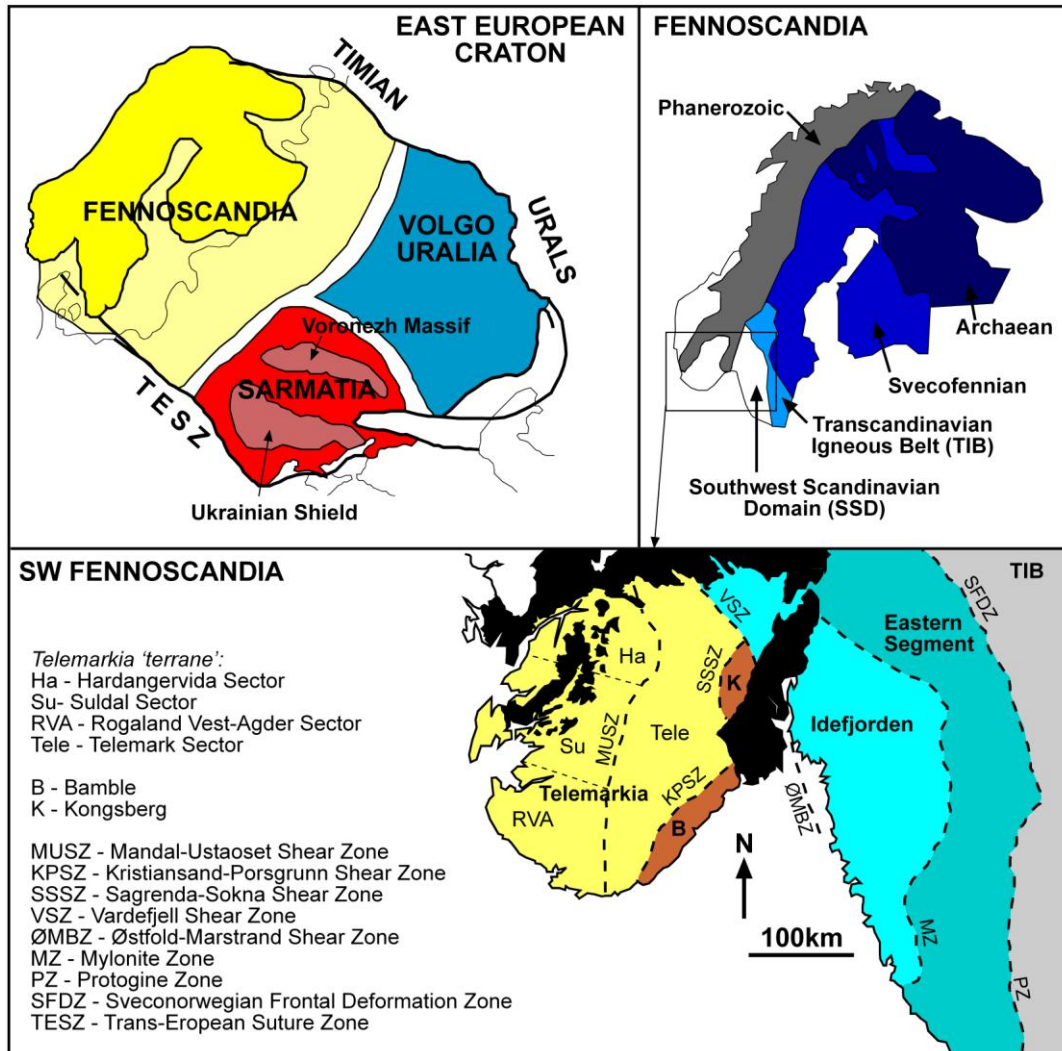


Figure 2.1. Map of the East European Craton, Precambrian domains within Fennoscandia and terranes within the Southwest Scandinavian Domain. After Bogdanova et al. 2008; Bingen et al. 2008a.

The Bamble and Kongsberg blocks are grouped together by Bingen et al. (2005b), who consider them to be a collision zone between the Telemarkia and the Idefjorden domains. The Bamble and Kongsberg domains both include gneiss and granitoids units similar in age and composition to the Telemarkia and Idefjorden terranes that bound them (Åhäll & Connelly 2008; Andersen et al. 2002b; Bingen et al. 2005b), i.e. subduction-related arc plutonics and volcanics of Hisingen age (1.59-1.52 Ga; Åhäll & Connelly 2008). Metasedimentary units within the domain were deposited between the Telemarkian and Sveconorwegian periods (de Haas et al. 1999, 2002; Bingen et al. 2001; Åhäll et al. 1998; Knudsen et al. 1997).

The crust west of the Bamble-Kongsberg domain has been grouped into a single terrane (Telemarkia; Bingen et al. 2005b) that comprises four sectors; the Telemark Sector in the east, and the Rogaland, Suldal and Hardangervidda Sectors in the west. The latter three forming the Hardangervidda-Rogaland Block of Andersen et al. (2005), or the Rogaland-Vest-Agder Sector of Berthelsen (1980).

The Telemark Sector features a >10km thick succession of supracrustals comprising the 1.5->1.35 Ga Vestfjorddalen, and 1.16-1.10 Ga Sveconorwegian Supergroups (Laajoki et al. 2002). The Vestfjorddalen Supergroup comprises the bimodal 1.51 Ga Rjukan Group and the overlying sedimentary Vindeggan Group. Bimodal magmatism is related to continental extension that occurred inboard of a subduction zone in a setting similar to the Granite-Rhyolite provinces in the mid-continental US (Slagstad et al. 2009). The Vemork Formation that is part of the Rjukan Group is dominated by metabasalt units; an intercalated metavolcanite is dated at 1495 ± 2 Ma (Laajoki & Corfu 2007). The 5km thick Vindeggan group comprised mostly of quartz-rich strata; a cross-cutting diabase intrusion dated at 1347 ± 4 Ma (Corfu & Laajoki 2008) places a minimum age constraint on sedimentary deposition within the group. The Sveconorwegian Supergroup comprises bimodal volcanic and sedimentary sequences deposited between 1.17 and 1.12 Ga (Laajoki et al. 2002; Bingen et al. 2003), that formed in extensional basins inboard of a continental arc (Brewer et al. 2004), or in a Basin and Range setting (Bingen et al. 2003). Intrusions in the Telemark Sector include 1.19-1.13 Ga A-type plutons (Bingen et al. 2003), and a 1.03 Ga suite transitional between calc-alkaline and A-type (Bingen & van Breemen, 1998). The Setesdal region is host to the oldest crust recognised in Telemark, the Asen tonalite (1555 ± 29 Ma; Pedersen et al. 2009). The main group of gneisses in the Setesdal region have ages of 1.32-1.22 Ga (Pedersen et al. 2009). At 1.2-1.2 Ga, juvenile granitoids intruded the gneisses in the Setesdal region; in the Vråvatn Complex in central Telemark, juvenile magmatism is dated at ~ 1.2 Ga (Andersen et al. 2007b; Pedersen et al. 2009).

In the Hardangervidda Sector (Figure 2.1) a gneiss complex comprises metasediments interlayered with granitic gneisses, the latter has been dated at ~ 1.65 Ga (Ragnhildsvet et al. 1994). A quartzofeldspathic gneiss yields a bimodal distribution of zircon ages, initially interpreted as gneiss crystallisation at 1.67 Ga and migmatisation at 1.47 Ga (Sigmond et al. 2000), and later interpreted as a paragneiss unit (Bingen et al. 2005b). Detrital zircon populations from metasediments in the area include Archaean to Mesoproterozoic components, with deposition constrained to later than 1.54 Ga (Bingen et al. 2001).

The geology of the Suldal Sector (Figure 2.1) can be divided into two parts, the 'basement' and the autochthonous/allochthonous nappes of Caledonian age. The basement was originally divided into three parts, supracrustal belts, a gneiss complex, and igneous intrusions; with the latter being both older and younger than the supracrustals (Sigmond 1978). All of these rocks formed in three

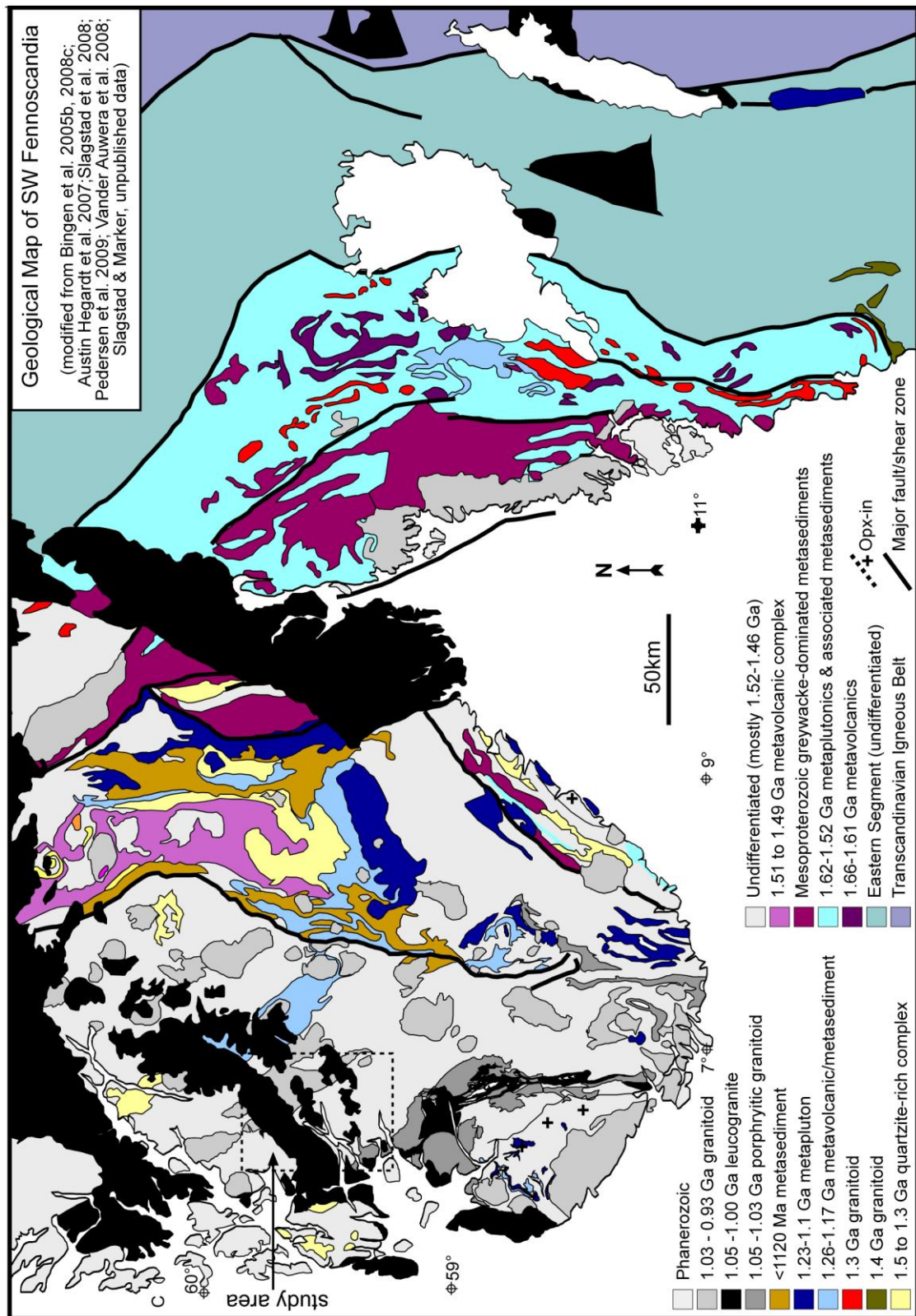


Figure 2.2. Geological map of SW Fennoscandia, (see Figure 3.1 for study area).

separate Proterozoic events. The gneiss complex, most supracrustals and many of the intrusions are dated between 1540 and 1480 Ma (Bingen et al. 2005b; Slagstad et al. 2008). One supracrustal belt, Sæsvatn-Valldall, is younger and formed at 1260-1210 Ma (Bingen et al. 2002; Brewer et al. 2004).

A few granitoid intrusions within the sector have Sveconorwegian ages (Andersen et al. 2002a, 2007a; Bingen et al. 2005b; Slagstad et al. 2008).

Supracrustal rocks in the Suldal Sector have been mapped as three belts: Grjotdokka-Nesflaten, Suldal-Åkrafjord and Sæsvatn-Valldall (Sigmond 1978). The Grjotdokka-Nesflaten belt has not been directly dated, but surrounding conformable gneiss dated at 1499 ± 12 Ma, lead Bingen et al. (2005b) to interpret a ~1500 Ma age for the belt. Deformed porphyritic granodiorite gneiss lenses that occur in the Suldal-Åkrafjord belt are dated at 1497 ± 12 and 1496 ± 12 Ma (Bingen et al. 2005b); the age of volcanism in this belt is thus also interpreted to be ~1500 Ma. The Sæsvatn-Valldall belt has a metarhyolite at its base dated at 1259 ± 2 Ma (Brewer et al. 2004), and a sandstone at its top that is younger than 1211 ± 18 Ma (based on the oldest dated zircon grain; Bingen et al. 2002). The belt formed in a marginal continental setting (Bingen et al. 2002), probably in a back-arc environment (Brewer et al. 2004).

The Rogaland Sector (Figure 2.1) comprises similar Telemarkian (1.52-1.48 Ga) rocks to those found in the Suldal Sector. Metasedimentary units are commonly interleaved with orthogneisses in the Rogaland Sector (Slagstad & Marker pers. comm. 2008), whereas they are rare in the Suldal and Hardangervidda Sectors. Concordant and deformed amphibolitic sheets found within the Rogaland gneisses have a Large-Ion-Lithophile-Element enriched N-MORB type signature (Slagstad & Marker pers. comm. 2008), are interpreted to have formed in an ocean-forming rifting event prior to the Sveconorwegian collision (Slagstad et al. 2008). The ~1500 Ma gneisses in the Rogaland Sector are typically migmatitic and highly deformed; less-deformed gneisses and granitoids are also found within the sector which are ~1200-1220 Ma in age (Slagstad et al. 2008).

The Sirdal Zone (Slagstad et al. 2008) is a broad region dominated by porphyritic granitoids and leucogranites, including the 1050 Ma Feda suite (Bingen et al. 1993; Bingen & van Breemen 1998). The granitoids may have an origin as an active continental margin that existed just prior to Sveconorwegian collision (Bingen & Van Breemen 1998; Slagstad et al. 2008), or an origin from partial melting of pre-existing crust with an arc signature as a consequence of crustal thickening during the Sveconorwegian orogeny (Bingen et al. 2008c). The Sirdal Zone may have formed from the partial subduction of the Rogaland Sector under the Suldal Sector during the early stages of the Sveconorwegian orogeny (Slagstad et al. 2008).

Late-Sveconorwegian (i.e. post-collisional/post-kinematic) granites intrude all of the Sectors. A broad region of granite plutons extends north to south and parallel to the Mandal-Ustaoset Line that divides the Telemark Sector from the Hardangervidda-Suldal-Rogaland Sectors. This alignment has been related to granite plutonism along lithospheric weaknesses that formed during the Sveconorwegian orogeny (Bogaerts et al. 2003; Duchesne et al. 1999). The ~930 Ma Rogaland anorthosite complex (Schärer et al. 1996) is the youngest of the late-Sveconorwegian intrusions in the region.

The Suldal and Hardangervidda Sectors are overlain by the Hardangervidda-Ryfkykle Nappe Complex (Andresen & Færseth 1982; see Chapter 7), which was thrust onto the basement during the Caledonian orogeny (e.g. Gee et al. 1975). The deformation of the basement related to this orogeny is minimal and limited to a zone (<10m) of weak shearing only seen in some places. Together the nappes and basement have been weakly folded into large open folds (Sigmond 1978).

Within the Suldal sector, metamorphism has been dated by the Re-Os method on Cu-Mo mineral occurrences (Stein & Bingen 2002), with rocks from the Sæsvatn-Valldall belt recording various stages of metamorphism and deformation: onset of greenschist facies metamorphism and deformation at 1047 ± 2 Ma, peak ductile deformation at 1032 ± 2 Ma, incipient extension/relaxation at 1025 ± 2 Ma and full relaxation (and brittle deformation) at 1017 ± 2 Ma (Stein & Bingen 2002). Within the RVA sector, high-grade metamorphism has been attributed to the intrusion of the Rogaland Igneous Complex (Tobi et al. 1985), it has now been shown that high-grade metamorphism occurred prior to the intrusion, and a UHT overprint was locally induced due to contact metamorphism from the igneous complex (Möller et al. 2002). Within the UHT isograd surrounding the Rogaland Igneous Complex, zircon growths believed to be metamorphic reveal high-grade metamorphism at 1000 Ma (M1), ultra-high grade metamorphism at 930 Ma (M2), and later high-grade metamorphism related to M2 at 910 Ma (M3) (Möller et al. 2002, 2003). Re-Os dating of molybdenite records granulite-facies metamorphism at 973 ± 4 Ma, that probably resulted from regional decompression towards the end of a prolonged period of metamorphism (1.03-0.97 Ga) (Bingen & Stein 2003). The origin of regional/local metamorphism and structural deformation outside of the area affected by the Rogaland Igneous Complex, is not constrained, but has been postulated to be Sveconorwegian in age (Bingen, cited in Bingen et al. 2005b).

2.2 Geology of the Suldal Sector

2.2.1 Description of units

The basement rocks (that are assumed to be 1540-1480 Ma in age) are predominantly grey orthogneisses that are variably deformed and recrystallised, and likely represent mid-crustal to supracrustal igneous protoliths. Primary contacts and igneous structures have been obscured by the deformation and recrystallisation, such that a lithostratigraphy and chronology of events is difficult to elucidate.

As stated above, the original mapping defined three separate supracrustal belts; however, banded fine-grained gneisses interpretable as supracrustal rocks outcrop throughout most of the Sector. The discrimination of the Suldal-Akrafjord belt as a separate unit is therefore abandoned; although, one sequence of banded fine-grained rocks that outcrops east of Sauda is distinguished as a separate unit. This belt, referred to here as the Zinc Mine Banded Gneiss, forms a coherent block of banded and layered gneisses that have a single structural fabric, and is bound by undeformed granites and

Caledonian nappes. A few samples were taken from the Grjotdokka-Nesflaten belt in the Nesflaten area, the term 'Nesflaten Suite' is used when referring to this study area.

Sauda Grey Gneiss

The term Sauda Grey Gneiss (referred to as Grey Gneiss) refers to the bulk of the crystalline basement rocks, except for undeformed to weakly deformed granitoids that are assumed to be Sveconorwegian in age, the Zinc Mine Banded Gneiss and Nesflaten Suites, and the amphibolite suite. The Grey Gneiss is a heterogeneous complex of orthogneisses, comprising gabbro, diorite, granodiorite and tonalite compositions, along with minor granite-syenite. The complex is dominated by fine to medium-grained porphyritic grey gneisses. Some outcrops feature banding, commonly between aphyric and phyrlic units, likely representing volcanic tuff/ignimbrite/lava (i.e. supracrustal) layers. Medium-grained porphyritic gneisses likely represent hypabyssal/upper crustal intrusions. Gneisses with evidence for a non-igneous epiclastic origin (i.e. paragneiss) were not observed.

Sauda Grey Gneiss orthogneisses comprise plagioclase, biotite, amphibole and varying quartz contents, with minor K-feldspar in more silicic compositions. Accessory phases include abundant titanite which commonly forms coronas around ilmenite, apatite, epidote in the more mafic lithologies, and zircon in the more evolved lithologies. The amphibole is a hornblende in more pristine samples, but is commonly retrogressed to actinolite. Alteration of feldspar to sericite is widespread in most samples and biotite is commonly altered to chlorite.

Enclaves are common within the grey gneisses, and are of variable lithologies. The most common are fine-grained mafic to felsic xenoliths within granodioritic gneisses, but also displayed are tonalitic/granitic enclaves in more mafic units, often interpretable as disaggregated veins/dykes. Some outcrops include evidence of magma mingling, the best example of this comprises aphyric granodioritic gneiss mingling with aphyric dioritic gneiss; margins between the two lithologies are rounded. Partial melting within the Grey Gneiss is evident in some outcrops, usually without large-scale separation of leucosome and melanosome. In a few outcrops, leucosomes of tonalitic material have formed a network of cm- scale veins which are normally sub-parallel to the structural fabric. A few outcrops of fine-grained banded gneiss exhibit patch-leucosome formation, with new growth of hornblende within the leucosomes.

Zinc Mine Banded Gneiss

The Zinc Mine Banded Gneiss (ZMBG) is a succession of fine to medium-grained banded gneisses that outcrop in the valley east of the town of Sauda. Compositions range from basalt to rhyolite, but the suite is dominated by dacitic to rhyolitic compositions. The gneisses are commonly porphyritic with <10mm size phenocrysts of K-feldspar and quartz, in thin-section these are often aggregates of both quartz and feldspar. Interlayered and conformable with fine-grained gneisses are a few 10cm's

to <50m layers of coarse porphyritic granodiorite (augen gneisses). These are interpreted as hypabyssal intrusions which are likely to be comagmatic with the surrounding gneisses. The mineralogy of the ZMBG is comparable to that of the Sauda Grey Gneiss.

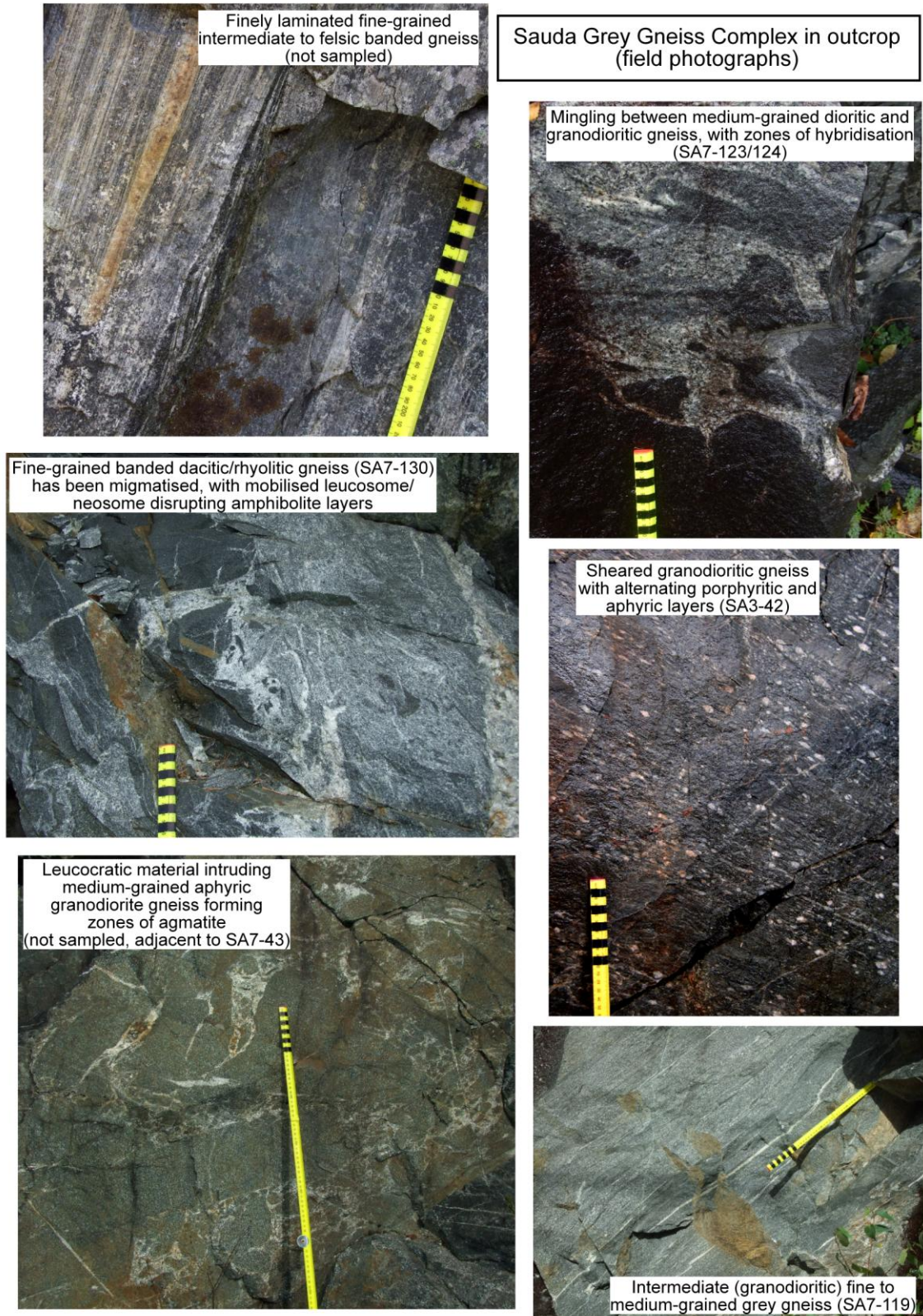


Figure 2.3. Field photographs of Sauda Grey Gneiss outcrops

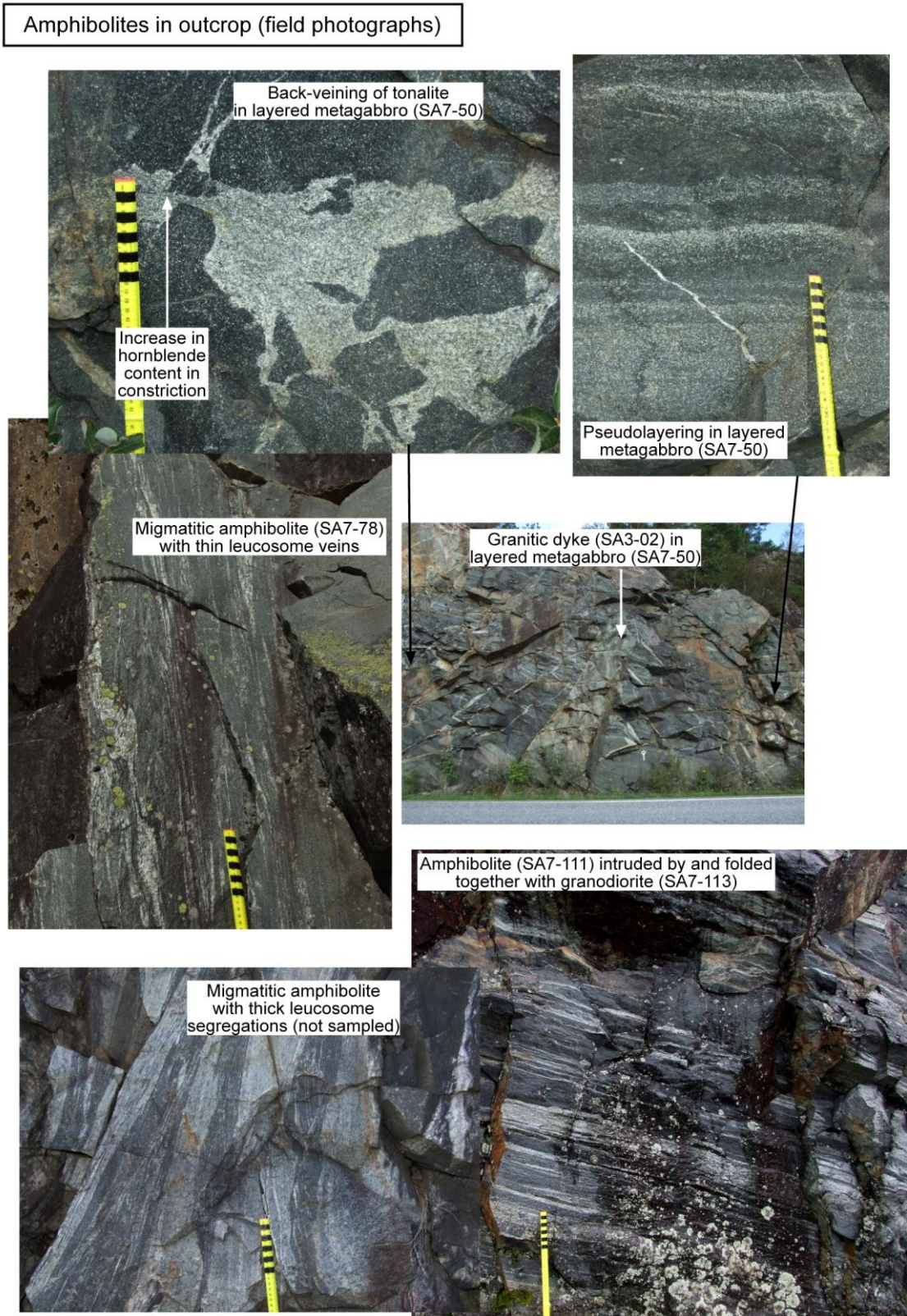


Figure 2.4. Field photographs of various amphibolite outcrops

Nesflaten Suite

The Nesflaten Suite comprises gneisses ranging from basalt to rhyolite in composition. Outcrops of gneiss with fine (<10cm) alternations of mafic and felsic compositions exist, as do mica-rich quartz-feldspar layers; some of these may have epiclastic origins. As well as abundant hornblende and

plagioclase, garnet and staurolite are recorded from one unit. Exposures of the belt in the north display networks of white granite/pegmatite intruding the gneiss complex; these are likely connected to a Sveconorwegian pluton.

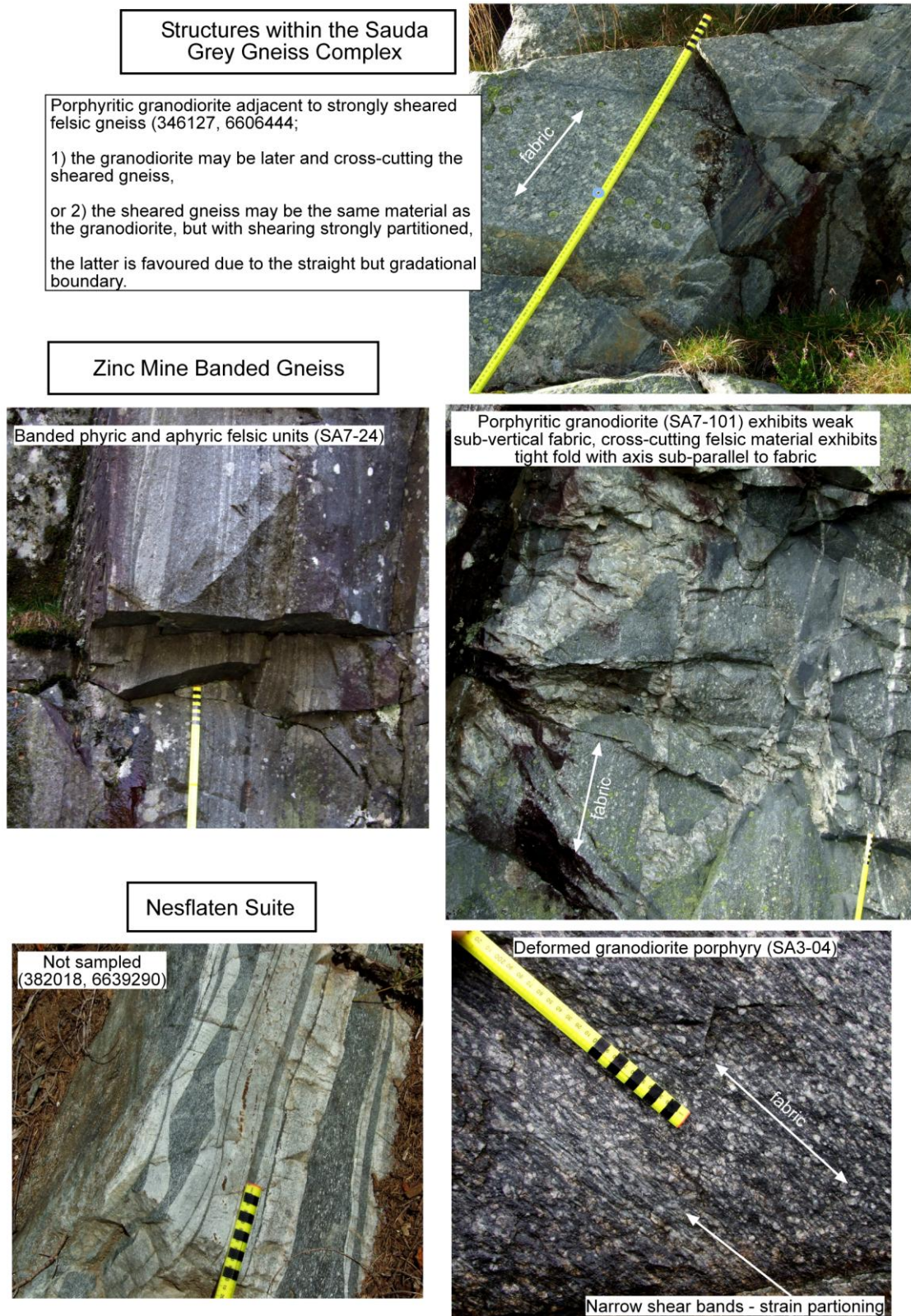


Figure 2.5. Field photographs of the Grey Gneiss, Zinc Mine Banded Gneiss and Nesflaten Suite.

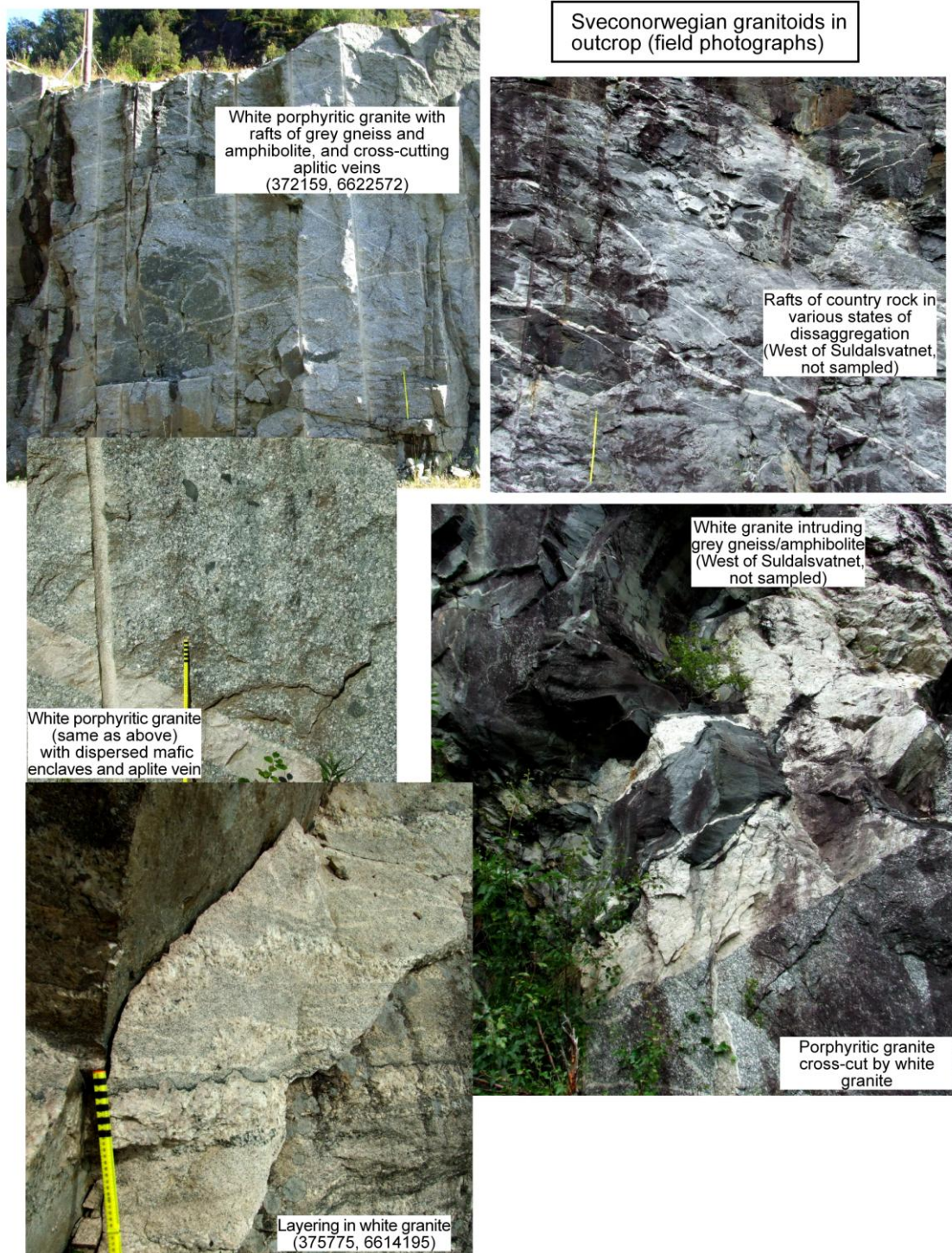


Figure 2.6. Field photographs of various outcrops of the Storlivatnet pluton

Amphibolites

Numerous mafic bodies that are metamorphosed to metabasites/amphibolites are found within the gneisses and granitoids; this suite is separated from the Grey Gneiss on rather subjective grounds, the separation is largely based on field-relations. Lithologies that are true amphibolites, or are more felsic but rich in amphibole and grade into more mafic lithologies, or are mafic enclaves within other lithologies, are grouped as the amphibolite suite. Undeformed dykes that have straight-

margins and intrude all other suites are not included in this suite. However, some dykes/sills cross-cut the fabric in the grey gneiss but are weakly deformed themselves, and these are included. Undeformed to weakly deformed gabbroic bodies are common, these are commonly heterogeneous

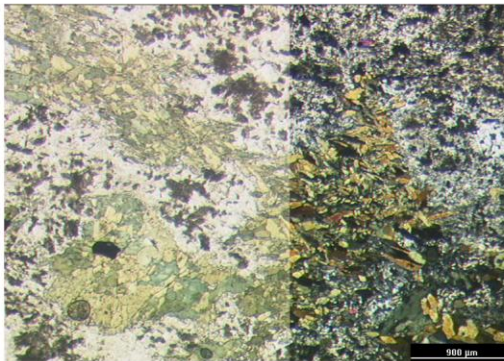


Figure 2.7. Aggregates of polygonal amphibole surrounded by plagioclase-rich matrix, aggregates likely replaced larger phenocrysts of olivine and pyroxene. Plagioclase is heavily altered to sericite. (*Amphibolites- Medium-grained layered amphibolite - SA7-50*)

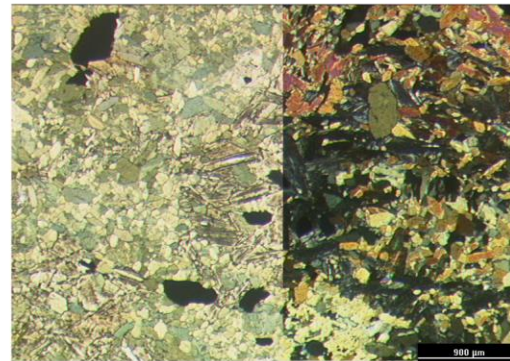


Figure 2.8. Patch of chlorite (centre) replacing biotite grains, relatively coarse anhedral Fe-Ti oxide grains, and polygonal amphibole grains. (*Amphibolites- Medium-grained layered amphibolite - SA7-50*)

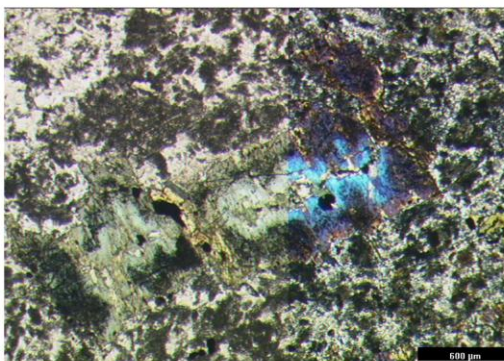


Figure 2.9. Subidioblastic amphibole grain with corona that contains fine-grained Fe-Ti oxide grains. Matrix is dominated by seritised feldspar. (*Amphibolites- Medium-grained layered amphibolite - SA7-50*)



Figure 2.10. Subidiomorphic elongate amphibole grains forming a fabric with quartz and altered feldspar grains. Small rounded apatite grains can be seen in some amphibole grains. (*Sauda Grey Gneiss - Fine-grained aphyric diorite gneiss, SA7-77*)

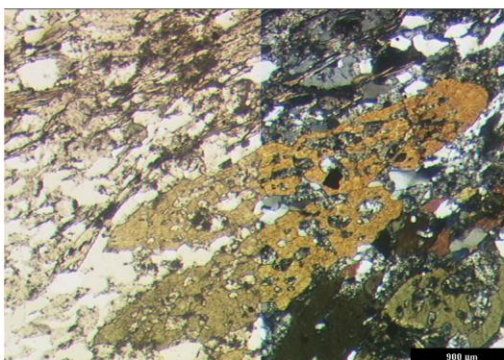


Figure 2.11. Elongate poikiloblastic amphibole grains that are subparallel to the fabric. Matrix is composed of finer-grained quartz and altered biotite and feldspar. (*Sauda Grey Gneiss - Medium-grained hornblende-phyric granodiorite gneiss, SA7-115*)

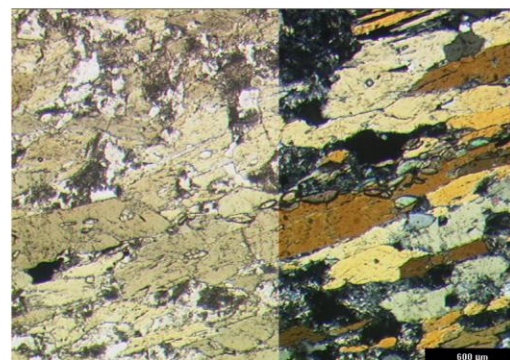


Figure 2.12. Elongate subidiomorphic biotite and amphibole grains, with small idiomorphic titanite grains forming a band that is parallel to the fabric and biotite cleavage (centre). (*Amphibolites- Medium-grained amphibolitic gneiss, SA7-114*)

bodies, ranging from coarse-grained plagioclase-porphyritic diorites to fine-grained massive gabbro, often with a network of narrow (<10cm) leucosome veins running through them. Southwest of the town of Sauda, there is a layered gabbro body. The rhythmic layering is nearly flat-lying, repeats every 10-15cm's and comprises retrogressed hornblende at the base, grading into plagioclase at the

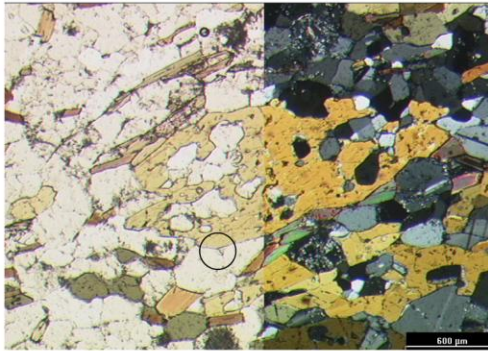


Figure 2.13. Poikiloblastic hornblende grain with straight margins and well-developed triple-junctions with plagioclase and quartz grains (e.g. black circle).
(Nesflaten - Medium-grained aphyric diorite gneiss, 375910, 6608495)

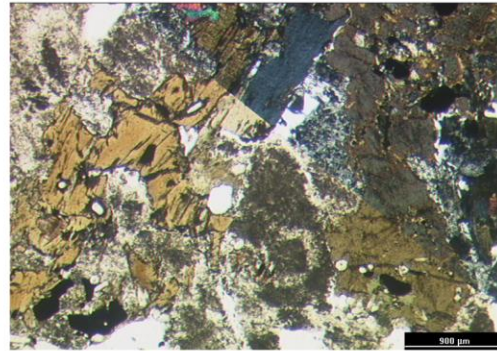


Figure 2.14. Xenoblastic biotite and hornblende with chlorite forming after biotite (top centre). Feldspars are heavily altered to sericite. Small apatite grains can be seen in the mafic minerals.
(Amphibolites - Coarse-grained amphibolite SA3-49)

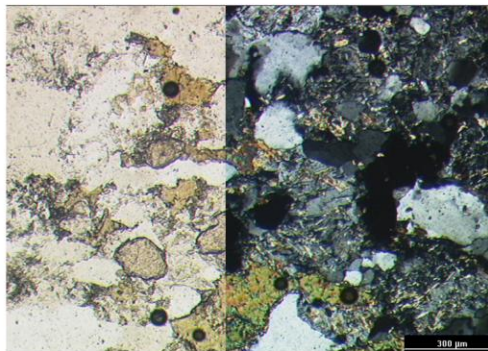


Figure 2.15. Subidiomorphic garnet grains along with xenoblastic biotite and a quartz-feldspar matrix. Sericite grains are visible, forming after feldspar.
(Zinc Mine Suite - Fine-grained aphyric felsic gneiss, SA3-63)

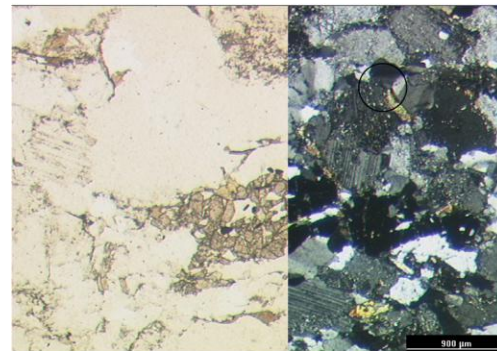


Figure 2.16. Xenoblastic garnet grain along with minor fine-grained biotite and epidote. Original twinning can be seen in plagioclase grains. Quartz extinction is undulose (black circle).
(Zinc Mine Suite - Medium-grained aphyric granodioritic gneiss, SA3-67)

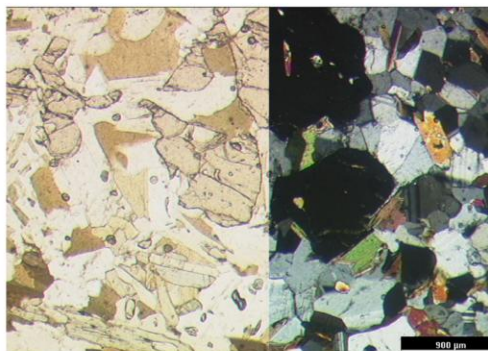


Figure 2.17. Subidiomorphic garnet grains along with subidioblastic hornblende and biotite grains. Feldspar is relatively unaltered.
(Nesflaten - Medium-grained aphyric mica-rich quartz-feldspar schist, 378082, 6614677)

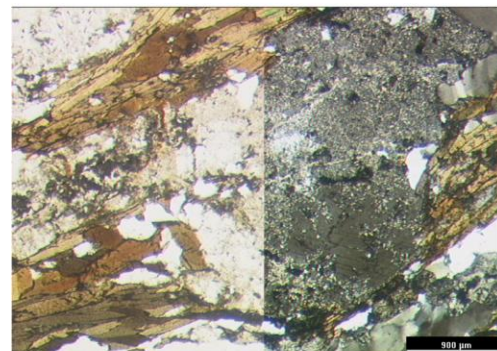


Figure 2.18. Elongate biotite laths forming a fabric which is bent around an augen composed of sericitised feldspar grains.
(Sauda Grey Gneiss - Medium-grained porphyritic granodiorite gneiss, adjacent to SA3-42)

top. The layered body is intruded by an undeformed 1-2m wide tonalitic dyke, and within the surrounding area is disaggregated by more granitic material. The tonalite comprises plagioclase, quartz and biotite, with retrogression to sericite, epidote and chlorite. It appears to be the same composition as the top of the rhythmic gabbro layers, thus, the tonalite is interpreted to be a

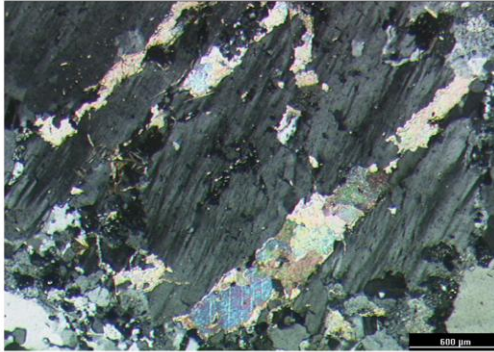


Figure 2.19. Calcite veins within large deformed mesoperthite grain.
(Sauda Grey Gneiss- Deformed feldspar-phyric granodiorite gneiss - SA3-04)

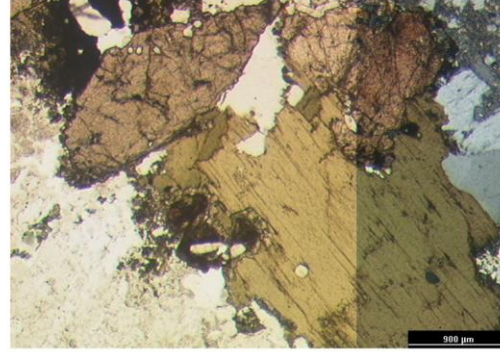


Figure 2.20. Large anhedral biotite and titanite grains forming a restitic clot. Pseudo-hexagonal apatite grains are visible in the mafic minerals. Coarse biotite grains are rimmed with finer biotite, epidote and titanite grains.
(Sveconorwegian intrusion - Undeformed porphyritic biotite granite, SA3-01)



Figure 2.21. Deformed biotite grain surrounded by finer biotite grains (top right), altered and twinned plagioclase (left of centre), surrounded by perthitic feldspar, and quartz grain with undulose extinction (bottom right).
(Sveconorwegian intrusion - Undeformed porphyritic biotite granite, SA3-01)



Figure 2.22. Myrmekite development (left of centre) on edge of K-feldspar, anhedral titanite grain (right of centre), and chlorite after biotite (top right).
(Sveconorwegian intrusion - Undeformed porphyritic biotite granite, SA7-80)

comagmatic back-veining feature which occurred in a brittle environment. Deformed within the grey gneiss and porphyritic granitoids are numerous mafic enclaves. These comprise biotite and amphibole with minor plagioclase and quartz, and resemble the mafic units within supracrustal belts. The age of the amphibolites is generally unconstrained. The tonalitic dyke that intrudes the layered gabbro is ~1500 Ma in age (see Chapter 3), thus, this gabbro is part of the ~1500 Ma magmatic event, or potentially could be older.

Granitoids

Weak to moderately deformed coarse-grained porphyritic granodiorites occur as sheets within the Grey Gneiss complex, ranging from metres to tens of metres in width. These are conformable to the

fabric of the Grey Gneiss, and generally have graded boundaries into the Grey Gneiss lithologies. Undeformed bodies of porphyritic granite also occur; these have varying mafic content, grading from porphyritic biotite-hornblende granodiorites to porphyritic biotite granites, and probably represent zoned plutonic bodies. The distinction between ~1500 Ma plutonic bodies and those of Sveconorwegian age is unclear, as both deformed and undeformed examples of each exist. Bodies of leucogranite occur also, generally in association with porphyritic granites. Again the age of these is problematic, as both ~1500 Ma and ~1050 Ma examples have been dated (Slagstad et al. 2008).

2.2.2 Structure

The Sauda Grey Gneiss Complex contains a structural fabric which has variable imprint across the region. The strongest deformation is recorded by proto-mylonitic banded units; phenocrysts within these are stretched but do not record an interpretable sense of shear. The majority of the outcrops record a sub-vertical L-fabric. Strain-shadow formation may have been strong during the main deformation phase, because undeformed outcrops occur adjacent to highly deformed outcrops. Within single lithologies, strain localisation into cm's and 10cm's scale is common. The boundaries between different lithologies are diffuse due to recrystallisation and the variable strain. The complex nature of the outcrops probably reflects multiple phases of intrusions, which in turn have intruded and deformed supracrustal units.

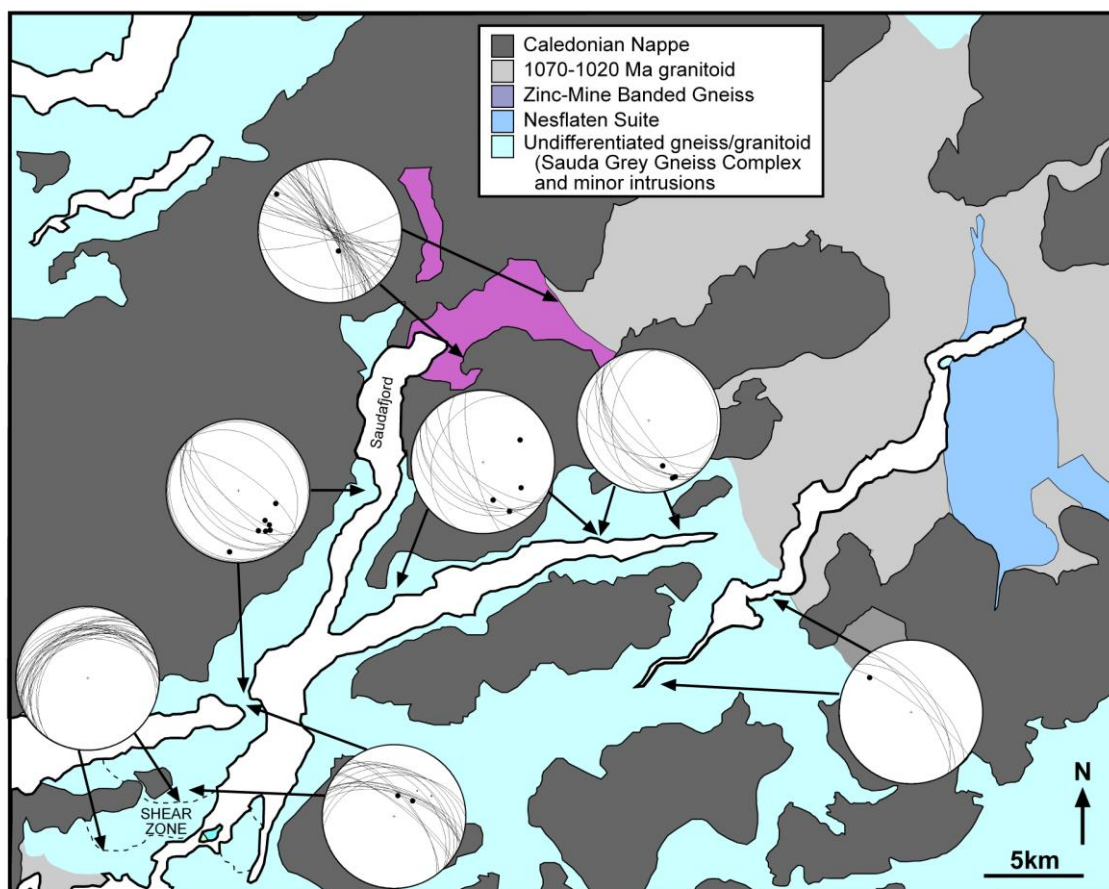


Figure 2.23. Map of the study area with lower-hemisphere stereonet showing planes and lineations (black spots), arrows define the transect that the structural data were obtained from for each plot.

The dominant strike trend is NW-SE (see Figure 2.23); although fold closures were not seen in the field, the main regional structure is that of tight to isoclinal folding with sub-vertical fold axis that trend NW-SE. Lineations dip to the southeast predominantly, suggesting stretching along the NW-SE fold-axis, and also that the fold-axis may be dipping to the southeast. A broad zone of strong shear that occurs to the southwest of Saudafjord (SHEARZONE in Figure 2.23) has a strike perpendicular (NE-SW) to the regional strike trend. Within both the ZMBG and Nesflaten Suite, a strong sub-vertical S-fabric is penetrative in a NNE-SSW direction, and phenocrysts are commonly stretched into augen.

The age and origin of deformation within the region is not constrained, but is generally considered to be Sveconorwegian (Bingen et al. 2005b). The complex nature of many outcrops is probably related to intrusion-related deformation during the main magmatic event (i.e. inferred to be Telemarkian ~1500 Ma). The regional NW-SE strike trend must be younger than the ~1500 Ma magmatic episode, because it affects all of the units except for the undeformed granite plutons; thus, this strike direction likely formed in relation to regional Sveconorwegian deformation and metamorphism (see next section), but this has yet to be demonstrated. The broad NW-SE strike direction is compatible with compression in a NE-SW direction, as would be expected with Sveconorwegian collision with an indenter from the SW. However, the Sveconorwegian collision may have been oblique (Park et al. 1991; Romer 1996; Stephens et al. 1996; Bingen et al. 2001), in which case the dominant strike trend may reflect strain partitioning in a transpressional regime. The dominant strike direction in the Hardangervidda Sector is E-W (Sigmond 1998), suggesting there may be more complexity to the regional structures than determined and discussed here.

2.2.3 Metamorphism (summary)

The petrography of orthogneisses from the Grey Gneiss, Zinc Mine Banded Gneiss and Nesflaten Suite, indicates widespread regional metamorphism that peaked at amphibolite-facies (see figures 2.7 to 2.22) No examples of retrogression from granulite-facies are observed, and also, no relic igneous pyroxenes or olivines are observed. In some lithologies actinolite and epidote are the peak-metamorphic minerals, indicating lower-amphibolite-facies has been reached; in other examples hornblende and garnet are preserved, suggesting middle-amphibolite-facies. Retrogression from hornblende to actinolite is observed, as is retrogression from biotite to chlorite. Alteration of feldspars to sericite and sausserite is widespread. Veins are commonly quartz dominated, but occasionally calcite filled. Metamorphic amphibole and plagioclase commonly are fabric-forming, suggesting peak metamorphism was likely synchronous with regional deformation. Metamorphic aureoles relating to undeformed granitoids were not observed.

2.3 Conclusions

The basement in the Suldal Sector is dominated by orthogneisses that are assumed to be 1540-1480 Ma in age (Bingen et al. 2005b; Slagstad et al. 2008); based on their petrology, petrography and

intrusive-relations, they are interpreted as mid- to upper-crustal, hypabyssal and supracrustal igneous rocks, intercalated together during multiple periods of intrusive activity during evolution of a mature volcanic arc. This arc complex was intruded by composite granitoid plutons during the Sveconorwegian orogeny. Mafic intrusions are related to the main arc event, but also cross-cut interpreted Telemarkian structures, and occasionally cross-cut Sveconorwegian granitoids. Metamorphism and regional deformation likely occurred (but this is not yet demonstrated) during the main collisional phase of the Sveconorwegian orogeny, with the undeformed granitoids intruding during a later phase of the orogeny. Some structures probably also formed during the Telemarkian arc event, as multiple phases of intrusion would lead to complex cross-cutting relations. The regional peak-metamorphic grade reached was middle-amphibolite-facies; retrogression to lower-amphibolite and upper-greenschist facies is common. Partial melting is observed in many outcrops, attesting to relatively high-temperatures. Leucosomes are commonly sub-parallel to the fabric, suggesting this partial melting may have been facilitated by shear deformation. Such partial melting and synchronous regional deformation are observed in other mid-crustal gneiss complexes, including those that formed during the same orogenic period (e.g. Muskoka domain of the Laurentian Grenville Province; Slagstad et al. 2005).

A chemical abrasion LA-ICP-MS and ID-TIMS U-Pb study of Mesoproterozoic magmatism in the Suldal Sector; constraints on Telemarkian and Sveconorwegian crustal evolution

Aim - In this Chapter U-Pb zircon ages using LA-ICP-MS are presented for gneisses and granitoids from the Suldal Sector; TIMS analyses are presented for a selection of the dated rocks to compare the precision and accuracy of the methods. The applicability of a chemical abrasion zircon treatment is assessed for use with the LA-ICP-MS method.

3.1 Introduction

In U-Pb geochronology, the Isotope Dilution Thermal Ionisation Mass Spectrometry (ID-TIMS) method has long been recognised as producing the highest level of precision. Using an ion probe (Secondary Ion Mass Spectrometry – SIMS) however, can give much greater levels of resolution, as individual growth zones of minerals can be targeted with the ion beam. Although being the most precise, TIMS analyses are also the most costly; SIMS analyses are also costly, but less so than TIMS. The recent advances in Laser Ablation Inductively Coupled Mass Spectrometry (LA-ICP-MS) has led to a vast increase in the number of U-Pb analyses being achieved globally, partly because laser ablation systems can be coupled to already existing ICP-MS machines. This latter method is less costly than TIMS and SIMS and produces a greater number of results per machine time. The spatial resolution capabilities using LA-ICP-MS are greater than using TIMS, since the beam can be aimed at specific growth zones, but is typically less resolute than SIMS due to a greater beam diameter. The precision of LA-ICP-MS in reported U-Pb ages is variable, but is much less than that of TIMS and typically similar to that of SIMS. Some users regard LA-ICP-MS as more of a reconnaissance tool, and is useful for guiding further work prior to more precise TIMS analyses; the method has seen its greatest U-Pb based use in detrital zircon studies, and is also commonly used in Precambrian studies where high-precision is not always necessary. However, the overall precision typically reached (~1%) is up to a factor of 10 worse than ID-TIMS. A goal in LA-ICP-MS U-Pb geochronology is to improve analytical protocols that achieve precision on U-Pb ages that more closely approach the precision of ID-TIMS, and that result in a high proportion of concordant analyses.

The chemical abrasion method (Mattinson 2005) is now routinely used in TIMS U-Pb zircon geochronology to produce concordant populations that will give a precise age. Variably discordant data are one factor that limits the overall precision of LA-ICP-MS geochronology; this study assesses the use of chemical abrasion for increasing the precision in this method.

3.2 Geological Framework

Samples were taken from the Suldal Sector, SW Norway (see Chapter 2). A range of lithologies with a variety of deformation states were sampled in order to help constrain tectonothermal events in the region. Previous U-Pb studies suggest that much of the exposed basement formed in the period from 1520 to 1480 Ma (Bingen et al. 2005b; Slagstad et al. 2008). However, many of the ages obtained are imprecise ($> \pm 10$ Ma), meaning that a relative chronology of events within the region is difficult to establish. Sampled units included the Zinc Mine Banded Gneiss (Figure 3.1); concordant porphyritic lenses within this sequence are dated at 1497 ± 12 and 1496 ± 12 Ma (Bingen et al. 2005b). The Nesflaten Suite is also targeted; this belt has not been previously dated, but conformable and surrounding gneiss gives an age of 1499 ± 12 Ma (Bingen et al. 2005b). Within the Sauda Grey Gneiss Complex (Figure 3.1), amphibolite, granodioritic and granitic gneisses were sampled. Deformed and undeformed coarse-grained granitoids that were expected to give Sveconorwegian ages were also targeted; previously published ages exist for granitoids of 1065 ± 75 and 1018 ± 33 (Bingen et al. 2005b). Sample locations for previous U-Pb determinations are shown in figure 3.1.

3.3 Methodology

U-Pb geochronology was determined on zircons by laser ablation multi-collector inductively coupled plasma mass spectrometry (LA-MC-ICP-MS), with a subset of samples being dated also by isotope dilution thermal ionisation mass spectrometry (ID-TIMS); both at the NERC Isotope Geosciences Laboratory, Nottingham.

Zircons were separated from coarsely crushed whole-rock samples using the following techniques, disk-milling, sieving to remove the $>300 \mu\text{m}$ fraction, Wilfley water table separation, heavy liquid separation, and finally Frantz magnetic separation. Zircons from the non-magnetic fraction were picked under alcohol; for LA-ICP-MS, zircons were mounted in 1 inch diameter epoxy resin mounts and polished to expose an equatorial section through the grains. A fraction of each sample was chemically abraded prior to mounting to remove portions of grains that have undergone lead loss (Mattinson 2005). For the chemical abrasion, a bulk zircon fraction from each sample was annealed in a muffle furnace at 850°C for 60 hours in a quartz beaker with a loose-fitting lid. The zircon crystals were washed in warm 4N HNO_3 , and rinsed in ultra-pure water to remove surface contamination. The annealed and cleaned bulk zircon fraction was then chemically abraded in $\sim 200 \mu\text{l}$ 29N HF and $\sim 20 \mu\text{l}$ 8N HNO_3 at 120°C for 12 hours. The abraded fraction was then washed several times in ultra-pure water, washed in warm 3N HCl for several hours on a hot plate, and then rinsed again in ultra-pure water and 8N HNO_3 before picking. A few analyses were conducted on zircons that were not annealed or abraded, and were mounted on double-sided tape on a glass slide.

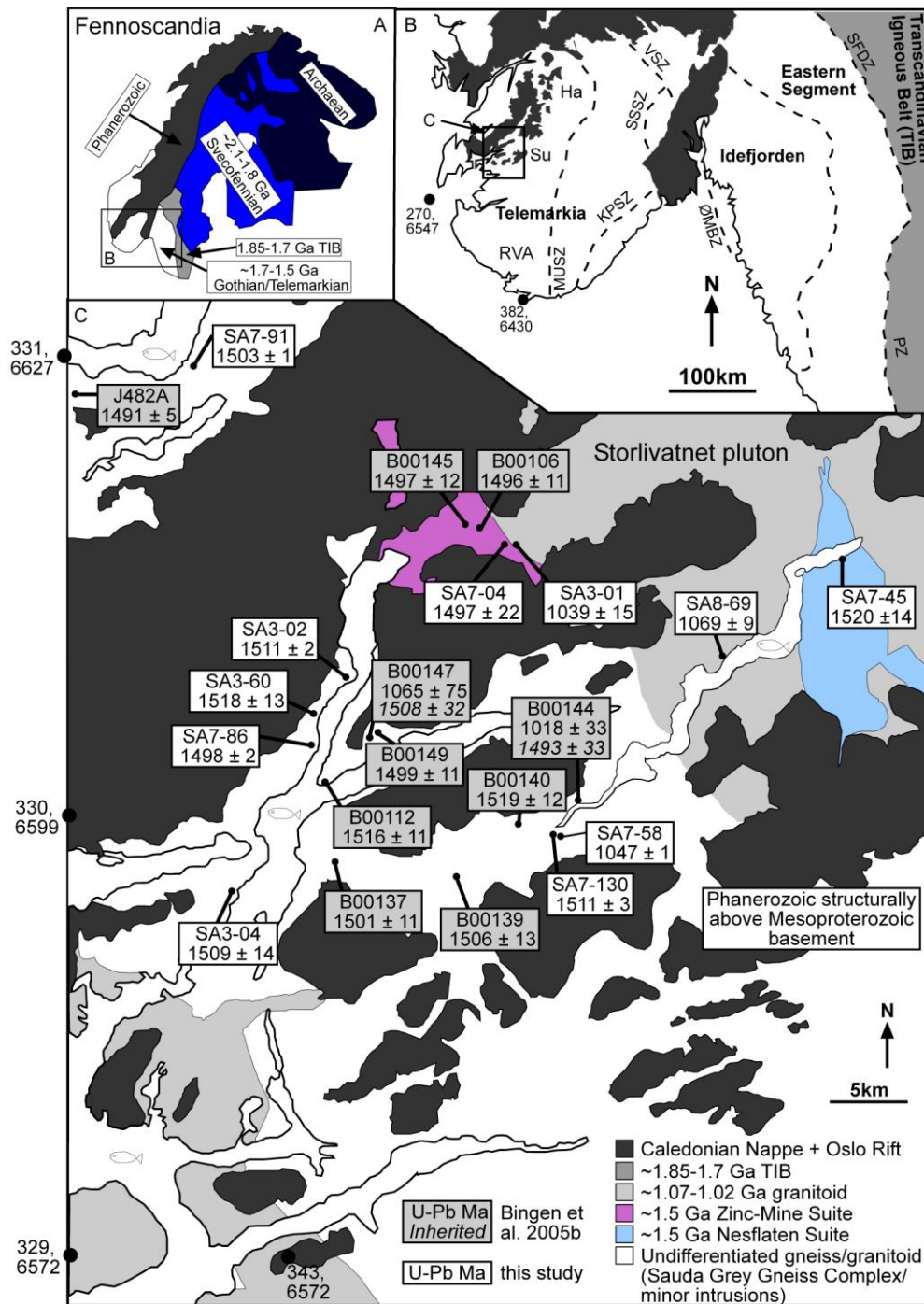


Figure 3.1. A) Geological sketchmap of the main geological provinces in the Fennoscandian Shield. B) Sketchmap of SW Fennoscandia showing the division of lithotectonic domains. C) Sketchmap showing the sample localities and new and previously published ages. Ha = Hardangervidda Sector, Su = Suldal Sector, RVA = Rogaland Vest-Agder Sector, TIB = Transcandinavian Igneous Belt, MUSZ = Mandal-Ustaoset Shear Zone, KPSZ = Kristiansand-Porsgrunn Shear Zone, SSSZ = Saggrenda-Sokna Shear Zone, VSZ = Vardefjell Shear Zone, ØBZ = Østfold Marstrand Boundary Zone, SFDZ = Sveconorwegian Frontal Deformation Zone, PZ = Protogine Zone (modified from Bingen et al. 2005b). Errors on ages are quoted at 2σ . Grid co-ordinates are zone 32V UTM.

For LA-MC-ICP-MS, the procedures were similar to those outlined in Horstwood et al. (2003). The analyses used a Nu Plasma HR multi-collector inductively coupled plasma mass spectrometer (MC-ICP-MS), coupled to a 193 nm solid state (UP193SS, New Wave Research) Nd:YAG laser ablation system, and an in-house designed low volume 'zircon ablation cell' based on the design principles

of Bleiner & Gunther (2001). Helium gas was introduced to the ablation cell to transport the ablated sample material. Solutions were aspirated using a Nu Instruments DSN-100 de-solvating nebulizer using an ESI PFA-50 nebuliser.

The counting array involved measurement of ^{238}U , ^{235}U , $^{205}\text{Pb}/\text{Tl}$, ^{203}Pb , and ^{202}Hg on Faraday cups, and ^{207}Pb , ^{206}Pb , and $^{204}\text{Pb}/\text{Hg}$ on discrete dynode ion-counting detectors. Tuning of the MC-ICP-MS at the start of each analytical session was achieved with the aspiration of a 500ppt solution of ^{205}Tl - ^{235}U . Ion counter to-Faraday gains were determined using a 100ppt ^{205}Tl - ^{235}U solution by jumping the ^{205}Tl peak through each ion counter and comparing the equivalent Faraday signal. During the ablation analyses a $^{205}\text{Tl}/^{235}\text{U}$ solution was simultaneously aspirated, this allows for an improved correction of instrumental mass bias and plasma induced inter-element fractionation. The isobaric interference of ^{204}Hg on ^{204}Pb was corrected by simultaneous measurement of ^{202}Hg (assuming $^{204}/^{202}\text{Hg} = 0.229887$).

Large rasters are preferred to static spots, as these limit the amount of fractionation at the ablation site (Horstwood et al. 2003); however, the zircon fragments used in this study were relatively small and thus limited the size of raster. In 2008, the analyses were conducted with a $20\mu\text{m} \times 20\mu\text{m}$ raster using a $15\mu\text{m}$ spot at a rate of $15\mu\text{m}$ per second. 12 passes of the raster gave 40 seconds of analysis time, a washout of 30 seconds was allowed in between each analysis. The laser was set to 70% power at 5Hz, giving a fluence averaging $4.5 \text{ J}/\text{cm}^3$. In 2009, a $25\mu\text{m}$ spot and a $25\mu\text{m} \times 25\mu\text{m}$ raster made with a $15\mu\text{m}$ spot were used; again at $15\mu\text{m}$ per second, meaning 8 passes gave 40 seconds of analysis. Instead of a 30 second washout, the laser was warmed-up for 15 seconds prior to opening the shutter. 70-80% power and 5Hz were used, giving an average fluence of $2 \text{ J}/\text{cm}^3$.

Primary standards used were Plešovice (Sláma et al. 2008) in 2008, and 91500 (Wiedenbeck et al. 1995) in 2009. These matrix-matched primary standards were analysed at regular intervals during each analytical session. The deviation of the average daily $^{207}\text{Pb}/^{206}\text{Pb}$ and $^{206}\text{Pb}/^{238}\text{U}$ values of the primary standard compared to the true value were used to normalize the sample data. The latter corrects for inter-element fractionation, whilst the former corrects for any drift or offset in the ion-counter gains recorded previously. To take account of the errors associated with the normalization process, the reproducibility of the primary standard ratios is propagated into the uncertainty of the sample ratios. A combination of GJ-1 (Jackson et al. 2004), 91500 or Plešovice were used as secondary standards to monitor the precision and accuracy of each analytical session.

Data were reduced and errors propagated using an in-house spreadsheet calculation package, with ages determined using Isoplot 3 (Ludwig 2003). Analyses that recorded $\ll 0.01\text{mV}$ ^{207}Pb were rejected, and those that recorded a ^{204}Pb signal of >300 cps were assessed for possible common-Pb contributions and rejected where required.

The average reproducibility of the $^{207}\text{Pb}/^{206}\text{Pb}$ and $^{206}\text{Pb}/^{238}\text{U}$ ratios on the primary standards was 0.65 and 0.99% respectively for 91500, and 0.79 and 1.00% for Plešovice (1σ). The average reproducibility of the secondary standards, after normalization to the primary standard, was 0.74 and 1.22% for $^{207}\text{Pb}/^{206}\text{Pb}$ and $^{206}\text{Pb}/^{238}\text{U}$ respectively on GJ-1, and 0.56 and 1.40% for Plešovice. The secondary standards gave $^{206}\text{Pb}/^{238}\text{U}$ ages of 602.02 ± 13.08 Ma (2σ) for GJ-1 (accepted $^{207}\text{Pb}/^{206}\text{Pb}$ age 609 Ma, but its $^{206}\text{Pb}/^{238}\text{U}$ age is accepted as ~ 602 -604 Ma due to its slight normal discordance; Jackson et al. 2004), and 339.54 ± 12.99 Ma for Plešovice (accepted age 337.13 Ma; Sláma et al. 2008); and are thus accurate within 1.2% (2σ) (see Figure 3.4).

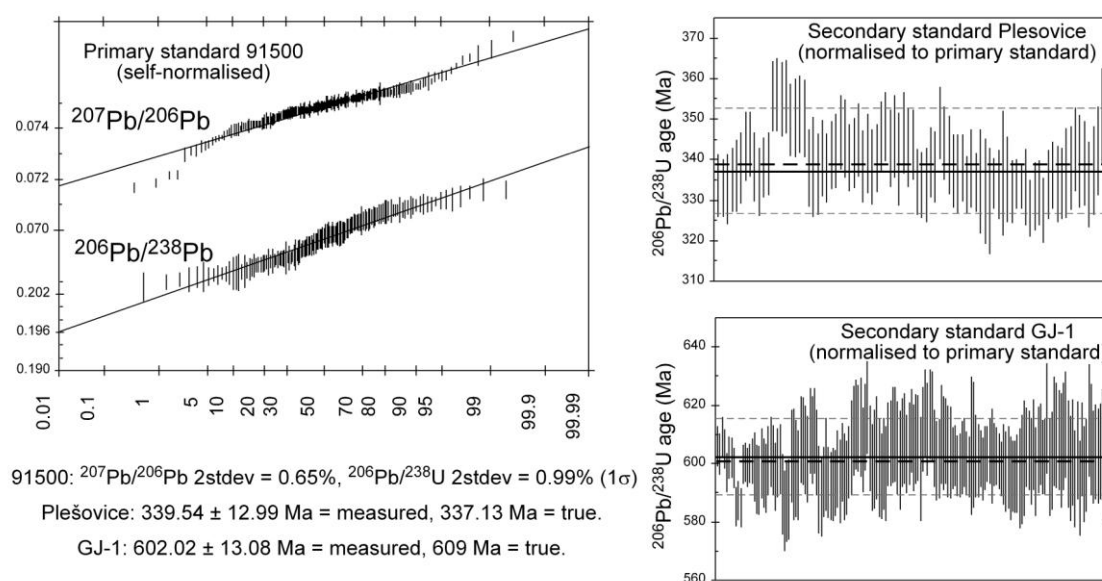


Figure 3.2. U-Pb data on standards run during the LA-ICP-MS analytical sessions.

For ID-TIMS analyses, zircons were subject to a modified version of the chemical abrasion technique (see previous section). After this treatment, the zircons were sequentially washed in dilute high purity HCl, HNO₃ and water prior to dissolution. Zircon was dissolved in Parr vessels in 120 μl of 29 M HF with a trace of 30% HNO₃ at 210 °C for 48 h, dried to fluorides, and then re-dissolved in 6 M HCl at 180 °C overnight. U and Pb were separated using an HCl-based anion-exchange chromatographic procedure (Krogh 1973). Pb and U were loaded together on a single Re filament in a silica-gel/phosphoric acid mixture (Gerstenberger & Haase 1997). TIMS analyses utilised the EARTHTIME ^{205}Pb - ^{233}U - ^{235}U (ET535) tracer solution. Measurements were performed on a Thermo Triton TIMS. Lead analyses were measured in dynamic mode on a MassCom SEM detector and corrected for $0.16 \pm 0.04\%$ / a.m.u. mass fractionation. Linearity and dead-time corrections on the SEM were monitored using repeated analyses of NBS 982, NBS 981 and U500. Uranium was measured in static Faraday mode on 10^{11} ohm resistors or for signal intensities < 15 mV, in dynamic mode on the SEM detector. Uranium was run as the oxide and corrected for

isobaric interferences with an $^{18}\text{O}/^{16}\text{O}$ composition of 0.00205 (determined through direct measurement at NIGL).

Loading blanks were <0.1 pg Pb and total procedural blanks were <1.5 pg Pb and <0.1 pg U, respectively. U-Pb dates and uncertainties were calculated using the algorithms of Schmitz and Schoene (2007) and a $^{235}\text{U}/^{205}\text{Pb}$ ratio for ET535 of $100.21 \pm 0.1\%$. All common Pb in the analyses was attributed to blank and subtracted based on the isotopic composition and associated uncertainties analysed over time. The $^{206}\text{Pb}/^{238}\text{U}$ ratios and dates were corrected for initial ^{230}Th disequilibrium using a $\text{Th}/\text{U}_{[\text{magma}]}$ of 4 ± 1 applying the algorithms of Crowley et al. (2007). All analytical uncertainties are calculated at the 95% confidence interval; all sources of uncertainty include the systematic error from tracer calibration and ^{238}U decay constant.

3.4 Sample Descriptions

3.4.1 SA3-02 tonalite dyke (Sauda Grey Gneiss Complex)

SA3-02 is an undeformed tonalitic dyke that intrudes a rhythmically layered metagabbro. The sample comprises strained quartz, coarse-grained heavily sericitised plagioclase feldspar, fine-grained biotite retrogressed to chlorite, and epidote. Zircon, titanite and Fe-Ti oxides occur as accessory phases. The dyke is 1-2m wide and has straight-sided margins. A network of at least two sets of veins cross-cuts the metagabbro; these are the same material as the dyke. Magma-mingling textures, including rounded margins to gabbroic enclaves in the tonalitic material, suggest a back-veining origin to some or all of the tonalite. In this scenario, the tonalite may have originated as a highly evolved differentiate of the gabbro that has intruded into the gabbro during cooling. The straight-sides to the dyke suggest it intruded in a brittle deformation regime.

3.4.2 SA8-45 banded felsic gneiss (Nesflaten Suite)

SA8-45 is a sheared banded fine to medium-grained felsic gneiss. The sample comprises aligned biotite laths, recrystallised quartz and variably sericitised feldspar. Titanite and zircon occur as accessory phases. The gneiss is taken from the Nesflaten Suite that outcrops around the northern extent of Suldalsvatnet. In the area, basaltic to dacitic fine-grained banded gneisses dominate, and generally feature a strong vertical fabric with weak shearing.

3.4.3 SA7-04 rhyodacitic gneiss (Zinc Mine Banded Gneiss)

SA7-04 is a sheared fine-grained grey gneiss with scattered phenocrysts of sericitised feldspar and ribbons of quartz. Fine-grained biotite lathes are unaltered and aligned with the fabric. Zircon occurs as an accessory phase. The gneiss is taken from the Zinc Mine Banded Gneiss, 1km from the granite SA3-01. The banded gneiss in this area is variable, comprising narrow mafic schists, and

dominated by phyric and aphyric granodioritic to granitic banded gneisses. The gneisses are sheared, and feature a vertical fabric.

3.4.4 SA7-86 metagabbro (Amphibolite)

SA7-86 is an amphibolite from a coarse-grained pegmatitic clot (~1m diameter) in a metagabbro body. The sample comprises feldspar heavily altered to sericite and sausserite, hornblende partially retrogressed to actinolite, biotite retrogressed to chlorite, and epidote. Abundant titanite, zircon and a Fe-Ti oxide occur as accessory phases. The metagabbro body is a ~2km wide body within the Sauda Grey gneiss on the west side of Saudafjord, parts of the metagabbro feature narrow felsic leucosomal veins. Within this 20km stretch of outcropping gneisses, a number of metagabbro bodies exist, including the layered gabbro mentioned above. Due to deformation and recrystallisation these bodies grade into the granodioritic gneisses so that the intrusive relationships cannot be determined. The sampled pegmatitic clot is free from deformation.

3.4.5 SA7-58 biotite porphyritic granite (Sveconorwegian intrusion)

SA7-58 is a coarse-grained porphyritic granite comprising perthite and plagioclase, variably altered to sericite, strained quartz, and finer-grained strained biotite and titanite. Fe-Ti oxides, allanite, apatite and zircon occur as accessory phases. The granite is very weakly deformed, and intrudes and cross-cuts sheared basaltic-rhyolitic bimodal banded gneisses (including SA7-130). In this area (south of Suldalsvatnet), a variety of porphyritic granites intrude the supracrustals and gneissic basement; these are inferred to be of Sveconorwegian age.

3.4.6 SA7-130 banded rhyodacitic gneiss (Sauda Grey Gneiss Complex)

SA7-130 is a fine-grained felsic gneiss comprising fine-grained equigranular granoblastic quartz and feldspar, and biotite laths aligned with the fabric. Concentrations of biotite and Fe-Ti oxide grains occur in weakly developed bands. Zircon and titanite occur as accessory phases. The banded gneiss is highly sheared and occurs with subordinate amphibolite layers, protoliths to the gneisses may have been bimodal volcanic tuffs, and thus the area was originally mapped as supracrustals (Sigmond 1975). Undeformed porphyritic granite (including SA7-58) intrudes the gneisses.

3.4.7 SA7-91 biotite granite (Sauda Grey Gneiss Complex)

SA7-91 is an undeformed porphyritic granite, comprising medium to coarse-grained perthitic feldspar that is variably altered to sericite, surrounded by a fine-grained granoblastic quartz matrix. Altered biotite, epidote and Fe-Ti oxides occur together in the matrix. Zircon occurs as an accessory phase. The granite is a >2km wide body on the southern side of Åkrafjord. Margins of the granite were not seen. To the north of the granite, gabbro-granodiorite-granite gneisses similar to those around Saudafjord occur. An undeformed 3m wide mafic dyke cuts through the granite outcrop.

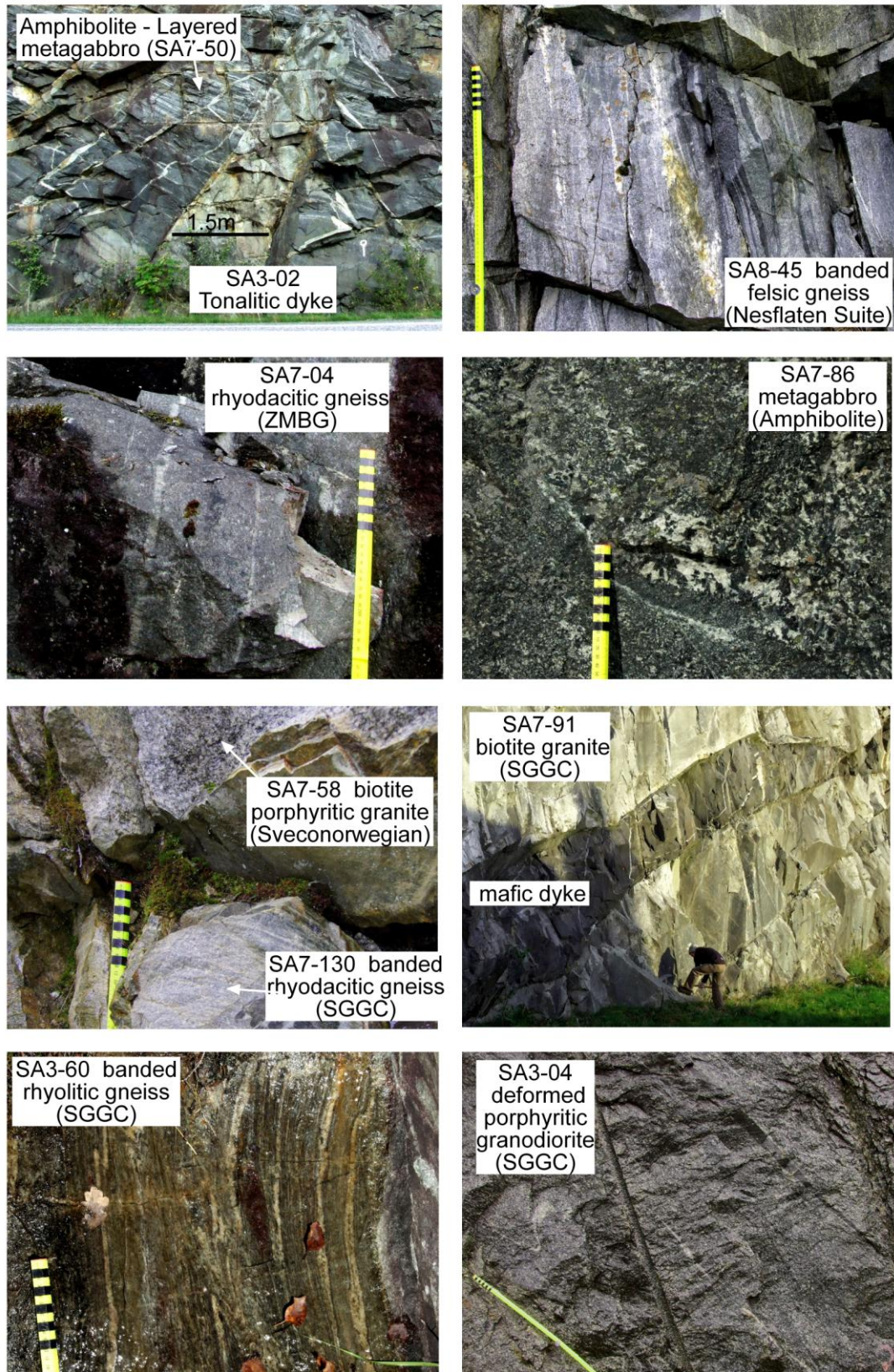


Figure 3.3. Field photographs of sample localities for U-Pb dating, SGGC = Sauda Grey Gneiss Complex; ZMBG = Zinc Mine Banded Gneiss.



Figure 3.4. Field photographs of sample localities for U-Pb dating.

3.4.8 SA3-60 banded rhyolitic gneiss (Sauda Grey Gneiss Complex)

SA3-60 is a felsic gneiss comprising equigranular fine-grained quartz and sericitised feldspar with a slight granoblastic texture, and small clots and schlieren of Fe-Ti oxides, altered biotite and titanite. Apatite and zircon occur as accessory phases. The felsic gneiss is highly sheared and isoclinally folded, and may have originated as a banded rhyolite. The felsic gneiss occurs as a 20m wide zone within a heterogeneous outcrop of fine to medium grained diorite to granodioritic gneisses.

3.4.9 SA3-04 granodiorite gneiss (Sauda Grey Gneiss Complex)

SA3-04 is a sheared granodiorite gneiss exhibiting an augen texture. The sample comprises strained quartz, heavily sericitised and sausseritised feldspar, deformed into ribbons and augen, surrounded by fine-grained quartz, feldspar, biotite, epidote and titanite. Zircon and rare apatite occur as accessory phases. The augen gneiss outcrops on the periphery of a 5km wide zone dominated by a high sense of shear; zones of proto-mylonite have formed commonly in the centre of this zone. The protoliths in this region likely included high-level porphyries, and both phytic and aphyric tuffs. Rare highly stretched xenoliths of mafic material occur in the sampled outcrop.

3.4.10 SA3-01 biotite-hornblende porphyritic granite (Sveconorwegian intrusion)

SA3-01 is an undeformed coarse-grained feldspar-phyric granite with abundant glomerocrysts of hornblende, biotite and titanite. Accessory phases include zircon and apatite. SA3-01 is from a large (>50km²) pluton that intrudes the zinc-mine supracrustals on its western edge. The sample is taken from adjacent to the zinc mine, 200m from the boundary with the Zinc Mine Banded Gneiss; at the boundary zone xenoliths of the supracrustals can be seen in the granite.

3.4.11 SA8-69 porphyritic granodiorite (Sveconorwegian intrusion)

SA8-69 is a granodiorite containing seriate-textured phenocrysts of feldspar (typically mesoperthite), quartz, hornblende and biotite. Apatite, zircon and abundant titanite occur as accessory phases. Alteration of feldspar to sericite is abundant. The sample is from a heterogeneous

outcrop comprising diorite/granodiorite gneisses and porphyries; the granite is folded and weakly sheared with finer-grained gneisses and felsic veins.

3.5 Results

The ages quoted are based on mean $^{207}\text{Pb}/^{206}\text{Pb}$ ages of mainly concordant points, as opposed to mean $^{206}\text{Pb}/^{238}\text{U}$ or concordia ages; $^{207}\text{Pb}/^{206}\text{Pb}$ ages are the most appropriate for material of this age, and for data with a degree of discordance. The errors on the mean ages derived from LA-ICP-MS data are calculated using two standard deviations of the mean, as this does not have the effect of reducing the uncertainty in large populations. All errors are quoted at 2σ unless stated.

3.5.1 SA3-02 tonalite dyke (Sauda Grey Gneiss Complex)

LA-ICP-MS:

Nine chemically abraded grains and seven non-abraded grains were analysed. The nine abraded analyses are reversely discordant (-1.2 to -4.4%) and provide a weighted mean average $^{207}\text{Pb}/^{206}\text{Pb}$ age of 1513 ± 5 Ma (MSWD = 0.52). The seven non-abraded analyses are concordant to slightly reversely discordant (0 to -2.1%) and provide a weighted mean average $^{207}\text{Pb}/^{206}\text{Pb}$ age of 1521 ± 5 Ma (MSWD = 0.87). The two mean $^{207}\text{Pb}/^{206}\text{Pb}$ ages are in error of each other, but have a slight offset. The weighted mean $^{207}\text{Pb}/^{206}\text{Pb}$ age of all fifteen analysis is 1516 ± 14 Ma (MSWD = 1.03).

TIMS:

Four analyses on chemically abraded grains are slightly discordant (0.2 to 1.4%), and provide a weighted mean $^{207}\text{Pb}/^{206}\text{Pb}$ age of 1511.1 ± 1.6 Ma (MSWD = 1.4; 95% conf.). Although reversely discordant, the chemically abraded grains analysed by LA-ICP-MS are closer in age to the TIMS analyses than the non-abraded grains.

3.5.2 SA8-45 banded felsic gneiss (Nesflaten Suite)

LA-ICP-MS:

Sixteen chemically abraded grains, and 8 non-abraded grains were analysed; both rasters and spots were used to compare each method. Of the spot analyses, 6 were chemically abraded grains and 6 were non-abraded grains. The chemically abraded grains were all reversely discordant, two of which to a large degree (-33.2 and -37.1%). The non-abraded grains were slightly reversely discordant (c. -2 to -6%), and two were normally discordant (+2.5 and +21.5%). The raster analyses have less discordance and less variation, being concordant to reversely discordant (0.2 to 12%), except for one grain that has normal discordance (5%) but is slightly older ($^{207}\text{Pb}/^{206}\text{Pb}$ age of 1554 ± 14 Ma). Six grains were analysed by spots then rasters; 5 out of the 6 grains were more concordant when rasters were used. There is no offset in the mean $^{207}\text{Pb}/^{206}\text{Pb}$ age between spots and rasters, both are 1519 Ma. A weighted mean $^{207}\text{Pb}/^{206}\text{Pb}$ age using 18 analysis (including 2 rejected)

is given at 1520 ± 14 Ma (MSWD = 1.06); this age is interpreted as the best estimate of crystallisation of the protolith to the gneiss.

3.5.3 SA7-04 rhyodacitic gneiss (Sauda Grey Gneiss Complex)

LA-ICP-MS:

Twentyone grains were analysed in total, 9 of these were rejected due to high common lead contents. 7 chemically abraded grains fall on concordia but with a spread of $^{207}\text{Pb}/^{206}\text{Pb}$ ages from 1466 to 1531 Ma. 5 non-abraded grains are discordant (+3.2 to +27.2%), and give varying $^{207}\text{Pb}/^{206}\text{Pb}$ ages; these are 1421 Ma (N=2), 1461 Ma, 1546 Ma, and 1620 Ma. The younger three grains when combined with the concordant grains fall on a regression line between 1493 ± 18 and 308 ± 160 Ma; if the 1535 Ma grain is included as well, then the regression gives an upper intercept of 1494 ± 25 Ma and a lower intercept of 176 ± 230 Ma. The 1620 Ma grain is interpreted to be an inherited grain; although the discordance of this analysis (16.4%) means that this age only gives an indication of the true age of the grain, it may be much older if non-zero Ma lead-loss events have affected the zircon. The spread in ages of concordant abraded grains may reflect a Proterozoic lead-loss event, or may reflect some inheritance of slightly older zircons with the true age being closer to 1470 Ma than the mean age, or may reflect a combination of both lead-loss and inheritance that cannot be distinguished with this dataset.

TIMS:

Five analyses on abraded grains are discordant and fall on a regression line (MSWD = 8.8) that is similar to that given by the LA-ICP-MS analyses. The upper intercept of this regression at 1497 ± 22 Ma overlaps the mean age of the concordant LA-ICP-MS analyses (1495 Ma). The lower intercept is imprecise (401 ± 140 Ma) but may reflect a lead-loss event related to the Caledonian orogeny. The 1497 Ma age is interpreted to be the best estimate of the crystallisation age of the protolith of this gneiss.

3.5.4 SA7-86 metagabbro (Amphibolites)

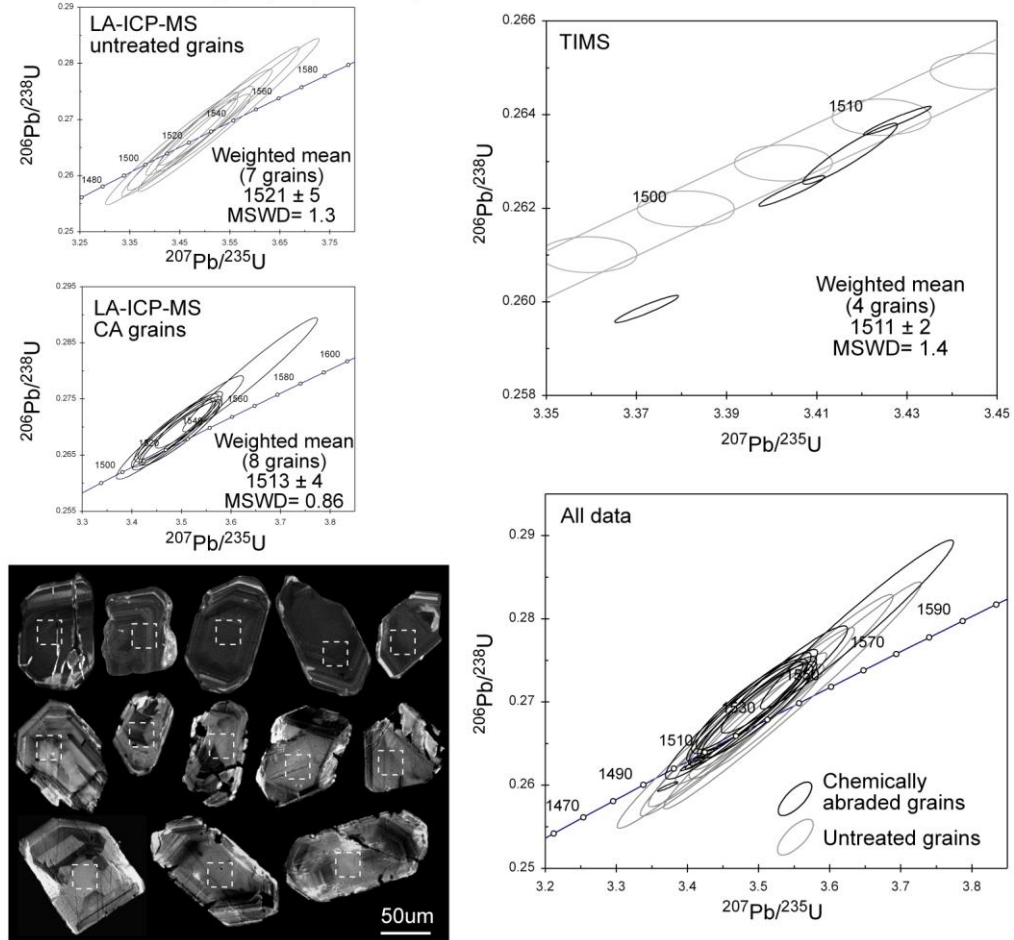
LA-ICP-MS:

21 chemically abraded grains, 10 in the first analytical session, and 11 in the second were analysed. The 21 analyses provide a weighted mean $^{207}\text{Pb}/^{206}\text{Pb}$ age of 1508 ± 10 Ma (MSWD = 0.36). All of the analyses are slightly discordant (+1.1 to +4.5). The second analytical session had lower precision on the $^{206}\text{Pb}/^{238}\text{U}$ ratio than the first, and the mean $^{207}\text{Pb}/^{206}\text{Pb}$ ages of the two sessions are slightly different; the first session gave 1506.0 ± 4.1 Ma (MSWD = 0.43) and the second gave 1512.9 ± 7.5 Ma (MSWD = 0.047). Despite the offset, all of the analyses are in error of each other.

TIMS:

Five chemically abraded grains are concordant to slightly normally discordant, and don't give overlapping $^{207}\text{Pb}/^{206}\text{Pb}$ ages. The weighted mean of the two most concordant grains is 1497.6 ± 1.5 (MSWD = 3.2), and is interpreted as the best estimate of the crystallization age of the metagabbro.

SA3-02 tonalite dyke (Amphibolite)



SA8-45 banded felsic gneiss (Nesflaten Suite)

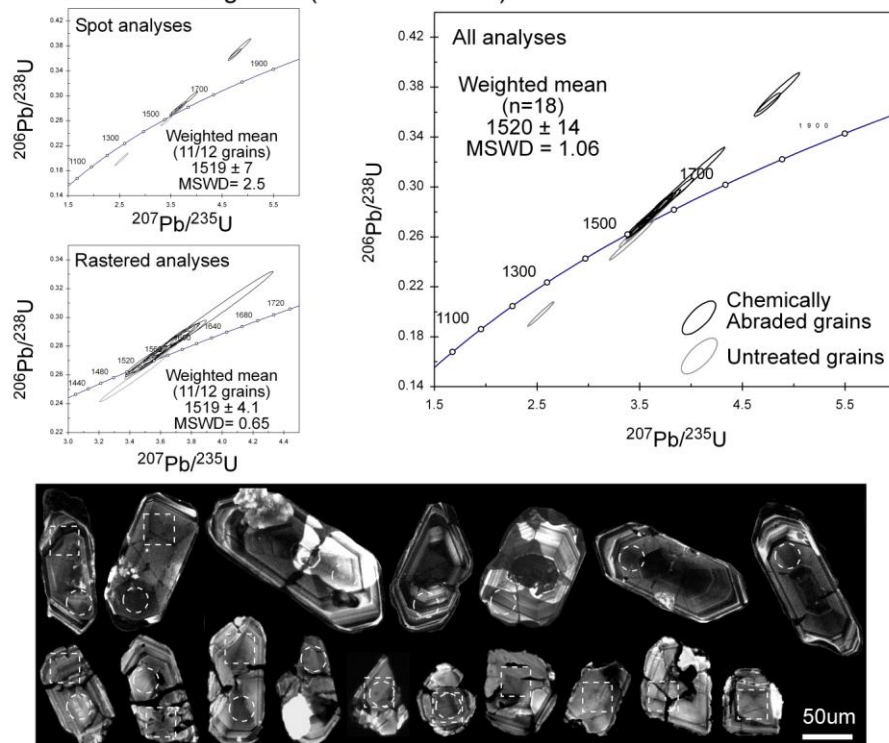
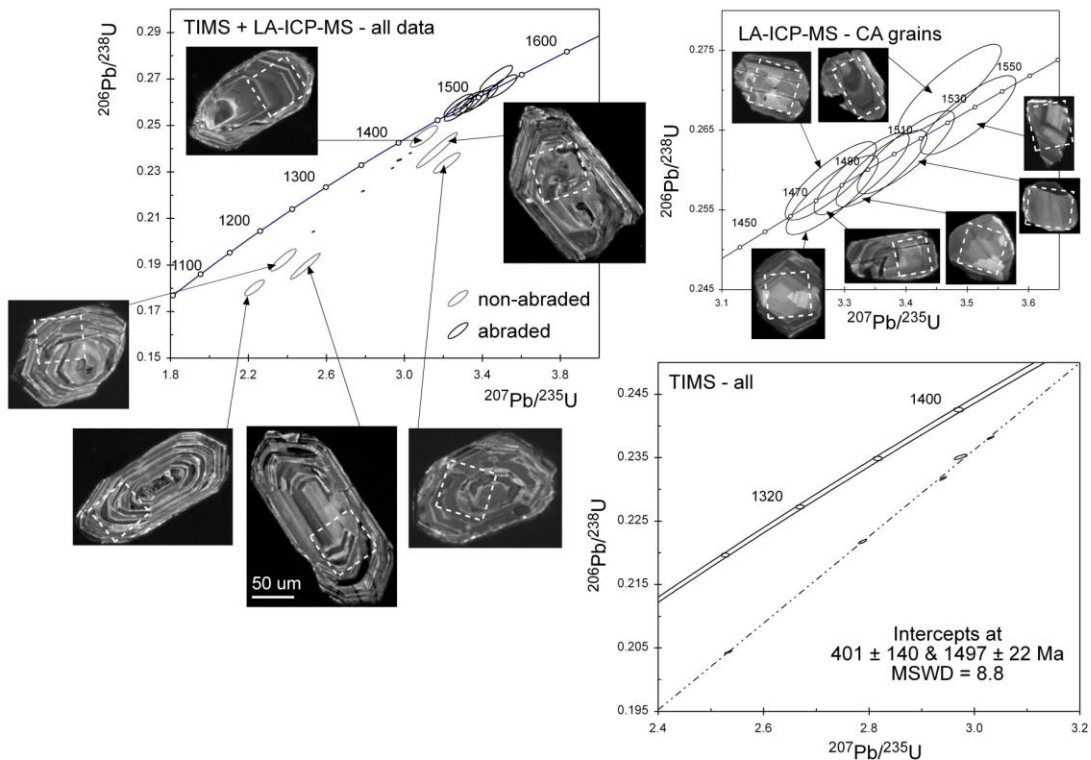


Figure 3.5. Results from U-Pb dating for SA3-02 and SA8-45. All errors are 2σ . all weighted mean ages are $^{207}\text{Pb}/^{206}\text{Pb}$. Dashed white squares are raster ablation sites, and circles are spot sites.

SA7-04 rhyodacitic gneiss (Zinc Mine Banded Gneiss)



SA7-86 Pegmatitic zone of metagabbro (Amphibolites)

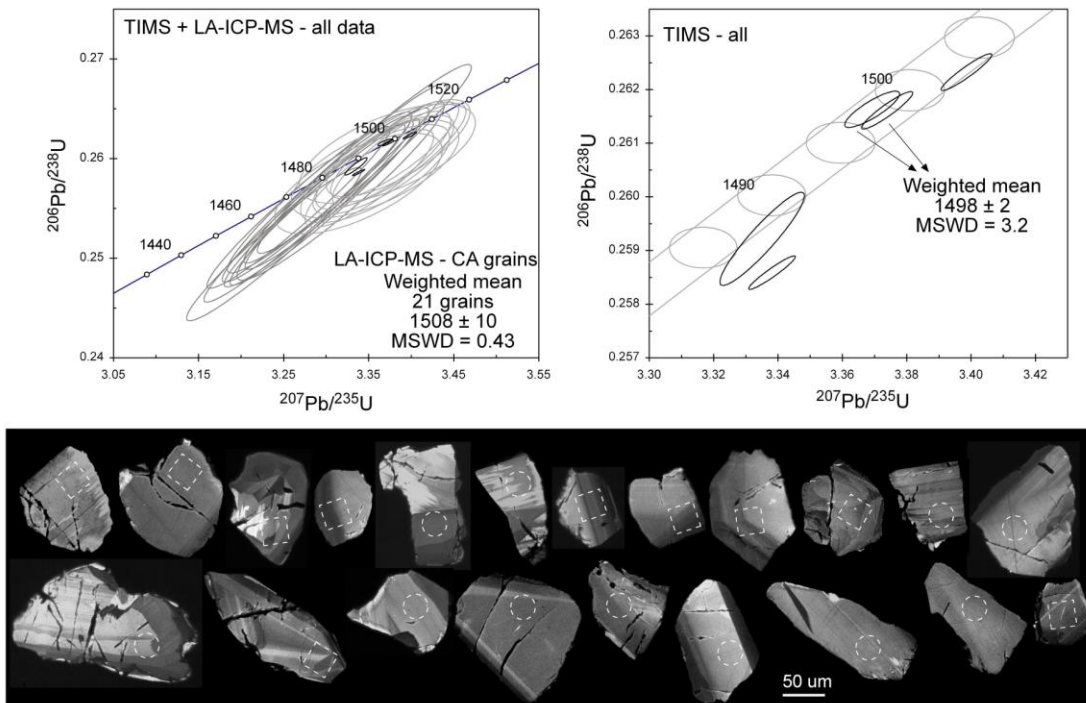
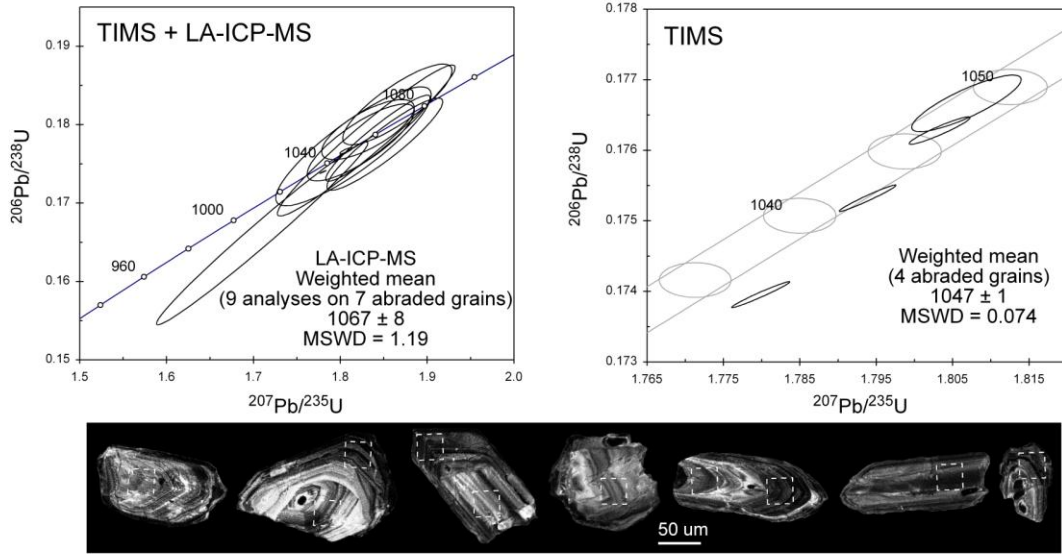
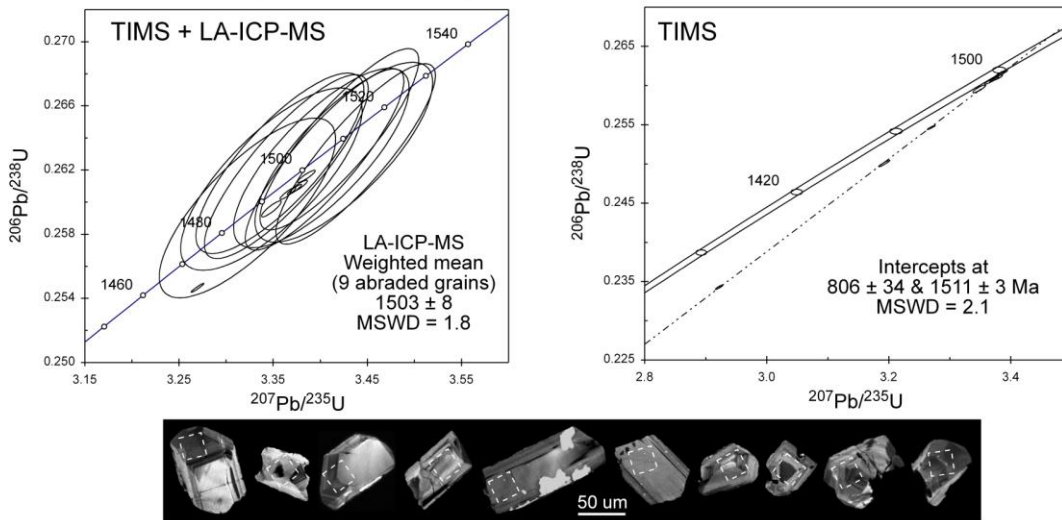


Figure 3.6. Results from U-Pb dating for SA7-04 and SA7-86. All errors are 2σ . all weighted mean ages are $^{207}\text{Pb}/^{206}\text{Pb}$. Dashed white squares are raster ablation sites, and circles are spot sites.

SA7-58 porphyritic biotite granite (Sveconorwegian intrusion)



SA7-130 rhyodacitic gneiss (Sauda Grey Gneiss Complex)



SA7-91 biotite granite (Sauda Grey Gneiss Complex)

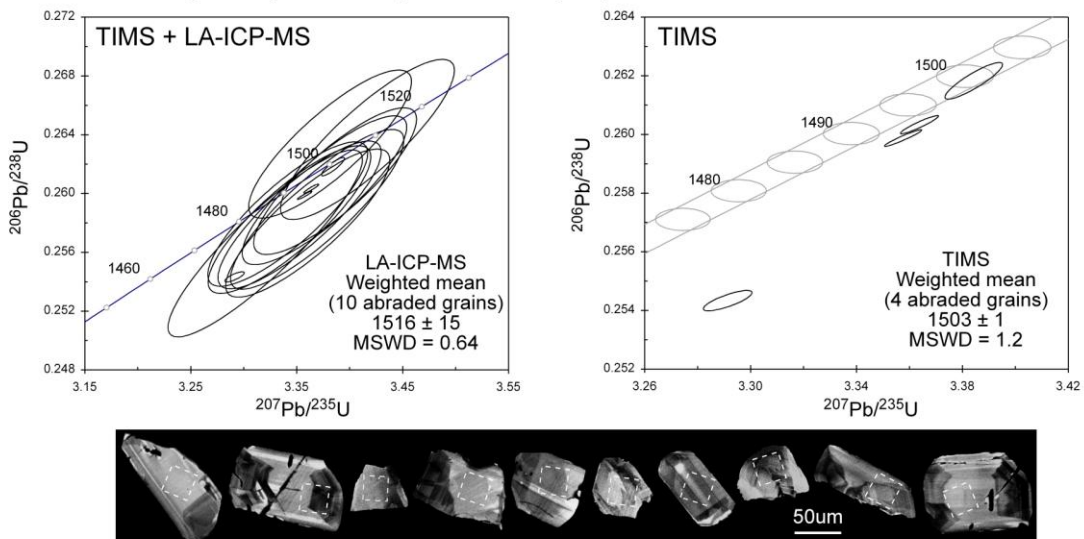
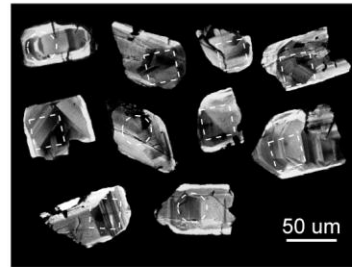
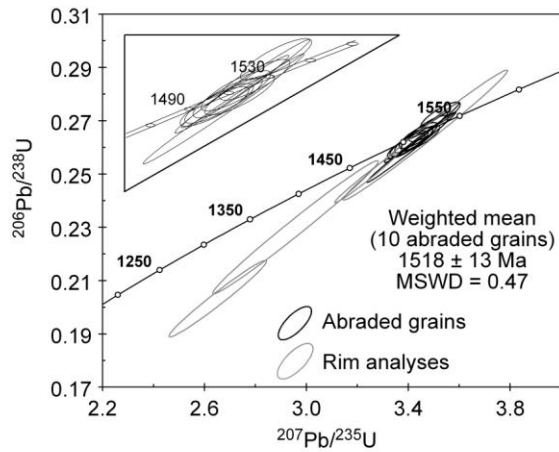
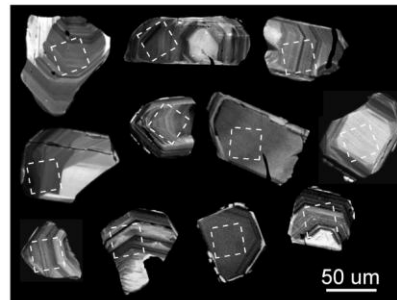
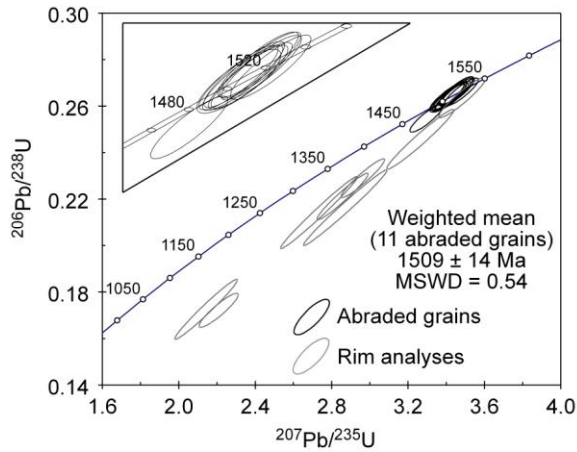


Figure 3.7. Results from U-Pb dating for SA7-58, SA7-130 and SA7-91. All errors are 2σ . all weighted mean ages are $^{207}\text{Pb}/^{206}\text{Pb}$. Dashed white squares are raster ablation sites, and circles are spot sites.

SA3-60 banded rhyolitic gneiss (Sauda Grey Gneiss Complex)



SA3-04 granodiorite gneiss (Sauda Grey Gneiss Complex)



SA3-01 biotite-hornblende porphyritic granite (Sveconorwegian intrusion)

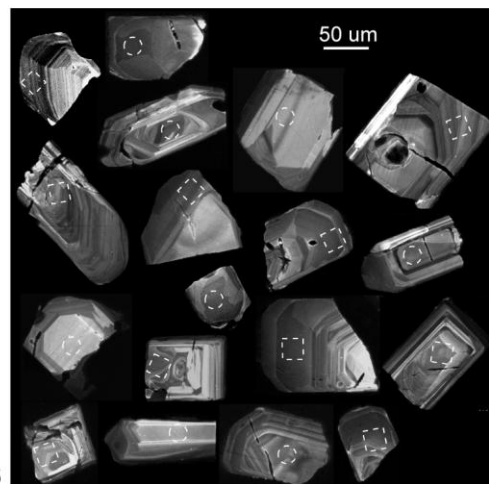
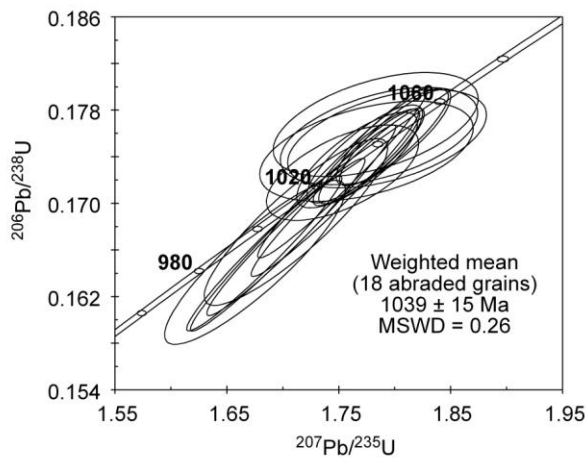


Figure 3.5. Results from U-Pb dating for SA3-60, SA3-04 and SA3-01. All errors are 2σ . all weighted mean ages are $^{207}\text{Pb}/^{206}\text{Pb}$. Dashed white squares are raster ablation sites, and circles are spot sites.

SA8-69 Deformed porphyritic granodiorite

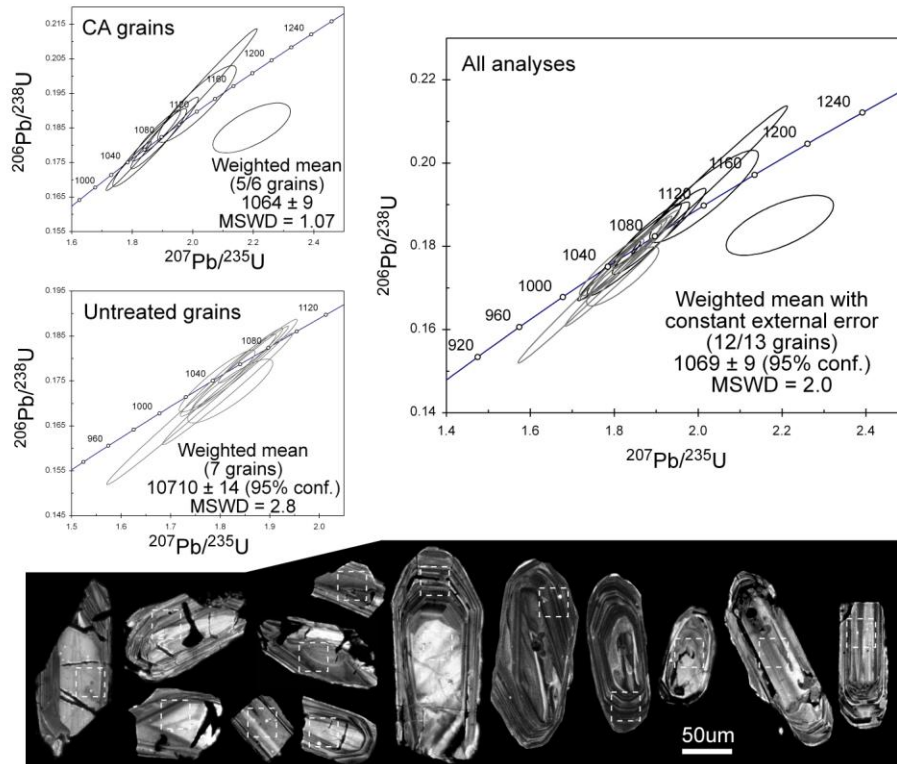


Figure 3.9. Results from U-Pb dating for SA8-69. All errors are 2σ . all weighted mean ages are $^{207}\text{Pb}/^{206}\text{Pb}$. Dashed white squares are raster ablation sites, and circles are spot sites.

Other $^{207}\text{Pb}/^{206}\text{Pb}$ ages are 1494, 1500 and 1507 Ma; the oldest two of these may represent some inheritance of slightly older material during intrusion and crystallisation of the gabbroic body. Although inheritance (and zircon crystallisation in general) is typically low in mafic rocks, examples are documented such as those found in a mid-ocean ridge setting (Schwartz et al. 2005). The 1498 Ma age is interpreted as the best estimate of crystallisation of the amphibolites.

3.5.5 SA7-58 biotite porphyritic granite (Sveconorwegian intrusion)

LA-ICP-MS:

9 analyses on non-abraded grains give a weighted mean $^{207}\text{Pb}/^{206}\text{Pb}$ age of 1068 ± 30 Ma (MSWD = 1.19). The $^{207}\text{Pb}/^{206}\text{Pb}$ ages have a slight spread, ranging from 1048 to 1084 Ma; and the data have variable discordance (-3 to 6.9%).

TIMS:

4 chemically abraded grains give a weighted mean $^{207}\text{Pb}/^{206}\text{Pb}$ age of 1047 ± 1 Ma (MSWD = 0.074); the analyses are concordant to slightly normally discordant. 6 of the LA-ICP-MS just overlap ($\pm 2\sigma$) with the TIMS analyses, whereas 3 grains are older and don't overlap. Given that a similar granitoid from the same region (SA8-69) has an older 1068 Ma age (see Section 3.5.11); the spread in ages in this granite may represent zircon growth during a prolonged crystallisation and/or

multiple-phase intrusion of this composite pluton. The 1047 Ma TIMS age is interpreted as the best estimate of the age of crystallisation of this granite however.

3.5.6 SA7-130 banded rhyodacitic gneiss (Sauda Grey Gneiss Complex)

LA-ICP-MS:

9 analyses on chemically abraded grains are fairly concordant (-1.3 to +1.2%), and give a weighted mean $^{207}\text{Pb}/^{206}\text{Pb}$ age of 1503 ± 11 (MSWD = 1.8; error calculated using a constant external error for each data point of 20)

TIMS:

8 chemically abraded grains give a regression with an upper intercept at 1511 ± 3 Ma and a lower intercept at 806 ± 34 Ma (MSWD = 2.1). The 8 analyses are variably normally discordant. The TIMS upper intercept age is interpreted as the best estimate of crystallisation of the protolith. The lower intercept although not falling at an exact Sveconorwegian age, may represent lead-loss during this orogenic period.

3.5.7 SA7-91 biotite granite (Sauda Grey Gneiss Complex)

LA-ICP-MS:

10 chemically abraded grains were analysed. The analyses are slightly discordant (-0.7 to +2.9%), and give a weighted mean $^{207}\text{Pb}/^{206}\text{Pb}$ age of 1516 ± 15 Ma (MSWD = 0.64).

TIMS:

4 chemically abraded grains give a weighted mean $^{207}\text{Pb}/^{206}\text{Pb}$ age of 1503 ± 1 Ma (MSWD = 1.2). The analyses are concordant to slightly normally discordant. This TIMS age is interpreted as the best estimate of crystallisation of the granite.

3.5.8 SA3-60 banded rhyolitic gneiss (Sauda Grey Gneiss Complex)

LA-ICP-MS:

10 chemically abraded grains, 7 in the first session, 3 in the second, and 4 non-abraded rim analyses were conducted. The chemically abraded analyses are fairly concordant (2.7 to -2.8% discordance), and give a weighted mean $^{207}\text{Pb}/^{206}\text{Pb}$ age of 1518 ± 13 Ma (MSWD = 0.47). The four rim analyses have large uncertainties ($^{206}\text{Pb}/^{238}\text{U} \pm \sim 3$ to 9% 2σ) and are discordant (21.6 to 1%), but have $^{207}\text{Pb}/^{206}\text{Pb}$ ages overlapping those of the abraded grains. The upper intercept age of these four grains at ~ 1521 Ma and a lower intercept at ~ 0 Ma, suggests a lack of Precambrian lead-loss events affecting the zircon grains.

3.5.9 SA3-04 granodiorite gneiss (Sauda Grey Gneiss Complex)

LA-ICP-MS:

Eleven chemically abraded grains were analysed, along with nine non-abraded grains for rim analyses using tape-mounting. The eleven abraded grains provide a concordia age of 1509 ± 4 Ma,

with all but one grain being concordant; the weighted mean $^{207}\text{Pb}/^{206}\text{Pb}$ age is 1509 ± 14 Ma (MSWD = 0.54). One of the rim analyses was rejected due to high common lead, the other eight are imprecise, and have a large degree of normal discordance, but point towards an upper intercept at ~ 1509 Ma, and a lower intercept at zero. The rim data suggest no lead-loss events are recorded in the zircon grains. The 1509 Ma $^{207}\text{Pb}/^{206}\text{Pb}$ age is interpreted to represent crystallisation of the porphyry.

3.5.10 SA3-01 biotite-hornblende porphyritic granite (Sveconorwegian intrusion)

LA-ICP-MS:

18 analyses were done in two sessions, 11 in the first and 7 in the second. All of the analyses are concordant to slightly discordant (less than 5%), and were conducted on chemically abraded grains. A weighted mean average $^{207}\text{Pb}/^{206}\text{Pb}$ age is given by all 18 analyses of 1039 ± 15 Ma (MSWD = 0.26). No obviously inherited grains are recorded. Zircons are all oscillatory zoned with some discordance between zones visible on many grains. Central and outer zones have been analysed, but with no difference in age recorded. The discordant zoning likely represents replenishment of the cooling magma in combination with movement of the magma mush, but within the timeframe of analytical uncertainty (<15 Ma). The 1039 Ma age is interpreted as recording the crystallisation age of the granite.

3.5.11 SA8-69 deformed porphyritic granodiorite (Sveconorwegian intrusion)

LA-ICP-MS:

14 analyses were conducted on 14 grains, 7 chemically abraded grains and 6 non-abraded grains. 6 out of the 7 abraded grains are concordant to slightly reversely discordant (-7.9 to $+2\%$), and give a weighted mean $^{207}\text{Pb}/^{206}\text{Pb}$ age of 1064 ± 9 Ma (MSWD = 1.07). The rejected grain is discordant ($+18.2\%$) and has a $^{207}\text{Pb}/^{206}\text{Pb}$ age of 1339 Ma. 7 analyses on the 6 non-abraded grains are concordant to slightly normally discordant (-0.9 to $+7.1\%$), and give a weighted mean $^{207}\text{Pb}/^{206}\text{Pb}$ age of 1070 ± 14 Ma (MSWD = 3; 95% conf.). The grain with both a core and outer growth-zone analysed gave an older age for the outer growth-zone (1095 ± 17 Ma) compared to the core (1051 ± 27 Ma); these ages are just in error of each other and indicate that the outer growth zone does not represent a younger magmatic/metamorphic growth. The weighted mean $^{207}\text{Pb}/^{206}\text{Pb}$ age of all the analyses (except the 1339 Ma grain) is 1069.3 ± 8.7 Ma (MSWD = 2; 95% conf.); this age is calculated using a constant external error, and is interpreted to be the best estimate of crystallisation of the granitoid.

3.6 Discussion

3.6.1 Chemical abrasion for laser ablation studies

High-precision and high-accuracy U-Pb geochronology can be achieved more effectively with zircon data that lack discordance due to lead-loss. The chemical abrasion method (Mattinson 2005) removes domains which have lost lead, thus, residual zircon that is dated is considered to contain U-Pb systematics that have remained in a closed-system. Chemical abrasion involves two main steps, annealing with high temperatures and abrasion with strong acid at moderate temperatures. Annealing is undergone at temperatures of 800-1100°C, with the aim of removing low to moderate lattice damage from natural alpha, alpha recoil and spontaneous fission processes (Mattinson 2005). The method of annealing prior to chemical abrasion limits leaching effects that have been observed in previous studies (e.g. Mattinson 1997). Chemical abrasion following annealing can be achieved with one step or multi-step partial dissolution. During multi-step partial dissolution where the temperature is raised during each subsequent analysis, the steps typically remove zones with decreasing U+Th contents (Mattinson 2005). Previous to the combined annealing and abrading method, most laboratories used the ‘air abrasion’ method (Krogh, 1982), which removed outer zones of zircons which are typically more discordant; this method doesn’t penetrate cracks and fractures in zircon grains however. Identifying inheritance in zircon grains may become more straightforward using the chemical abrasion method, as the effects of lead-loss are reduced (Mattinson 2005).

For ion microprobe and laser-ablation methods, annealing of radiation damage is considered to remove heterogeneities related to U-Pb fractionation during alpha recoil, as well as radiation damage, thus providing a more homogeneous zircon grain that will feature smoother sputtering during ablation. (Romer 2003; Mattinson 2005). Most LA-ICP-MS U-Pb analyses are routinely conducted on grains that are untreated, except perhaps for a clean in weak acid. The method employed here used a single step chemical abrasion (120°C for 12 hours in Hf and minor HNO₃). For most samples, especially the older Telemarkian gneisses, this provided what can be described as an ‘overkill’ method, given that on average less than 5 to 10% of the original material was salvageable after chemical abrasion. For the undeformed granitoids where larger prismatic zircons were abraded, slightly more material was available after abrasion.

The results show that this single-step overkill method was successful in producing single populations of concordant material. Most of the LA-ICP-MS analyses fall into relatively tight groups with overlapping error ellipses. Where analyses were conducted in two different sessions on the same sample (e.g. SA7-86 and SA3-01), the offset between analyses in the different sessions highlights how reproducible the individual sessions were. Several of the samples gave analyses which were reversely discordant (e.g. SA3-02, SA8-45 and SA8-69). Reverse discordance is primarily produced by analytical artifacts, and only extremely rarely by natural processes. Where analyses were conducted on both untreated and abraded grains, the abraded grains were more reversely discordant. Also, in an example where both raster and spot analyses were conducted

(SA8-45), the spots gave greater reverse discordance than the rasters. Reverse discordance is only affecting the abraded grains, and is enhanced when using static spot analyses; this effect is therefore interpreted to represent a matrix-matching issue.

Inter-element fractionation is a major factor impacting on laser ablation analyses, Horn et al. (2000) showed that this fractionation can be related to the ablation pit depth, and is inversely exponentially correlated with spot size. A number of methods have been employed to limit such fractionation, such as rastering over large areas to limit pit depth (Horstwood et al. 2003), soft-ablation where laser power is increased slowly throughout the analyses (Hirata 1997), and active-focusing where the laser focus is changed throughout the analyses (Hirata & Nesbitt 1995). The method employed within this study was to use rasters, however, the small zircon sizes, especially after chemical abrasion, meant that rasters still involved 6 to 10 passes over the same area.

If the inter-element fractionation during analyses of the standard is similar to that of the unknowns, then the impact on the overall analyses will be limited. This is why zircon standards are used to normalize zircon unknowns (i.e. matrix-matching). Studies have shown however that the use of zircon standards for non-zircon unknowns such as monazite and titanite, can provide precise and accurate analyses if methods such as rastering are employed to reduce inter-element fractionation (Horstwood et al. 2006; Storey et al. 2006). The abraded zircon grains analysed within this study exhibited fractures, cracks and features that suggested they were rather skeletal. These features do exist in the large fragments of standard zircons (e.g. 91500). Thus, the matrix-matching effect is reduced. During analyses, ablation of more skeletal grains would lead to a greater degree of inter-element fractionation that was not copied during ablation of the standard. This difference in fractionation is interpreted to be the cause of reverse discordance. The worst case of reverse discordance (SA8-45) was achieved using zircons that exhibit the greatest amount of cracks, providing further evidence for the matrix-matching issue described.

Reverse discordance due to inter-element fractionation should occur directly away from 0 Ma lead-loss. Real lead-loss on the other hand may have not occurred at 0 Ma. Therefore, the intercept of discordant analyses (i.e. $^{207}\text{Pb}/^{206}\text{Pb}$ age), may not reflect the true age of the grain (see Figure 3.10). A difference in $^{207}\text{Pb}/^{206}\text{Pb}$ age of the average of the untreated versus abraded grains is visible in SA3-02 (1521 ± 12 versus 1513 ± 10 Ma), and in SA8-69 (1070 ± 14 versus 1064 ± 9 Ma), and may reflect this effect. The accuracy of the final age is affected by this analytical artifact, and therefore need to be limited as much as possible.

The accuracy of some of the LA-ICP-MS ages determined in this study can be analysed by comparing with the TIMS ages. In five out of the six samples, the difference between the LA-ICP-MS and TIMS ages is less than 1% (0.27 to 0.86%). This overlap in ages can be viewed

qualitatively by observing the TIMS error ellipses falling within the LA-ICP-MS error ellipses in figures 3.5 to 3.7. In one example the difference between the two ages is closer to 2%; however, in this example (SA7-58) the LA-ICP-MS age is derived from a large spread in $^{207}\text{Pb}/^{206}\text{Pb}$ ages, with older ages possibly representing inheritance of older material. Again, the TIMS ellipses fall within the majority of the error ellipses of the LA-ICP-MS analyses. The variation between mean $^{207}\text{Pb}/^{206}\text{Pb}$ ages derived from chemically abraded and untreated grains where analysed, is also less than 1% for each sample (SA3-02, S8-45, SA8-69). The combined LA-ICP-MS and ID-TIMS study clearly shows that LA-ICP-MS analyses are accurate and in good agreement with reference values for both standards and unknowns as determined by accompanying ID-TIMS data.

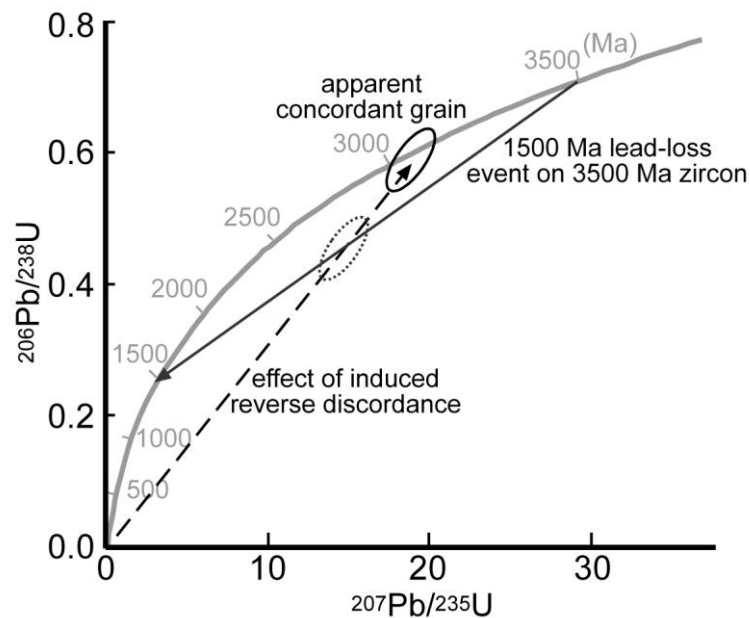


Figure 3.10. U-Pb concordia plot, showing example of how analytical induced reverse discordance may effect a zircon which has non-zero lead-loss. A grain which was formed at 3500 Ma and exhibited lead-loss at 1500 Ma should fall on a tie-line between these two ages, but reverse discordance away from 0 Ma may push the grain onto concordia giving a spurious and meaningless age.

The overall precision on the LA-ICP-MS ages is equal or better than most published Precambrian ages on similar rocks that have been observed during review of the literature in this thesis; also the populations of zircons exhibit much less scatter throughout a suite of metaigneous samples than any observed in recent literature. In future, perhaps a less radical chemical abrasion step would be advisable, as this would leave zircon fragments which were larger, allowing for larger rasters, as well as less skeletal fragments which would limit inter-element fractionation issues. Analyses of untreated grains are also useful to check what effect the chemical abrasion has had in relation to non-zero lead-loss and inheritance.

3.6.2 1.5 Ga Telemarkian crustal growth

From previous work, the crust within the Suldal Sector formed during the 1520-1480 Ma Telemarkian period (Bingen et al. 2005b). Combining the previously published ages with those in this study, the time-span for magmatism within this region is 1489 to 1520 Ma without errors included; including 2σ errors the minimum time span is 1492 to 1509 Ma, whereas the maximum time span is 1475 to 1534 Ma. If unpublished ages from the Suldal Sector are included of 1475 ± 8 , 1484 ± 10 , 1486 ± 4 and 1521 ± 6 Ma (Slagstad & Marker 2009, unpublished data), then the maximum age range is slightly increased; but overall the 1520-1480 Ma age span of Bingen et al. (2005b) is fairly appropriate. This 40 million year age span is appropriate for a continental crust-building long-lived mature volcanic arc or active continental margin. Within this time frame the crust likely underwent phases of compression and extension, as these may occur in cycles of ~10 million years in an accretionary orogen (Collins 2002).

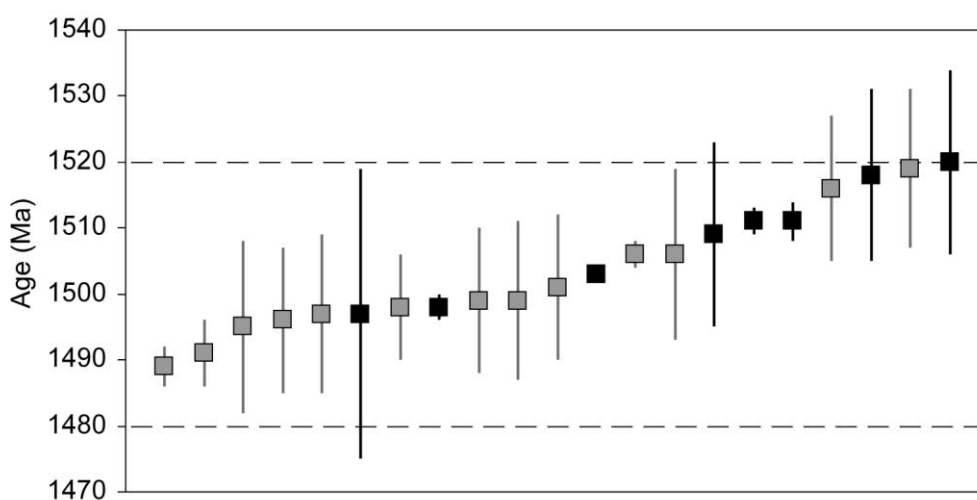


Figure 3.11. Compilation of published ages (grey squares) and those determined in this study (black squares) from the Suldal Sector. Published ages are Bingen et al. (2005b). Error bars are 2σ . Dashed lines mark the 1520-1480 Ma Telemarkian time span.

The hitherto undated Nesflaten Suite has an age of 1520 ± 14 Ma, suggesting it formed in the earlier part of the Telemarkian period. The sample from the Zinc Mine Banded Gneiss did not yield a precise age, but the estimate provided here of 1497 ± 22 Ma overlaps the previous ages on concordant porphyritic layers (1497 ± 12 and 1496 ± 12 Ma; Bingen et al. 2005b). The Sauda Grey Gneiss yielded ages of 1518 ± 13 , 1511 ± 3 , 1509 ± 14 and 1503 ± 1 Ma; all of these ages fall in the earlier part of the Telemarkian period. The overlap between the Zinc Mine Banded Gneiss, Nesflaten Suite and Sauda Grey Gneiss agrees with the interpretation that the supracrustal belts defined by the earlier mapping (Suldal-Åkrafjord and Grjotdokka-Nesflaten; Sigmond 1978), do not form separate belts that lie upon an older gneissic basement, but are all part of the same event (see Chapter 2). The age of the metagabbro (SA7-86) at 1498 ± 2 Ma confirms that this member of the ‘amphibolite’ suite (see Chapter 2) is part of the Telemarkian event. The 1511 ± 2 Ma age for an

undeformed tonalite dyke that intrudes a layered metagabbro suggests the gabbroic body (another member of the amphibolite suite), is of Telemarkian age, and also fairly early on in the Telemarkian period.

Undeformed units are dated at 1511 ± 2 (SA3-02) and 1503 ± 1 Ma (SA7-91), whereas deformed units are both older and younger than these ages. This suggests that deformation was not penetrative, but instead was partitioned, with certain units escaping either both Telemarkian and Sveconorwegian fabric-forming deformation. This means that a relative chronology based on structural fabrics is potentially misleading; such chronologies have been used in the past to help define tectonothermal events, for example in the Idefjorden terrane various granitoids were grouped based on their state of deformation (Åhäll et al. 1990). The use of structural fabrics in this way is advised against, given that strain can be highly localized over a range of scales.

In-situ U-Pb geochronological methods are useful for indentifying inheritance in magmatic suites since large zircon populations can be dated, and older cores that represent inherited zircons that have been overgrown can be analysed. About 350 zircons have now been analysed from Telemarkian rocks in the Suldal Sector. In this large population only one grain is outside of the error of the Telemarkian age span, this grain is discordant (+16.4%) and has a $^{207}\text{Pb}/^{206}\text{Pb}$ age of 1620 Ma. The lack of inheritance in Telemarkian rocks suggests limited amounts of older material were available for inheritance, or that the magmas were capable of dissolving any inherited zircon (see discussion in Chapter 5). Some inheritance of Telemarkian age material during the prolonged Telemarkian event is suggested by the data, for example in SA7-86 precise TIMS $^{207}\text{Pb}/^{206}\text{Pb}$ ages spread from 1507 to 1495 Ma, with 1498 ± 2 Ma being the interpreted age of crystallisation. Cathodoluminescence images of the zircons (Figures 3.5 to 3.9), show that each sample comprises a population of zircons that have similar characteristics, which is compatible with their interpreted igneous origin. The zircons are mostly elongate and oscillatory zoned, and lack any obvious inherited cores or discontinuities. Zircons from SA7-86 are unzoned to weakly zoned and are fragments of larger zircons ($>300 \mu\text{m}$), which is compatible with their interpreted crystallisation in a mafic composition.

3.6.3 Sveconorwegian events

The Sveconorwegian orogeny (e.g. Gaál & Gorbatshev, 1987; Bingen et al. 2008a) involved continent-continent collision between Fennoscandia and another continent of unknown origin. Sveconorwegian events within SW Fennoscandia have been split into four distinct phases (Bingen et al. 2008c). The Arendal phase (1140-1080 Ma) involved collision between the Telemarkia and Idefjorden terranes, and the thrusting of the Bamble-Kongsberg terrane over Telemarkia (Bingen et al. 2008c). The Agder phase (1050-980 Ma) represents the main continent-continent collisional

phase, with the collision possibly being oblique (Bingen et al. 2008c). Crustal thickening and associated regional metamorphism is estimated to have peaked at 1035 Ma (Bingen et al. 2008c).

Within the Suldal sector, metamorphism has been dated by the Re-Os method on Cu-Mo mineral occurrences (Stein & Bingen 2002), with the Sæsvatn belt recording various stages of metamorphism and deformation: onset of greenschist facies metamorphism and deformation at 1047 ± 2 Ma, peak ductile deformation at 1032 ± 2 Ma, incipient extension/relaxation at 1025 ± 2 Ma and full relaxation (and brittle deformation) at 1017 ± 2 Ma (Stein & Bingen 2002). Monazite analyses in a ~1500 Ma gneiss to the south of the Suldal Sector give a younger age of 1005 ± 7 Ma, interpreted to represent amphibolites-facies metamorphism (Bingen et al. 2008b). A titanite age of 1009 ± 10 Ma from the 1035 Ma Rosskreppfjord granitoid (Andersen et al. 2002a) provides further evidence for metamorphism of this age. From analyses of all available geochronological data, Bingen et al. (2008b) define M1 as regional medium-pressure protracted metamorphism that peaked in granulite-facies, and occurred from 1035 to 970 Ma. M2 peaked at 930-920 Ma and is related to intrusion of the Rogaland Anorthosite Complex, but did not affect the Suldal Sector (Bingen et al. 2008b). The crust in the Suldal sector is inferred to be in a brittle regime by 970 Ma, with regional decompression occurring from 970 to 955 Ma (Bingen et al. 2008b).

Separate rim analyses were conducted on two deformed units (SA3-60, SA3-04); for each of these samples the discordant rim analyses point towards lead-loss at ~0 Ma, suggesting there is no observable imprint from the Sveconorwegian orogeny on the U-Pb systematics. Only one sample (SA7-130) has an imprecise lower intercept that is near the range of the Sveconorwegian orogeny (at 806 ± 34 Ma). This sample is highly deformed and some parts of the outcrop feature leucosome formation, however, the fabric and leucosomes are cross-cut by SA7-58 dated at 1047 ± 1 Ma; this suggests that the 806 Ma age is unrelated to the deformation or partial melting of the sample. Overall, the imprint of the Sveconorwegian orogeny recorded in the Telemarkian basement in this U-Pb dataset is non-existent to minimal.

Four main magmatic suites are defined in Telemarkia that occur within the main Sveconorwegian orogenic period. These are the Feda Suite (~1050 Ma), Fennefoss Suite (~1035 Ma), Hornblende-Biotite Granite Suite (~970-930 Ma) and the Rogaland AMC Suite (~930 Ma) (Schärer et al. 1996; Bingen & van Breemen 1998; Andersen et al. 2002a, 2007a). The Feda Suite may have been produced in an active margin setting that existed just prior to continent-continent collision (Slagstad et al. 2008; Bingen & van Breemen 1998), or may represent melting of previous arc-related crust as a result of crustal thickening (Bingen et al. 2008c). The HBG Suite is considered to be post-collisional and likely formed via fractional crystallisation of mafic lower crust (Vander Auwera et al. 2003; 2008; Bogaerts et al. 2003, 2006; Bingen et al. 2006). The Rogaland AMC Suite intruded

contemporaneously with the latter stages of the HBG Suite, and likely formed from an anhydrous mafic lower crust (e.g. Longhi et al. 1999; Bolle et al. 2003).

This study has shown that a composite pluton, named here the Storlivatnet pluton, has ages of 1069 ± 9 Ma, 1047 ± 1 , 1039 ± 15 Ma (this study) and 1021 ± 8 Ma (MM26181; Slagstad & Marker 2009, unpublished). The oldest age (~ 1069 Ma) is from a strongly deformed porphyritic granitoid. The next youngest ages of 1047 and 1039 Ma are from relatively undeformed porphyritic granitoids (although some undulose extinction is observed). Thus, it can be inferred that deformation of the oldest granitoid occurred after 1069 ± 9 and prior to 1047 ± 1 Ma. It is not known whether the deformation of this granitoid is related to the NW-SE striking fabric-forming deformation that affects much of the older Telemarkian crust; but the data suggest at least some deformation occurred early on and perhaps slightly older than the Agder phase (1050-980 Ma) of the Sveconorwegian orogeny in the Suldal Sector.

The oldest Sveconorwegian granitoids dated hitherto, are the Mandal-Svindal Unit ($1051^{+2}_{-.8}$ Ma), Veggja-Leland Unit ($1051^{+2}_{-.8}$ Ma) and the Liland Unit ($1051^{+2}_{-.4}$ Ma), all belonging to the Feda Suite (Bingen & van Breemen 1998). The 1069 ± 9 Ma age for the Storlivatnet pluton pushes back the recorded onset of Sveconorwegian magmatism by some 18 million years. Bingen et al. (2008c) suggest that the Feda Suite may have formed by melting of older crust due to crustal thickening. Crustal thickening is inferred to have peaked at 1035 Ma (Bingen et al. 2008b); however, for crustal thickening to have produced all of the early-Sveconorwegian granitoids it must have occurred as early as ~ 1070 Ma, for which there is no direct evidence of. An alternative explanation is that the early-Sveconorwegian magmatism was related to subduction along a continental arc that was active just prior to continent-continent collision; such an explanation has already been postulated for the Feda Suite (Bingen et al. 1993; Bingen & van Breemen 1998; Slagstad et al. 2008). The deformation that occurred between 1069 and 1047 Ma (see above) is compatible with magmatism in an arc setting (at 1069 Ma) prior to collision and deformation in the Suldal Sector (at $<1069 >1047$ Ma), and followed by crustal thickening (at ~ 1035 Ma; Bingen et al. 2008b).

The only other event in the region of comparable age to the 1069 Ma Storlivatnet granitoid is that of deposition of the Kalhovde Formation in the adjacent Telemark Sector (Bingen et al. 2003). The age of deposition of this unit is interpreted to be $<1065 \pm 11$ Ma based on an average of the six youngest detrital grains (Bingen et al. 2003); although, the youngest individual grains have $^{207}\text{Pb}/^{206}\text{Pb}$ ages at 1035 ± 31 , 1054 ± 11 , 1059 ± 19 and 1061 ± 11 . This unit likely formed in an extensional setting, interpreted to have during regional thermal subsidence following 1.17-1.14 Ga volcanism (Bingen et al. 2003). This setting is at odds with a model whereby crustal thickening has produced the entire early-Sveconorwegian magmatic suite. Thus, a subduction-zone setting is preferred for the early stages of Sveconorwegian magmatism (Feda Suite). Brewer et al. (2002) advocate a continental

back-arc setting for 1.17-1.13 Ga volcano-sedimentary units within the Telemark Sector, suggesting that subduction-margin processes occurred until at least 1.16 Ga in the region. A subduction origin for the early-Feda magmatism suggests the subduction-margin was active until ~1050 Ma, just prior to continent-continent collision. Further evidence for a subduction-zone setting at ~1060 Ma is discussed in Chapter 8.

3.7 Conclusions

11 new ages are presented for gneisses/granitoids within the Suldal Sector, southwest Norway. Three ages from a composite pluton (Storlivatnet) that has both deformed and undeformed lithologies gave 1039 ± 15 , 1047 ± 1 and 1069 ± 9 Ma, and therefore these ages extend the age range of early-Sveconorwegian magmatism. Deformation of this pluton is inferred to have occurred between 1069 ± 9 and 1047 ± 1 . Calc-alkaline gneiss/granite/gabbro units that comprise the variably deformed basement in the region are Telemarkian in age, ranging from 1497 ± 22 to 1520 ± 14 Ma; within this crystalline basement, the Nesflaten and Zinc Mine Banded Gneiss ‘supracrustal’ belts formed contemporaneously with orthogneisses of the Sauda Grey Gneiss Complex. The influence of later orogenic events on the U-Pb systematics of the Telemarkian rocks is minimal. Pre-Telemarkian inheritance in Telemarkian rocks is almost non-existent (only one grain >1600 Ma is recorded).

Chemical abrasion is successful in producing relatively tight single-age populations of zircon fragments. However, chemical abrasion can cause matrix-matching issues such as inter-element fractionation; the use of large rasters is suggested for analyses, and fractured/skeletal grains should be avoided. Both the accuracy and precision of final ages using LA-ICP-MS and chemical abrasion are less than 1%, the ages determined are within 1% of the TIMS ages also. Slight offsets between different sessions and untreated versus abraded grains versus TIMS ages, suggests this method is limited to 1% precision on material of this age.

Table 3.1 Results of LA-ICP-MS and TIMS U-Pb study. ¹ = 2 standard errors, ² = 2 standard deviations, ³ = determined using constant external error, CA = chemically abraded.

Sample	Abraded?	Spot/Raster	Concordance	weighted mean ^{7/6} age	2 σ^1	2 σ^2	MSWD	n	TIMS	MSWD	n	% variation TIMS-vs. LA	% variation CA vs. non-CA
SA3-01	CA	Raster	-3 to +4.7	1039.2	5.6	15.0	0.26	18					
	CA	Raster	-4.4 to -1.2	1512.7	4.1	9.9	0.86	8					
	non-CA	Raster	-2.1 to 0	1521.1	5.3	12.3	1.30	7					
	Both	Raster		1516.3	3.4	13.7	1.03	15	1511.1 (^{7/6} age)	1.4	4	-0.66	0.55
SA3-04	CA	Raster	-1.1 to +2.8	1508.6	5.8	14.0	0.54	11					
	CA	Raster	-2.8 to +2.7	1518.0	6.0	12.9	0.47	10					
SA7-04	CA	Raster	-3.3 to +0.7	1495.0	20.0	5.00	5.00	7	1497.0 (upper int.)	401.00	5	0.27	
	non-CA	Raster	+3.2 to +24.9	1434.0	57.0	5.70	5.70	3		140.0 (lower intercept)			
	non-CA	Raster	+27.2	1535.8	13.2	inherited?							
	non-CA	Raster	+16.4	1619.9	14.4	inherited?							
SA7-58	non-CA	Raster	-3 to +6.9	1067.6	8.3	29.8	1.19	9	1046.7 (^{7/6} age)	0.1	4	1.96	
SA7-86	CA	Raster	+1.1 to +4.5	1507.6	3.6	9.7	0.43	21	1497.6 (^{7/6} age)	1.5	2	0.66	
									1500.4 (^{7/6} age)	1.7			
SA7-91	CA	Raster	-0.7 to +2.9	1516.0	6.0	15.2	0.64	10	1507.2 (^{7/6} age)	1.8	4	0.86	
SA7-130	CA	Raster	-1.3 to +1.2	1503.1 (1502.0) ³	7.6 (11.0)	30.6	1.80	9	1511.0 (upper int.)	2.6	8	0.52	
									806.00 (lower intercept)	34.0			
SA8-45	CA	Spot	-37.1 to -3.9	1512.2	9.8		2.50	6					0.51
	non-CA	Spot	-5.8 to +21.5	1520.0	19.0		7.70	6					
	CA	Raster	-12 to -0.4	1517.9	4.3		0.46	10					1.50
	non-CA	Raster	-1 to +5	1541.0	170.		7.60	2					
	CA	All	-37.1 to -0.4	1515.4	3.2		1.30	16					0.63
	non-CA	All	-5.8 to +21.5	1525.0	16.0		8.80	8					
SA8-69	All	All	(6 rejected)	1520.0	7.0	14.0	1.06	18					
	CA	Raster	-7.9 to +2	1064.1	9.1		1.07	6					0.55
	non-CA	Raster	-0.9 to +7.1	1070.0	14.0		3.00	7					
	All	Raster		1067.7 (1069.3) ³	8.4 (8.7)		2.00	13					

The petrogenesis of 1.5 Ga magmatism in the Suldal Sector

Aim – In this chapter, whole-rock geochemical data from the ~1.5 Ga basement in the Suldal Sector are presented; the data are used to develop a model for the petrogenesis and tectonic setting of the main lithologies.

4.1 Introduction

The tectonic setting and petrogenesis of the crystalline basement rocks within the Telemarkia terrane is uncertain, primarily due to the scarcity in published geochemical data. Unpublished preliminary geochemical data on lithologies in the Suldal Sector suggest an active continental margin setting (Bingen et al. 2005b). Coeval volcanism in the Telemark Sector is bimodal with an A-type geochemical signature, and interpreted to have occurred in a continental ‘within-plate’ setting (Menuge & Brewer 1996), possibly in relation to extension in a ‘behind-arc’ convergent-margin setting (Slagstad et al. 2009). Abundant 1.52-1.48 Ga ages across the region suggest that the Telemarkia terrane was a location of substantial continental growth during this period (Bingen et al. 2005b; 2008a). The Gothian period (1.65-1.52 Ga) that occurred prior to the Telemarkian (1.52-1.48 Ga) period, built the Fennoscandian crust that is exposed to the east of Telemarkia, and is interpreted as an accretionary orogen with a single progressively maturing volcanic arc that is variably distal to Fennoscandia (Andersen et al. 2004a), or as several volcanic arcs accreted shortly after formation (Brewer et al. 1998; Åhäll & Connelly 2008). The Telemarkian crust may represent an extension of this accretionary orogen or may form an exotic microcontinent that was accreted during the Sveconorwegian orogeny (Åhäll & Connelly 2008; Bingen et al. 2005b).

4.2 Geological Framework

The Suldal Sector is an informal term for the central part of the west half of the Telemarkia terrane (Bingen et al. 2005b). It comprises a crystalline basement dominated by heterogeneous orthogneisses that are intruded by Sveconorwegian granitoids. Similar orthogneisses outcrop in the surrounding Hardangervidda, Rogaland and Telemark Sectors. The studied orthogneisses in the Suldal Sector have petrology, petrography and field-relations interpreted to represent mid- to supracrustal arc-related intrusions and volcanics (see Chapter 2). Gneisses sampled for geochemical analyses that are discussed in this chapter are taken from the region around the Sauda and Suldal communes (Figure 4.1). In the study area, the basement has been split up into the Sauda Grey Gneiss Complex, the Nesflaten Suite, the Zine Mine Banded Gneiss, Amphibolites and Granitoids (see Chapter 2), and are all 1.52-1.48 Ga in age (see Chapter 3).

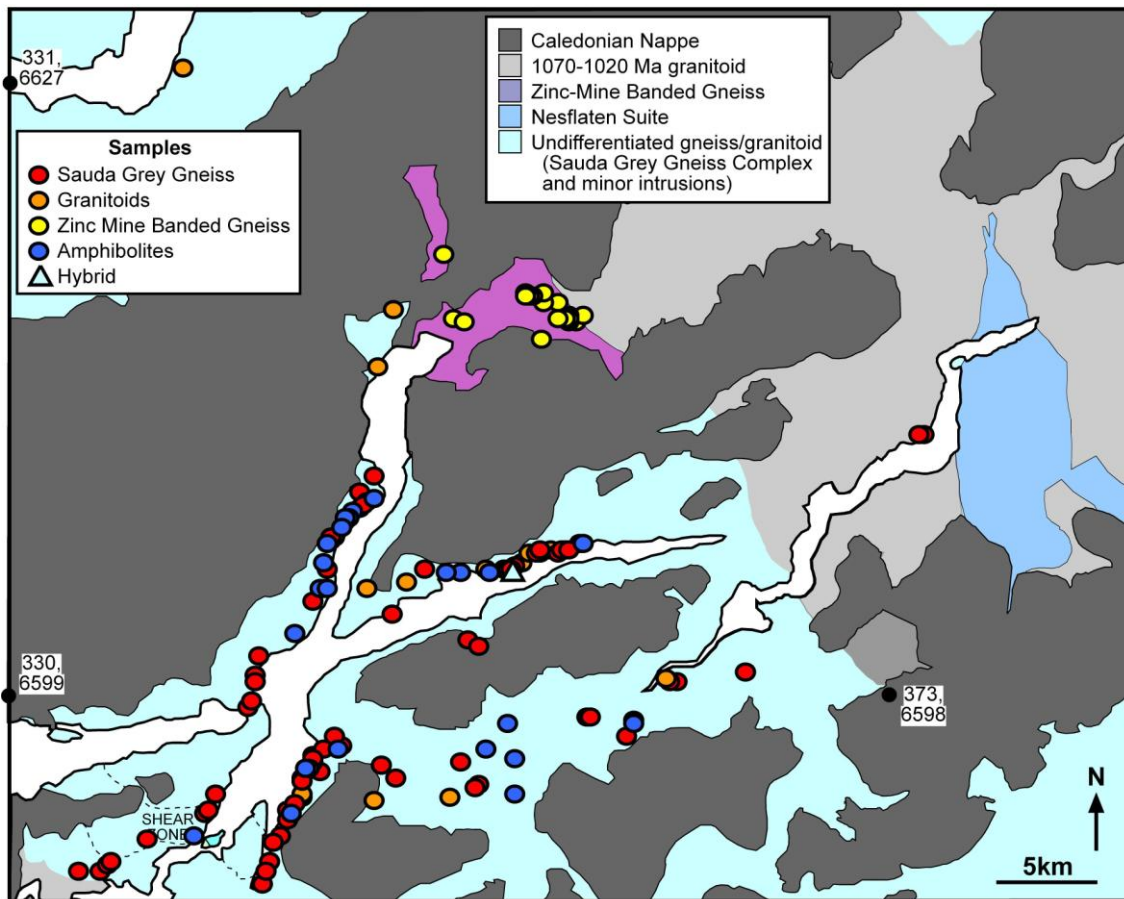


Figure 4.1. Geological map of the study area showing the sample localities. Modified from Sigmond (1975).

4.3 Geochemistry

4.3.1 Analytical Techniques

Samples were analysed by XRF at the University of Leicester, UK, and by XRF and ICP-MS at the Geological Survey of Norway, Norway. The methods are outlined in the appendices. For XRF analyses at the University of Leicester, repeat analysis of certified reference materials gives a precision (2σ) for major elements of <5% for SiO_2 , TiO_2 , Al_2O_3 , Fe_2O_3 , and MgO , <10% for MnO , CaO and Na_2O , and 11% for K_2O ; precision on the trace elements is <10% at contents over 15ppm.

4.3.2 Element Mobility

The rocks studied are orthogneisses that have been metamorphosed under amphibolite-facies and variably retrogressed in the greenschist facies, thus, their geochemistry has been liable to variable element enrichment and depletion. In this chapter, element concentrations of the rocks are used to determine their petrogenesis, the mobility of these elements should therefore be acknowledged.

Large-ion-lithophile-elements (LILE; e.g. Rb, Ba, K and Sr) are generally considered to be mobile, whereas high-field-strength elements (HFSE; e.g. Th, Nb, P, Ti, Hf, Zr, Y), rare-earth-elements (REE) and transition metals (e.g. Ni, V, Cr and Co) are considered to be immobile (Rollinson

1993). Most major elements form definable trends in Harker diagrams, although K_2O and Na_2O are relatively scattered (Figure 4.3); this is expected given the abundant alteration of feldspar to sericite (see Chapter 2). Other LILE such as Rb and Sr also define very scattered trends. Transition metals such as Co and V form well-defined trends, whereas HFSE such as Nb and Zr display scattered trends. This scatter may be caused by the samples not representing a single co-magmatic suite, but arising from multiple magmatic suites all with slightly different 'liquid lines of descent'; given that the samples span a period of >15 million years, this is considered to be highly probable. In evolved samples, the varying fractionation and accumulation of accessory phases which have high partition coefficients for Zr and Nb (such as zircon, titanite and rutile) will also cause scatter.

The ability to distinguish a distinctive suite (the tholeiitic amphibolites; see following sections), suggests limited mobility of elements. In summary, the geochemistry allows for a rough approximation of original protolith compositions; with discrimination based on HFSE rather than LILE favoured for petrogenetic interpretations.

4.3.3 Souda Grey Gneiss Association

The grey gneiss a calcic to calc-alkaline differentiation trend, is magnesian, metaluminous to weakly peraluminous, and sub-alkaline (see Figure 4.2). The samples range from quartz gabbro and diorite, through tonalite, to granodiorite and granite (QAP), and are not adakitic but fall in the field of normal arc rocks (Sr/Y vs Y; Figure 4.2). In Harker diagrams (Figure 4.3) the major elements display defined trends but with variable scatter. Al_2O_3 and TiO_2 are roughly constant up to approximately 60% SiO_2 then decrease. CaO, MgO, MnO and Fe_2O_3 display negative trends, with a visible inflection in MgO at 55% SiO_2 . P_2O_5 defines a negative trend above 65 % SiO_2 , and a scattered slightly positive trend at lower SiO_2 content. Na_2O defines a poor trend, but seems to display an increase up to 60% SiO_2 , then a constant trend. K_2O defines a positive trend with significant scatter; an inflection at 69% marks an increase in K_2O .

The grey gneiss exhibits a variety of trends in trace elements relative to SiO_2 (Figures 4.4 & 4.5). Rb and Ba both increase but exhibit considerable scatter, especially in Rb in evolved samples. Sr shows a negative correlation after ~65 % SiO_2 , but is widely scattered at lower SiO_2 . Ni, Cr, Co and V all show negative trends with silica enrichment (Cr and Ni not shown), but with some variation between them. V displays a rather consistent and well-defined trend from ~200ppm to 0ppm with a possible inflection to a shallower trend at 63% SiO_2 . Co displays a similar trend to that of V, decreasing from ~50ppm to 3ppm, again with an inflection at 63%. Both Nb and Zr show slightly increasing trends with SiO_2 , but there is considerable scatter. LREEs exhibit scattered trends especially in evolved samples, but show a general increase with silica enrichment. MREEs also show scattered positive trends. HREEs show scattered trends, but are fairly constant up to ~69% SiO_2 , then display a sudden increase in most of the evolved samples.

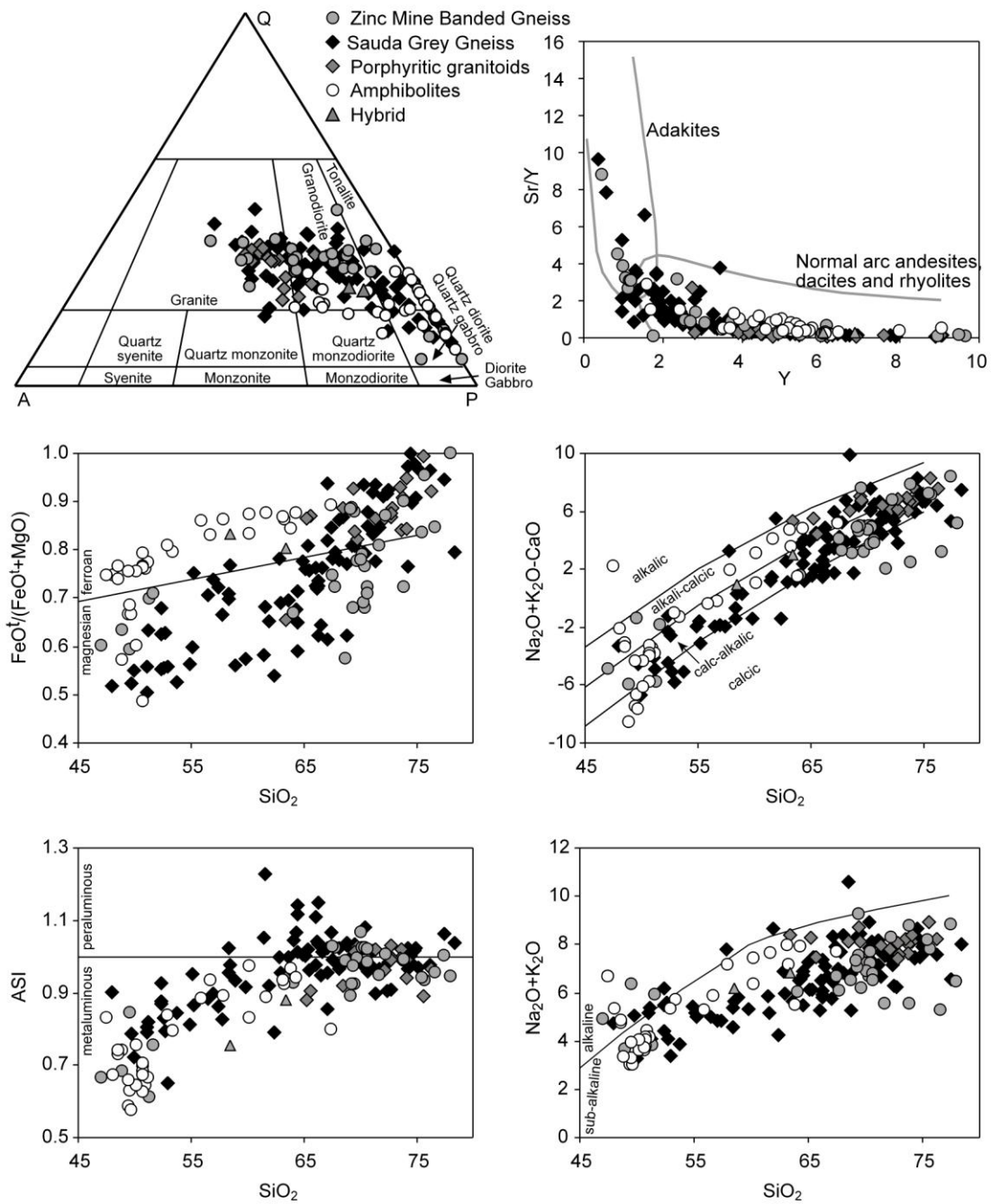


Figure 4.2. Geochemical classification of magmatic suites in the Suldal Sector. QAP = Quartz, Alkali-Feldspar, Plagioclase - IUGS classification, based on normative calculations; Y versus Sr/Y after Defant & Drummond (1990); $FeO^*/(FeO+MgO)$ (Fe^*), Na_2O+K_2O-CaO (Modified Alkali Lime Index), ASI (Aluminium Saturation Index - molar $Al_2O_3/CaO+Na_2O+K_2O$) after Frost et al. (2001). Sub-alkaline/alkaline field (Na_2O+K_2O) after Irvine & Baragar (1971).

In Primitive Mantle normalised spider diagrams (Figure 4.6) all lithologies show enrichment in all elements relative to Primitive Mantle. The greatest enrichment is that of the LILE, with Rb contents 30 to 300 times greater than Primitive Mantle. Strong depletion relative to other elements is seen in Nb, Ta, Sr, P and Ti. The depletion in Nb and Ta is recorded in basaltic compositions, and is

relatively constant with increasing silica enrichment. Sr, P and Ti are only slightly depleted in the basaltic samples, but exhibit a much greater degree of depletion with increasing silica enrichment.

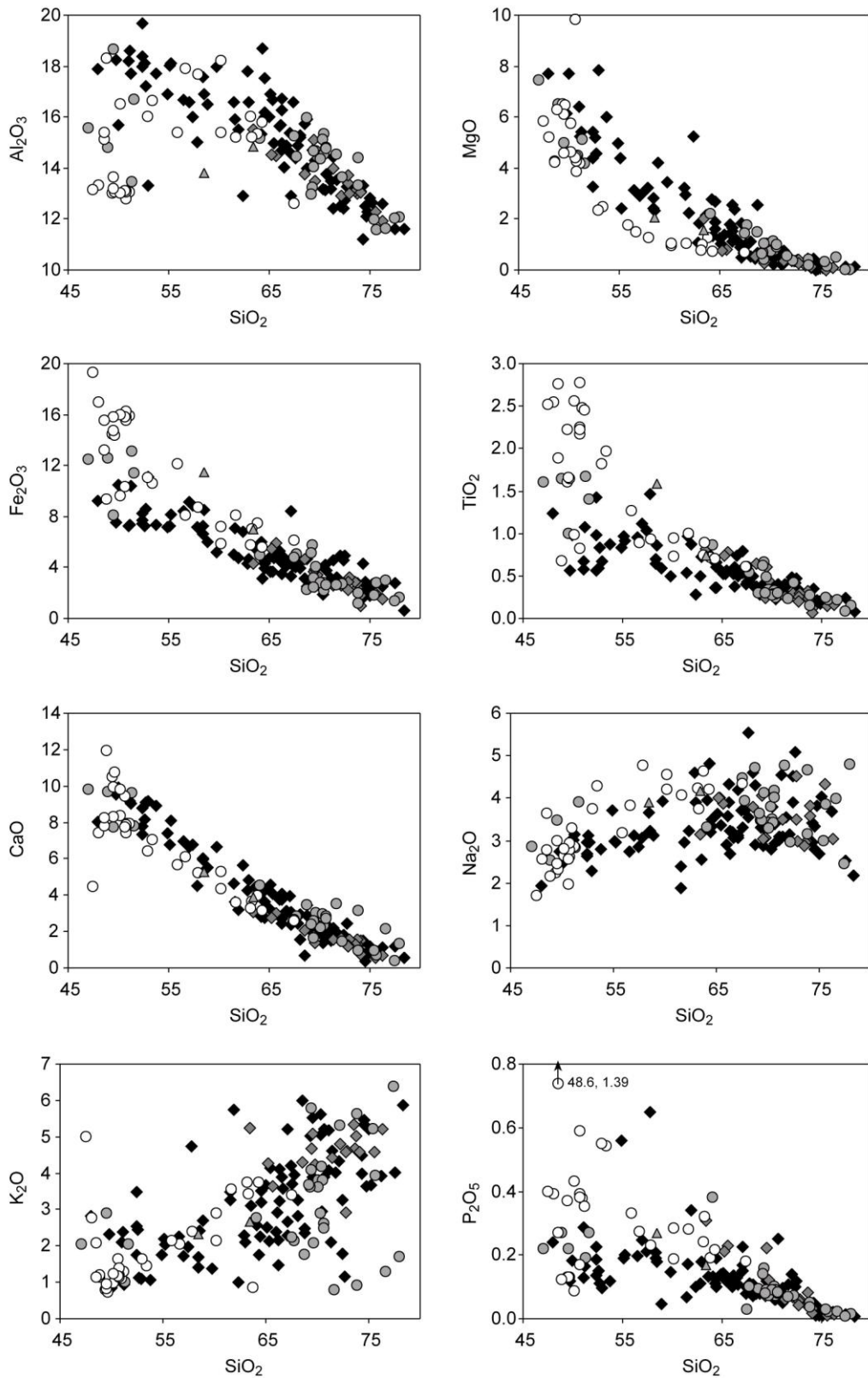


Figure 4.3. Major element oxides versus SiO_2 for magmatic suites in the Suldal Sector. Symbols as in figure 4.2.

In chondrite normalised REE spider diagrams (Figure 4.7), all lithologies show LREE enrichment relative to MREE, LREE enrichment relative to HREE, and only slight MREE enrichment relative to HREE. The amount of LREE to MREE enrichment is relative constant up to 60% SiO₂, then

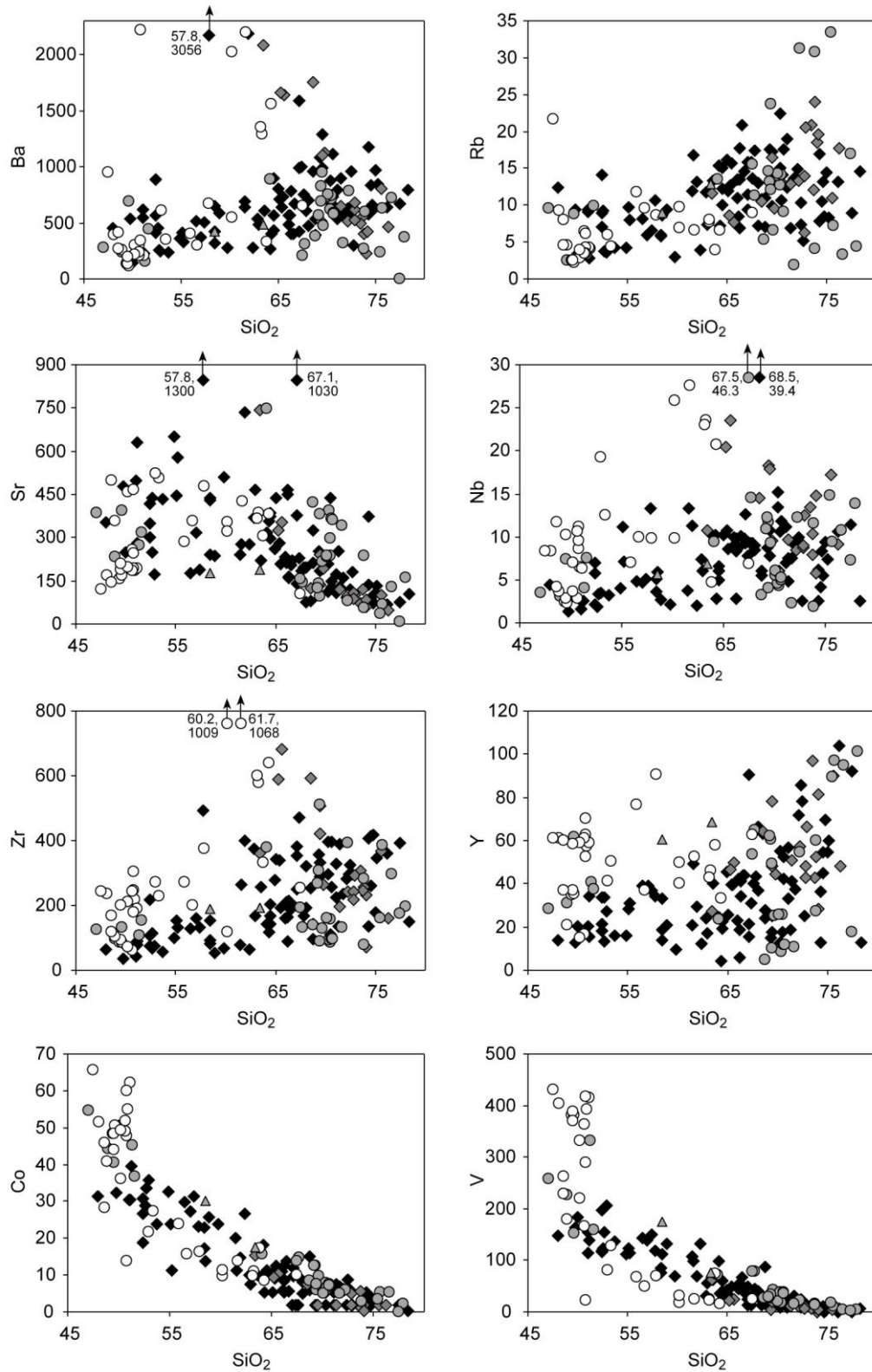


Figure 4.4. Selected trace elements versus SiO₂ for magmatic suites in the Suldal Sector. Symbols as in figure 4.2.

increases in more evolved samples. LREE to HREE enrichment is fairly constant throughout the suite, but exhibits large scatter in samples between >68% SiO₂. MREE to HREE enrichment slightly decreases with silica enrichment. Total REE contents show a positive but scattered trend. In basaltic samples both small negative and positive Eu anomalies are exhibited, with increasing silica

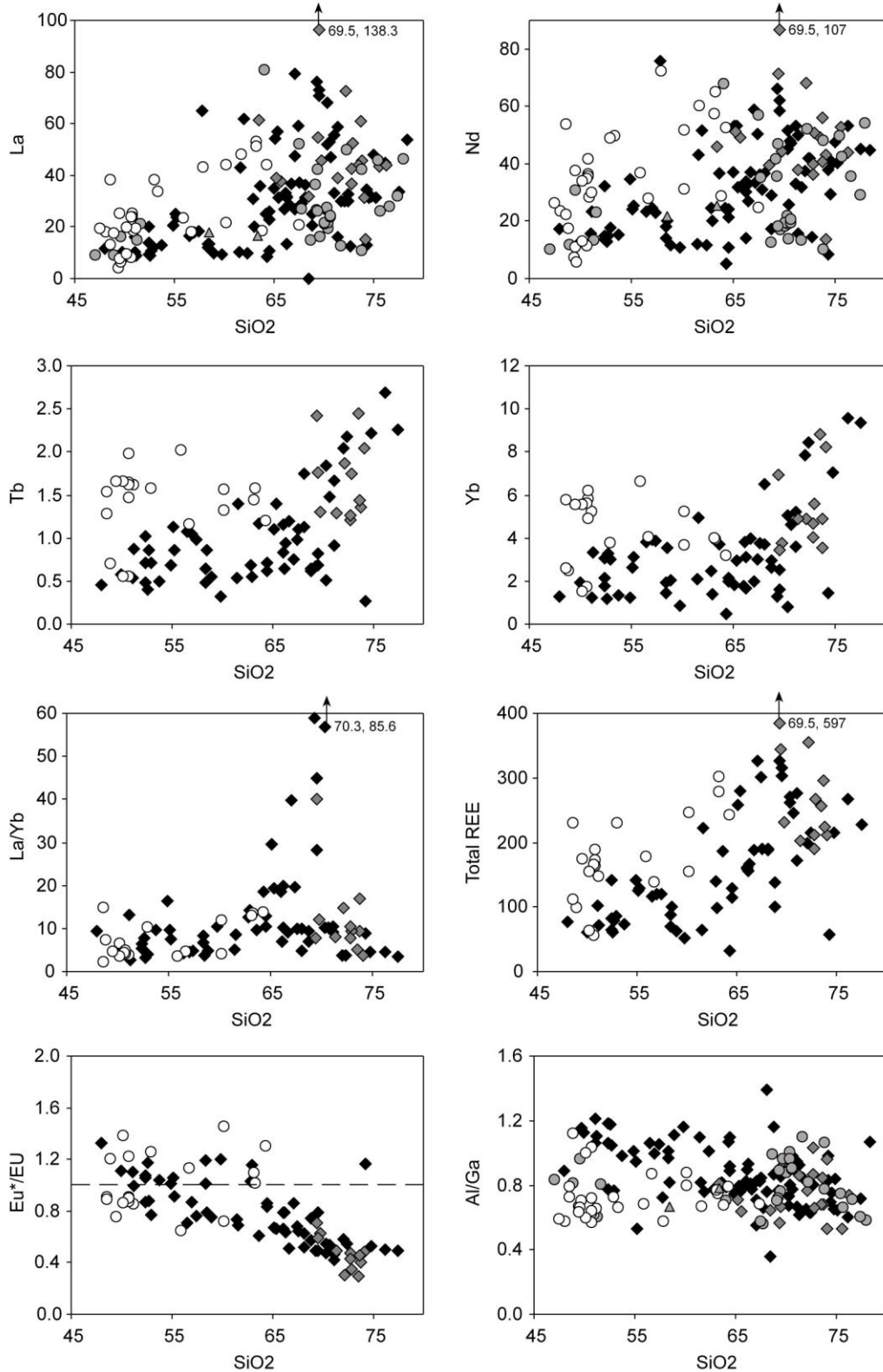


Figure 4.5. Selected trace and REE elements versus SiO₂ for magmatic suites in the Suldal Sector. Eu* = Eu/(√Sm*√Gd). Symbols as in figure 4.2.

enrichment the Eu anomaly becomes progressively more negative (Eu^*/Eu ; Figure 4.6). In the normalised spider diagrams the samples generally plot sub-parallel to each other. A few evolved

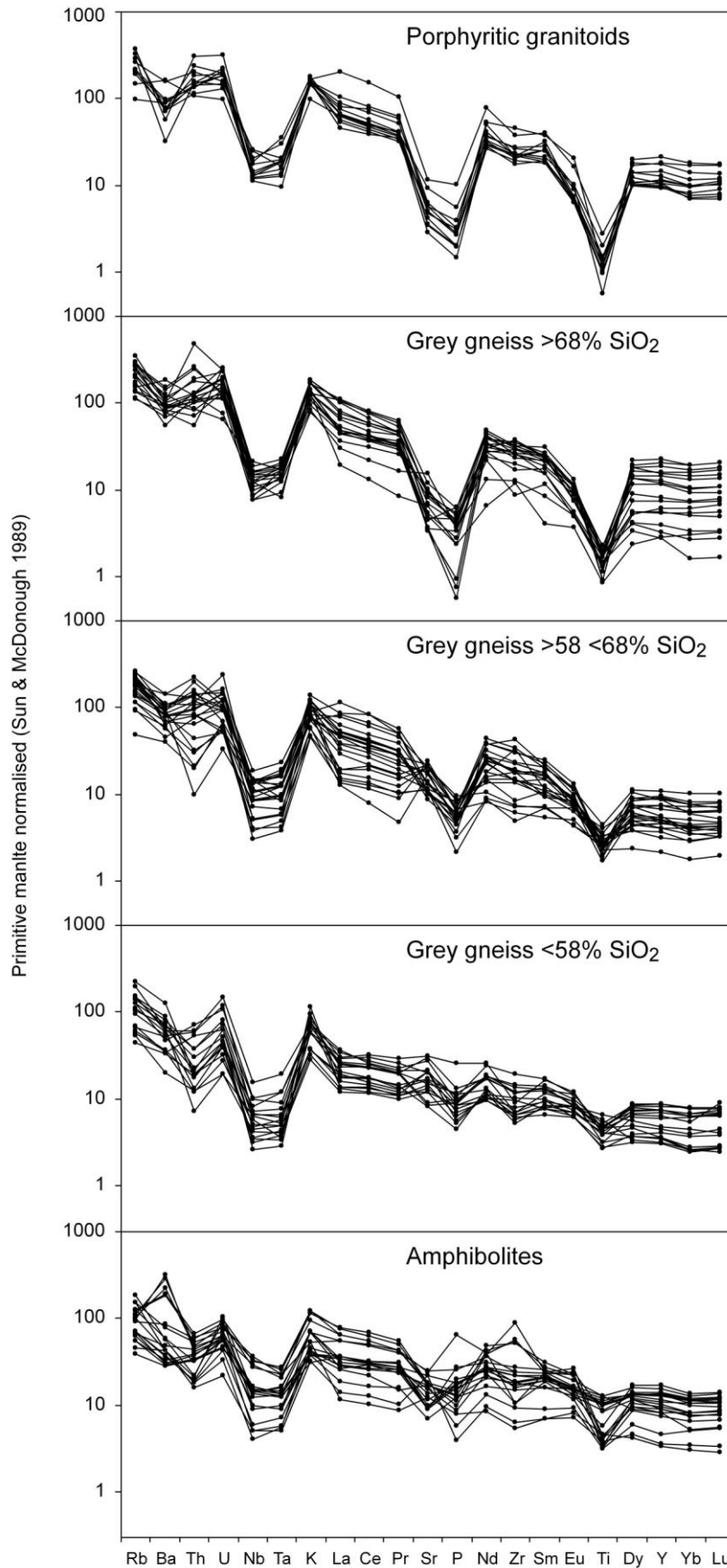


Figure 4.6. Primitive mantle normalised (Sun & McDonough 1989) spider-diagrams.

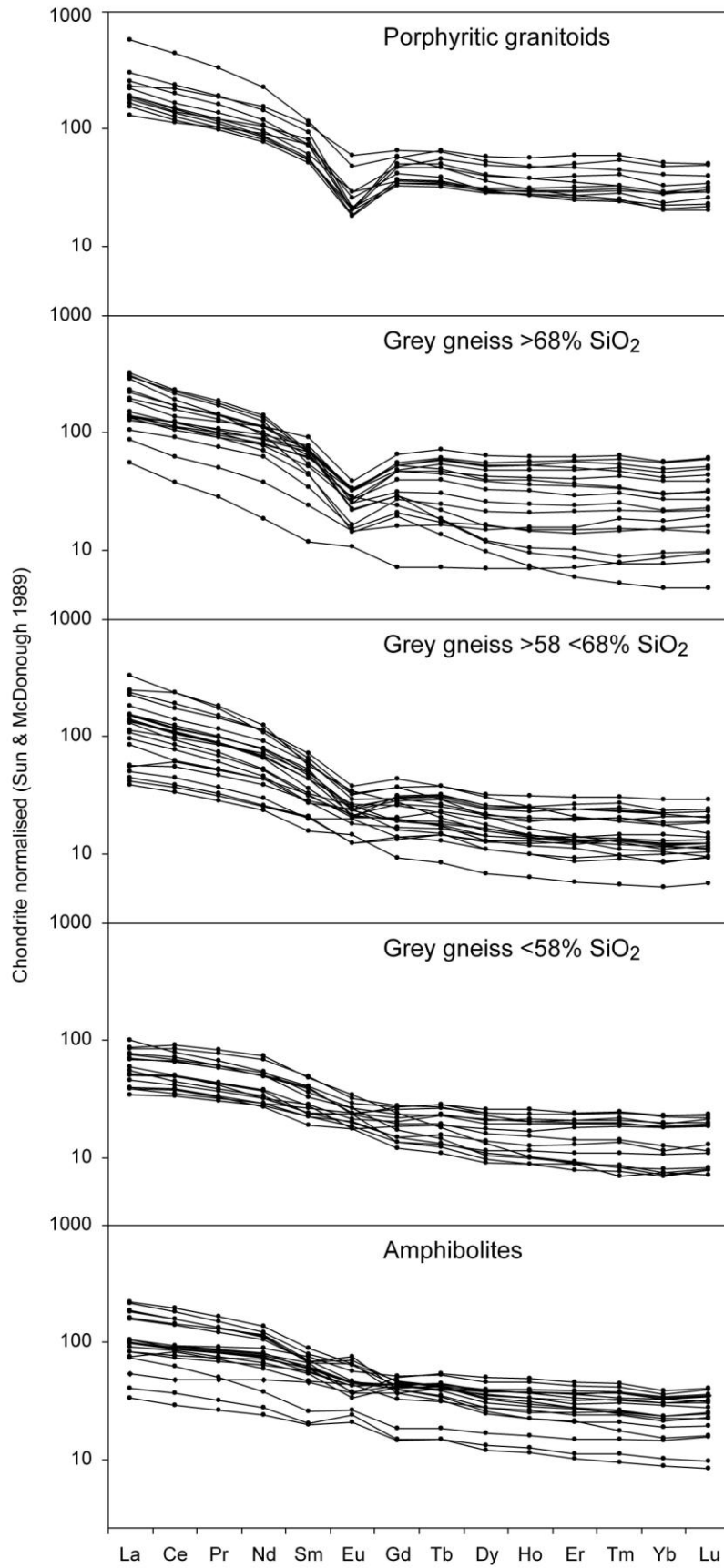


Figure 4.7. Chondrite normalised (Sun & McDonough 1989) spider-diagrams.

samples display less enriched profiles, two of which have positive Eu anomalies; these samples likely represent residual melts or cumulates with cumulative feldspar.

4.3.4 Zinc Mine Banded Gneiss

The Zinc Mine Banded Gneiss is a succession of calc-alkaline, metaluminous to weakly peraluminous and magnesian orthogneisses. The sample selection is bimodal in terms of silica content although intermediate compositions were observed in the field; differentiation trends are therefore not well-defined. Both the mafic and felsic populations show considerable scatter, but broadly correlate with trends shown by the Grey Gneiss. The REE were not measured on the ZMBG, but La and Y contents are similar to that of the Grey Gneiss, suggesting similar LREE to HREE fractionation and enrichment levels.

4.3.5 Amphibolites

As discussed in Chapter 2, the amphibolites are not amphibolites *sensu stricto*, but are a suite largely comprising amphibolites *sensu stricto*, but also comprising amphibole-rich intermediate to felsic lithologies which are spatially related to amphibolite units. The amphibolites are calc-alkaline to alkali-calcic, ferroan, metaluminous and sub-alkaline (Figure 4.2). The suite displays a differentiation trend on the Harker diagrams that is well-defined above ~53% SiO₂; at lower SiO₂ the trend is near vertical such that the samples appear to be scattered in some elements. In MgO, Co and V, the amphibolites have a well-defined negative trend throughout, in other elements (P₂O₅, Al₂O₃, TiO₂, Sr) the amphibolites increase steeply to ~53% SiO₂ then have a shallow negative trend, and in some elements (REE, Nb, Zr) the amphibolites increase steeply at first then increase more gradually after ~53% SiO₂. Some of the most primitive samples of the amphibolites suite (high MgO, and low SiO₂), exhibit positive Eu anomalies and are less-enriched in REE (see Figure 4.7); these samples likely represent magmas that are cumulative in feldspar.

Above ~53% SiO₂ the trends displayed by the amphibolites are generally sub-parallel to the Sauda Grey Gneiss trends, except that depletion or enrichment relative to the Grey Gneiss is evident in most major and trace elements. In the major elements the amphibolites have higher TiO₂, Na₂O, P₂O₅ and Fe₂O₃, lower Al₂O₃ and CaO, and similar K₂O contents. In the trace elements the amphibolites have higher Nb, Y, Zr, and V, and similar Rb and Ba; Co is higher in the most mafic amphibolites, but then drops off to a lower trend than that of the Grey Gneiss; Sr displays similar behavior to Al₂O₃ and is low at the mafic end-member, but then has similar contents to that of the Grey Gneiss; and Al/Ga, which can be used to indicate feldspar fractionation is lower in the amphibolites. At similar SiO₂, the REE display greater enrichment in the amphibolites relative to the Grey Gneiss (see Figure 4.5), although the LREE/MREE, LREE/HREE and MREE/HREE are similar between the two suites. In the Primitive Mantle normalized plot (Figure 4.7) the amphibolites exhibit similar depletions to those displayed by the Grey Gneiss. In summary, the

amphibolites have similar LILE (except for Sr), greater contents of incompatible elements, and higher Fe/Mg than the Grey Gneiss.

4.3.6 Granitoids

The granitoids are porphyritic, granodioritic to granitic, calc-alkaline, metaluminous to weakly peraluminous and sub-alkaline (Figure 4.2). The majority of the samples plot in the ferroan field (Fe*), however, this does not mean they have evolved from less-differentiated ferroan magmas, since at high silica content most magmas become enriched in Fe* (Frost et al. 2001). The granitoids have similar major and trace element contents to those in the Sauda Grey Gneiss (Figures 4.3 to 4.6). In Primitive Mantle normalized diagram (Figure 4.7) the granitoids display similar enrichment and depletions to those of the most evolved members of the Grey Gneiss Suite.

4.4 Petrogenesis

The Zinc Mine Banded Gneiss and granitoids were only studied at a reconnaissance level, thus their petrogeneses is not discussed separately. These suites have petrographic and petrologic similarities to the Sauda Grey Gneiss and are of the same age; therefore they are assumed to have a similar petrogenetic origin.

4.4.1 Grey Gneiss

The LILE enrichment and depletion in Nb, Ta, P and Ti are all characteristic of magmas produced in a supra-subduction zone setting. LILE enrichment (Rb, Ba, K) is generally attributed to addition of these elements from subduction zone fluids (e.g. Saunders et al. 1991). Depletion in Nb and Ta has been related to both retention of phases that accommodate these elements in the downgoing slab and to the immobility of these elements relative to LILE (e.g. Saunders et al. 1980; Green et al. 1981; McCulloch & Gamble 1991; Kelemen et al. 1993; Brenan et al. 1994). The fact that the basaltic compositions exhibit Nb and Ta depletion is compatible with a pre- crustal-differentiation origin for this depletion. Ti and P exhibit greater depletion with increasing SiO₂, therefore they are related to processes occurring during differentiation. Ti is likely depleted by fractionation of Fe-Ti oxides and titanite, and P is depleted by fractionation of apatite. The HFSE enrichment in the Grey Gneiss is typical of continental arc magmas. This enrichment, which is not typically observed in intra-oceanic arcs, is often related to an enriched source, e.g. asthenospheric mantle as opposed to depleted mantle, and/or to crustal contamination (i.e. the 'within-plate' component; Pearce 1983).

Evolved compositions have various origins in arc magmatic suites. Simplistically these involve fractional crystallisation with or without assimilation (e.g. Bowen 1928; Reagan et al. 2003; Kuritani et al. 2005; Greene et al. 2006), or partial melting of already crystallised crust (e.g. Tamura & Tatsumi 2002; Smith et al., 2003; Vogel et al. 2006). In reality both of these mechanisms likely occur together; in oceanic arcs where older silicic crust may not exist, the emplacement of mafic

sills, remelting of previous sills, fractionation of both mafic sills and partial melts, and mixing between different compositions, can lead to a crustal section with a range of compositions typical of volcanic arcs (i.e. a deep hot crustal zone; Annen et al. 2006).

Straight-lines on differentiation trends are indicative of magma mixing. Within the Grey Gneiss, straight-lines in Harker diagrams are exhibited in some elements, but the existence of inflections in many elements suggests fractional crystallisation played a significant role in differentiation. The sudden increase in REE, Zr, Y and K at ~69% SiO₂ means that intermediate compositions do not fall on a mixing array between felsic and mafic end-members, excluding a mixing-hypothesis for intermediate compositions. Inflections occur at lower SiO₂ also, for example MgO at ~55-60% SiO₂ and Na₂O and Al₂O₃ at ~60-65% SiO₂, and in trace elements at ~63% SiO₂ (Ga) and ~60-65% (Sr, Co). Thus, basaltic andesite compositions do not correspond to mixtures between basaltic and andesitic members, excluding a mixing-process at low silica enrichment. At 50 % SiO₂, Ni does not fall on a trend but is widely scattered, suggesting variable olivine content in the basaltic end-members. The evidence noted above points towards fractional crystallisation from mafic end-members, as opposed to mixing between mafic and silicic end-members, for the main process of differentiation within the suite. However, this does not exclude a partial melting process for differentiation. The discrimination between partial melting and fractional crystallisation can be achieved using the changes in REE abundance with magma differentiation (Brophy 2008). In the Grey Gneiss, the slightly increasing LREE, and constant HREE at intermediate compositions are most compatible with fractionation of basalt in the lower crust with amphibole present, and the enrichment in all REE at high silica content is compatible with mid-to upper-crustal fractionation of basalt where amphibole is not present (Brophy 2008).

High-silica melts generally contain crystallising phases that have high partition coefficients for LREE, MREE, and HREE (e.g. zircon, allanite, apatite, monazite). Within the Grey Gneiss suite, a sudden increase is seen in MREE and HREE at ~69% SiO₂. If this point marks the onset of crystallisation of certain accessory phases, then the sampled orthogneisses must contain accumulations of these phases, as opposed to originating as residual liquids. Apatite is found in most samples with SiO₂ greater than 60%, thus, it is not expected to cause the change at ~69%. Monazite is not recorded in any of the samples and is thus assumed not to be a fractionating phase. Zircon has $D_{\text{LREE}} < D_{\text{MREE}} < D_{\text{HREE}}$ and allanite has $D_{\text{LREE}} > D_{\text{MREE}} > D_{\text{HREE}}$, thus, zircon is the most likely candidate for controlling the observed REE changes. An increase in Zr at ~69 % corresponds to the MREE and HREE increase, supporting the hypothesis that this phase is responsible for the change in REE concentrations. However, samples with low HREE samples do not have corresponding low Zr values, invalidating this hypothesis. Another phase that accommodates both Zr and REE is amphibole. The termination of amphibole as a fractionating phase would produce an increase in

REE and Zr, as these would no longer be removed from the melt. As D_Y in amphibole is greater than 1, the constant Y abundances and then sudden increase at ~69% support this notion. Thus, in agreement with the trends modelled by Brophy (2008), it is suggested that the change in REE concentrations in the Grey Gneiss suite is strongly controlled by amphibole fractionation.

Along with amphibole, the role of other fractionating minerals can be assessed using major and trace element changes with differentiation. The increase in the size of the negative Eu anomaly with differentiation indicates plagioclase was fractionating throughout the entire differentiation process. The inflection in the Al_2O_3 and Sr trends indicate that plagioclase had a greater control on differentiation after ~60 % SiO_2 . Decreases in CaO, MgO, and Fe_2O_3 , and increases in Na_2O and K_2O with differentiation, are compatible with fractionation of clinopyroxene. Decreases in transition metals (Ni, Co, V), MgO and Fe_2O_3 are compatible with fractionation of Fe-Ti oxides. In summary, the trends displayed are typical of POAM - Plagioclase, olivine (and/or orthopyroxene), clinopyroxene (and/or amphibole) and magnetite fractionation; such fractionation is typical in arc suites for the formation of andesitic compositions from mafic parent melts (Gill 1981).

To assess whether the crystallizing phases determined above are compatible with the REE trends, a simple fractional crystallisation model was tested (Figure 4.8; Table 4.1). There are inherent problems with modelling of trace elements (see Rollinson 1993); particularly of concern are the partition coefficients used, as these are dependent on factors which are often not controlled in the modelling, i.e. temperature, oxygen fugacity, pressure, and H_2O activity. Partition coefficients also vary as the melt evolves. However, modelling can still provide a useful indication of what assemblages are compatible with the observed trends. REE concentrations were modelled in two stages using Rayleigh fractional crystallisation; these stages comprise the fractionation of an average mafic Grey Gneiss composition to produce an andesitic composition, and the fractionation of an average andesitic composition to produce a dacitic composition. At higher silica contents trace elements become highly dependent on accessory phases such as zircon, thus, rhyolitic compositions were not modelled. In the first stage, a best fit is achieved with 30-40% fractionation of an assemblage comprising plagioclase, clinopyroxene, hornblende and magnetite. In the second stage, a best fit is achieved by 30-40% fractionation of an assemblage similar to that in stage 1, but with greater plagioclase content and the addition of minor apatite content. These assemblages are similar to those modelled in other Precambrian continental arcs (Slagstad et al. 2004).

In summary the major, trace and REE trends within the Grey Gneiss suite suggest that it formed by fractional crystallisation of a basaltic parent melt, with multiple stages of fractionation probably occurring at different levels in the crust. This scenario is compatible with a deep hot crustal zone setting (Annen et al. 2006). The geochemistry of the studied suites suggests formation in a volcanic

arc setting. The range and abundance of evolved compositions is suggestive of a mature island arc or continental arc; this inferred tectonic setting for the Grey Gneiss suite is here named the Suldal arc.

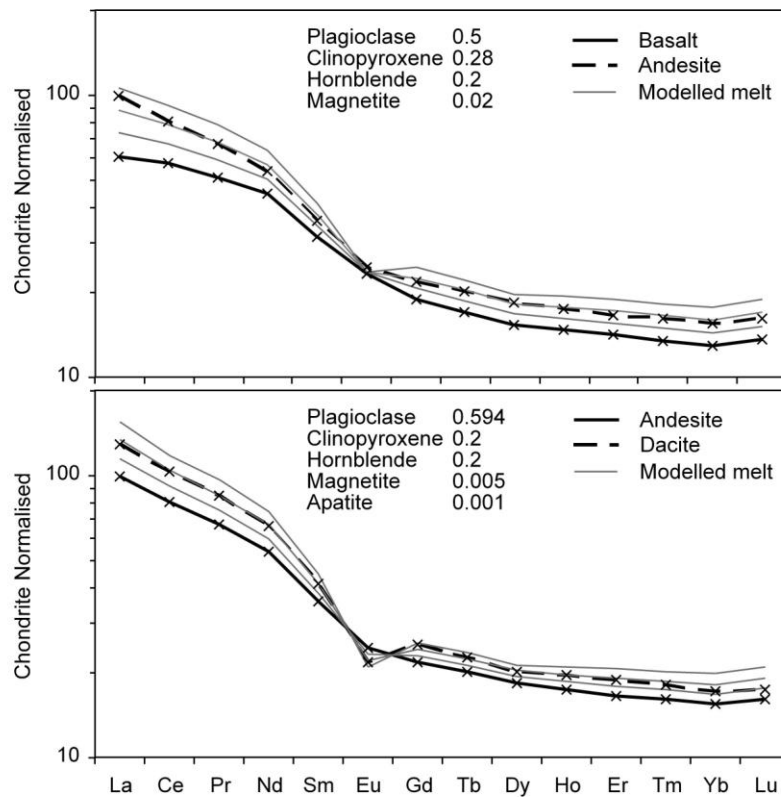


Figure 4.8. Rayleigh fractional crystallisation modelling of REE contents in the Sauda Grey Gneiss. Basalt, Andesite and Dacite are average REE contents of the Grey Gneiss from 45-55%, 55-63% and 63-67% SiO₂ respectively. Modelled melts are shown at 20% increments. Results and partition coefficients are shown in table 4.1.

4.4.2 Amphibolites

The amphibolites, although displaying similar trends to the Grey Gneiss Suite, exhibit features that are typical of 'A-type' rocks, i.e. low CaO, high Fe/Mg and Ga/Al, and enrichment in incompatible elements (Whalen et al. 1987; Collins 1982). A-type magmas are typical of post-collisional and extensional tectonic settings, but are not typical of the main arc-forming stage in subduction-zone settings (Bonin 2007). In the Suldal Sector, at least some of the amphibolites crystallised during the ~1500 Ma event (see Chapter 3). Thus, formation of the amphibolites for at least some of the samples must have occurred contemporaneously with formation of the Grey Gneiss suite. Different mafic bodies within the study area have different structural fabrics recorded in them, with some being undeformed dyke-like intrusions; this suggests that emplacement of these magmas may have occurred on multiple occasions since the ~1500 Ma event. The gabbro bodies that are inferred to be ~1500 Ma are typically less deformed than the Grey Gneiss they intrude, suggesting the amphibolites may have intruded in a later stage of arc development than the bulk of the Grey Gneiss, however, one sample of amphibolite is an enclave from within highly deformed Grey

Gneiss, suggesting earlier or concomitant formation. Also, two samples from a zone of magma mingling ('hybrid' in figures 4.2 to 4.5), have major and trace element contents that straddle the magnesian Grey Gneiss and ferroan amphibolite trends, suggesting some mingling has occurred between these magma series upon intrusion. The A-type amphibolite suite is interpreted to have evolved contemporaneously with the Grey Gneiss suite, thus, the cause of the compositional difference between the two suites is likely related to changes during magma differentiation, changes in source conditions, and/or changes in the source material.

As previously discussed, fractionating phases in the Grey Gneiss suite likely included plagioclase, olivine, pyroxene, amphibole, olivine and Fe-Ti oxides. The amphibolites have higher Ga and lower CaO and Al₂O₃, this can be explained by leaving a plagioclase residue in the parent melt. The lower MgO in the amphibolites, suggests a greater olivine residue. V is higher in the more mafic end of the amphibolite suite, but has a sharp decrease so that intermediate compositions have lower V than the Grey Gneiss. TiO₂ is also initially much higher in the amphibolites. The trends in Ti and V suggest that residual Fe-Ti oxides were less important in the parent melt of the amphibolites, but probably formed part of the fractionating assemblage later on in the differentiation. The compositional differences discussed so far can be related to an increase in residual plagioclase and olivine in the amphibolites, and an increase in residual Fe-Ti oxides in the Grey Gneiss suite.

The amphibolites also show an increase in the HFSE, MREE and HREE (i.e. the incompatible elements), whereas the LILE are similar between the two suites. Increases in incompatible elements can be related to either smaller degrees of partial melting, or partial melting of a mantle source that is less depleted by previous melt extraction (enriched mantle). Isotope data can often aid the discrimination between these processes. Hafnium in zircon data on two amphibolite samples (SA7-86, ROG525; chapter 5) suggest that the source was similar in terms of crustal versus mantle contribution. 'Enriched mantle' sources, which in arc/back-arc settings are generally related to asthenospheric mantle input, typically lack a negative Nb anomaly. The amphibolites have a negative Nb anomaly similar to that of the Grey Gneiss, suggesting a similar mantle source, or at least that the mantle sources underwent the same modification by subduction-zone fluids. The geochemical data thus suggest that two processes are responsible for the development of the two suites, the fractionating assemblage, and the degrees of partial melting.

The amphibolite suite is likely produced by fractionation of a parent magma with residual plagioclase and olivine (\pm clinopyroxene/hornblende), whereas the Grey Gneiss includes Fe-Ti oxide as a residual phase. Differences in the stability of crystallizing phases during magma differentiation depend on a number of intensive parameters, namely temperature, pressure, oxygen fugacity and water activity. Experimental studies have demonstrated the significance of water

content in primary basaltic magmas, in particular an increase in the water content leads to the early appearance of Fe-Ti oxides and the suppression of plagioclase crystallization (Gaetani et al. 1993; Sisson & Grove 1993; Kawamoto 1996). An increase in pressure leads to the reversal of this, with earlier plagioclase crystallisation and a greater proportion of plagioclase relative to Fe-Mg silicates (Grove et al. 2003). Oxygen fugacity generally correlates with water activity, with reducing conditions normally being relatively anhydrous and oxidizing conditions being hydrous. The effect of oxygen fugacity has similar effects to that of water, although water has a much greater effect than oxygen fugacity or pressure (Hamada & Fuji 2008). Oxygen fugacity controls the stability of Fe-Ti oxides (Feig et al. 2006; Botcharnikov et al. 2008), with magnetite crystallizing first in conditions above fayalite-magnetite-quartz (FMQ), and ilmenite appearing first in conditions below FMQ (Toplis & Carroll 1995).

The relative amount of Fe-Ti oxide to plagioclase crystallisation has a strong control on magma differentiation. If Fe-Ti oxides crystallize early, then the magma will become increasingly enriched in silica, and enrichment in iron will be suppressed; thus, the melts will follow a calc-alkaline trend. If Fe-Ti oxides do not crystallize early on, then the melt will become progressively enriched in iron, and form a tholeiitic trend. This leads to the general inference that calc-alkaline magma suites are relatively hydrous and oxidizing, and tholeiitic magma suites are anhydrous and reducing (Sisson & Grove 1993; Baker et al. 1994).

Tholeiitic (ferroan) magmas are typical of oceanic island arcs, where the crust is relatively thin, however, there are examples where they occur in the same volcanic arc as calc-alkaline (magnesian) magmas, for example in the Cascades (Baker et al. 1994), the Aleutians (Kay et al. 1982) and in Japan (Hunter 1988; Sakuyama 1981). The formation of tholeiitic and calc-alkaline trends in the same volcanic system has been explained by the difference in intensive parameters, for example Baker et al. (1984) advocate a deep source control on magma trends whereby the water content in the mantle varies, causing differences in fractionating assemblages in the parent magmas. At Aso volcano, SW Japan, a shallow level control is advocated for differentiation of tholeiitic and calc-alkaline trends (Hunter 1998); whereby predominantly tholeiitic magmas evolve to calc-alkaline magmas with a change in the fractionating assemblage, but also with a decrease in crustal contamination. This is contrary to the general belief that calc-alkaline magmas involve greater amounts of crustal contamination (e.g. Grove & Baker 1984; Myers et al. 1984; Fujinawa 1988; Hora et al. 2009). Hora et al. (2009) advocate a shallow-level control on differentiation of tholeiitic to calc-alkaline suites, but where tholeiitic magmas evolve to calc-alkaline magmas via assimilation of crust/melts. In this model, tholeiitic series are 'clean' and characterized by rapid magma throughput and minimal crustal contamination, whereas calc-alkaline magmas are 'dirty', involving compartmentalized, stagnant assimilation-prone magma differentiation (Hora et al. 2009).

From the examples listed above, it would seem that the petrogenesis of the amphibolites evolving contemporaneously with the Grey Gneiss, could be explained by either a shallow- or deep-level control on the intensive parameters, which in turn affected the fractionation assemblage. However, on closer examination of the amphibolite suite, it appears such iron-enrichment is not comparable with examples such as those listed above, and requires further explanation.

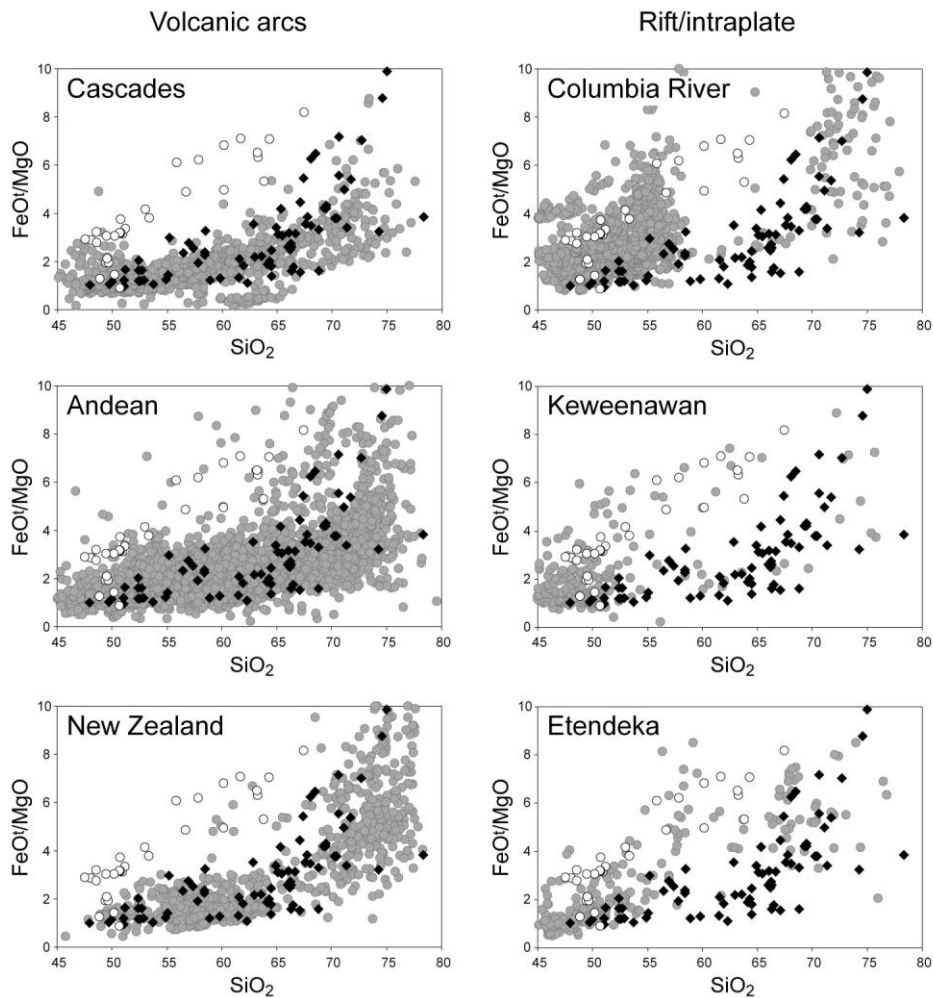


Figure 4.9. SiO_2 versus $\text{FeO}^{\text{t}}/\text{MgO}$ for selected continental arc and continental rift data (grey circles) compared with the Suda Grey Gneiss (black diamonds) and amphibolite (white circles) suites. Data from the Georoc database (<http://georoc.mpch-mainz.gwdg.de>)

Figure 4.9 shows data from the Grey Gneiss and amphibolite suites compared to published data from a variety of continental arc and continental rift settings. Such extreme iron enrichment in basaltic lithologies is rare to non-existent in arc settings, but is more common in continental rift settings, particularly in the Columbia River Flood Basalts (CFB). Such iron-rich mafic rocks are commonly referred to as ferrobasalts, notable examples include oceanic islands (Galapagos, Baitis & Lindstrom 1980; Thingmuli, Carmichael 1964), continental rifts (Snake River Plain, Leeman et al. 1976), layered intrusions (Skaergaard; Wager 1960) and residual magmas associated with

anorthosite massifs (Laramie Anorthosite Complex; Scoates et al. 1996). These examples exhibit lithologies with similar iron contents to that recorded in the amphibolites suite (Figure 4.10a).

Extreme iron enrichment can be achieved by differentiation of parent magmas involving no Fe-Ti crystallization but dominant plagioclase crystallisation in the early stages of differentiation, such that iron is enriched, and silica is not enriched and possibly even depleted. This differentiation has been reproduced experimentally at low pressure to explain the origin of oceanic tholeiites and the Skaergaard trend (e.g. Spulber & Rutherford 1983; Toplis & Carroll 1985; Snyder et al. 1993; Thy et al. 2006), but does not explain formation in settings with thick continental crust such as the Snake River Plain. Recent studies however have focused on this latter setting; experiments with low water contents at a variety of pressures have been conducted to try and reproduce the compositions seen in the Snake River Plain and in other iron-enriched magma series (Villiger et al. 2004; Nekvasil et al. 2001; 2004; Whitaker et al. 2007; 2008). The results from Whitaker et al. (2007) are displayed in figure 4.10b; the experiments were conducted on an olivine tholeiite with reducing conditions ($\Delta\text{FMQ} \sim -2$), low water activity (0.05 wt% H_2O), and pressures from 0 to 9.3 Kbar. At all pressures, magma differentiation involved significant iron enrichment and a lack of silica enrichment. Also shown on figure 4.10b are experimental data from Sisson et al. (2005), which are similar to the original calc-alkaline experiments of Sisson & Grove (1993); iron enrichment during magma differentiation varies according to a change in oxygen fugacity, but silica is highly enriched leading to calc-alkaline differentiation trends. In summary, experimental data show that water content has a critical control on fractionating assemblage, and thus, whether tholeiitic or calc-alkaline trends are followed. The amphibolite suite must have formed in conditions with very low water activity similar to that advocated for continental rift ferrobasalts, and the Grey Gneiss suite likely formed in hydrous conditions similar to those recorded in modern arcs.

The threshold water content at which iron-enriched tholeiitic trends will form instead of more typical silica-enriched calc-alkaline trends, is not well constrained, but is inferred to be between 0.5 and 0.8 wt% H_2O at 9.3 Kbar using continental rift starting materials (Nekvasil et al. 2001). The scarcity of iron-enriched magma series occurring in volcanic arcs suggests that the crust in this setting typically has a higher water content than this threshold. Where iron-enriched compositions are more common, e.g. oceanic islands and continental rifts, there is typically a plume-related source advocated for formation of the magma series; this mantle source is inferred to be drier and more reducing than in arc settings (e.g. Christiansen & McCurry 2009), and in some examples, such as the Etendeka-Parana flood basalts province, the iron-enrichment may even be enhanced by further processes such as iron-rich streaks in the mantle plume (Gibson et al. 2000; Ewart et al. 2004).

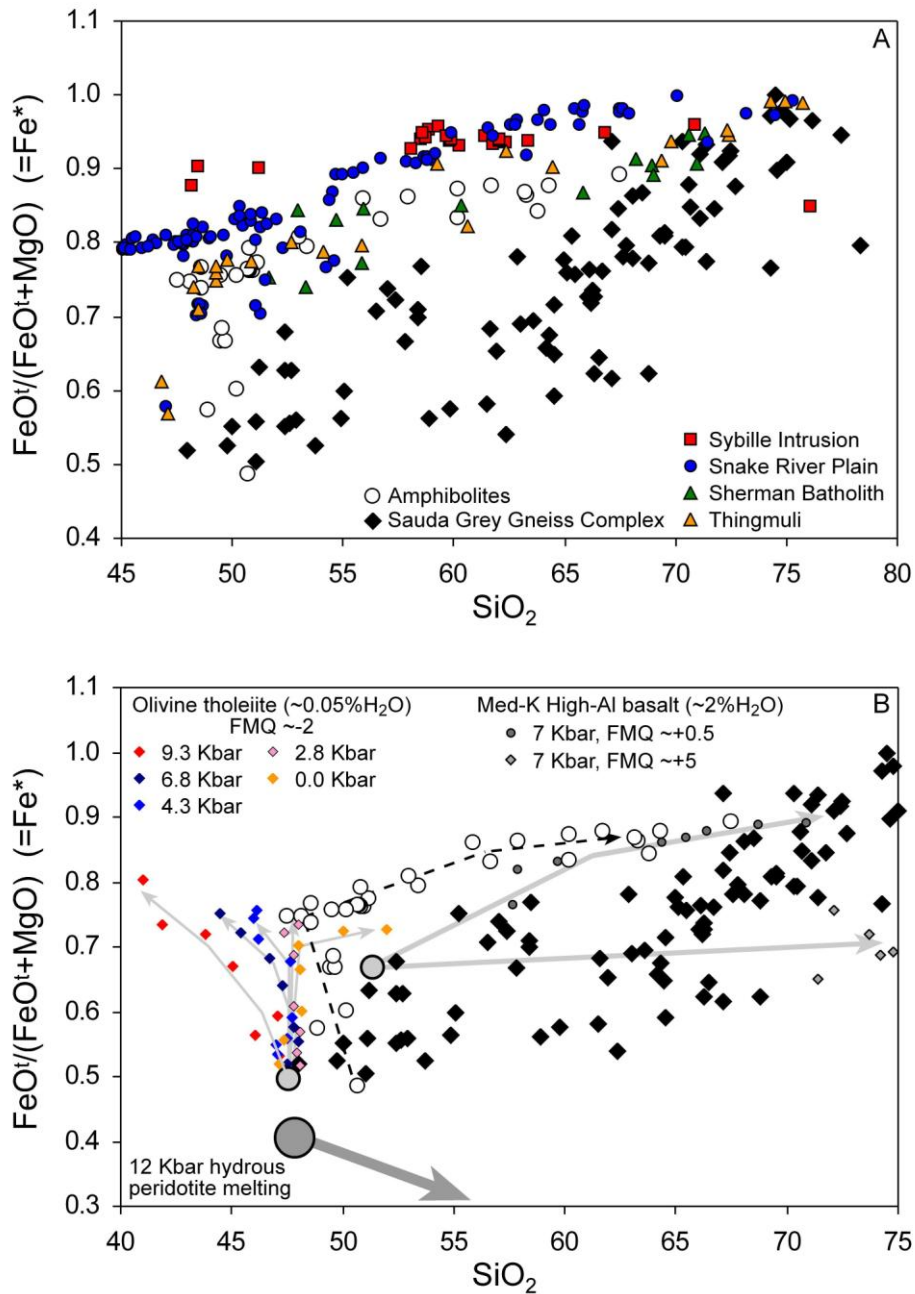


Figure 4.10. A) SiO_2 versus Fe^* (Frost et al. 2001) for the Suda Grey Gneiss and amphibolite suites compared with data from Thingmuli (Iceland; Carmichael 1964), the Craters of the Moon suite in the Snake River Plain (Stout et al. 1994; Hooper 2000; McCurry et al. 2008; Putirka et al. 2009), the Sherman Batholith (Proterozoic tholeiitic A-type pluton in Wyoming; Frost et al. 1999), and the Sybille intrusion (residual tholeiitic rocks associated with the Proterozoic Laramie Anorthosite Complex, Mitchell et al. 1996; Scoates et al. 1996).

B) The Suda Grey Gneiss and amphibolite suite compared with experimental data using anhydrous olivine tholeiite (Whitaker et al. 2007), hydrous medium-K high-Al basalt (Sisson et al. 2005) and hydrous peridotite (Gaetani & Grove 1998). Grey lines show the approximate differentiation trends for experimental data; black dotted line shows the evolution of the amphibolite suite.

The contemporaneous formation of continental rift-like tholeiitic (ferroan) amphibolites (at least on this coarse Precambrian timescale), with the subduction-related calc-alkaline (magnesian) Grey Gneiss suite, is rather anomalous within the global rock record. As stated previously, the

compositional difference between the two suites is likely related to changes during magma differentiation, changes in source conditions, or changes in the source material. The previous sections have discussed changes in source conditions that form tholeiitic versus calc-alkaline magma series. To further assess whether different sources were involved, the trace element content of the two suites can be examined; this is shown in figure 4.11 using primitive mantle normalized plots and trace element ratio binary plots. The amphibolites feature similar LILE and HFSE enrichment to the Grey Gneiss suite, similar LILE/HFSE ratios, and a similar to slightly less-negative Nb anomaly. In the Th/Yb versus Ta/Yb and the Nb/Y versus Zr/Y plots, the amphibolites overlap the Grey Gneiss, and exhibit similar degrees of subduction-zone related enrichment. The data indicate a similar subduction-zone related source for the amphibolites as for the Grey Gneiss; if the source for the amphibolites was related to a mantle plume or asthenospheric mantle, then the data should fall within the tramlines on the Ta/Yb versus Th/Yb and Zr/Y versus Nb/Y diagrams, and should lack a Nb anomaly.

On the basis of comparison with experimental data and geochemical data, the petrogenesis of the amphibolites suite is inferred to have involved a source similar to that of the Grey Gneiss, but with crystallisation under different intensive parameters, namely very low water content (<0.5% H₂O) and reducing conditions ($\Delta FMQ \sim -1$ to -2). How such conditions prevailed in an arc setting remains speculative, and due to the lack of other comparable suites in the rock record, may be a rare sequence of events. One similar example but with less extreme end-member compositions, may provide a more recent analogue however for the setting of this Telemarkian magmatism. Shuto et al. (2006) describe a model for the petrogeneses of magmatic suites that developed during the opening of the Japan sea; in their model, the early stages of the Japan sea opening (Early Miocene) involved asthenospheric mantle upwelling with partial melting of the overlying lithosphere and continental rifting; partial melting of the lower crust forming continental-rift silicic magmas. This process of continental rift magmatism is similar to that advocated for the Rjukan rift in central Telemarkia (Menuge & Brewer 1996; Sigmond et al. 1997; Slagstad et al. 2009), in which partial melting of crust formed the Rjukan rhyolites at ~1500 Ma (Dahlgren et al. 1990). The geochemistry of basaltic magmatism that occurred in the Rjukan Rift (Vemork formation) is shown in figure 4.11 for comparison; compared to the Grey Gneiss and amphibolites, the Vemork basalts are much less LILE-enriched, lack a Nb anomaly, and fall within the tramlines in the Zr/Y versus Nb/Y plot, therefore they are compatible with an origin in the asthenospheric mantle.

The opening of the Rjukan rift in the Telemark Sector (and the related asthenospheric mantle upwelling), occurred contemporaneously with the amphibolite and Grey Gneiss magmatic suites in the neighbouring Suldal Sector. A tectonic model for the evolution of these magmatic suites is shown in figure 4.11. It is inferred that extension of the overriding plate (Telemarkia) that was

likely related to slab-rollback, caused localized extension of the crust forming the Rjukan rift (Slagstad et al. 2009). Extension of the lithosphere allowed uprise of asthenospheric mantle, this uprising mantle produced the Rjukan rhyolites via crustal anatexis, and later produced basaltic magmatism after further crustal extension. At the same time, dehydration melting in the mantle wedge above the subducting slab was producing typical arc magmatism (Sauda Grey Gneiss). At certain points in time, dry and reducing conditions existed in the zone of melt generation, such that the tholeiitic amphibolite suite was produced. Differentiation of the tholeiitic magma series may have been aided by crustal extension, allowing rapid magma uprise without crustal contamination (e.g. Hora et al. 2009). The prevalence of reducing and dry conditions may have been aided by the uprise of asthenospheric mantle; this mantle uprise is interpreted to be a source of heat but not a source of material for the generation of the amphibolites.

As stated above, the existence of dry and reducing conditions in a supra-subduction setting is rare. Known water contents of arc magmas are up to 6 wt% (Sisson & Layne 1993). The average oxygen fugacity of arc magmas is estimated to be ΔFMQ -1 to +2 whereas the upper mantle has a range from ΔFMQ -4 to +2, and the lower mantle is much more reducing at ΔFMQ <-5 (Carmichael & Ghiorso 1990; Parkinson & Arculus 1999; McCammon 2005; Rowe et al. 2009). The oxygen fugacity of lower arc crust has been estimated for the Talkeetna arc to be ΔFMQ +1 \pm 1 (Behn & Kelemen 2006). The increased oxygen fugacity in arc magmas relative to the mantle has been attributed to the addition of volatiles derived from dehydration of the subducting slab; in a study of volcanic arc magmas from the Cascades arc, oxygen fugacity was correlated with fluid-mobile trace element and LREE contents (Rowe et al. 2009). In the Taupo volcanic zone of New Zealand, oxygen fugacity is correlated with slab-derived fluids such as Ba and Cl (Deering et al. 2010). In the latter study a temporal change is observed from wet-oxidising magmas to dry-reducing magmas, and is thus related to a decrease in the flux of subduction-related volatiles. Average oxygen fugacity in the Taupo magmas ranges from ΔFMQ +0.5 to +1.5, and the change occurs over \sim 100,000 years. A temporal change like this may have existed in the Suldal arc, but would be difficult to distinguish on a Precambrian timescale. The range in oxygen fugacity in this example is much less extreme than that required to produce the variation between the iron-enriched tholeiitic amphibolite suite and the calc-alkaline Grey Gneiss suite.

The cause of dry and reducing conditions during early differentiation of the amphibolite suite remains speculative, since its geochemistry is indicative of subduction-zone enrichment in

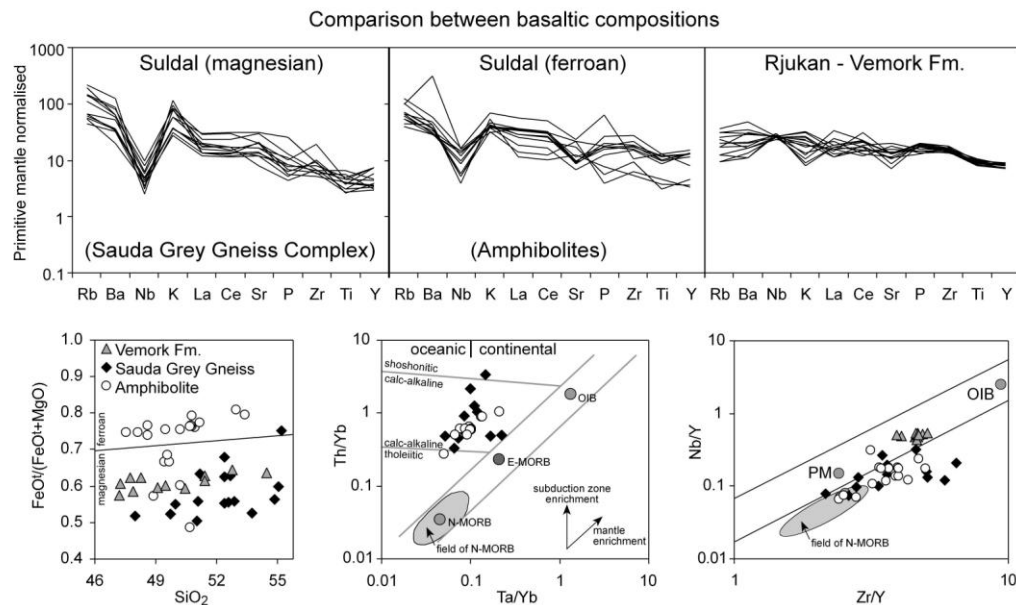
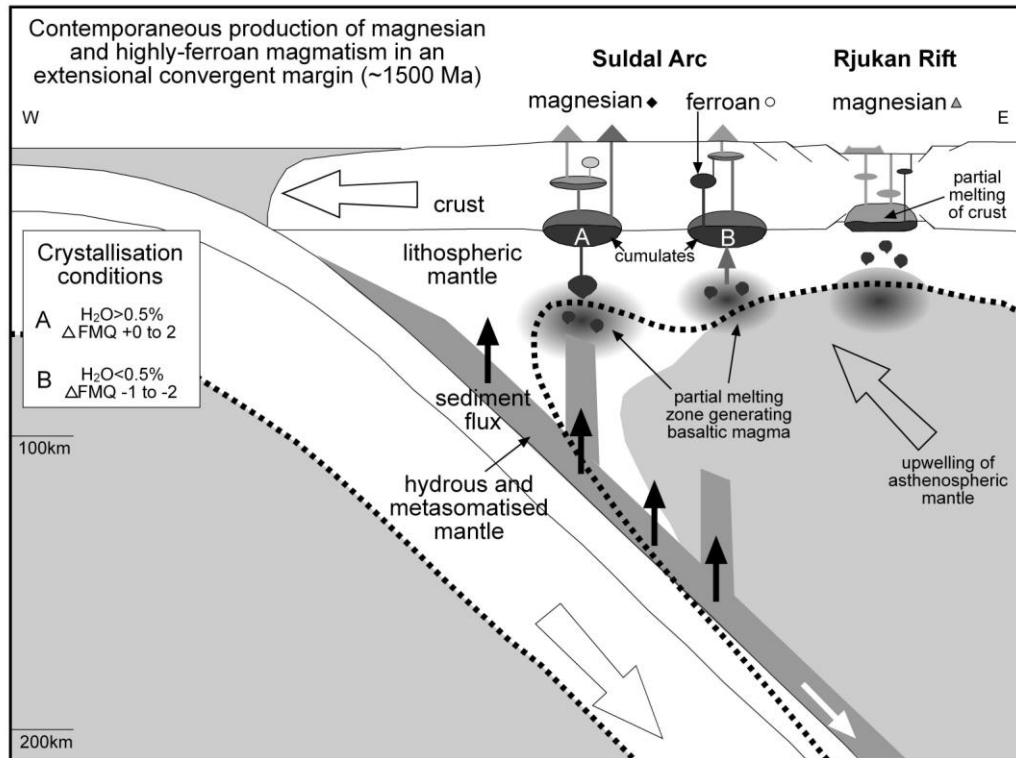


Figure 4.11. Schematic model for the tectonic setting of ~1500 Ma magmatism in Telemarkia. The magnesian Sauda Grey Gneiss suite is formed by melting in the mantle wedge with a subduction-zone fluid and sediment flux typical of continental arcs; the ferroan amphibolite suite had a similar parent magma but formed in anhydrous and reducing conditions. The magnesian rhyolites (Tuddall Fm) of the Rjukan Rift in the Telemark Sector formed by crustal anatexis fluxed by asthenospheric mantle, and the basalts (Vemork Fm) formed after underplating by asthenospheric mantle. Plots of mafic end-members of the three suites are shown to compare geochemistry; the Grey Gneiss and amphibolite suites have similar signatures (subduction-related), and the Vemork Fm has a significantly different signature (asthenospheric mantle input). Subduction zone model modified from Shuto et al. (2006); FeO_t/FeO_t+MgO versus SiO₂ after Frost et al. (2001); Th/Yb versus Ta/Yb after Pearce (1982); Nb/Y versus Zr/Y after Fitton et al. (1997).

fluids/volatiles. A possible explanation is that at certain points in time during the evolution of the Suldal Arc, basaltic parent magmas forming in a hot deep crustal zone were dehydrated; this

occurred through a decrease in subduction-zone fluid flux, and to successive melt production and heating from magmatic underplating; this would have left the magma dehydrated but not refractory (Landenberger & Collins 1996), and would also have a higher solidus than normal hydrous arc magma. The extra heat required for melting of dehydrated mafic crust was likely provided by asthenospheric mantle upwelling; also, an extensional setting meant that melts could intrude along weaknesses into the upper crust, and thus avoid assimilation of surrounding wet and oxidizing crust.

4.5 Discussion

4.5.1 Origin of A-type granites.

If the tholeiitic (ferroan) amphibolites differentiated into granitic compositions, then based on their geochemistry these would fall into the category of A-type granites (low CaO, high Fe/Mg and Ga/Al, and enriched incompatible elements); they would thus provide a genetic link between tholeiitic mafic magmas and A-type felsic magmas. The amphibolite suite has differentiated into granodioritic compositions that are coarse-grained porphyritic amphibolites bodies. At high silica contents calc-alkaline (magnesian) trends converge with ferroan trends, hindering the distinction between different granite suites (Frost et al. 2001). On the Fe* versus SiO₂ plot (Figure 4.2) a couple of the granitoids fall on the ferroan trend; these coarse-grained porphyritic granitoids are similar to other granites in the region, including those that are Sveconorwegian in age. Thus, it cannot be determined without further dating, whether the amphibolite suite has fully differentiated into A-type granites, or whether such lithologies in the region are only related to Sveconorwegian magmatism.

The connection between tholeiitic (i.e. ferroan and anhydrous source) magmas, and A-type granites, is known as the tholeiite connection (Frost & Frost 1997). This model is postulated for the petrogenesis of Proterozoic Rapakivi-type granites (e.g. Sherman Batholith, US), and involves the intrusion of tholeiitic basalts into the lower crust, remelting of these basalts, and the intrusion of subsequent melts into the middle crust to form A-type plutons. This is a similar mechanism to that proposed for the amphibolite suite, except that in the Frost & Frost (1997) model, an asthenospheric source is required for the initial intrusion of tholeiitic basic magmas into the base of the crust. In the model proposed here an asthenospheric mantle is required for heating but not for the source; the tholeiitic source is derived from dehydrating of normal depleted mantle arc magmas.

A-type granites are commonly associated with extensional and 'anorogenic' settings (Windley 1993; Bonin 2007). This study has indicated the formation of A-type magmas in an arc setting; this has previously been recorded in Proterozoic arc settings (e.g. Slagstad et al. 2004; Zhao et al. 2008). In the Mesoproterozoic Muskoka domain in the Grenville province, Slagstad et al. (2004) suggest intra-arc extension has allowed the sourcing of asthenospheric mantle for formation of tholeiitic

parent magmas. In a Neoproterozoic arc on the edge of the Yangtze block, Zhao et al. (2008) suggest A-type plutons have formed by remelting of TTG-type crust that has been dried out (i.e. charnockitisation), by sustained heating from a magmatic underplate. The model proposed here includes elements of both of these examples, i.e. intra-arc extension, dehydration of mafic crust induced by magmatic underplating, and asthenospheric mantle upwelling to provide further heat for melting of the dehydrated crust.

4.6 Conclusions

The major, trace and REE trends within the Sauda Grey Gneiss suite suggest that it formed by multiple stages of fractionation at different levels in the crust, in a deep hot crustal zone setting (Annen et al. 2006). The fact that both ferroan (amphibolites) and magnesian (Grey Gneiss) trends are recorded in upper crustal intrusive rocks, suggests that melts were able to fractionate in relatively closed-systems. However, in this hot crustal environment, it is likely that some magma batches underwent mixing; the magma mingling seen in the field is evidence of mafic magmas intruding more felsic magma bodies. Partial melting of crystallised magma bodies by the heat of later intrusions may occur in this environment. The production of evolved rocks via fractional crystallisation requires large volumes of residual cumulate rocks to be produced. These may be present in the lower crust, but also may have been returned to the mantle (Kay & Kay 1985; Arndt & Goldstein 1989).

The geochemistry of the magma suites suggests formation in a volcanic arc setting. The degree of LREE enrichment is significantly greater than that observed in oceanic island arcs (e.g. Talkeetna, Clift et al. 2005; Greene et al. 2006), and complete differentiation from mafic to felsic compositions requires a greater differentiation column than typical oceanic island arcs. Thus, the Suldal arc probably developed on thickened crust, such as in a mature island arc or continental arc. However, the geochemistry of the arc rocks is compatible with fractional crystallisation of mantle-derived basalt in relatively closed-systems, without obvious assimilation of previously formed crust. Although the data cannot exclude the existence of pre-existing crust, they do not require it. Bimodal continental rift magmatism in the adjacent Telemark Sector, occurring contemporaneously with arc magmatism in the Suldal Sector, suggests that the crust was undergoing extension during the ~1.5 Ga period. Thus, a thin ensilic crust is interpreted to be the most likely candidate for the substrate of the Suldal Arc. Arcs developed on ensilic crust can occur outboard of continental shields as continental ribbons, or on attenuated parts of continental crust; both of these features are typical of retreating accretionary orogens (Cawood et al. 2009).

Highly iron-enriched tholeiitic magma series were able to differentiate during the evolution of the Suldal arc. Such compositions are rare in the rock record, and in continental settings are typically

related to anorogenic plume-related magmatism. The formation of such compositions is postulated to be a function of very dry and reducing conditions existing during magma differentiation; the cause of such conditions in a supra-subduction setting is anomalous, but linked to dehydration and subsequent melting, both possibly as a consequence of asthenospheric mantle upwelling that produced coeval continental rift magmatism in the adjacent Telemark Sector.

Table 4.1. Results of Rayleigh fractional crystallisation modelling of REE contents in the Sauda Grey Gneiss. Each successive melt is modelled at 20% fractional crystallisation. Partition coefficients from Arth (1976), Fujimaki et al. (1984), Dostal et al. (1983), Shock (1979), Gill (1981) and Philpotts & Schnetzler (1970).

		La	Ce	Nd	Sm	Eu	Gd	Dy	Er	Yb	Lu
Averages	Basalt	60.32	57.30	44.31	31.12	23.20	18.71	15.25	13.97	12.82	13.44
	Andesite	98.21	80.38	53.21	35.42	24.23	21.73	18.25	16.51	15.40	15.98
	Dacite	127.46	102.46	65.42	41.14	21.71	24.86	20.09	18.78	17.13	17.22
Kd Stage 1	Plagioclase	0.148	0.111	0.090	0.039	1.126	0.031	0.023	0.020	0.023	0.019
	Olivine	0.007	0.006	0.006	0.007	0.007	0.010	0.013	0.026	0.049	0.045
	Clinopyroxene	0.056	0.150	0.310	0.500	0.510	0.610	0.680	0.650	0.620	0.560
	Hornblende	0.250	0.843	1.340	1.804	1.200	2.017	2.024	1.740	1.642	1.563
	Magnetite	1.500	1.500	3.000	3.000	2.000	1.000	1.000	1.000	1.000	1.000
Kd Stage 2	Plagioclase	0.302	0.221	0.149	0.102	1.214	0.067	0.050	0.045	0.041	0.046
	Olivine	0.007	0.006	0.006	0.007	0.007	0.010	0.013	0.026	0.049	0.045
	Clinopyroxene	0.056	0.508	0.645	0.954	0.681	1.350	1.460	1.330	1.300	1.200
	Hornblende	0.544	0.843	1.340	1.804	1.557	2.017	2.024	1.740	1.642	1.563
	Magnetite	0.200	0.200	0.300	0.300	0.250	0.250	0.250	0.250	0.250	0.250
	Apatite	20.00	34.70	57.10	62.80	30.40	56.30	50.70	37.20	23.90	20.00
Modelled melts Stage 1		72.60	67.05	49.99	34.18	23.27	20.41	16.58	15.41	14.23	15.03
		87.38	78.45	56.39	37.53	23.35	22.27	18.02	17.00	15.79	16.81
		105.17	91.80	63.62	41.21	23.42	24.29	19.58	18.75	17.52	18.80
Modelled melts Stage 2		114.30	91.13	59.40	38.13	23.01	22.87	19.18	17.74	16.70	17.47
		133.01	103.33	66.31	41.03	21.84	24.07	20.15	19.06	18.10	19.09
		154.79	117.15	74.03	44.16	20.74	25.34	21.17	20.47	19.62	20.87

Continental recycling in arc magmas: Hf-O isotope constraints on Telemarkian (1.52-1.48 Ga) magmatism

Aim - In this chapter, zircon Hf and O isotope data from various arc-type lithologies from the Suldal Sector are presented. The data are used to constrain the possible crustal and mantle components that have contributed to ~1.5 Ga arc magmatism in Telemarkia, and deduce the amount of continental growth that has occurred during this magmatic episode.

5.1 Introduction

Recent advances in the in-situ measurement of isotopes in the accessory mineral zircon have led to its common use as a tool for refining the petrogenesis of igneous rocks (e.g. Hawkesworth & Kemp 2006). The ability to measure both hafnium and oxygen isotopes on zircon grains that have also been dated by U-Pb, allows for the discrimination of multiple magmatic sources that typically cannot be constrained using whole-rock methods. For example, U-Pb zircon ages can point to older crustal contaminants that have added inherited zircons to a magma, Hf isotopes can be used to determine the crustal residence age of the magma that a zircon crystallised in, and oxygen isotopes can be used to constrain where older components were recycled into the magma (in the mantle or in the crust).

The recycling of pre-existing continental crust, including sedimentary material, to arc magmas has long been recognized (e.g. Armstrong 1971; Hildreth & Moorbath 1988; Plank & Langmuir 1993). Numerous studies have sought to constrain whether continental crust has been recycled into the arc magmas in the mantle, via subduction of sediments, or in the crust, via contamination and assimilation (e.g. Hawkesworth et al. 1979; Thirlwall & Graham 1984; Gasparon et al. 1994). Both of these processes likely occur together in the same subduction zone; however it is useful to discriminate between them to determine the volume and rate that previously formed continental crust is being recycled. The end-member processes are termed mantle recycling and intracrustal recycling; the latter can be broken down into infracrustal recycling, whereby previously formed igneous crust (such as ancient underplated material) is recycled into the magma, and supracrustal recycling, whereby sedimentary material is recycled into the magma. Studies aiming at differentiating these processes have commonly combined radiogenic isotopes (e.g. Sr, Nd, Hf) with a stable isotope (O) (e.g. James 1981; Davidson 1985).

Determining the mantle versus crustal input to different granitoid types in different geodynamic settings has long been a focus of petrogenetic studies. The geochemical classification of granitoid suites is commonly used to infer tectonic settings and/or mantle versus crustal sources. For example, with the alphabet classification scheme (Chappell & White 1974), I-type granites typically

have an inferred igneous and/or mantle source and occur in arc settings, S-type granites have inferred sedimentary sources and occur in collisional settings, and A-types have inferred mantle or mixed sources and occur in anorogenic sources (see reviews by Barbarin 1999; Frost et al. 2001). However, recent studies combining zircon U-Pb, Hf and O, have demonstrated that both sedimentary and mantle material have been involved in the petrogenesis of all of these granite types in a variety of settings (e.g. I-type, Kemp et al. 2007; S-type, Appleby et al. 2009; A-type granites, Be'eri-Shlevin et al. 2009). Thus, granitoids with a variety of geochemical signatures and in a variety of tectonic settings may involve both recycling of previously formed continental crust and formation of new crust by juvenile mantle input.

The crystalline basement in SW Fennoscandia comprises various Palaeo- to Mesoproterozoic terranes that comprise deformed plutonic and volcanic arc-like lithologies, and have been reworked during the Sveconorwegian (Grenvillian) and Caledonian orogenies (e.g. Gaál & Gorbatshev, 1987; Bingen et al. 2008a). The evolution of the ~1.7 to 1.5 Ga crust can be described by two end-member models: 1) where Palaeoproterozoic crust underlies the entire region and has been recycled during younger magmatic episodes (Andersen et al. 2002b, 2004a, 2009b), or 2) where the various terranes represent accreted juvenile arcs with limited contribution from older material (Brewer et al. 1998; Åhäll & Connelly 2008). Various isotope data point to a contribution from Palaeoproterozoic crust to Gothian (~1.7-1.55 Ga) and younger magmatism (1.2-0.93 Ga; Andersen 1997, 2001, 2002b, 2004a, 2007b, 2009b; Andersen & Griffin 2004), but the lack of isotope data from ~1.5 Ga Telemarkian crust hinders the testing of the above models; to resolve this, this study presents U-Pb, Hf and O data from Telemarkian (~1.5 Ga) magmatic rocks in the Suldal Sector, which are used to constrain if and what older crust has been recycled during their petrogenesis.

5.2 Geological Setting

The Fennoscandian Shield comprises an Archaean core in the northwest; surrounding this are younger arcs and microcontinents that amalgamated during the Svecofennian orogeny at ~ 2.1-1.9 Ga (Korja et al. 2006; Lahtinen et al. 2009). At ~1.85 Ga a subduction zone initiated on the southwest margin (present-day position) of the continent, producing the Transcandinavian Igneous Belt (TIB; see Högdahl et al. 2004). The terranes to the southwest of the TIB that comprise the Southwest Scandinavian Domain (SSD), can be interpreted as forming in continental and island arcs along a long-lived subduction margin that progressively moved away from the Fennoscandian continent (Åhäll & Connelly 2008), in a retreating accretionary orogen (Cawood et al. 2009).

The SSD comprises terranes (*senso lato*) aged ~1.69 to 1.48 Ga that progressively young to the west. The youngest of these, Telemarkia, makes up the crust west of the Oslo Rift (Bingen et al. 2005b). The oldest identified igneous unit within Telemarkia is the 1.55 Ga Åsen metatonalite

(Pedersen et al. 2009); this is the only unit older than 1.52 Ga, and its origin remains uncertain. The main continental growth episode of the Telemarkia terrane is defined as 1.52-1.48 Ga (Bingen et al. 2005b; 2008a), and is known from dating plutonic and volcanic orthogneisses from across the region. Other major tectonostratigraphic units within Telemarkia include the ~1.5 Ga Vestfjorddalen supergroup which has been related to continental extension behind a subduction margin (Slagstad et al. 2009), supracrustal sequences dated at 1260-1220 and 1170–1140 Ma that are also related to extensional settings behind a subduction margin (Bingen et al. 2002; Brewer et al. 2004), and early- to late-Sveconorwegian intrusions dated between 1.05 and 0.93 Ga (Andersen et al. 2002a, 2007a; Bingen & van Breemen 1998; Schärer et al. 1996). Various sedimentary units within Telemarkia that were deposited between ~1.6 and 1.1 Ga, comprise Palaeoproterozoic and late Archaean detrital zircons (Åhäll et al. 1998; de Haas et al. 1999; Bingen et al. 2001b, 2003); this suggests that during the Mesoproterozoic the terrane was located near to an older continent.

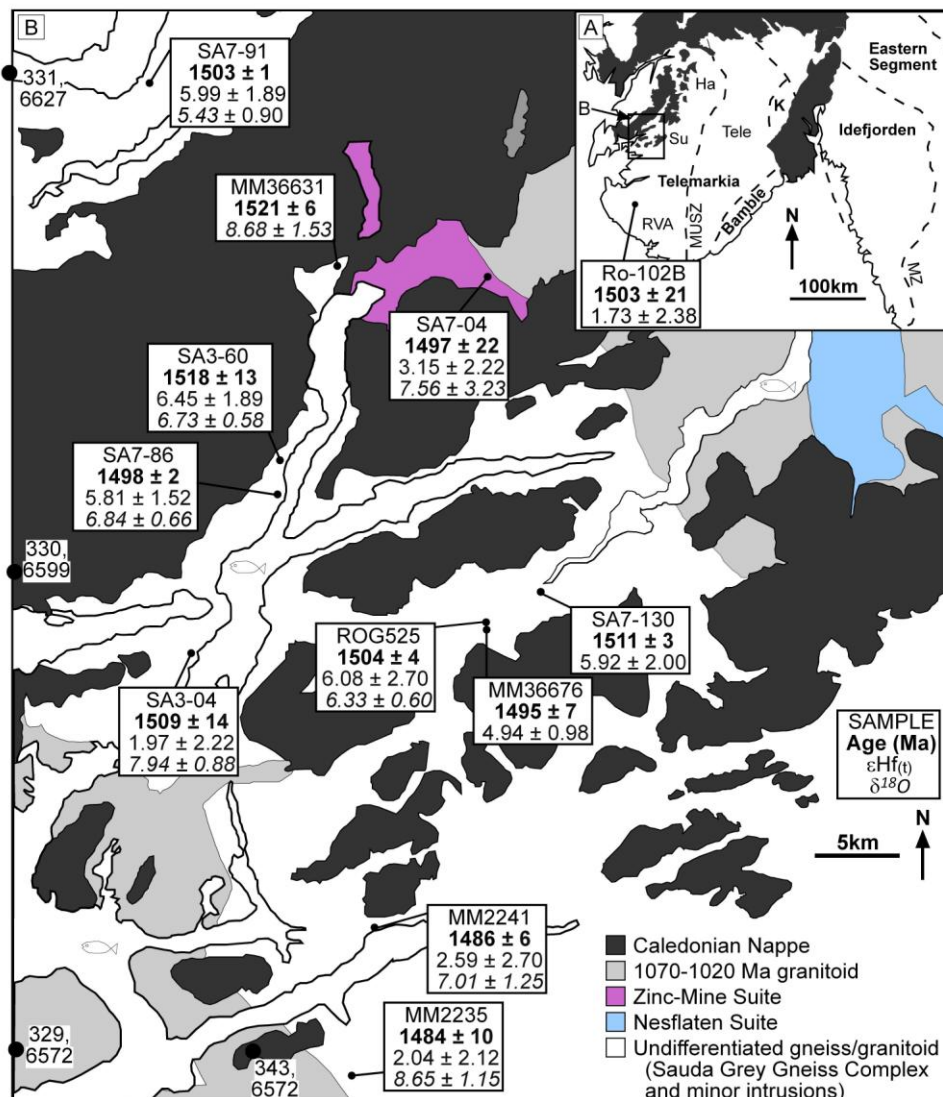


Figure 5.1. A) Lithotectonic domains of SW Fennoscandia. Ha = Hardangervidda Sector, Su = Suldal Sector, RVA = Rogaland Vest-Agder Sector, Tele = Telemark Sector, K = Kongsberg terrane, MZ = Mylonite Zone, MUSZ = Mandal-Ustaoset Shear Zone. B) Geological sketchmap showing the sample localities from the Suldal Sector along with U-Pb ages and average Hf and O isotope values. (Modified from Bingen et al. 2005b).

The samples in this study are taken from the Suldal Sector in and around the Sauda and Suldal communes (Figure 5.1), except for one sample from further south in the Rogaland Vest-Agder Sector. The basement in these areas comprises variably fine to coarse-grained lithologies metamorphosed in amphibolite-facies, and that are interpreted to represent different exposures through an arc complex (Chapter 2). The geochemistry of these lithologies is compatible with formation in an arc setting via fractional crystallisation of mantle-derived mafic melts (Chapter 4). Brief sample descriptions are given in Table 5.1; further details of samples collected within this study (SAX-XX sample number), are provided in Chapter 3. Separated zircons have a range of morphologies, but are generally prismatic, oscillatory-zone and elongate, as is typical of igneous zircons (Figure 5.2). The more mafic lithologies (SA7-86 and ROG525) exhibit larger zircons which were fragmented during separation, and feature less distinct oscillatory-zoning or are sector zoned. Distinctive core and rim/overgrowth relationships are lacking in all samples; discontinuities in zoning do exist in some grains, but the style of zoning across these is similar, suggesting an origin related to replenishment of magma during crystallisation, as opposed to overgrowth on inherited zircons. U-Pb ages were obtained from multiple growth zones are similar in age also (see Chapter 3; Slagstad & Marker 2009, unpublished data).

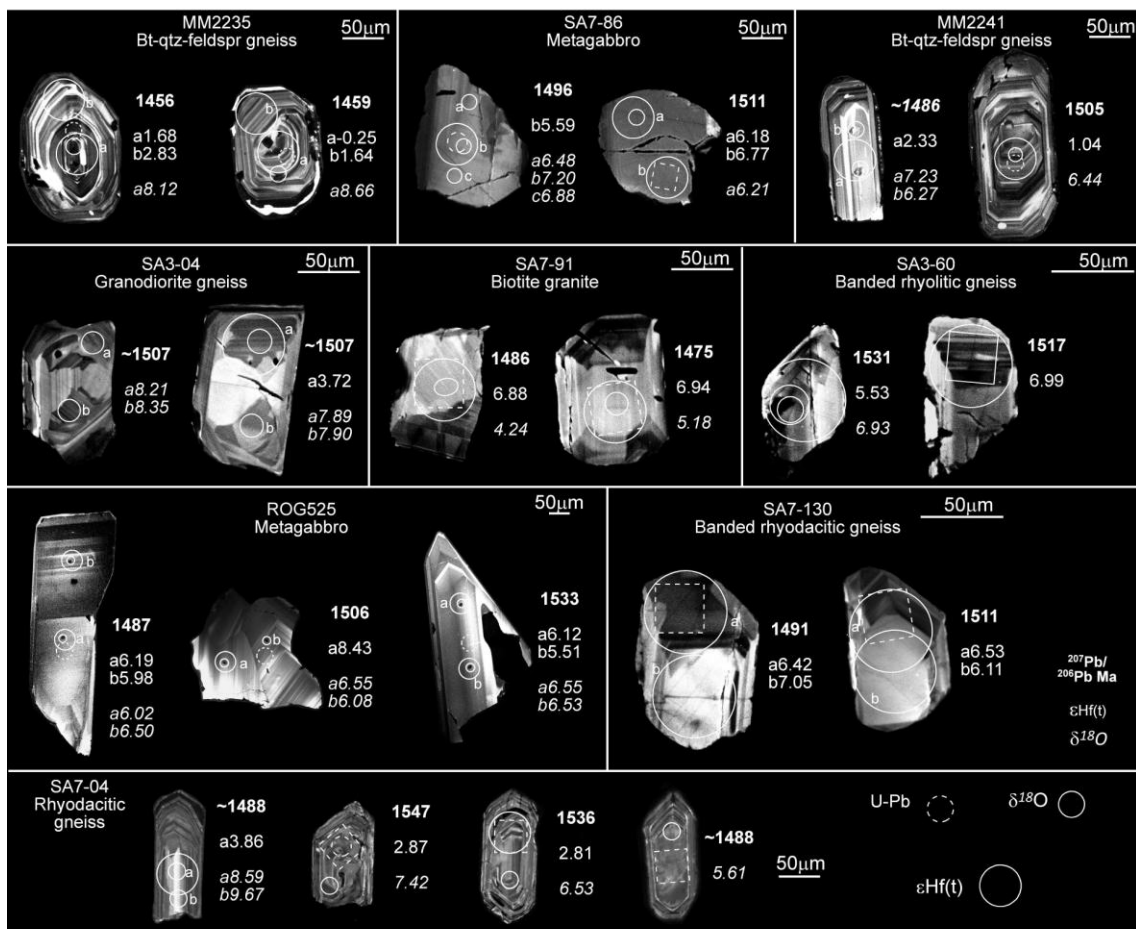


Figure 5.2. CL images of selected zircons showing position of individual U-Pb, Hf and O analyses.

Table 5.1. Sample descriptions. ^aU-Pb dating by LA-ICP-MS/TIMS at NIGL, Nottingham (Chapter 3); ^b U-Pb dating by Ion-microprobe at NORDSIM, Stockholm (Slagstad & Marker, unpublished data); ^c U-Pb dating by LA-ICP-MS at Norwegian Geological Survey, Trondheim (Slagstad & Marker, unpublished data). T_{Zr-C} = zircon saturation temperature (Watson & Harrison 1983), calculated from whole-rock geochemical data in table 10.x.

Sample	Unit	Lithology	Deformation	Field relations	T _{Zr} °C
SA3-04 ^a 1509 ± 6	Sauda Grey Gneiss Complex	Coarse-grained porphyritic felsic gneiss	Strongly deformed	Wide (>100m) unit within a region on strongly sheared porphyritic gneisses	781
SA3-60 ^a 1518 ± 6	Sauda Grey Gneiss Complex	Light grey fine- grained felsic gneiss	Strongly deformed	Narrow (<20m) unit within a heterogeneous body of mafic to felsic gneisses	859
SA7-04 ^a 1497 ± 22	Zinc Mine Banded Gneiss	Light grey fine- grained felsic gneiss	Strongly deformed	Narrow (<20m) unit within heterogeneous banded gneiss sequence	727
SA7-130 ^a 1511 ± 3	Sauda Grey Gneiss Complex	Grey fine-grained banded gneiss	Strongly deformed	Felsic unit from a bimodal gneiss sequence that is disrupted by Sveconorwegian granitoids	850
SA7-86 ^a 1498 ± 2	Amphibolites	Pegmatitic zone of hornblende gabbro	Weakly deformed	Coarse-grained part of a heterogeneous mafic body (~1km wide)	812
SA7-91 ^a 1503 ± 1	Sauda Grey Gneiss Complex	Medium-grained biotite granite	Undeformed	Massive granite body that intrudes more deformed and heterogeneous gneisses	854
MM2235 ^b 1484 ± 10	Sauda Grey Gneiss Complex	Grey fine-grained biotite gneiss	Strongly deformed	Narrow (<10m) unit within heterogeneous banded gneiss sequence	771
MM2241 ^b 1486 ± 6	Sauda Grey Gneiss Complex	Grey fine-grained biotite gneiss	Strongly deformed	Narrow (<10m) unit within heterogeneous banded gneiss sequence	807
ROG525 ^b 1504 ± 4	Amphibolites	Medium-grained hornblende gabbro	Undeformed	Mafic body, contacts not observed	n/a
MM36676 ^b 1495 ± 7	Amphibolites	Coarse-grained hornblende granite	Weakly deformed	Intrusive sheets in gabbro (ROG525)	712
MM36631 ^b 1521 ± 6	Sauda Grey Gneiss Complex	Light grey fine- grained felsic gneiss	Strongly deformed	Narrow (<20m) unit within heterogeneous banded gneiss sequence	n/a
Ro-102B ^c 1503 ± 21	Undefined (gneiss complex)	Grey migmatitic felsic gneiss	Strongly deformed	Narrow (<10m) unit within heterogeneous banded gneiss sequence	n/a

5.3 Analytical Methods

5.3.1 Zircon U-Pb isotopes

Zircons were analysed either by LA-ICP-MS at the NERC Isotope Geosciences Laboratory, UK, (data presented in chapter 3), or by ion microprobe at the NORDSIM facility, Sweden (unpublished data; Slagstad & Marker 2009). $^{207}\text{Pb}/^{206}\text{Pb}$ ages are given in Table 10.18.

5.3.2 Zircon Hf isotopes

Lu-Hf isotope analyses were determined at the NERC Isotope Geosciences Laboratory, UK, using a Nu-Plasma HR MC-ICP-MS coupled to a 193 nm solid state (UP193SS, New Wave Research) laser ablation system. Helium gas was added to the laser ablation cell, and argon gas was added after ablation via a NU-Plasma DSN-100 desolvating nebuliser, whilst aspirating a 2% HNO_3 +0.1 molar Hf acid solution to help maintain constant plasma conditions.

The analyses were performed on zircons mounted in epoxy blocks; all mounts were cleaned with weak acid before Hf analysis, and mounts that had been used for SIMS analyses had their gold coating removed prior to cleaning. Analyses were carried out on top of the ion-microprobe or laser-ablation pit when possible, so that Hf analysis could be paired with the dated portion of the zircon.

The isotopes ^{173}Yb , $^{174}(\text{Yb, Hf})$, ^{175}Lu , $^{176}(\text{Yb, Lu, Hf})$, ^{177}Hf , ^{178}Hf , and ^{179}Hf were measured on Faraday cups in a static sequence. The isobaric interference of ^{176}Yb was corrected using the method of Nowell & Parrish (2001); JMC475 Hf standard solutions were measured prior to each analytical session which were variably doped with Yb (0 to 40ppb), the true value of $^{176}\text{Yb}/^{173}\text{Yb}$ is then calculated using a regression. This true $^{176}\text{Yb}/^{173}\text{Yb}$ value is used to subtract ^{176}Yb from the 176 peak. The interference of ^{176}Lu on ^{176}Hf was corrected by measuring the interference-free ^{175}Lu isotope and using a value of 0.02653. Corrections were applied during each analysis after an inverse mass bias correction using the measured $^{179}\text{Hf}/^{177}\text{Hf}$ ratio, this allows for absolute differences between the Hf and Yb mass bias. The $^{178}\text{Hf}/^{177}\text{Hf}$ stable isotope ratio is used to monitor data quality.

A spot diameter of 50 μm , 10 Hz repetition rate and ablation time of 60 seconds were used, resulting in total Hf signals of 5 to 9V. All data were normalised to the $^{176}\text{Hf}/^{177}\text{Hf}$ of the JMC475 reference solution assuming a value of 0.282160. The $^{176}\text{Lu}/^{177}\text{Hf}$ ratio was normalised to the reference material using values of 0.000311 for 91500 and 0.000042 for Mud Tank (Woodhead & Hergt 2005). Data were reduced off-line using time-resolved analyses; this allows for the selection of stable portions of analyses and the identification of ablation through different growth zones or into the epoxy mount. All uncertainty components, including those for age and normalisation, were factored into the final uncertainty quoted. Analytical uncertainties for unknowns were propagated by quadratic addition to include the standard error of the mean of the analysis and the

reproducibility of the primary ablation reference material. The reproducibility of the standards was better than 1 epsilon unit; the final analytical uncertainty of the unknowns is typically between 1 and 2 epsilon units.

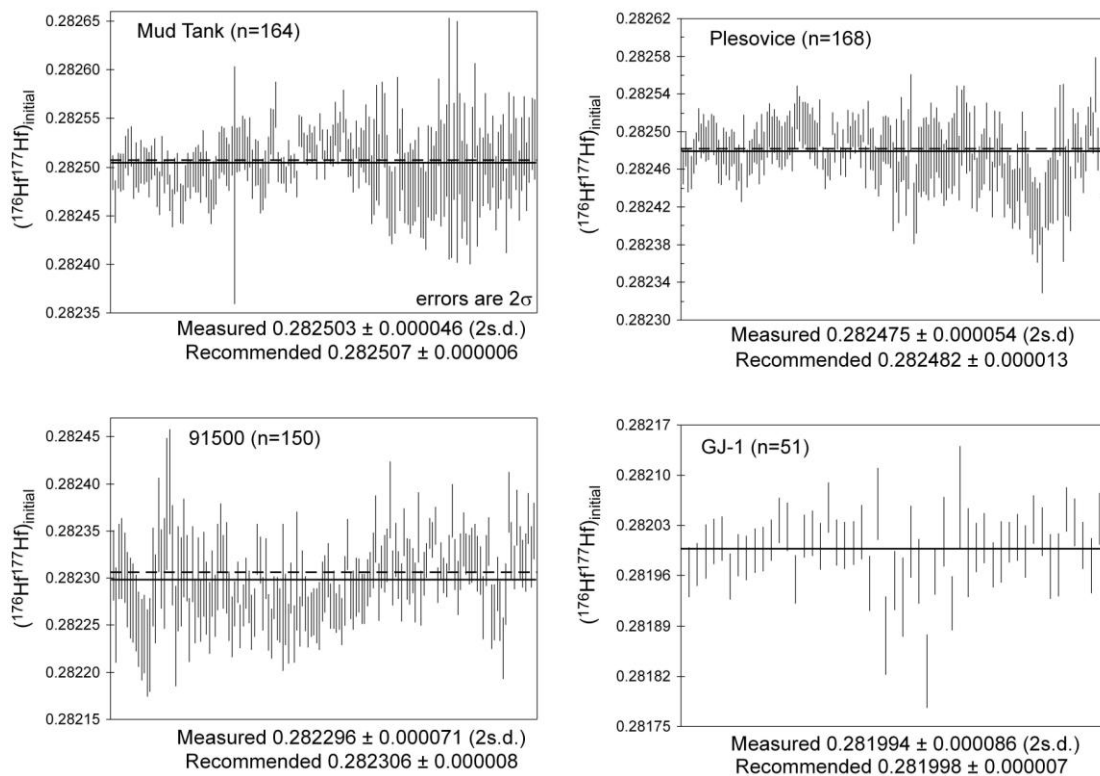


Figure 5.3. Reproducibility of the $^{176}\text{Hf}/^{177}\text{Hf}$ ratio in secondary standards across all of the analytical sessions. Recommended values from Jackson et al. (2004), Woodhead & Hergt (2005) and Sláma et al. (2008).

Hf analyses were conducted on concordant (>95 % concordance) grains where possible; less than 10% of the data are obtained on discordant grains. The $^{176}\text{Hf}/^{177}\text{Hf}_{\text{initial}}$ value measured on discordant grains is within error of the average $^{176}\text{Hf}/^{177}\text{Hf}_{\text{initial}}$ of the sample, indicating that any disturbance of the Lu-Hf system during events that have caused lead-loss is negligible, and thus that the spread in $^{176}\text{Hf}/^{177}\text{Hf}_{\text{initial}}$ within each sample does not represent metamorphic disturbance.

During analytical sessions in 2009, the measured $^{178}\text{Hf}/^{177}\text{Hf}$ ratio was sometimes below the recommended value (1.4723; Patchett & Tatsumoto 1981). In some samples $^{176}\text{Hf}/^{177}\text{Hf}_{\text{initial}}$ correlates with $^{178}\text{Hf}/^{177}\text{Hf}$, whereas in other samples $^{176}\text{Hf}/^{177}\text{Hf}_{\text{initial}}$ seems unaffected (Table 10.18). The analyses where the $^{178}\text{Hf}/^{177}\text{Hf}$ ratio is significantly low have $^{176}\text{Hf}/^{177}\text{Hf}_{\text{initial}}$ values that are within analytical uncertainty (2σ) of the sample mean; thus these data have not been rejected, but it is worth noting that the total range in ϵHf for some samples maybe over estimated due to this analytical error.

Epsilon Hf values were calculated using the decay constant $\lambda(^{176}\text{Lu})=1.867 \cdot 10^{-11}$ (Söderlund et al. 2004), CHUR parameters of Bouvier et al. (2008), and the depleted mantle model (DM) of Griffin

et al. (2000); the depleted mantle model of Pietranik et al. (2009) is also shown in figure 5.7 for comparison. Model ages are calculated using $^{207}\text{Pb}/^{206}\text{Pb}$ ages with $^{176}\text{Hf}/^{177}\text{Hf}_{\text{initial}}$ and $^{176}\text{Lu}/^{177}\text{Hf}$ ratios. The Lu/Hf ratio in a zircon is typically much lower than that of the magma that the zircon crystallised in, therefore, single-stage model ages calculated using the Lu/Hf of the zircon (T_{DMZ}) will be erroneously low. An alternative method is to calculate a two-stage model age using the Lu/Hf ratio of the whole-rock from which the zircon was extracted, as this provides a best estimate for the Lu/Hf of the magma. Whole-rock measurements were not made during this study, thus, known average Lu/Hf ratios of crustal reservoirs can be used instead. Commonly used ratios include 0.022 for mafic crust (Vervoort & Patchett 1996), 0.093 for felsic crust (Amelin et al. 1999), and 0.015 for average continental crust (Griffin et al. 2000). In this study, two-stage model ages are presented using a Lu/Hf of 0.015 (T_{DMC}).

5.3.3 Zircon oxygen isotopes

Oxygen isotope data were obtained at the University of Edinburgh, UK, using a Cameca ims-1270 ion microprobe following methods outlined in Appleby et al. (2009) and Kemp et al. (2007). Analysed zircons were mounted in epoxy blocks, cleaned in weak acid and gold-coated. The analyses were conducted after U-Pb and Hf analyses, so the mounts were lightly polished using diamond paste to remove any significant topography caused by previous ablation.

A 6nA primary $^{133}\text{Cs}^+$ ion beam with a diameter of $\sim 20\ \mu\text{m}$ was used, with the charge being neutralised using a normal-incidence electron flood gun. Secondary ions were extracted at 10kV. $^{18}\text{O}^-$ and $^{16}\text{O}^-$ ions were measured simultaneously on dual Faraday cups. Each analysis involved pre-sputtering for 50 seconds, followed by data collection in 10 cycles, with 4 seconds of acquisition per cycle. The secondary yield of ^{18}O was typically between 5×10^6 and 8×10^6 counts per second.

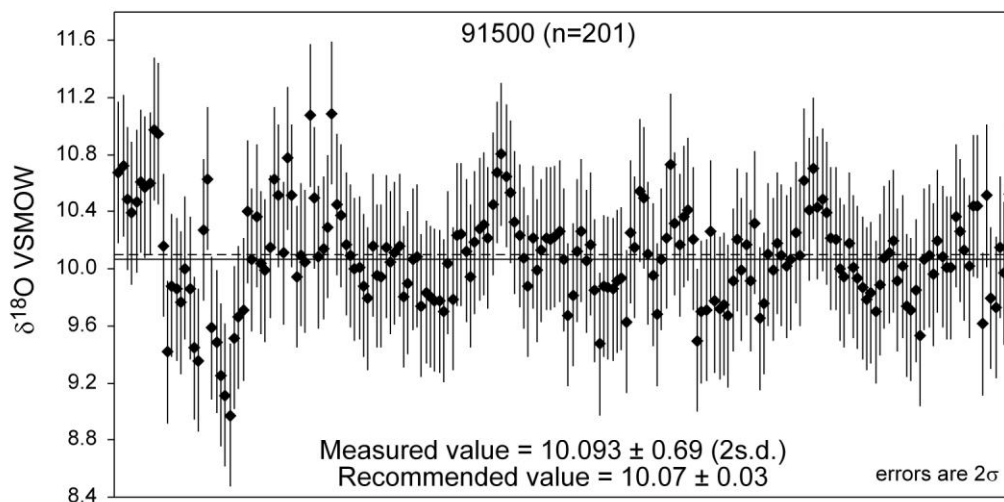


Figure 5.4. Reproducibility of $\delta^{18}\text{O}$ in the 91500 primary standard across the analytical session. Recommended value from Valley (2003).

To correct for instrumental mass bias and instrumental drift all data were normalised to 91500 ($\delta^{18}\text{O} = 10.07 \pm 0.03\text{‰}$; Valley 2003). This standard zircon was analysed in blocks of 5 to 10 after every 10 to 20 analyses of unknowns. The beginning of each analytical session involved measurement of 40-60 analyses of a combination of 91500 and in-house standards (KIM/Temora). The unknown analyses were normalised to the daily average $^{18}\text{O}/^{16}\text{O}$ value obtained for 91500, or if instrumental drift was recognised, the data were normalised to the linearly interpolated $^{18}\text{O}/^{16}\text{O}$ value derived from analyses of the bracketing 91500 standard. The external precision based on analysis of the standard was 0.69‰ (2σ) across the whole analytical session (Figure 5.4). This value is used as the final uncertainty on the unknowns as it gives the most conservative estimate of the uncertainty.

5.4 Results

5.4.1 Zircon Hf isotopes

The results of the Hf analyses are plotted in Figure 5.5. Each sample has a mean value falling between CHUR and depleted mantle (DM); the total ϵHf range across the samples is from ~ -1 to $+10$. The range in ϵHf for each sample varies from ~ 1.5 to 6 epsilon units (MSWD 0.4 to 5); for some of the samples this range is within analytical uncertainty (MM36631, MM36676, SA3-60, SA7-91; MSWD 0.4 to 1.4). None of the samples have outliers which are not within error (2σ) of other analyses within the sample population. 20 of the analyses lack U-Pb data from the analysed zircon; however, the U-Pb data from these samples suggests the zircons represent single igneous populations (Chapter 3), and therefore the intrusion age provides a robust estimate for the age of crystallisation of the zircons. The lack of anomalously low $^{176}\text{Hf}/^{177}\text{Hf}_{\text{initial}}$ values in any of the samples, suggests that none of the analysis were conducted on grains inherited from much older crust (>300 Myrs).

Multiple Hf analyses from the same zircon grain are within analytical uncertainty of each other (see Figure 5.2 & Table 10.18); the maximum variation between multiple analyses that are aimed at the same portion of zircon is 2.03 epsilon units with an average variation of only 0.76 epsilon units ($n=11$), the maximum variation between analyses on different parts of the same zircon grain is 1.89 epsilon units with a average of 0.96 epsilon units ($n=8$). Thus, in this dataset there is no evidence for variation between outer and inner zircon zones, suggesting little evolving heterogeneity in the magmas, in contrast to selected previous studies (Kemp et al. 2007; Appleby et al. 2008; Be'eri Shlevin et al. 2009).

The data exhibit a subtle temporal correlation, with ϵHf decreasing with decreasing intrusion age (Figure 5.5). The data do not exhibit a clear correlation between ϵHf and SiO_2 , the latter being used to represent the degree of magma differentiation. The two most mafic samples (ROG525 and SA7-86) have mean ϵHf values of $\sim +6$ and $\sim +5.5$ respectively, which are similar to the mean values of the most differentiated samples (SA7-91, SA3-60). The most enriched (lowest ϵHf) samples are Ro-

102B (migmatitic grey gneiss), SA3-04 (porphyritic granodiorite), and MM2235 and MM2241 (dacitic quartz-feldspar gneisses).

Two-stage model ages using a Lu/Hf of 0.015 (T_{DMC}) for the samples range from 1530 to 2173 Ma, with the average of each sample ranging from 1611 to 2016 Ma. The model ages are ~100 to 500 million years older than the intrusion ages.

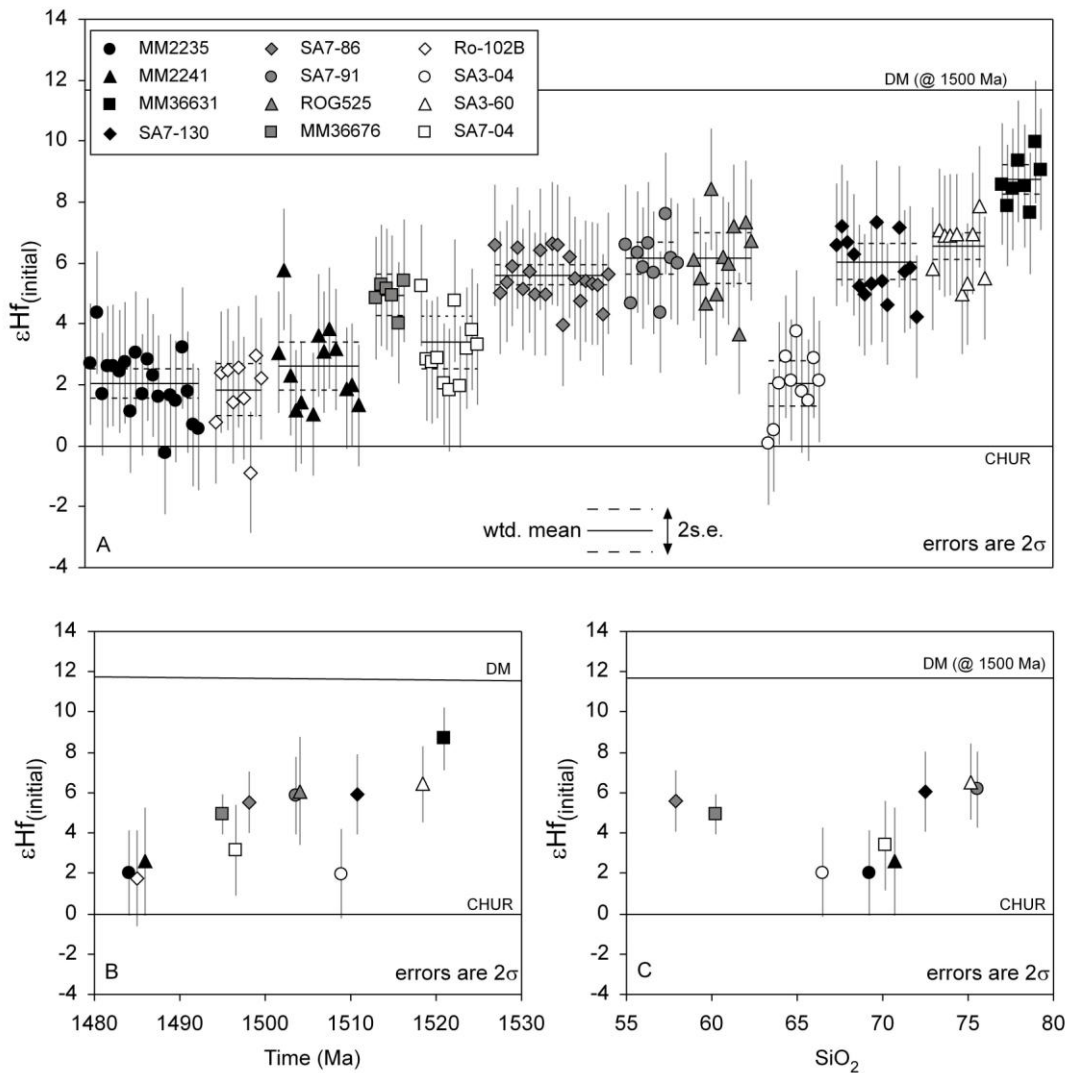


Figure 5.5. Results of in-situ Hf analyses. (A) $\epsilon Hf_{(initial)}$ plotted against arbitrary units, for each sample the weighted mean and 2s.e. are shown as a black solid line and block dotted lines respectively. (B) $\epsilon Hf_{(initial)}$ versus the intrusion age of the sample. Error bars are 2s.d. of the mean (C) $\epsilon Hf_{(initial)}$ versus whole-rock SiO_2 . Error bars are 2s.d. of the mean. DM is depleted mantle model of Griffin et al. (2000) and CHUR uses values according to Bouvier et al. (2008).

5.4.2 Zircon oxygen isotopes

A subset of 8 samples were analysed for $\delta^{18}O$ (Figure 5.6). The average $\delta^{18}O$ of each sample varies from $+5.43 \pm 0.9$ to $+8.65 \pm 1.15$ ‰. Five of the samples have variation which does not exceed analytical uncertainty (ROG525, SA3-04, SA3-60, SA7-86, SA7-91; MSWD = 0.7 to 1.7), and two of the samples have variation slightly outside of the analytical uncertainty suggesting real

geological heterogeneity (MM2235, MM2241; MSWD = 2.8 & 3.3). One sample (SA7-04) exhibits a significant range in $\delta^{18}\text{O}$ (MSWD = 22); this sample has been affected by lead-loss (see Chapter 3), has metamict and/or alteration textures visible in CL (Figure 5.2), and under normal light the zircons have an opaque milky colour. The sample was taken from near the contact with a Sveconorwegian granite which features hydrothermal mineralisation, thus, it is suggested that the variation in $\delta^{18}\text{O}$ within this sample may represent post-crystallisation alteration.

Multiple $\delta^{18}\text{O}$ ratios measured on the same zircon grain have variation of up to 1.01 ‰, which is slightly outside of analytical uncertainty (± 0.69 ‰), these multiple analyses were not conducted on distinguishable growth zones; such analysis of clearly different growth zones was hampered by the limited availability of material to analyse. As with the Hf analyses, the O isotopes do not exhibit a clear correlation with SiO_2 (Figure 5.6). The sample closest to the mantle value (5.3 ± 0.3 ‰) is a granite (SA7-91), samples with averages above the mantle value are dioritic (ROG525, SA7-86) to rhyolitic (SA3-60, MM2241), and the highest mean $\delta^{18}\text{O}$ belongs to a dacitic gneiss (MM2235).

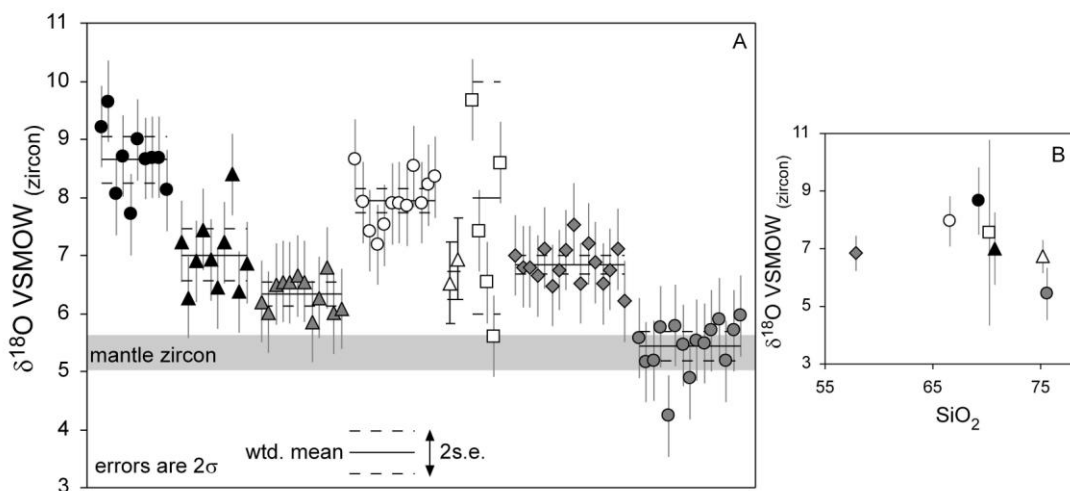


Figure 5.6. Results of in-situ oxygen analyses. (A) $\delta^{18}\text{O}$ VSMOW_(zircon) plotted against arbitrary units; for each sample the weighted mean and 2s.e. are shown as a black line and block dotted lines respectively. (B) $\delta^{18}\text{O}$ VSMOW_(zircon) versus whole-rock SiO_2 . Error bars are 2s.d. of the mean. DM is depleted mantle model of Griffin et al. (2000) and CHUR values are from Bouvier et al. (2008). Symbols as in figure 5.5.

5.5 Discussion

Before discussing the possible mantle and crustal contributions to Telemarkian magmatism, constraints from previous studies are evaluated.

5.5.1 Previous isotopic constraints

Whole-rock Sm-Nd data exist for a number of different magmatic suites within SW Fennoscandia. The Trossodal rhyolite formation in the Sæsvatn-Valldal supracrustal belt (Suldal Sector), is postulated to have formed by crustal anatexis in a back-arc setting by mafic underplating and

asthenospheric uprise (Brewer et al. 2004); whole-rock Sm-Nd analyses constrain ϵ_{Nd} at 1260 Ma to be 0.6 and -3.3, equivalent to model ages of 1730 and 2000 Ma (Brewer et al. 2004). The Tuddall rhyolite formation of the Vestfjorddalen supergroup (Telemark Sector), also formed by crustal anatexis as a consequence of mafic underplating and asthenospheric uprise (Menuge & Brewer 1996); whole-rock Sm-Nd analyses give a range of model ages from 1506 to 1779 Ma. Late Gothian granitoids in the Bamble-Kongsberg and Idefjorden terranes intruding at 1522 to 1615 Ma (Hisingen Suite and Göteborg-Åmål Belt; Figure 5.7), have Nd model ages of 1570 to 1760 Ma (Andersen et al. 2002b). Late-Sveconorwegian granitoids from across SW Fennoscandia have Nd model ages in the range of 1300-1600 Ma (Andersen et al. 2001). By combining Nd with Sr and Pb isotopes, Andersen et al. (1997, 2001), have constrained the composition of a crustal component that they suggest has been involved in the source of Sveconorwegian intrusions, as well as in earlier 1.5 to 1.2 Ga magmatic suites (Andersen et al. 2002b, 2007b, 2009b; Andersen & Griffin 2004). This crustal component, termed the ‘normal deep crust’ (see Andersen et al. 2001), is regarded to be moderately LILE-enriched (i.e. similar to upper crust composition) and at least 1.7 Ga age.

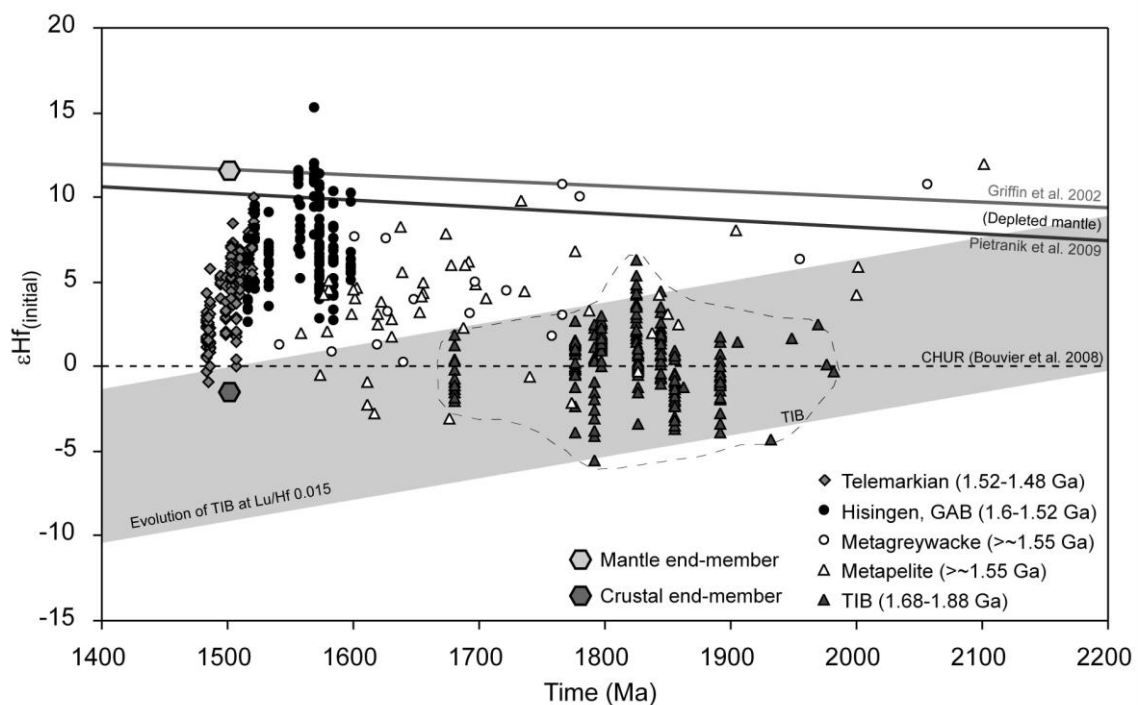


Figure 5.7. Time (Ma) versus $\epsilon_{\text{Hf}}(\text{initial})$ for zircons from SW Fennoscandia. Telemarkian data from this study; Hisingen and GAB are calc-alkaline granitoids from the Bamble, Kongsberg and Idefjorden terranes (Andersen et al. 2002b, 2004a); metagreywacke and metapelite zircons are from units deposited at ~1550 Ma in the Idefjorden terrane (Andersen et al. 2004a); TIB data are granitoids from the Transcandinavian Igneous Belt (Andersen et al. 2009a). Mantle and crustal end-members are those discussed in the text. The grey bar represent the evolution of TIB granitoids using $\text{Lu}/\text{Hf} = 0.015$.

In-situ Hf zircon analyses have been conducted on ~0.93-1.1 Ga Sveconorwegian intrusions from across Telemarkia, ~1.3-1.2 gneisses in the Telemark Sector, ~1.52-1.62 Ga calc-alkaline granites in the Bamble-Kongsberg and Idefjorden terranes, and ~1.85-1.66 Ga Transcandinavian Igneous Belt granitoids (Andersen et al. 2002b, 2004a, 2007b, 2009a, 2009b; Andersen & Griffin 2004;

Pedersen et al. 2009). The ϵ_{Hf} of the ~1.52-1.66 Ga granitoids is close to that of the depleted mantle, suggesting limited involvement of older crust (see Figure 5.7). The ϵ_{Hf} of <1.5 Ga magmatic rocks is compatible with mixing between depleted mantle and a source equivalent to the ~1.52-1.62 Ga granitoids. A few inherited zircons in Sveconorwegian granites, some of which are Palaeoproterozoic in age, have relatively low ϵ_{Hf} , and therefore cannot be produced by remelting of 1.52-1.62 Ga crust alone; these have been cited as evidence for the existence of Palaeoproterozoic crust at depth underlying southern Norway (Andersen et al. 2002b, 2009b; Andersen & Griffin 2004; Pedersen et al. 2009).

Scherstén (2002) provide the least equivocal evidence for older crust at depth, with a Re-Os age of 1887 Ma for an ultramafic lens within the Mylonite Zone that divides the Eastern Segment (comprising reworked 1.6-1.7 Ga TIB crust) from the Idefjorden terrane (1.66-1.55 Ga crust). However, this indicates that ~1.9 Ga crust may reside at depth below younger ~1.7 Ga TIB crust, but does provide evidence for older crust underlying the Telemarkia terrane.

5.5.2 Zircon inheritance

The issue of inherited zircons and their origin is important, since such evidence has been used in other accretionary orogens to infer older crust existing at depth; by doing this, the interpreted amount of continental growth versus the amount of continental recycling in these accretionary orogens is dramatically decreased. Examples include the 1.7-1.8 Ga Yavapai-Mazatzal province in Laurentia (Hill & Bickford 2001), the Central Asian Orogenic Belt (Kröner et al. 2007), and the Arabian-Nubian Shield (Hargrove et al. 2006; Ali et al. 2009b). However, whether such inherited zircons can be used to infer an older deep crust is a matter of contention, for example, older zircon ‘only indicates the presence of older zircons, not the presence of extensive tracts of older crust’ (from a discussion in Liégeois & Stern 2010 centred on the Arabian-Nubian Shield). Liégeois & Stern (2010) suggest that because zircons are stable in the mantle, they can be introduced into juvenile magmas through a number of ways, including delamination of older crust into the mantle, subduction of ocean crust and sediments, and zircon growth in the oceanic crust itself. Glacial deposits have also been cited as a method of introducing older zircons onto juvenile crust (e.g. Ali et al. 2009a).

As previously stated, Sveconorwegian granitoids within Telemarkia contain some Palaeoproterozoic inherited zircons. These Sveconorwegian granitoids intrude Telemarkian basement that lack inherited zircon (see Chapter 3). Although the existence of inherited zircons has commonly been used as evidence for assimilation of older crust, the lack of inherited zircons does not indicate the non-existence of older crust.

If a magma is hot enough (typically greater than 850°C; Watson 1996), then any zircon assimilated will dissolve unless suitably large in size (>120 µm radius); the temperature that zircon can crystallize at is dependent on the zirconium concentration of the melt (T_{Zr} ; Watson & Harrison 1983). A study by Miller et al. (2003) showed that inheritance-rich granitoids have a mean T_{Zr} of 766°C, whereas inheritance-poor granitoids have a mean of 837°C. The T_{Zr} of the samples in this study is variable, ranging from 712 to 859°C (Table 5.1), and spans the range of both inheritance-poor and inheritance-rich granitoids. However, Kemp et al. (2005) concluded that T_{Zr} was unreliable at estimating the initial temperature of magma bodies, and showed that low T_{Zr} in evolved compositions may be an underestimate, and reflect fractional crystallisation from zircon-undersaturated melts, such that the magma was initially capable of dissolving zircon, but after fractionation the residual liquids were capable of precipitating zircon.

The general lack of inheritance in the studied Telemarkian rocks can be explained by any crustal input being zircon-free (i.e. dominantly mafic), or that the melts were capable of dissolving any assimilated zircon; however, for the latter to happen in all lithologies with a range of geochemical compositions is considered unlikely. Younger Sveconorwegian intrusions feature Palaeoproterozoic inherited zircons, however, sedimentary rocks within the region have detrital zircon populations that include an abundance of Palaeoproterozoic and sometimes Archaean zircons (de Haas et al. 1999; Bingen et al. 2001b; Andersen et al. 2004b; Åhäll et al. 1998). Therefore, if Sveconorwegian granitoids assimilated such sediments prior to their crystallisation, then the need for Palaeoproterozoic igneous crust at depth is negated. In summary, the evidence from U-Pb zircon ages does not provide significant support for a Palaeoproterozoic deep crust underlying Telemarkia, unless such crust is dominantly mafic and zircon-free.

5.5.3 Geochemical indicator of sources

If significant assimilation of crustal material occurs during differentiation of a magma suite, then this may impart an imprint on the magma suite's geochemistry. Detecting the input of older crust formed in an arc setting to younger arc magmas may be difficult though, especially if metamorphic recrystallisation renders mineral chemistry ineffective. If a magma assimilated, or is a partial melt of a metasedimentary rock, then it will typically be peraluminous in nature; this feature led to the discrimination of S-type granites which are highly peraluminous and have inferred supracrustal sources (Chappell & White 1974). The metaluminous to weakly peraluminous nature of the Telemarkian rocks is more typical of I-type granites, i.e. those that have igneous precursors, and suggests limited involvement of supracrustal sources. However, recent zircon isotope studies in the Lachlan orogen, have shown that supracrustal input to I-type granites can go undetected in whole-rock geochemical/isotopic data (Kemp et al. 2007). The geochemistry of the studied Telemarkian rocks suggests formation by fractional crystallization of mafic parent magmas (see Chapter 4); the data do not exclude the assimilation of pre-existing crust, but do not require it.

5.5.4 Nature of crustal and mantle components

Zircon Hf isotopes

The Hf model ages are 100-500 million years older than the crystallisation ages of the samples, suggesting that they did not form purely by intrusion of depleted mantle, but involved contribution from older material, or alternatively mantle that was more chondritic. Involvement of older material can occur via source contamination, whereby subducted sediments mix with depleted mantle, or by crustal contamination, whereby depleted mantle is mixed with older material during differentiation in the crust. Long-term subduction of sediments leads to enrichment of the mantle region, with a migration in composition away from pristine depleted mantle; this can lead to juvenile mantle-derived magmas that have an isotope signature that has departed from the depleted mantle. Granitoids that intruded in the Gothian period (Hisingen and GAB suite; Figure 5.7), have ϵHf values equivalent to the depleted mantle; suggesting that during this time-period the mantle was not significantly enriched. The range of ϵHf in the Telemarkian samples is on average lower than that of the Gothian rocks (Figure 5.7), suggesting either an increase in the influence of older subducted sediment, an increase in contamination of older material in the crust, or that the crustal contaminant itself was older. The latter is not expected, since the terranes young to the west, and no older crust is exposed in the Telemarkia terrane. Mixing between depleted mantle and a component similar to Transcandinavian Igneous Belt (TIB) crust can produce the appropriate ϵHf values of the Telemarkian rocks (Figure 5.7).

Zircon oxygen isotopes

The mantle is a remarkably homogeneous oxygen isotope reservoir, with igneous zircons formed in equilibrium with the mantle having an average $\delta^{18}\text{O}$ of $5.3 \pm 0.3 \text{ ‰}$ (Valley et al. 1998). High magmatic $\delta^{18}\text{O}$ values ($>6.5\text{‰}$) are attributed to melting or assimilation of sediments, altered volcanics, or other supracrustal rocks affected by low-temperature alteration, whereas low magmatic $\delta^{18}\text{O}$ values are attributed to incorporation of material that has undergone high temperature alteration (Valley et al. 2005). Oxygen isotopes can therefore be used to discriminate source contamination (mantle recycling) from crustal contamination (intracrustal recycling), since source contamination will lead to enriched radiogenic isotope signatures, but with oxygen isotopes retaining a mantle signature. The $\delta^{18}\text{O}_{\text{zircon}}$ of Telemarkian rocks in this study are well above the range of mantle values (Figure 5.6), suggesting intracrustal recycling and a significant involvement of a component with high- $\delta^{18}\text{O}$.

Hf-O modelling

The Hf and O data form a binary array in Hf-O space (Figure 5.8), with a low- ϵHf , high- $\delta^{18}\text{O}$ (crustal) end-member and a high- ϵHf , low- $\delta^{18}\text{O}$ (mantle) end-member, thus input of an older crustal component can be modelled by two-component mixing, as has been achieved in previous studies combining Hf-O or Nd-O data (e.g. Peck et al. 2004; Lackey et al. 2005; Kemp et al. 2007). These

previous studies resolved AFC and bulk-mixing curves based on known crustal and mantle end-members; in this study there is a lack of data to constrain the crustal end-member, as no older crust or metasediments are exposed within the region; however, speculative end-members can be model based on previous whole-rock studies.

The crustal end-member can be constrained by the lowest $\epsilon\text{Hf}_{(1500 \text{ Ma})}$ value (~ 0) and the highest $\delta^{18}\text{O}$ value (~ 10), and conversely the mantle-like end-member can be constrained by the highest $\epsilon\text{Hf}_{(1500 \text{ Ma})}$ value (~ 8.3) and the lowest $\delta^{18}\text{O}$ value (equivalent to the mantle value at ~ 5.3). For the crustal end-member a composition similar to that of young TIB crust is used (Figure 5.7); this corresponds in age to the ‘normal deep crust’ component advocated by Andersen et al. (2001, 2002b, 2009b). The ϵHf of this crustal end-member is similar to a metagreywacke unit from the Idefjorden terrane (Figure 5.7), indicating that material with an appropriate age, Hf signature and sedimentary nature, does exist within the region. A $\delta^{18}\text{O}$ value of 14 is used for the crustal component, and is based on an estimated average value for sedimentary rocks (Simon & Lécuyer 2005). The mantle end-member uses ϵHf and $\delta^{18}\text{O}$ values appropriate for depleted mantle at 1500 Ma.

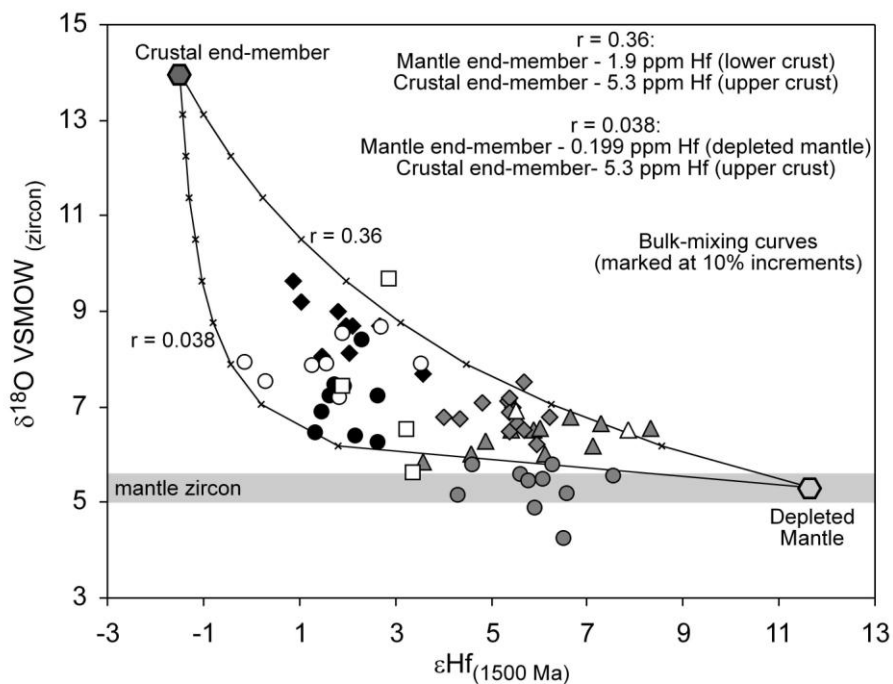


Figure 5.8. $\epsilon\text{Hf}_{(1500 \text{ Ma})}$ versus $\delta^{18}\text{O VSMOW}_{(\text{zircon})}$ for zircons of this study. Bulk-mixing curves and mantle and crustal end-members are discussed in the text. Symbols as in figure 5.5.

The use of either AFC or bulk-mixing modelling will result in similar mixing curves, but with different proportions of end-members (Kemp et al. 2007). In this study a simple two-component mixing model was employed, since Hf or O do not correlate with indices of differentiation (e.g.

SiO₂, figures 5.5 and 5.6), as would be expected with an AFC process. Since the oxygen content is assumed to be similar in mantle and crustal rocks, the shape of the mixing curves depends on the Hf concentration of the end-members. The two curves shown (Figure 5.8) use depleted mantle (0.199ppm; Salters & Stracke, 2004) or lower crustal (1.9ppm; Rudnick & Gao 2003) values for the mantle end-member, combined with an upper crustal value (5.3ppm; Rudnick & Gao 2003) for the crustal end-member. Using depleted mantle combined with upper crustal values is compatible with a source contamination model; whereas using lower crust combined with upper crust values is compatible with a crustal contamination model. The data fall between the two curves, suggesting (assuming that the end-members are appropriate) that mixing is not limited to contamination in the mantle region, but has involved crustal input higher in the magmatic plumbing system. Alternative values could be chosen iteratively to fit the data; however, for any curve that falls through the data and uses the same end-member values, the mixing proportions will be similar. The Hf-O mixing curves indicate that 10-50% of the crustal component is required.

5.5.5 Processes of continental recycling

Addition of a crustal component to mantle-derived magmas can be achieved by a number of processes. As discussed previously, the $\delta^{18}\text{O}$ signature is too high to be compatible with contamination in the mantle via subducted high- $\delta^{18}\text{O}$ material. This is based on the assumption however, that the mantle is homogeneous in $\delta^{18}\text{O}$. Although this is normally the case (e.g. Valley et al. 1998), there are some examples where enrichment via mantle processes has led to an increase in $\delta^{18}\text{O}$ recorded in magma suites. In mantle domains enriched by subducted sediment (i.e. EM2), $\delta^{18}\text{O}$ in olivine is increased from 5.2 to 5.7 (Workman et al. 2008); this is modeled as 2-3% sediment input. In the Banda arc, $\delta^{18}\text{O}_{\text{zircon}}$ values are ~5.5 to 6.5 ‰ (Vroon et al. 2001), with the increase from the mantle value being related to 1-5% subducted sediment input. In settings where the subducted slab itself is postulated to have had an input to arc magmatism, $\delta^{18}\text{O}_{\text{melt}}$ values reach ~8 ‰ (Setouchi belt, Japan; Bindeman et al. 2005). In all of these examples, the enrichment in $\delta^{18}\text{O}$ is much smaller than that recorded in the Telemarkian rocks (up to $\delta^{18}\text{O}_{\text{zircon}}$ ~10 ‰), suggesting processes additional to mantle recycling are required.

In Kamchatka, arc basalts across the region have high- $\delta^{18}\text{O}$ (up to 8.5‰ $\delta^{18}\text{O}_{\text{melt}}$). The occurrence of these high- $\delta^{18}\text{O}$ basalts is accounted for by one or more of three processes: 1) crustal contamination of mantle-like magmas with high- $\delta^{18}\text{O}$ (~10‰) sediments in the lower or middle crust, 2) addition of high- $\delta^{18}\text{O}$ (~10-20‰) slab fluids into the magma generation zone, or 3) parental basalts were derived by melting of thickened lower crust that already had high- $\delta^{18}\text{O}$ (~6.5-7.2‰) (Bindeman et al. 2004). These processes can also be applied to this study; slab-fluid addition would require excessive amounts of fluids (Bindeman et al. 2004), and the ϵ_{Hf} of this component is likely to not have been evolved enough, since the subducting ocean crust will have been relatively young. Further to this, Hf has variably conservative behaviour; some studies have shown that it can be

mobilized in slab fluids (Woodhead et al. 2001; Barry et al. 2006), whereas others recorded immobile behavior (Pearce et al. 1999). Crustal assimilation is not advocated in the Kamchatkan example because of energy conservation considerations (Bindeman et al. 2004). However, high amounts of assimilant are advocated in the Lachlan orogen (Kemp et al. 2007). In the Telemarkian rocks up to 50% assimilant is required using the proposed end-members, and is achievable according to the model of Kemp et al. (2007). Melting of an older high- $\delta^{18}\text{O}$ source is advocated for the Kamchatkan arc basalts, with this source being volcanic material such as high- $\delta^{18}\text{O}$ hydrated metabasalt (Bindeman et al. 2004); the high- $\delta^{18}\text{O}$ values are derived from deep-seated enrichment by slab fluids, or by low-temperature alteration followed by burial by tectonic and magmatic processes. For the Telemarkian magmatism, both crustal assimilation and melting of older high- $\delta^{18}\text{O}$ crust are concluded to be possible processes.

Discriminating between the different processes requires examining evidence outside of the zircon data. For the Telemarkian rocks, a variety of evidence points to input of the crustal component occurring within the parent magma source zone: 1) the lack of zircon inheritance is suggestive of introduction in the lower crust where magmatic temperatures are higher, and where zircon-free material is more likely to reside; 2) the geochemistry of the suite points to extensive fractional crystallisation of mafic parent magmas without crustal assimilation during differentiation; 3) data on zircon core-rim pairs are lacking, but repeat analyses on the same grains, whether on the same growth zone, or on different growth zones, are generally within analytical uncertainty of each other, suggesting that the crustal component was not introduced during the later stages of zircon crystallization; 4) a granitic sample with the most mantle-like values suggests that a degree of closed-system differentiation was able to occur; 5) Hf and O do not correlate with indices of differentiation (SiO_2 ; Figures 5.5 and 5.6), as would be expected with an AFC process; 6) no definitively older metasedimentary rocks are found outcropping within the region, either as outcrop or as enclaves within the magmatic rocks. All of the evidence above is compatible with a setting in which the crustal component is mixed with depleted mantle or young mantle-derived material, in a lower crustal melting region, similar to the deep hot crustal zone setting (Annen et al. 2006), advocated in the Lachlan orogen (Kemp et al. 2007), or the Melting Assimilation Storage and Homogenisation (MASH) zone, advocated in the Andean arc (Hildreth & Moorbath 1988).

Establishing how a high- $\delta^{18}\text{O}$ source resided in the lower crust prior to Telemarkian arc magmatism is speculative. Possible processes could include burial of volcano-sedimentary rocks during repeated opening and closing of back-arc and fore-arc basins during tectonic switching (i.e. repeated compression and extension; Collins 2002) in an accretionary orogen; such a process is responsible for granite formation and continental growth in the Lachlan orogen (Kemp et al. 2007; Kemp et al. 2009). Another process is underthrusting and underplating of subducted oceanic crust and overlying sediments to the lower crust during preceding subduction stages; such a process is advocated as a

way of inputting high- $\delta^{18}\text{O}$ sources to the melt region of the Sierra Nevada batholith (Lackey et al. 2005). Tectonic burial of a crustal component would possibly lead to localised variation in radiogenic isotope signatures; based on previous isotopic constraints, the existence of an older crustal component at depth is widespread beneath SW Fennoscandia. Another process described previously is enrichment of mafic lower crust by slab fluids during previous periods of subduction (Bindeman et al. 2004); whether this can occur to the extent required in the Telemarkian example is yet to be constrained, as no such examples exist in the literature.

The Suldal arc is suggested to be built on attenuated continental crust (see Chapter 4), such crust may be relatively immature in composition (i.e. mafic), and comprise low-temperature altered material in its upper portions; thus, building a continental arc on such crust may involve mobilisation of older high- $\delta^{18}\text{O}$ material. Further evidence is required to establish how exactly a high- $\delta^{18}\text{O}$ source had an input to the Telemarkian arc magmatism. Repeated episodes of compression/extension in a retreating accretionary orogen is likely to result in burial of high- $\delta^{18}\text{O}$ material; stretching of such crust into attenuated margins and continental ribbons is likely to produce widespread domains with possible high- $\delta^{18}\text{O}$ signatures. Thus, retreating accretionary orogens provide a setting where assimilation of older sedimentary material may be prone to occur. Irrespective of the exact mechanism for producing a high- $\delta^{18}\text{O}$ source, it is the mixing of this source in the melt generation zone that can be gleaned from the available data. By mixing in the source region, any characteristic geochemical signature that the high- $\delta^{18}\text{O}$ source may have is homogenized with a mantle-derived subduction-zone signature (i.e. in a MASH zone). Bulk-mixing in this MASH zone is heterogeneous, such that daughter magmas can exhibit variably enriched Hf and O isotope signatures (Figure 5.5 and 5.6). The high- $\delta^{18}\text{O}$ source could have included zircon-bearing felsic material, but in this case the melt generation zone must have been hot and zircon-undersaturated such that zircon was dissolved; more likely is that the high- $\delta^{18}\text{O}$ source was dominantly mafic, and comprised hydrated metabasalt as advocated for Kamchatkan arc magmas (Bindeman et al. 2004).

5.6 Conclusions

The Hf-O data in this study indicate that Telemarkian magmatism involved significant recycling of previously formed continental crust, with bulk-mixing calculations indicating 10-50% involvement of a component that has an average model age of ~2.15 Ga. This continental material was recycled within the crust (intracrustal recycling), comprised sedimentary material, and was mixed with mantle-derived material in the lower crust in a MASH zone (Hildreth and Moorbath 1988). The data do not exclude the existence of the 'normal deep crust' component of Andersen et al. (2001; 2004a, 2009b). It is suggested that the existence of older crust residing at depth in the Telemarkia terrane, is due to the fact Telemarkian arc magmatism was built upon crust that comprised Gothian-age

(>1600 Ma) sedimentary material. The continental building of Telemarkian and Gothian age crust occurred in a retreating accretionary orogen, which likely featured tectonic burial of sedimentary material, addition of mantle-derived melts to arc magmatism, and mobilization of older crustal material in melt generation zones. A modern analogue for this is the southwestern Pacific, which comprises oceanic and continental arcs at varying levels of maturity, which feature varying amounts of older ensilic crust, but generally all include continental growth via juvenile mantle addition.

Geochemical and Hf-O constraints on the petrogenesis of early- to late-Sveconorwegian magmatism in S. Norway

Aim – In light of the new U-Pb ages for Sveconorwegian magmatism (see Chapter 3), the petrogenesis and tectonic setting of the different magmatic suites in southern Norway is discussed, basing observations on new in-situ Hf and oxygen isotope data combined with whole-rock geochemistry.

6.1 Introduction

During the Sveconorwegian orogeny, southern Norway was intruded by voluminous suites of granite *sensu lato*; these include suites of both I- and A-type affinity, with the latter including an Anorthosite-Mangerite-Charnockite (AMC) body. The abundance of large anorthosite massifs such as these is a unique feature of the middle Proterozoic. The origin of A-type granites, including Rapakivi-type suites which are commonly associated with AMC suites, is an ongoing matter of debate within igneous petrology (e.g. Martin 2006); understanding the petrogenesis of these magma series can inform us about processes of crustal formation and differentiation. Several processes are favoured for the genesis of A-type granites, including melting of granulitic refractory crust (Collins 1982; Clemens 1986; Whalen et al. 1987), melting of tonalitic crust (Anderson 1983; Creaser 1991; Patiño Douce 1997), and derivation from mafic crust (Frost & Frost 1997; Anderson et al. 2003). Recent studies using the accessory mineral zircon have constrained mixed mantle and crustal sources for both I and A-type granites (e.g. Peck et al. 2004; Kemp et al. 2006; Appleby et al. 2009; Be'eri Shlevin et al. 2009).

In southern Norway, four main suites of magmatism occurred around the period of the Sveconorwegian orogeny (1050-920 Ma). These are the Feda suite (I-type) at ~1050 Ma (Bingen et al. 1993; Bingen & van Breemen 1998), the Fennefoss suite at ~1035 Ma (Bingen & van Breemen 1998), the A-type Hornblende-Biotite-Granite (HBG) suite at 970-930 Ma (Andersen et al. 2002a, 2007a; Vander Auwera et al. 2003), and the Rogaland AMC suite at ~930 Ma (Schärer et al. 1996). Peak crustal thickening related to continent-continent collision occurred at ~1035 Ma (Bingen et al. 2008c), such that the Feda and Fennefoss suite are considered to be early- to syn-collisional suites, and the HBG and AMC suites are considered to be post-collisional. This study (see Chapter 3) has shown that undeformed granites normally grouped under the HBG suite are as old as 1047 Ma, and therefore pre-collisional in age, and also that deformed porphyritic granitoids (e.g. Feda suite) can be extended in their age range back to 1069 Ma. The emplacement of the HBG suite, although considered to be post-collisional, is controlled by orogenic structures (Duchesne et al. 1999; Bolle et al. 2003b); the suite intruded during phases of crustal doming that is related to the gravitational collapse of the Sveconorwegian orogen (Andréasson and Rodhe 1994; Romer 1996; Bingen et al.

2006). As a consequence of their different geodynamic setting, the petrogenesis of different suites is typically discussed separately.

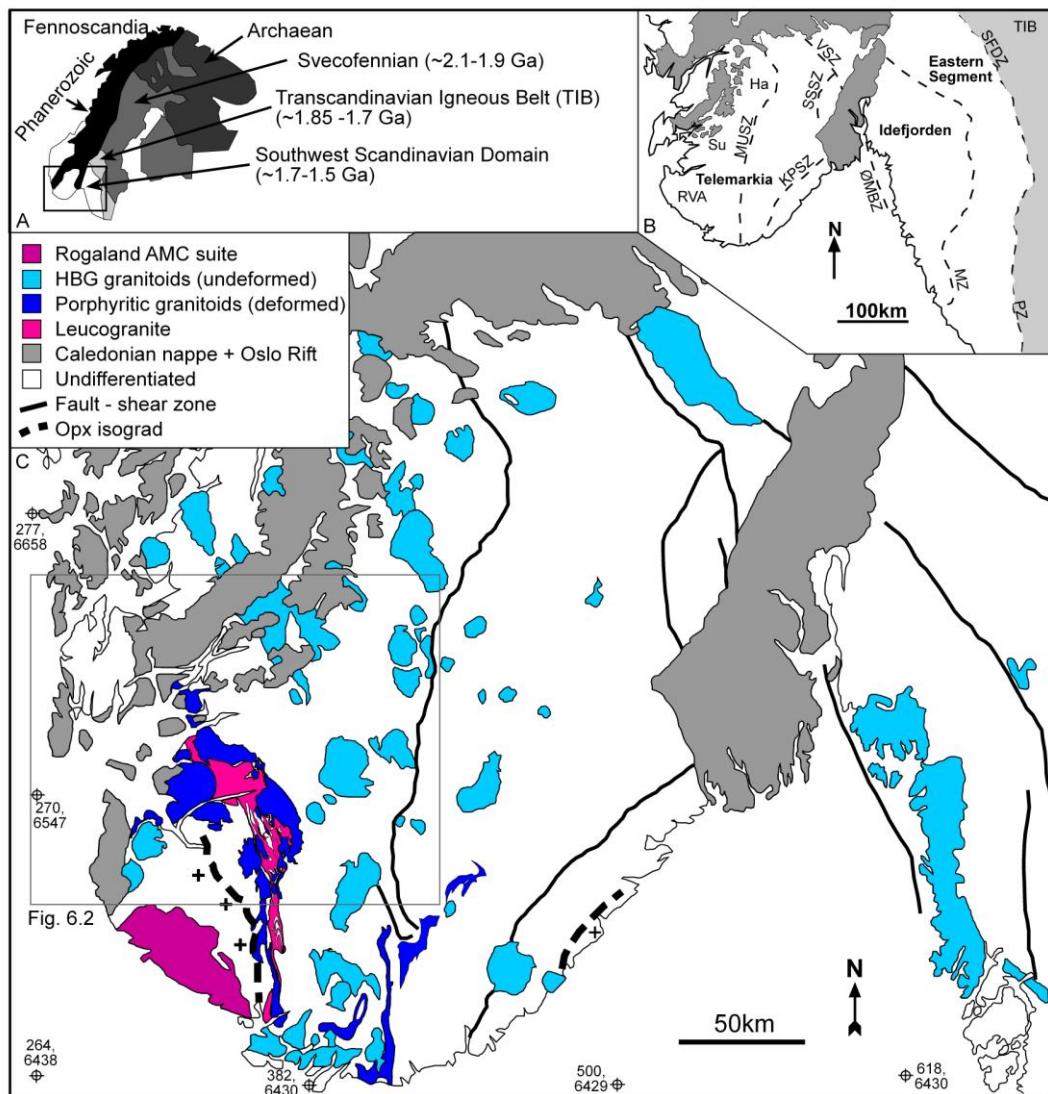


Figure 6.1. A) Sketchmap of Fennoscandia showing the main geological provinces. B) Sketchmap of SW Fennoscandia showing the division of lithotectonic domains (after Bingen et al. 2005b). C) Map of southern Norway showing the location of Sveconorwegian granitoid suites (modified from Bingen et al. 2005b; Vander Auwera et al. 2008; Slagstad et al. 2008). Ha = Hardangervidda Sector, Su = Suldal Sector, RVA = Rogaland Vest-Agder Sector, TIB = Transcandinavian Igneous Belt, MUSZ = Mandal-Ustaøset Shear Zone, KPSZ = Kristiansand-Porsgrunn Shear Zone, SSSZ = Saggrenda Sokna Shear Zone, VSZ = Vardefjell Shear Zone, ØBZ = Østfold Marstrand Boundary Zone, SFDZ = Sveconorwegian Frontal Deformation Zone, PZ = Protogine Zone. Grid co-ordinates are UTM zone 32V.

6.2 Previous studies

The HBG suite is defined as a ferro-potassic A-type suite (Vander Auwera et al. 2003), and is ferroan, metaluminous to weakly peraluminous, and features enriched incompatible elements as well as enriched large ion lithophile elements (LILE). Vander Auwera et al. (2003) showed that the HBG suite defines a differentiation trend from 50 to 77% SiO₂; this trend is interpreted to represent extreme fractional crystallisation from basaltic parent magmas. Such parental basaltic parent magmas are postulated to be partial melts of a hydrous mafic and potassic source lying in the

lithospheric upper mantle, or the mafic lower crust derived from it (Vander Auwera et al. 2003). Differentiation via fractional crystallisation without assimilation is corroborated by data from the Lyngdal-Tranevåg Suite (Bogaerts et al. 2003). Analysing natural and experimental data, and using trace element modeling, Vander Auwera et al. (2008) showed that both 73% fractional crystallization of an amphibole-bearing gabbroic cumulate subtracted from the parent mafic composition, and 30% non-modal batch melting of an amphibolitic source equivalent in composition to the mafic facies, produce a monzodioritic liquid that is appropriate to be a parent magma to the HBG suite.

Bogaerts et al. (2006) conducted crystallisation experiments on members of the Lyngdal Suite; comparison with natural data suggest crystallisation of a monzodioritic parent at 2-5 Kbar, with 5-6 wt% water and oxygen fugacity of NNO to NNO+1. An oxygen fugacity above NNO is also indicated by the assemblage magnetite+quartz+titanite (Vander Auwera et al. 2003). The high crystallisation temperature and water content of the Lyngdal Suite are suggested to be too high for primary magmas produced by partial melting of the crust (Bogaerts et al. 2006), with fractionation from mafic magmas being more likely. Using geothermobarometers (hornblende-plagioclase and Al-in-hornblende), crystallisation pressures are estimated at 1.3 to 2.7 Kbar for members of the HBG suite (Vander Auwera et al. 2003). Given the 5-6 wt% H₂O content for the Lyngdal granodiorite (Bogaerts et al. 2006), the monzodioritic parent is calculated to have been 4.05 to 4.85 wt% H₂O, and the amphibolitic source for this parent to have been 1.51 to 1.74 wt% H₂O (Vander Auwera et al. 2008).

Andersen et al. (2001) group post-collisional granitoids in Telemarkia into three groups based on isotopic and trace element compositions; Group 1 (normal-Sr) granites have >150 ppm Sr, ⁸⁷Rb/⁸⁶Sr <5, Sri_{930Ma} <0.710 and εNd <0; Group 2 (low-Sr) have <150 ppm Sr, ⁸⁷Rb/⁸⁶Sr >5, Sri_{930Ma} >0.710 and εNd <0; Group 3 comprises one granite from the south of the Telemark Sector that has Sri_{930Ma} <0.710 and εNd >0. Most of the HBG suite falls into Group 1, whereas plutons in the north of the Telemark Sector fall into Group 2.

The gneissic country rocks exposed in Rogaland have too high a ⁸⁷Sr/⁸⁶Sr ratio to be involved in the petrogenesis of Group 1 HBG granitoids (Bogaerts et al. 2003; Vander Auwera et al. 2003). The restricted Sr range also suggests (but is not restricted to) contamination by a Rb-depleted (i.e. granulitic lower crust) source (Vander Auwera et al. 2003). The absence of a correlation between SiO₂ and Sr_i or εNd suggests assimilation is not controlling the isotope signatures of the HBG suite (Bogaerts et al. 2003).

Andersen et al. (2001) postulate various crustal end-members found within southern Norway; 'CA' is moderately LILE-enriched deep crust with a T_{DM} of 1.9 Ga and has a composition similar to

‘upper continental crust’; ‘CB’ also has a T_{DM} of 1.9 Ga, is more LILE-enriched and is equivalent to metasedimentary gneisses in the Bamble terrane; ‘CC’ has a T_{DM} of 1.7 Ga with highly radiogenic $^{87}\text{Sr}/^{86}\text{Sr}$. Bolle et al. (2003a) postulate two different crustal end-members for Sr-Nd mixing calculations, ‘C1’ has a T_{DM} of 1.8 Ga and is LILE-enriched, and ‘C2’ has a T_{DM} of 1.9 Ga and is moderately LILE-enriched. Mixing between a depleted mantle component and CA/C2 (moderately LILE-enriched, normal-Sr, 1.7-1.9 Ga in age) crustal end-member can produce the isotope signature of Group 1 granites in Telemark and Rogaland with 30-70% of the crustal end-member. Binary mixing between these two end-members requires 20-40% crustal contamination to produce the composition of the monzodioritic parent liquid to the HBG Suite (Vander Auwera et al. 2008). This amount of contamination is suggested to be unrealistic, but can be lowered to 10-20% by using higher Sr and Nd contents (Vander Auwera et al. 2008). Group 2 granites require the CC (highly radiogenic $^{87}\text{Sr}/^{86}\text{Sr}$) end-member to be involved. Whereas the isotope compositions of Nd and Sr in the crustal and mantle end-members can be related to non-element selective bulk-mixing processes, the lead-isotope systematics require element selective processes such as fluid-exchange (Andersen et al. 2001).

Andersen et al. (2002b, 2007b, 2009b) and Andersen & Griffin (2004) present in-situ hafnium zircon data for various Sveconorwegian granitoids from across southern Norway. The Hf data corroborate with whole-rock Nd data, in terms of the relative amounts of mantle and older crust required in bulk-mixing calculations. Scarce inherited zircon signatures (see Figure 6.12) are inferred by these authors to confirm the presence of older Palaeoproterozoic crust at depth. However, as discussed by Liégeois and Stern (2010), inherited zircons do not confirm the existence of older crust; they only confirm that older zircons were available for assimilation. The most radiogenic (but non-outlying and non-inherited) Hf isotope composition of the Sveconorwegian granites requires involvement from a source with $\epsilon\text{Hf}_{950\text{Ma}} \sim -4$, which approximates to a model age of 1950 Ma (2-stage using Lu/Hf 0.015; Andersen et al. 2002b). Hf data on gneisses in central Telemark and younger granitoids suggest depleted mantle input to magmatism at ~ 1.2 Ga (Andersen et al. 2007b), that later formed a source involved in the Sveconorwegian magmatism (Andersen et al. 2009b). The range in ϵHf for individual plutons reaches >8 epsilon units; this is suggested by Andersen et al. (2009b) to be incompatible with closed-system differentiation of a homogeneous parental magma, however, closed-system differentiation from a heterogeneous source is not considered by the authors.

Andersen et al. (2002b) stated that mid-Proterozoic (i.e. 1.5-1.6 Ga) calc-alkaline protoliths are unlikely to have been a source for the Sveconorwegian granitoids in Telemarkia, because no such rocks exist in the region. However, this has recently been shown to not be the case, in fact widespread exposed crust in Telemarkia is constructed of calc-alkaline Telemarkian (1.52-1.48 Ga) gneiss (Bingen et al. 2005b, see Chapters 2-5).

The Rogaland AMC suite involved fractional crystallisation of a mafic anhydrous parent magma under low oxygen fugacity (Vander Auwera & Longhi 1994; Vander Auwera et al. 1998; Longhi et al. 1999), with anorthosite bodies forming by diapiric rise of plagioclase accumulations (Emslie 1985; Longhi et al. 1993). Fractional crystallization of the parent magmas involved crustal contamination, with different magma batches undergoing varying degrees of contamination (Bolle et al. 2003a); the crustal contaminant is represented by moderately to strongly-LILE enriched gneisses 1.5-1.9 Ga in age. Re-Os isotope data from the AMC suite suggest formation by melting of a mafic lower crust that is 1400-1550 Ma in age (Schiellerup et al. 2000).

The Feda suite is high-K, calc-alkaline, metaluminous, and displays characteristics typical of continental arc granites (Bingen & van Breemen 1998). It has been modelled via bulk-mixing of ultra-potassic-mantle and crustal components (Bingen et al. 1993). Andersen et al. (2001) showed that 20-35% crustal contamination using CA/C2 and depleted mantle end-members can produce the required isotopic compositions. Although the fields for Feda granitoids and Group 1 granites overlap in Nd and Sr space, lead isotope data indicate that the Group 1 granites cannot be formed purely by remelting of Feda granitoids (Andersen et al. 2001).

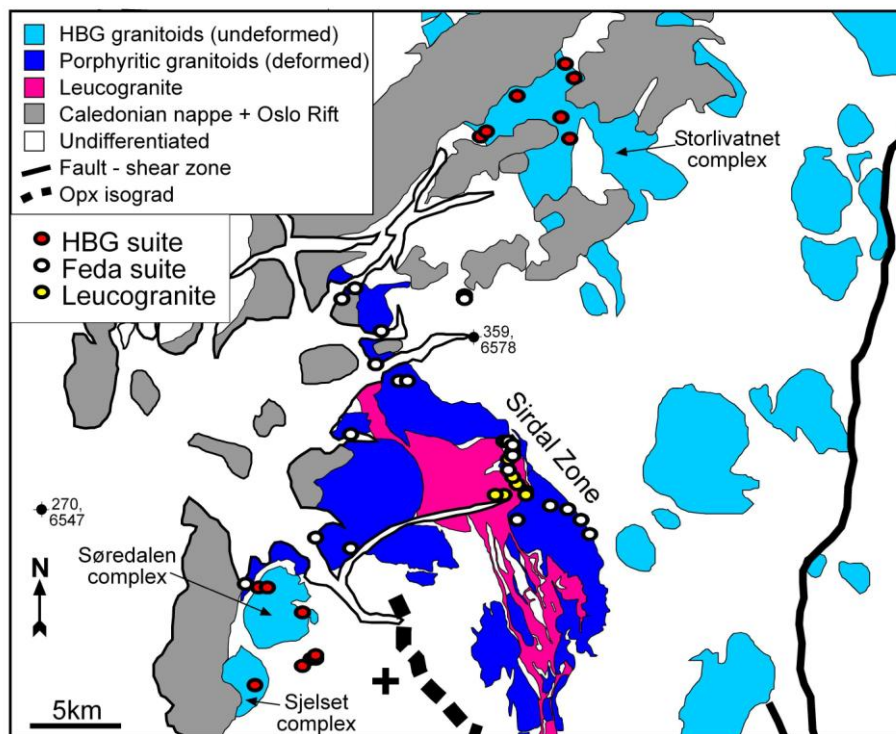


Figure 6.2. Geological map with sample localities of this study. (see Figure 6.1 for references)

The Fennefoss suite comprises similar augen gneisses to that of the Feda suite, but with a geochemical signature transitional between A-type and subduction-zone related; this signature is interpreted to represent the last vestiges of a subduction regime (Bingen & van Breemen 1998).

6.3 Analytical Methods

Whole-rock geochemistry was conducted using methods outlined in Chapter 4; hafnium and oxygen isotope analyses were conducted using methods outlined in Chapter 5.

6.4 Petrography and geochemistry

6.4.1 The HBG suite

Samples of the HBG suite in this present study come from the Storlivatnet intrusive complex in the Suldal Sector and from the Sjelset and Sjøredalen intrusive complexes in the RVA Sector (Figure 6.2). The Storlivatnet complex contains various units, both deformed and undeformed, with ages at 1021 ± 8 Ma, 1039 ± 15 and 1069 ± 9 Ma (see Chapter 3). The dominant lithology is a coarse-grained porphyritic granite comprising K-feldspar, altered plagioclase, quartz and biotite; hornblende is present in some units, and titanite is often intergrown with biotite. The Sjøredalen intrusive complex contains medium to coarse grained undeformed and deformed granitic units, with ages at 991 ± 35 and 1003 ± 43 Ma. The granites are composed of K-feldspar, plagioclase and quartz, with minor biotite and muscovite, and variable amounts of garnet; up to 20% garnet occurs where the granites contain inclusions and schlieren of pelite. The Sjelset intrusive complex comprises both ~ 930 and ~ 990 Ma units; the latter is sampled in this study. The sampled granite is dated at 993 ± 16 Ma, and comprises K-feldspar, quartz, altered plagioclase, biotite and muscovite.

The geochemistry of the HBG granites is compared with other members of this suite in figures 6.3 to 6.6. The HBG granites are metaluminous to weakly peraluminous, ferroan (except one sample), and calc-alkalic to alkali-calcic (Figure 6.3). In their major and trace element contents the samples of this study mostly overlap those of previous studies (Figures 6.4 & 6.5); SiO₂ content ranges from 68.7 to 76.4 %. The HBG suite forms bell-shaped trends in some elements (e.g. Ba, Nb and Zr), positive trends in others (e.g. Rb), and negative trends in others (e.g. Sr, V); inflections in these trends occur at ~ 60 - 65% SiO₂. On the primitive-mantle normalised plot (Figure 6.7), the HBG suite exhibits relative depletions in Ba, Nb, Sr, P, Eu and Ti. These can be related to fractionation of feldspar (Ba, Sr and Eu), apatite (P) and titanite/Fe-Ti oxides (Ti). The depletion in Nb is typical of subduction-related magmas, suggesting the HBG granites formed by remelting or fractionation of subduction-related parent magma. The HBG granites exhibit enrichment in LILE and HSFE, and positive LILE/HFSE and LREE/HREE ratios.

6.4.2 The Feda suite

The Feda suite refers to ~ 1050 to ~ 1020 Ma megacrystic (alkali-feldspar) granitoids that form the Sirdal Zone; the Sirdal zone is defined as the zone separating the Suldal sector to the northeast from the Rogaland sector to the southwest (Slagstad et al. 2008). The Sirdal zone comprises large

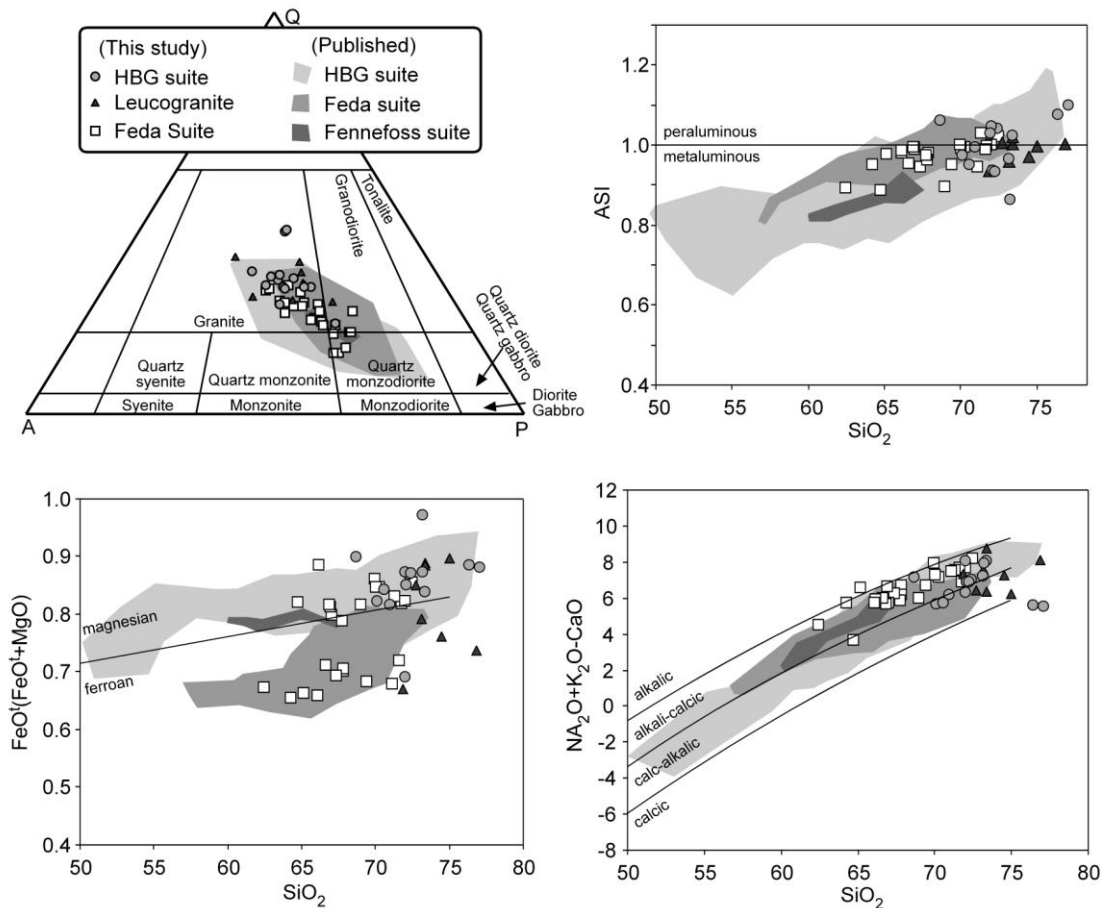


Figure 6.3. Geochemical classification diagrams for granitoid suites in southern Norway. Data for Late-granite, leucogranite and Feda granitoid from this study; HBG Suite from Auwera et al. (2003); Feda Suite and Fennefoss Suite from Bingen et al. (1993). ASI (aluminium saturation index), $\text{FeO}^t/(\text{FeO}^t+\text{MgO})$ (i.e. Fe^*) and $\text{Na}_2\text{O}+\text{K}_2\text{O}-\text{CaO}$ (i.e. MALI) from Frost et al. (2001).

volumes of megacrystic granitoid gneiss, leucocratic granite-pegmatite, and smaller volumes of medium-grained biotite-granite. The term ‘Feda’ Suite originally referred to ~1050 Ma augen gneisses outcropping to the south of the RVA Sector (Bingen et al. 1993; Bingen & van Breemen 1998), and is retained here for all porphyritic granitoids of this age that outcrop in the Sirdal Zone. The Feda granitoids are undeformed to moderately deformed, but folded by large, open folds with wavelengths of up to several kilometres (Slagstad & Marker 2009, pers. comm.). Samples within this study are dated at 1019 ± 10 , 1027 ± 24 , 1043 ± 6 , and 1046 ± 3 Ma (Slagstad & Marker 2009, unpublished data). The granitoids are granodioritic to granitic, and typically exhibit large (1-2cm) K-feldspar phenocrysts, sometimes red in colour. The matrix is composed of altered plagioclase, quartz and K-feldspar, with biotite in all samples, and hornblende, titanite and epidote being minor minerals in some units.

Previous geochemical data from the Feda suite (Bingen et al. 1993) is shown for comparison with the new data in figures 6.3 to 6.6. The Feda suite ranges from quartz monzodiorite and granodiorite to granite, is metaluminous to weakly peraluminous, and alkali-calcic (Figure 6.3). On the Fe^* classification ($\text{FeO}^t/(\text{FeO}^t+\text{MgO})$; Frost et al. 2001) the previous Feda data exhibit a magnesian

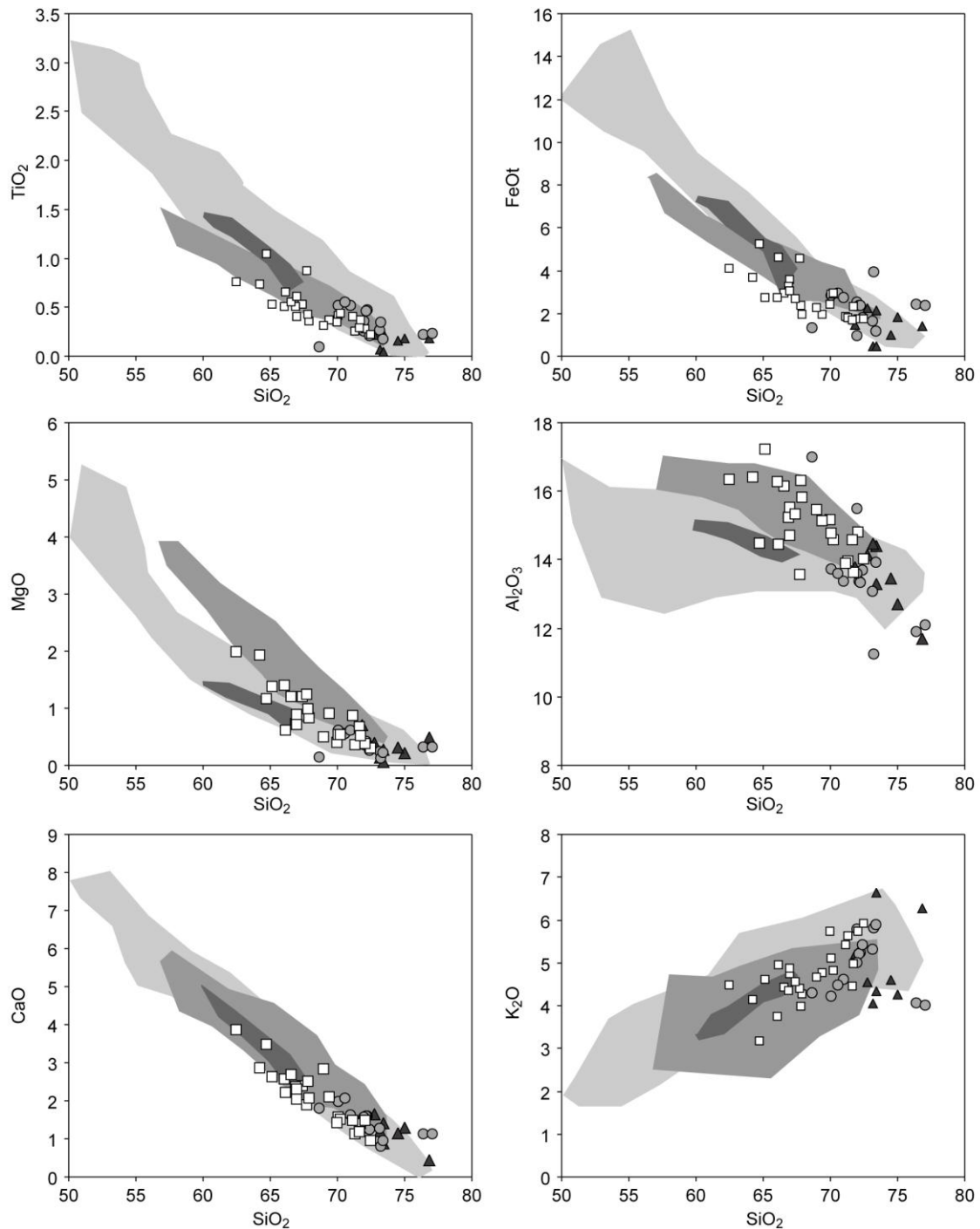


Figure 6.4. Harker diagrams for selected major elements. Symbols as in figure 6.3.

trend; data from this study fall into two groups, one that overlaps the previous magnesian trend, and one that overlaps the ferroan HBG suite. In major and trace element contents the Fedra suite exhibits trends that are similar to the previous Fedra data; however some of the new data is different in that they overlap the HBG trends. The trends between the Fedra and HBG suites are typically sub-parallel, but with varying contents of some elements. For example, in major element contents the Fedra suite has lower TiO₂ and FeOt, and greater MgO and Al₂O₃; in trace element contents the Fedra suite has lower Nb and Zr, greater Sr, and similar Ba and Rb (Figures 6.4 and 6.5). The Fedra suite

exhibits relative depletions in Nb, P, Eu and Ti (Figure 6.7); the depletions in P, Eu, and Ti are all to a lesser extent than in the HBG suite. The LILE are similarly enriched to that of the HBG suite, but the HFSE are less enriched. The LREE enrichment relative to HREE enrichment is also greater in the Feda Suite (La/Y; Figure 6.6).

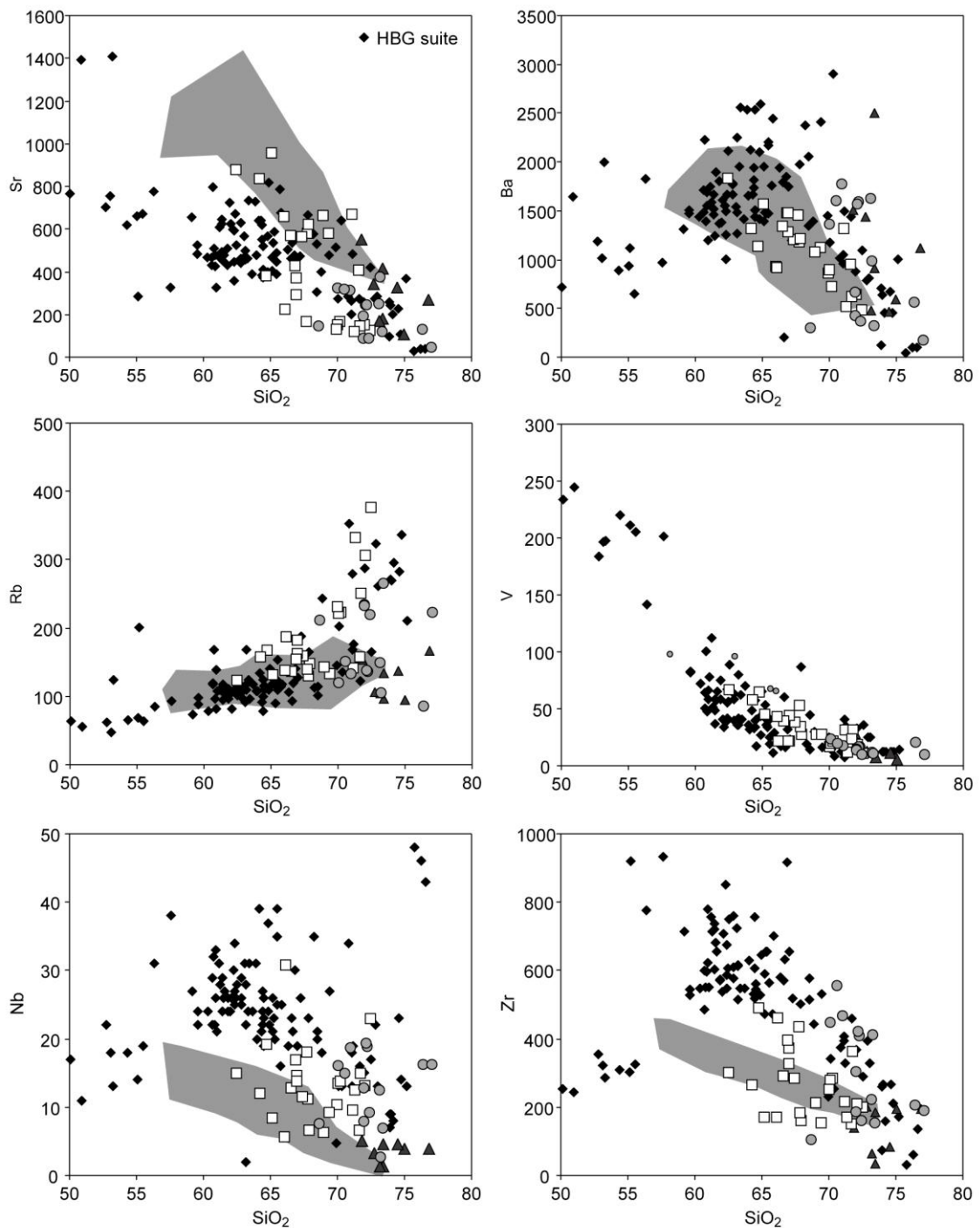


Figure 6.5. Harker diagrams for selected trace elements. Symbols as in figure 6.3 except for the HBG suite which is plotted at black diamonds.

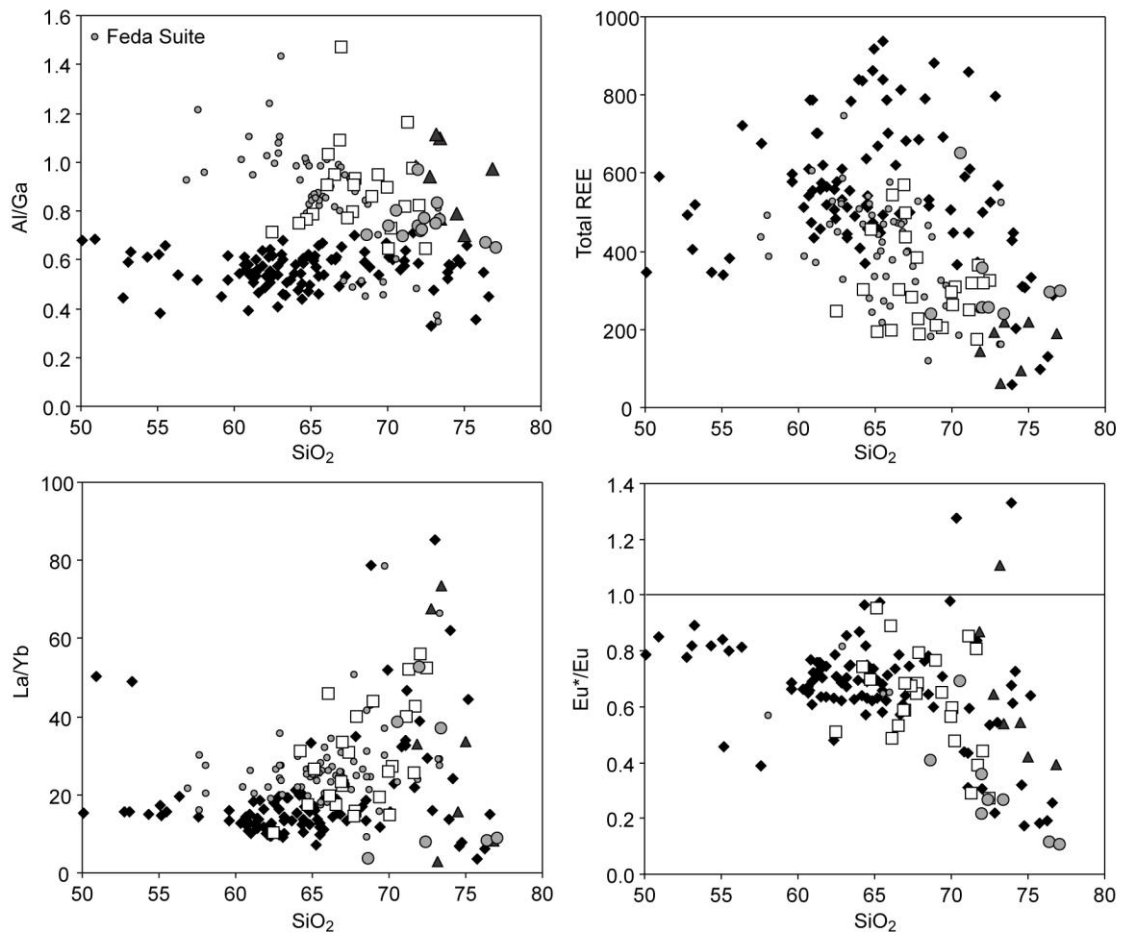


Figure 6.6. SiO_2 versus Al/Ga, Total REE contents, La/Yb and Eu^*/Eu . $\text{Eu}^* = \text{Eu}/(\sqrt{\text{Sm}^*}\sqrt{\text{Gd}})$. Symbols as in figure 6.4 except for the Feda Suite which is plotted as small grey-filled circles.

6.4.3 Leucogranites

Leucocratic granite and pegmatite are found within the Sirdal zone, and are characterised by gradual transitions, on a several-meter scale, between coarse-grained granite and pegmatite. Inclusions of fine-grained migmatitic paragneiss are found abundantly in parts of the leucocratic granite-pegmatite. Samples are dated at 1021 ± 61 , 1025 ± 25 , and 1045 ± 13 Ma (Slagstad & Marker 2009, unpublished data). The sampled leucogranites are typically medium-grained biotite granite, comprising K-feldspar, quartz, altered plagioclase and biotite. Some areas are rich in inclusions of amphibolite or gneiss; within these, opaque minerals, titanite and zircon are more abundant, sometime forming schlieren.

The leucogranites straddle the boundary between metaluminous and peraluminous, are variably ferroan/magnesian and calc-alkalic to alkali-calcic (Figure 6.3). In major and trace element contents the leucogranites roughly overlap the evolved members of the HBG suite (Figures 6.4 to 6.6). In the primitive mantle normalised plot (Figure 6.7) the leucogranites exhibit depletions in Ba, Nb, Sr, P, Eu and Ti; the depletions are similar in extent to those of the HBG suite. The LILE/HFSE and LREE/HREE enrichment in the leucogranites is similar to that of the Feda Suite (Figures 6.6 to 6.7).

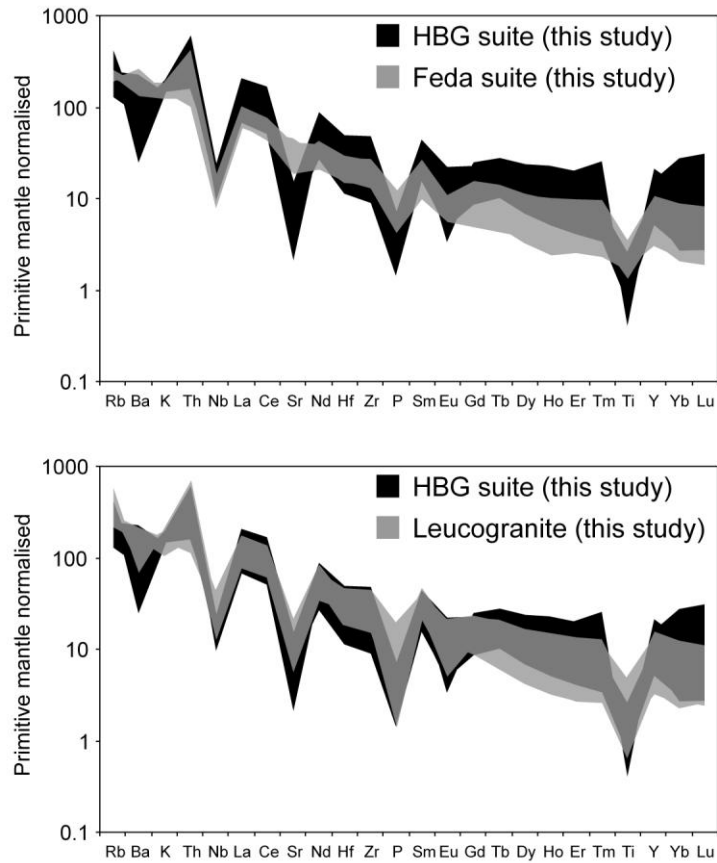


Figure 6.7. Primitive mantle (Sun & McDonough 1989) normalised plots comparing the HBG, Feda and Leucogranite suites.

6.4.4 Zircon saturation temperature

Figure 6.8 shows zirconium content plotted against $M ((Na+K+2Ca)/Al*Si)$ for the samples in this study, along with zircon saturation isotherms from Watson & Harrison (1983). The magnesian members of the Feda suite fall close to the 800°C isotherm, whereas the ferroan members extend to higher temperatures similar to those of the HBG suite. The leucogranites have relatively low temperatures (<810°C).

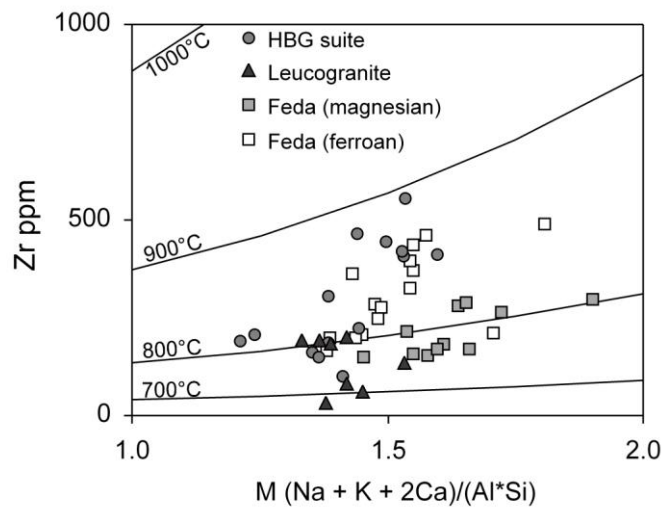


Figure 6.8. $M ((Na+K+2Ca)/(Al*Si))$ versus Zr ppm for granite suites of this study, isotherms are zircon saturation temperature (calculated from Watson & Harrison 1983).

6.5 Results - Hf isotopes

Hf isotopes were measured in 12 granitoids from across the study area (Figure 6.9). Two of these samples (MM2230 and MM26297) are from the leucogranite belt within the Sirdal Zone (Figure 6.2), and include inherited zircons that are ~1500 Ma in age; the ϵ_{Hf} of these inherited zircons is between +7.51 and 12.74). Disregarding the inherited zircons, the total range in ϵ_{Hf} across all samples (6.5 epsilon units) is fairly narrow considering the number of samples. The mean of each sample varies from ϵ_{Hf} -0.78 to +2.57. Within each sample the range in ϵ_{Hf} is limited, with the MSWD being between 0.03 and 2.3 for 10 out of 11 samples. The sample with a higher MSWD (MM26302) features two analyses that have higher ϵ_{Hf} that are out of the range of the entire suite. This is the only sample with a convincing degree of geological heterogeneity; analytical uncertainty can explain the heterogeneity within the other samples. Two stage model ages (T_{DMC}) range from 1474 Ma to 1887 Ma.

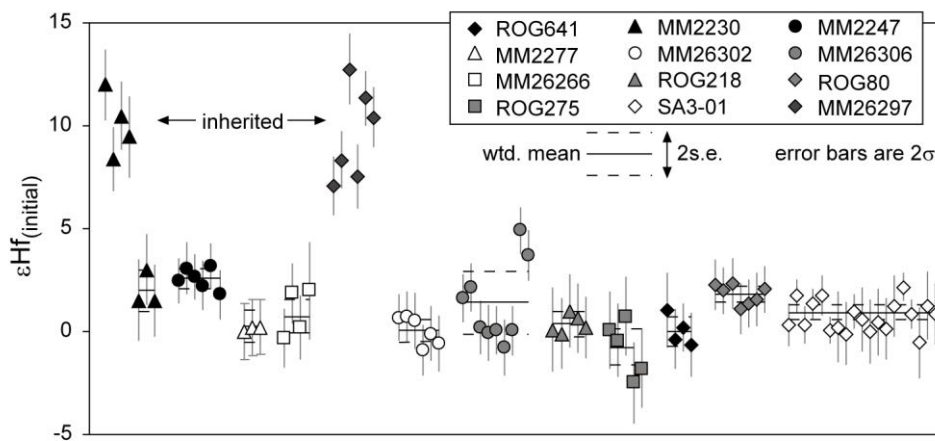


Figure 6.9. Results of in-situ Hf analyses; $\epsilon_{\text{Hf}}(\text{initial})$ is plotted against arbitrary units. For each sample the weighted mean and 2s.e. are shown as a black solid line and block dotted lines respectively. From MM26297, only ~1500 Ma inherited zircons were analysed for Hf; U-Pb analyses reveal a ~1045 Ma population of magmatic zircons.

6.6 Results - Oxygen isotopes

Oxygen isotope data was determined on a subset of six samples (Figure 6.10). The total range in $\delta^{18}\text{O}$ is from +4.66 to +12.09‰. Five of the samples have means (+5.74 to +7.07‰) that are slightly above the mantle value ($5.3 \pm 0.3\text{‰}$), and one sample (MM26306) has values that are much higher (mean = +11.63 ‰). The range in each sample is variable; in three samples (MM26306, ROG641 and SA3-01) the range is within analytical uncertainty (MSWD = 0.69 to 1.7), and in the other three samples (MM2247, MM26032 and ROG80) the range likely represents geological heterogeneity (MSWD = 3.2 to 8.1).

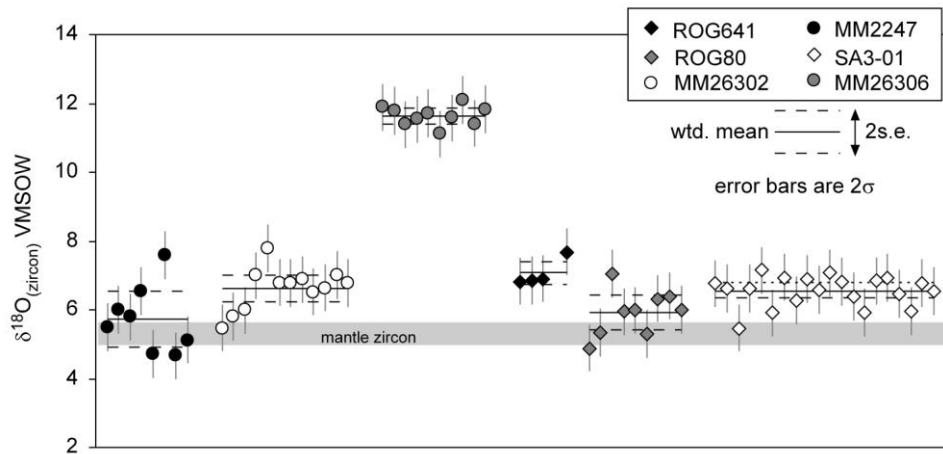


Figure 6.10. Results of in-situ oxygen analyses; $\delta^{18}\text{O VSMOW}_{(\text{zircon})}$ plotted against arbitrary units. For each sample the weighted mean and 2s.e. are shown as a black solid line and block dotted lines respectively. Mantle zircon = $\delta^{18}\text{O } 5.3 \pm 0.3 \text{ ‰}$ (Valley et al. 1998).

6.7 Discussion

6.7.1 Hf-O constraints on magma source

Figure 6.11 shows ϵHf versus time for the granitoids of this study along with published data from the region. The ϵHf of the Feda suite is remarkably similar to that of the HBG Suite; there is no temporal change in ϵHf either, with granitoids across the Sveconorwegian period all having similar values. The range in ϵHf for an individual sample in this study was typically smaller than that measured in previous studies (Andersen et al. 2002a, 2007b, 2009b); whether this is due to real geological variation or an analytical effect is difficult to constrain, since previous studies include a greater number of analyses per sample.

The Sveconorwegian granitoids intrude 1.5-1.6 Ga crust that is calc-alkaline and rather juvenile in nature (Chapter 5; Andersen et al. 2002a), the evolution of this crust is shown in Figure 6.11; also shown is the evolution of ~1.7-1.9 Ga Transcandinavian Igneous Belt (TIB) crust. The Sveconorwegian granitoids largely overlap with the 1.5-1.6 Ga crust, suggesting that remelting of 1.5-1.6 Ga crust to produce the younger granitoids is compatible with the Hf isotope data. Outliers in the previously published data that have low ϵHf (see Figure 6.11) have been used as evidence for an older >1.7 Ga component to be involved in the petrogenesis of the late-Sveconorwegian granitoids (Andersen et al. 2002b; 2007b; 2009b). These potentially inherited zircons are small in number, they lack U-Pb data in some cases, and in others the U-Pb data is not discussed in terms of discordance/metamorphic disturbance; the evidence for a >1.7 Ga component based on these zircons is therefore unpersuasive.

The mantle is a remarkably homogeneous oxygen isotope reservoir, with igneous zircons formed in equilibrium with the mantle having an average $\delta^{18}\text{O}$ of $5.3 \pm 0.3\text{‰}$ (Valley et al. 1998). High

magmatic $\delta^{18}\text{O}$ values ($>6.5\%$) are attributed to melting or assimilation of sediments, altered volcanics, or other supracrustal rocks affected by low-temperature alteration, whereas low magmatic $\delta^{18}\text{O}$ values are attributed to incorporation of material that has undergone high temperature alteration (Valley et al. 2005). Oxygen isotopes can therefore be used to discriminate mantle recycling from intracrustal recycling.

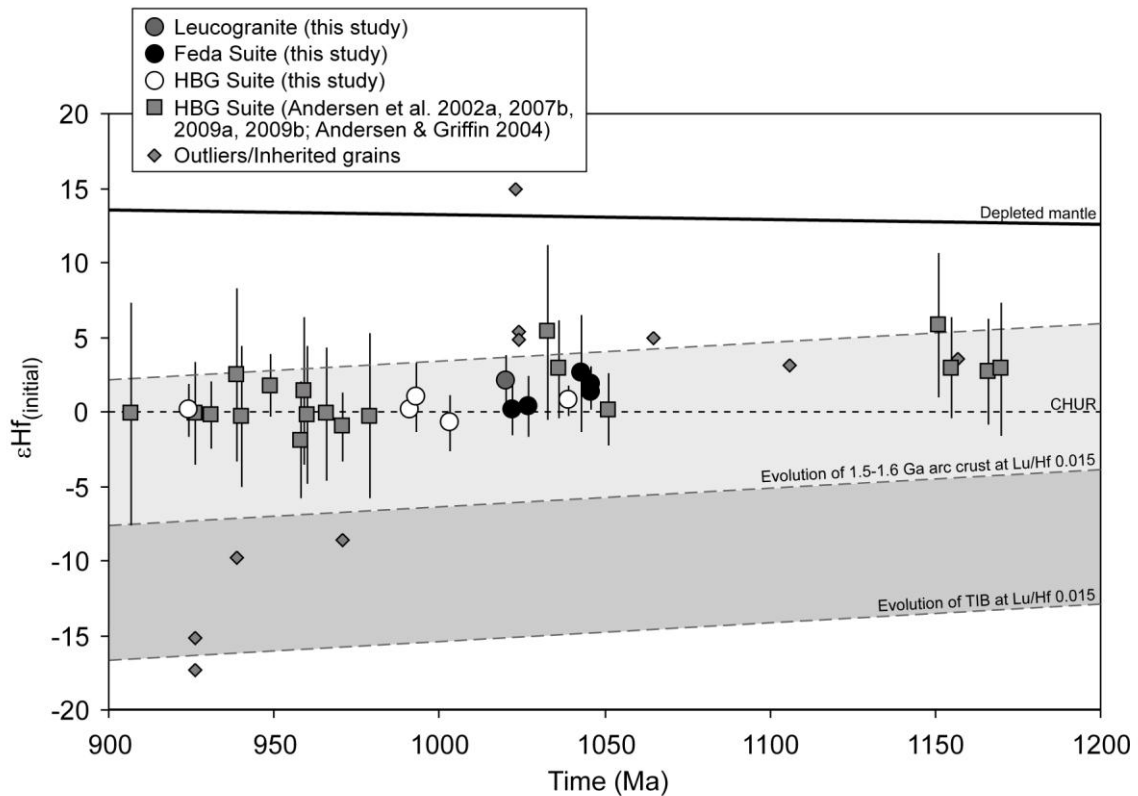


Figure 6.11. $\epsilon\text{Hf}_{(\text{initial})}$ versus intrusion age (Ma) for Sveconorwegian granitoids. The field for 1.5-1.6 Ga granitoids is based on data from Andersen et al. (2002b) and Chapter 5. The field for TIB (1.7-1.9 Ga) crust is based on data from Andersen et al. (2009a). The evolution of these fields uses an average crustal Lu/Hf value of 0.015. Depleted mantle (DM) is based on Griffin et al. (2000), and CHUR uses values of Bouvier et al. (2008). Error bars represent 2s.d. of the mean.

Oxygen isotopes are similar for both Feda suite granitoids (MM2247, MM26302, and ROG80) and HBG granitoids (ROG641, SA3-01). The average values are above the mantle range, suggesting a magmatic source with a high- $\delta^{18}\text{O}$, such as weathered continental crust. The origin of the highest- $\delta^{18}\text{O}$ granitoid (MM26306) is discussed in section 6.7.5. In summary, the Hf-O isotope data suggest a similar source is likely for both ferroan and magnesian magmas, and for early- syn- and late-orogenic suites.

6.7.2 Formation of silicic melts - magma mixing versus fractional crystallization

An origin for the HBG suite via fractional crystallisation has been advocated in various studies (Vander Auwera et al. 2003, 2008; Bogaerts et al. 2003, 2006). Andersen et al. (2009b) disagree with this model, instead, they suggest a model whereby silicic end-members have been formed by

crustal anatexis, and these have mixed with differentiated and contaminated mantle-derived mafic end-members. The bell-shaped trends observed in some trace element harker diagrams are pivotal to this debate (see Figure 6.12). Vander Auwera et al. (2003) suggest the bell-shape is due to a change in fractionating phases such that certain trace elements behave incompatibly during early fractional crystallisation, turning to compatible behavior during fractionation of more evolved magmas. A lack of magma-mixing between mafic and silicic end-members means that samples do not fall within the bell-shape. Andersen et al. (2009b) propose that mafic magmas have differentiated producing positive trends at low silica content, silicic melts are formed by partial melting of crustal rocks, and that the negative trend after ~55% SiO₂ is due to mixing between these silicic melts and the differentiated mafic melts. In this case, mixing should occur between silicic melts and mafic compositions at varying degrees of differentiation, such that a variety of mixing lines are produced (see Figure 6.12c); the lack of such mixing lines in the data is suggested by Andersen et al. (2009b) to reflect a lack of local homogenization. Andersen et al. (2009b) also point out that the HBG trend discussed by Vander Auwera et al. (2003, 2008) is made up of unimodal or bimodal clusters, and that individual plutons do not exhibit single differentiation trends (see Figure 6.12a).

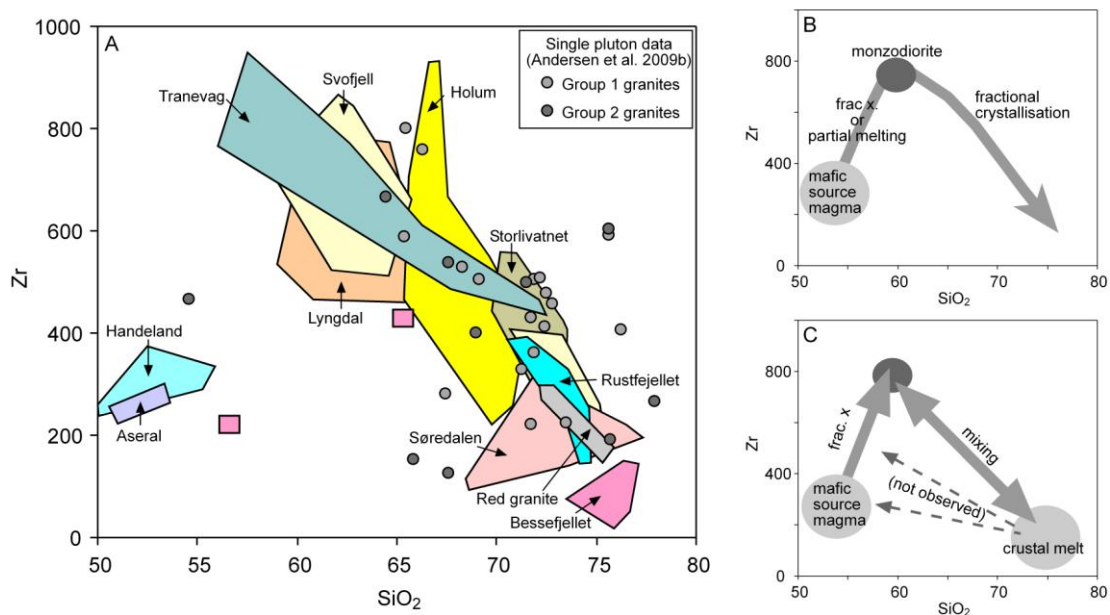


Figure 6.12. A) SiO₂ versus Zr for plutons within southwest Norway. Aseral, Handeland, Svofjell, Lyngdal, Holum, Rustfjället, Red granite and Bessefjället are members of HBG suite shown in figures 6.3 to 6.6 (from Vander Auwera et al. 2008 & Bogaerts et al. 2003); Storlivatnet and Soredalen are members of HBG suite from this study; other data points represent other individual plutons in the region (from Andersen et al. 2009b). B) evolution of the HBG trend via fractional crystallisation of a mafic parent magma (see text) C) evolution of the HBG trend via mixing between mafic parent magmas, and silicic melts derived from crustal anatexis. (see text for explanation of these models).

In response to these arguments it is worth pointing out that typical models for formation of granite plutons, involve segregation of felsic melts, collection of these melts into larger bodies, and buoyant uprise of these bodies via varying dyking/stopping mechanisms (e.g. Marsh 1992; Brown 1994; Petford et al. 2000). Therefore, mafic and intermediate compositions are often going to be located at

deeper crustal levels than that of the felsic plutons. The density contrast between mafic/intermediate and felsic melts means that even if all melts are mobilized, the felsic magmas will rise highest in the crust. Arguments against differentiation of felsic plutons from mafic magmas have often cited the argument of a lack of exposed mafic to intermediate crust (e.g. Haapala et al. 2005), however, these are hindered by the fact that exposure at the surface is typically constrained to a certain crustal level (normally upper-crustal). As pointed out by Vander Auwera et al. (2008), if the HBG suite was formed by fractionation of a lower crustal mafic parent magma, then the mafic residues are likely to still reside in the lower crust, or to have been returned to the mantle.

The trends in figure 6.12 are compatible with differentiation of a parent magma with ~57% SiO₂ and ~800 ppm Zr, to more evolved composition with lower Zr. This parent magma is indicated by Bogaerts et al. (2003, 2006) to be a monzodioritic composition. Using experimental and natural data, Vander Auwera et al. (2008) show that this monzodiorite composition can be produced by both fractional crystallisation and partial melting of an amphibolitic source magma. The new data presented here overlap the previous HBG data, and do not help resolve the issue over which petrogenetic process is responsible. However, the petrogenetic model proposed later in this chapter advocates differentiation from mafic parent magmas, either by fractional crystallisation, partial melting or more likely by both processes; in so doing this the model does not contradict the experimental data or modelling of natural data, but also aims to account for the isotopic constraints that Andersen et al. (2001, 2002b, 2007b, 2009b) outline in their petrogenetic models.

6.7.3 Geochemical constraints on magma source

For Sveconorwegian magmatism, Bingen et al. (1993) advocate a change in Fe* over time, with early granitoids (Fedra suite) having low Fe*, late granitoids (HBG suite) being highest in Fe*, and the Fennefoss suite falling in the middle. The data presented here shows that although the granitoids <1000 Ma are all ferroan (high Fe*), early granitoids are both magnesian (low Fe*) and ferroan; therefore the geochemistry is changing spatially and not just temporally. The ferroan samples have higher TiO₂, FeO^t, and incompatible elements (e.g. Nb, Zr, REE), lower MgO, Al₂O₃ and Al/Ga, and greater depletion in Ba, Sr, P and Eu (Figures 6.4 to 6.7). These characteristics are all typical features of A-type granites (e.g. Whalen 1987; Collins 1982), and can be explained by a greater degree of plagioclase fractionation (which lowers Ba, Sr, Eu in residual melts), lesser degree of apatite and Fe-Ti oxide fractionation (which lower Fe, Ti and P), and either smaller degrees of partial melting or melting of an enriched source (to account for the increase in incompatible elements). A-type granites form at higher temperatures than I-type granites (Collins 1982; Clemens et al. 1986). The difference between zircon saturation temperatures of the magnesian and ferroan granitoids (see Figure 6.8) is compatible with the ferroan members of the Fedra suite being more closely related to A-type magma series.

Changes between the amount of plagioclase fractionation versus the amount of Fe-Ti oxide fractionation can be related to intensive parameters during melt generation. An increase in water content promotes the stability of plagioclase and reduces the stability of Fe-Ti oxides (Gaetani et al. 1993; Sisson & Grove 1993), an increase in oxygen fugacity has the same effect although to a lesser extent (Toplis & Carroll 1995; Feig et al. 2006; Hamada & Fuji 2008), and an increase in pressure has the reverse effect (Grove et al. 2003). Water content also has the effect of lowering the solidus, meaning that the degree of melting will be increased in hydrous conditions (Baker et al. 1994), as is consistent with the incompatible element contents. The importance of plagioclase fractionation for producing A-type magmas means they typically have anhydrous sources advocated. It could thus be inferred that the source conditions for the magnesian granites were hydrous and more oxidising, and for the ferroan granites were anhydrous and reducing. This is contradicted however by experiments on the parent to the Lyngdal granodiorite, suggesting crystallization at 2 to 4 Kbar from a magma with 5 to 6 % H₂O at an fO_2 of NNO to NNO+1 (Bogaerts et al. 2006). Such oxidizing and hydrous conditions have been recognised in other A-type granites, and form a subset classified as oxidized A-type granites (Dall'Agnol et al. 1999; Dall'Agnol & Oliveira 2006); such granites typically contain >4 wt% H₂O and can be derived from lower crustal igneous quartzo-feldspathic sources (Dall'Agnol & Oliveira 2006).

Trends for the Feda and HBG suites do not appear to converge at low silica contents, although this conclusion is hampered by the lack of mafic (<57% SiO₂) compositions in the Feda suite. At ~57% SiO₂ the two trends are markedly different in major and trace element contents, therefore, the monzodiorite parent magma that evolved to form the HBG suite (Vander Auwera et al. 2008), is not suitable for forming the Feda suite. Thus, formation of these two suites may have involved either a different source magma, or different conditions during fractionation/melting of this source to produce different parent magmas.

The Hf-O isotope data, and previous Nd and Sr data (Bingen et al. 1993; Andersen et al. 2001), point to a similar source in terms of isotope signatures for both the Feda and HBG suites. The similarity in geochemical enrichment (see Figure 6.7), except for elements related to plagioclase/Fe-Ti oxide fractionation, is also striking. The negative Nb anomaly in both suites is suggestive of a source with a subduction-zone influence, as opposed to asthenospheric mantle which typically lacks a Nb anomaly (e.g. Thompson 1983; Fitton et al. 1997). Both whole-rock and isotope geochemistry point to a similar source for the HBG and Feda suites; thus, the influence of crystallisation conditions is advocated for the changes in geochemistry.

In the model of Vander Auwera et al. (2008), the monzodiorite parent magmas to the HBG suite contain 4.05-4.85 wt% H₂O, likely formed by partially melting of amphibolite with 1.5-1.7 wt%

H₂O, which originated by fractionation or partial melting of a lower crustal source with 0.34-0.85 wt% H₂O. The Fedra suite source magmas likely contained a greater water content than this, so that Fe-Ti oxide relative to plagioclase stability was increased, therefore hindering iron enrichment and producing more magnesian compositions; and also producing greater degrees of partial melting. The greater water content in the Fedra suite is compatible with their postulated supra-subduction zone origin (Bingen et al. 1993; Bingen & van Breemen 1998; Slagstad et al. 2008). Over time the Sveconorwegian magma suites become entirely ferroan, this temporal change can be related to a decrease in the water content of the magma sources over time. A temporal decrease in water content can be related to dehydration via successive melting and heating from magmatic underplating (Landenberger & Collins 1996). Since continent-continent collision occurred by 1035 Ma (Bingen et al. 2008c), any flux of water related to a postulated subduction zone will have been cut off by ~1035 Ma.

As noted previously, as well as the HBG suite being ferroan, some members of the Fedra suite are also ferroan (including MM26306 - 1046±3 and ROG218 – 1027±24 Ma). Thus, an explanation of the ferroan and magnesian trends must allow for their contemporaneous formation (at least at a >1 Myr timescale). To account for this, a suggested model (Figure 6.13) involves: 1) melting of mafic lower crust to form parent magmas that evolve to magnesian Fedra granitoids, 2) dehydration zones occurring above the melt generation zones, and 3) melting of the dehydrated lower crust for form parent magmas that evolve to ferroan Fedra granitoids. This model is based on that proposed for the Triassic I and A-type granites of the Chaelundi Complex, Australia (Landenberger & Collins 1996). Generation and ascent of early formed magnesian magmas leaves the crust relatively anhydrous but not refractory (chemically depleted); this crust will stay anhydrous unless new hydrous mantle-derived arc magmas are intruded. Remelting of this refractory crust is only achievable at high temperatures (>900°C; Landenberger & Collins 1996); this can occur during prolonged periods of magma underplating, but may require thinning of the crust and heat from asthenospheric mantle (Zhao et al. 2008).

Two possibilities exist for the origin of the heterogeneity in water content in the Sveconorwegian lower crust, 1) that the lower crust was already low in water content prior to the Sveconorwegian orogeny, and that increased water content occurred when there was sufficient volatile flux from subduction, or 2) that the crust didn't have low water content prior to the Sveconorwegian orogeny, and that dehydration zones that sourced ferroan magmas were formed by continued heating and extraction of melts. Given that there is evidence for magmatic underplating and A-type magmatism prior to the Sveconorwegian orogeny, i.e. 1.2 Ga juvenile magmatism in Telemark (Andersen et al. 2007b), and 1.16 Ga charnockite intrusions in Rogaland Vest-Agder (Zhou et al. 1995), it is postulated that the crust was already low in water content prior to the Sveconorwegian orogeny.

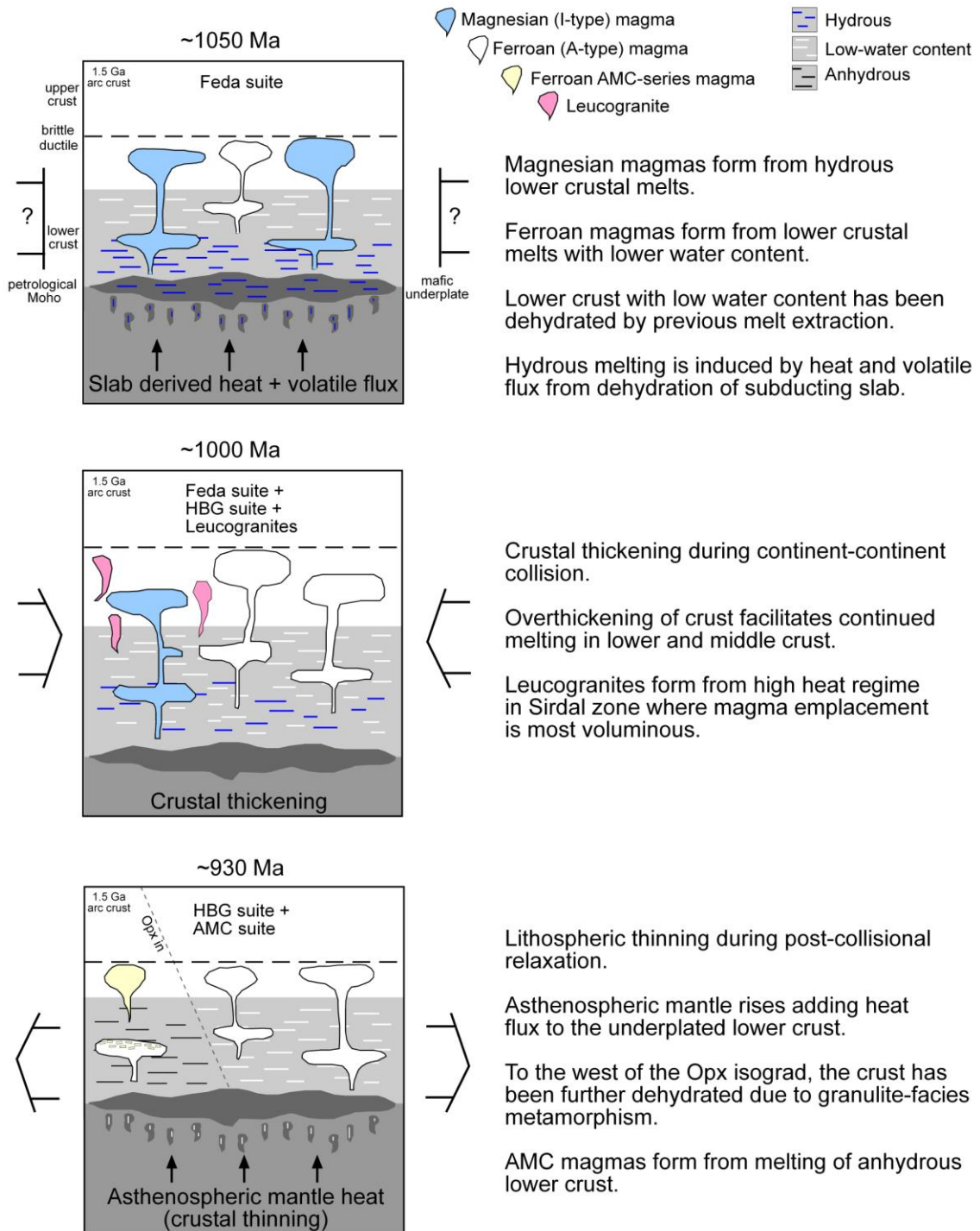


Figure 6.13. Petrogenetic model for the formation of the Feda, HBG and AMC suites; see text for explanation. Modified from Vander Auwera et al. (2008).

6.7.4 Leucogranite formation

The leucogranites (MM2230 and MM26207) have Hf isotopic signatures similar to the HBG and Feda suite (Figure 6.10). The geochemistry of the samples is rather scattered, but in general the data fall on trends that overlap with the Feda suite (Figures 6.3 to 6.6). In the primitive mantle normalised diagram (Figure 6.7) the leucogranites have similar LILE and HFSE enrichments to that of the Feda suite; depletions in Ba, Sr, P, Eu and Ti fall between those of the Feda and HBG suite.

The leucogranite samples have higher silica content than the Fedra suite, and are found spatially with Fedra granitoids. For these reasons, it is hypothesised that the majority of the leucogranites represent highly differentiated members of the Fedra suite.

6.7.5 Continental recycling during Sveconorwegian magmatism

The Hf and oxygen isotopes point to a similar source for both magnesian and ferroan granitoids, and also for early-, syn- and late-Sveconorwegian suites. This source included a component that is substantially greater in age than the granitoids; average model ages fall in the region of 1700 to 1900 Ma. The $\delta^{18}\text{O}$ data suggest that this older component comprised a high- $\delta^{18}\text{O}$ source, such as weathered sediments, thus, the magmatism involved recycling of continental material via intracrustal processes.

The Hf-O data can be produced by remelting of 1.5-1.6 Ga crust that has a high- $\delta^{18}\text{O}$ signature, however, previously determined whole-rock isotope and geochemical studies have shown that both a mantle and crustal component was involved in the petrogeneses of the early- and late-Sveconorwegian granitoids (Bingen et al. 1993; Vander Auwera et al. 2003; Bogaerts et al. 2003; Andersen et al. 2001). For example, Nd and Sr measured on late-Sveconorwegian granitoids in Rogaland, points to bulk mixing between 45-70% depleted mantle, and 30-55% of a crust component (the 'normal deep crust'; Andersen et al. 2001). To compare the new Hf-O data with previously published models, bulk-mixing calculations are discussed.

Figure 6.14 shows ϵ_{Hf} versus $\delta^{18}\text{O}$ that is measured on the same zircons. Shown on this diagram is the range in Hf-O that ~1.5-1.6 Ga crust would have at 950 Ma (based on data presented in Chapter 5). C1 is a crustal component correlative in age with the 1.7-1.9 Ga deep crustal component of Andersen et al. (2001; 2007b; 2009b), and has a high- $\delta^{18}\text{O}$ of +12 compatible with a sedimentary origin. C2 is a crustal component that is equivalent in age to C1, but has a mafic $\delta^{18}\text{O}$ signature; this component is therefore compatible with ancient underplated material. C3 is a crustal component that is young relative to the magmatism (i.e. <1200 Ma), and has high- $\delta^{18}\text{O}$ of +11; this component is compatible with an origin as young weathered sediments that have been derived from the Fennoscandian continent.

Since the oxygen content is assumed to be similar in mantle and crustal rocks, the shape of the mixing curves depends on the Hf concentration of the end-members. The curves shown use either depleted mantle (0.199ppm; Salters & Stracke 2004) or lower crustal (1.9ppm; Rudnick & Gao 2003) values for the mantle end-member, combined with an upper crustal value (5.3ppm; Rudnick & Gao 2003) for the crustal end-member. Using depleted mantle combined with upper crustal values is compatible with a source contamination model; whereas using lower crust combined with upper crust values is compatible with a crustal contamination model. The majority of the granitoids

in this study can be modelled with bulk-mixing between older crustal components that are variable in oxygen values (C1 and C2), with a depleted mantle contribution of 50-70%.

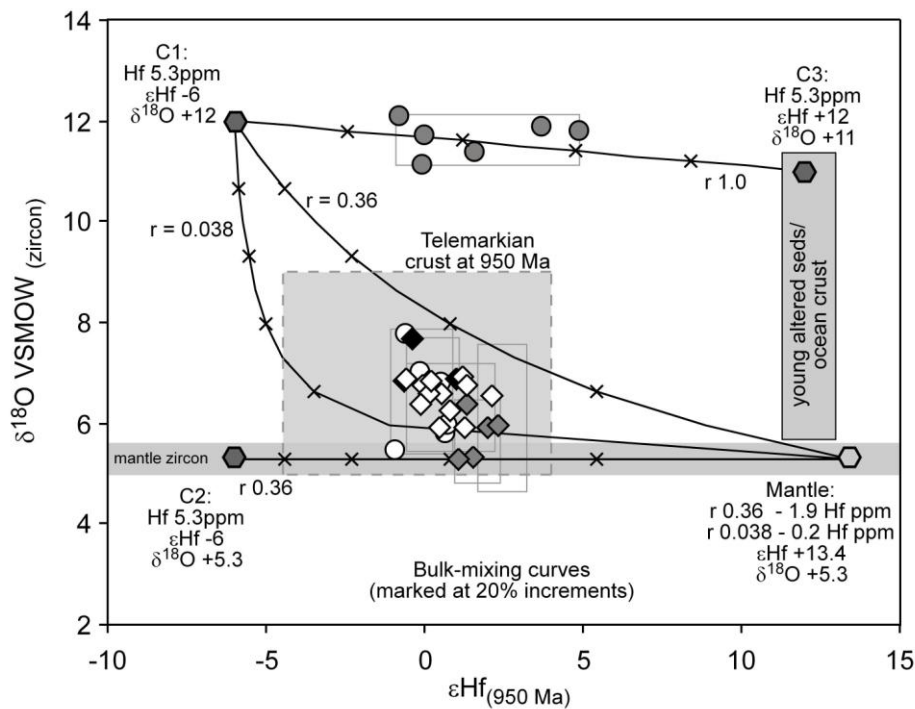


Figure 6.14. $\epsilon\text{Hf}_{(950 \text{ Ma})}$ versus $\delta^{18}\text{O VSMOW}_{(\text{zircon})}$ that are measured in the same zircon domains. The grey dashed box represents average 1.5-1.6 Ga crust at 950 Ma, based on HF-O data in Chapter 5. Values for crust and mantle end-members are discussed in the text. Curves are derived from bulk-mixing calculations, with dashes marking 20% increments. The filled grey bar represents values for young altered ocean crust and overlying sediments. The grey unfilled boxes represent the total range in ϵHf and $\delta^{18}\text{O}$ for each sample. (Symbols as in Figure 6.9).

An anomalously high- $\delta^{18}\text{O}$ granitoid (MM26306) does not fit an array between the depleted mantle and C1/C2 components, and instead suggests mixing with alternative end-members. It may simply be a case that the crust is highly heterogeneous in oxygen, and that the small sample population of this study has fortuitously fallen into two clusters. However, an alternative process is suggested that accounts for the array displayed by the high- $\delta^{18}\text{O}$ granite. This process involves mixing between young high- $\delta^{18}\text{O}$ sediments (C3) and older high- $\delta^{18}\text{O}$ crust (C1). The mixing proportions for this granite require 40-70% of the older crustal component. The introduction of the C3 component to a lower crustal melt generation zone may have occurred via underthrusting during subduction that preceded the continent-continent collision. Such a scenario is advocated for the Grenvillian Frontenac terrane in Laurentia (Peck et al. 2004). However, in this example a whole terrane exhibited a much higher oxygen value than the adjacent terranes. In the example discussed here, it is a single granite that has a much higher $\delta^{18}\text{O}$ value than surrounding granites. Thus, this model is rather speculative and requires further data to be tested. It is worth noting that the geochemistry of the high- $\delta^{18}\text{O}$ granitoid is indistinguishable from granitoids with lower $\delta^{18}\text{O}$; thus highlighting how in-situ zircon data can recognise magma source changes that whole-rock data cannot distinguish.

Mixing calculations in this study are compatible with the Nd-Sr mixing calculations of Andersen et al. (2001), which suggest 30-55% of a crustal component for the HBG suite and 20-35% for the Feda suite; with the crustal component having a $T_{DM}(Nd)$ of 1.9 Ga. The mixing calculations of previous studies, and those described above, do not include the presence of ~1.5 Ga crust. Since crust of such age dominates the exposed upper-crust in the region, it likely did have a contribution to Sveconorwegian magmatism. Evidence for this is provided by ~1.5 Ga inherited zircons in various granites (Table 10.4; Bingen et al. 2005b; Andersen et al. 2009b). Andersen et al. (2009b) advocate three crustal sources for Sveconorwegian granitoids: 1.7 Ga granitoids similar to young members of the TIB, 1.5 Ga felsic igneous rocks, and 1.2 Ga juvenile granitoids; these crustal sources are indicated to have mixed with juvenile mantle-derived material. This hypothesis is compatible with the Hf-O data presented in this study, however, it is expected that the C1 and DM end-members probably contributed much less material than that indicated by two-component mixing, and that the Telemarkian crust had a much larger contribution. In summary, the Hf-O data suggest supracrustal material (weathered sediments) contributed to the magma source of the Sveconorwegian granitoids. The magma source is equivalent to both 1.5 Ga crust, and to a mixture of older crust (~1.7 Ga) and mantle. In-situ Hf data from previous studies have recorded zircon inheritance that suggests input of older (>1.7 Ga) and younger (~1.2 Ga) components.

6.7.6 Reconciling the Hf-O and geochemical constraints

The following two notions can be reconciled into one model that accounts for all of the data: 1) The whole-rock geochemistry of the granitoids suggests derivation from mafic lower crust, which likely occurred via partial melting and fractionation of mafic lower crustal melts to form mafic/intermediate parent magmas, and fractionation of these parent magmas to form the various granitoids (Vander Auwera et al. 2003, 2008; Bogaerts et al. 2003; 2006). 2) The Hf and O (along with previous Hf, Nd and Sr) isotope data indicate contribution from crust that is ~1.5 Ga, ~1.7-1.9 Ga, and ~1.1-1.2 Ga in age, combined with younger mantle-derived material (Andersen et al. 2001, 2002a, 2007b, 2009b; Bingen et al. 1993; Bogaerts et al. 2003).

The origin of a high- $\delta^{18}O$ signature in the older crustal components is largely related to burial of late Palaeoproterozoic supracrustal material and its remobilisation during ~1.5 Ga Telemarkian magmatism (see Chapter 5); continental crust formation via arc magmatism at ~1.5 Ga would have left a residual mafic lower crust that retained a high- $\delta^{18}O$ signature, and a geochemical signature typical of subduction-related magmatism. Underplating may have occurred at 1.2 Ga (Andersen et al. 2007b), adding mafic crust with mantle-like isotopic signatures to the lower crust. During the Sveconorwegian period, the mafic lower crust, in particular its base, will have acted as a zone of mixing, assimilation, storage and homogenisation (i.e. MASH zone; Hildreth & Moorbath 1988). Melting in this MASH zone region produced parent magmas to the Sveconorwegian magmatic

suites. The rather homogeneous isotope and geochemical signatures thus result from derivation from a homogenised mafic lower crustal source. Differences in granite geochemistry result from varying water content (along with smaller effects of oxygen fugacity and pressure). Formation of the Rogaland AMC suite from the same mafic lower crustal source region is compatible with this model; Re-Os data suggest derivation from 1.4-1.55 Ga mafic lower crust (Schiellerup et al. 2000), and Nd-Sr suggest >1.5 Ga crustal components and <1.2 Ga mantle components (Menuge 1988; Bolle et al. 2003a).

6.7.7 Geodynamic setting

The protracted period of magmatism (~1070-920 Ma) requires a significant heat source; this in turn can be related to the tectonic setting and geodynamic regime of the crust in question. The Feda Suite has an ambiguous origin, either relating to crustal thickening during the Sveconorwegian orogeny, or to the late stage of an active continental margin that existed prior to continent-continent collision (e.g. Bingen et al. 2008c). Early Sveconorwegian granites dated at 1039-1069 Ma are emplaced in a region that suffered little effects of the Sveconorwegian orogeny (Slagstad et al. 2008; Chapter 3), and metamorphism related to crustal thickening is not recorded until 1035 Ma (Bingen et al. 2008b), thus, a subduction-setting is favoured for the early-Sveconorwegian granitoids. This setting will also provide a volatile flux for producing the hydrous magmas (magnesian members of the Feda suite). During the peak continent-continent collision phase, the crust is inferred to be overthickened (Bingen et al. 2008b); this may have provided further heat for lower crustal melting. Between 980 and 940 Ma the geodynamic regime in the region changed from compressional to extensional (Bingen et al. 2008b), voluminous granitoid emplacement in this period suggests a continued heat flux to the lower crust. The late-Sveconorwegian granites <970 Ma, have been explained by rise of asthenosphere after delamination of underthrust lithosphere (Vander Auwera et al. 2003; Duchesne et al. 1999); this model is partly explained by the linear alignment of the HBG Suite in relation to the Mandal-Ustaoset Shear Zone. Thus, the origin of heat flux to the lower crust has varied over the Sveconorwegian period; however, there are no distinct pauses or changes in magmatism that can identify a change in geodynamic regime.

6.7.8 Continental growth during Sveconorwegian magmatism

Determining the extent of juvenile mantle addition to the magmatic suites has its inherent problems; the low Lu/Hf of both zircons and crustal rocks means that even in a hundred million years, the measured $^{176}\text{Hf}/^{177}\text{Hf}$ ratio will not change significantly enough to be discernable. For example, in this study the mantle component in bulk-mixing modelling is calculated using depleted mantle at 950 Ma, however, the youngest mantle contribution could be mafic underplate that is as old as 1.2 Ga (Andersen et al. 2007b). Thus, the data point to contribution from mantle that is 1.2 Ga or younger, but also indicate a significant proportion of recycled crust that is ~1.5 Ga and older. Overall, the Sveconorwegian period has seen a significant degree of remobilisation of older crust,

and a limited volume of crustal growth (mantle addition). This crustal remobilisation (or intracrustal recycling), where felsic plutons form in the upper crust and mafic residues are produced in the lower crust, is an important process that aids the stratification and differentiation of the continental crust.

6.8 Conclusions

Voluminous granitic magmatism occurred in southwest Norway from ~1070 to 920 Ma. All granitoids display features associated with subduction-related magmatism, i.e. alkali-calcic to calc-alkaline, metaluminous to weakly peraluminous, and depletion in Nb, Ti, and P. The early- to syn-Sveconorwegian granitoids feature both magnesian (I-type) and ferroan (A-type) magma series. The late-Sveconorwegian granitoids are more iron-enriched and have a greater A-type signature. The Fennefoss suite (not sampled; Bingen & van Breemen 1998) has geochemistry transitional but more towards the ferroan suites. The change between ferroan and magnesian magma series can be explained by changes in crystallising conditions (namely the water content) as opposed to changes in magma source.

Magmatism prevailed during differing geodynamic regimes, from supra-subduction, to collisional, and then to extensional. Throughout these different regimes the heat source will have varied; however, both the magma source and the process of granite production likely stayed the same. The Hf-O data suggest the magma source involved a large contribution from crust ~1.5 Ga and older, as well as a contribution from mantle-derived material that is 1.2 Ga or younger. This magma source was mafic lower crust that had homogeneous isotopic and geochemical characteristics imparted from previous magmatic episodes, and that was partially melted and fractionated to form parent magmas to the individual granitoid suites.

This study highlights: 1) how weathered continental crust may contribute to the source of I and A-type granitoids, 2) how such granitoids can form in a variety of tectonic settings as long as there is significant heat flux, and 3) how the conditions in the melt generation zone impart the strongest control on the geochemistry and petrography of granitoid suites.

The 1.24 Ga Grossæ-Totak suite, a new age confirms an old correlation in the Telemark supracrustals, southern Norway

Aim – This chapter presents the first U-Pb age from the Grossæ-Totak belt in the Telemark Sector. Correlations between this and other supracrustal belts within SW Fennoscandia are discussed, as is the tectonic setting of ‘interorogenic’ units within the region.

7.1 Introduction

From ~1800 to 1500 Ma, Fennoscandia is considered to have grown along its southwestern margin via oceanward migration of a long-lived subduction zone (Åhäll & Connelly 2008), i.e. a retreating accretionary orogen (Cawood et al. 2009). The Telemarkia block is suggested to represent a continuation of this south-westerly growth, thereby extending continental growth via arc magmatism to at least ~1460 Ma (see Chapters 4, 6 and 9; Slagstad et al. 2008). Following the 1.8-1.46 Ga growth of SW Fennoscandia, the crustal domains were subject to repeated episodes of magmatism. These have previously been referred to as interorogenic events (Åhäll & Connelly 1998; Bingen et al. 2003); however, it is now increasingly recognised that these magmatic events likely occurred in response to convergent-margin processes on the SW margin of Fennoscandia (Brewer et al. 2004; Söderlund et al. 2005; Söderlund & Ask 2006).

Within the Telemarkia terrane, the Suldal and Hardangervidda Sectors are home to the Sæsvatn-Valldall rift basin that formed at ~1.26 to 1.21 Ga (Bingen et al. 2002; Brewer et al. 2004). In the Telemark Sector, rift basins formed earlier at ~1.5 Ga (Vestfjordallen Supergroup, Laajoki et al. 2002; Dahlgren 1990), and later at ~1.16 Ga (Sveconorwegian Supergroup, Laajoki et al. 2002, Bingen et al. 2003). In the Setesdal region of southern Telemark, supracrustal deposition and calc-alkaline plutonism occurred between 1320 and 1200 Ma (Pedersen et al. 2009); the exact tectonic setting during this period is undefined, but the geochemistry points to a supra-subduction zone setting. The extensional basins that formed in the Telemarkia terrane are typically not correlated across the Mandal-Ustoaset Shear Zone which separates the Suldal and Rogaland Sectors from the Telemark Sector (Figure 7.1). In the original mapping of this region (Sigmond 1975, 1978), the Grossæ-Totak supracrustal belt in Telemark was speculatively correlated with the Sæsvatn-Valldall supracrustal belt in Suldal. Since then, this correlation has not existed in the published literature; the Grossæ-Totak belt is not included in published map figures and is not defined in the tectonostratigraphy e.g. Corfu & Laajoki 2008), but is assumed to correlate with the younger 1.17-1.14 Ga Sveconorwegian Supergroup (Bingen, pers. comm. 2010).

7.2 Geological Setting

The Telemarkia block comprises four sectors; the Telemark Sector in the east, and the Rogaland, Suldal and Hardangervidda Sectors in the west. In Hardangervidda the oldest outcropping rocks may be as old as 1.65 Ga (Ragnhildsvet et al. 1994). However, gneisses with >1.5 Ga zircon ages have since been interpreted as paragneiss units (Bingen et al. 2005b). In all of the sectors the basement comprises volcanic-plutonic gneisses and granitoids that are 1.55-1.46 in age and likely formed in a continental arc setting (Bingen et al. 2005b; Chapter 4). The Sæsvatn-Valldall supracrustal belt formed within the Suldal Sector at 1.26-1.21 Ga (Bingen et al., 2002; Brewer et al., 2004). At 1.22-1.16 Ga, orthopyroxene-bearing granitoids intruded the Rogaland Sector (Slagstad et al. 2008; Zhou et al. 1995). Abundant metasediments within the Rogaland Sector, including those with passive-margin facies, are suggested to have formed within an extensional basin that formed as Rogaland rifted away from Suldal (Slagstad et al. 2008). The Sirdal Zone (Slagstad et al. 2008) that divides the Rogaland and Suldal Sectors comprises ~1.05 Ga porphyritic granitoids that formed as a result of convergent-margin magmatism possibly related to the subduction of Rogaland under the Suldal Sector (Slagstad et al. 2008), although they may also reflect crustal melting after thickening during the early stage of the Sveconorwegian orogeny (Bingen et al. 2008c). Late-Sveconorwegian granites (0.98-0.93 Ga; Andersen et al. 2002a, 2007a) and a 0.93 Ga Anorthosite-Mangerite-Charnockite complex (Schärer et al. 1996) intruded the Rogaland and Suldal Sectors after the main collisional phase of the Sveconorwegian orogeny.

The Telemark Sector features a >10km thick succession of supracrustals comprising the 1.5->1.35 Ga Vestfjorddalen, and 1.16-1.10 Ga Sveconorwegian Supergroups (Laajoki et al. 2002). The Vestfjorddalen Supergroup comprises the bimodal 1.51 Ga Rjukan Group and the overlying sedimentary Vindeggan Group. Bimodal magmatism is related to continental extension that occurred inboard of a subduction zone in a setting similar to the Granite-Rhyolite provinces in the mid-continental US (Slagstad et al. 2009). The Vemork Formation that is part of the Rjukan Group is dominated by metabasalt units; an intercalated metavolcanite is dated at 1495 ± 2 Ma (Laajoki & Corfu 2007). The 5km thick Vindeggan group comprised mostly of quartz-rich strata; a cross-cutting diabase intrusion dated at 1347 ± 4 Ma (Corfu & Laajoki 2008) places a minimum age constraint on sedimentary deposition within the group. The Sveconorwegian Supergroup comprises bimodal volcanic and sedimentary sequences deposited between 1.17 and 1.12 Ga (Laajoki et al. 2002; Bingen et al. 2003), that formed in extensional basins inboard of a continental arc (Brewer et al. 2004), or in a Basin and Range setting (Bingen et al. 2003). Intrusions in the Telemark Sector include 1.22-1.2 Ga juvenile granitoids (Andersen et al. 2007b), 1.19-1.13 Ga A-type plutons (Bingen et al. 2003), and a 1.03 Ga suite transitional between calc-alkaline and A-type (Bingen & van Breemen 1998). The Setesdal valley in the southwest of the Telemark Sector is host to the

oldest crust recognised in the sector, the Asen tonalite (1555 ± 29 Ma), and calc-alkaline gneisses and supracrustals formed between 1.32-1.14 Ga (Pedersen et al. 2009).

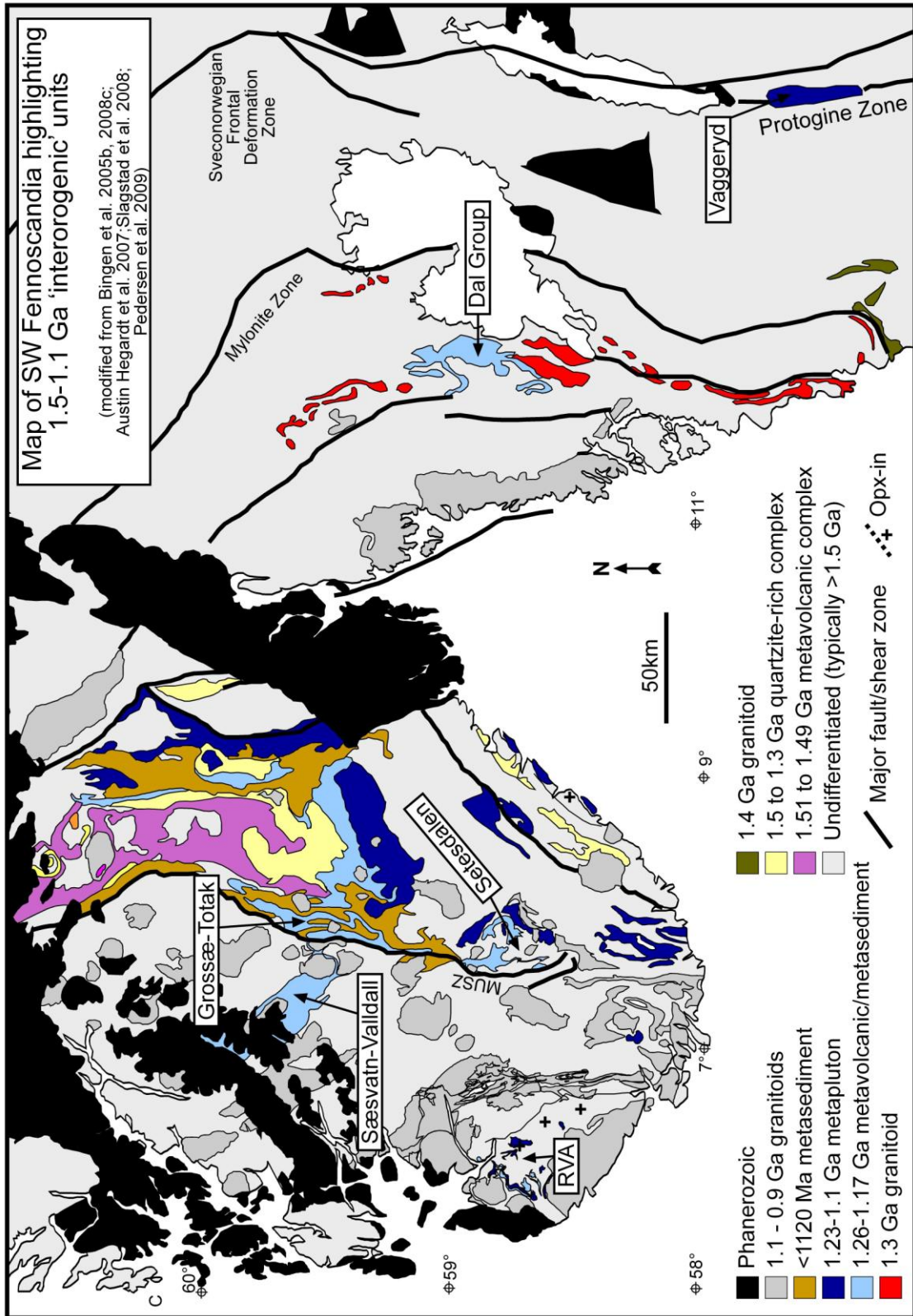


Figure 7.1. Map of SW Fennoscandia highlighting post-1.5 Ga and pre-Sveconorwegian units. RVA = Rogaland Vest-Agder, MUSZ = Mandal-Ustaøset Shear Zone.

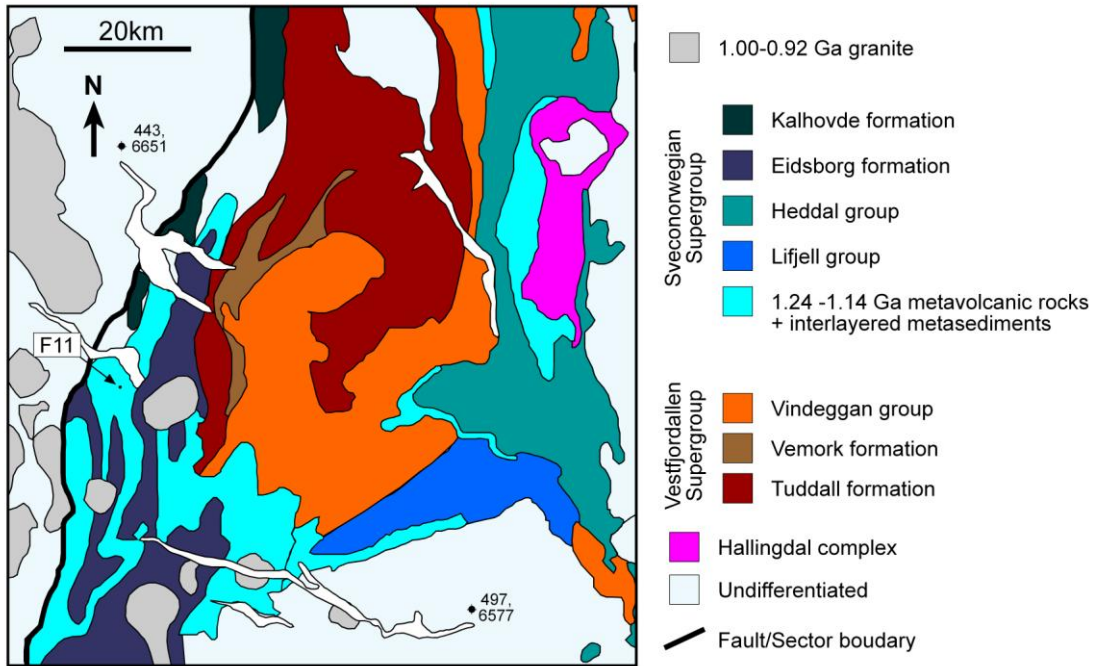


Figure 7.2. Map of the southern part of the Telemark supracrustals, showing the location of the dated Fjellhovdane metarhyolite (F11). Modified after Bingen et al. (2003) and Corfu & Laajoki (2008).

7.3 Sample description and results

The sample that has been dated is a metarhyolite from the Fjellhovdane unit towards the base of the Totak sequence (Figure 7.3), and formed part of the study of the Telemark supracrustals undertaken by Brewer (1985). The sample comprises fine-grained quartz and feldspar, with epidote, Fe-Ti oxides and rare muscovite; coarser quartz grains have developed into stringers. Zircon occurs as an accessory phase.

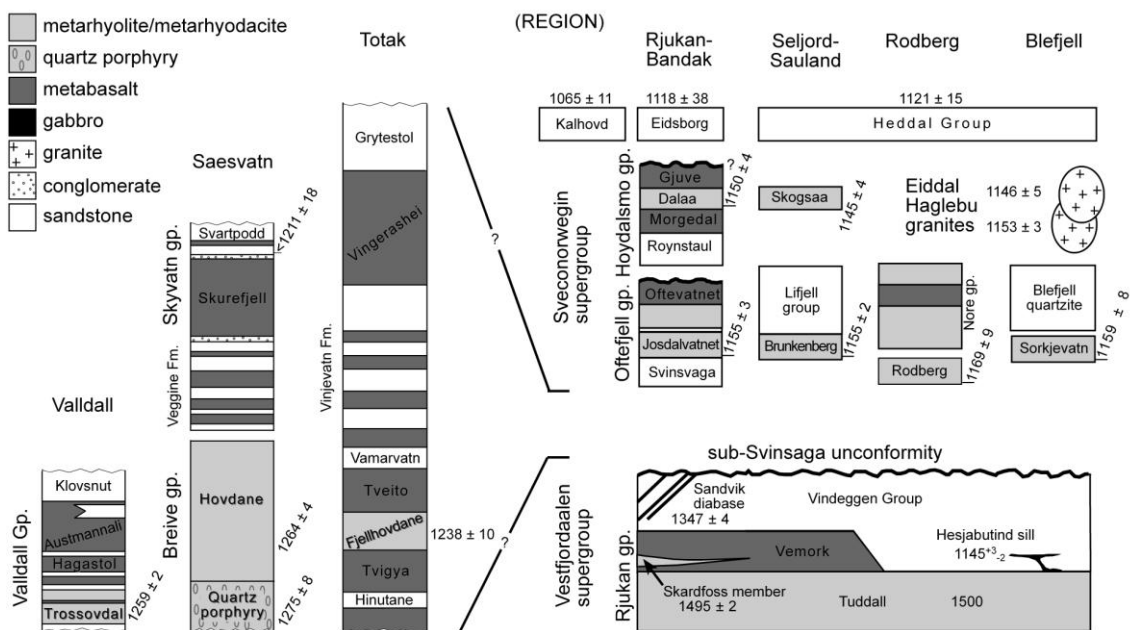


Figure 7.3. Stratigraphy of supracrustal belts within Telemarkia, based on Sigmond (1978), Bingen et al. (2002), Brewer et al. (2004) and Corfu & Laajoki (2008).

U-Pb geochronology used the LA-ICP-MS method outlined in Chapter 3; the zircons were not chemically abraded. 18 analyses provide a weighted mean $^{207}\text{Pb}/^{206}\text{Pb}$ age of 1238 ± 10 Ma (MSWD = 3.6), using an external error of 34 Ma. This age is interpreted to reflect the crystallisation of the rhyolite.

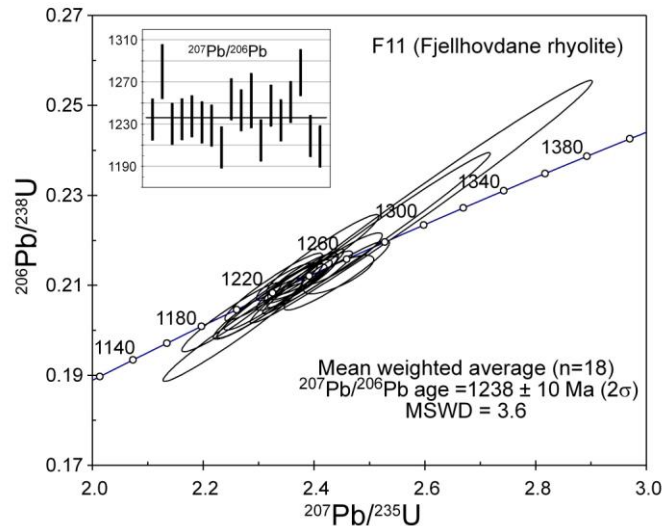


Figure 7.4. U-Pb concordia showing results of LA-ICP-MS dating of the Fjellhovdane rhyolite.

7.4 Discussion

In regional maps, the Grossæ-Totak supracrustal belt is grouped under the Sveconorwegian Supergroup, and is thus assumed to have a 1.17-1.14 Ga depositional age. The 1236 Ma age of the Fjellhovdane rhyolite shows that the Grossæ-Totak belt is older than the Sveconorwegian Supergroup, and is in fact much closer in age to the Sæsvatn-Valldal Belt in the Suldal Sector (1.26-1.21 Ga; Bingen et al. 2002; Brewer et al. 2004). As well as a similar age, the Grossæ-Totak and Sæsvatn-Valldal belts have similar characteristics that suggest they formed by similar tectonic and magmatic processes, namely, early rhyolitic volcanism followed by voluminous basaltic volcanism, with intercalated quartz-rich sediments (Brewer et al. 2004). The geochemistry and whole-rock Nd and Hf isotope systematics of the Sæsvatn-Valldal Belt are interpreted to represent rhyolite formation by crustal anatexis, early basaltic volcanism involving significant crustal contamination, and later basaltic volcanism tapping a mantle source and undergoing less crustal contamination (Brewer et al. 2004). The initial crustal anatexis is produced by basalt intrusion into the crust as a consequence of lithospheric thinning (Brewer et al. 2004). The geochemistry of the Grossæ-Totak rhyolites is similar to the Trossodal rhyolites of the Sæsvatn-Valldal belt (Figure 7.5), suggesting that similar crustal rocks underwent melting to form the rhyolites. Both suites feature highly enriched LILE, enriched HFSE, elevated LILE/HFSE ratios, and relative depletion in Nb, Sr, P and Ti. These features are suggestive of a continental arc setting (Wilson 1989; Pearce 1982). In the Suldal Sector, Telemarkian rocks likely formed in a continental arc setting (Chapter 4), and thus

provide a potential candidate for crustal protoliths that underwent melting to form the rhyolites in the Sæsvatn-Valldall belt. In the Telemark sector, similar age lithologies are not recorded at the surface, which is largely due to the more widespread younger sedimentary cover in this region. Assuming the Fjellhovdane rhyolite formed by the same tectonothermal process as for the formation of the Trossovdal rhyolite, the geochemistry suggests that continental arc rocks are located at depth within the Telemark Sector, lending support to the hypothesis that the Telemark block grew by continental arc magmatism in the Telemarkian period (Bingen et al. 2005b).

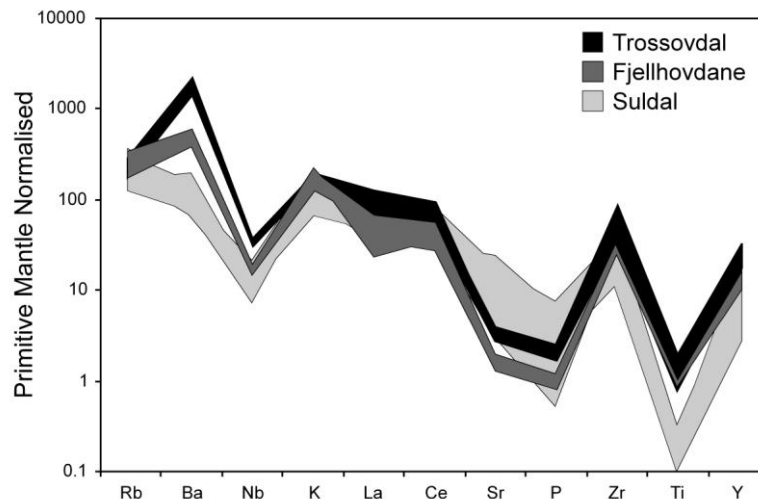


Figure 7.5. Primitive Mantle normalised (Sun & McDonough, 1989) plot for felsic units within the Sæsvatn-Valldall belt (Trossovdal), Grossæ-Totak belt (Fjellhovdane) and metaplutonic/volcanic basement within the Suldal Sector (Sauda). Trossovdal data from Brewer et al. (2004); Suldal data from Chapter 4.

Gneisses of the Vravatn Complex in Telemark are slightly younger than the Grossæ-Totak belt, with ages of ~1220-1200 Ma, and have Hf isotope signatures that suggest formation with a significant depleted mantle input (Andersen et al. 2007b). This juvenile magmatism is interpreted to reflect an episode of mafic underplating in the region (Andersen et al. 2007b). In the Setesdal region, south of the Grossæ-Totak belt, supracrustals were deposited between 1320 and 1200 Ma (Pedersen et al. 2009). Hf isotopes from this region suggest that a change in magmatism from a dominantly older crustal input to a juvenile input occurred between 1220 and 1215 Ma (Pedersen et al. 2009). This provides further supporting evidence for mafic underplating of the crust. The deposition of volcanic and sedimentary rocks with associated juvenile mafic intrusions, spanning the period from 1320 to 1200 Ma, is probably linked to the same long-lived tectonic process. This involved mafic underplating and intrusion, crustal anatexis, and continental sedimentation in rift basins. As suggested by Brewer et al. (2004), the lithospheric extension that allowed for these processes was likely linked to extension of the overriding plate in a subduction setting, i.e. the extensional basins are back-arc expressions of a long-lived convergent margin. Continental arc rocks of equivalent age are not recorded in the region, although the Tromøy Block located off the

southeast coast of Telemarkia does have a postulated island-arc origin (Knudsen & Andersen 1999), attesting to convergent margin processes in the region. If a continental arc located to the west of Telemarkia did exist at 1300-1200 Ma, then this crust must have been recycled by subduction erosion, or translated to a different continental region during the Sveconorwegian orogeny.

In the eastern parts of the Southwest Sveconorwegian Domain (SSD) the magmatic record for the 1300-1200 Ma time period is dominated by mafic magmatism in localised extensional settings. This includes the 1300 Ma Våstergotland dolerite suite in the Idefjorden terrane, the 1.27-1.26 Ga Central Scandinavian Dolerite Group across central Scandinavia, and the 1.22-1.2 Ga Protogine Zone dolerites in the Eastern Segment/Idefjorden terrane boundary zone (Söderlund et al. 2005). The latter features granite and syenite intrusions as well as mafic magmatism (Johansson 1990).

The 1300-1200 Ma events in Telemarkia are distinct from those in the eastern part of the SSD, i.e. in the west there was basin formation with deposition of sediments and associated bimodal volcanism, and in the east there was localised mafic magmatism with minor felsic magmatism. This contrast lead Corfu & Laajoki (2008) to suggest a more outboard and exotic origin for the Telemarkia terrane, as similar characteristics are recorded in the Composite Arc Belt of the Grenville province in Laurentia (Carr et al. 2000). However, the Dal Group in the Eastern Segment is an extensional basin that is interpreted to be a more distal equivalent of ~1.16 Ga supracrustals in the Sveconorwegian Supergroup (Bandak Group; Brewer et al. 2002). The Dal Group comprises quartzite, slate, mafic volcanics, and arkose that are interpreted as forming in a rift basin (Alm et al. 1997; Lundberg 1973), with deposition bracketed between 1.05 and 1.33 Ga (Romer & Smeds 1996; Piontek et al. 1998). Thus, although the timing of Dal Group deposition is not well constrained, it provides a link between the western and eastern parts of the SSD.

At ~1300-1200 Ma, the contrast between extensional basin formation in Telemarkia and formation of discrete mafic intrusions in Idefjorden and further east, may be a consequence of the difference in thermal properties of the crust. The younger Telemarkia block may have been a warmer, more mobile and thus weaker domain, whereas the older Idefjorden and Eastern Segment were probably colder, thicker and stronger crustal domains. This difference led to broad and widespread extension in Telemarkia and discrete more localized extension in the east.

7.5 Conclusions

A U-Pb age of 1238 ± 10 Ma for the Fjellhovdane rhyolite indicates that the Grossæ-Totak supracrustal belt is older than the Sveconorwegian Supergroup (1.17-1.14 Ga), and overlaps in age with the Sæsavtn-Valldal supracrustal belt (1.26-1.21 Ga). This confirms a correlation made by Sigmond (1978) in the original mapping of the region. This age widens the temporal and spatial

extent of 1300-1200 Ma magmatism, and suggests that the tectonostratigraphy of the supracrustals in the Telemark Sector needs revision. The Grossæ-Totak belt is interpreted to be part of a widespread extensional phase affecting southern Norway, which occurred in response to a convergent margin that likely existed to the west of the current Norwegian coastline.

In-situ U-Pb and Hf isotopes constrain the age & provenance of the Hardangervidda-Ryfylke Nappe Complex, SW Norwegian Caledonides

Aim - This chapter presents the first U-Pb and Lu-Hf data from Caledonian nappe units exposed in the Suldal Sector; the data are used to constrain the age and provenance of nappe units from a variety of structural levels. Correlations with nappe complexes elsewhere are discussed, as are insights into the Mesoproterozoic history of Fennoscandia.

8.1 Introduction

The Scandian phase of the Caledonian orogeny resulted in the continental margin of Fennoscandia being subducted underneath Laurentia, imbricated and thrust eastwards onto the foreland, with nappe displacements of up to several hundreds of kilometres (Roberts & Gee 1985). The Caledonian nappes have been traditionally divided into the Lower, Middle and Upper Allochthons. The Lower Allochthon comprises Precambrian basement and overlying cover sediments that can be correlated with autochthonous units; the Middle Allochthon comprises allochthonous Fennoscandian Precambrian basement and cover sediments from the continental margin and ocean-continent transition zone; the Upper Allochthon comprises lower Iapetus-derived oceanic units; and above this the Uppermost Allochthon comprises exotic units that are inferred to have a Laurentian ancestry (e.g. Gee 1975; Roberts & Gee 1985; Stephens & Gee 1985; Roberts 2003).

The Precambrian crystalline units found within the Caledonian nappes likely are parts of the Fennoscandian basement and record the Mesoproterozoic growth of Fennoscandia, including the continent's evolution during the amalgamation and break-up of the supercontinent Rodinia. Thus, the information recorded in the Caledonian nappe units is relevant to aid our understanding of palaeotectonics in the Precambrian of the Baltic Shield. Studies of the Scandinavian Caledonides have traditionally focussed on key areas (e.g. the Western Gneiss Region), leaving other regions less understood. The Hardangervidda-Ryfylke Nappe Complex (HRNC) in SW Norway is one such area, having received little attention since being mapped in the seventies (Naterstad et al. 1973; Andresen 1974; Sigmond 1975). The lack of U-Pb geochronology conducted on this nappe complex is especially hindering correlation with units elsewhere in Scandinavia.

8.2 Geological Setting

The allochthonous rocks south of the Hardangerfjord were grouped together as the Hardangervidda-Ryfylke Nappe Complex by Naterstad et al. (1973). In the Haukelisater-Røldal area, the HRNC can be subdivided into three allochthonous units (Andresen & Færseth 1982), these are (from the base

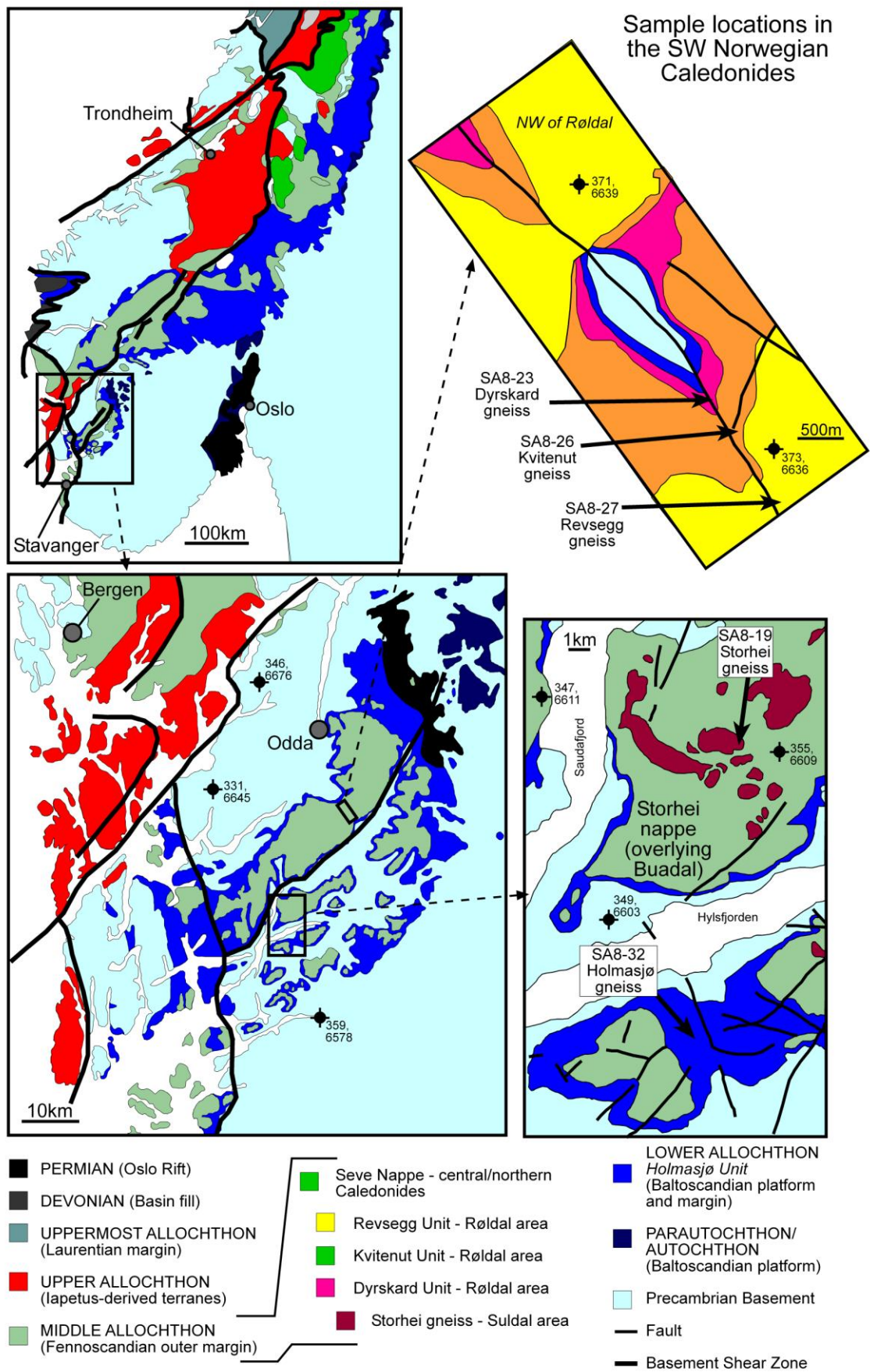


Figure 8.1. Geological map of the southern Norwegian Caledonides, and sample localities (indicated by arrows). After Gee et al. 2008; Sigmond 1975.

upwards) the Holmasjø allochthon, Nupsfonn allochthon, and the Dyrskard-Kvitenut-Revsegg allochthon. These units are separated by ductile shear zones that formed in amphibolite-facies (Andresen 1974). Southwest of Haukelisater-Røldal in the Sauda-Suldal area, two nappe units have been recognised, these are the Buadal and Storhei units (Sigmond 1978). The same units cannot be traced all the way from Hardangervidda southwest to the coast, this is due to both displacement along shearzones within the nappe complex, and the limited extent of some units; however, similarities in the general structure of the complex do exist in all areas. Thus, the term Hardangervidda-Ryfylke Nappe Complex and its reference to the entire complex of nappes outcropping south of the Hardangerfjord are kept here. The following is a summary of published data on the nappe units of the HRNC that are sampled in this study; for further review the reader is referred to Sigmond (1978) and Andresen & Færseth (1982).

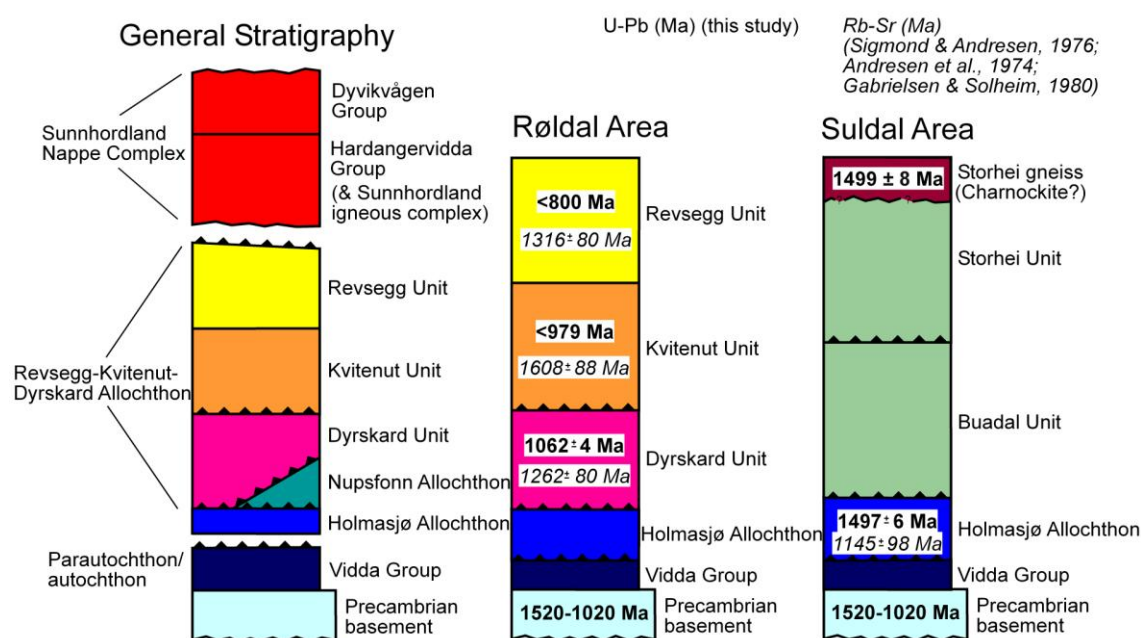


Figure 8.2. Tectonostratigraphy of the Hardangervidda-Ryfylke Nappe Complex, including new and published ages. Modified from Sigmond (1978) and Andresen & Færseth (1982).

8.2.1 Holmasjø unit (Lower Allochthon)

The Holmasjø unit comprises non-calcareous schists and phyllites commonly interspersed with thin quartzite layers and pods. The unit is metamorphosed in greenschist facies, with biotite and garnet formation recorded in some areas, although retrogression to chlorite is widespread (Naterstad et al. 1973). Polyphase deformation is evident in the unit. Low-angle thrust faults dip northwest and trend northeast-southwest; the transport direction along these is thought to be to the southeast and east, but with the dominant deformation phase being that of extension or back-thrusting to the northwest (Andresen & Færseth 1982). Locally, faults cut down into the basement so that basement slices can be found along the base of the unit (Andresen & Færseth 1982). Phyllites were dated in the Hardangervidda region by whole-rock Rb-Sr, giving an age of 409 ± 15 Ma (Andresen et al. 1974).

The basal allochthon in the Suldal region, which has been correlated with the Holmasjø unit, contains a metaandesite that has been dated by whole-rock Rb-Sr at 1145 ± 98 Ma (Sigmond & Andresen 1976). Holmasjø Unit phyllites in the study area are thought to represent a deeper water facies of the Cambrian to Lower Ordovician sediments of the Parautochthonous Vidda Group (Andresen 1978); in this case the Precambrian metaandesite may represent a thin thrust slice of crystalline basement caught up with younger cover sediments.

8.2.2 Storhei unit (Middle Allochthon)

The Storhei unit is dominantly composed of layered gneisses, with subordinate augen gneiss, quartzite and amphibolite layers; the layered gneisses may have supracrustal origins (Sigmond 1978). Previous work suggests that the top of the unit comprises charnockitic gneisses, with acid to basic compositions and both foliated and massive varieties (Sigmond 1978). Diabase dykes with garnet and clinopyroxene intrude the charnockitic gneisses (Sigmond 1978). The layered gneisses are amphibolite-grade, with staurolite occurring west of Saudafjord (Sigmond 1978). The charnockitic rocks have reached granulite-facies, with the assemblage clinopyroxene-hypersthene-garnet-plagioclase-quartz recorded in massive gneisses; in the foliated rocks this is present as relics or has been replaced by amphibolite-facies assemblages (Sigmond 1978). No rocks within the Storhei or underlying Buadal nappe have been previously dated. The boundary between the Storhei and underlying units is a mylonitic thrust zone, but is gradational in terms of lithological change (Sigmond 1978).

8.2.3 Dyrskard unit (Middle Allochthon)

The Dyrskard unit is composed of volcanic and sedimentary supracrustal rocks, dominated by metabasalts, metarhyolites and quartzites (Andresen & Gabrielsen 1979). From the base upwards the unit comprises 1) banded supracrustal gneisses, 2) quartzite, feldspathic sandstones and mica schists with minor basic to intermediate metavolcanics, 3) amphibolites with quartzite and marble horizons, and 4) acid metavolcanics (Gabrielsen 1980). Metabasalts have a restricted extent, whereas the metarhyolites are widespread (Gabrielsen 1980). Kyanite in a mica-schist, a plagioclase-amphibole-garnet assemblage in the amphibolites, and the lack of migmatization, attest to medium-grade metamorphism under relatively high pressure (Sigmond 1978). Chlorite after biotite/amphibole records retrogression in greenschist-facies (Andresen 1974). Polyphase deformation is evident within the unit; the oldest phase occurred prior to thrusting of the overlying nappe units, and the youngest phase represents Caledonian folding (Sigmond 1978). Five samples from varying lithologies gave a whole-rock Rb-Sr isochron of 1289 ± 80 Ma (Andresen et al. 1974). Another age determination was made at c. 1520 Ma (Gabrielsen & Solheim, in Gabrielsen & Solheim 1980), with the authors concluding that the 1289 Ma age was a mixed age and unreliable.

Thrust zone blastomylonites that occur between the Dyrskard and the overlying Kvitenut unit have also been dated by whole-rock Rb-Sr, giving an age of 1504 ± 41 Ma (Gabrielsen et al. 1979).

8.2.4 Kvitenut unit (Middle Allochthon)

The Kvitenut unit comprises quartzofeldspathic gneisses with subordinate calc-silicate rocks and migmatized gneisses. The lowermost part of the unit features mylonitic gneisses, whereas migmatite formation occurs in the upper part of the unit (Naterstad et al. 1973). Minor lithologies within the banded gneisses include marble, mica schist, diopside fels and plagioclase-diopside-epidote rocks (Andresen 1974). Gneissic intrusive bodies ranging from gabbro to granite that cut earlier fabrics are common, but do not cut the boundary into the underlying Dyrskard unit (Naterstad et al. 1973; Andresen & Færseth 1982). The migmatization and development of schlieren in amphibolitic rocks, and the sillimanite/kyanite assemblages attest to medium- to high-grade metamorphism under medium to high pressure (Sigmond 1978). However, most of the unit has been retrogressed to amphibolite facies (Andresen 1974). The unit features multiple stages of deformation, most of which occurred in amphibolite-facies conditions and are interpreted as pre-Caledonian (Andresen & Færseth 1982). Some of the deformation occurred prior to thrusting of the unit above the underlying Dyrskard unit. An amphibolite gneiss has been dated by whole-rock Rb-Sr at 1643 ± 88 Ma (Andresen et al. 1974), which was interpreted as a metamorphic age.

8.2.5 Revsegg unit (Middle Allochthon)

The Revsegg unit is composed of muscovite-biotite gneisses with quartzo-feldspathic pods, concordant boudins of amphibolite and some cross-cutting intrusive bodies (Naterstad et al. 1973). The dominant rock type is a two-mica gneiss that has a variably developed schistosity. Interbedded with the mica gneiss is a hornblende-biotite gneiss that is commonly boudinaged. Large intrusive bodies are not found, but minor bodies of granodiorite and quartz-diorite apparently postdate the peak metamorphism and earliest structures (Andresen & Færseth 1982). The Revsegg unit is interpreted to have been deposited on the underlying Kvitenut unit (Naterstad et al. 1973), although this remains to be proven. The mineral assemblage biotite-muscovite-garnet-sillimanite/kyanite suggests medium-grade metamorphism under medium pressure (Sigmond 1978). The deformation recorded in the Revsegg unit is similar to that in the Kvitenut complex. Revsegg gneisses have been dated by whole-rock Rb-Sr and give ages of 440 ± 250 Ma (Andresen et al. 1974) and 1316 ± 80 Ma (Gabrielsen & Solheim 1980). The latter age was interpreted as a mixed age but constraining a minimum age for deposition, and the younger age indicates an influence from the Caledonian orogeny.

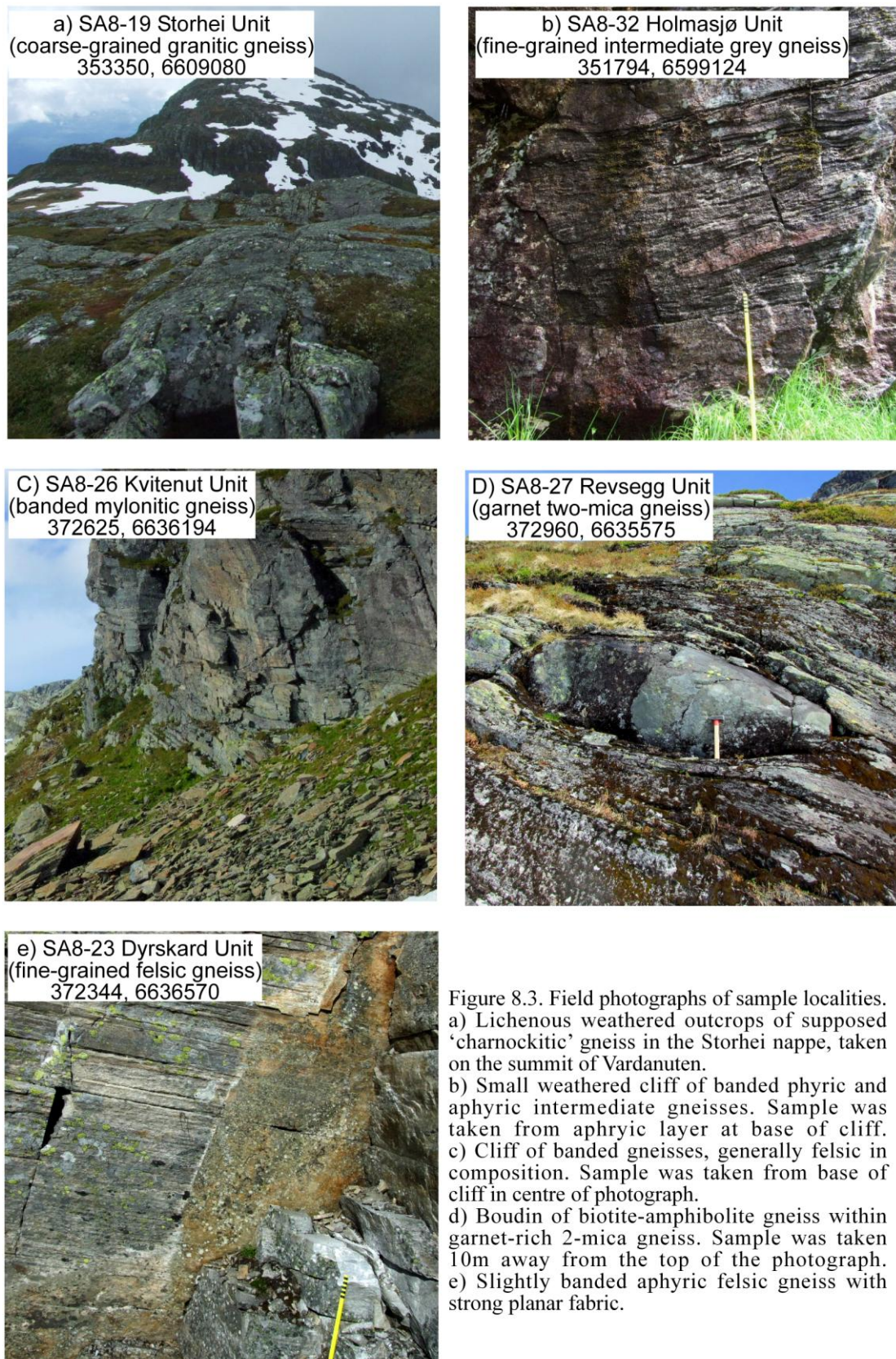


Figure 8.3. Field photographs of sample localities. a) Lichenous weathered outcrops of supposed ‘charnockitic’ gneiss in the Storhei nappe, taken on the summit of Vardanuten. b) Small weathered cliff of banded phryic and aphyric intermediate gneisses. Sample was taken from aphyric layer at base of cliff. c) Cliff of banded gneisses, generally felsic in composition. Sample was taken from base of cliff in centre of photograph. d) Boudin of biotite-amphibolite gneiss within garnet-rich 2-mica gneiss. Sample was taken 10m away from the top of the photograph. e) Slightly banded aphyric felsic gneiss with strong planar fabric.

8.3 Rationale for isotope work

The scarcity of Rb-Sr age determinations and the questions over their reliability in mixed age populations, and the lack of any U-Pb dating, means a number of key issues relating to the HRNC

remain unresolved. For example: 1) does the tectonostratigraphy represent sequential emplacement of nappe units from more distal locations upon more proximal units, i.e. does the stratigraphically highest unit represent the most distal unit? 2) related to the former question, do the nappe units young upwards as would be expected from simple imbrication and stacking of the continental margin? 3) what age are the cross-cutting rocks described in some units and do they correlate with

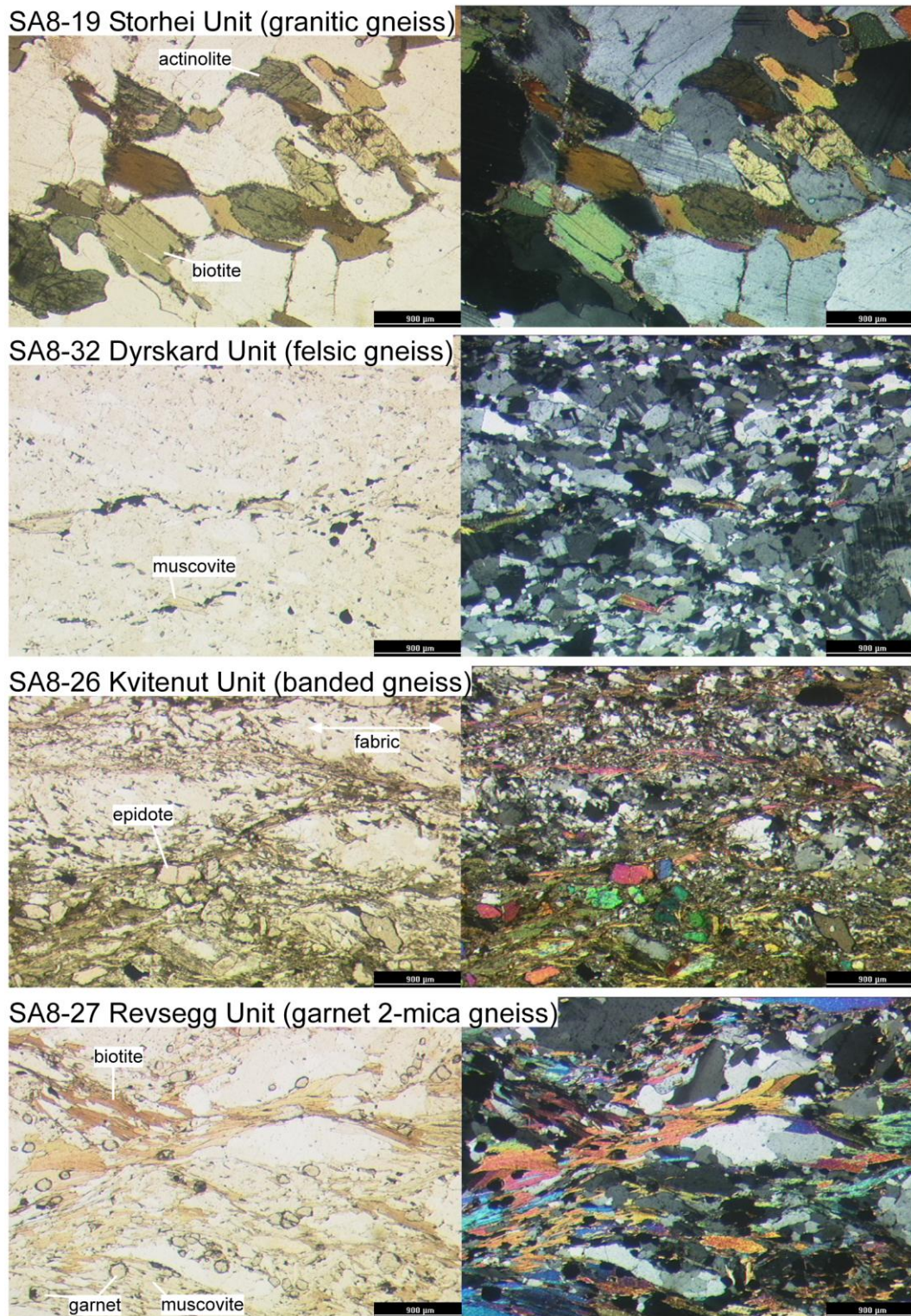


Figure 8.4. Thin section photomicrographs of sampled Middle Allochthon gneisses.

Sveconorwegian, Neoproterozoic or Caledonian events recorded elsewhere? 4) Do any of the nappe units correlate with Mesoproterozoic autochthonous rocks within the region? To answer some of these questions, one sample was collected and analysed from each of five different nappe units.

8.4 Sample Description

8.4.1 SA8-32 Holmasjø Unit (fine-grained intermediate grey gneiss)

SA8-32 is an aphyric massive fine-grained grey gneiss of intermediate composition. The sampled outcrop comprises decimetre scale bands of aphyric and feldspar-phyric units of similar composition that feature a weakly developed planar fabric. The outcrop was poorly exposed so that tracing with other units was not possible, but the location matches the description of metaandesitic gneisses previously dated at 1145 Ma (Sigmond & Andresen 1976). The sample is composed of fine to medium-grained quartz, feldspar, amphibole, biotite and epidote, with abundant retrogression of biotite and amphibole to chlorite. Separated zircons are prismatic, elongate and feature oscillatory zoning. Some grains feature truncations between cores and outer zones, and many feature thin CL-bright rims.

8.4.2 SA8-19 Storhei Unit (coarse-grained granitic gneiss)

SA8-19 is a weakly deformed coarse-grained granitic gneiss. The sample was taken from poorly exposed weathered outcrops on the summit of Vardanuten. Other lithologies in the area include white feldspar-rich veins, and migmatitic gneisses with well-developed leucosome formation. The location correlates with the charnockitic gneisses mapped by Sigmond (1975). The sample comprises quartz, feldspar, actinolite and biotite. The mafic minerals are variably distributed and occur as individual laths, schlieren, or up to 3cm-across aggregates in less-foliated areas. Feldspars are both plagioclase and microcline, and also feature myrmeckite development. Opaque grains are complex and include rutile overgrowths on ilmenite. Exsolution textures are visible in the opaques and in the other mafic minerals. Although no pyroxene or garnet was observed, the exsolution and overgrowth textures suggest a possible relic high-grade metamorphism. Separated zircons are generally elongate and oscillatory zoned, often featuring irregular zones or embayments that may represent alteration and/or metamictisation. Truncations between core and outer zones exist in some grains, and a few also feature CL-bright rims.

8.4.3 SA8-23 Dyrskard Unit (fine-grained felsic gneiss)

SA8-23 is a fine-grained quartz-feldspar gneiss with a strong planar fabric. The outcrop features bands (likely originating as bedding) of this felsic gneiss, along with bands of more intermediate composition which are typically feldspar phyric. The outcrop matches the description of acidic banded gneisses that occur in the upper parts of the Dyrskard Unit (Gabrielsen 1980). The sample is composed of fine-grained quartz, feldspar, biotite, muscovite, epidote and opaque grains. A fabric is

seen as alignment of mica laths, and development of coarser bands of quartz and feldspar. The geochemistry of the sample (figure 8.7) indicates a rhyolitic protolith was likely for this sample. Separated zircons are prismatic, generally elongate, and feature regular oscillatory-zoning. There is a lack of truncations between growth zones, and the grains do not exhibit any metamorphic or alteration rims.

8.4.4 SA8-26 Kvitenu Unit (mylonitic banded gneiss)

SA8-26 is a mylonitic gneiss comprising mm- to cm-scale alternating pink, grey and black bands. The sample is taken from the base of a cliff which is interpreted to be the base of the unit; the outcrop comprises mylonitic banded gneisses of varying composition. Felsic bands within the sample comprise quartz, feldspar, and minor biotite, epidote and titanite grains. The more mafic bands comprise a much greater content of biotite, but also feature abundant coarse grains of titanite, epidote minerals and a pale amphibolite. These grains are fairly spherical and rounded, and likely originate as phenocrysts that have been rounded during mylonitisation. The protolith of the sample is not obvious, the description of the unit refers to granodioritic and granitic gneisses (Naterstad et al. 1973), which is generally appropriate for the sampled outcrop; however, it is not clear whether the alternating bands of different composition represent sheared igneous lithologies, or banding due to a sedimentary origin. Separated zircons are of various morphologies and textures, commonly oscillatory zoned, but also sector zoned and some with no obvious zonation; the variety of zircons suggests a sedimentary protolith may be appropriate. CL-bright rims occur on some grains not treated by chemical abrasion (see 8.6); after treatment the chemically abraded grains are often skeletal.

8.4.5 SA8-27 Revsegg Unit (garnet two-mica gneiss)

SA8-27 is a mica-rich gneiss quartz-feldspar gneiss, with quartz and feldspar occurring as both fine-grained matrix minerals, and also as cm-scale pods. Boudinaged amphibolite pods exist in the sampled area and are concordant to the structural fabric. The sample represents the two-mica gneiss that occurs in the basal part of the unit (Naterstad et al. 1973). Biotite and muscovite are the dominant minerals, and form an anastomosing extensional shear fabric. Garnet is abundant, and forms small euhedral grains that are both cross-cutting and aligned to biotite cleavage. Chlorite that has replaced biotite during retrogression is weakly developed. Kyanite was not seen in the thin section but was abundant in the mineral separate, and thus likely forms distinct horizons within the gneiss. Separated zircons exhibit a wide variety of morphologies and textures, which is compatible with a sedimentary origin for the protolith; the abundance of mica suggests a semi-pelitic composition. The chemically abraded grains are typically skeletal, whereas the untreated grains are rounded and commonly feature oscillatory zoning.

8.5 Analytical Methods

Analytical methods follow those described in Chapter 3 (U-Pb), Chapter 4 (whole-rock geochemistry) and Chapter 5 (Lu-Hf).

8.6 Results – U-Pb

8.6.1 SA8-32 Holmasjø Unit (fine-grained intermediate grey gneiss)

Ten non-abraded zircon grains were analysed and all gave nearly concordant ages. Nine out of ten analyses provide a weighted mean $^{207}\text{Pb}/^{206}\text{Pb}$ age of 1497 ± 6 Ma, with a MSWD of 2.3. The rejected analysis has a slightly younger $^{207}\text{Pb}/^{206}\text{Pb}$ age of 1464 ± 10 Ma, and may reflect modest lead-loss due to Sveconorwegian or Caledonian events. The 1497 Ma age is interpreted to represent the crystallisation age of the igneous protolith.

8.6.2 SA8-19 Storhei Unit (coarse-grained granitic gneiss)

Nineteen chemically abraded zircons grains were analysed; these were all nearly concordant but gave a spread of ages. Nine overlapping grains form a defined group at 1480 ± 20 to 1512 ± 12 Ma. Three overlapping grains form a slightly younger group at 1421 ± 22 to 1456 ± 19 Ma. Five concordant grains are dated at 1198 ± 18 , 1251 ± 32 , 1302 ± 18 , 1323 ± 25 , 1365 ± 26 Ma. The two youngest grains are dated at 1021 ± 23 and 1024 ± 27 Ma. Some of the ~1100-1400 Ma grains appear to have analyses that overlap different growth zones; however this is not applicable to all of this population. The age population is interpretable in a number of ways. The sample may represent a sedimentary protolith with a detrital zircon population. Or, the sample may represent a ~1500 Ma protolith with Sveconorwegian overprinting, with ages representing mixtures of these ages. Or, the sample may represent a ~1500 Ma protolith with younger ages representing lead-loss, and Sveconorwegian ages representing new growth. The ~1500 Ma population of zircons feature similar oscillatory zoning and morphologies, with dark outer growth bands. Younger grains also feature similar characteristics. The two Sveconorwegian grains feature more diffuse zoning and less prismatic morphology. A sedimentary origin of these zircons is thus unlikely as a greater variety of morphologies is likely to exist in this case. Since some of the analyses cross different growth zones, some mixing between ~1500 Ma and ~1000 Ma may have occurred. The favoured interpretation is that the two Sveconorwegian grains are new zircon growth during this orogenic event. Lead-loss may have produced some of the younger ages, but is unlikely to be the sole cause in the spread of ages. Thus, the age population is interpreted as a ~1500 Ma protolith age, and a zircon-growth event at ~1020-1030 Ma.

8.6.3 SA8-23 Dyrskard Unit (fine-grained felsic gneiss)

Eleven chemically abraded zircon grains were analysed; these were all relics of oscillatory-zoned prismatic grains. All eleven analyses provide a weighted mean $^{207}\text{Pb}/^{206}\text{Pb}$ age of 1062 ± 4 Ma with

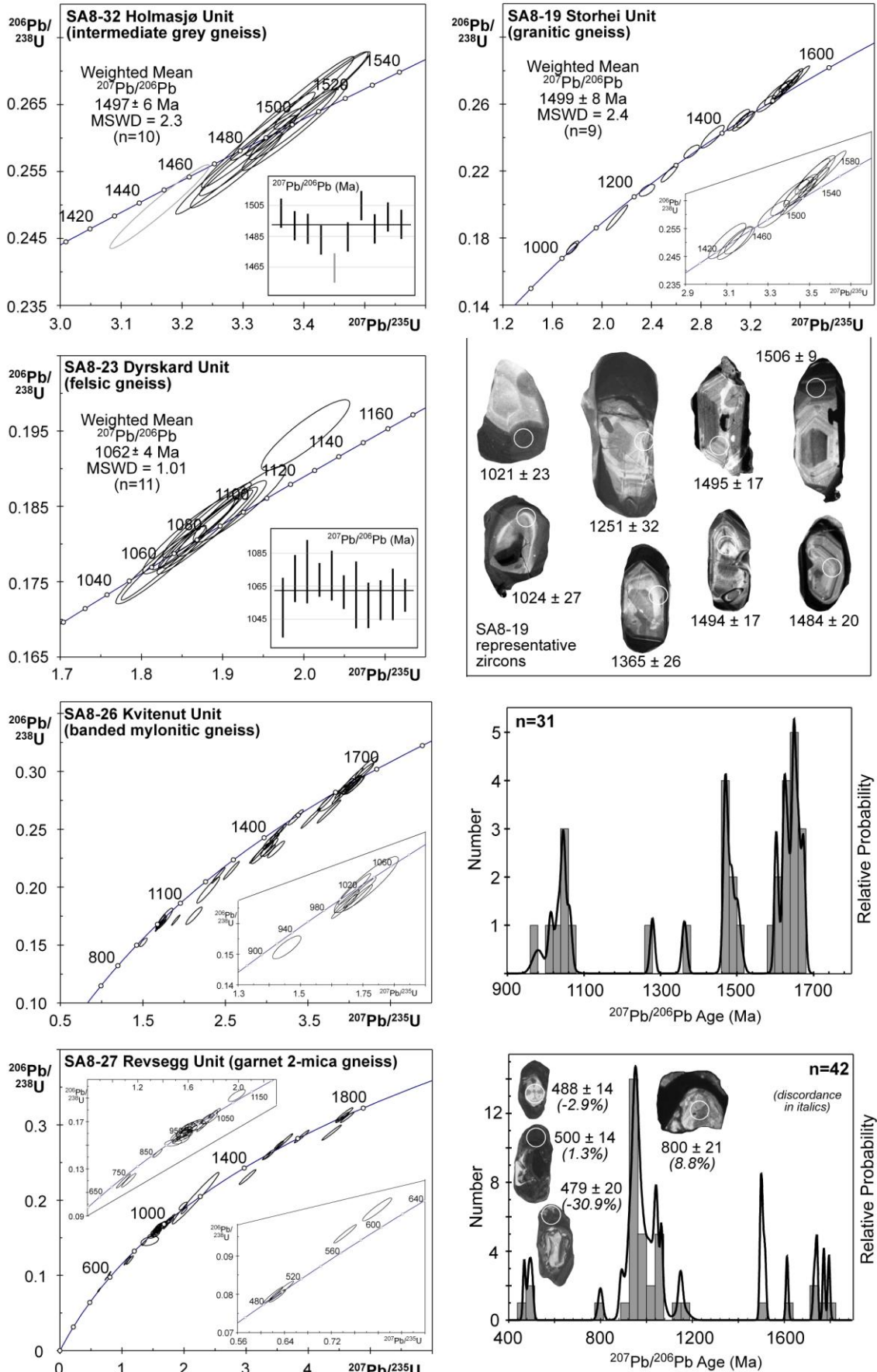


Figure 8.5. Selection of zircon grains and results of U-Pb dating, shown as concordia plots and cumulative probability plots for detrital samples (excluding grains with >10% discordance).

a MSWD of 1.01. The analyses are concordant to weakly reversely discordant; one grain is strongly reversely discordant, but has a $^{207}\text{Pb}/^{206}\text{Pb}$ age that is equivalent to the mean of the group at 1060 ± 20 Ma. The reverse discordance is likely related to inter-element fractionation differences between the sample and standard as a consequence of chemical abrasion (see Chapter 3). The 1062 Ma age is interpreted to represent crystallisation of the igneous protolith.

8.6.4 SA8-26 Kvitenuit Unit (mylonitic banded gneiss)

41 chemically abraded zircon grains were analysed. 4 inferior analyses were rejected due to high common lead or low ^{207}Pb signals. 6 of the accepted grains have normal discordance greater than 10%. A multi-age population is exhibited, ranging from 979 to 1674 Ma. On the cumulative probability plot three major peaks are displayed at 1.01 to 1.06 Ga, 1.46 to 1.5 Ga, and at 1.6 to 1.67 Ga. These correspond to early- Sveconorwegian, Telemarkian and early-Gothian magmatic episodes respectively. There are two other concordant grains dated at 1278 ± 12 , and 1362 ± 13 Ma. The youngest grain has a $^{207}\text{Pb}/^{206}\text{Pb}$ age at 979 ± 29 Ma. The analyses were nearly all conducted on inner cores of grains. Each peak in the cumulative probability plot is represented by zircons with varying morphologies and zoning patterns, suggesting a detrital origin for the zircons, and thus a sedimentary origin for the protolith. The grains are sub-rounded which is compatible with this interpretation, although the chemical abrasion has masked this to an extent. The youngest grain suggests deposition of the protolith after 979 ± 29 Ma, multiple analyses of this grain would have been preferred to confirm this age, as some lead-loss may have effected this grain. A significant population (n=6) of varying morphologies ranging from 1013 to 1062 Ma indicates the maximum age of deposition is younger than this population.

8.6.5 SA8-27 Revsegg Unit (garnet two-mica gneiss)

30 chemically-abraded zircon grains and 31 untreated grains were analysed. 2 analyses were rejected due to high common lead or a low ^{207}Pb signal. 5 of the accepted grains had discordance greater than 10%. A multi-age population is exhibited, ranging from 800 to 1795 Ma. On the cumulative probability plot a major peak is displayed at 0.9 to 1.06 Ga (27 grains). Smaller peaks are at 1.73 to 1.8 Ga (4 grains), at 1.5 Ga (4 grains) and at 1.15 Ga (2 grains). Two other grains are concordant at 0.8 and 1.61 Ga. The three youngest grains have ages of 468 ± 11 , 500 ± 14 , and 488 ± 14 , and occur on CL-dark outer zones and a bright metamict core respectively. The range in morphologies and zoning patterns is compatible with a detrital origin. The ~940 to 960 Ma grains exhibit a range in morphologies, mostly with oscillatory zoning; the 800 Ma analysis is from a core of a grain with zoning typical of igneous zircons. The 470-500 Ma analyses are conducted on outer growth-zones and a metamict core, and are interpreted as zircon growth and metamictisation during early-Caledonian events. In this case, deposition is constrained to be younger than the ~940-960 Ma population, and possibly as young as <800 Ma if this grain represents a true detrital age.

8.7 Results – Hf

Each of the three samples interpreted as having igneous origins (SA8-32, SA8-19, SA8-23) has a range in $\epsilon\text{Hf}_{(T)}$ of three to four epsilon units, which is within the range of analytical error (typically $\pm 2\epsilon$). Weighted average $\epsilon\text{Hf}_{(T)}$ values are 6.0 ± 1.0 for SA8-32 (MSWD = 2.2), 2.5 ± 0.9 for SA8-23 (MSWD = 1.9) and 2.1 ± 1.0 for the ~1500 Ma population of SA8-19 (MSWD = 1.5). These values overlap the field for autochthonous basement of Sveconorwegian and Telemarkian age (Figure 8.6).

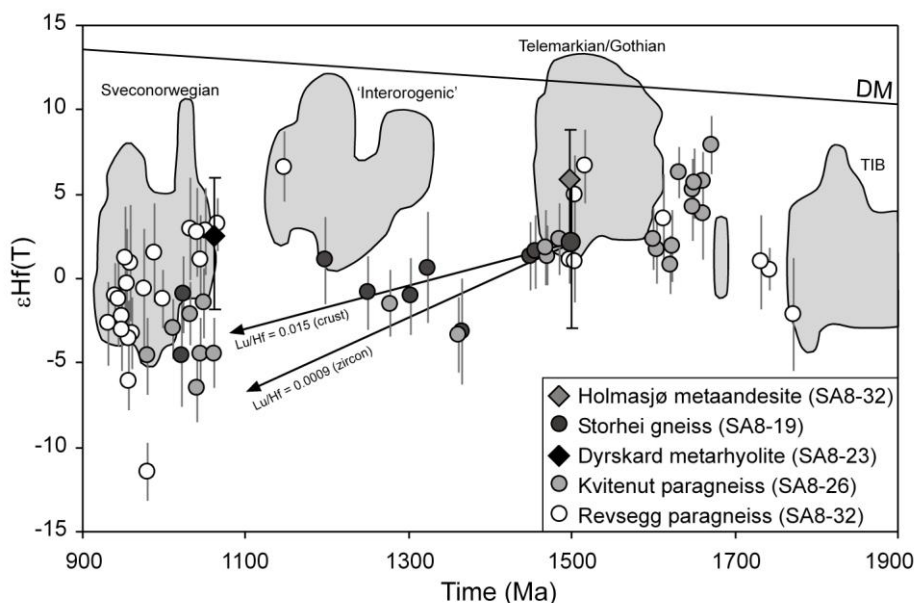


Figure 8.6. $\epsilon\text{Hf}_{(T)}$ vs. Time (Ma) for HRNC gneisses compared with data for autochthonous basement rocks in SW Fennoscandia (grey fields). Fields are plotted from data in Chapters 5 and 6, and Andersen et al. 2002b, 2004a, 2007b, 2009a; Andersen & Griffin 2004; Pedersen et al. 2009. SA8-23 and SA8-32 are shown as weighted mean averages with the black error bars representing the total range of values including 2sigma error. The 1500 Ma population of SA8-19 is also shown as a weighted mean value. The rest of the SA8-19 data and SA8-27 and SA8-26 are shown as individual analyses with grey error bars representing 2sigma. The depleted mantle (DM) value of Griffin et al. (2000) is used, along with the CHUR values of Bouvier et al. (2008).

The evolution of Lu-Hf in a closed-system zircon will be different to that in a piece of crust due to the difference in the abundance of these elements. Evolution lines are drawn in figure 8.6 for typical continental crust ($\text{Lu}/\text{Hf} = 0.015$) and for the average zircon concentration ($\text{Lu}/\text{Hf} = 0.0009$), starting at the 1500 Ma population of SA8-19. The younger zircons of this sample have errors in $\epsilon\text{Hf}_{(T)}$ which overlap both of these evolution lines, thus, the Hf data cannot distinguish between a lead-loss or mixed age origin for these younger grains.

The detrital samples (SA8-26 and SA8-27) have $\epsilon\text{Hf}_{(T)}$ that broadly correlate with the autochthonous basement rocks (Figure 8.6). There is an abundance of 1650-1700 Ma age grains that do not correlate in age with the basement, however, this likely results from sampling bias, since

1650-1700 Ma age rocks are common within the Eastern Segment and within the Western Gneiss Region (e.g. Tucker et al. 1990; Åhall & Connelly 2008) but do not have published Hf data.

8.8 Discussion

8.8.1 Origin of the nappe units

Holmasjø Allochthon

The ~1500 Ma age for the intermediate gneiss (SA8-32) from the Holmasjø allochthon correlates with the Telemarkian (1520-1480) age for much of the autochthonous basement within the region (Bingen et al. 2005b; see Chapter 3). Thrust faults within the unit have been observed to cut down locally into this autochthonous basement (Andresen & Færseth 1982). The displacement of the unit is in the order of several tens of kilometres (Andresen & Færseth 1982). Thus, it seems likely that the sample is from a slice of basement that is locally derived (<100km displacement), and has been imbricated with younger allochthonous phyllites during Caledonian thrusting.

Storhei Gneiss

The Buadal and Storhei nappe units that make up the crystalline allochthonous units in the Suldal region have little known about them. In the sampled area (east of Saudafjord) the rocks are assigned to the Storhei Nappe, with charnockites occurring in the upper section (Sigmond 1978). The relationship between the charnockitic rocks and the amphibolite-facies gneisses that comprise the rest of the unit is unknown (Sigmond 1978). During this study, the relationship between supposed charnockitic rocks and other gneiss units was not observed due to poor exposure. Definite charnockite lithologies were also not observed, even when they were previously mapped as charnockite. Thus, the possible relic granulite-facies history of gneisses in the Storhei Unit remains to be explored.

The ~1500 Ma age and $\varepsilon_{\text{Hf}(T)}$ of the Storhei gneiss is similar to that of the Telemarkian age crust that dominates the autochthonous rocks (Figure 8.6). Based on the assumption that the sampled rock has an igneous origin, the Storhei nappe likely comprises Telemarkian crust that existed northwest of the present coastline prior to Caledonian shortening. It is not known whether the sampled gneiss has been disrupted by younger intrusive units, or if high-grade metamorphism occurred at ~1020 Ma or at a younger age. However, granulite-facies rocks are recorded at Stavsnuten in the Kvitenut unit (Andresen 1974), therefore a possible correlation with this adjacent Middle Allochthon unit may exist in terms of metamorphic history.

Dyrskard Unit

The quartzite-dominated sediments and bimodal volcanics of the Dyrskard Unit are interpreted to have formed in a continental margin environment (Gabrielsen 1980). The geochemistry of the dated

metarhyolite (Figure 8.7) has a signature indicative of a supra-subduction setting (e.g. enriched LILE & negative Nb, Ti, P anomalies). The geochemistry is strikingly similar to metarhyolites (Trossovdal Fm.) of the ~1260 Ma Saesvatn-Valldall sequence that are interpreted to have formed in a continental-rift or back-arc (Bingen et al. 2002; Brewer et al. 2004), that also comprise bimodal volcanics and intercalated sediments. The 1062 Ma age and geochemistry for the Dyrs kard metarhyolite is also correlative with autochthonous early-Sveconorwegian granitoids that occur in the region (Chapter 6). These granitoids are related to an E/NE dipping subduction zone that was active prior to continent-continent collision at ~1035 Ma (Bingen & van Breemen 1998; Slagstad et al. 2008), although granitoids of this suite have also been interpreted to result from crustal thickening during Sveconorwegian orogenesis (Bingen et al. 2008c). The geochemistry and sedimentology of the Dyrs kard supracrustals is interpreted here to represent deposition in a shallow marine environment located on a fore- or retro-arc foreland basin. This is compatible with the existence of an early Sveconorwegian arc located on the Fennoscandian margin (Slagstad et al. 2008).

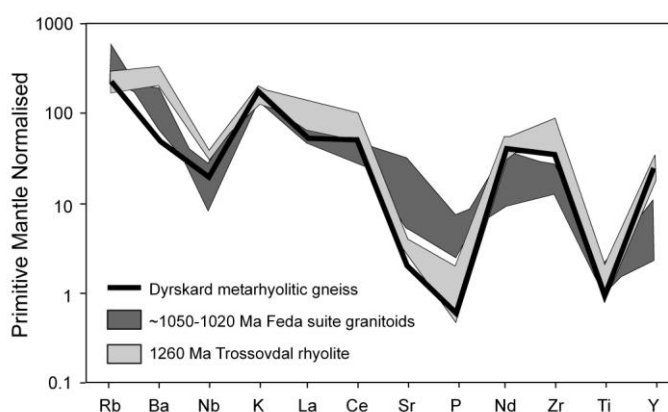


Figure 8.7. Primitive mantle normalised (Sun & McDonough 1989) plot of the Dyrs kard metarhyolitic gneiss (SA8-23) compared with the ~1260 Ma Trossovdal metarhyolite (Brewer et al. 2004), and ~1050 Ma Feda suite granitoids (see Chapter 6).

Kvitenut and Revsegg Units

The Kvitenut and Revsegg metasedimentary gneisses were deposited after the main Sveconorwegian orogenic phase within the region (1035-1000 Ma; Bingen et al. 2008c), with single detritus zircon ages suggesting deposition after 979 Ma for the Kvitenut Unit, and possibly as young as <800 Ma for the Revsegg Unit. There are no exact minimum age constraints on the deposition of the sediments, except that they have been deformed during Caledonian orogenesis, with interpreted new zircon growth at ~500 Ma in the Revsegg Unit.

The Revsegg paragneiss contains a much greater content of Sveconorwegian age zircons than the Kvitenut paragneiss, with fewer early-Mesoproterozoic zircons (see Figure 8.8). This may be

related to uplift and increased weathering of the Sveconorwegian-aged crust during the early Neoproterozoic, as has been interpreted for correlative deposits in NW Scotland (Kirkland et al. 2008b). The oldest grains in both samples are c. 1700 Ma, suggesting that 1500-1700 Ma Telemarkian-Gothian crust may have had enough relief to inhibit flow of detritus from Archaean-Palaeoproterozoic sources, this feature has also been attributed for sedimentary deposits in Scotland and Greenland (Cawood et al. 2004).

The metasedimentary lithologies within the Kvitenut and Revsegg units are poorly described; however, the Kvitenut Unit is dominated by quartz-feldspar-rich gneisses, whereas the Revsegg Unit is dominated by mica-rich gneisses. Thus, it seems reasonable to interpret the Revsegg Unit as having a more distal marine origin than the Kvitenut Unit, with mica gneisses in the former representing more pelitic protoliths.

Late Mesoproterozoic to Neoproterozoic sedimentary sequences are found throughout the North Atlantic Region, in both autochthonous and allochthonous positions, for a review of ages and correlations see Cawood et al. (2007) and Kirkland et al. (2008b). In the Scandinavian Caledonides, detrital zircons from sedimentary units have been dated hitherto from allochthonous units in south-central Norway (Valdres; Bingen et al. 2005a, 2009), in the central Norwegian-Swedish Caledonides (Seve-Köli nappes; Ladenberger et al. 2009), and in the northernmost Norwegian Caledonides (Kalak Nappe Complex; Kirkland et al., 2006, 2007).

The Kalak Nappe Complex (KNC) has been assigned to the Upper Allochthon but has a debated origin. Recent work has postulated an exotic origin for the KNC, based on the fact that 850-690 Ma igneous intrusions dated within the allochthon are not found in the Fennoscandian autochthon (Kirkland et al. 2006, 2007; Corfu et al. 2007). However, palaeocurrent data from sediments in the lower part of the KNC favour a Fennoscandian source (Roberts 2007). As highlighted by Roberts (2007), the argument for an exotic origin of the KNC is based on negative evidence, i.e. the fact that igneous rocks of the appropriate age are not currently known from the autochthon. The Kvitenut and Revsegg units may provide insight into this argument, as they comprise metasedimentary rocks that correlate in depositional age with those in the KNC (<~980 Ma), and that are cross-cut by igneous units.

In the central Scandinavian Caledonides, the allochthonous rocks from bottom to top are: mylonitic granites and psammites, the Särvi Nappes, the Seve Nappe Complex (SNC) and the Köli Nappes. These originate as the imbricated Fennoscandian basement, continental margin sediments, continent-oceanic transition zone, and Iapetus-derived oceanic terranes. The Dyrskard-Kvitenut-Revsegg allochthon can be correlated with the lower part of the sequence, comprising basement

slices and shallow marine to continental shelf deposits. The U-Pb detrital signatures recorded from the Kvitenut and Revsegg units are also comparable to metasedimentary units from the lower Seve nappe (Ladenberger et al. 2009), which has deposition <850 Ma, and peaks at 1000, 1400 and 1650 Ma.

In the Seve-Köli Complex, the Seve nappe units have reached granulite-facies metamorphism during Caledonian orogenesis (Claesson 1987), whereas the underlying Sarv and Offerdal nappes and the overlying Köli nappes are lower grade. This has led to the ductile extrusion of the high-grade Seve Nappe Complex being compared to the channelised flow model for the Himalayan orogeny (Ladenberger et al. 2009). The Dyrskard-Kvitenut-Revsegg allochthons has similarities to the SNC, with the central Kvitenut complex preserving higher-grade metamorphism and migmatization than the overlying Revsegg and underlying Dyrskard units. Further work is needed to elucidate whether these units were extruded in a large orogen-scale channel, or whether they were emplaced as separate nappe complexes at different times.

Metasedimentary units within Scotland correlate in age with the studied Kvitenut and Revsegg paragneisses. Detrital age patterns show some similarities; however, those in Scotland have been correlated with a Laurentian source (see Cawood et al. 2007). In the central Scandinavian Caledonides, sedimentary units from both the Lower and Middle Allochthons have been dated using detrital zircons (Bingen et al. 2005a; 2009). The zircon populations are similar to those dated here from the HRNC, and to those from the other regions discussed above, however, a population of grains at 620 ± 14 Ma in the Lower Allochthon constrains an Ediacaran maximum age of deposition (Bingen et al. 2005a). Because the minimum age of deposition for the sedimentary units is not constrained, it is not known whether the Kvitenut and Revsegg Units correlate with this Ediacaran period of deposition, or with older Tonian (1000-850 Ma) deposits such as those in the Kalak Nappe Complex.

Distinguishing between a Laurentian and a Fennoscandian source is problematical, as the tectonothermal evolution of both continents is very similar throughout the Palaeo- to Mesoproterozoic. In a recently proposed model, post-Sveconorwegian sedimentation occurred in the North Atlantic region in the Asgard sea that formed by the clockwise rotation of Fennoscandia in relation to Laurentia (Cawood et al. 2010); the sedimentary successions were affected by tectonothermal events (Renlandian – 980-910 Ma and Knoydartian – 830-710 Ma), defining the Valhalla Orogen. Events in the Valhalla orogen are tectonically discrete from those in the Sveconorwegian orogen, as they formed in an external accretionary orogen as opposed to the interior Sveconorwegian orogen (Cawood et al. 2010). Gaining further knowledge of the

tectonothermal events that have affected the HRNC will be useful in constraining correlations between this exterior orogen with events that affected the interior of the Rodinia supercontinent.

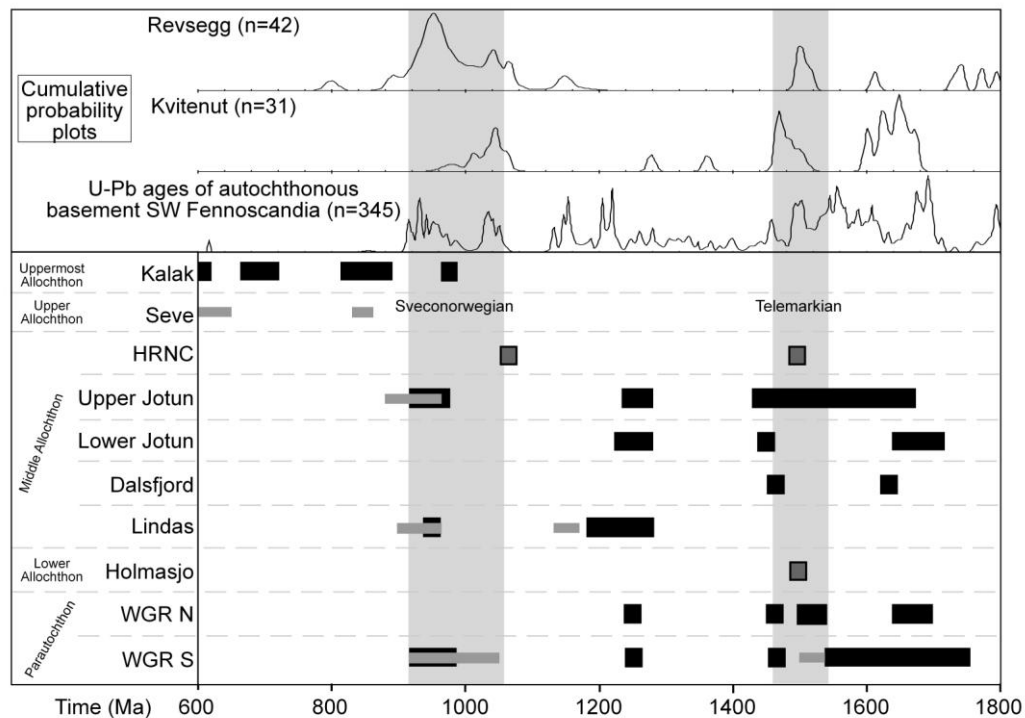


Figure 8.8. (Top) Cumulative probability plots of detrital units within the HRNC (Revsegg and Kvitenut) compared with ages from the autochthonous basement within SW Fennoscandia (compilation from Bingen & Solli 2009). (Bottom) Age compilation of magmatic (black bars) and metamorphic/anatectic (grey bars) events within Scandinavian Caledonian terranes, compared with protolith ages determined in this study (dark grey boxes). Grey vertical bars represent the time periods of the main Sveconorwegian orogenic phase and Telemarkian continental growth (Bingen et al. 2008a). See Table 8.1 for compilation of age data.

8.8.2 Gothian-Telemarkian continental growth

In Fennoscandia, the autochthonous basement underlying the Caledonian nappes youngs to the southwest, with the crust being divided into Transcandinavian Igneous Belt (TIB) 1850-1700 Ma, Gothian 1700-1520 Ma, and Telemarkian 1520-1480 Ma terranes (Åhäll & Connelly 2008; Bingen et al. 2008a). Crystalline units within the allochthonous nappes have similar ages to the autochthonous basement that underlies them, for example in the Telemark Sector the HRNC comprises ~1500 Ma rocks overlying ~1500 Ma basement, and to the north of this, the Jotun Nappe comprises 1650 Ma rocks that likely overlie 1650 Ma Gothian crust (Lundmark & Corfu 2008). The original position of the crystalline nappe units was likely to the west/northwest of their current position, and outboard of the current coastline. Thus, the southwesterly younging age pattern of the crust likely existed prior to any Caledonian orogenesis, and extended out to several hundred kilometres offshore of the current coastline (Figure 8.9).

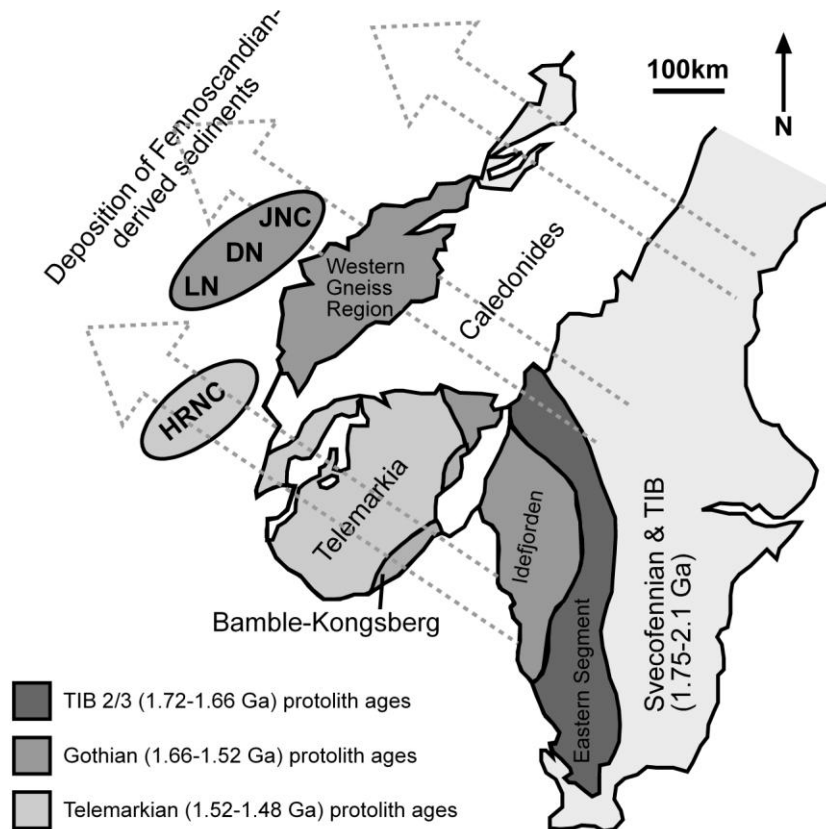


Figure 8.9. The postulated original position of Middle Allochthon nappe units in the southern Scandinavian Caledonides is shown as grey ellipses. The dashed arrows show the likely post-Sveconorwegian shedding of detritus from the Fennoscandian continent into basins that formed sedimentary units in the upper parts of the Middle Allochthon (e.g. Kvitnut and Revsegg units). HRNC, Hardangervidda-Ryfylke Nappe Complex; JNC, Jotun Nappe Complex; DN, Dalsfjord Nappe; LN, Lindas Nappe (modified from Lundmark & Corfu 2008).

8.8.3 Sveconorwegian orogeny in SW Norway

Bingen et al. (2008c) divide the Sveconorwegian orogeny into a time-frame of four periods, based on events that occur throughout SW Fennoscandia. The Arendal Phase (1140-1080 Ma) is related to the collision between Telemarkia and the Idefjorden terrane, forming the highly tectonised Bamble and Kongsberg terranes, with the only effect of this in southwest Norway being continental sedimentation resulting from localised uplift (Bingen et al. 2008c). The Agder Phase (1050-980 Ma) corresponds to the main orogenic phase with continent-continent collision, and crustal thickening that peaked at ~1035 Ma (Bingen et al. 2008c). In Telemarkia the ~1050 Ma Feda Suite is related to either east-dipping subduction prior to continent-continent collision, or to melting of older calc-alkaline crust during crustal thickening (Bingen & van Breemen 1998; Bingen et al. 2008c; Slagstad et al. 2008). The ~1062 Ma age for the Dyrskard supracrustals, and their likely setting in an extensional basin above a supra-subduction zone, is much more compatible with a continental-arc origin rather than a crustal thickening origin for the Feda granitoids.

8.9 Conclusions

U-Pb geochronology of allochthonous units within the HRNC has shown that the units are much younger than previously interpreted from Rb-Sr dates. The basal allochthon contains an intermediate igneous unit dated at $1493 \pm$ Ma, interpreted to be a locally derived thrust slice of basement. In the Storhei Nappe, a granitic gneiss is dated at ~ 1500 Ma, and features Sveconorwegian metamorphism at 1020 Ma. Thus, Telemarkian age crust likely extended much further northwest than the current coastline prior to Caledonian shortening. The Dyrskard Unit is dated at ~ 1062 Ma, and is interpreted as a supracrustal sequence deposited in a shallow basin in a supra-subduction setting. This adds evidence to the argument that the early-Sveconorwegian history included continental arc magmatism (Feda suite) at ~ 1060 -1040 Ma. The Kvitenuit and Revsegg units contain sedimentary paragneisses deposited after the main Sveconorwegian orogenic phase < 950 -980 Ma. Further work is needed to establish the minimum age of deposition. Cross-cutting units in these allochthons may correlate with those in the Kalak Nappe Complex, aiding the debate on the origin of this allochthonous complex.

Table 8.1 Compilation of ages for Figure 8.8

Metamorphism and anatexis age:			Ma	±	
Middle South	Upper Jotun	Djupevik Leucosome	892	4	Lundmark & Corfu 2008
Middle South	Upper Jotun	Syenite to monzonite	907	11	Scharer 1980
Middle South	Upper Jotun	Granite	909	4	Lundmark et al. 2007
Middle South	Upper Jotun	Anorthosite, Hurrungane	913	3	Lundmark & Corfu 2008
Middle South	Lindås Nappe	Granulite, Holsnoy	929	1	Bingen et al. 2001a
Windows South	WGR	Granite, Hafslø	930	10	Corfu 1980
Middle South	Lindås Nappe	Charnockite, Lygra	932	+28/-36	Bingen et al. 2001a
Middle South	Lindås Nappe	Retrograded granulite, Radøy	933	2	Bingen et al. 2001a
Middle South	Upper Jotun	Anatexis, Hurrungane	934	3	Lundmark et al. 2007
Middle South	Upper Jotun	Granite, Hurrungane	934	1	Lundmark et al. 2007
Middle South	Upper Jotun	Qtz-Monzonite and gabbro	941	10	Lundmark et al. 2007
Windows South	WGR	Quartz-monzonite, Hisarøy	949	3	Røhr et al. 2004
Middle South	Upper Jotun	Anatexis, Hurrungane	954	3	Lundmark et al. 2007
Windows South	WGR	Quartz-monzonite, Hisarøy	987	10	Røhr et al. 2004
Windows South	WGR	Granite, Hafslø	1014	35	Corfu 1980
Middle South	Lindås Nappe	Granulite, Gaupas	1151	5	Burton et al. 1995
Windows South	WGR	Granite, Hafslø	1518	17	Corfu 1980
Protolith age:			Ma	±	
Kalak Nappes	Havvatnet imbricate	Litlefjord pegmatite	826	±5.4	Kirkland et al. 2006
Kalak Nappes	Havvatnet imbricate	Revsneshamn pegmatite	833	±8.9	Kirkland et al. 2006
Kalak Nappes		Granitic dikelet near Lillefjord pluton	834	±19	Corfu et al. 2007
Kalak Nappes	Havvatnet imbricate	Revsneshamn granite	839	±9.7	Kirkland et al. 2006
Kalak Nappes	Havvatnet imbricate	Litlefjord granite, 2 samples	841	±6.5	Kirkland et al. 2006
Seve Nappes	Kebnekaise Nappe	Vistas Granite, Kebnekaise Mts	845	±14	Paulsson & Andréasson 2002
Kalak Nappes	Sorøy-Seiland	Eidvågvatnet foliated granite	851	±5	Kirkland et al. 2008a
Kalak Nappes	Sorøy-Seiland	Nordneset foliated granite	853	±4	Kirkland et al. 2008a
Kalak Nappes	Sorøy-Seiland	Lillefjord granitic gneiss	876	±9	Corfu et al. 2007
Middle South	Upper Jotun	Leucosome in garnet granulite, Djupevik	892	±4.4	Lundmark et al. 2008
Middle South	Upper Jotun	Granitic pegmatite, Rambera	927	±2.0	Lundmark et al. 2008
Middle South	Upper Jotun	Granitic pegmatite, Hurrungane	927	±3.2	Lundmark et al. 2008
Windows South	WGR	Granodiorite dyke, Ornfjell	942	+5/-3	Tucker et al. 1990
Middle South	Upper Jotun	Zoned granitic pegmatite, Hurrungane	942	±2.7	Lundmark et al. 2008
Windows South	WGR	Pegmatite dyke, discordant, Breidalsvatnet	943	±5	Tucker et al. 1990
Middle South	Upper Jotun	Allanite-bearing pegmatite dyke, Hurrungane	950	±1.3	Lundmark et al. 2007
Middle South	Lindås Nappe	Jotunite-mangerite pluton Radøy, mafic granulite	951	±2	Bingen et al. 2001aa
Middle South	Lindås Nappe	Jotunite-mangerite pluton Radøy, retrogranulite	951	+10/-4	Bingen et al. 2001
Windows South	WGR	Granodiorite dyke, Djupvatnet	951	+5/-3	Tucker et al. 1990
Middle South	Upper Jotun	Granitic neosome in banded anatexite, Hurrungane	954	±3	Lundmark et al. 2007
Windows South	Øye-Vang	Granite, Øye	954	+41/-33	Corfu 1980
Middle South	Upper Jotun	Massif anorthosite, Gudvangen quarry	965	±3.8	Lundmark et al., 2008a
Windows South	WGR	Jølster granite, porphyritic quartz syenite	966	±3	Skår & Pedersen, 2003
Kalak Nappes	Kolvik nappe	Siedgoaivi granite	973	±4.2	Kirkland et al., 2006
Windows South	WGR	Granite, Havslø	976	±8	Corfu, 1980
Kalak Nappes	Kolvik nappe	Hårvika granite, Harvikneset	978	±9.1	Kirkland et al., 2006
Kalak Nappes	Olderfjord nappe	Repvåg granite	981	±6.9	Kirkland et al., 2006
Middle southern	HRNC	Dyrskard metarhyolite	1062	5	this study
Middle South	Risberget Nappe	Augen gneiss, S of Oppdal	1189	±1	Handke et al., 1995
Middle South	Risberget Nappe	Augen gneiss, Kjöra, Rønningen	1189	±3	Handke et al., 1995
Middle South	Risberget Nappe	Augen gneiss, Brattvåg, Verpholmen	1190	±2.8	Handke et al., 1995

Middle South	Lindås Nappe	Charnockite gneiss, Lygra	1237	+43/-35	Bingen et al., 2001a
Windows South	WGR	Hustad igneous complex, coronitic gabbro/dolerite	1251	±3	Austrheim et al., 2003
Middle South	Upper Jotun	Gabbro, Høgeloft, Tyn	1252	+28/-25	Schärer, 1980
Middle South	Upper Jotun	Quartz monzonitic gneiss, Rambera	1257	±22	Lundmark et al., 2007
Middle South	Upper Jotun	Dioritic gneiss, Rambera	1257	±22	Lundmark et al., 2007
Middle South	Upper Jotun	Leirungsmyran gabbroic complex, pegmatite pod	1450	±3	Corfu & Emmett, 1992
Windows South	WGR	Coronitic metagabbro, Selsnes	1461	±2	Tucker et al., 2004
Middle South	Dalsfjord Nappe	Pegmatitic gabbro, Stordalsvatn	1464	±6	Corfu & Andersen, 2002
Middle southern	HRNC	Holmasjø metaandesite	1497	6	<i>this study</i>
Middle southern	HRNC	Storhei gneiss	1499	8	<i>this study</i>
Middle South	Dalsfjord Nappe	Svarthumlevatnet pegmatitic leucocratic vein	1507	±4	Austrheim & Corfu, 2009
Windows South	WGR	Mølmesdal gabbro complex, gabbro pegmatite	1621	±3	Skår & Pedersen, 2003
Middle South	Upper Jotun	Alkali granite gneiss, Hurrungane	1630	±30	Lundmark et al., 2007
Windows South	WGR	Quartz syenite gneiss and leucosomes, Sognefjord	1633	±8	Skår & Pedersen, 2003
Windows South	Grong-Olden	Coarse-grained granite, Blåfjellhatten granite	1633	±2.9	Roberts et al., 1999
Middle South	Upper Jotun	Anatectic granitic gneiss, Galbergstjernet	1634	±5	Lundmark et al., 2007
Middle South	Upper Jotun	Charnockitic two-pyroxene granulite, Hurrungane	1634	±3.6	Lundmark et al., 2007
Middle South	Dalsfjord Nappe	Monzonite, Altøy	1634	±3	Corfu & Andersen, 2002
Windows South	WGR	Quartz diorite, Altøy, Vikanes unit	1641	±2.3	Skår et al., 1994
Windows South	WGR	Quartz monzonitic granulite, Vilsvikvågen, Hisarøya	1646	±110	Røhr et al., 2004
Windows South	WGR	granite gneiss, Åndalsnes	1647	ca.	Tucker et al., 1990
Windows South	WGR	Microcline granite gneiss, Hindrem	1652	ca.	Tucker et al., 1990
Windows South	WGR	Granite gneiss, Ingdøl	1653	±2	Tucker et al., 1987
Windows South	WGR	Hustad igneous complex, foliated granite	1653	±2	Austrheim et al., 2003
Windows South	WGR	Hustad complex, monzodiorite, Lakseberga	1654	±1	Austrheim et al., 2003
Windows South	WGR	Leucogabbro gneiss, Damvatnet	1657	+5/-3	Tucker et al., 1990
Windows South	WGR	Granite gneiss, Frei Island	1658	±2	Tucker et al., 1990
Windows South	WGR	Migmatite gneiss, Åstfjord, 2 samples	1659	±2	Tucker et al., 1990
Windows South	WGR	Migmatitic gneiss, tonalitic gneiss, Våvatnet	1659	ca.	Tucker et al., 1990
Windows South	WGR	Granitic gneiss, Meisingset	1659	ca.	Tucker et al., 1990
Windows South	WGR	Tonalite gneiss, Asprong	1659	ca.	Tucker et al., 1990
Windows South	WGR	Migmatitic gneiss, grey tonalite gneiss, Karøydalen	1660	ca.	Tucker et al., 1990
Windows South	WGR	Granite gneiss, Ålvund	1660	ca.	Tucker et al., 1990
Middle South	Upper Jotun	Jotunite gneiss, Fannaråken	1660	±2.1	Lundmark et al., 2007
Windows South	WGR	Granite gneiss, Sagfjorden	1661	±2	Tucker et al., 1990
Windows South	WGR	Layered migmatite gneiss, Breidalsvatnet	1662	+41/-29	Tucker et al., 1990
Windows South	WGR	Granite gneiss, Sundalsøra	1664	ca.	Tucker et al., 1990
Middle South	Lower Jotun	Quartz monzonite, tyn	1666	+26/-23	Schärer, 1980
Windows South	WGR	Granite migmatite gneiss, Smiset	1672	ca.	Tucker et al. 1990
Windows South	WGR	Granite gneiss, Selsjord, Dombås	1678	ca.	Tucker et al. 1990
Windows South	WGR	Migmatite gneiss, leucosome + host, Tingvoll	1686	±2	Tucker et al. 1990
Windows South	WGR	Granite migmatite gneiss, Solsnes	1686	ca.	Tucker et al. 1990
Middle South	Lower Jotun	Syenitic to monzonitic gneiss, Tyn	1694	±20	Schärer 1980
Middle North	Akkajaure Nappes	Felsic dyke, Sarek	1731	±5	Rehnström 2003
Middle North	Akkajaure Nappes	Ruovddevåre syenite	1744	±10	Rehnström 2003
Middle North	Akkajaure Nappes	Ruovddevåre syenite	1761	±9	Rehnström 2003
Windows North	West Troms	Plagioclase phyrlic dyke, Ytre Kårvika	1767	±5	Kullerud et al. 2006
Windows North	Rombak	Granite intruding supracrustal belt, Gautelis	1770	±9.7	Romer et al. 1991
Windows North	West Troms	Plagioclase phyrlic dyke, Blombakk	1772	±9	Kullerud et al. 2006
Windows North	Lofoten	Borge pluton, felsic pegmatite cutting gabbro	1773	±2	Corfu 2004
Windows North	West Troms	Foliation-cutting granite dyke, Kattfjord complex	1774	±5	Corfu et al. 2003a
Seve Nappes	Skárjá Nappe	Banded granitic gneiss, Skárjá gneiss	1776	±4	Rehnström et al. 2002
Middle North	Akkajaure Nappes	Tielma magmatic complex, syenite, Sarek	1776	±7	Rehnström 2003
Windows North	Rombak	Granite, Sjangel	1778	±19	Romer et al. 1991
Middle North	Akkajaure Nappes	Granite dyke, upper thrust sheet 5	1779	±7	Rehnström & Corfu 2004
Middle North	Akkajaure Nappes	Phenocryst gneissic granite, upper thrust sheet 5	1780	±2	Rehnström & Corfu 2004
Windows North	Lofoten	Flagstadøy complex, pegmatite in Napp gabbro	1789	±2	Corfu 2004
Windows North	Lofoten	Torset pluton, granite, Langøy	1789	±1	Corfu 2004
Windows North	West Troms	Ersfjord granite, Kvaløya	1792	±5	Corfu et al. 2003a
Windows North	Lofoten	Flagstadøy complex, pegmatitic pod in gabbro	1793	±4	Corfu 2004
Middle North	Akkajaure Nappes	Granite dyke cutting granite-diorite	1795	±4	Rehnström & Corfu 2004
Windows North	Lofoten	SW Lofoten pluton, Ballsdad mangerite, Vestvågøy	1795	±1	Corfu 2004
Windows North	Nordland windows	Monzonite gneiss, migmatitic, Træna	1795	±3	Skår 2002
Windows South	Central Norway	Coarse porphyritic granite, Geitfjell granite	1795	+52/-49	Johansson et al. 1993
Windows North	Fagervik complex	Tjukkfjellet granite, Seiland	1796	±3	Kirkland et al. 2008
Windows North	Lofoten	Raftsund pluton, charnockite, Austvågøy	1796	±2	Corfu 2004
Windows North	Lofoten	Borge pluton, gabbro, Vestvågøy	1796	±1	Corfu 2004
Windows North	Lofoten	Eidsfjord complex, anorthosite, Langøy	1796	±2	Corfu 2004
Windows North	Vesterålen	Amphibolite enclave, Ryggedalen	1796	±2	Corfu 2007
Windows North	Rombak	Granite, Svartdal	1796	±5.2	Romer et al. 1991
Windows North	Nordland windows	Protolith of migmatite leucosome, Sjøna	1797	±3	Larsen et al. 2002
Windows North	Nordland windows	Quartz monzonite gneiss, Sjøna	1797	±3	Skår 2002
Windows North	Vesterålen	Felsic granulite, Vikan, Straumfjorden	1798	±1	Corfu 2007
Middle North	Akkajaure Nappes	Granite, granite-diorite mingling, lower thrust sheet	1800	±2	Rehnström & Corfu 2004
Windows North	Lofoten	Sund-Ølkona pluton, mangerite, Flakstadøy	1800	±2	Corfu 2004
Windows North	Lofoten	Eidsfjord complex, monzonite, Langøy	1800	±3	Corfu 2004
Windows North	Rombak-Kuokkal	Granite, Vassijaure	1800	±4	Rehnström & Torsvik 2003
Windows North	Nordland windows	Syenite gneiss, Nesøy	1800	±3	Skår 2002
Windows North	Nordland windows	Syenite gneiss, Høgtuva, Melfjell	1800	±2	Skår 2002
Windows North	Vesterålen	Mafic granulite, enclave in Vikan gneiss	1804	±1	Corfu 2007
Windows South	Central Norway	Weakly deformed tonalite	1818	±6	Schouenborg et al. 1991
Windows North	Lofoten	Hopen pluton, charnockite, Austvågøy	1860	±5	Corfu 2004
Windows North	Lofoten	Hopen pluton, mangerite, Austvågøy	1864	±1	Corfu 2004
Windows North	Hinnøy	Felsic granulite, Blokkneset, Blokken, Sigerfjord	1870	ca.	Corfu 2007
Windows North	Ritsem window	Ritsem granite	1871	±11	Rehnström & Corfu 2004
Windows North	Lofoten	Lødingen pluton, granite, Hinnøy	1873	±2	Corfu 2004

Discussion

9.1 Crustal evolution in the Telemarkian (1.52-1.48 Ga) period

Based on their petrology, petrography and intrusive-relations, the orthogneisses exposed in the Suldal Sector are thought to represent mid- to upper-crustal, hypabyssal and supracrustal igneous rocks, intercalated together during the evolution of a mature volcanic arc complex (Chapter 2). This interpretation is backed up by the whole-rock geochemistry of the orthogneisses, which exhibit typical calc-alkaline subduction-related signatures (Chapter 3). This arc is referred to as the Suldal arc; U-Pb geochronology of various lithologies suggests that it was active from ~1475 to 1521 Ma (Chapter 3).

The geochemistry of the Suldal arc is indicative of continental crust that is thickened relative to typical island arc crust, suggesting a mature island arc or continental arc setting. In continental arcs, magmatism may be dominated by recycling of pre-existing crust as opposed to addition of new crust (i.e. mantle addition). Coeval continental-rift magmatism in the adjacent Telemark Sector involved voluminous magmatic underplating, and felsic magmatism derived from crustal anatexis, suggesting a significant thickness of lithosphere must have existed prior to 1.5 Ga. Zircon inheritance is often used to infer older deep crust; inheritance is almost non-existent in Telemarkian magmatism (see Chapter 3), meaning that such an inference cannot be made based on the zircon data.

As discussed in Chapters 4 and 5, Andersen et al. (2001, 2002b, 2004a, 2007b, 2009b), Andersen & Griffin (2004) and Pedersen et al. (2009) advocate the existence of a pre-1.5 Ga deep crust throughout southwest Fennoscandia; they base this hypothesis on scant inherited zircons in younger <1.5 Ga intrusions, low ϵ_{Hf} in a few <1.5 Ga zircons, and Nd and Sr isotopes in 1.5-1.6 Ga and <1.5 Ga granitoids that depart from a depleted mantle signature. The Hf-O data presented in Chapter 4 confirms that a component older than 1.5 Ga and comprising a high- $\delta^{18}\text{O}$ signature (e.g. weathered sediments), made a contribution to the 1.5 Ga Suldal arc magmatism. The addition of such a component did not occur purely by mantle recycling, i.e. contamination from subducted sediments, but must have involved some recycling of this older component within the crust (intracrustal recycling). However, intracrustal recycling of an older sedimentary component does not prove the existence of an extensive older deep crust; intracrustal recycling requires burial and remobilisation of older sediments, which can occur via a number of processes, such as closure of back-arc basins and underthrusting at subduction margins.

Combining all of the evidence, it is suggested that the Suldal arc and its ensialic back-arc rift (the Rjukan Rift in Telemark), developed on an attenuated continental margin which comprised a degree

of older Gothian-aged (>1600 Ma) sediments; although, an origin on a rifted continental fragment cannot be discounted.

9.1.1 ‘Indigenous’ or ‘Exotic’ Telemarkia

Traditionally, the crust of the SSD was interpreted to have grown by successive westward accretion (e.g. Berthelsen 1980; Gaál & Gorbatshev 1987). Later on, the crust west of the Oslo rift (e.g. Telemarkia) was inferred to be a crustal block >1.65 Ga in age, based on limited zircon U-Pb ages (Ragnildstevt et al. 1994; Schärer et al. 1996; Birkeland et al. 1997). This led to a number of suggestions that the crust west of the Oslo rift formed a separate continental block or ‘proto SW-Norway’; this block may have accreted between 1.58 Ga and 1.5 Ga (Åhäll et al. 1998, 2000, or during the Sveconorwegian orogeny (Cornell & Austin Hedgart 2004). The zircon evidence can now be regarded as inconsequential, because the U-Pb ages are interpreted to have a detrital origin (Bingen et al. 2005b). The crust exposed at the surface of the SSD has a general east to west younging pattern, which can be inferred to represent a younging of the crustal domains, and therefore a possible origin as sequentially accreted terranes. However, as pointed out by Pedersen et al. (2009), models which are based on the age of exposed crust, in some cases fail to account for the age of the deep crust. Conversely, it is argued that models using in-situ U-Pb-Hf data to account for the age of the deep crust, in some cases *explicitly* imply features such as extensive Palaeoproterozoic crust at depth, where the data only indicate that such crust *may* exist (Pedersen et al. 2009; Andersen et al. 2009b).

Formation of the Suldal arc is inferred to have occurred above an east-dipping subduction zone (see Chapter 4). Calc-alkaline granitoids formed in the Idefjorden terrane as young as 1.49 Ga (Pózer Bue 2008), and are likely related to the youngest expression of east-dipping subduction that formed the Hisingen Suite continental arc (Åhäll & Connelly 2008). The coexistence of this arc with the 1.5 Ga Suldal arc in Telemarkia can be explained by two models: 1) where the arcs formed above the same subduction zone, and were later translated by strike-slip faulting to their current position, and 2) where two different subduction zones produced two contemporaneous arcs. The first model is compatible with the strike-skip terrane model advocated by Andersen et al. (2004a), de Haas et al. (1999) and Bingen et al. (2001b), and originally proposed by Torske (1985). The second model is consistent with an exotic microcontinent model for Telemarkia (Bingen et al. 2005b), but is suggested to be incompatible with the isotope data (Andersen et al. 2001, 2002b, 2004a, 2009b).

There is some limited structural evidence for the terrane displacement model, including coeval sinistral strike-slip and reverse dip-slip sense of shear on the mylonite zone, characteristic of a transpressive tectonic regime (Stephens et al. 1996), and early SE-directed movements that were later partitioned into sinistral strike-slip movements (Park et al. 1991). U-Pb ages of detrital zircons

in various metasedimentary units also provide evidence for this model. Metasedimentary units deposited during the Telemarkian period (those that are >1.48 Ga), contain abundant Palaeoproterozoic zircons, particularly correlating in age with the ~ 1.75 -1.9 Ga Transcandinavian Igneous Belt; they also contain Archaean zircons. There is a relative lack of zircons in the 1.7-1.6 Ga age bracket that correspond to the age of the crust to the east of Telemarkia; such zircons are abundant however in metasedimentary units within the Idefjorden Terrane. This suggests that the Telemarkia terrane was proximal to TIB and Svecofennian age parts of the Fennoscandian continent (or another continent of similar age), and was not shielded from such detritus by the Idefjorden terranes; the detrital zircon data are therefore compatible with a strike-slip displacement model (see Figure 9.1).

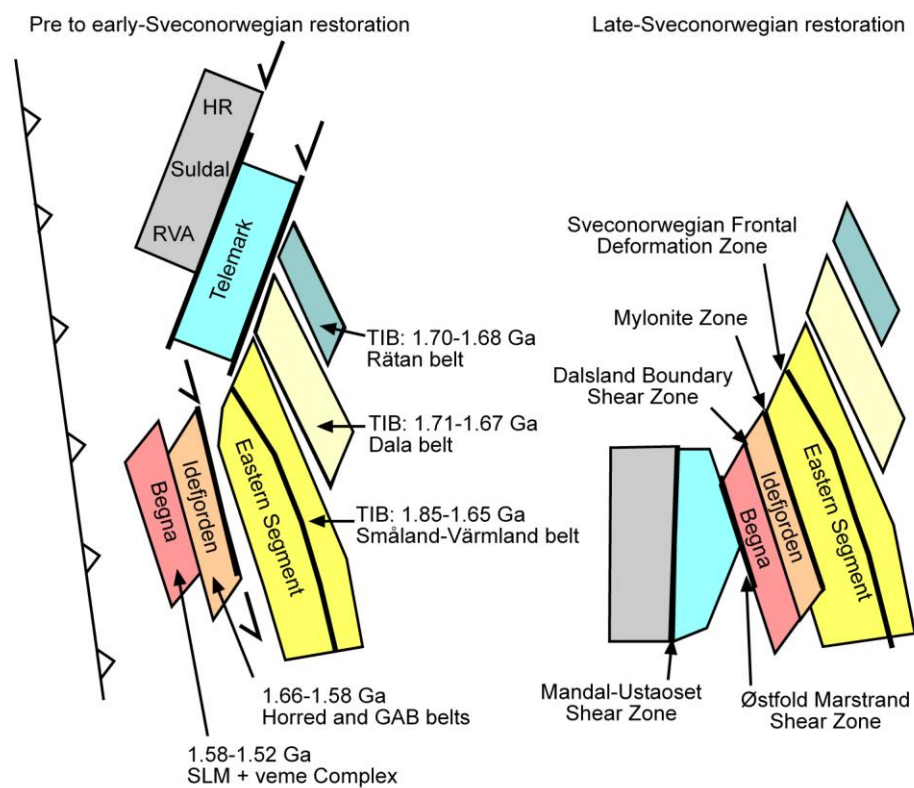


Figure 9.1. Strike-slip terrane displacement model, showing major lithotectonic domains and their relative motion (after Bingen et al. 2001b).

Whether the Telemarkia terrane is ‘indigenous’ or ‘exotic’ can be put down to semantics. For example, Japan has an origin as a rifted fragment of the Eurasian continent (e.g. Tamaki 1995); since rifting it has suffered a different history to that of the Eurasian continent, but after future closing of the Pacific Ocean (e.g. Maruyama et al. 2007) Japan will be accreted back onto Eurasian continental crust. After this juxtaposition, a study of the isotopic characteristics of the Japanese lower crust, and that of the adjacent Eurasian lower crust, may find very similar isotopic signatures due to their pre-rifting mutual history. The isotopic similarities of the lower crust could be used to

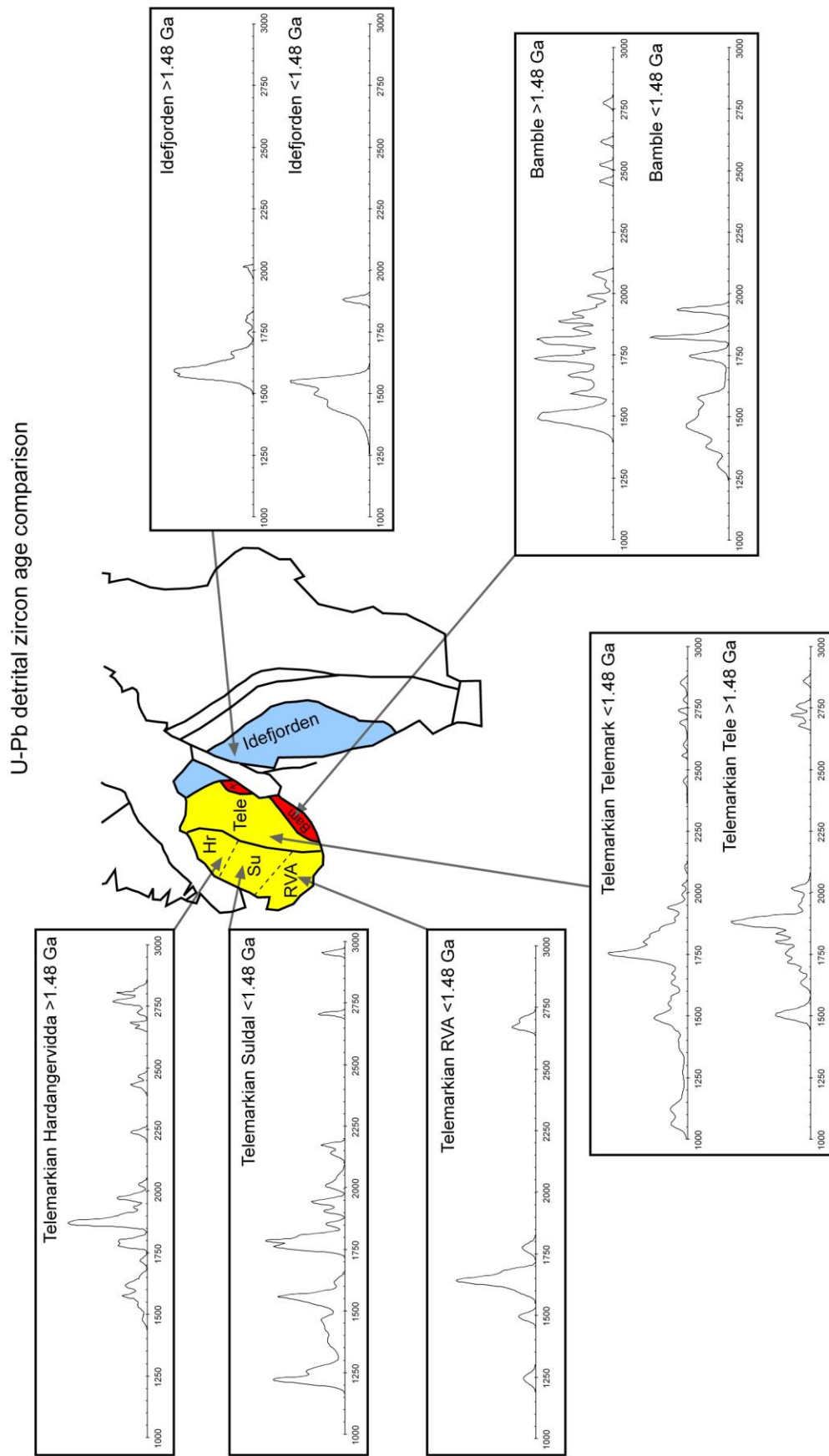


Figure 9.2. Compilation of detrital zircon U-Pb data for SW Fennoscandia, from Knudsen (1997), Åhäll et al. (1998), de Haas et al. (1999), Bingen et al. (2001b, 2002, 2003), Andersen et al. (2004a, 2004b),

interpret an ‘indigenous’ origin for the Japanese terranes, or, the contrasting characteristics of the upper crust could be used to interpret an ‘exotic’ origin.

Andersen et al. (e.g. 2004a, 2009b) use the isotopic signatures of magmatic rocks across SW Fennoscandia to interpret an indigenous origin for Telemarkia. Cornell & Austin Hedgardt (2004) use the contrasting ages of granites exposed at the surface across the Mylonite Zone to interpret an exotic origin for both the Idefjorden and Telemarkia terranes. The model described in the next section aims to satisfy all of the data.

9.1.2 A retreating accretionary orogenic model

Combining all of the previous geochronology and geochemical considerations, Åhäll & Connelly (2008) present a model for the evolution of SW Fennoscandia, from formation of the TIB to the end of the Gothian period (1.52 Ga). In their model, the various lithotectonic domains represent near-continuous oceanward-stepping (westward) crustal growth along a long-lived subduction zone; changes from continental to oceanic arcs are attributed to advance and retreat of Fennoscandia relative to the subduction trench. This geodynamic setting is consistent with a retreating accretionary orogen (Cawood et al. 2009); the advance and retreat of a subduction trench in relation to the continent is termed tectonic switching, and is an efficient way of producing continental crust (Collins 2002; Kemp et al. 2009). In their model, Åhäll & Connelly (2008) do not specifically refer to the nature of the lower crust, or the radiogenic isotopic characteristics of the crustal domains; their continental growth calculations however, do imply a relatively juvenile nature throughout. Åhäll & Connelly (2008) end their model at 1.52 Ga, based on the assumption that this is the age of the youngest subduction-related magmatism recorded in the Gothian terranes, but suggest that Telemarkia may represent a younger continuation of this oceanward-stepping westward crustal growth. The conclusions from this study indicate that their suggestion is consistent with the data, and thus it is postulated that the growth of Telemarkia is related to a long-lived subduction zone that also produced the Gothian terranes, and was initiated during TIB continental arc magmatism. As pointed out by Åhäll & Connelly (2008), Telemarkia may have been originally located further north along the margin of Fennoscandia (see Figure 9.1), but a southern continuation of Telemarkia or another crustal segment likely existed in its place, and was subsequently translated elsewhere; Telemarkia thus provides a proxy for the crust that existed outboard of the Idefjorden terranes.

The following issues have already been raised: 1) is Telemarkia indigenous or exotic to Fennoscandia? and 2) does Telemarkian growth represent recycling of older Fennoscandian crust or is Telemarkia a juvenile terrane? In the model of a retreating accretionary orogen, these issues are answered in the following way: 1) Telemarkia is built on attenuated continental crust of Fennoscandian origin, this explains the similarities in radiogenic isotopic character of the deep crust across the region; however, it is not unconceivable that the Telemarkian segment of crust rifted

away from the Fennoscandian continent, thus forming a continental ribbon (or microcontinent). Jostling between this and other terranes during the Sveconorwegian orogeny, means the Telemarkia block could be regarded as ‘exotic’ according to some terrane criteria, but its overall origin is with that of a SW Fennoscandian accretionary orogen, thus an ‘indigenous’ origin is preferred. 2) Because Telemarkia was built on a thin continental substrate, the arc magmatism involved a degree of recycling of this older continental crust; Telemarkia is therefore not considered to be an ‘accreted juvenile arc’. Conversely, Telemarkian magmatism is not likened to Andean-type settings where thick continental crust exists and continental recycling dominates over mantle addition; a preferred analogue for Telemarkia is that of modern arcs in the western Pacific that originate as rifted continental ribbons, such as Japan.

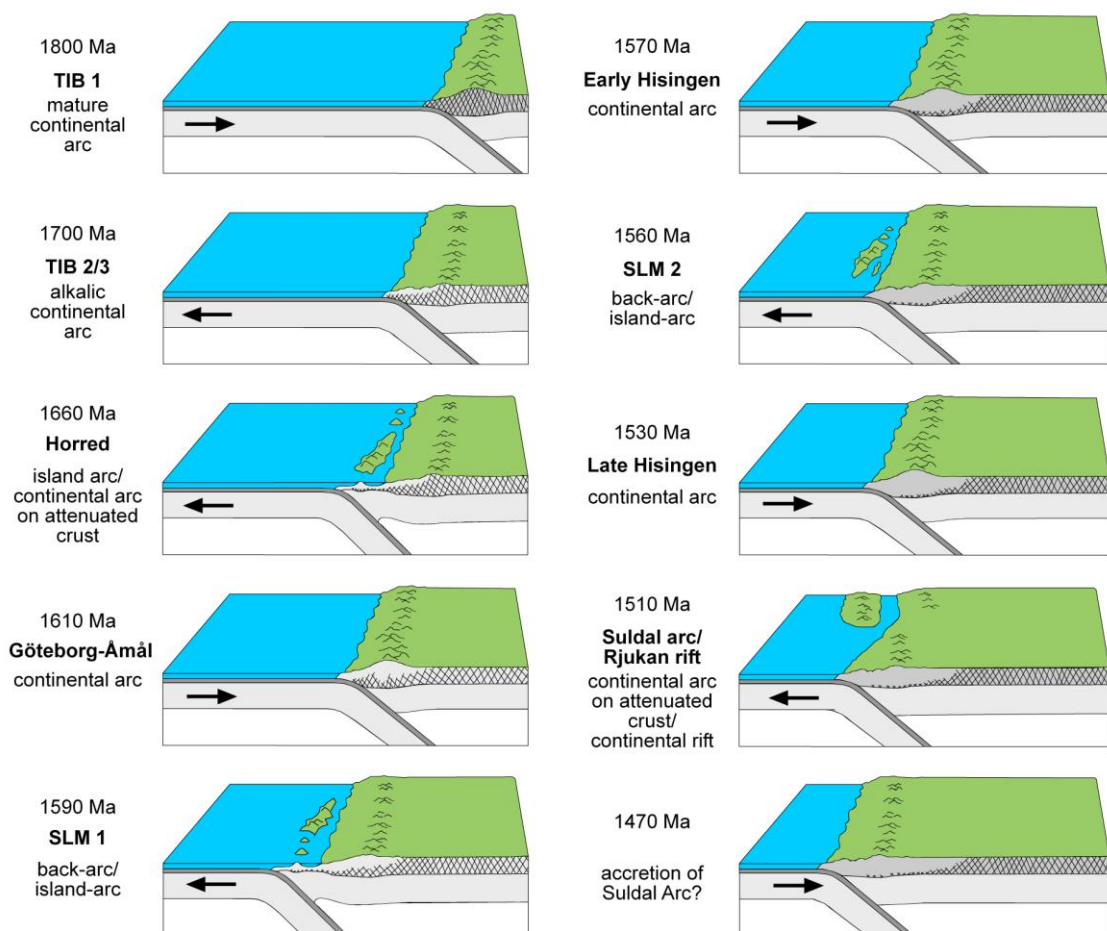


Figure 9.3. Simplified model of a retreating accretionary orogen to explain the westward growth of continental crust in SW Fennoscandia in various arc settings. The continuous east-dipping subduction zone and attenuation of the continental margin means that the isotopic characteristics of the deep crust are retained for large horizontal distances. TIB = Transcandinavian Igneous Belt, SLM = Stora Le Marstrand, black hatching refers to crust of late-Palaeoproterozoic age. (Modified from Åhäll & Connelly 2008).

9.2 Crustal evolution in the Sveconorwegian (1.06-0.92 Ga) period

New U-Pb ages (Chapter 3) show that the Storlivatnet plutonic complex in the Suldal Sector does not fall into the group of post-collisional Sveconorwegian granites, as it formed much earlier; U-Pb

ages from the plutonic complex date intrusions at 1039 ± 15 , 1047 ± 7 and 1069 ± 9 Ma. Deformation of the pluton is inferred to have occurred between 1047 ± 7 and 1069 ± 9 Ma; although this provides evidence for Sveconorwegian deformation within the region, the effect of this orogeny on the U-Pb systematics within the basement rocks is minimal (see Chapter 3). Inheritance of >1.5 Ga crust was not recorded in Sveconorwegian rocks of this study.

Early to pre-Sveconorwegian granitoids feature both I-type and A-type geochemistry, post-collisional granites are all A-type; the origin of these two suites can be explained by changes in water content (and oxygen fugacity) in the melting region (see Chapter 6). A supra-subduction zone setting is favoured for the pre-collisional granites; this setting provided hydrous conditions for formation of I-type magmas. Subsequent granite suites formed in a collisional setting with crustal thickening, and then a post-collisional setting with associated crustal thinning. Throughout these different geodynamic regimes the heat flux that is required to produce granitic magmatism will have changed, however, Hf-O data suggest that the magma source stayed the same (see Chapter 6). The magma source advocated for the Sveconorwegian magmatism involved a large contribution from 1.5 Ga crust, and a smaller contribution from mantle-derived material that is ~ 1.2 Ga or younger. The magma source was mafic lower crust that had isotope and geochemical characteristics imparted from previous magmatic episodes. Partial melting and fractionation of this mafic lower crust produced parent magmas that then evolved to granitoid intrusions.

The conclusions of this study confirm that the Sveconorwegian period largely involved recycling and remobilisation of pre-existing continental crust, as opposed to addition of new crust.

9.3 The 'interorogenic' period

The period after Telemarkian continental growth and before Sveconorwegian reworking, i.e. 1.46-1.06 Ga, features intermittent and generally localised periods of magmatism and sedimentation. Magmatic activity is dominated by mafic volcanism, but also includes felsic volcanism which is likely a result of crustal anatexis produced by heat from mafic intrusions. In Telemarkia, volcanism is typically associated with sedimentation in rift basins, whereas in the Idefjorden and Eastern Segment terranes, magmatism is associated with crustal lineaments or mafic dyke swarms (see Chapter 7). Both the formation of extensional basins and the intrusion of mafic dyke swarms, can be related to inboard effects of a convergent margin existing to the west of the present-day coastline (Brewer et al. 2002; Brewer et al. 2004; Söderlund et al. 2006; Chapter 7); although the 1.2 Ga Tromøy block is the only preserved arc crust of this age (Knudsen & Andersen 1999). This interpretation means that convergent margin activity is recorded in SW Fennoscandia from ~ 1.8 Ga (Transcandinavian Igneous Belt) to ~ 1.05 Ga (Feda Suite; see Chapter 6). It is also worth noting that 1.69-1.50 Ga A-type Rapakivi suites in Sweden and Finland have also been interpreted as distal

affects of convergent margin activity on the southwestern Fennoscandian margin; this is based on a temporal and spatial trend for the A-type suites that matches that of westward arc magmatism in the Idefjorden and Telemarkian terranes (Åhäll et al. 2000). Some ~1.85-1.75 Ga A-type suites in Finland have post-collisional tectonic settings advocated, i.e. magmatism related to lithospheric thinning after crustal relaxation (Eklund et al. 1998; Väisänen et al. 2000; Kurhila et al. 2010). In accepting the above interpretations, it is worth pointing out that for a 1 Gyr period (~1.8 to ~0.8 Ga) all tectonothermal, magmatic and sedimentary events in Fennoscandia can be in some way related to convergent margin tectonism, and thus, there is no call for any deep-seated mantle anomalies to explain any particular events.

9.3.1 The Hallandian-Danopolonian event

The term Hallandian was coined by Hubbard (1975) for metamorphism, anatexis and magmatic events around ~1.4 Ga in southwest Sweden. Christoffel et al. (1999) later defined the Hallandian as a thermo-magmatic event in the 1.44-1.38 Ga period. The term Danopolonian was used by Bogdanova et al. (2001) for tectonothermal events in the East European Craton between 1.5 and 1.4 Ga, and was related to a possible collisional orogeny between Baltica and another continent (probably Amazonia). More recently the informal term Hallandian-Danopolonian has emerged, and can be ascribed to any tectonothermal event in the 1.46-1.38 Ga period.

Ages between 1.46 and 1.42 Ga for new zircon growth/recrystallisation have been reported in veined gneisses in the south of the Eastern Segment (Christoffel et al. 1999; Söderlund et al. 2002). Magmatism in the Eastern Segment includes granitic to monzonitic intrusions ~1.4 to 1.36 Ga in age (Åhäll et al. 1997; Andersson et al. 1999, 2002; Christoffel et al. 1999; Möller et al. 2007); these include dehydrated charnockitic granites. Dehydration of a localised zone (<10m) of pre-1.46 Ga granitoid has been dated at 1397 ± 4 Ma (Rimša et al. 2007). On Bornholm Island to the east of the Eastern Segment, granites and orthogneisses have crystallisation ages from ~1475 to 1445 Ma (Zarinš & Johansson 2008); an east-west trend is interpreted to have formed synchronously with the magmatism, and titanite ages are coeval to slightly younger than the magmatic ages suggesting slow-cooling.

In the Idefjorden terrane to the west of the Eastern Segment, there are bimodal granite-gabbro intrusions dated at ~1.5 Ga (Åhäll & Connelly 1998), ~1.46 Ga dolerite dyke swarms (Hageskov 1997; Åhäll & Connelly 1998), and intermittent granite magmatism at ~1.34 to 1.25 Ga (Persson et al. 1983; Piontek et al. 1998; Austin Hegardt et al. 2007). No well constrained 1.46-1.42 Ga zircon growth has been recorded from the Idefjorden terrane; the lack of Hallandian-Danopolonian metamorphism in the Idefjorden terrane is one of the arguments used for its exotic origin (Andersson et al. 2002; Cornell & Austin Hegardt et al. 2004).

Brander & Söderlund (2008) note that in the Hallandian-Danopolonian period there is a predominance of mafic intrusions in the north and felsic intrusions in the south, and interpret this as possibly being related to distal effects of an orogeny in the south. However, some of these mafic intrusions can also be interpreted as distal effects of convergent margin tectonism in the west (see Chapter 7; Söderlund et al. 2005). The Hallandian-Danopolonian event has not affected the Telemarkia terrane, and thus could be assumed to have only affected inboard terranes. However, it is possible that the Hallandian-Danopolonian did affect terranes to the west of Idefjorden, but that these terranes have now been replaced by the unaffected Telemarkia terrane, which until the Sveconorwegian was located further north along the Fennoscandian margin (see Figure 9.1).

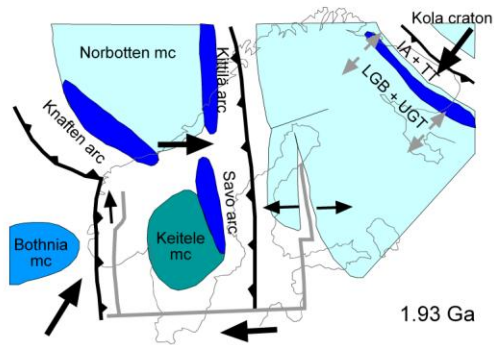
Contemporaneous with 1.5-1.6 Ga arc magmatism and 1.46-1.38 Ga tectonothermal events in the southwest of Fennoscandia, the central and eastern parts of the East European Craton were host to rifting events; these can be interpreted as both back-arc responses to Hallandian-Danopolonian convergence, and to abortive break-up of the East European Craton (see Bogdanova et al. 2008 and references within).

9.4 A tectonic synthesis

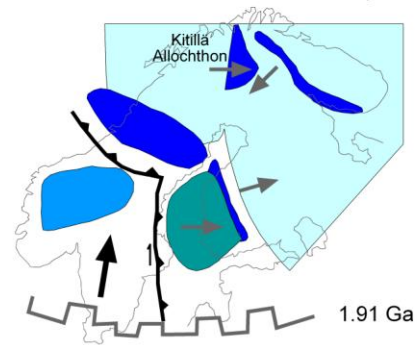
Figure 9.4 depicts the building of Fennoscandia during the Proterozoic; the pre-1.85 Ga configurations are modified from Korja et al. (2006) and Lahtinen et al. (2009). During the period between 2.0 Ga and 1.8 Ga, various Archaean continental blocks amalgamated in collisional orogenies (Lapland-Savo, Fennia, Svecobaltic and Nordic orogens; Lahtinen et al. 2009); caught up within these orogenic belts were juvenile Palaeoproterozoic arc and microcontinental blocks. As well as collisional orogenies, the 2.1-1.8 Ga period involves retreating (Tersk, Kittilä, Savo and Häme) and advancing (Tampere, Bergslagen and TIB1) accretionary orogenic belts (Lahtinen et al. 2009). By 1.8 Ga, the Palaeoproterozoic and Archaean domains were amalgamated into a stabilised craton; Sarmatia and Volgo-Uralia had also amalgamated by this time to form the East European Craton (Bogdanova et al. 2008).

Subduction on the south and west margins of Fennoscandia that formed the TIB1 continental arc, marks the beginning of a long-lived retreating accretionary orogen. This accretionary belt was active until Sveconorwegian continent-continent collision at ~1.05 Ga. Crustal additions related to this accretionary belt are ~1.75 to ~1.48 Ga in age (Gothian and Telemarkian). The period between 1.48 and 1.05 Ga involved little net crustal addition; the preserved crust was likely in back-arc and inboard positions relative to the convergent margin, and outboard juvenile crust that may have been produced during this time has likely been lost via both subduction erosion, and terrane displacement.

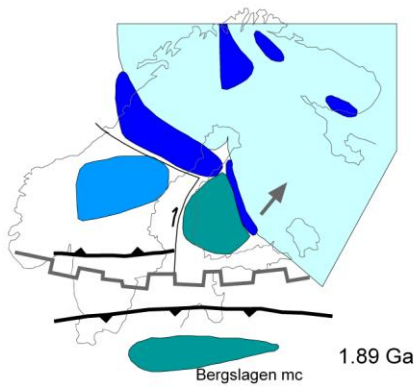
Subduction and back-arc rifting in the Lapland-Kola area, westwards subduction under the Keitele mc and Norbotten mc, and subduction to the NE under the Norbotten mc and east under the Keitele mc.



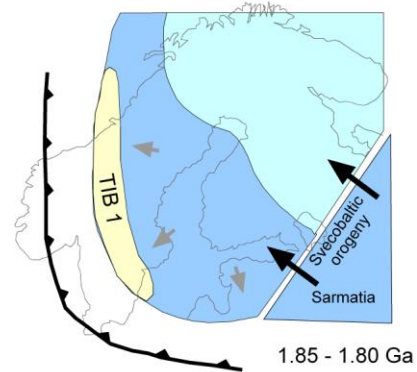
Peak of the Lapland-Kola and Lapland-Savo orogenies. Initial stage of collision of the Bothnian mc with the Norbotten and Keitele mc. Initiation of Northern and Central Svecofennian Subprovinces.



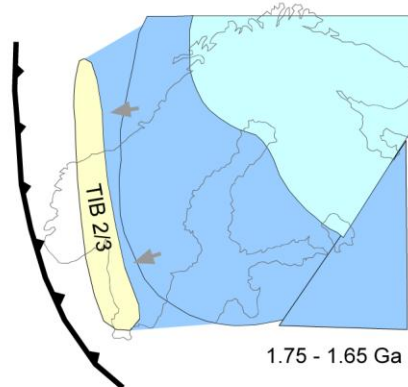
Beginning of the Fennian orogeny. As a result of locking of northward subduction under the Keitele mc, the southern ocean is consumed by subduction to the south under the combined Häme island arc and Bergslagen mc. After amalgamation of the Bothnian mc, another subduction zone is formed at its southern margin.



Archaean and Palaeoproterozoic crust has formed and is largely stabilised. Subduction initiates to the north and east, large-scale extension takes place in the hinterland, and Fennoscandia amalgamates with Sarmatia.



The subduction zone migrates oceanward relative to Fennoscandia. TIB 2/3 arc rocks form in an extensional continental arc.



Overall the subduction zone is migrating oceanward, but periodic trenchward movement accretes Gothian and Telemarkian arc terranes to Fennoscandia. By 1.5 Ga most of the Fennoscandian crust is stabilised.

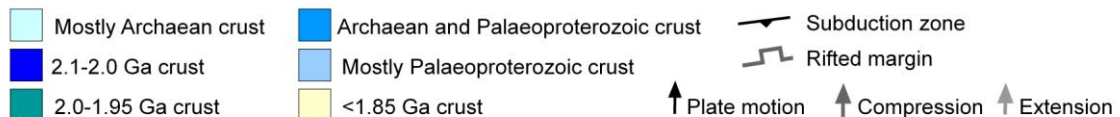
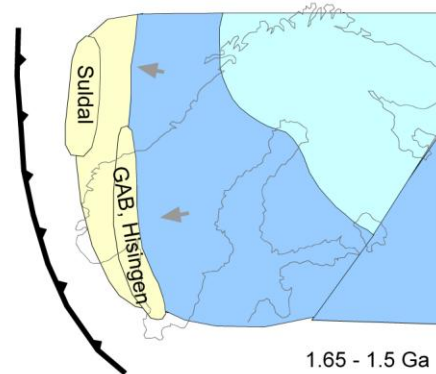


Figure 9.4. A schematic model for the amalgamation of Fennoscandian continental crust during the Palaeo- to Mesoproterozoic (modified from Korja et al. 2006; Lahtinen et al. 2009). mc = microcontinent, IA = Inari Area, TT = Tersk Terrane, LGB = Lapland-granulite Belt, UGT = Umba Granulite Terrane, GAB = Göteborg-Åmål Belt, TIB = Transcandinavian Igneous Belt.

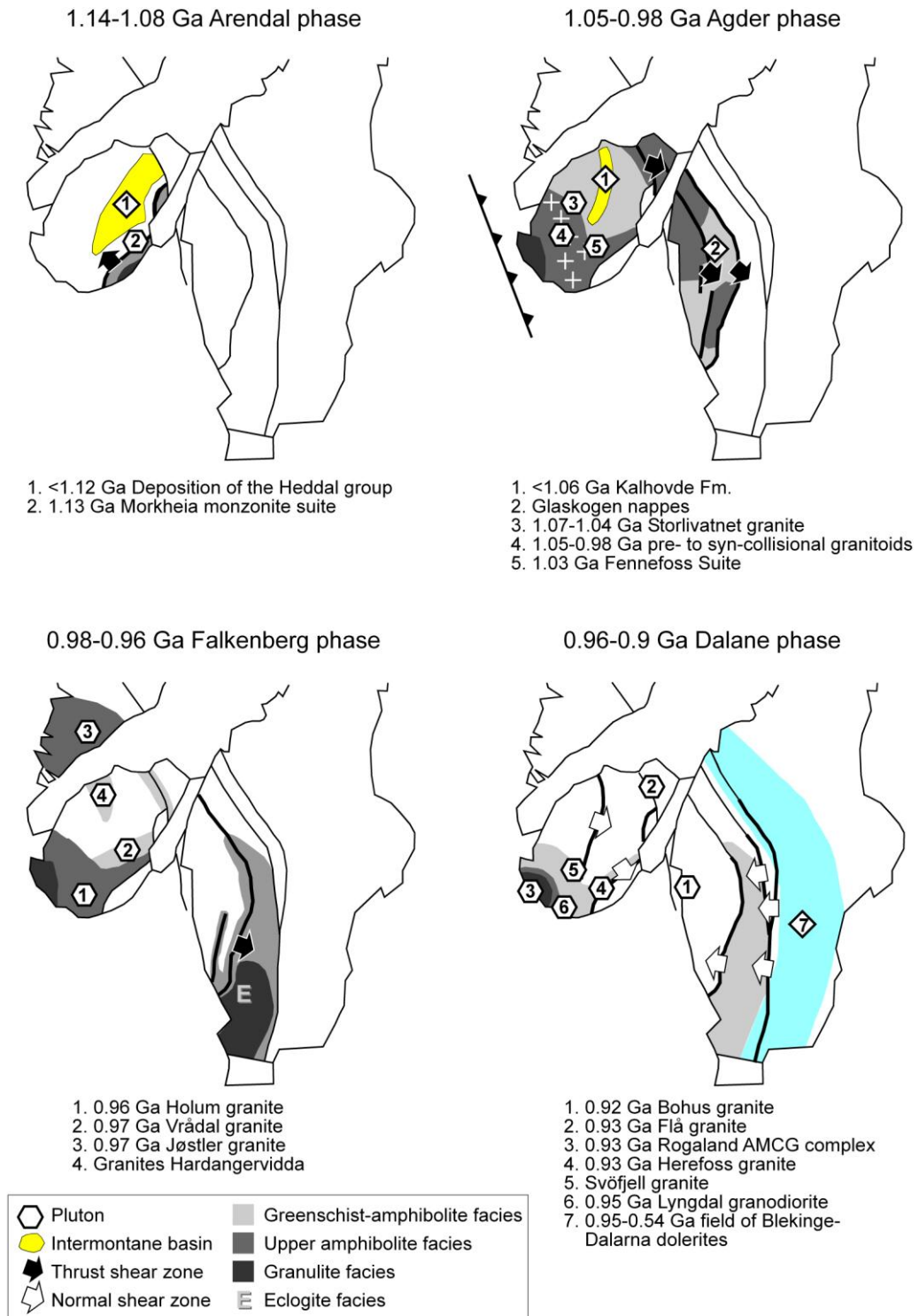


Figure 9.5. The distribution of metamorphism, magmatism and sedimentary basins during the Sveconorwegian orogeny (modified from Bingen et al. 2008c; Bogdanova et al. 2008).

Figure 9.5 depicts the Sveconorwegian orogeny in Fennoscandia, modified from Bingen et al. (2008c) and Bogdanova et al. (2008). Modifications to the model include the addition of the 1.07-1.04 Ga Storlivatnet pluton, and an east-dipping subduction zone that produced the >1.04 Ga granitoids.

9.5 Reading the isotope barcode

The tectonic model discussed in the previous section features a retreating accretionary orogen that was active from ~1850 Ma to 1050 Ma. The period of accretion was concluded by ~1030 Ma with a major continent-continent collision and reworking and reorganisation of terranes. The onset of this accretionary orogen is defined by an active continental margin that reworked previously formed crust (the Transcandinavian Igneous Belt); accretionary orogenesis also occurred prior to the TIB continental arc event, but the TIB allows for a convenient separation between >1.85 Ga Svecofennian and <1.8 Ga Gothian to Sveconorwegian events.

In the Gothian-Telemarkian orogen, the oldest (and exposed) upper crust youngs to the west, from ~1750 Ma in the east (Eastern Segment) to ~1480 Ma in the west (Suldal/Rogaland). Various episodes of arc magmatism have been recognised from combined field, geochemical and geochronological data, including Horred (1.66 Ga), Göteborg-Åmål (1.61-1.59 Ga), Hisingen (1.59-1.52 Ga), and Telemarkian (1.52-1.48 Ga) (Åhäll & Connelly 2008 and references within; Chapters 2 to 5). Back-arc and fore-arc sequences with arc-dominated greywacke sediment are generally restricted to the Idefjorden terrane, but are also found in the Bamble and Kongsberg collisional terranes. Younger extensional basins with continental or shallow sedimentation are found across the Telemarkia terranes, and magmatism that is not clearly arc-related occurs in various discrete episodes throughout the discussed time period (see Chapter 7 and section 9.3).

The Lachlan orogen in SE Australia is a younger example of a retreating accretionary orogen, where the coupling of arc and back-arc, and magmatic, metamorphic and sedimentary processes are well-documented (e.g. Collins 2002; Kemp et al. 2009; Foster et al. 2009). One method of continental crust formation in this orogen is the formation of S-type granites during closure of back-arc basins. These granites form during a compressional state of the orogen, and have the most evolved Nd and Hf signatures relative to other suites in the orogen (Kemp et al. 2009). During the maximum extensional state of the orogen, A-type granites with the most depleted Hf and Nd signatures are produced (Kemp et al. 2009). I-type granites occur during the initial extensional phases in back-arc and fore-arc settings, and have mixed mantle and sedimentary isotope signatures (Kemp et al. 2007). The temporal variation in the isotopic signature of different granitoid suites is correlative with the geodynamic setting of magmatism. In its simplest terms, the amount of mantle addition to magmatism increases during the maximum extensional state of the orogen; this may reflect a variety of processes such as intrusion into thinned crust and/or intrusion along extensional structures, as well as a decrease in sediment-subduction or subduction-erosion. In the Lachlan orogen, the thickness of crust is postulated as the underlying cause of varying mantle/crustal contributions (Kemp et al. 2009).

Whereas the Lachlan orogen features marginal basins and large volumes of turbiditic sediments (Foster et al. 2009), the orogen studied here features voluminous arc crust, with limited volume of turbidites. Kemp et al. (2009) suggest such features are related to a quasi-stationary subduction zone, such as the Canadian Cordillera. In the Lachlan orogen the crust has been shortened by ~75% (Foster et al. 2009), in the Fennoscandian orogen, it is likely to be less than 50% given the lack of ocean basin formation. This difference in extension has produced the variance in volume of sediment versus igneous crust. The Fennoscandian orogen is also eroded to a deeper crustal level, implying that a greater volume of supracrustal material may have existed originally.

9.5.1 Source versus time

Figure 9.6a shows a compilation of published and new Hf isotope data for SW Fennoscandian autochthonous basement domains. The data fall into clusters that from oldest to youngest are TIB1 and TIB2/3 arc-related units; Göteborg-Åmål, Hisingen and Telemarkian arc-related units; ~1.3-1.1 Ga interorogenic units; and 1.06-0.92 Ga Sveconorwegian granitoid units. Ranging from ~1.6 to 0.92 Ga are mafic intrusions that intrude terranes east of the Oslo Rift. The inter-orogenic rocks likely formed in a supra-subduction zone setting (see Chapter 7), particularly those in the Setesdalen region (Pedersen et al. 2009). Figure 9.6b shows averages of the data using 25 Myr bins; this enables the general trend in ϵ_{Hf} to be visualised.

TIB 1 and TIB 2/3 magmatism can be related to continental arc magmatism that involved a large proportion of recycling of pre-existing Svecofennian crust. The switch to arc magmatism forming the Göteborg-Åmål Belt (GAB) and Hisingen Suite (Åhäll & Connelly 2008), involved a change to a greater degree of mantle input; this change is interpreted to reflect slab rollback so that magmatism intrudes thinner crust, and that magmatism is more distal to the continent so that the volume of older subducted sediment is decreased. Between 1.6 and 1.5 Ga there were multiple episodes of back-arc/fore-arc sediment deposition (Stora Le-Marstrand formations), and accretion of arc-derived blocks (Åhäll & Connelly 2008); however, the data cannot pick out differences in mantle input at this timescale. During the following Telemarkian period, arc magmatism featured a slightly decreasing apparent mantle input. The Telemarkian arc were likely built upon the same crust that the GAB and Hisingen arcs were built upon, and features a slightly increased amount of crustal reworking.

The interorogenic period is represented by units within central and southern Telemarkia; this period begins with a relatively dominant mantle signature, which then decreases until ~1.22 Ga. At ~1.2 Ga there is another change to a greater mantle input, which again decreases over time. These perturbations in ϵ_{Hf} over time can be related to periods of maximum slab retreat at ~1.35 and ~1.2 Ga, such that magmatism occurred in extensional settings or in thinned crust, where crustal

assimilation was limited. There were no perturbations relating to increased mantle input in the Sveconorwegian period, suggesting that the magmatism involved significant reworking of crust.

Mafic intrusions do not fall on the depleted mantle trend; this can be explained by two models, 1) where the mafic intrusions result from melting of older mafic lower crust, and therefore have evolved ϵ_{Hf} signatures, or 2) where the mafic intrusion result from enriched mantle domains. The latter was favoured by Söderlund et al. (2005), who postulated enrichment of lithospheric mantle via previous subduction episodes; however, some of the contemporaneous arc-related granitoids have more depleted signatures suggesting that a depleted mantle reservoir must have been available. Either the mafic intrusions and arc-related granitoids tapped different mantle sources, or the mafic intrusions comprise a degree of crustal anatexis or assimilation. Most of the mafic intrusions broadly correlate in time with inferred periods of extension; the ~0.95 Ga mafic intrusions can be explained by lithospheric thinning during orogenic collapse.

Perturbations in the ϵ_{Hf} trend to increased mantle input can largely be explained by slab retreat, extensional tectonics, and an increase in mantle addition to magmas; perturbations away from the mantle curve can be explained by compressive or collisional tectonics, and reworking of pre-existing crust. Therefore in its simplest terms, these trends can be interpreted in the context of continental growth versus continental recycling (Figure 9.6b).

9.5.2 Comparison with other evidence

The temporal isotope trend provides a barcode of inferred compressional and extensional events that can be correlated with geodynamic events interpreted from alternative evidence; such evidence is documented below:

9.5.2.1 Compressive phases

Pre-1.65 Ga deformation in the Idefjorden and Eastern Segment is poorly constrained. As discussed previously, some deformation may be related to Hallandian-Danopolonian events. Owing to the existence of sedimentary units within the Idefjorden terrane, 1.6-1.5 Ga events are well-constrained compared to other time periods.

Deformation of the Horred arc, which is related to its accretion onto the Fennoscandian continent, is older than a cross-cutting granite at 1578 ± 7 Ma; with the switch from island arc to continental arc magmatism at 1634 Ma suggesting accretion by this time (Åhäll & Connelly 2008). Volcano-sedimentary units within the Amal formation, of which a rhyolite is dated at 1631 ± 3 Ma, contain source material from an adjacent granite dated at 1634 ± 3 Ma, suggesting rapid unroofing of a magmatic arc at 1.63 Ga (Åhäll & Connelly 2008). A sandstone unit with 1.62 to 1.59 Ga and a few older zircon grains is suggestive of closure of Göteborg-Åmål basins by this time (Åhäll &

Connelly 2008). Deposition and deformation of SLM 1 rocks is constrained to be younger than 1591 ± 8 Ma by the youngest detrital zircon (Åhäll et al. 1998), and older than 1587 ± 3 Ma based on a cross-cutting intrusion (Connelly & Åhäll 1996; Åhäll et al. 1998). Deposition of SLM 2 rocks is bracketed by the youngest detrital zircon to be <1.56 Ga, with cross-cutting intrusions at 1545 ± 5 Ma and 1546 ± 7 Ma suggesting accretion by this time (Åhäll & Connelly 2008). Regional migmatization related to accretion of SLM 2 rocks is estimated at 1.54 Ga from U-Pb data on zircon rims (Åhäll & Connelly 2008). Åhäll & Connelly (2008) distinguish three phases of Hisingen magmatism, at 1.59-1.56 Ga, 1.56-1.55 Ga, and 1.55-1.52 Ga; the youngest phase truncates fabrics in the earlier phases. Deformation is bracketed between 1563 ± 2 and 1558 ± 2 Ma, and between 1555 ± 2 and 1553 ± 2 Ma (Connelly & Åhäll 1996; Åhäll & Connelly 2008) from deformed host rocks and post-kinematic dykes.

Zircon growth at ~ 1.46 - 1.42 Ga in Eastern Segment gneisses suggests a high-grade compressive event (see 9.3.1); however such an event is not recorded in the terranes that the ϵ_{Hf} data are derived from. Deformation is not recorded after this event until the Sveconorwegian period. At ~ 1140 Ma high-grade metamorphism is attributed to collision between the Telemarkia and Idefjorden terranes, and formation of the Bamble and Kongsberg tectonised terranes (Bingen et al. 2008c). At ~ 1100 - 1080 Ma high-grade metamorphism propagated locally into the Idefjorden terrane; the main continent-continent collision phase with associated regional metamorphism occurred between 1050 and 980 Ma (Bingen et al. 2008c).

9.5.2.2 *Retreating phases*

Evidence for slab retreat could be interpreted in the form of extensional basins; within SW Fennoscandia these include: Stora Le Marstrand 1 (~ 1.59 Ga), Stora Le Marstrand 2 (~ 1.55 Ga), the Rjukan Rift (~ 1.51 Ga), the Sæsvatn-Valldall Belt (~ 1.26 - 1.21 Ga), and formations within the Sveconorwegian Supergroup (1.19-1.14 Ga). The mafic intrusions at ~ 1.6 , ~ 1.56 , ~ 1.46 , ~ 1.27 , ~ 1.22 , and ~ 0.95 - 0.97 Ga (Söderlund et al. 2005), can also be interpreted in the context of extensional phases.

In general, major compressional phases (high-grade metamorphism) correlate with gaps in the magmatic record, indicating a lack of magma production during these periods. Minor compressional phases, such as those between 1.6 and 1.5 Ga, do not have a resolvable effect on the isotope trend. The ages of extensional basins and mafic intrusion correlate fairly well with the slab retreat phases inferred from the isotope trends. The 1140-1080 Ma magmatic gap (that was previously recognised by Bingen et al. 2008c) correlates with the interpreted collision between Telemarkia and Idefjorden; this would explain the lack of magmatism in this central region of SW Fennoscandia. The lack of magmatism on the western margin of the region however, is interpreted to reflect a compressive period where previously formed crust was removed via subduction erosion; this can be used to

partly explain the lack of 1.3-1.14 Ga arc crust to the west of Telemarkia, which would correlate with the back-arc basins preserved within Telemarkia.

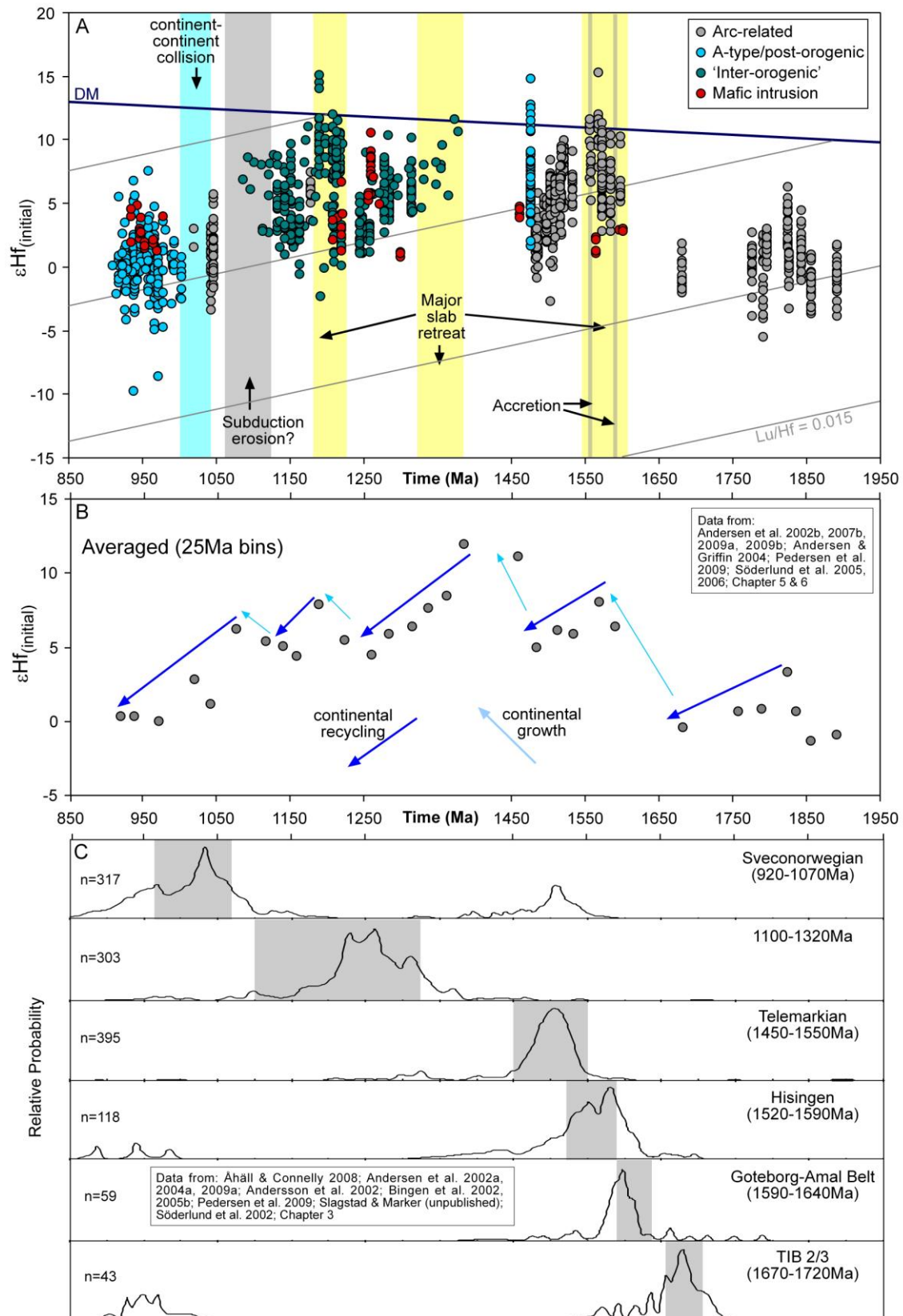


Figure 9.6. A) Compilation of $\epsilon\text{Hf}_{(\text{initial})}$ zircon and whole-rock data from units with igneous prothyls within SW Fennoscandia, plotted versus time (Ma). DM is depleted mantle of Griffin et al. (2000); reference lines are showing evolution of crust with $\text{Lu}/\text{Hf} = 0.015$. B) All $\epsilon\text{Hf}_{(\text{initial})}$ data averaged at 25 Ma bins. C) Compilation of $^{207}\text{Pb}/^{206}\text{Pb}$ zircon ages from various time periods within SW Fennoscandia, shown as cumulative probability plots. Grey bars represent the range of magmatic ages for each period.

9.5.3 Zircon Inheritance

Zircon inheritance has been repeatedly discussed within this study; in Figure 9.6c, a compilation of zircon $^{207}\text{Pb}/^{206}\text{Pb}$ ages for different age bracketed periods is shown. The periods interpreted as reflecting continental arc magmatism are the GAB and Hisingen, these feature a greater proportion of older zircons than the TIB 2/3 and Telemarkian periods which are interpreted to reflect magmatism on attenuated continental crust in extensional settings. The lack of inheritance in the 1100-1320 Ma interorogenic units is compatible with their largely juvenile origin; whereas the abundance of ~1.5 Ga zircons in Sveconorwegian units is compatible with them involving a large proportion of crustal recycling (see Chapter 6). Thus, the interpreted geodynamic settings of these periods are compatible with the pattern of zircon inheritance.

9.6 Supercontinents and global correlations

9.6.1 A global accretionary orogen?

The Proterozoic history of other continents is briefly discussed to examine the extent of 1.8-1.0 Ga accretionary orogens.

9.6.1.1 *Laurentia*

Similarities between the Late Palaeoproterozoic to Mesoproterozoic history of Fennoscandia and Laurentia (Figure 9.7) were observed over two decades ago (Gower 1985; Hoffman 1988). The widely accepted extension of the Grenville orogen in Laurentia to the Sveconorwegian orogen in SW Fennoscandia, means that this connection, known as NENA (Northern Europe North America; Gower et al. 1990), has formed an integral part of most reconstructions of Rodinia (e.g. Li et al. 2008; Evans 2009). Correlations between late-Palaeoproterozoic orogenic belts, and the pre-Sveconorwegian growth of these continents, mean that the NENA connection is also generally correlated at least as far back as the formation of the NUNA (a.k.a Columbia) supercontinent (e.g. Hoffmann 1997; Zhao et al. 2002).

Whitmeyer & Karlstrom (2007) present a comprehensive tectonic model for the continental growth of Northern America during the Proterozoic; in this model, Laurentia grew along its southern margin from 1.8-1.0 Ga by progressive addition of dominantly juvenile arcs and oceanic terranes, in a setting analogous to modern day Indonesia. Crustal provinces in southern Laurentia include the Yavapai province (1.80-1.70 Ga) accreted during the 1.71-1.68 Ga Yavapai orogeny; the Mazatzal province (1.70-1.65 Ga) added during the 1.45-1.30 Ga tectonic event associated with A-type intracratonic magmatism; and the Llano-Grenville province (1.30-1.00 Ga) added during the 1.30-0.95 Ga Grenville orogeny (Whitmeyer & Karlstrom 2007).

In the easternmost part of the Grenville Province, crustal provinces include pre-Labradorian (1800-1770 Ma), early Labradorian (1680-1655 Ma), Mid-to late-Labradorian (1650-1630 Ma), Pinwarian (1520-1460 Ma), Mid-Grenvillian (1040-1020 Ma) and late to post-Grenvillian (1000-940 Ma) events (Gower et al. 2008). This crustal province, which is the closest spatially in Laurentia to Fennoscandia (excluding Greenland), has a strikingly similar history to that of SW Fennoscandia. Telemarkian magmatism in Fennoscandia has a direct correlation with the Pinwarian event, which also involves arc magmatism built upon Labradorian crust (Gower 1996; Gower et al. 2008). Further south, the Muskoka domain in the southwestern Grenville Province also has a striking similarity to Telemarkian events, with coeval to younger continental arc magmatism from 1480 to 1430 Ma, which involves intra-arc extension and contemporaneous A-type magma generation in a back-arc environment (Slagstad et al. 2004). The extent of Telemarkian age crust in Laurentia is extended across the continent by isotopic mapping using Nd model ages; Dickin & Higgins (1992) suggest a vast region of the central Grenville Province was part of a 1.5 Ga crust-forming event.

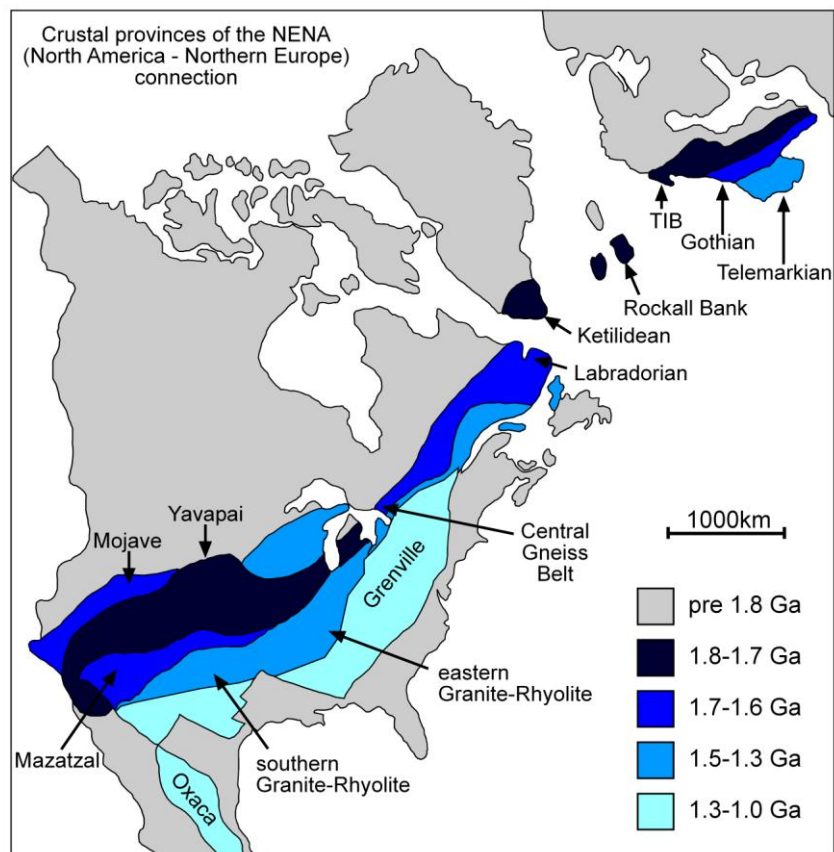


Figure 9.7. 1.8 - 1.0 Ga Crustal provinces in Laurentia and Fennoscandia (after Karlstrom et al. 2001).

As well as Fennoscandia, Laurentia is correlated eastward with Greenland and parts of the British Isles. The 1.9-1.78 Ga Makkovik province in the easternmost part of the Grenville Province is related to a continent margin setting with both juvenile Palaeoproterozoic and reworked Archaean components (Kerr et al. 1996; Ketchum et al. 2001). The Makkovik province is correlated with the

Ketilidean province of southern Greenland, which is a dominantly juvenile arc located on the edge of an Archaean domain (Chadwick & Garde 1996; Garde et al. 2002). Makkovikian-Ketilidean and pre-Labradorian provinces are correlated with the ~1.75 Ga Rockall Bank (Morton & Taylor 1991), the Rhinns complex in the Inner Hebrides (Muir et al. 1994), and the Annagh gneiss complex in Ireland (Menuge & Daly 1994). These dominantly juvenile belts which formed on the exterior of Palaeoproterozoic and Archaean domains are broadly correlative with the formation of the Transcandinavian Igneous Belt on the southwestern edge of the Fennoscandian continent.

9.6.1.2 Amazonia

The Amazonian craton comprises an Archaean core which is flanked to the southwest by successively younging Palaeo- to Mesoproterozoic lithotectonic domains, this feature is similar to that of the Fennoscandian Shield, and has led to correlations being made across the two continents (Geraldes et al. 2001; Cordani et al. 2009; Johansson 2009). The major geological provinces are: Central Amazonian (CAP - >2.3 Ga), Maroni-Itacaiúnas (MIP – 2.2-1.95 Ga), Ventuari-Tapajós (VTP – 1.95-1.80 Ga), Rio Negro-Juruena (RNJP – 1.8-1.55 Ga), Rondonian-San Ignacio (RSIP – 1.55-1.3 Ga) and Sunsás (SP – 1.3-1.0 Ga) (Tassinari et al. 1999). The VTP, RNJP and part of the RSIP represent a vast area of juvenile continental crust that was formed by accretion of magmatic arcs, whereas the younger domains are dominated by crustal reworking (Tassinari et al. 1999; Geraldes et al. 2001). The 1.55-1.30 Ga Rondonian-San Ignacio province involves a collisional orogeny involving a possible microcontinent, accretionary belts, and inboard plutonism (Cordani et al. 2009); a distinct correlation can be made with events of this age in Fennoscandia.

9.6.1.3 Australia

During the amalgamation of Rodinia, eastern Australia is typically connected to Laurentia either in the western US (AUSWUS, Karlstrom et al. 1999, 2001) or in northern Canada (SWEAT, Dalziel 1991; Hoffman 1991). A link between these continents is also made for the Nuna supercontinent, in which Australia is typically placed in a SWEAT-type position to the northwest of Laurentia (Betts et al. 2008). Palaeomagnetic data suggest Australia and Laurentia were contiguous from 1730-1595 Ma, but also permit a continued association until ~1200 Ma (Payne et al. 2009). However, a 1.6-1.5 Ga hotspot track in eastern Australia suggests that Laurentia and Australia diverged during this period, with Laurentia staying at low latitudes, and Australia drifting to high latitudes (Betts et al. 2007). Events in the 1.8-1.6 Ga period are particularly linked across Australia and Laurentia. In this period episodic orogenesis occurred along the southern margin of the Australian continent above a north-dipping subduction system, with the pattern of accretion suggesting southward migration of the subduction zone via slab rollback and oceanward stepping behind accreted blocks (Betts & Giles, 2006). Episodes of accretion that link Laurentia with Australia include the ~1780 Ma Yapunka-Yamba-Bow Medicine orogens, the ~1.74-1.7 Ga Strangeways-Kimban-Nimrod-Yavapai orogens, and the 1.65-1.64 Ga Leibig-Kararan-Maztazal orogens (Betts et al. 2008). Some of the

evidence used to infer a subduction zone setting on the southern margin has been refuted (Payne et al. 2010); instead convergence may have occurred under the eastern margin of the continent (Payne et al. 2009). The 1.5-1.4 Ga period is host to extension, basin formation and anorogenic magmatism (Betts & Giles 2006; Wade et al. 2007). After 1.5 Ga the South Australian Craton (Mawsonland) is postulated to have broken away from the North Australian Craton, and then to have reattached during the 1.33-1.1 Ga Albany-Fraser-Musgrave orogenies (Giles et al. 2004). The Australian continent appears to have had a more complex history of accretion, orogenesis and break-up than the southern margin of Laurentia and its extension into Fennoscandia; during the 1.8-1.5 Ga period it can still be considered to be part of an accretionary orogen, but a part which featured more recycling of older crust than juvenile addition (Betts et al. 2008).

9.6.1.4 China

China is split into two cratons, the South China Craton (SCC) and North China Craton) NCC; the SCC appears to be poorly constrained in terms of its Proterozoic history and lacks palaeomagnetic key poles, it therefore doesn't feature in some Nuna supercontinent reconstructions or has an unconstrained placement (e.g. Zhao et al. 2002). The NCC comprises two separate blocks, namely the Western Block and Eastern Block; these two blocks amalgamated in the late Palaeoproterozoic at ~1.85 Ga, forming the Trans-North China Orogen (Zhao et al. 2001; 2002; Santosh 2010). The NCC is included in the Nuna supercontinent in a variety of positions; some models have connected the Trans-North China Orogen with other Palaeoproterozoic orogens such as those in India (Zhao et al. 2004, 2006), whereas others have connected the Northern Hebei orogen that forms the northern margin of the NCC with other Palaeoproterozoic orogens (Kusky et al. 2007 GR, Kusky & Santosh 2009; Santosh 2010).

The 1.8-1.4 Ga Xiong'er belt in the southwestern margin of the NCC is interpreted by some to occur in a continental rift environment (Zhao et al. 2002; Peng et al. 2008), whereas others advocate a continental margin setting (Zhao et al. 2003, 2009; He et al. 2008, 2010). The Xiong'er belt is bounded to the south by the 1.6-1.4 Ga Kuanping ophiolite Complex; combining this with the arc setting for the Xiong'er belt, Zhao et al. (2003) suggest that the southern margin of the NCC was bordered by a 1.8-1.3 Ga subduction related belt. If the accretionary margin postulate is accepted, then the NCC must have faced an open ocean along its southwestern margin for this time period; it therefore seems credible to place NCC in the context of a Nuna supercontinent based on this accretionary margin (see Figure 9.8).

The 1.6-1.2 Ga Zhaertai-Bayan Obo rift zone along the northern margin of the NCC is interpreted to result from fragmentation of the NUNA supercontinent (Zhao et al. 2003). A correlation between 1.35 Ga diabase sills in the NCC with 1.4-1.3 Ga mafic dyke swarms in Laurentia, Fennoscandia, Siberia, Australia and Antarctica (Ernst et al. 2008), led Zhang et al. (2009) to infer that the NCC

was part of Nuna until at least this time. Based on extensional magmatism, others consider the NCC to have been involved in break-up of Nuna by 1.6 Ga (Rogers & Santosh 2002).

9.6.2 Proterozoic supercontinents

The 1.8-1.0 Ga long-lived convergent orogen of Karlstrom et al. (2001) can be extended across at least the Amazonia, Fennoscandia, Laurentia, Antarctica, Australia and North China cratons. This accretionary orogen formed on the margin of these continents after the formation of the ~1.8 Ga Nuna supercontinent. Supercontinents may form by two end-member mechanisms: introversion in which interior ocean floor is preferentially subducted, and extroversion in which exterior ocean floor is preferentially subducted (Murphy & Nance 2003). When a supercontinent breaks-up, the trailing edge of dispersing continents will comprise passive margins flanking relatively new oceanic lithosphere, whilst the leading edges will comprise subduction margins that recycle and accrete older mantle lithosphere that surrounded the supercontinent (Murphy et al. 2009).

The Nuna supercontinent partially broke-up at 1.8-1.5 Ga; after this time the continents dispersed before amalgamating again to form the supercontinent Rodinia at ~1.0 Ga. During dispersal, the 1.8-1.3 Ga global accretionary belt can be interpreted in the context of a leading edge, where it recycled the exterior ocean, and accreting oceanic terranes. During retreating phases of this accretionary belt, oceanward migration of the subduction zone trench must have exceeded migration of the continent, allowing for slab rollback. During advancing phases the oceanward migration of the continent would have recycled any oceanbound terranes and lithosphere in an Andean-type setting. The dominance of arc-related 1.8-1.5 Ga crust, and lack of arc-related 1.5-1.1 Ga crust in Fennoscandia, suggests that the margin was dominantly retreating prior to 1.5 Ga, and dominantly advancing after 1.5 Ga.

The idea of the 1.8-1.3 Ga accretionary orogen acting as a leading edge forms the basis of the supercontinent reconstruction shown in Figure 9.8. This reconstruction is largely based on that of Zhao et al. (2002), which was later modified by Zhao et al. (2004) and Hou et al. (2008a). The major change from this previous model is that the global 1.8-1.3 Ga accretionary belt now includes the southwestern margin of the North China Craton, and the southern margin of Australia and its Mawsonland counterpart. The continents are arranged so that the 1.8-1.3 Ga belt forms an exterior belt encircling the supercontinent; this differs from previous reconstructions in which the accretionary belts have only occurred on one side of the supercontinent (e.g. Zhao et al. 2002; Hou et al. 2008; Bispo-Santos et al. 2008). This postulated reconstruction is not constrained by palaeomagnetic data, but does comprise individual fits between continents and some generalised global fits that have been constrained by palaeomagnetism.

During break-up of the Nuna supercontinent after 1.8 Ga, Laurentia and Fennoscandia likely stayed together to at least 1.25 Ga, (Buchan et al. 2000); Amazonia may also have been connected to Fennoscandia until the Sveconorwegian orogeny (Johansson 2009), or may have broken off earlier to then re-amalgamate at ~1.45 Ga (Bogdanova et al. 2001, 2008). Australia may have stayed connected to Laurentia till the formation of Rodinia (Karlstrom et al. 2001). During the formation of Rodinia, the accretionary belt in Laurentia and Baltica then became host to a global-scale interior orogen, the Grenville Belt. To go from an exterior to interior belt, the supercontinent must have extroverted. This is compatible with the postulated rotation of the East European Craton (Starmer 1996), and collision of Amazonia with Laurentia and the EEC (Johansson 2009; Gower et al. 2008; Li et al. 2008).

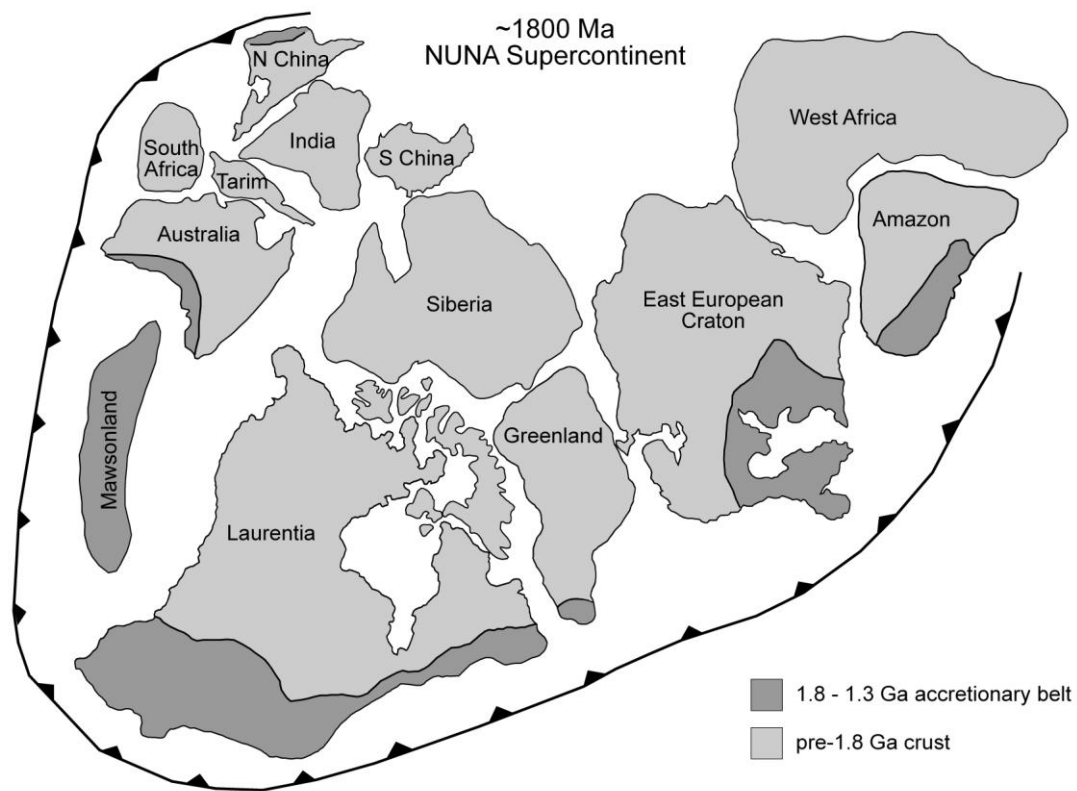


Figure 9.8. Late Palaeoproterozoic reconstruction of Nuna. Laurentia - Australia - Mawsonland fit modified from Betts et al. (2008); Laurentia - Greenland - East European Craton - Amazon fit modified from Pesonen et al. (2003) and Bispos-Santos et al. (2008); India - N China, Amazon - W Africa - Laurentia - Siberia - Greenland, and S Africa - Australia - Tarim fit modified from Zhao et al. (2002) and Hou et al. (2008a). The location of the S China block is currently unconstrained.

In this model of extroversion of Nuna to form Rodinia, both continental growth and recycling were focussed along the edges of continents as they consumed oceanic lithosphere during their dispersal. Minor amounts of continental growth will have occurred within the interior of the supercontinent during rifting events; some of this rifting is evident as major radiating dyke swarms, i.e. Mackenzie dyke swarm, which has led to inferences about the role of mantle plumes in the break-up of supercontinents (Ernst & Buchan 2002; Hou et al. 2008b).

9.7 Continental growth – a final comment

Whitmeyer & Karlstrom (2007) in their model of Proterozoic growth of Laurentia, present a model of continental growth termed the ‘arc-accretion-assembly-stabilization’ model, which can be applied to accretionary orogens. This model involves three processes; the first comprises accretion of mafic, intermediate and felsic material from the mantle via subduction processes during the multistage evolution of outboard arcs. The second process involves assembly of a mixture of juvenile terranes and older crustal fragments during a series of orogenic episodes, with the style of deformation being subduction-dominated; this multistage assembly includes continental growth via crustal thickening, tectonic imbrications and further differentiation and modification of crust during suturing. The third process involves stabilisation of continental crust via crustal melting, this melting is initiated by crustal thickening and results in periods of late-orogenic granitoid magmatism that stitch sutures and aid the differentiation of the crust.

The arc-accretion-assembly-stabilization model and the processes described above provide a suitable explanation for the formation of Fennoscandian continental crust. The Archaean domains were formed by 2.5 Ga; whether they were formed by subduction-related or geodynamic processes different to those seen today is an interesting topic, but is outside the realm of this thesis. The 2.1-1.8 Ga Svecofennian period saw the multistage assembly of these Archaean domains along with the assembly of arcs and microcontinents at differing stages of maturity. Orogenesis, crustal thickening and orogenic collapse, meant the Palaeoproterozoic and Archaean domains of Fennoscandia were largely stabilised by 1.8 Ga. Further crustal differentiation occurred during repeated episodes of intraplate, commonly A-type, granitoid genesis; these can be related to lithospheric extension associated with distal effects of convergent margin tectonism, and post-orogenic crustal relaxation. After 1.8 Ga the southwest margin of Fennoscandia involved further multistage accretion of largely juvenile crust; this crust was stabilised and differentiated during Sveconorwegian collisional orogenesis (and possibly Hallandian-Danoplionian orogenesis). Since the Sveconorwegian orogeny, the continental crust of Fennoscandia has only seen minor crustal additions such as those in the Oslo Rift (see Larsen et al. 2008), but has suffered major tectonic (as opposed to magmatic) remobilisation of crust along its margins, i.e. during the Caledonian and Timanian orogenies (see Gee et al. 2008).

In Chapter 1, the apparent episodic nature of continental crustal growth was cited, along with the concept that such apparent episodicity may arise from preservational bias in the rock record. This concept suggests that the dominant setting for producing continental crust is at subduction zone margins, but within this setting there is poor potential for preservation; in collisional settings there is little new crust produced, but this setting has a large potential for preservation; and in extensional

settings there is limited zircon-producing crust formed, and this may also have a poor preservational potential (Hawkesworth et al. 2009). Because of this bias, it is likely that periods when collisional settings were most prolific, i.e. when supercontinents amalgamate, will appear to have the greatest amount of crustal growth. The similarity in peaks of crystallisation age with ages of supercontinents (see Figure 1.1), suggests this concept holds true. The peaks in crystallisation age at 1.9 Ga and 2.7 Ga also match up with peaks in juvenile crustal addition, suggesting there was large-scale formation of crust, as well as reworking in collisional settings.

Using Fennoscandia as an example, we can gain some insight in to this important period. During the 2.1-1.8 Ga period, major crustal additions comprised 2.1-2.0 Ga microcontinents with an undefined history, >2.02-1.83 Ga juvenile arcs, and magmatic addition in continental arcs at 1.89 and 1.8 Ga (Lahtinen et al. 2009). There is a lack of 2.5-2.1 Ga age crust, and few detrital zircons have been found within this age range (Lahtinen et al. 2009); suggesting that crustal formation was limited, and that any such crust produced was not preserved. This gap in the 2.5-2.1 Ga period correlates globally (see Figure 1.1). Using the preservation bias concept (Hawkesworth et al. 2009), this period likely involved a lack of collisional orogenies, this in turn can be interpreted as reflecting rifting of the Superia and Slavia cratons (Bleeker 2003). The 1.9 Ga peak in zircon crystallisation ages (and juvenile crustal addition) has previously been linked to a mantle superplume (Condie 2002), but the width of the peak and the existence of a number of individual peaks within the zircon record (Condie et al. 2009), means that a single plume event cannot explain the data. It is suggested that the apparent increase in crustal growth is likely a consequence of both preservation bias during amalgamation of the Nuna supercontinent, but also of increased production of 2.1-1.9 Ga crust via tectonic switching in retreating accretionary orogens that formed just prior to collision. Apparent episodicity of crustal formation is a result of preservational bias that can be linked to formation and break-up of supercontinents on a global scale, but on a regional scale can be linked to episodic migration of subduction zone margins.

Accretionary orogens are the dominant setting for growth and differentiation of continental crust; modern examples can be found in the western Pacific (mainly retreating) and in the eastern Pacific (i.e. Andes; mainly advancing). Ancient examples may have been completely recycled by younger events, however, well-preserved examples exist from a variety of ages (e.g. the 1.8-1.1 Ga belt of SW Fennoscandia and Laurentia, the 1000-325 Ma Central Asian Orogenic Belt, and the 515-330 Ma Tasmanides of eastern Australia); each of these provide a 'tectonic dynasty' for the study of crustal processes (see Åhäll & Larson 2000 and references within).

9.7.1 A final comment on the final comment - continental versus crustal growth

Discussion within this thesis has involved settings, rates and relative amounts of continental growth. It is important to highlight that in the context of this study, continental growth refers to localised

addition of juvenile mantle-derived material to the continental crust. Such addition does not imply a net addition to the volume of global continental crust, since at any one time the loss of continental crust globally may outweigh the addition of continental crust. Also, within the context of continental crust, this study has not considered the lithospheric mantle. There is evidence that the sub-continental lithospheric mantle (SCLM) under a large proportion (>70%) of the continental crust is Archaean in age (Begg et al. 2009; Griffin et al. 2009); suggesting that Archaean SCLM has a higher preservation potential than young continental crust. If global crustal growth models account for both the SCLM and the overlying continental crust, the increase in crustal volume since the Archaean will be near zero (Begg et al. 2009).

Appendix

XRF methodology and precision

Samples were prepared for XRF analysis by removing their weathered surfaces, broken up using a mechanical jaw-splitter, crushed to a coarse powder using an engineer's fly press, and milled to a fine powder in agate pots. At the University of Leicester samples were analysed on a Philips PW1400 X-ray fluorescence spectrometer (sample numbers SA3-XX) or a PANalytical Axios Advanced XRF spectrometer (sample numbers SA7-XX and SA8-XX). There was no significant difference between results from the two instruments.

Loss on ignition was determined from powders dried overnight at 105°C, then ignited at 950°C for 1 hour. Major elements were determined on fused glass beads prepared from ignited powders, with a sample to flux ratio of 1:5, 80% Li metaborate: 20% Li tetraborate flux; the results are quoted as component oxide weight percent, re-calculated to include LOI. Trace elements were analysed on 32mm diameter pressed powder briquettes, prepared from 10g fine ground powder mixed with ~20-25 drops 7% PVA solution and pressed at 10 tons per square inch.

Components with concentrations below the lower limit of detection reported as bdl. LLDs calculated from $3\text{-}\sigma$ for the background determination. At the Norwegian Geological Survey, samples (sample numbers MMxxxxxx and ROGxxx) were analysed on a PANalytical Axios Advanced XRF spectrometer using methods similar to those above, and on a Finnigan MAT ICP-MS (Y, Zr, Nb, REE, Ta, Hf, Th and U), see Flem et al. (2005) for full description of the methods.

Table 10.1 Average precision and lower limits of detection (LLD) based on repeat analyses of CRMs, major element data from the Norwegian Geological Survey has a similar precision to those from University of Leicester.

	Precision 2 σ %	LLD	Precision (UoL)		LLD	Precision (NGU)			
			@ >15ppm 2 σ %	@ <15ppm 2 σ (ppm)		@ <50ppm 2 σ %	@ >50ppm 2 σ %		
SiO₂	1.2	0.015							
TiO₂	3.2	0.002	Cr	5.5	5.0	0.7	Cr	<10	<5
Al₂O₃	1.9	0.008	Ni	1.4	4.3	0.6	Ni	<10	<5
Fe₂O₃	1.4	0.001	V	1.4	12.3	0.8	V	<10	<5
MnO	6.0	0.001	Co	6.3	7.4	0.8	Co	<10	<5
MgO	3.8	0.048	Sc	22.9	12.0	0.9	Sc	<20	<10
CaO	6.3	0.001	Zn	2.0		0.7	Zn	<10	<5
Na₂O	6.3	0.014	Ga	6.5		0.4	Ga	<10	<5
K₂O	11.0	0.002	Zr	4.5		0.2	Zr	<20	<10
P₂O₅	8.3	0.001	Nb	1.9	5.1	0.2	Nb	<10	<5
			Th	4.7	4.3	0.4	Th	<10	<5
			U	3.0	11.3	0.4	U	<10	<5
			Pb	6.8	4.6	0.5	Pb	<10	<5
			Sr	0.7	1.1	0.2	Sr	<10	<5
			Rb	4.4	4.0	0.2	Rb	<10	<5
			Ba	6.3	10.0	2.9	Ba	<20	<10
			Cs		6.4	1.4	Cs	<50	<25
			La	8.0	9.9	1.7	La	<20	<10
			Ce	8.1	19.5	6.6	Ce	<30	<15
			Nd	7.9	13.6	2.4	Nd	<20	<10
			Y	5.8	0.7	0.2	Y	<10	<5

Sample	MM 036632	MM 036707	MM 036717	MM 036720	MM 036724	MM 036730
UTM x	348322	347157	354445	354919	355941	347641
UTM y	6616123	6603168	6604423	6604757	6604923	6613373
Age	Telemarkian	Telemarkian	Telemarkian	Telemarkian	Telemarkian	Telemarkian
Suite	Granitoid	Granitoid	Granitoid	Granitoid	Granitoid	Granitoid
Lithology	Deformed grey porphyritic biotite-hornblende granitoid	Deformed porphyritic biotite-granite	Deformed dark grey fine-porphyritic granitoid	Deformed dark grey porphyritic biotite-granitoid	Deformed dark grey porphyritic biotite-granitoid	Weakly deformed grey porphyritic biotite-hornblende granitoid
Mineralogy		Ksp, Pl, Qz, Ep, Bt, Acc- Opq, Tt	Qz, Ksp, Pl, Bt, Ep	Qz, Ksp, Pl, Bt, Ep + Opq		
Geochem	x	x	x	x	x	x
REE	x	x	x	x	x	x
Thin section		x	x	x		
Other						

Sample	ROG396	ROG400	ROG401	ROG402	ROG413	ROG416
UTM x	344634	344093	344067	344078	350990	347437
UTM y	6595471	6594399	6593551	6593803	6593628	6593415
Age	Telemarkian	Telemarkian	Telemarkian	Telemarkian	Telemarkian	Telemarkian
Suite	Granitoid	Granitoid	Granitoid	Granitoid	Granitoid	Granitoid
Lithology	Porphyritic granitoid	Porphyritic granitoid	Porphyritic granitoid	Porphyritic granitoid	Coarse-grained porphyritic granite	Porphyritic granitoid
Mineralogy						
Geochem	x	x	x	x	x	x
REE	x	x	x	x	x	x
Thin section						
Other						

Sample	MM 026153	MM 026173	MM 036672	MM 036673	MM 036676	MM 036677
UTM x	343454	338888	352723	353796	356627	354078
UTM y	6592899	6591831	6595827	6596944	6595116	6593768
Age	Telemarkian	Telemarkian	Telemarkian	Telemarkian	Telemarkian	Telemarkian
Suite	Amphibolite	Amphibolite	Amphibolite	Amphibolite	Amphibolite	Amphibolite
Lithology	Deformed fine-grained amphibolite	Deformed massive amphibolite	Undeformed metagabbro	Weakly deformed hornblende quartz-diorite	Coarse-grained hornblende-granite	Deformed dark grey hornblende-quartz-diorite
Mineralogy					K-sp + Plag + Qtz + Amph (act) + Opq + Ep + acc.tit	
Geochem	x	x	x	x	x	x
REE	x	x	x	x	x	x
Thin section					x	
Other					U-Pb-NS,Hf-O	

Sample	MM 036681	MM 036682	MM 036686	MM 036692	MM 036693	MM 036694
UTM x	345295	344831	345144	345953	345932	346424
UTM y	6603186	6603219	6604380	6606022	6606001	6606658
Age	Telemarkian	Telemarkian	Telemarkian	Telemarkian	Telemarkian	Telemarkian
Suite	Amphibolite	Amphibolite	Amphibolite	Amphibolite	Amphibolite	Amphibolite
Lithology	Undeformed medium-grained metadiorite	Metadiorite, scattered feldspar phenocrysts	Weakly deformed black amphibolite	Fine-grained black amphibolite	Fine-grained black amphibolite	Weakly deformed med.-grained porphyritic gabbro
Mineralogy	Pl, Amph, Qz, Bt, Opq, Chl - Acc - Ap, Ep					Pl, Bt, Qz, Tt, Acc - Opq, Ap, Ep
Geochem	x	x	x	x	x	x
REE	x	x	x	x	x	x
Thin section	x					x
Other						

Sample	MM 036695	MM 036698	MM 036699	MM 036711	MM 036712	MM 036713
UTM x	346319	346039	346015	350822	351583	353018
UTM y	6606505	6606404	6606353	6603975	6603907	6603991
Age	Telemarkian	Telemarkian	Telemarkian	Telemarkian	Telemarkian	Telemarkian
Suite	Amphibolite	Amphibolite	Amphibolite	Amphibolite	Amphibolite	Amphibolite
Lithology	Deformed coarse-grained porphyritic gabbro	Deformed fine-grained massive amphibolite	Deformed fine-grained massive amphibolite	Undeformed porphyritic hornblende-biotite granodiorite	Undeformed porphyritic hornblende-biotite granodiorite	Weakly deformed porphyritic hornblende granitoid
Mineralogy	Pl + Bt + Qz + Tt + Acc - Opq + Ap + Ep			Pl + Qz + Ksp + Bt + Amph + Acc - Opq + Tt + Ap	Pl + Qz + Ksp + Bt + Amph + Acc - Opq + Tt + Ap	Pl + Ksp + Qz + Amph + Bt + Acc - Opq + Tt + Ap
Geochem	x	x	x	x	x	x
REE	x	x	x	x	x	x
Thin section	x			x	x	x
Other						

Sample	ROG394	ROG421	ROG399	ROG525	MM 2235	MM 2241
UTM x	345803	354199	344289	356618	348106	349390
UTM y	6595821	6595345	6594908	6595498	6570396	6578545
Age	Telemarkian	Telemarkian	Telemarkian	Telemarkian	Telemarkian	Telemarkian
Suite	Amphibolite	Amphibolite	Amphibolite	Amphibolite	Grey Gneiss	Grey Gneiss
Lithology	Amphibolite	Amphibolite	Amphibolite	Medium-grained hornblende gabbro	Banded fine-grained grey biotite gneiss	Banded fine-grained grey biotite gneiss
Mineralogy				Pl + Amph + Qz + Ksp + Ep + Chl + Opq	Qz + Pl + Ksp + Bt + Chl + Acc - Opq + Ap	Qz + Pl + Ksp + Bt + Chl + Acc - Opq + Ap
Geochem	x	x	x	x	x	x
REE	x	x	x	x	x	x
Thin section				x	x	x
Other				U-Pb-NS,Hf-O	U-Pb-NS,Hf-O	U-Pb-NS,Hf-O

Sample	MM 026152	MM 026157	MM 026160	MM 026161	MM 026166	MM 026170
UTM x	343401	344535	336908	336803	339975	339629
UTM y	6592974	6595278	6587700	6587753	6593759	6593023
Age	Telemarkian	Telemarkian	Telemarkian	Telemarkian	Telemarkian	Telemarkian
Suite	Grey Gneiss	Grey Gneiss	Grey Gneiss	Grey Gneiss	Grey Gneiss	Grey Gneiss
Lithology	Deformed grey gneiss, diffusely porphyritic	Massive dark grey fine-grained grey gneiss	Grey biotite gneiss, med.-grained, diffusely banded	Grey biotite gneiss, med.-grained, diffusely banded	Weakly deformed porphyritic diorite	Deformed dark grey diorite with hornblende spots
Mineralogy	Pl + Qz + Ksp + Bt + Amph + Acc - Opq + Ep + Ap					
Geochem	x	x	x	x	x	x
REE	x	x	x	x	x	x
Thin section	x					
Other						

Sample	MM 026171	MM 026181	MM 026263	MM 026265	MM 036575	MM 036576
UTM x	339456	338373	351926	352436	345495	343349
UTM y	6592844	6588018	6600846	6600597	6596435	6592617
Age	Telemarkian	Telemarkian	Telemarkian	Telemarkian	Telemarkian	Telemarkian
Suite	Grey Gneiss	Grey Gneiss	Grey Gneiss	Grey Gneiss	Grey Gneiss	Grey Gneiss
Lithology	Deformed fine-grained grey biotite-gneiss	Fine-grained diffusely banded biotite-gneiss	Fine-grained dark grey porphyritic gneiss	Fine-grained dark grey porphyritic gneiss	Deformed fine-grained dark grey porphyritic gneiss	Deformed fine-grained dark grey porphyritic gneiss
Mineralogy						
Geochem	x	x	x	x	x	x
REE	x	x	x	x	x	x
Thin section						
Other						

Sample	MM 036577	MM 036591	MM 036594	MM 036595	MM 036600	MM 036601
UTM x	344087	334955	334829	334497	333330	334950
UTM y	6594373	6590672	6590472	6590203	6590247	6590560
Age	Telemarkian	Telemarkian	Telemarkian	Telemarkian	Telemarkian	Telemarkian
Suite	Grey Gneiss	Grey Gneiss	Grey Gneiss	Grey Gneiss	Grey Gneiss	Grey Gneiss
Lithology	Deformed fine-grained dark grey porphyritic gneiss	Deformed fine-grained grey porphyritic gneiss	Deformed fine-grained dark grey gneiss			
Mineralogy						
Geochem	x	x	x	x	x	x
REE	x	x	x	x	x	x
Thin section						
Other						

Sample	MM 036631	MM 036671	MM 036674	MM 036675	MM 036678	MM 036683
UTM x	348858	351638	352446	352254	359462	345258
UTM y	6616037	6595280	6594152	6594065	6596440	6604120
Age	Telemarkian	Telemarkian	Telemarkian	Telemarkian	Telemarkian	Telemarkian
Suite	Grey Gneiss	Grey Gneiss	Grey Gneiss	Grey Gneiss	Grey Gneiss	Grey Gneiss
Lithology	Deformed light grey fine-grained gneiss	Undeformed porphyritic metadiorite	Massive hornblende quartz-diorite	Deformed fine-grained dark grey porphyritic gneiss	Deformed fine-grained dark grey biotite gneiss	Undeformed coarse-grained hornblende-biotite granitoid
Mineralogy	Pl + Qz + Ksp + Ms + Bt + Acc - Opq					Qz + Pl + Ksp + Bt + Amph + Ep + Acc - Tt
Geochem		x	x	x	x	x
REE	x	x	x	x	x	x
Thin section	x					x
Other	U-Pb-NS, Hf-O					

Sample	MM 036688	MM 036690	MM 036700	MM 036701	MM 036702	MM 036704
UTM x	345444	345613	346799	347079	346991	347497
UTM y	6605437	6605587	6606932	6607172	6606998	6608282
Age	Telemarkian	Telemarkian	Telemarkian	Telemarkian	Telemarkian	Telemarkian
Suite	Grey Gneiss	Grey Gneiss	Grey Gneiss	Grey Gneiss	Grey Gneiss	Grey Gneiss
Lithology	Fine-grained massive dark grey gneiss	Fine-grained massive dark grey gneiss	Massive fine-grained biotite-hornblende grey gneiss	Massive fine-grained biotite-hornblende grey gneiss	Massive fine-grained biotite-hornblende grey gneiss	Fine-grained grey gneiss with quartz lamellae
Mineralogy						
Geochem	x	x	x	x	x	x
REE	x	x	x	x	x	x
Thin section						
Other						

Sample	MM 036706	MM 036710	MM 036680	MM 036714	MM 036715	MM 036716
UTM x	346743	348284	359804	354244	353728	353779
UTM y	6607670	6602040	6597146	6604274	6604119	6604134
Age	Telemarkian	Telemarkian	Telemarkian	Telemarkian	Telemarkian	Telemarkian
Suite	Grey Gneiss	Grey Gneiss	Grey Gneiss	Grey Gneiss	Grey Gneiss	Grey Gneiss
Lithology	Deformed greenish grey massive quartz-diorite	Deformed medium-grained porphyritic grey granodiorite	Fine-grained light grey gneiss	Fine-grained grey gneiss	Medium-grained hornblende diorite	Medium-grained hornblende diorite
Mineralogy	Pl + Amph + Qz + Ksp + Acc - Ep	Pl + Qz + Bt + Ksp + Acc - Ep				
Geochem	x	x	x	x	x	x
REE	x	x	x	x	x	x
Thin section	x	x				
Other						

Sample	MM 036721	MM 036722	MM 036725	MM 036726	MM 036727	MM 036728
UTM x	355193	355280	355427	356619	356461	356309
UTM y	6604831	6604847	6604887	6604998	6604978	6604825
Age	Telemarkian	Telemarkian	Telemarkian	Telemarkian	Telemarkian	Telemarkian
Suite	Grey Gneiss	Grey Gneiss	Grey Gneiss	Grey Gneiss	Grey Gneiss	Grey Gneiss
Lithology	Fine-grained massive dark grey gneiss	Fine-grained massive dark grey gneiss with hornblende	Fine-grained massive dark grey gneiss	Deformed light grey scattered porphyritic grey gneiss	Deformed dark grey small porphyritic metadiorite	Deformed light grey scattered porphyritic gneiss
Mineralogy				Qz + Pl + Ksp + Bt + Amph + Tt + Acc - Ep	Pl + Amph + Ksp + Qz + Tt + Chl + Acc - Ep	Pl + Amph + Ksp + Qz + Bt + Tt + Chl + Acc - Ep
Geochem	x	x	x	x	x	x
REE	x	x	x	x	x	x
Thin section				x	x	x
Other						

Sample	Ro-102B	ROG339-1	ROG339-2	ROG340	ROG369	ROG393
UTM x	344250	357733	357733	357601	344901	345891
UTM y	6510480	6597315	6597315	6597216	6594801	6595966
Age	Telemarkian	Telemarkian	Telemarkian	Telemarkian	Telemarkian	Telemarkian
Suite	Grey Gneiss	Grey Gneiss	Grey Gneiss	Grey Gneiss	Grey Gneiss	Grey Gneiss
Lithology	Deformed grey migmatitic gneiss	Deformed fine-grained grey gneiss	Deformed fine-grained grey gneiss	Deformed medium-grained grey gneiss	Deformed medium-grained porphyritic grey gneiss	Deformed fine-grained porphyritic grey gneiss
Mineralogy						
Geochem	x	x	x	x	x	x
REE	x	x	x	x	x	x
Thin section						
Other	U-Pb-NGU,Hf					

Sample	ROG395	ROG397	ROG398	ROG403	ROG404	ROG405
UTM x	345145	344576	344306	343761	343312	342955
UTM y	6595826	6595353	6594918	6593317	6592601	6591765
Age	Telemarkian	Telemarkian	Telemarkian	Telemarkian	Telemarkian	Telemarkian
Suite	Grey Gneiss					
Lithology	Deformed fine-grained grey gneiss					
Mineralogy						
Geochem	x	x	x	x	x	x
REE	x	x	x	x	x	x
Thin section						
Other						

Sample	ROG406	ROG407	ROG408	ROG409	ROG410	ROG411
UTM x	342735	342453	342330	342124	347762	348534
UTM y	6591576	6590679	6590245	6589555	6595136	6594400
Age	Telemarkian	Telemarkian	Telemarkian	Telemarkian	Telemarkian	Telemarkian
Suite	Grey Gneiss					
Lithology	Deformed fine-grained grey gneiss					
Mineralogy						
Geochem	x	x	x	x	x	x
REE	x	x	x	x	x	x
Thin section						
Other						

Sample	SA7-80	SA7-91	SA7-92	SA7-128	SA7-129	SA7-133
UTM x	348988	338383	359281	353598	352845	361341
UTM y	6603505	6627090	6642829	6604075	6604012	6599002
Age	Telemarkian	Telemarkian	Telemarkian	Telemarkian	Telemarkian	Telemarkian
Suite	Granitoid	Granitoid	Granitoid	Granitoid	Granitoid	Granitoid
Lithology	Weakly deformed coarse-grained biotite-hornblende granite	Undeformed medium grained biotite granite	Deformed medium-grained biotite granite	Undeformed coarse-grained porphyritic granodiorite	Undeformed coarse-grained porphyritic granite	Undeformed coarse-grained porphyritic granite
Mineralogy		Qz + Ksp + Pl + Bt + Ep + Acc - Opq + Ap	Qz + Ksp + Pl + Bt + Ep + Acc - Opq + Ap		Ksp + Qz + Pl + Bt + Amph + Acc - Opq + Ap + Ep	
Geochem	x	x	x	x	x	x
REE						
Thin section			x		x	
Other		U-Pb-NIGL,Hf-O				

Sample	SA8-016	SA7-123	SA7-124	SA3-02	SA3-49	SA7-38
UTM x	356709	353964	353964	347387	345238	346143
UTM y	6640857	6604111	6604110	6607361	6603123	6606454
Age	Telemarkian	Telemarkian	Telemarkian	Telemarkian	Telemarkian	Telemarkian
Suite	Granitoid	Hybrid	Hybrid	Amphibolite	Amphibolite	Amphibolite
Lithology	Undeformed coarse-grained grey granite	Fine-grained dark grey gneiss	Fine-grained grey gneiss	Undeformed coarse-grained tonalite	Weakly deformed coarse-grained porphyritic gabbro	Weakly deformed massive medium-grained diorite
Mineralogy				Pl + Q + Amph + Bt + Chl + Ep + Opq + Acc - Ap	Amph + Pl + Qz + Bt + Chl + Ksp + Opq	
Geochem	x	x	x	x	x	x
REE						
Thin section				x	x	
Other				U-Pb-TIMS		

Sample	SA7-79	SA7-86	SA7-104	SA7-111	SA7-112	SA7-114
UTM x	345227	345526	343753	357352	357352	357352
UTM y	6605324	6603195	6601103	6605321	6605321	6605321
Age	Telemarkian	Telemarkian	Telemarkian	Telemarkian	Telemarkian	Telemarkian
Suite	Amphibolite	Amphibolite	Amphibolite	Amphibolite	Amphibolite	Amphibolite
Lithology	Deformed felsic part of veined gabbro	Pegmatitic zone of hornblende gabbro	Deformed fine-grained dark grey gneissic enclave	Deformed fine-grained black amphibolite	Deformed fine-grained black amphibolite	Deformed fine-grained black amphibolite with felsic segregations
Mineralogy		Amph + Pl + Tt + Acc - Ap + Qz				
Geochem	x	x	x	x	x	x
REE						
Thin section		x				
Other		U-Pb-TIMS,Hf-O				

Sample	SA7-131	SA7-132	SA3-04	SA3-08	SA3-23	SA3-42
UTM x	359893	359892	340220	361603	349912	336568
UTM y	6596991	6596990	6593772	6598858	6604108	6591640
Age	Telemarkian	Telemarkian	Telemarkian	Telemarkian	Telemarkian	Telemarkian
Suite	Amphibolite	Amphibolite	Grey Gneiss	Grey Gneiss	Grey Gneiss	Grey Gneiss
Lithology	Deformed fine-grained black amphibolite	Deformed fine-grained black amphibolite	Deformed coarse-grained porphyritic granodiorite	Undeformed medium-grained granodiorite	Weakly deformed coarse-grained granodiorite	Deformed fine-grained felsic grey gneiss
Mineralogy	Amph + Pl + Bt + Qz + Ksp + Acc + Tt + Opq		Pl + Qz + Ksp + Bt + Tt + Acc - Ap	Pl + Amph + Bt + Ep + Qz + Ksp + Tt + Acc - Opq	Pl + Qz + Ksp + Bt + Acc - Opq + Tt + Ap	Qz + Pl + Ksp + Bt + Chl
Geochem	x	x	x	x	x	x
REE						
Thin section	x		x	x	x	x
Other			U-Pb-NIGL,Hf-O			

Sample	SA3-46	SA3-51	SA3-52	SA3-60	SA7-43	SA7-47
UTM x	341723	345602	346944	345387	345920	345475
UTM y	6598875	6605605	6607002	6605374	6606001	6605499
Age	Telemarkian	Telemarkian	Telemarkian	Telemarkian	Telemarkian	Telemarkian
Suite	Grey Gneiss	Grey Gneiss	Grey Gneiss	Grey Gneiss	Grey Gneiss	Grey Gneiss
Lithology	Deformed medium-grained intermediate grey gneiss	Deformed medium-grained hornblende-bearing grey gneiss	Deformed medium-grained intermediate grey gneiss	Deformed banded felsic grey gneiss	Deformed banded felsic grey gneiss	Deformed banded felsic grey gneiss
Mineralogy	Pl + Qtz + Amph + Bt + Ksp + Acc - Tt + Opq + Ap	Pl + Amph + Qz + Bt + Chl	Qz + Pl + Ksp + Bt + Acc - Opq	Pl + Qz + Ksp + Bt + Acc - Tt + Opq + Grt		
Geochem	x	x	x	x	x	x
REE						
Thin section	x	x	x	x		
Other				U-Pb-NIGL,Hf-O		

Sample	SA7-61	SA7-77	SA7-82	SA7-84	SA7-85	SA7-101
UTM x	365167	345598	341789	341721	341511	344525
UTM y	6599387	6605586	6599190	6598858	6597713	6602581
Age	Telemarkian	Telemarkian	Telemarkian	Telemarkian	Telemarkian	Telemarkian
Suite	Grey Gneiss	Grey Gneiss	Grey Gneiss	Grey Gneiss	Grey Gneiss	Grey Gneiss
Lithology	Deformed fine-grained felsic aphyric grey gneiss	Deformed medium-grained hornblende-bearing grey gneiss	Weakly deformed coarse-grained granodiorite	Deformed fine-grained felsic grey gneiss	Deformed medium-grained grey gneiss, sparsely feldspar-phyric	Weakly deformed coarse-grained granodiorite
Mineralogy		Pl + Amph + Bt + Chl + Qz + Ksp + Ep				
Geochem	x	x	x	x	x	x
REE						
Thin section		x				
Other						

Sample	SA7-103	SA7-105	SA7-106	SA7-107	SA7-113	SA7-115
UTM x	343752	341998	341576	341576	357352	357232
UTM y	6601105	6600110	6598030	6598030	6605321	6605241
Age	Telemarkian	Telemarkian	Telemarkian	Telemarkian	Telemarkian	Telemarkian
Suite	Grey Gneiss	Grey Gneiss	Grey Gneiss	Grey Gneiss	Grey Gneiss	Grey Gneiss
Lithology	Deformed fine-grained felsic grey gneiss	Weakly deformed coarse-grained granodiorite	Deformed felsic gneissic enclave	Deformed medium-grained grey gneiss, sparsely feldspar-phyric	Deformed medium-grained granodiorite	Deformed medium-grained granodiorite
Mineralogy						Pl + Amph + Qz + Ksp + Bt + Chl
Geochem	x	x	x	x	x	x
REE						
Thin section						x
Other						

Sample	SA7-119	SA7-125	SA7-130	SA7-134	SA8-56	SA8-57
UTM x	356737	353964	359894	357715	374291	374291
UTM y	6605029	6604112	6596991	6597286	6610312	6610312
Age	Telemarkian	Telemarkian	Telemarkian	Telemarkian	Telemarkian	Telemarkian
Suite	Grey Gneiss	Grey Gneiss	Grey Gneiss	Grey Gneiss	Grey Gneiss	Grey Gneiss
Lithology	Deformed fine-grained felsic grey gneiss	Undeformed medium-grained granodiorite	Deformed banded felsic grey gneiss	Deformed banded felsic grey gneiss	Undeformed coarse-grained porphyritic granodiorite	Deformed fine-grained dark grey gneiss
Mineralogy				Qz + Pl + Ksp + Bt + Amph + Opq		
Geochem	x	x	x	x	x	x
REE						
Thin section				x		
Other			U-Pb-TIMS, HF-O			

Sample	SA8-64	SA8-65	SA3-62	SA3-63	SA3-66	SA3-67
UTM x	361852	361852	351175	357478	355182	351678
UTM y	6598854	6598854	6613340	6615601	6616561	6614399
Age	Telemarkian	Telemarkian	Telemarkian	Telemarkian	Telemarkian	Telemarkian
Suite	Grey Gneiss	Grey Gneiss	Zinc Mine Suite	Zinc Mine Suite	Zinc Mine Suite	Zinc Mine Suite
Lithology	Deformed fine-grained light grey gneiss	Deformed medium-grained porphyritic grey gneiss	Deformed medium-grained banded grey gneiss	Deformed medium-grained light grey gneiss	Deformed medium-grained light grey gneiss	Deformed medium-grained light grey gneiss
Mineralogy			Qz + Ksp + Pl + Acc + Bt + Ep + Tt + Opq	Qz + Pl + Ksp + Bt + Acc - Opq + Grt + Ep	Qz + Pl + Ksp + Bt + Amph + Acc - Tt + Opq	Qz + Pl + Ksp + Bt + Acc - Grt + Opq + Ep
Geochem	x	x	x	x	x	x
REE						
Thin section			x	x	x	x
Other						

Sample	SA7-04	SA7-05	SA7-11	SA7-12	SA7-14	SA7-16
UTM x	357114	357489	356816	356817	356692	356522
UTM y	6615430	6615470	6615678	6615678	6615513	6615595
Age	Telemarkian	Telemarkian	Telemarkian	Telemarkian	Telemarkian	Telemarkian
Suite	Zinc Mine Suite	Zinc Mine Suite	Zinc Mine Suite	Zinc Mine Suite	Zinc Mine Suite	Zinc Mine Suite
Lithology	Deformed medium-grained light grey biotite gneiss	Deformed coarse-grained porphyritic granodiorite	Deformed fine-grained dark grey gneiss	Deformed medium-grained lgrey biotite gneiss	Deformed fine-grained dark grey gneiss	Deformed medium-grained porphyritic granodiorite
Mineralogy	Pl + Qz + Ksp + Bt	Pl + Qz + Ksp + Bt + Amph + Acc - Opq			Amph + Pl + Qz + Bt + Ksp + Opq	
Geochem	x	x	x	x	x	x
REE						
Thin section		x			x	
Other	U-Pb-TIMS,Hf-O					

Sample	SA7-18	SA7-19	SA7-20	SA7-21	SA7-22	SA7-23
UTM x	356274	356274	356274	356274	356274	356170
UTM y	6615648	6615648	6615648	6615648	6615648	6615549
Age	Telemarkian	Telemarkian	Telemarkian	Telemarkian	Telemarkian	Telemarkian
Suite	Zinc Mine Suite	Zinc Mine Suite	Zinc Mine Suite	Zinc Mine Suite	Zinc Mine Suite	Zinc Mine Suite
Lithology	Deformed fine-grained dark grey gneiss	Deformed medium-grained felsic vein/band	Deformed medium-grained grey banded biotite gneiss	Deformed fine-grained felsic vein/band	Deformed fine-grained felsic vein/band	Deformed medium-grained porphyritic grey gneiss
Mineralogy	Qz + Pl + Ksp + Bt + Ms + Ep + Acc - Tt					Qz + Pl + Ksp + Bt + Acc - Ep + Tt + Opq
Geochem	x	x	x	x	x	x
REE						
Thin section	x					x
Other						

Sample	SA7-24	SA7-27	SA7-109	SA7-136	SA7-138	SA7-140
UTM x	355610	354987	347446	350880	350808	354658
UTM y	6616321	6616753	6608199	6617983	6618582	6616673
Age	Telemarkian	Telemarkian	Telemarkian	Telemarkian	Telemarkian	Telemarkian
Suite	Zinc Mine Suite	Zinc Mine Suite	Zinc Mine Suite	Zinc Mine Suite	Zinc Mine Suite	Zinc Mine Suite
Lithology	Deformed medium-grained porphyritic grey gneiss	Deformed fine-grained grey gneiss	Deformed fine-grained banded light grey gneiss	Deformed fine-grained banded light grey gneiss	Deformed medium-grained grey gneiss	Deformed fine-grained light grey gneiss
Mineralogy	Qz + Pl + Ksp + Bt + Acc - Ep + Tt + Ap	Qz + Pl + Ksp + Bt + Acc - Ep + ap		Pl + Amph + Ep + Chl + Acc - Qz + Opg + Tt	Pl + Qz + Amph + Ksp + Ep + Acc - Opg	
Geochem	x	x	x	x	x	x
REE						
Thin section	x	x		x	x	
Other						

Sample	SA7-141	SA7-142	SA7-143	SA8-45	SA3-01a	SA3-01b
UTM x	354686	354876	354819	376752	357948	357948
UTM y	6616754	6616569	6616681	6613070	6615161	6615161
Age	Telemarkian	Telemarkian	Telemarkian	Telemarkian	Sveconorwegian	Sveconorwegian
Suite	Zinc Mine Suite	Zinc Mine Suite	Zinc Mine Suite	Nesflaten	HBG	HBG
Lithology	Deformed fine-grained banded light grey gneiss	Deformed fine-grained grey gneiss	Deformed porphyritic medium-grained grey gneiss	Deformed medium-grained banded biotite-gneiss	Undeformed coarse-grained porphyritic biotite granite	Undeformed coarse-grained porphyritic biotite granite
Mineralogy					Ksp + Pl + Qz + Bt + Tt + Acc - Ap	Ksp + Pl + Qz + Bt + Tt + Acc - Ap
Geochem	x	x	x		x	x
REE						
Thin section					x	x
Other				U-Pb-NIGL	U-Pb-NIGL,Hf-O	

Sample	SA7-58	SA7-65	SA8-50	SA8-51	SA8-52	SA8-54
UTM x	359965	375658	358960	365238	373897	373298
UTM y	6596954	6626611	6616661	6623402	6629309	6619421
Age	Sveconorwegian	Sveconorwegian	Sveconorwegian	Sveconorwegian	Sveconorwegian	Sveconorwegian
Suite	Suite	HBG	HBG	HBG	HBG	HBG
Lithology	Undeformed coarse-grained porphyritic granite	Undeformed coarse-grained porphyritic biotite granite	Undeformed coarse-grained porphyritic biotite granite with pink feldspar	Undeformed fine-grained granite	Undeformed coarse-grained porphyritic biotite granite	Undeformed coarse-grained white granite
Mineralogy						
Geochem		x	x	x	x	x
REE						
Thin section						
Other	U-Pb-TIMS					

Sample	MM 02277	MM 026183	MM 026226	ROG 190	ROG 197	ROG 200
UTM x	325424	375014	315203	324908	327033	327378
UTM y	6526915	6615718	6613355	6517359	6518349	6518699
Age	Sveconorwegian	Sveconorwegian	Sveconorwegian	Sveconorwegian	Sveconorwegian	Sveconorwegian
Suite	HBG	HBG	HBG	HBG	HBG	HBG
Lithology	Massive medium-grained leucocratic granite	Undeformed coarse-grained white biotite-granite	Massive granite	Garnet-granite, associated with pelite	Undeformed medium-grained garnet-granite	Deformed garnet-granite
Mineralogy	Ksp + Qz + Pl + Bt + Grt + Chl + Acc - Ap + Opq		Qz + Ksp + Pl + Bt + Chl + Acc - Ap + Opq			
Geochem	x	x		x	x	x
REE	x	x		x	x	x
Thin section	x		x			
Other	U-Pb-NS,Hf		U-Pb-NS,Hf			

Sample	ROG 203	ROG 245	ROG 275	ROG 641	MM 02105	MM 02214
UTM x	327858	316703	318862	330123	332637	333807
UTM y	6519377	6531446	6531428	6508272	6585303	6539047
Age	Sveconorwegian	Sveconorwegian	Sveconorwegian	Sveconorwegian	Sveconorwegian	Sveconorwegian
Suite	HBG	HBG	HBG	HBG	Feda	Feda
Lithology	Foliated garnet-granite	Weakly deformed medium-grained garnet-granite	Garnet-granite	Granite associated with Faurefjell metaseds	Deformed porphyritic granodiorite	Deformed coarse-grained porphyritic biotite-granite
Mineralogy						
Geochem	x	x	x		x	x
REE	x	x	x		x	x
Thin section						
Other			U-Pb-NS, Hf	U-Pb-NS,Hf-O		

Sample	MM 02247	MM 026182	MM 026199	MM 026255	MM 026302	MM 026303
UTM x	338597	335158	364670	334332	342702	344910
UTM y	6572694	6587408	6544077	6560297	6570573	6570265
Age	Sveconorwegian	Sveconorwegian	Sveconorwegian	Sveconorwegian	Sveconorwegian	Sveconorwegian
Suite	Feda	Feda	Feda	Feda	Feda	Feda
Lithology	Deformed grey porphyritic biotite-hornblende granite	Weakly deformed porphyritic granodiorite	Weakly deformed grey porphyritic granite	Deformed porphyritic biotite-granite	Porphyritic granite	Porphyritic granite
Mineralogy	Ksp + Qz + Plg + Bt + Tt + Opq + Acc - Ep + Ap	Ksp + Qz + Pl + Bt + Tt + Acc - Opq + Ep + Ap			Ksp + Qz + Pl + Bt + Chl + Acc - Opq + Ap	
Geochem	x	x	x	x	x	x
REE	x	x	x	x	x	x
Thin section	x	x			x	
Other	U-Pb-NS,Hf-O				U-Pb-NS,Hf-O	

Sample	MM 026306	MM 99208	ROG 13-1	ROG 15	ROG 16	ROG 218
UTM x	340075	359185	362877	363301	363845	314258
UTM y	6579722	6480785	6558911	6558756	6558173	6532437
Age	Sveconorwegian	Sveconorwegian	Sveconorwegian	Sveconorwegian	Sveconorwegian	Sveconorwegian
Suite	Feda	Feda	Feda	Feda	Feda	Feda
Lithology	Undeformed porphyritic granite	Porphyritic granitoid	Deformed porphyritic granitoid	Deformed porphyritic granitoid	Deformed porphyritic granitoid	Porphyritic granite, large zrn sep. sample
Mineralogy						
Geochem	x	x	x	x	x	x
REE	x	x	x	x	x	x
Thin section						
Other	U-Pb-NS,Hf-O					U-Pb-NS,Hf

Sample	ROG 23	ROG 256	ROG 257	ROG 27	ROG 2A	ROG 34
UTM x	364079	355088	355185	363949	378768	363661
UTM y	6557117	6586267	6585284	6556165	6544483	6553510
Age	Sveconorwegian	Sveconorwegian	Sveconorwegian	Sveconorwegian	Sveconorwegian	Sveconorwegian
Suite	Feda	Feda	Feda	Feda	Feda	Feda
Lithology	Deformed porphyritic granitoid	Deformed porphyritic granitoid	Deformed porphyritic granitoid	Deformed porphyritic granitoid with red feldspar	Deformed porphyritic granitoid	Deformed porphyritic granitoid with red feldspar
Mineralogy						
Geochem	x	x	x	x	x	x
REE	x	x	x	x	x	x
Thin section						
Other						

Sample	ROG 43	ROG 71	ROG 72	ROG 75	ROG 80	ROG329
UTM x	366261	373508	376216	380509	371806	327835
UTM y	6549586	6546690	6546418	6541581	6546058	6540728
Age	Sveconorwegian	Sveconorwegian	Sveconorwegian	Sveconorwegian	Sveconorwegian	Sveconorwegian
Suite	Feda	Feda	Feda	Feda	Feda	Feda
Lithology	Deformed porphyritic granitoid with red feldspar	Deformed porphyritic granitoid				
Mineralogy						
Geochem	x	x	x	x	x	x
REE	x	x	x	x	x	x
Thin section						
Other					U-Pb-NS,Hf-O	

Sample	MM 02230	MM 026191	MM 026297	MM 026298	MM 026299	ROG 28
UTM x	350409	362621	361312	361046	360948	363525
UTM y	6554133	6549102	6548784	6548791	6549097	6555933
Age	Sveconorwegian	Sveconorwegian	Sveconorwegian	Sveconorwegian	Sveconorwegian	Sveconorwegian
Suite	Leucogranite	Leucogranite	Leucogranite	Leucogranite	Leucogranite	Leucogranite
Lithology	Massive medium-grained light grey biotite granite	Coarse-grained leucocratic granite	Leucocratic granite	Leucocratic granite	Leucocratic granite	Undeformed medium-grained leucocratic granite
Mineralogy	Ksp + Qz + Pl + Bt + Acc - Opq + Ap	Qz + Pl + Ksp + Bt + Chl + Acc - Opq + Ap	Ksp + Qz + Pl + Bt + Chl + Tt + Opq + Acc - Ap			
Geochem		x	x	x	x	x
REE		x	x	x	x	x
Thin section	x	x	x			
Other	U-Pb-NS,Hf		U-Pb-NS,Hf			

Sample	ROG 30-1	ROG 33	ROG 45	SA8-19	SA8-23a	SA8-23b
UTM x	364734	364407	366293	353350	372344	372344
UTM y	6551294	6552651	6549215	6609080	6636570	6636570
Age	Sveconorwegian	Sveconorwegian	Sveconorwegian	Caledonian	Caledonian	Caledonian
Suite	Leucogranite	Leucogranite	Leucogranite	Storhei	Dyrskard	Dyrskard
Lithology	Undeformed medium-grained leucocratic granite	Leucogranite	Leucogranite	Deformed coarse-grained granitoid	Deformed fine-grained light grey gneiss	Deformed fine-grained light grey gneiss
Mineralogy				PL + Qz + Ksp + Bt + Amph + Opq + Acc - Ap + Ep	Qz + Pl + Ksp + Bt + Opq + Acc - Ep	Qz + Pl + Ksp + Bt + Opq + Acc - Ep
Geochem	x	x	x		x	x
REE	x	x	x			
Thin section				x	x	x
Other				U-Pb-NIGL,Hf	U-Pb-NIGL,Hf	

Sample	SA8-26	SA8-27	SA8-32
UTM x	372625	372960	351794
UTM y	6636194	6635575	6599124
Age	Caledonian	Caledonian	Caledonian
Suite	Kvitenut	Revsegg	Holmasjø
Lithology	Deformed mylonitic banded grey gneiss	Deformed biotite-muscovite quartz-feldspar gneiss	Deformed grey gneiss
Mineralogy	Qz + Pl + Ksp + Bt + Ms + Grt + Ep + Acc - Opq	Qz + Pl + Ksp + Ms + Bt + Grt + Ep + Acc - Opq	
Geochem			
REE			
Thin section	x	x	
Other	U-Pb-NIGL,Hf	U-Pb-NIGL,Hf	U-Pb-NIGL,Hf

Table 10.2. Sample details. Co-ordinates are UTM zone 32V. Pl = Plagioclase, Qz = Quartz, Ksp = K-feldspar, Amph = Amphibole, Bt = Biotite, Ap = Apatite, Ep = Epidote, Chl = Chlorite, Ms = Muscovite, Grt = Garnet, Opq = Opaques. In other- U-Pb-NIGL = dated by LA-ICP-MS at NIGL, U-Pb-TIMS = dated by TIMS and LA-ICP-MS at NIGL, U-Pb- NS = dated by ionprobe at Nordsim, U-Pb-NGU = dated by LA-ICP-MS at NGU, Hf = in-situ hafnium analyses by LA-ICP-MS at NIGL, O = oxygen isotope analysis by ionprobe at Edinburgh.

Sample	MM 036632	MM 036707	MM 036717	MM 036720	MM 036724	MM 036730	ROG396	ROG400	ROG401	ROG402	ROG413
UTM x	348322	347157	354445	354919	355941	347641	344634	344093	344067	344078	350990
UTM y	6616123	6603168	6604423	6604757	6604923	6613373	6595471	6594399	6593551	6593803	6593628
Suite	Granitoid										
SiO ₂	72.20	69.80	72.80	72.80	73.70	71.40	74.10	73.50	73.80	72.90	69.50
Al ₂ O ₃	12.90	14.40	13.40	13.70	13.30	14.00	13.10	13.10	13.00	13.00	13.50
Fe ₂ O ₃	2.62	3.39	2.83	2.22	2.75	2.57	1.75	2.87	2.42	3.26	3.84
TiO ₂	0.29	0.44	0.26	0.21	0.33	0.26	0.12	0.25	0.22	0.30	0.60
MgO	0.36	0.66	0.39	0.28	0.47	0.36	0.09	0.19	0.22	0.38	0.66
CaO	1.65	2.32	1.28	1.20	1.56	1.54	1.50	1.29	1.30	1.60	1.38
Na ₂ O	3.00	3.08	4.53	3.49	2.97	3.51	3.58	2.89	2.99	3.00	3.03
K ₂ O	4.81	4.25	2.91	4.59	4.68	4.43	4.56	5.34	5.01	4.60	5.09
MnO	0.03	0.05	0.05	0.05	0.04	0.04	0.04	0.05	0.03	0.05	0.06
P ₂ O ₅	0.07	0.12	0.06	0.04	0.08	0.06	0.03	0.04	0.04	0.06	0.22
LOI	0.71	1.26	0.61	0.75	0.57	0.76	0.72	0.30	0.39	0.39	0.66
Total	98.70	99.80	99.10	99.30	100.00	98.90	99.60	99.80	99.40	99.50	98.50
Ba	516	1120	622	685	553	648	222	499	401	530	1100
Co	5.9	6.8	5.1	bdl	5.7	bdl	bdl	bdl	bdl	bdl	bdl
Cr	bdl	9.6	bdl	8.0	bdl						
Ga	16.8	15.5	13.0	15.8	15.7	16.3	24.7	19.2	19.1	19.7	20.2
Nb	8.5	9.5	8.8	9.0	7.9	9.7	14.8	13.5	10.4	12.5	17.9
Ni	bdl	2.1	bdl	bdl	bdl	2.3	2.5	2.4	2.2	3.1	bdl
Pb	16.0	13.1	10.7	15.2	13.9	12.5	29.0	32.3	33.1	31.7	32.4
Rb	133	95	63	139	121	129	185	209	240	206	165
Sc	bdl	5.4	5.6	5.7	5.7	bdl	bdl	7.6	bdl	8.0	6.9
Sr	100	193	107	87	121	120	60	72	76	102	241
Ta	0.5	0.6	0.5	0.8	0.4	0.8	1.2	1.4	0.8	0.8	0.7
Th	15.7	9.0	12.2	11.6	11.6	13.2	13.1	12.6	25.9	20.2	17.4
U	4.0	2.1	3.1	4.4	3.9	3.0	4.7	3.9	6.8	4.1	3.3
V	11.0	21.3	10.8	6.9	15.1	11.2	bdl	6.1	8.6	12.0	20.7
Y	57.4	44.4	42.6	48.0	43.1	50.7	81.3	96.7	52.3	66.2	48.0
Zn	35.1	58.9	46.5	41.8	42.2	41.7	51.7	59.7	53.7	66.2	89.9
Zr	241.9	262.6	242.9	217.8	246.5	196.6	231.9	305.9	255.6	291.5	421.0
Hf	6.8	7.6	7.5	7.3	6.9	6.1	8.0	9.9	8.2	8.6	10.7
La	72.4	45.7	42.5	36.8	61.0	39.2	31.3	44.2	45.6	52.5	138.3
Ce	144.8	92.1	84.5	72.3	123.2	77.6	68.9	86.1	89.5	102.4	269.4
Pr	17.1	11.0	10.1	8.7	14.5	9.4	9.8	11.4	10.3	11.5	28.3
Nd	68.2	44.6	39.9	36.3	56.3	37.8	43.2	49.3	40.9	50.8	106.9
Sm	14.2	9.4	8.3	7.9	11.4	8.5	11.2	12.5	8.7	11.1	17.7
Eu	1.2	1.7	1.2	1.0	1.5	1.2	1.7	1.2	1.1	1.2	2.8
Gd	10.4	7.4	6.7	7.0	8.5	7.0	9.8	11.8	7.5	9.6	11.9
Tb	1.9	1.3	1.2	1.3	1.4	1.3	2.1	2.4	1.4	1.7	1.8
Dy	10.4	7.4	7.3	7.5	7.6	8.0	12.4	14.8	7.8	10.2	9.1
Ho	2.1	1.6	1.6	1.7	1.5	1.8	2.7	3.2	1.6	2.2	1.7
Er	5.9	4.3	4.5	5.0	4.1	5.3	8.3	10.0	4.8	6.6	4.5
Tm	0.8	0.6	0.7	0.8	0.6	0.8	1.4	1.5	0.8	1.0	0.6
Yb	4.9	3.8	4.0	4.7	3.6	4.9	8.2	8.8	4.9	5.6	3.5
Lu	0.7	0.6	0.7	0.8	0.6	0.8	1.2	1.3	0.7	0.9	0.5

Sample	ROG416	MM 026153	MM 026173	MM 036672	MM 036673	MM 036677	MM 036681	MM 036682	MM 036686	MM 036692	MM 036693
UTM x	347437	343454	338888	352723	353796	354078	345295	344831	345144	345953	345932
UTM y	6593415	6592899	6591831	6595827	6596944	6593768	6603186	6603219	6604380	6606022	6606001
Suite	Granitoid	Amphibolt									
SiO ₂	69.40	51.18	50.77	48.90	56.70	60.20	53.00	50.20	50.70	55.90	48.60
Al ₂ O ₃	15.10	13.03	13.03	18.30	17.90	18.20	16.00	16.50	13.00	15.40	15.10
Fe ₂ O ₃	3.65	15.84	15.48	9.36	8.11	5.86	11.00	9.59	10.30	12.10	15.50
TiO ₂	0.25	2.45	2.16	0.67	0.88	0.73	1.81	0.99	0.82	1.26	1.88
MgO	0.26	4.17	4.28	6.27	1.48	1.05	2.35	5.74	9.80	1.77	4.27
CaO	1.73	7.93	7.82	11.90	6.09	5.28	6.40	9.77	9.41	5.67	7.81
Na ₂ O	4.07	2.85	2.92	2.14	3.82	4.21	3.73	2.63	1.97	3.17	3.63
K ₂ O	4.67	1.29	1.13	1.18	2.04	2.13	1.62	0.96	1.63	2.12	1.13
MnO	0.08	0.21	0.22	0.16	0.13	0.09	0.17	0.13	0.16	0.17	0.26
P ₂ O ₅	0.07	0.35	0.38	0.12	0.27	0.19	0.55	0.09	0.17	0.33	0.27
LOI	0.78	0.59	1.04	1.49	0.93	0.62	1.22	1.60	1.56	1.17	1.14
Total	100.00	99.89	99.22	100.00	98.30	98.50	97.90	98.20	99.50	99.00	99.50
Ba	512	207	202	257	301	547	609	300	300	403	265
Co	bdl	62.0	60.0	40.8	15.6	11.4	21.7	36.1	51.7	24.0	45.7
Cr	bdl	53.0	56.0	46.0	8.5	6.9	5.1	82.3	629.0	4.9	bdl
Ga	26.8	20.0	23.0	16.4	20.7	20.8	22.1	16.6	12.6	22.6	19.1
Nb	18.3	6.3	9.6	3.6	10.0	9.9	19.3	3.6	2.8	7.0	4.2
Ni	bdl	31.0	28.0	5.3	bdl	bdl	bdl	11.2	105.0	bdl	bdl
Pb	26.2	bdl	bdl	17.2	19.0	13.7	17.1	14.7	18.3	26.4	25.4
Rb	133	43	35	45	96	98	59	29	65	118	45
Sc	bdl	36.0	39.0	43.2	22.4	15.1	20.4	28.3	31.6	25.7	35.7
Sr	135	191	246	356	358	321	522	460	258	285	145
Ta	0.8	0.4	0.5	0.2	0.7	0.7	0.9	0.2	0.2	0.4	0.3
Th	9.6	3.2	2.9	1.6	1.8	4.5	5.0	1.3	1.5	1.9	1.6
U	2.8	1.3	1.0	1.3	2.2	1.5	1.9	0.5	0.7	1.9	0.9
V	5.5	414.0	417.0	180.0	49.8	31.5	79.9	219.0	167.0	67.2	262.0
Y	78.3	59.1	52.5	20.8	37.0	49.9	41.0	15.1	16.4	76.9	60.2
Zn	80.5	131.0	134.0	78.5	117.0	81.0	147.0	78.8	83.2	137.0	142.0
Zr	508.0	189.1	178.5	104.4	199.2	116.9	272.6	71.1	60.4	271.4	168.0
Hf	11.5	5.6	5.6	2.8	4.6	3.2	6.2	1.9	1.7	7.4	4.9
La	54.6	19.5	23.8	17.7	18.1	21.5	38.0	9.6	8.0	23.3	12.8
Ce	134.6	45.4	54.4	38.5	51.0	52.0	86.7	22.4	17.8	55.5	29.5
Pr	16.3	6.6	7.6	4.2	6.5	7.1	11.1	2.8	2.4	7.6	4.4
Nd	71.5	29.7	35.4	17.5	27.9	31.2	48.9	12.8	11.2	36.6	22.2
Sm	16.5	8.6	8.4	4.0	7.1	8.3	10.4	3.1	3.1	10.3	7.0
Eu	3.4	2.5	2.5	1.5	2.6	2.0	4.1	1.4	1.2	2.2	2.2
Gd	13.4	9.1	8.9	3.8	6.7	8.5	9.4	3.0	3.0	10.2	7.7
Tb	2.4	1.6	1.5	0.7	1.2	1.6	1.6	0.6	0.6	2.0	1.5
Dy	13.4	10.0	9.2	4.3	7.0	8.9	8.4	3.1	3.3	12.7	9.6
Ho	2.7	2.1	1.9	0.9	1.4	1.9	1.7	0.6	0.7	2.8	2.1
Er	7.8	5.5	4.9	2.5	4.1	5.3	4.6	1.7	1.9	7.5	6.0
Tm	1.2	0.8	0.8	0.4	0.7	0.8	0.6	0.2	0.3	1.1	1.0
Yb	6.9	5.2	4.9	2.5	4.0	5.2	3.8	1.5	1.7	6.6	5.7
Lu	1.0	0.8	0.7	0.4	0.6	0.8	0.6	0.2	0.2	1.0	0.9

Sample	MM 036695	MM 036694	MM 036698	MM 036699	MM 036711	MM 036712	MM 036713	ROG394	ROG399	ROG421	MM 026152
UTM x	346319	346424	346039	346015	350822	351583	353018	345803	344289	354199	343401
UTM y	6606505	6606658	6606404	6606353	6603975	6603907	6603991	6595821	6594908	6595345	6592974
Suite	Amphibolt	Grey Gneiss									
SiO2	50.80	60.20	50.70	50.80	63.30	64.30	63.20	50.20	49.50	48.60	70.64
Al2O3	13.10	15.40	13.10	12.80	15.20	15.80	16.00	13.00	13.20	15.40	13.77
Fe2O3	15.80	7.15	15.80	16.20	6.99	5.60	5.71	16.00	15.80	13.20	3.81
TiO2	2.25	0.95	2.22	2.77	0.89	0.70	0.74	2.55	2.22	2.76	0.41
MgO	4.44	0.94	4.40	3.84	0.99	0.71	0.78	4.64	4.59	4.22	0.61
CaO	7.75	4.32	7.74	7.42	3.62	3.11	3.27	8.35	8.27	8.22	2.40
Na2O	2.60	4.55	2.55	2.76	3.75	4.19	4.22	2.81	2.98	2.77	3.40
K2O	1.18	2.88	1.16	1.38	3.41	3.73	3.72	1.23	0.94	2.08	3.89
MnO	0.23	0.15	0.24	0.23	0.12	0.09	0.09	0.22	0.23	0.18	0.07
P2O5	0.39	0.28	0.38	0.59	0.32	0.22	0.24	0.43	0.37	1.39	0.09
LOI	1.23	2.00	1.23	0.92	0.84	0.61	0.60	0.48	0.70	1.00	0.61
Total	99.80	98.80	99.50	99.70	99.40	99.00	98.60	99.90	98.80	99.80	99.69
Ba	2220	2020	233	342	1290	1560	1350	220	200	415	737
Co	13.9	9.7	48.9	47.6	11.0	8.4	9.7	49.2	44.0	28.3	7.0
Cr	bdl	bdl	33.5	7.8	bdl	bdl	bdl	43.3	41.0	bdl	21.0
Ga	20.9	19.4	18.2	20.0	20.4	20.1	20.9	21.9	20.8	21.3	14.0
Nb	11.1	25.8	10.6	8.6	23.6	20.8	23.0	7.0	10.2	11.7	11.8
Ni	bdl	bdl	19.9	7.6	bdl	bdl	bdl	34.6	23.9	bdl	bdl
Pb	15.0	14.5	31.1	26.8	20.2	13.3	18.5	14.6	14.2	14.5	23.0
Rb	62	70	35	42	77	66	80	39	25	79	176
Sc	16.9	15.2	34.8	36.5	13.6	10.2	13.9	32.7	29.1	20.2	bdl
Sr	465	354	186	191	384	380	364	195	210	500	147
Ta	0.6	0.9	0.6	0.5	1.1	0.8	1.1	0.4	0.5	0.6	0.8
Th	3.5	4.2	3.3	3.8	5.1	4.0	5.7	2.8	2.8	2.8	16.2
U	1.2	1.7	1.2	1.4	1.6	1.3	2.1	1.2	1.0	1.2	4.8
V	22.0	17.7	364.0	289.0	24.6	16.3	22.4	332.0	369.0	228.0	20.0
Y	62.6	40.3	61.1	70.3	45.8	33.3	42.8	59.0	58.6	37.2	52.7
Zn	145.0	123.0	142.0	149.0	125.0	102.0	107.0	138.0	145.0	139.0	118.0
Zr	246.7	1008.6	243.4	304.1	577.2	640.6	599.9	210.9	201.4	117.2	258.8
Hf	6.9	21.1	6.8	8.2	14.0	14.9	14.9	6.0	5.9	3.0	8.7
La	24.8	43.7	23.5	25.3	53.0	44.1	51.3	19.9	25.1	38.2	47.2
Ce	55.2	97.4	53.3	57.6	120.6	96.9	111.2	47.1	57.1	89.2	98.0
Pr	7.6	11.9	7.5	8.6	15.3	11.7	13.8	7.0	8.2	11.9	11.6
Nd	36.2	51.7	34.8	41.7	64.9	52.4	57.4	33.8	37.6	53.9	47.3
Sm	9.7	10.6	9.2	11.5	13.8	10.3	12.1	9.3	9.2	10.6	9.7
Eu	2.6	4.4	2.6	3.3	3.8	3.8	3.7	2.6	2.2	2.7	1.6
Gd	8.9	8.1	8.4	10.7	9.6	7.6	8.8	9.0	8.7	8.1	8.2
Tb	1.6	1.3	1.6	2.0	1.6	1.2	1.4	1.7	1.7	1.3	1.5
Dy	10.1	7.0	9.7	11.6	8.5	6.3	7.8	9.8	9.7	6.5	8.4
Ho	2.3	1.5	2.1	2.6	1.8	1.3	1.6	2.1	2.1	1.3	1.8
Er	6.4	3.9	6.1	7.1	4.6	3.4	4.5	6.1	5.9	3.5	4.8
Tm	1.0	0.6	0.9	1.1	0.7	0.5	0.6	0.9	0.9	0.5	0.8
Yb	5.8	3.7	5.6	6.2	3.9	3.2	4.0	5.5	5.5	2.6	4.6
Lu	0.9	0.6	0.9	1.0	0.6	0.5	0.6	0.8	0.9	0.4	0.7

Sample	MM 026157	MM 026160	MM 026161	MM 026166	MM 026170	MM 026171	MM 026181	MM 026263	MM 026265	MM 036575	MM 036576
UTM x	344535	336908	336803	339975	339629	339456	338373	351926	352436	345495	343349
UTM y	6595278	6587700	6587753	6593759	6593023	6592844	6588018	6600846	6600597	6596435	6592617
Suite	Grey Gneiss										
SiO ₂	62.88	66.03	65.35	53.74	55.08	64.49	68.80	74.30	64.50	52.90	68.10
Al ₂ O ₃	17.82	15.63	16.68	17.72	18.04	17.54	13.97	13.30	16.00	13.30	15.20
Fe ₂ O ₃	4.31	5.25	3.71	7.38	7.30	3.91	4.68	1.64	4.34	11.10	4.38
TiO ₂	0.50	0.57	0.52	0.87	0.97	0.36	0.32	0.18	0.60	0.68	0.49
MgO	1.08	1.78	0.79	6.00	4.40	1.90	2.54	0.45	2.69	7.85	1.11
CaO	4.27	3.78	4.11	8.94	6.75	4.30	3.47	1.48	3.62	9.16	2.95
Na ₂ O	4.59	2.90	4.00	2.79	2.98	3.21	2.91	3.42	3.50	2.30	3.54
K ₂ O	2.28	2.37	2.12	1.08	2.21	2.26	2.34	3.98	3.20	1.11	3.28
MnO	0.05	0.08	0.05	0.13	0.12	0.05	0.10	0.04	0.06	0.19	0.06
P ₂ O ₅	0.11	0.10	0.13	0.12	0.19	0.10	0.08	0.05	0.13	0.10	0.11
LOI	1.28	1.14	0.67	1.30	1.96	1.96	0.14	0.58	1.19	1.05	0.76
Total	99.17	99.63	98.12	100.07	100.00	100.07	99.35	99.40	99.90	99.70	99.90
Ba	538	565	643	238	417	570	540	576	434	243	705
Co	10.0	11.0	9.0	24.0	24.0	11.0	15.0	bdl	11.1	35.7	4.9
Cr	25.0	45.0	29.0	204.0	113.0	81.0	89.0	7.0	98.0	770.0	21.9
Ga	23.0	19.0	21.0	18.0	19.0	16.0	12.0	13.5	18.0	17.4	20.0
Nb	7.4	9.9	10.7	3.2	11.1	6.1	5.5	6.2	6.6	3.5	9.0
Ni	6.0	5.0	6.0	36.0	25.0	10.0	11.0	2.7	28.2	60.7	4.7
Pb	bdl	bdl	12.0	bdl	bdl	12.0	bdl	31.9	21.7	21.3	35.8
Rb	117	110	127	43	97	101	70	169	150	36	131
Sc	10.0	23.0	18.0	33.0	26.0	21.0	19.0	bdl	6.2	33.3	9.3
Sr	371	233	281	432	445	384	214	136	297	171	196
Ta	0.5	0.8	0.5	0.2	0.8	0.4	0.5	0.6	0.5	0.2	0.7
Th	8.0	7.1	16.6	4.6	5.1	8.2	4.7	6.0	9.7	1.0	11.1
U	3.1	1.2	2.2	1.3	3.1	3.0	5.3	2.8	5.0	0.6	5.3
V	32.0	49.0	29.0	136.0	123.0	36.0	87.0	8.8	61.4	206.0	41.0
Y	24.1	23.2	39.9	16.2	28.5	23.2	24.3	13.0	22.7	27.1	37.1
Zn	45.0	89.0	67.0	82.0	82.0	57.0	59.0	29.0	54.9	115.0	66.9
Zr	374.6	159.0	339.1	58.5	152.2	167.1	96.9	135.3	202.2	76.4	191.3
Hf	11.6	5.2	10.7	2.0	4.8	5.2	3.1	4.5	5.3	2.4	5.7
La	31.0	32.4	57.0	13.1	25.3	25.8	25.0	13.2	22.8	12.2	36.2
Ce	57.3	64.7	116.5	27.1	45.0	52.7	55.4	23.2	47.6	30.6	74.1
Pr	6.6	7.9	13.8	3.5	5.8	6.1	7.0	2.3	5.3	3.9	8.7
Nd	24.6	31.4	53.3	15.5	24.4	24.2	29.1	8.7	21.3	17.6	36.5
Sm	5.0	6.7	11.1	3.7	5.7	4.8	5.2	1.8	4.3	4.2	7.8
Eu	1.5	1.5	2.2	1.2	1.9	1.2	0.9	0.6	1.0	1.0	1.5
Gd	3.9	5.3	9.1	3.1	5.0	4.0	4.3	1.5	3.4	3.8	6.4
Tb	0.7	0.8	1.4	0.5	1.1	0.7	0.6	0.3	0.6	0.7	1.1
Dy	4.2	4.5	7.7	2.7	4.8	4.1	4.1	1.7	3.6	4.4	6.6
Ho	0.8	0.8	1.4	0.6	1.3	0.8	0.8	0.4	0.8	1.0	1.4
Er	2.3	2.1	3.4	1.5	2.7	2.2	2.3	1.2	2.3	3.0	4.0
Tm	0.4	0.3	0.5	0.2	0.7	0.3	0.4	0.2	0.3	0.5	0.6
Yb	2.5	1.8	3.0	1.4	2.6	2.0	2.6	1.5	2.2	3.0	3.7
Lu	0.4	0.2	0.4	0.2	0.7	0.3	0.4	0.2	0.3	0.5	0.6

Sample	MM 036577	MM 036591	MM 036594	MM 036595	MM 036600	MM 036601	MM 036671	MM 036674	MM 036675	MM 036678	MM 036680
UTM x	344087	334955	334829	334497	333330	334950	351638	352446	352254	359462	359804
UTM y	6594373	6590672	6590472	6590203	6590247	6590560	6595280	6594152	6594065	6596440	6597146
Suite	Grey Gneiss										
SiO ₂	71.10	67.10	69.50	70.30	65.10	69.30	52.40	58.40	58.40	74.80	72.10
Al ₂ O ₃	13.20	15.40	14.60	14.50	16.90	14.70	19.70	17.60	17.60	12.30	12.50
Fe ₂ O ₃	3.10	4.58	2.50	1.90	3.71	2.68	7.72	6.63	7.26	2.57	4.94
TiO ₂	0.28	0.59	0.37	0.31	0.53	0.41	1.43	0.69	0.65	0.20	0.48
MgO	0.24	0.91	0.53	0.44	1.05	0.57	3.29	2.44	2.81	0.05	0.44
CaO	1.53	3.98	1.73	1.39	4.56	1.94	8.82	6.00	5.98	0.72	1.50
Na ₂ O	3.02	3.08	2.89	3.33	3.63	3.30	2.63	3.67	3.20	3.82	3.15
K ₂ O	5.17	2.67	5.54	5.61	2.51	5.02	1.77	1.69	1.40	3.64	4.34
MnO	0.05	0.06	0.03	0.03	0.05	0.03	0.10	0.10	0.10	0.05	0.08
P ₂ O ₅	0.05	0.15	0.12	0.09	0.15	0.13	0.19	0.19	0.21	0.01	0.14
LOI	0.33	1.14	0.78	0.71	1.32	0.65	1.78	1.16	1.61	0.26	0.28
Total	98.00	99.60	98.60	98.70	99.50	98.80	99.90	98.50	99.20	98.40	99.90
Ba	791	989	990	738	708	1080	414	421	322	614	626
Co	bdl	bdl	bdl	bdl	5.2	bdl	26.7	17.3	23.0	bdl	6.3
Cr	10.0	9.1	bdl	4.8	15.3	4.7	9.8	24.3	26.1	bdl	bdl
Ga	19.7	21.6	19.3	21.4	22.4	19.1	18.5	18.2	17.4	18.9	19.2
Nb	11.1	9.8	10.7	13.5	10.3	8.7	5.8	5.2	3.6	5.5	9.1
Ni	2.5	bdl	2.2	2.1	4.9	bdl	bdl	4.8	11.4	bdl	bdl
Pb	41.8	27.9	40.9	45.0	27.5	36.4	15.7	10.0	10.6	11.7	19.0
Rb	190	115	173	224	120	176	70	59	59	85	149
Sc	5.6	8.5	bdl	bdl	5.5	bdl	34.8	15.2	14.7	bdl	19.1
Sr	108	379	183	209	436	255	349	438	430	73	93
Ta	0.8	0.5	0.6	0.9	0.4	0.3	0.5	0.3	0.2	0.4	0.6
Th	15.2	11.1	20.8	41.0	13.6	22.3	1.1	1.8	6.4	9.7	8.9
U	3.4	2.1	2.7	5.0	1.4	2.6	0.8	1.3	2.5	2.3	3.6
V	8.1	24.5	20.5	17.4	29.5	23.0	197.0	77.3	85.9	bdl	17.7
Y	57.0	21.4	25.4	12.6	25.5	14.8	21.3	18.6	14.2	69.4	71.6
Zn	53.8	85.8	63.5	72.1	64.5	58.2	66.1	76.3	80.3	45.4	118.0
Zr	329.1	381.4	332.2	297.0	342.2	355.4	73.6	153.5	82.0	416.3	283.7
Hf	9.3	9.9	8.9	8.1	8.8	9.9	2.0	3.8	2.1	11.8	8.1
La	55.4	79.3	71.0	68.2	54.4	76.4	14.0	13.4	12.0	31.7	30.2
Ce	105.6	145.8	138.5	118.6	107.2	142.3	30.7	33.8	27.3	75.7	67.6
Pr	13.2	15.8	16.0	12.4	12.6	17.2	3.6	4.2	3.4	9.0	8.7
Nd	53.2	58.9	62.3	45.2	53.2	66.3	15.1	18.2	14.0	40.5	37.7
Sm	11.4	8.8	10.2	6.9	10.0	10.7	3.7	4.3	3.1	10.6	9.4
Eu	1.4	2.0	1.3	0.8	1.9	1.3	1.4	1.4	1.2	1.8	1.8
Gd	9.7	5.7	6.0	4.0	7.6	6.0	4.0	3.9	2.9	10.8	9.9
Tb	1.7	0.8	0.8	0.5	1.1	0.7	0.7	0.7	0.5	2.2	2.0
Dy	9.8	3.9	4.1	2.5	5.3	2.9	4.1	3.6	2.8	13.3	12.2
Ho	2.0	0.8	0.8	0.4	0.9	0.5	0.9	0.8	0.6	3.0	2.8
Er	5.9	2.1	2.5	1.0	2.4	1.4	2.3	2.1	1.4	8.4	7.9
Tm	0.9	0.3	0.4	0.1	0.3	0.2	0.4	0.3	0.2	1.2	1.3
Yb	5.2	2.0	2.5	0.8	1.8	1.3	2.2	2.0	1.4	7.0	7.8
Lu	0.8	0.3	0.4	0.1	0.3	0.2	0.3	0.3	0.2	1.1	1.2

Sample	MM 036683	MM 036688	MM 036690	MM 036700	MM 036701	MM 036702	MM 036704	MM 036706	MM 036710	MM 036714	MM 036715
UTM x	345258	345444	345613	346799	347079	346991	347497	346743	348284	354244	353728
UTM y	6604120	6605437	6605587	6606932	6607172	6606998	6608282	6607670	6602040	6604274	6604119
Suite	Grey Gneiss										
SiO ₂	70.30	51.10	52.40	52.60	58.90	52.70	77.50	61.50	68.80	68.10	57.40
Al ₂ O ₃	13.20	18.60	18.00	18.10	16.50	17.20	11.60	16.60	15.90	15.30	16.00
Fe ₂ O ₃	4.01	7.36	7.42	7.24	6.02	8.59	2.79	5.04	2.49	3.91	8.90
TiO ₂	0.36	0.68	0.57	0.60	0.60	0.83	0.25	0.54	0.28	0.39	1.03
MgO	0.24	5.24	5.41	5.19	4.21	4.57	0.14	3.25	0.66	0.56	3.06
CaO	1.82	9.14	7.34	8.19	5.53	9.13	1.19	4.66	2.91	1.60	6.80
Na ₂ O	2.79	3.01	2.68	3.13	3.11	2.96	2.52	2.39	4.30	5.54	2.85
K ₂ O	5.05	2.37	3.49	2.46	2.70	1.14	4.02	3.47	2.48	2.84	1.99
MnO	0.05	0.12	0.14	0.13	0.10	0.14	0.06	0.07	0.05	0.06	0.13
P ₂ O ₅	0.06	0.29	0.14	0.15	0.05	0.11	0.02	0.07	0.08	0.07	0.21
LOI	0.46	1.63	1.98	1.61	1.64	1.62	0.91	1.90	0.83	0.68	1.33
Total	98.30	99.50	99.60	99.40	99.30	99.00	101.00	99.50	98.80	99.00	99.70
Ba	880	619	882	453	583	257	674	640	388	478	501
Co	5.2	30.5	30.8	28.9	25.7	33.5	bdl	20.0	6.1	8.1	31.4
Cr	4.3	64.2	65.9	66.2	55.9	143.0	8.4	32.1	6.6	bdl	25.5
Ga	18.0	15.3	15.2	15.4	14.8	16.4	16.2	15.1	18.3	11.0	15.2
Nb	15.1	2.5	2.2	1.8	2.7	3.4	11.4	3.8	6.0	8.4	5.2
Ni	bdl	32.4	25.4	23.3	10.0	10.4	bdl	11.7	2.4	bdl	21.4
Pb	19.5	14.3	13.5	12.0	8.7	12.9	10.1	5.6	7.8	3.8	20.6
Rb	150	93	141	93	94	38	89	119	110	72	66
Sc	10.0	20.7	21.8	23.0	17.3	28.0	bdl	12.2	bdl	7.6	23.6
Sr	113	630	301	439	239	249	78	241	325	75	188
Ta	0.7	0.1	0.2	0.1	0.2	0.2	0.7	0.2	0.7	0.7	0.3
Th	7.3	1.5	1.7	2.5	3.7	1.5	7.2	2.8	10.0	8.7	3.2
U	1.3	0.9	0.8	1.1	1.1	1.0	3.0	1.1	3.2	2.5	1.5
V	9.8	115.0	119.0	124.0	133.0	154.0	bdl	107.0	15.6	30.1	151.0
Y	54.9	15.5	18.2	13.6	21.0	34.0	92.0	21.0	27.7	66.6	37.0
Zn	70.0	89.6	87.8	69.0	57.5	83.1	117.0	54.2	49.9	73.6	76.5
Zr	396.0	77.5	106.4	68.6	55.1	114.4	393.0	78.9	142.1	320.8	131.9
Hf	10.6	2.1	2.8	2.0	1.9	3.1	11.6	2.3	4.3	9.9	4.2
La	52.1	16.1	9.4	9.2	9.9	10.7	33.5	10.5	20.5	31.5	18.4
Ce	104.3	41.2	23.6	23.1	22.8	25.5	74.3	23.8	38.7	64.2	43.8
Pr	12.6	5.4	3.0	3.1	2.9	3.3	9.9	2.8	4.5	8.0	5.4
Nd	51.7	23.5	13.7	12.7	11.8	15.1	45.3	12.2	17.5	36.8	23.1
Sm	10.7	5.1	3.4	2.9	3.1	4.3	11.9	3.2	3.7	9.6	5.9
Eu	1.9	1.5	1.1	1.0	0.7	1.2	1.9	0.7	0.8	1.6	1.4
Gd	10.7	3.6	2.8	2.5	2.7	4.2	11.4	2.8	3.2	9.6	5.3
Tb	1.8	0.5	0.5	0.4	0.5	0.9	2.3	0.5	0.6	1.7	1.0
Dy	10.1	2.7	2.9	2.3	3.3	5.4	14.2	3.2	3.8	10.7	6.1
Ho	2.2	0.6	0.6	0.5	0.7	1.2	3.2	0.7	0.9	2.4	1.3
Er	6.1	1.5	1.8	1.3	2.0	3.5	9.7	2.1	2.6	6.7	3.9
Tm	0.9	0.2	0.3	0.2	0.3	0.6	1.5	0.3	0.5	1.1	0.6
Yb	5.1	1.2	1.8	1.2	2.1	3.3	9.3	2.1	3.0	6.5	3.9
Lu	0.8	0.2	0.3	0.2	0.3	0.5	1.5	0.3	0.5	1.0	0.6

Sample	MM 036716	MM 036721	MM 036722	MM 036725	MM 036726	MM 036727	MM 036728	ROG339-1	ROG339-2	ROG340	ROG369
UTM x	353779	355193	355280	355427	356619	356461	356309	357733	357733	357601	344901
UTM y	6604134	6604831	6604847	6604887	6604998	6604978	6604825	6597315	6597315	6597216	6594801
Suite	Grey Gneiss										
SiO ₂	56.50	51.20	57.00	50.00	71.10	54.90	59.80	72.40	76.20	63.00	67.40
Al ₂ O ₃	16.70	17.70	16.60	15.70	13.50	16.90	18.00	12.40	12.60	16.60	16.60
Fe ₂ O ₃	8.44	10.40	9.19	10.50	2.76	7.15	5.18	4.61	2.55	4.63	4.11
TiO ₂	0.96	1.07	1.12	0.98	0.36	0.84	0.50	0.42	0.19	0.73	0.40
MgO	3.14	5.43	2.93	7.70	0.49	4.99	3.44	0.38	0.08	1.86	0.67
CaO	6.95	9.03	6.66	9.94	1.95	7.39	6.67	1.84	1.16	4.86	2.60
Na ₂ O	2.75	3.15	3.11	2.44	3.09	3.70	3.92	3.91	3.68	3.89	3.70
K ₂ O	2.25	0.95	1.72	0.84	4.08	1.76	1.39	3.25	3.93	2.11	4.21
MnO	0.12	0.16	0.13	0.16	0.05	0.12	0.08	0.10	0.07	0.06	0.06
P ₂ O ₅	0.20	0.17	0.25	0.18	0.10	0.56	0.15	0.10	0.02	0.18	0.08
LOI	1.28	0.99	0.97	1.06	0.73	1.25	1.04	0.24	0.20	0.54	0.91
Total	99.30	100.00	99.70	99.40	98.20	99.60	100.00	99.70	101.00	98.50	101.00
Ba	512	230	370	140	533	363	281	600	644	484	1000
Co	29.8	39.7	27.3	50.6	5.3	32.6	23.9	bdl	bdl	7.6	bdl
Cr	28.0	108.0	bdl	235.0	bdl	83.9	49.3	5.4	bdl	33.7	8.8
Ga	15.7	16.0	16.6	13.9	14.3	16.7	15.5	19.6	20.8	21.7	20.1
Nb	4.8	2.5	4.7	2.9	7.0	4.1	2.2	9.9	10.6	6.0	7.8
Ni	20.9	19.7	bdl	111.0	bdl	84.7	41.0	<2	3.5	3.7	2.4
Pb	21.7	18.7	15.1	16.3	12.2	7.2	3.7	25.3	25.3	18.3	22.5
Rb	81	28	59	34	124	43	31	104	132	74	159
Sc	23.8	30.0	22.5	34.4	7.0	18.8	14.2	12.4	14.8	6.1	5.8
Sr	178	280	319	248	172	649	510	100	70	468	231
Ta	0.2	0.2	0.3	0.2	0.5	0.1	0.2	0.6	0.7	0.4	0.5
Th	1.9	1.6	4.9	1.0	11.0	1.8	1.7	8.7	10.7	5.5	18.9
U	1.0	0.7	2.5	0.4	4.1	1.3	1.4	2.7	4.0	2.0	2.4
V	143.0	140.0	139.0	183.0	22.2	113.0	70.1	10.0	bdl	56.2	14.2
Y	39.2	34.0	38.8	20.3	33.4	16.0	9.8	85.8	103.9	16.9	31.0
Zn	85.4	89.7	92.2	76.7	38.3	75.2	49.1	100.0	119.0	75.5	47.7
Zr	127.3	89.3	159.0	73.3	223.4	100.7	67.8	297.1	361.5	166.8	471.1
Hf	3.9	2.5	4.1	1.8	6.3	2.4	1.8	9.2	10.6	4.8	14.1
La	16.8	9.1	17.7	8.1	33.1	20.5	9.3	32.8	44.8	20.3	59.2
Ce	40.4	21.5	41.7	20.4	69.4	56.1	20.6	69.7	83.3	38.2	146.0
Pr	5.3	3.0	5.5	2.7	8.5	7.9	2.5	9.3	11.8	4.7	13.7
Nd	23.6	13.7	24.8	12.8	33.0	34.9	10.9	42.1	53.4	20.3	50.5
Sm	6.1	4.0	6.2	3.4	6.8	7.3	2.4	11.0	13.9	4.2	9.3
Eu	1.3	1.4	1.7	1.2	0.9	2.0	0.8	1.9	2.2	1.4	1.7
Gd	5.6	4.5	5.5	3.1	5.6	4.9	1.9	10.8	13.5	3.3	6.1
Tb	1.1	0.9	1.1	0.6	0.9	0.7	0.3	2.2	2.7	0.6	1.0
Dy	6.5	5.3	6.2	3.5	5.4	3.4	1.7	13.1	16.1	2.8	5.5
Ho	1.5	1.2	1.3	0.7	1.2	0.6	0.4	3.0	3.5	0.6	1.1
Er	4.0	3.4	3.9	2.1	3.5	1.5	0.9	9.3	10.4	1.5	3.2
Tm	0.6	0.5	0.6	0.3	0.6	0.2	0.1	1.4	1.6	0.2	0.5
Yb	3.8	3.3	3.9	1.9	3.6	1.3	0.9	8.4	9.6	1.4	3.0
Lu	0.6	0.5	0.6	0.3	0.6	0.2	0.1	1.3	1.5	0.2	0.5

Sample	ROG393	ROG395	ROG397	ROG398	ROG403	ROG404	ROG405	ROG406	ROG407	ROG408	ROG409
UTM x	345891	345145	344576	344306	343761	343312	342955	342735	342453	342330	342124
UTM y	6595966	6595826	6595353	6594918	6593317	6592601	6591765	6591576	6590679	6590245	6589555
Suite	Grey Gneiss										
SiO ₂	66.20	63.60	61.60	55.20	67.60	66.10	52.40	48.00	69.50	66.30	66.70
Al ₂ O ₃	16.30	15.30	15.90	18.10	14.40	15.70	18.40	17.90	14.30	14.70	14.90
Fe ₂ O ₃	4.35	5.50	7.05	8.16	4.03	4.95	8.21	9.28	3.00	4.67	4.14
TiO ₂	0.52	0.77	0.97	0.91	0.43	0.56	0.98	1.24	0.38	0.60	0.50
MgO	1.53	2.17	2.94	2.41	1.01	1.38	4.39	7.72	0.62	2.54	1.16
CaO	3.76	4.46	3.63	8.08	2.72	3.88	7.78	8.04	2.19	2.67	3.17
Na ₂ O	3.90	2.55	1.87	2.95	3.31	3.57	2.96	1.94	3.31	2.70	3.07
K ₂ O	2.18	3.10	3.28	2.04	3.69	2.92	2.54	2.82	3.88	3.22	3.59
MnO	0.06	0.07	0.08	0.10	0.07	0.07	0.11	0.13	0.04	0.07	0.06
P ₂ O ₅	0.14	0.13	0.17	0.20	0.10	0.13	0.23	0.24	0.10	0.11	0.11
LOI	1.05	1.39	2.11	1.47	0.65	0.73	1.96	2.56	0.90	2.12	0.90
Total	100.00	99.10	99.60	99.70	98.00	100.00	100.00	99.90	98.20	99.70	98.30
Ba	566	607	695	326	757	484	567	453	1290	781	667
Co	5.3	10.0	11.2	11.4	bdl	6.1	18.8	31.4	bdl	8.7	5.6
Cr	32.1	59.7	120.0	8.6	16.7	54.7	94.3	346.0	5.2	113.0	17.4
Ga	18.2	18.7	19.4	34.2	17.0	19.6	23.8	20.1	16.7	18.3	19.3
Nb	8.3	10.5	13.3	7.2	9.2	9.2	7.1	4.5	7.8	9.8	10.1
Ni	4.2	7.1	16.3	bdl	4.4	9.9	27.4	99.5	<2	17.1	5.2
Pb	18.5	21.4	21.8	13.7	38.3	27.6	42.0	13.1	25.0	16.8	19.5
Rb	86	133	168	79	136	135	89	124	98	135	146
Sc	10.3	8.8	15.9	10.3	bdl	10.0	17.3	18.2	bdl	9.7	9.8
Sr	465	220	278	580	184	211	416	352	184	160	222
Ta	0.3	0.7	1.0	0.5	0.7	0.7	0.4	0.2	0.5	0.7	0.7
Th	7.0	10.0	12.0	6.1	12.0	6.9	3.1	0.6	10.4	9.2	11.8
U	1.1	1.9	3.2	2.3	2.1	2.1	1.7	0.4	1.6	2.5	3.4
V	45.3	61.8	98.8	115.0	31.5	46.8	117.0	148.0	16.5	49.2	38.5
Y	18.6	40.0	49.2	31.2	40.4	42.5	33.7	14.1	17.8	34.0	43.8
Zn	59.0	70.1	90.5	40.0	69.9	79.6	108.0	110.0	57.4	67.3	51.0
Zr	162.8	256.2	264.3	132.0	192.7	211.6	218.4	64.8	288.4	214.0	204.3
Hf	5.0	7.5	7.8	3.9	5.7	5.6	5.3	1.7	7.4	5.8	5.6
La	33.4	35.7	43.2	23.8	37.1	26.7	20.0	11.9	73.2	32.0	36.6
Ce	66.3	72.0	85.5	48.0	76.4	60.4	52.5	30.1	133.3	67.5	72.4
Pr	7.4	8.8	10.7	6.3	8.8	7.7	7.0	4.0	14.6	7.9	8.6
Nd	30.4	36.8	43.2	25.4	36.3	33.5	32.4	17.3	58.5	32.3	37.1
Sm	5.5	7.8	9.0	5.5	7.2	7.6	7.6	3.5	8.3	6.6	8.0
Eu	1.2	1.4	1.9	1.5	1.4	1.5	1.9	1.4	1.7	1.2	1.2
Gd	4.0	6.3	7.6	4.8	5.9	6.2	5.7	2.8	4.9	5.4	6.4
Tb	0.6	1.2	1.4	0.9	1.1	1.2	1.0	0.5	0.7	0.9	1.2
Dy	3.3	6.6	8.1	4.9	6.1	6.2	5.8	2.5	3.0	5.4	6.5
Ho	0.7	1.4	1.8	1.1	1.3	1.4	1.1	0.5	0.6	1.2	1.4
Er	1.9	4.0	5.1	3.2	3.9	4.0	3.3	1.5	1.7	3.3	4.4
Tm	0.2	0.6	0.8	0.5	0.6	0.6	0.5	0.2	0.2	0.5	0.7
Yb	1.7	3.7	4.9	3.1	3.8	3.8	3.1	1.3	1.6	3.1	4.0
Lu	0.3	0.5	0.7	0.5	0.6	0.6	0.5	0.2	0.2	0.5	0.6

Sample	ROG410	ROG411	SA7-92	SA7-128	SA7-80	SA7-91	SA7-129	SA7-133	SA8-016	SA7-123	SA7-124
UTM x	347762	348534	359281	353598	348988	338383	352845	361341	356709	353964	353964
UTM y	6595136	6594400	6642829	6604075	6603505	6627090	6604012	6599002	6640857	6604111	6604110
Suite	Grey Gneiss	Grey Gneiss	Granitoid	Hybrid	Hybrid						
SiO ₂	64.30	58.50	76.29	65.65	74.13	75.57	65.27	63.46	68.54	63.42	58.48
Al ₂ O ₃	18.70	16.90	0.16	0.78	0.06	0.15	0.74	0.82	0.64	0.74	1.59
Fe ₂ O ₃	3.11	8.51	11.91	14.48	13.03	12.28	14.54	15.50	13.75	14.86	13.81
TiO ₂	0.37	0.86	1.49	5.91	0.95	2.00	5.47	4.31	4.67	7.00	11.51
MgO	1.34	2.31	0.02	0.11	0.04	0.03	0.09	0.06	0.07	0.13	0.17
CaO	4.16	5.33	0.11	0.80	0.16	0.00	0.77	2.04	0.53	1.55	2.06
Na ₂ O	4.81	3.23	0.68	3.04	0.74	0.57	2.79	3.06	2.04	3.88	5.28
K ₂ O	1.75	2.43	3.05	3.87	3.82	4.34	4.02	3.16	3.80	4.16	3.89
MnO	0.04	0.13	5.21	3.63	4.60	4.57	4.26	5.24	4.30	2.68	2.31
P ₂ O ₅	0.11	0.18	0.01	0.23	0.02	0.01	0.21	0.31	0.09	0.17	0.27
LOI	1.39	1.40	0.34	0.85	0.36	0.39	0.56	1.31	0.46	0.88	0.66
Total	100.00	99.80	99.28	99.34	97.90	99.91	98.72	99.27	98.91	99.47	100.02
Ba	401	646	468	1641	422	803	1661	2086	1757	482	420
Co	5.3	13.7	1.8	10.5	bdl	2.0	9.4	15.3	7.4	17.5	30.1
Cr	22.3	6.6	4.0	2.1	7.4	bdl	bdl	45.0	1.9	2.3	bdl
Ga	17.5	20.6	16.1	22.6	13.5	23.1	20.5	19.1	21.2	19.0	20.6
Nb	2.9	5.9	9.1	23.5	5.7	17.2	20.5	10.7	14.5	6.8	5.7
Ni	7.7	bdl	bdl	bdl	bdl	bdl	bdl	31.1	bdl	bdl	bdl
Pb	15.6	14.9	19.0	16.0	34.3	7.0	18.0	28.0	18.9	13.2	11.4
Rb	72	87	178	77	196	110	87	117	105	128	89
Sc	bdl	15.4	4.3	16.0	3.6	1.5	11.4	8.8	9.1	15.3	25.9
Sr	358	240	47	355	83	100	325	742	125	190	178
Ta	0.2	0.4									
Th	2.5	0.8	17.7	4.1	12.7	12.0	5.3	7.2	15.8	4.4	5.3
U	1.2	0.7	5.6	2.6	5.9	4.2	2.5	1.3	8.7	2.7	3.1
V	35.0	111.0	7.4	24.0	5.3	4.4	22.9	62.7	29.1	76.2	175.0
Y	4.3	33.2	47.9	49.9	28.2	90.2	46.6	27.3	64.1	68.6	60.4
Zn	35.1	99.7	35.9	105.5	18.4	113.0	104.4	70.2	88.9	147.1	119.4
Zr	118.2	93.3	162	684	71	367	589	359	593	192	189
Hf	2.9	2.5									
La	8.7	13.3	44.0	37.5	15.5	43.3	39.2	61.6	31.9	16.7	17.9
Ce	13.8	37.2	94.7	86.6	24.5	95.0	91.2	109.3	70.7	39.3	40.9
Pr	1.3	4.5									
Nd	5.1	20.3	44.0	49.4	13.6	52.8	51.3	45.9	39.7	25.4	21.8
Sm	0.8	4.9									
Eu	0.7	1.2									
Gd	0.7	4.2									
Tb	< 0.1	0.9									
Dy	0.6	5.2									
Ho	0.1	1.1									
Er	0.4	3.3									
Tm	< 0.1	0.5									
Yb	0.5	3.5									
Lu	0.1	0.5									

Sample	SA3-02	SA3-49	SA7-38	SA7-79	SA7-86	SA7-104	SA7-111	SA7-112	SA7-114	SA7-131	SA7-132
UTM x	347387	345238	346143	345227	345526	343753	357352	357352	357352	359893	359892
UTM y	6607361	6603123	6606454	6605324	6603195	6601103	6605321	6605321	6605321	6596991	6596990
Suite	Amphibolite	Amphibolt									
SiO2	63.83	53.40	61.70	67.50	57.91	50.95	49.46	49.69	49.57	48.12	47.54
Al2O3	0.71	1.96	1.00	0.61	0.93	2.48	1.60	1.64	1.66	2.54	2.51
Fe2O3	15.35	16.65	15.21	12.59	17.66	12.98	13.01	13.03	13.62	13.32	13.12
TiO2	7.40	10.56	8.09	6.12	8.68	15.83	14.45	14.34	14.70	16.98	19.25
MgO	0.07	0.13	0.14	0.13	0.11	0.22	0.24	0.23	0.24	0.28	0.26
CaO	1.24	2.46	1.02	0.67	1.25	4.48	6.50	6.44	6.10	5.18	5.84
Na2O	3.96	7.06	3.57	2.57	5.22	7.88	10.51	10.73	9.93	7.41	4.45
K2O	4.62	4.28	4.07	4.34	4.76	3.28	2.24	2.31	2.45	2.55	1.69
MnO	0.86	1.44	3.55	3.38	2.39	1.11	0.80	0.73	0.81	2.77	5.00
P2O5	0.19	0.54	0.28	0.18	0.23	0.38	0.13	0.13	0.13	0.39	0.40
LOI	1.48	1.12	0.99	0.69	0.73	0.89	1.03	1.05	1.18	0.64	0.81
Total	99.71	99.59	99.62	98.77	99.87	100.47	99.97	100.32	100.39	100.16	100.88
Ba	363	375	2195	651	671	228	132	118	135	389	953
Co	0.8	bdl	13.8	10.2	16.3	54.8	48.3	50.4	48.2	51.6	65.6
Cr	6.8	16.0	bdl	bdl	7.0	39.0	155.0	155.6	135.7	33.7	32.5
Ga	20.8	37.4	22.8	18.4	30.8	21.0	19.4	18.5	20.7	23.1	22.2
Nb	26.0	53.8	27.5	6.9	9.8	6.4	2.4	2.3	2.8	8.4	8.4
Ni	1.7	6.5	bdl	bdl	bdl	26.9	25.6	24.7	22.2	25.9	29.9
Pb	41.9	47.9	11.0	17.4	13.6	6.4	5.4	4.7	6.6	6.2	7.5
Rb	430	1223	65	89	87	34	25	22	25	93	217
Sc	19.6	24.1	15.9	17.1	17.1	36.6	52.1	51.2	49.3	39.8	37.2
Sr	320	527	426	106	476	186	157	167	189	170	121
Ta											
Th	5.8	4.2	3.2	9.1	6.1	2.7	0.2	bdl	0.9	2.0	3.1
U	2.1	0.3	1.9	4.3	2.4	2.0	1.1	0.7	1.3	1.7	2.6
V	71.5	118.0	25.0	24.5	68.8	391.9	380.6	381.8	387.5	403.2	429.5
Y	62.8	57.0	52.7	62.6	90.6	57.1	35.1	35.5	37.1	61.1	61.2
Zn	68.7	162.5	161.2	100.4	132.3	138.0	109.1	106.1	119.2	153.6	206.9
Zr	324	220	1068	255	376	217	85	86	93	237	243
Hf											
La	2.5	1.4	48.1	20.5	43.0	18.4	4.0	6.5	7.5	17.8	19.1
Ce	24.4	42.6	108.2	42.4	106.0	47.5	10.7	11.8	14.7	35.1	46.2
Pr											
Nd	0.0	0.0	60.3	24.7	72.0	28.2	7.4	5.7	10.9	23.5	26.3
Sm											
Eu											
Gd											
Tb											
Dy											
Ho											
Er											
Tm											
Yb											
Lu											

Sample	SA3-08	SA3-04	SA3-42	SA3-46	SA3-51	SA3-52	SA3-60	SA7-43	SA7-47	SA7-61	SA7-77
UTM x	361603	340220	336568	341723	345602	346944	345387	345920	345475	365167	345598
UTM y	6598858	6593772	6591640	6598875	6605605	6607002	6605374	6606001	6605499	6599387	6605586
Suite	Grey Gneiss										
SiO2	57.80	66.52	74.99	66.30	51.05	71.36	75.18	67.15	71.39	68.53	49.75
Al2O3	1.47	0.74	0.18	0.60	0.58	0.29	0.22	0.79	0.41	0.38	0.57
Fe2O3	15.02	14.04	12.84	14.99	18.22	14.46	12.64	12.93	12.42	15.03	18.27
TiO2	7.17	4.76	1.77	4.91	7.28	2.84	2.68	8.41	4.57	3.55	7.55
MgO	0.08	0.06	0.01	0.06	0.11	0.03	0.06	0.15	0.06	0.05	0.13
CaO	3.22	2.36	0.16	1.66	6.43	0.74	0.08	0.50	0.29	1.46	6.15
Na2O	4.52	2.89	1.20	2.47	9.23	2.18	1.02	3.05	1.93	3.71	9.57
K2O	3.06	3.19	2.70	3.24	3.05	4.56	4.04	4.19	3.10	3.95	2.75
MnO	4.75	3.90	5.22	4.11	2.09	2.09	3.68	2.29	4.60	1.84	2.31
P2O5	0.65	0.13	0.02	0.12	0.13	0.06	0.01	0.17	0.06	0.08	0.12
LOI	1.28	0.97	0.45	1.22	1.82	0.94	0.25	0.46	0.42	0.80	1.82
Total	99.02	99.56	99.55	99.69	100.00	99.53	99.86	100.08	99.24	99.38	98.99
Ba	3056	418	984	800	513	615	863	426	896	505	532
Co	23.3	81.6	0.0	16.8	85.8	0.0	89.3	12.1	6.7	11.7	32.5
Cr	42.1	6.4	5.5	10.1	4.9	5.9	9.5	bdl	bdl	18.5	94.6
Ga	20.6	31.2	45.7	36.5	16.1	18.4	31.3	23.3	20.0	15.9	15.9
Nb	13.4	29.5	46.1	32.4	15.3	10.4	36.7	12.7	7.6	2.4	1.3
Ni	37.4	21.0	9.8	8.8	3.6	3.6	17.6	bdl	bdl	8.6	32.9
Pb	27.5	231.8	154.1	196.6	101.8	73.7	84.0	13.0	16.2	6.5	5.5
Rb	106	120	305	83	16	762	bdl	95	131	74	94
Sc	13.2	11.3	9.6	11.9	25.4	6.0	6.9	15.5	12.9	8.3	28.7
Sr	1300	215	114	172	523	263	139	140	131	425	478
Ta											
Th	5.8	23.3	23.7	17.8	3.6	13.2	13.7	5.9	7.8	4.1	0.0
U	0.9	7.4	3.1	4.6	2.1	3.1	0.5	3.4	2.3	0.9	0.9
V	118.2	59.1	7.3	48.2	147.9	18.7	8.7	12.9	16.3	51.9	163.1
Y	34.3	45.8	57.7	43.0	22.1	21.1	66.4	90.5	41.2	8.6	13.0
Zn	103.7	66.8	11.4	71.0	86.1	32.1	89.2	150.5	71.8	51.0	84.8
Zr	494	203	180	190	53	141	354	353	389	76	36
Hf											
La	65.2	1.3	1.4	0.5	0.0	1.0	1.7	26.7	58.9	27.8	10.4
Ce	140.1	18.0	3.5	16.6	33.1	10.8	3.0	57.8	111.4	48.5	20.9
Pr											
Nd	75.7	25.7	0.0	0.7	33.4	0.0	0.0	33.5	50.2	20.3	12.1
Sm											
Eu											
Gd											
Tb											
Dy											
Ho											
Er											
Tm											
Yb											
Lu											

Sample	SA7-82	SA7-84	SA7-85	SA7-101	SA7-103	SA7-105	SA7-106	SA7-107	SA7-113	SA7-115	SA7-119
UTM x	341789	341721	341511	344525	343752	341998	341576	341576	357352	357232	356737
UTM y	6599190	6598858	6597713	6602581	6601105	6600110	6598030	6598030	6605321	6605241	6605029
Suite	Grey Gneiss										
SiO ₂	74.61	65.48	64.96	70.44	64.50	70.62	78.37	67.81	66.26	62.34	71.76
Al ₂ O ₃	0.22	0.56	0.57	0.23	0.66	0.40	0.08	0.49	0.37	0.28	0.41
Fe ₂ O ₃	12.12	14.96	16.02	14.69	16.17	13.12	11.62	14.87	16.71	12.91	13.53
TiO ₂	2.16	4.75	4.78	2.82	4.48	4.18	0.64	4.39	3.51	6.86	3.20
MgO	0.04	0.08	0.07	0.03	0.05	0.05	0.01	0.06	0.06	0.12	0.05
CaO	0.22	1.37	1.24	0.66	1.60	0.52	0.15	1.01	1.13	5.26	0.53
Na ₂ O	0.82	3.01	3.28	2.11	2.78	1.63	0.54	2.45	4.08	5.66	1.95
K ₂ O	2.79	3.36	3.60	3.79	3.34	2.93	2.17	3.71	4.32	3.24	3.54
MnO	5.45	4.14	3.68	2.94	3.53	5.20	5.87	3.97	1.47	1.02	4.01
P ₂ O ₅	0.04	0.12	0.14	0.06	0.19	0.25	0.01	0.11	0.13	0.10	0.11
LOI	0.70	1.03	1.22	1.16	1.47	0.73	0.40	0.94	1.47	1.35	0.60
Total	99.17	98.86	99.58	98.95	98.75	99.63	99.85	99.81	99.50	99.15	99.69
Ba	659	729	807	671	896	1118	792	604	401	282	572
Co	4.2	12.4	10.3	6.9	11.2	6.6	bdl	9.1	8.5	26.6	7.0
Cr	bdl	15.2	2.7	5.0	14.1	bdl	3.6	13.9	3.6	356.6	5.3
Ga	16.1	19.8	21.4	18.3	17.7	17.0	10.9	22.5	17.9	12.8	16.0
Nb	8.4	8.6	10.2	6.0	5.0	10.6	2.5	9.2	2.8	2.1	7.5
Ni	bdl	1.4	bdl	bdl	5.1	bdl	bdl	1.2	bdl	88.4	bdl
Pb	19.9	29.4	17.0	7.1	6.2	18.3	23.9	16.4	8.2	5.2	13.4
Rb	132	157	162	107	122	141	146	174	69	39	136
Sc	5.9	12.1	12.8	7.2	9.7	11.6	2.2	10.6	8.8	23.0	8.2
Sr	84	210	259	438	374	128	105	196	451	278	162
Ta											
Th	19.4	11.4	11.2	8.2	0.7	12.2	16.7	8.6	0.3	bdl	9.7
U	2.3	4.1	4.7	2.1	2.1	3.5	2.6	2.6	0.7	0.4	4.5
V	10.4	50.1	42.7	25.8	40.3	17.0	6.5	43.8	50.6	132.6	32.3
Y	45.2	39.4	45.3	17.9	19.3	42.6	12.8	43.4	5.7	12.1	37.7
Zn	29.9	78.1	73.8	33.9	46.2	68.4	12.8	74.4	50.6	83.6	46.6
Zr	260	192	280	110	142	398	148	168	89	65	236
Hf											
La	32.5	31.5	35.2	25.7	10.9	53.0	53.8	29.3	13.3	10.0	29.9
Ce	71.9	65.4	73.7	50.6	16.1	108.0	107.5	58.6	23.6	21.1	63.8
Pr											
Nd	40.7	32.0	37.0	25.8	10.9	47.9	44.6	31.2	14.3	11.8	31.9
Sm											
Eu											
Gd											
Tb											
Dy											
Ho											
Er											
Tm											
Yb											
Lu											

Sample	SA7-125	SA7-130	SA7-134	SA8-56	SA8-57	SA8-64	SA8-65	SA3-62	SA7-04	SA7-05	SA3-63
UTM x	353964	359894	357715	374291	374291	361852	361852	351175	357114	357489	357478
UTM y	6604112	6596991	6597286	6610312	6610312	6598854	6598854	6613340	6615430	6615470	6615601
Suite	Grey Gneiss	ZMBG	ZMBG	ZMBG	ZMBG						
SiO2	72.71	72.49	61.93	67.14	64.16	74.51	74.28	68.77	70.47	69.70	76.61
Al2O3	0.34	0.47	0.87	0.54	0.68	0.20	0.35	0.30	0.24	0.33	0.21
Fe2O3	13.26	12.76	15.50	14.58	15.34	12.53	11.22	15.96	15.32	14.66	11.62
TiO2	3.08	4.91	4.71	3.28	5.97	2.91	4.33	2.23	2.13	4.00	2.96
MgO	0.06	0.07	0.06	0.05	0.11	0.03	0.07	0.02	0.03	0.07	0.06
CaO	0.39	0.37	2.25	1.84	2.78	bdl	0.11	1.49	0.90	1.04	0.49
Na2O	2.47	1.72	3.19	2.39	2.84	0.39	0.80	3.42	2.67	3.04	2.12
K2O	5.10	4.51	2.95	3.12	3.96	3.33	2.96	4.72	3.51	4.12	3.99
MnO	1.16	1.78	5.73	5.20	2.56	5.32	4.50	1.77	4.18	2.07	1.28
P2O5	0.06	0.12	0.34	0.22	0.13	0.01	0.04	0.09	0.07	0.07	0.02
LOI	0.95	0.28	1.25	0.48	0.48	0.25	0.55	0.81	0.60	0.81	0.54
Total	99.57	99.48	98.79	98.84	99.02	99.49	99.21	99.57	100.13	99.94	99.90
Ba	301	963	2187	1585	268	838	1176	389	716	475	783
Co	6.1	8.7	14.7	9.8	18.3	2.5	5.4	23.1	5.9	9.7	bdl
Cr	15.3	7.6	47.5	48.1	109.7	bdl	bdl	4.0	9.5	0.3	27.3
Ga	16.5	20.1	20.3	17.6	19.4	18.0	13.5	18.6	15.3	15.2	31.4
Nb	2.6	9.4	11.3	9.3	10.2	4.2	2.5	8.2	4.3	9.3	33.0
Ni	bdl	bdl	33.3	34.0	32.6	bdl	bdl	5.2	0.9	bdl	62.6
Pb	15.4	8.0	25.2	33.9	17.9	31.5	17.1	57.7	23.7	8.9	34.6
Rb	52	74	132	159	154	106	79	58	129	65	1142
Sc	6.2	19.1	10.2	8.7	19.0	2.5	6.9	5.4	7.5	11.0	3.1
Sr	183	122	737	1030	315	94	374	442	299	216	134
Ta											
Th	6.6	8.3	8.0	10.9	6.3	5.7	7.0	13.2	9.4	5.9	9.6
U	2.7	3.1	0.8	4.1	2.7	1.7	2.2	3.1	5.6	4.1	4.9
V	19.2	23.9	69.8	48.6	98.4	7.3	9.9	21.5	24.0	43.0	3.0
Y	25.0	78.4	29.4	15.5	24.5	54.6	36.6	8.4	11.3	25.4	100.1
Zn	57.9	58.7	73.0	50.2	101.3	92.1	69.3	37.2	36.4	47.0	171.0
Zr	295	325	400	250	144	413	409	141	85	130	290
Hf											
La	12.4	29.8	61.8	47.7	25.2	31.3	34.4	0.2	19.4	16.3	1.0
Ce	26.3	67.5	122.6	86.7	43.9	61.7	66.5	9.4	31.8	32.3	7.2
Pr											
Nd	14.6	42.1	51.7	33.5	24.5	29.5	38.1	16.3	13.7	17.0	0.0
Sm											
Eu											
Gd											
Tb											
Dy											
Ho											
Er											
Tm											
Yb											
Lu											

Sample	SA3-66	SA3-67	SA7-10	SA7-11	SA7-12	SA7-14	SA7-16	SA7-19	SA7-18	SA7-20	SA7-21
UTM x	355182	351678	356818	356816	356817	356692	356522	356274	356274	356274	356274
UTM y	6616561	6614399	6615678	6615678	6615678	6615513	6615595	6615648	6615648	6615648	6615648
Suite	ZMBG										
SiO2	72.28	71.70	78.00	51.32	64.12	47.06	70.36	73.86	70.13	67.74	77.49
Al2O3	0.42	0.23	0.15	1.67	0.86	1.60	0.33	0.15	0.27	0.54	0.09
Fe2O3	13.63	14.55	12.07	13.46	15.16	15.58	15.12	14.41	14.37	14.45	12.04
TiO2	2.69	2.58	1.62	13.13	4.95	12.49	2.77	1.16	2.75	5.06	1.34
MgO	0.02	0.05	0.02	0.19	0.06	0.18	0.03	0.02	0.05	0.07	0.01
CaO	0.36	0.55	bdl	5.12	2.20	7.43	1.11	0.40	0.70	1.75	<0.045
Na2O	1.46	3.52	1.34	9.63	4.49	9.78	2.92	3.12	2.19	2.80	0.40
K2O	2.96	4.76	4.79	2.83	3.30	2.84	3.78	4.66	3.28	3.94	2.44
MnO	5.31	0.79	1.69	1.00	2.75	2.03	2.89	0.90	3.60	2.14	6.37
P2O5	0.07	0.07	0.01	0.19	0.38	0.22	0.10	0.05	0.09	0.10	0.01
LOI	0.39	0.80	0.21	0.99	1.05	0.86	0.43	0.58	1.21	0.53	0.21
Total	99.59	99.60	99.90	99.54	99.32	100.07	99.86	99.32	98.66	99.12	100.39
Ba	800	351	371	150	885	279	621	271	748	309	bdl
Co	bdl	2.6	2.2	45.3	15.7	54.7	7.8	2.9	5.1	14.7	bdl
Cr	1.4	2.1	1.3	122.9	73.0	169.4	33.7	4.9	5.1	95.3	2.1
Ga	51.6	15.6	20.7	22.3	21.6	18.8	16.9	13.6	16.4	25.7	20.0
Nb	48.9	9.8	13.9	4.1	9.4	3.5	4.6	1.8	6.0	14.6	7.3
Ni	20.0	0.6	bdl	22.3	25.7	112.8	6.0	2.0	bdl	17.3	bdl
Pb	336.7	20.4	16.7	12.0	16.3	12.8	16.3	16.3	11.6	14.8	25.2
Rb	49	211	43	40	135	96	127	40	144	112	170
Sc	7.2	5.2	4.7	40.4	11.9	33.2	8.8	5.6	5.7	14.4	1.2
Sr	80	354	159	273	747	385	394	239	239	145	8
Ta											
Th	32.6	5.4	18.4	3.8	17.3	0.1	7.8	0.8	10.2	8.5	6.1
U	7.1	2.1	4.0	2.7	4.6	0.7	2.1	1.9	3.7	3.0	2.4
V	20.0	7.7	4.7	331.5	71.0	257.9	38.7	16.2	20.0	79.0	3.1
Y	52.3	15.0	101.5	40.8	23.7	28.4	8.8	27.2	25.9	64.6	17.9
Zn	46.0	36.4	41.6	100.4	65.7	113.7	43.5	16.9	46.9	79.8	48.5
Zr	386	131	196	108	379	125	93	77	162	134	175
Hf											
La	1.4	0.8	46.1	14.9	80.6	9.0	27.1	10.9	21.5	26.7	31.9
Ce	9.2	6.4	97.7	28.6	161.0	20.4	46.8	12.1	38.6	58.7	62.3
Pr											
Nd	0.0	0.0	53.9	13.3	67.7	10.3	21.7	10.2	19.5	35.2	29.2
Sm											
Eu											
Gd											
Tb											
Dy											
Ho											
Er											
Tm											
Yb											
Lu											

Sample	SA7-22	SA7-23	SA7-24	SA7-27	SA7-109	SA7-136	SA7-138	SA7-140	SA7-141	SA7-142	SA7-143
UTM x	356274	356170	355610	354987	347446	350880	350808	354658	354686	354876	354819
UTM y	6615648	6615549	6616321	6616753	6608199	6617983	6618582	6616673	6616754	6616569	6616681
Suite	ZMBG										
SiO2	67.52	75.48	70.67	73.89	75.69	49.60	48.94	51.64	69.44	69.18	69.35
Al2O3	0.61	0.24	0.30	0.27	0.21	1.00	1.64	1.40	0.30	0.62	0.66
Fe2O3	15.25	11.96	14.80	13.30	11.56	18.67	14.82	16.66	14.65	12.95	13.23
TiO2	4.76	1.77	2.63	1.99	2.74	8.11	12.57	11.36	2.44	5.14	5.74
MgO	0.05	0.02	0.04	0.03	0.06	0.14	0.19	0.15	0.03	0.08	0.09
CaO	1.44	0.31	0.91	0.20	0.12	4.98	6.50	4.16	1.03	0.61	0.67
Na2O	2.62	0.96	2.81	0.96	0.66	7.72	9.64	7.77	2.60	2.41	2.48
K2O	4.47	3.00	4.17	3.15	3.86	3.46	2.52	3.89	3.47	3.62	3.47
MnO	2.22	5.20	2.60	5.61	3.92	2.88	1.13	2.04	4.08	3.68	3.59
P2O5	0.03	0.03	0.08	0.04	0.02	0.22	0.27	0.27	0.08	0.14	0.16
LOI	0.55	0.45	0.35	0.33	0.55	1.95	1.40	0.69	0.44	0.44	0.43
Total	99.53	99.42	99.36	99.76	99.38	98.73	99.62	100.02	98.58	98.88	99.86
Ba	207	235	592	595	625	690	240	447	823	567	686
Co	13.9	3.4	7.5	2.8	5.4	40.6	44.1	36.9	7.7	12.5	12.6
Cr	51.2	0.7	15.7	1.5	9.3	57.1	217.5	21.1	22.2	bdl	bdl
Ga	26.7	16.1	16.5	17.2	17.5	19.4	18.2	20.6	16.4	18.5	18.5
Nb	46.3	14.8	5.0	11.5	9.4	7.4	3.1	7.5	4.1	11.0	12.3
Ni	18.4	1.1	1.6	bdl	bdl	42.3	43.2	4.2	4.3	bdl	bdl
Pb	17.6	25.1	19.1	25.0	13.3	5.6	6.9	12.9	19.3	17.0	13.8
Rb	155	334	91	308	72	88	26	99	120	145	132
Sc	12.8	4.3	8.5	4.5	3.3	26.4	37.8	28.2	7.0	10.7	14.3
Sr	157	37	364	56	69	393	233	318	383	123	142
Ta											
Th	26.6	31.7	13.5	24.2	6.5	bdl	1.1	1.8	7.1	11.2	9.4
U	3.7	8.1	3.9	5.9	3.7	1.0	1.6	2.6	2.0	4.9	4.0
V	77.6	17.3	37.2	14.2	10.3	153.5	226.6	159.6	34.3	28.0	30.0
Y	53.7	89.5	11.8	60.1	96.8	61.6	30.8	37.6	9.9	62.1	60.6
Zn	133.7	35.2	38.9	35.9	94.2	81.5	91.3	108.9	41.8	68.1	82.8
Zr	194	160	95	284	387	133	97	155	89	269	306
Hf											
La	52.2	45.8	23.9	42.2	26.2	16.3	8.9	20.9	26.0	36.3	26.3
Ce	112.3	97.1	43.7	93.8	66.0	46.0	22.0	49.1	42.4	75.3	59.4
Pr											
Nd	56.9	49.7	19.6	48.0	42.5	30.6	11.9	23.2	18.2	41.6	35.3
Sm											
Eu											
Gd											
Tb											
Dy											
Ho											
Er											
Tm											
Yb											
Lu											

Sample	SA3-01a	SA3-01b	SA7-65	SA8-50	SA8-51	SA8-52	SA8-54	MM 02277	MM 026183	ROG 190	ROG 197
UTM x	357948	357948	375658	358960	365238	373897	373298	325424	375014	324908	327033
UTM y	6615161	6615161	6626611	6616661	6623402	6629309	6619421	6526915	6615718	6517359	6518349
Suite	HBG	HBG	HBG	HBG							
SiO2	72.27	72.14	73.23	70.99	75.54	73.20	70.09	72.02	70.59	76.40	77.10
Al2O3	13.34	13.36	12.62	13.37	13.08	13.07	13.72	15.47	13.60	11.90	12.10
Fe2O3	2.61	2.64	3.49	3.02	0.79	1.80	3.15	1.02	3.28	2.67	2.59
TiO2	0.46	0.46	0.36	0.51	0.09	0.27	0.51	0.25	0.55	0.21	0.23
MgO	0.36	0.42	0.28	0.61	bdl	0.24	0.61	0.41	0.55	0.31	0.32
CaO	1.60	1.60	0.81	1.62	0.82	1.26	1.98	1.26	2.07	1.11	1.13
Na2O	3.29	3.29	2.97	3.17	3.81	3.13	3.45	3.54	3.31	2.65	2.65
K2O	5.22	5.19	5.80	4.60	4.90	5.31	4.21	5.78	4.48	4.06	3.99
MnO	0.05	0.05	0.04	0.06	0.03	0.04	0.05	<0.01	0.06	0.04	0.04
P2O5	0.11	0.11	0.04	0.14	0.01	0.07	0.14	0.05	0.15	0.06	0.06
LOI	0.77	0.73	0.52	0.85	0.38	0.49	0.75	0.51	0.35	0.40	0.41
Total	100.06	99.97	100.16	98.95	99.44	98.87	98.66	100.33	98.99	99.80	101.00
Ba	1587	1569	981	1778	86	1628	1359	663	1603	558	171
Co	4	5	32	5	bdl	3	6	bdl	7	bdl	bdl
Cr	bdl	bdl	bdl	bdl	bdl	bdl	4	32	19	11	bdl
Ga	19	19	24	19	21	17	19	16	17	18	19
Nb	19	19	16	19	16	12	16	7.8	14.8	16.1	16.1
Ni	bdl	bdl	bdl	3							
Pb	27	29	15	23	50	26	20	33	19	27	37
Rb	136	138	105	133	369	149	120	232	150	85	223
Sc	7	7	32	9	5	4	9	bdl	bdl	11	6
Sr	240	241	256	307	49	245	317	187	314	126	44
Ta								0.2	1.0	0.3	0.3
Th	12	12	5	11	39	11	9	40.2	14.0	42.7	44.9
U								3.8	1.7	4.1	4.4
V	16	15	98	17	4	10	22	14	19	20	9
Y	59	60	90	55	12	33	54	7.7	51.0	96.5	88.3
Zn	68	68	779	85	36	52	75	39	82	78	48
Zr	405	418	569	463	111	220	445	184.4	552.6	203.0	186.6
Hf								6.5	15.2	7.0	6.8
La	90	87	46	99	23	62	85	55.5	140.0	46.3	46.9
Ce	181	181	111	209	40	122	182	119.5	296.1	104.0	106.1
Pr								13.2	33.5	13.1	13.4
Nd	84	83	59	95	16	56	82	46.4	121.0	57.8	59.3
Sm								8.8	19.8	16.7	17.2
Eu								0.8	3.7	0.6	0.5
Gd								5.8	13.5	14.2	14.7
Tb								0.8	1.9	2.9	2.9
Dy								2.4	10.6	17.2	16.9
Ho								0.2	1.8	3.6	3.6
Er								0.5	4.4	9.4	9.4
Tm								0.1	0.6	1.1	1.1
Yb								0.4	3.6	5.6	5.4
Lu								0.1	0.5	0.7	0.7

Sample	ROG 200	ROG 203	ROG 245	ROG 275	MM 02105	MM 02214	MM 02247	MM 026182	MM 026199	MM 026255	MM 026302
UTM x	327378	327858	316703	318862	332637	333807	338597	335158	364670	334332	342702
UTM y	6518699	6519377	6531446	6531428	6585303	6539047	6572694	6587408	6544077	6560297	6570573
Suite	HBG	HBG	HBG	HBG	Feda	Feda	Feda	Feda	Feda	Feda	Feda
SiO2	72.00	72.40	68.70	73.40	67.79	72.06	71.15	64.75	66.62	71.34	71.89
Al2O3	13.60	13.70	17.00	13.90	13.54	14.81	13.88	14.48	16.13	13.95	12.68
Fe2O3	2.77	1.96	1.43	1.26	5.05	1.94	2.05	5.81	3.24	1.97	1.43
TiO2	0.36	0.20	0.09	0.17	0.87	0.27	0.40	1.04	0.55	0.25	0.14
MgO	0.36	0.26	0.15	0.22	1.23	0.38	0.87	1.15	1.19	0.36	0.13
CaO	1.56	1.25	1.78	0.94	1.87	1.47	1.46	3.47	2.69	1.13	1.19
Na2O	2.87	2.87	4.63	3.12	3.32	3.39	3.53	3.94	4.21	3.07	2.72
K2O	5.00	5.41	4.28	5.87	4.40	5.73	5.42	3.17	4.43	5.61	5.74
MnO	0.02	0.04	0.08	0.02	0.08	0.02	0.03	0.10	0.05	0.03	0.02
P2O5	0.09	0.05	0.03	0.04	0.34	0.07	0.15	0.42	0.18	0.07	0.03
LOI	0.34	0.48	0.51	0.44	0.98	0.30	0.60	0.86	0.54	0.50	0.66
Total	98.90	98.60	98.70	99.40	99.47	100.43	99.54	99.18	99.82	98.29	96.63
Ba	428	366	297	320	1453	636	1310	1128	1343	509	588
Co	bdl	bdl	bdl	bdl	8	bdl	bdl	15	8	bdl	5
Cr	bdl	bdl	bdl	bdl	125	24	50	35	28	12	23
Ga	19	18	24	18	17	18	17	19	17	12	bdl
Nb	12.7	9.1	7.6	6.9	17.9	13.1	9.4	19.1	12.8	12.5	9.1
Ni	bdl	bdl	2	bdl	bdl	bdl	9	6	8	7	bdl
Pb	33	39	56	65	<10	29	29	20	27	33	28
Rb	233	219	210	265	139	306	141	167	136	331	190
Sc	bdl	bdl	bdl	bdl	bdl	bdl	bdl	16	14	bdl	bdl
Sr	84	83	139	115	163	146	664	377	565	114	121
Ta	0.3	0.2	0.5	0.2	1.1	0.5	1.1	1.2	1.1	0.6	0.3
Th	31.8	16.9	34.0	51.5	9.5	60.0	35.8	13.3	16.0	58.2	15.0
U	1.9	1.2	6.7	12.0	3.4	6.2	6.0	4.4	1.7	25.2	1.6
V	13	8	bdl	bdl	52	18	30	64	38	11	<10
Y	31.0	63.0	73.4	24.3	58.1	17.8	16.0	61.8	45.1	21.7	16.0
Zn	53	28	22	32	71	39	38	110	67	53	37
Zr	301.9	158.4	100.2	149.1	432.8	205.2	212.4	486.1	287.9	165.8	197.3
Hf	8.7	5.3	3.6	5.6	11.1	6.9	6.7	13.8	8.7	5.7	7.8
La	69.9	49.0	48.0	54.0	65.7	70.8	63.6	86.1	62.0	68.2	73.7
Ce	148.4	96.4	91.0	99.4	157.1	146.8	118.6	189.3	124.0	144.8	150.1
Pr	17.7	11.4	10.0	11.5	20.0	16.3	11.9	23.3	14.7	16.4	16.2
Nd	73.0	46.2	36.9	45.1	81.5	58.6	38.2	91.3	56.8	60.4	58.3
Sm	16.8	11.3	7.2	9.5	16.1	9.7	5.5	17.4	11.2	11.2	9.7
Eu	1.0	0.9	0.8	0.7	3.0	1.1	1.2	3.5	1.8	0.8	1.9
Gd	12.6	8.8	5.3	7.1	12.4	6.6	3.2	13.8	9.4	6.8	5.2
Tb	1.8	1.6	1.1	1.1	2.0	0.8	0.5	2.1	1.5	0.9	0.7
Dy	8.2	10.2	8.8	5.0	11.3	3.8	2.7	11.8	8.2	4.4	3.1
Ho	1.4	2.5	2.6	0.8	2.0	0.6	0.5	2.2	1.6	0.8	0.5
Er	2.6	8.0	9.7	1.9	5.5	1.4	1.4	5.4	3.9	1.8	1.3
Tm	0.3	1.2	1.9	0.3	0.8	0.2	0.3	0.8	0.6	0.2	0.2
Yb	1.3	6.4	13.6	1.5	4.6	1.3	1.6	5.0	3.6	1.3	1.1
Lu	0.2	1.0	2.3	0.2	0.7	0.2	0.2	0.8	0.5	0.2	0.2

Sample	MM 026303	MM 026306	MM 99208	ROG 13-1	ROG 15	ROG 16	ROG 218	ROG 23	ROG 256	ROG 257	ROG 27
UTM x	344910	340075	359185	362877	363301	363845	314258	364079	355088	355185	363949
UTM y	6570265	6579722	6480785	6558911	6558756	6558173	6532437	6557117	6586267	6585284	6556165
Suite	Feda	Feda	Feda	Feda	Feda	Feda	Feda	Feda	Feda	Feda	Feda
SiO ₂	66.17	67.02	62.47	70.28	70.01	70.06	72.50	66.12	66.96	66.88	64.25
Al ₂ O ₃	14.43	14.70	16.34	14.58	15.17	14.78	14.00	16.28	15.51	15.22	16.40
Fe ₂ O ₃	5.13	3.93	4.52	3.26	2.68	3.17	1.93	3.01	3.35	3.60	4.06
TiO ₂	0.65	0.61	0.75	0.43	0.34	0.41	0.22	0.50	0.40	0.50	0.73
MgO	0.60	0.89	1.98	0.53	0.39	0.52	0.30	1.40	0.70	0.73	1.93
CaO	2.20	2.30	3.85	1.49	1.42	1.57	0.94	2.55	2.04	2.36	2.86
Na ₂ O	3.15	3.27	3.90	3.83	3.63	3.72	3.17	4.53	3.84	3.69	4.41
K ₂ O	4.95	4.72	4.47	4.82	5.72	5.10	5.92	3.75	4.85	4.35	4.14
MnO	0.07	0.05	0.07	0.06	0.05	0.06	0.03	0.05	0.06	0.07	0.06
P ₂ O ₅	0.28	0.20	0.27	0.09	0.08	0.10	0.06	0.17	0.18	0.21	0.25
LOI	0.63	0.51	0.54	0.34	0.36	0.35	0.51	0.66	0.72	0.83	0.92
Total	98.27	98.21	99.17	99.70	99.86	99.86	99.50	99.01	98.62	98.41	100.00
Ba	918	1278	1834	716	860	892	482	932	1477	1475	1316
Co	10	7	11	5	6	bdl	bdl	7	7	8	10
Cr	36	27	34	11	26	17	5	38	12	35	69
Ga	14	10	23	20	17	23	22	18	bdl	14	22
Nb	30.7	13.7	14.8	13.7	10.3	13.4	22.9	5.6	14.6	16.8	12.0
Ni	6	bdl	22	8	7	<5	3	17	<5	<5	21
Pb	25	18	26	25	27	21	52	20	21	17	20
Rb	187	162	122	222	231	221	376	138	182	153	157
Sc	12	12	13	bdl	bdl	bdl	bdl	bdl	12	bdl	11
Sr	222	285	871	162	124	145	119	651	368	421	833
Ta	2.1	0.9	1.0	0.7	0.4	0.6	0.6	0.3	1.1	1.1	0.8
Th	19.0	18.9	0.5	23.7	26.3	21.3	53.4	10.4	12.1	14.6	17.9
U	2.3	2.3	0.5	2.3	2.4	3.0	20.4	0.9	4.4	3.1	2.1
V	21	43	66	21	16	19	10	42	21	21	57
Y	70.5	40.3	49.3	37.1	36.2	48.2	23.4	15.7	48.8	65.4	23.9
Zn	93	83	76	62	47	58	42	59	78	76	68
Zr	458.8	368.4	296.5	281.9	247.7	273.4	195.7	167.9	321.9	393.0	261.9
Hf	12.4	10.3	8.1	9.4	7.8	8.5	6.7	5.4	8.7	10.7	7.8
La	118.1	110.1	42.6	63.7	60.7	52.8	73.6	46.3	91.3	116.0	69.3
Ce	230.8	224.2	93.7	132.3	127.0	110.3	140.4	88.5	187.9	242.1	135.5
Pr	26.0	25.3	11.7	14.7	14.6	12.5	16.2	9.4	21.7	28.5	14.9
Nd	102.6	94.0	51.5	57.4	52.9	46.6	60.9	34.7	86.0	115.3	54.3
Sm	18.5	14.7	11.8	11.0	10.8	9.3	11.4	5.5	14.6	20.9	8.7
Eu	2.4	2.2	1.7	1.6	1.8	1.7	0.8	1.3	2.6	3.2	1.7
Gd	12.6	8.7	9.3	9.0	8.7	8.0	7.7	3.8	9.6	13.1	5.5
Tb	2.3	1.4	1.4	1.5	1.4	1.4	1.2	0.5	1.6	2.2	0.8
Dy	12.0	7.3	7.9	7.7	7.5	8.7	5.5	3.1	8.3	11.5	4.2
Ho	2.5	1.4	1.6	1.4	1.3	1.8	1.0	0.5	1.7	2.3	0.8
Er	6.6	3.6	4.6	3.4	3.2	4.6	2.3	1.3	4.5	5.9	2.2
Tm	0.9	0.6	0.7	0.5	0.4	0.6	0.3	0.2	0.7	0.9	0.3
Yb	6.0	3.3	4.3	2.4	2.3	3.6	1.4	1.0	4.1	5.0	2.2
Lu	0.8	0.5	0.6	0.3	0.3	0.4	0.2	0.1	0.6	0.7	0.3

Sample	ROG 2A	ROG 34	ROG 43	ROG 71	ROG 72	ROG 75	ROG329	MM 026191	MM 026297	MM 026298	MM 026299
UTM x	378768	363661	366261	373508	376216	380509	327835	362621	361312	361046	360948
UTM y	6544483	6553510	6549586	6546690	6546418	6541581	6540728	6549102	6548784	6548791	6549097
Suite	Feda	Leuco	Leuco	Leuco	Leuco						
SiO2	68.99	65.18	69.42	67.88	67.82	71.64	71.76	72.71	73.40	75.00	73.40
Al2O3	15.46	17.20	15.14	15.82	16.29	14.58	13.63	14.15	13.30	12.70	14.40
Fe2O3	2.48	3.02	2.15	2.13	2.61	1.88	2.56	2.47	2.38	2.03	0.50
TiO2	0.31	0.53	0.37	0.35	0.42	0.29	0.37	0.22	0.23	0.18	0.05
MgO	0.50	1.38	0.90	0.82	0.98	0.66	0.51	0.39	0.28	0.21	0.06
CaO	2.83	2.62	2.09	2.05	2.49	1.18	1.37	1.64	1.41	1.29	0.87
Na2O	4.15	4.56	4.01	4.48	4.68	4.39	3.32	3.54	3.42	3.29	3.02
K2O	4.65	4.61	4.77	4.25	3.98	4.45	4.96	4.55	4.35	4.26	6.63
MnO	0.04	0.05	0.04	0.03	0.04	0.03	0.04	0.02	0.03	0.02	bdl
P2O5	0.10	0.18	0.12	0.13	0.13	0.09	0.10	0.06	0.05	0.03	bdl
LOI	0.72	0.54	0.49	0.61	0.49	0.93	0.56	0.29	0.37	0.21	0.28
Total	100.22	99.85	99.49	98.55	99.93	100.12	99.17	100.03	99.20	99.20	99.20
Ba	1073	1567	1120	1212	1174	950	616	1445	915	598	2500
Co	bdl	9	bdl	5	7	bdl	8	bdl	bdl	bdl	bdl
Cr	19	47	42	31	36	23	20	19	bdl	bdl	bdl
Ga	18	22	16	17	18	15	bdl	15	17	18	13
Nb	6.2	8.4	9.1	6.6	11.1	6.5	14.9	3.3	4.5	3.9	1.3
Ni	6	15	13	11	10	10	bdl	bdl	bdl	bdl	bdl
Pb	34	28	27	24	27	23	22	30	38	36	47
Rb	142	131	132	147	129	157	250	106	96	95	134
Sc	bdl	bdl	10	bdl	11	bdl	bdl	bdl	bdl	bdl	bdl
Sr	657	953	573	617	576	404	143	340	176	105	411
Ta	0.6	0.8	1.0	0.6	1.1	0.8	0.6	0.1	0.1	0.1	bdl
Th	20.9	8.6	16.6	15.1	13.2	15.9	42.4	11.2	11.9	17.4	0.3
U	2.1	1.0	1.3	4.0	2.3	1.6	3.0	0.9	0.7	1.1	0.5
V	26	44	26	26	33	23	30	12	7	5	bdl
Y	15.2	17.0	28.1	13.8	28.5	17.1	24.9	9.7	11.8	24.3	0.9
Zn	43	56	50	47	63	45	62	41	34	22	6
Zr	210.0	167.6	150.2	155.5	179.9	147.8	360.3	199.2	183.3	191.8	33.0
Hf	6.9	5.5	4.8	4.7	5.5	4.8	10.5	7.0	6.4	7.9	1.1
La	53.7	40.3	50.3	43.6	50.5	43.6	83.9	43.2	45.6	43.0	3.0
Ce	97.0	86.0	87.0	85.0	98.5	78.0	158.1	84.8	91.5	86.3	5.1
Pr	9.7	9.9	9.0	9.0	10.7	7.9	18.2	10.3	11.0	10.6	0.5
Nd	33.1	36.6	33.3	32.4	40.5	27.9	70.6	37.9	47.2	44.7	1.8
Sm	5.1	5.9	5.9	5.3	6.8	4.4	11.7	7.0	9.1	10.6	0.3
Eu	1.0	1.5	1.1	1.1	1.3	1.0	1.2	1.2	1.3	1.3	1.0
Gd	3.4	3.8	4.3	3.3	4.8	3.0	8.1	4.4	6.3	8.5	0.3
Tb	0.5	0.6	0.8	0.5	0.8	0.5	1.1	0.6	0.8	1.4	bdl
Dy	2.4	3.0	4.4	2.5	4.1	2.8	5.0	2.4	3.3	6.4	bdl
Ho	0.5	0.6	0.9	0.4	0.9	0.5	0.9	0.4	0.5	1.0	bdl
Er	1.3	1.5	2.6	1.2	2.8	1.7	2.2	0.8	1.1	2.3	bdl
Tm	0.2	0.2	0.4	0.2	0.5	0.3	0.3	0.1	0.1	0.2	bdl
Yb	1.2	1.5	2.6	1.1	3.2	1.7	2.0	0.6	0.6	1.3	bdl
Lu	0.2	0.2	0.4	0.2	0.5	0.2	0.3	0.1	0.1	0.2	bdl

Sample	ROG 28	ROG 30-1	ROG 33	ROG 45	SA8-23a	SA8-23b
UTM x	363525	364734	364407	366293	372344	372344
UTM y	6555933	6551294	6552651	6549215	6636570	6636570
Suite	Leuco	Leuco	Leuco	Leuco	Dyrskard	Dyrskard
SiO ₂	71.87	76.85	73.17	74.50	76.13	75.99
Al ₂ O ₃	13.77	11.69	14.46	13.45	11.86	11.84
Fe ₂ O ₃	1.61	1.56	0.55	1.13	2.12	2.12
TiO ₂	0.28	0.18	0.07	0.16	0.20	0.20
MgO	0.71	0.50	0.13	0.32	0.11	0.08
CaO	1.50	0.45	1.20	1.16	0.45	0.44
Na ₂ O	3.63	2.26	4.77	3.83	3.45	3.48
K ₂ O	5.19	6.28	4.05	4.59	4.99	5.18
MnO	0.02	0.03	0.01	0.03	0.23	0.02
P ₂ O ₅	0.09	0.04	0.02	0.04	0.01	0.01
LOI	0.75	0.21	0.27	0.28	0.24	0.23
Total	99.41	100.05	98.69	99.50	99.79	99.59
Ba	1507	1117	484	467	344	347
Co	bdl	bdl	bdl	bdl	1.7	1.6
Cr	27	18	10	13	bdl	bdl
Ga	14	12	13	17	19.0	19.1
Nb	5.1	4.0	1.3	4.5	14.0	14.0
Ni	10	6	5	8	bdl	bdl
Pb	17	44	38	30	8.1	8.7
Rb	154	167	105	138	144	145
Sc	bdl	bdl	bdl	bdl	2.4	3.0
Sr	550	268	166	325	43	44
Ta	1.0	0.1	bdl	0.5		
Th	7.9	15.7	5.4	8.2	9.2	9.6
U	1.6	2.0	2.5	1.1	4.2	4.5
V	28	bdl	bdl	11	6.7	5.4
Y	11.9	44.7	33.5	18.6	110	112
Zn	35	33	17	32	24.9	25.4
Zr	136.6	194.3	61.5	82.4	379	388
Hf	4.5	8.1	2.3	3.6		
La	34.6	33.3	10.4	23.8	36.5	36.2
Ce	65.5	73.6	21.0	38.5	90.8	89.0
Pr	6.8	9.2	2.5	3.8		
Nd	25.2	37.4	9.3	13.9	54.3	56.1
Sm	3.8	8.4	2.3	2.6		
Eu	0.9	1.1	0.9	0.5		
Gd	2.5	8.0	2.7	2.5		
Tb	0.4	1.3	0.6	0.5		
Dy	2.1	7.5	4.1	2.8		
Ho	0.4	1.6	1.0	0.6		
Er	1.0	4.3	3.5	1.8		
Tm	0.2	0.6	0.6	0.3		
Yb	1.1	4.1	3.4	1.5		
Lu	0.2	0.6	0.6	0.2		

Table 10.3. Whole-rock geochemical data. HBG = Hornblende Biotite Granite Suite, Leuco = Leucogranite Suite, Grey Gneiss = Sauda Grey Gneiss Complex, ZMBG = Zinc Mine Banded Gneiss, Amphibolt = Amphibolite Suite. Data in italics are ICP-MS, all other data are XRF. bdl = below detection limit.

Date	Zr	Tm	204 cps	206Pb mV	207Pb mV	238U mV	Pb ppm	U ppm	207Pb/ 206Pb	1 σ %	207Pb/ 235U	1 σ %	206Pb/ 238U	Rho	207Pb/ 206Pb	2 σ	207Pb/ 235U	2 σ	206Pb/ 238U	2 σ	Disc.		
SA3-01	3.11.09	15	R CA	-163	1.80	0.11	8.75	9	57	0.0737	0.903	1.712	1.956	0.168	1.735	0.89	1034	36	1013	25	1003	32	2.96
SA3-01	3.11.09	33	R CA	-290	4.24	0.26	20.42	21	134	0.0738	0.432	1.709	2.195	0.168	2.152	0.98	1037	17	1012	28	1000	40	3.55
SA3-01	3.11.09	17	R CA	-25	11.40	0.72	53.97	55	353	0.0741	0.400	1.747	1.752	0.171	1.705	0.97	1045	16	1026	22	1017	32	2.73
SA3-01	3.11.09	13	R CA	-303	5.65	0.35	25.42	27	166	0.0737	0.400	1.754	1.773	0.173	1.727	0.97	1033	16	1029	23	1026	33	0.62
SA3-01	3.11.09	5	R CA	145	11.16	0.70	53.44	54	350	0.0739	0.400	1.703	1.697	0.167	1.649	0.97	1039	16	1010	21	996	30	4.12
SA3-01	3.11.09	4	R CA	17	6.67	0.42	32.39	32	212	0.0737	0.400	1.684	1.685	0.166	1.637	0.97	1033	16	1002	21	988	30	4.31
SA3-01	3.11.09	12	R CA	169	1.67	0.10	8.14	8	53	0.0737	0.923	1.675	1.972	0.165	1.743	0.88	1032	37	999	25	984	32	4.66
SA3-01	22.4.08	2	R CA	156	2.30	0.15	13.75	45	279	0.0738	0.669	1.773	1.190	0.174	0.985	0.83	1037	27	1036	15	1035	19	0.11
SA3-01	22.4.08	14	R CA	165	1.10	0.07	6.64	21	135	0.0737	1.254	1.753	1.585	0.173	0.969	0.61	1032	51	1028	20	1027	18	0.57
SA3-01	22.4.08	11	R CA	-130	5.97	0.39	35.84	116	727	0.0740	0.500	1.775	1.096	0.174	0.975	0.89	1041	20	1036	14	1034	19	0.74
SA3-01	22.4.08	7	R CA	133	1.88	0.12	11.38	36	231	0.0738	0.794	1.766	1.249	0.174	0.964	0.77	1035	32	1033	16	1033	18	0.21
SA3-01	22.4.08	24	R CA	134	5.32	0.35	32.40	103	657	0.0741	0.500	1.779	1.084	0.174	0.962	0.89	1045	20	1038	14	1034	18	1.05
SA3-01	22.4.08	29	R CA	355	2.43	0.16	14.60	47	296	0.0743	0.650	1.799	1.164	0.176	0.966	0.83	1048	26	1045	15	1043	19	0.47
SA3-01	22.4.08	19	R CA	199	0.76	0.05	4.63	15	94	0.0737	1.770	1.786	2.018	0.176	0.971	0.48	1033	72	1040	26	1044	19	-1.03
SA3-01	22.4.08	22	R CA	-106	0.72	0.05	4.34	14	88	0.0732	1.827	1.783	2.099	0.177	1.032	0.49	1018	74	1039	27	1049	20	-3.03
SA3-01	22.4.08	30	R CA	-124	0.75	0.05	4.64	15	94	0.0741	1.773	1.793	2.026	0.176	0.981	0.48	1044	72	1043	26	1043	19	0.13
SA3-01	22.4.08	38	R CA	-120	2.89	0.19	17.85	56	362	0.0743	0.547	1.799	1.105	0.176	0.960	0.87	1050	22	1045	14	1043	18	0.65
SA3-01	22.4.08	45	R CA	-101	0.69	0.04	4.29	13	87	0.0738	1.953	1.775	2.197	0.174	1.007	0.46	1035	79	1036	28	1037	19	-0.13
SA3-01	22.4.08	46	R CA	443	0.26	0.02	4.51	5	34	0.0720	4.660	4.743	4.772	0.176	1.029	0.22	986	490	4024	60	4043	20	-6.75
SA3-01	22.4.08	48	R CA	-99	0.62	0.04	3.74	42	76	0.0735	2.407	4.726	2.344	0.170	1.020	0.44	1028	85	4048	30	4044	49	4.34
SA3-01	22.4.08	40	R CA	74	0.50	0.03	2.96	40	60	0.0724	2.577	4.768	2.762	0.177	0.995	0.36	997	405	4034	35	4052	49	-5.50
SA3-01	22.4.08	49	R CA	436	0.62	0.04	3.80	42	77	0.0738	2.093	4.765	2.314	0.174	0.987	0.43	4035	85	4033	30	4032	49	0.30
SA3-02	14.5.09	1	R U	141	5.58	0.48	19.26	119	468	0.0945	0.350	3.460	1.304	0.266	1.256	0.96	1518	13	1518	20	1518	34	-0.02
SA3-02	14.5.09	2	R U	-145	5.14	0.44	17.23	110	419	0.0951	0.350	3.553	2.086	0.271	2.057	0.99	1531	13	1539	33	1545	56	-0.91
SA3-02	14.5.09	3	R U	-184	5.87	0.51	19.98	126	486	0.0949	0.350	3.502	1.107	0.268	1.050	0.95	1526	13	1528	17	1529	29	-0.19
SA3-02	14.5.09	4	R U	-148	6.83	0.59	23.21	146	564	0.0946	0.350	3.470	1.548	0.266	1.508	0.97	1519	13	1520	24	1521	41	-0.11
SA3-02	14.5.09	5	R U	-109	5.90	0.51	20.02	126	487	0.0945	0.350	3.513	1.471	0.270	1.429	0.97	1519	13	1530	23	1538	39	-1.28
SA3-02	14.5.09	7	R U	-217	3.99	0.34	13.62	85	331	0.0942	0.350	3.439	1.585	0.265	1.546	0.98	1512	13	1513	25	1515	42	-0.19
SA3-02	14.5.09	8	R U	-176	4.60	0.40	15.30	98	372	0.0946	0.350	3.554	1.616	0.272	1.578	0.98	1521	13	1539	25	1553	43	-2.13
SA3-02	14.5.09	10	R CA	-263	4.76	0.41	16.07	102	391	0.0940	0.350	3.496	1.078	0.270	1.020	0.95	1509	13	1526	17	1539	28	-1.97

Date	Zrn	Tm	204 cps	206Pb mV	207Pb mV	238U mV	Pb ppm	U ppm	207Pb/ 206Pb	1 σ %	207Pb/ 235U	1 σ %	206Pb/ 238U	Rho	207Pb/ 206Pb	2 σ	207Pb/ 235U	2 σ	206Pb/ 238U	2 σ	Disc.		
SA3-02	14.5.09	13	R CA	-292	5.94	0.51	19.92	127	485	0.0946	0.350	3.643	1.526	0.279	1.485	0.97	1520	13	1559	24	1588	42	-4.45
SA3-02	14.5.09	15	R CA	-419	4.79	0.41	16.15	102	393	0.0943	0.350	3.496	1.055	0.269	0.996	0.94	1514	13	1526	17	1535	27	-1.42
SA3-02	14.5.09	16	R CA	-76	5.18	0.44	17.92	111	436	0.0942	0.350	3.541	1.027	0.273	0.965	0.94	1512	13	1536	16	1554	27	-2.82
SA3-02	14.5.09	17	R CA	-159	3.11	0.27	10.55	67	257	0.0940	0.422	3.492	0.959	0.269	0.861	0.90	1508	16	1525	15	1538	24	-2.02
SA3-02	14.5.09	19	R CA	-336	3.23	0.28	11.04	69	269	0.0944	0.397	3.500	0.949	0.269	0.862	0.91	1516	15	1527	15	1535	24	-1.24
SA3-02	14.5.09	26	R CA	-276	3.46	0.30	11.85	74	288	0.0940	0.381	3.471	1.142	0.268	1.076	0.94	1508	14	1521	18	1530	29	-1.43
SA3-02	14.5.09	29	R CA	-100	4.29	0.37	14.46	92	352	0.0939	0.350	3.498	0.947	0.270	0.880	0.93	1506	13	1527	15	1541	24	-2.33
SA3-02	14.5.09	32	R CA	-49	3.46	0.30	11.65	74	283	0.0945	0.362	3.505	0.953	0.269	0.881	0.93	1518	14	1528	15	1536	24	-1.21
SA3-04	10.4.08	3	R CA	-39	1.90	0.16	7.48	42	177	0.0938	0.636	3.407	1.128	0.263	0.931	0.83	1505	24	1506	18	1507	25	-0.16
SA3-04	10.4.08	6	R CA	183	2.57	0.21	9.86	57	233	0.0943	0.500	3.458	1.058	0.266	0.933	0.88	1514	19	1518	17	1520	25	-0.41
SA3-04	10.4.08	16	R CA	308	6.73	0.56	26.36	149	622	0.0948	0.500	3.479	1.056	0.266	0.930	0.88	1525	19	1522	17	1521	25	0.28
SA3-04	10.4.08	17	R CA	120	6.27	0.51	25.23	138	595	0.0939	0.500	3.296	1.070	0.255	0.946	0.88	1505	19	1480	17	1463	25	2.84
SA3-04	10.4.08	26	R CA	253	4.09	0.34	15.79	91	373	0.0941	0.500	3.428	1.060	0.264	0.935	0.88	1511	19	1511	17	1511	25	0.00
SA3-04	10.4.08	28	R CA	270	7.47	0.62	29.17	165	688	0.0942	0.500	3.436	1.078	0.265	0.956	0.89	1512	19	1513	17	1513	26	-0.04
SA3-04	10.4.08	33	R CA	270	3.18	0.26	12.10	70	286	0.0938	0.500	3.416	1.075	0.264	0.951	0.89	1505	19	1508	17	1510	26	-0.38
SA3-04	10.4.08	36	R CA	382	6.25	0.51	23.99	138	566	0.0939	0.500	3.450	1.066	0.267	0.941	0.88	1506	19	1516	17	1523	25	-1.13
SA3-04	10.4.08	38	R CA	68	4.41	0.36	17.50	98	413	0.0936	0.500	3.407	1.060	0.264	0.935	0.88	1499	19	1506	17	1511	25	-0.76
SA3-04	10.4.08	47	R CA	195	9.17	0.76	36.05	203	851	0.0941	0.500	3.455	1.074	0.266	0.951	0.89	1509	19	1517	17	1523	26	-0.88
SA3-04	10.4.08	61	R CA	294	6.20	0.51	23.59	137	557	0.0937	0.500	3.419	1.078	0.265	0.955	0.89	1502	19	1509	17	1514	26	-0.77
SA3-04	15.5.09	a2	RIM	-52	4.06	0.35	14.06	123	1751	0.0963	0.500	3.265	2.197	0.246	2.140	0.97	1555	19	1473	34	1417	54	8.87
SA3-04	15.5.09	a4	RIM	90	13.00	1.08	52.43	393	6530	0.0926	0.500	2.734	3.003	0.214	2.961	0.99	1479	19	1338	44	1251	67	15.40
SA3-04	15.5.09	a12	RIM	6684	18.87	2.56	98.84	670	12308	0.1566	2.619	3.913	7.184	0.181	6.690	0.93	2419	89	1616	140	1074	131	56.64
SA3-04	15.5.09	a9	RIM	-9	24.39	2.06	91.92	737	11447	0.0939	0.500	2.964	1.569	0.229	1.487	0.95	1505	19	1398	24	1329	36	11.71
SA3-04	15.5.09	a9	RIM	216	24.07	1.96	120.57	727	15015	0.0901	0.636	2.143	3.117	0.173	3.052	0.98	1427	24	1163	42	1027	58	28.05
SA3-04	15.5.09	a16	RIM	44	6.28	0.55	20.63	190	2570	0.0958	0.500	3.484	1.439	0.264	1.349	0.94	1544	19	1524	22	1509	36	2.28
SA3-04	15.5.09	a22	RIM	154	27.32	2.38	103.86	825	12933	0.0963	0.500	2.871	3.108	0.216	3.067	0.99	1553	19	1374	46	1262	70	18.76
SA3-04	15.5.09	a18	RIM	18	28.82	2.43	114.70	871	14284	0.0937	0.500	2.858	1.917	0.221	1.851	0.97	1503	19	1371	28	1288	43	14.29
SA3-04	15.5.09	a7	RIM	138	27.11	2.29	136.08	819	16946	0.0931	0.765	2.209	1.901	0.172	1.741	0.92	1489	29	1184	26	1024	33	31.23

Date	Zrn	Tm	204 cps	206Pb mV	207Pb mV	238U mV	Pb ppm	U ppm	207Pb/ 206Pb	1 σ %	207Pb/ 235U	1 σ %	206Pb/ 238U	Rho	207Pb/ 206Pb	2 σ	207Pb/ 235U	2 σ	206Pb/ 238U	2 σ	Disc.		
SA3-60	2.11.09	19	R CA	-4	11.46	0.92	34.85	57	231	0.0943	0.500	3.461	1.711	0.266	1.636	0.96	1514	19	1518	27	1521	44	-0.48
SA3-60	2.11.09	8	R CA	308	22.22	1.79	69.71	110	463	0.0952	0.500	3.413	2.145	0.260	2.086	0.97	1531	19	1507	33	1490	55	2.69
SA3-60	2.11.09	2	R CA	-22	11.07	0.89	34.19	55	227	0.0944	0.500	3.431	1.541	0.264	1.468	0.95	1516	19	1511	24	1508	39	0.50
SA3-60	22.4.08	3	R CA	50	5.74	0.48	20.39	84	335	0.0949	0.500	3.448	0.911	0.263	0.762	0.84	1526	19	1515	14	1507	20	1.24
SA3-60	22.4.08	5	R CA	22	2.75	0.23	9.96	40	163	0.0945	0.500	3.481	0.927	0.267	0.781	0.84	1518	19	1523	15	1526	21	-0.51
SA3-60	22.4.08	6	R CA	46	6.48	0.53	24.05	95	395	0.0944	0.500	3.403	0.910	0.261	0.760	0.84	1516	19	1505	14	1497	20	1.28
SA3-60	22.4.08	4	R CA	-16	4.27	0.35	15.42	63	253	0.0940	0.500	3.527	0.935	0.272	0.791	0.85	1509	19	1533	15	1551	22	-2.81
SA3-60	22.4.08	11	R CA	-70	5.41	0.45	19.59	80	321	0.0943	0.500	3.440	0.910	0.264	0.760	0.84	1515	19	1513	14	1513	20	0.14
SA3-60	22.4.08	15	R CA	18	3.65	0.30	13.32	54	219	0.0944	0.500	3.393	0.905	0.261	0.755	0.83	1516	19	1503	14	1493	20	1.50
SA3-60	22.4.08	18	R CA	-28	3.98	0.33	14.45	59	237	0.0944	0.500	3.422	0.906	0.263	0.756	0.83	1517	19	1509	14	1504	20	0.85
SA3-60	15.5.09	a1	RIM	252	17.66	1.52	75.36	508	8921	0.0947	0.597	2.653	2.954	0.203	2.893	0.98	1522	23	1315	43	1193	63	21.62
SA3-60	15.5.09	a2	RIM	86	7.12	0.61	23.66	205	2801	0.0950	0.508	3.467	3.801	0.265	3.767	0.99	1529	19	1520	58	1513	101	1.01
SA3-60	15.5.09	a3	RIM	-251	11.41	0.97	39.52	328	4678	0.0944	0.500	3.237	1.577	0.249	1.557	0.99	1516	19	1466	24	1432	40	5.54
SA3-60	15.5.09	a4	RIM	-63	12.69	1.06	50.47	365	5975	0.0933	0.664	2.958	4.490	0.230	4.441	0.99	1493	25	1397	66	1335	106	10.62
SA7-04	23.4.08	8	R CA	-197	5.29	0.44	21.25	109	437	0.0952	0.500	3.501	0.909	0.267	0.759	0.83	1531	19	1528	14	1525	21	0.41
SA7-04	23.4.08	14	R CA	-3	2.64	0.21	10.88	55	224	0.0937	0.496	3.360	0.903	0.260	0.754	0.83	1502	19	1495	14	1491	20	0.72
SA7-04	23.4.08	12	R CA	-235	7.56	0.62	30.68	156	631	0.0940	0.500	3.400	0.954	0.262	0.813	0.83	1509	19	1504	15	1501	22	0.52
SA7-04	23.4.08	23	R CA	-210	3.89	0.32	16.18	80	333	0.0930	0.500	3.328	0.953	0.260	0.811	0.83	1488	19	1488	15	1487	22	0.03
SA7-04	23.4.08	25	R CA	10457	45.21	2.78	96.11	314	1977	0.2098	2.193	4.981	2.359	0.172	0.867	0.34	2904	71	1816	39	1024	46	64.73
SA7-04	23.4.08	20	R CA	-182	6.16	0.50	26.11	127	537	0.0926	0.500	3.280	0.936	0.257	0.792	0.83	1480	19	1476	14	1474	21	0.42
SA7-04	23.4.08	27	R CA	27947	48.97	5.75	146.29	362	3099	0.3461	0.578	6.744	4.179	0.141	1.017	0.85	3690	48	2078	20	852	46	76.92
SA7-04	23.4.08	11	R CA	141	6.68	0.55	27.38	138	563	0.0932	0.500	3.471	0.989	0.270	0.853	0.84	1492	19	1521	15	1541	23	-3.32
SA7-04	23.4.08	9	R CA	268	4.85	0.39	20.29	100	417	0.0919	0.500	3.277	0.925	0.259	0.779	0.83	1466	19	1476	14	1483	21	-1.18
SA7-04	23.4.08	3	R CA	1210	7.36	0.76	39.02	452	803	0.1171	3.761	3.486	4.064	0.216	1.598	0.37	1912	435	4524	62	4260	95	34.09
SA7-04	23.4.08	26	R CA	9434	40.13	2.25	44.54	209	916	0.2511	5.575	9.223	6.449	0.266	3.242	0.50	3192	476	2360	112	1622	87	52.31
SA7-04	23.4.08	5	R CA	4484	14.34	1.80	88.45	296	1819	0.1422	1.830	3.560	2.212	0.182	1.243	0.54	2254	63	1541	34	1076	25	52.29
SA7-04	23.4.08	6	R CA	531	45.33	1.24	99.39	317	1859	0.0929	0.480	2.412	0.936	0.188	0.919	0.98	1486	7	1246	13	1112	49	25.14
SA7-04	23.4.08	7	R U	155	12.48	0.98	76.98	258	1583	0.0898	0.500	2.231	0.923	0.180	0.776	0.83	1421	19	1191	13	1068	15	24.85
SA7-04	23.4.08	47	R U	241	40.52	0.87	62.02	217	1275	0.0954	0.352	2.492	4.261	0.189	1.211	0.96	1536	43	1270	18	1118	25	27.19
SA7-04	23.4.08	19	R U	-62	11.13	0.88	50.62	230	1041	0.0917	0.500	3.100	0.920	0.245	0.772	0.83	1460	19	1433	14	1414	20	3.17

Date	Zrn	Tm	204 cps	206Pb mV	207Pb mV	238U mV	Pb ppm	U ppm	207Pb/ 206Pb	1 σ %	207Pb/ 235U	1 σ %	206Pb/ 238U	Rho	207Pb/ 206Pb	2 σ	207Pb/ 235U	2 σ	206Pb/ 238U	2 σ	Disc.		
SA7-04	23-4-08	4	R-U	7766	9.69	1.94	36.69	200	755	0.2297	6.965	9.297	7.288	0.293	2.146	0.29	2368	223	3050	126	4659	62	45.64
SA7-04	23-4-08	2	R-U	708	40.47	0.96	61.67	216	4268	0.1048	0.539	2.844	4.234	0.197	1.107	0.89	4366	20	4711	48	4157	23	32.38
SA7-04	23-4-08	48	R-U	4295	42.62	1.18	84.25	261	4733	0.1079	0.887	2.574	4.181	0.173	0.780	0.61	4293	32	4764	47	4029	45	41.68
SA7-04	23-4-08	22	R-U	-115	9.77	0.76	58.67	202	1207	0.0898	0.500	2.379	1.127	0.192	1.010	0.88	1236	16	1421	16	1133	21	20.26
SA7-04	23-4-08	24	R-U	497	9.53	0.83	46.49	497	956	0.0998	0.388	3.218	0.864	0.234	0.769	0.89	4464	44	4620	43	4355	49	16.36
SA7-86	3.11.09	25	R CA	-93	7.32	0.58	23.73	36	158	0.0941	0.350	3.321	1.354	0.256	1.307	0.97	1486	13	1510	21	1470	34	2.65
SA7-86	3.11.09	31	R CA	50	4.79	0.38	15.35	24	102	0.0940	0.350	3.299	1.400	0.255	1.355	0.97	1481	13	1508	22	1462	35	3.10
SA7-86	3.11.09	22	R CA	-10	4.41	0.35	14.19	22	94	0.0940	0.350	3.247	1.317	0.250	1.270	0.96	1468	13	1508	20	1441	33	4.46
SA7-86	3.11.09	27	R CA	31	7.49	0.60	23.68	37	157	0.0942	0.350	3.306	1.400	0.255	1.355	0.97	1483	13	1511	22	1463	35	3.21
SA7-86	3.11.09	40	R CA	-246	3.63	0.29	11.54	18	77	0.0936	0.396	3.300	1.366	0.256	1.308	0.96	1481	15	1501	21	1468	34	2.21
SA7-86	3.11.09	36	R CA	-38	5.00	0.40	15.87	25	105	0.0935	0.350	3.276	1.369	0.254	1.323	0.97	1475	13	1497	21	1460	34	2.51
SA7-86	3.11.09	44	R CA	87	5.11	0.41	15.90	25	106	0.0938	0.350	3.331	1.488	0.258	1.447	0.97	1488	13	1504	23	1477	38	1.75
SA7-86	3.11.09	11	R CA	76	3.73	0.30	11.45	19	76	0.0939	0.380	3.353	1.557	0.259	1.509	0.97	1494	14	1506	24	1485	40	1.41
SA7-86	3.11.09	13	R CA	-130	5.58	0.44	17.53	28	116	0.0939	0.350	3.283	1.495	0.254	1.453	0.97	1477	13	1506	23	1457	38	3.25
SA7-86	3.11.09	28	R CA	-13	2.96	0.24	9.42	15	63	0.0943	0.459	3.325	1.520	0.256	1.450	0.95	1487	17	1514	23	1468	38	2.98
SA7-86	3.11.09	29	R CA	-66	4.95	0.40	15.84	25	105	0.0938	0.350	3.297	1.399	0.255	1.355	0.97	1480	13	1503	22	1464	35	2.60
SA7-86	23-4-08	1	R CA	-32	3.03	0.25	12.94	73	298	0.0941	0.500	3.385	0.901	0.261	0.750	0.83	1501	19	1511	14	1494	20	1.09
SA7-86	24-4-08	4	R CA	39	1.16	0.10	5.03	28	116	0.0940	0.982	3.376	1.235	0.260	0.750	0.61	1499	37	1508	19	1492	20	1.06
SA7-86	25-4-08	6	R CA	-58	1.83	0.15	7.91	44	182	0.0942	0.675	3.389	1.009	0.261	0.750	0.74	1502	25	1511	16	1495	20	1.08
SA7-86	26-4-08	7	R CA	-114	2.11	0.17	9.13	51	210	0.0941	0.578	3.372	0.947	0.260	0.750	0.79	1498	22	1510	15	1489	20	1.41
SA7-86	27-4-08	10	R CA	-395	1.95	0.16	8.48	47	195	0.0943	0.628	3.372	0.978	0.259	0.750	0.77	1498	24	1514	15	1487	20	1.79
SA7-86	28-4-08	18	R CA	-198	4.30	0.35	18.80	104	432	0.0943	0.500	3.355	0.901	0.258	0.750	0.83	1494	19	1515	14	1480	20	2.30
SA7-86	29-4-08	17	R CA	-380	1.29	0.11	5.67	31	130	0.0942	0.899	3.343	1.171	0.257	0.750	0.64	1491	34	1511	18	1477	20	2.26
SA7-86	30-4-08	14	R CA	-616	1.29	0.10	5.62	31	129	0.0942	0.912	3.362	1.181	0.259	0.750	0.64	1496	34	1511	18	1485	20	1.76
SA7-86	1.5.08	15	R CA	-402	3.90	0.32	16.92	94	389	0.0944	0.500	3.390	0.901	0.260	0.750	0.83	1502	19	1517	14	1492	20	1.64
SA7-86	2.5.08	23	R CA	-342	1.66	0.14	7.23	40	166	0.0943	0.728	3.362	1.045	0.258	0.750	0.72	1496	27	1515	16	1482	20	2.16
SA7-91	22-4-08	4	R CA	-241	4.01	0.33	16.22	74	306	0.0945	0.500	3.400	1.032	0.261	0.902	0.87	1504	19	1519	16	1494	24	1.66
SA7-91	22-4-08	9	R CA	291	5.97	0.50	24.54	110	462	0.0949	0.500	3.384	1.034	0.259	0.905	0.88	1501	19	1526	16	1482	24	2.89
SA7-91	22-4-08	13	R CA	161	3.31	0.27	13.73	61	259	0.0943	0.500	3.366	1.031	0.259	0.902	0.87	1497	19	1515	16	1484	24	2.07

Date	Zir	Tm	204		206Pb		207Pb		238U		Pb ppm	U ppm	207Pb/1 σ %		206Pb/1 σ %		Rho	207Pb/2 σ		206Pb/2 σ		Disc.
			cps	mV	mV	mV	235U	238U	235U	238U			206Pb	235U	206Pb	238U						
SA7-91 22.4.08	12	R CA	196	5.28	0.44	21.76	97	410	0.0942	0.500	3.365	1.017	0.259	0.886	0.87	1511	19	1496	16	1486	23	1.71
SA7-91 22.4.08	11	R CA	113	3.74	0.30	15.20	69	286	0.0936	0.500	3.405	1.022	0.264	0.891	0.87	1499	19	1506	16	1510	24	-0.70
SA7-91 22.4.08	15	R CA	169	4.88	0.40	20.57	90	387	0.0944	0.500	3.441	1.070	0.264	0.946	0.88	1517	19	1514	17	1512	25	0.34
SA7-91 22.4.08	17	R CA	230	4.31	0.36	18.13	79	342	0.0946	0.500	3.410	1.021	0.261	0.890	0.87	1520	19	1507	16	1497	24	1.52
SA7-91 22.4.08	19	R CA	155	4.22	0.35	17.73	77	334	0.0948	0.500	3.393	1.080	0.259	0.958	0.89	1525	19	1503	17	1487	25	2.45
SA7-91 22.4.08	30	R CA	129	3.63	0.30	15.09	67	284	0.0945	0.500	3.376	1.031	0.259	0.902	0.87	1518	19	1499	16	1485	24	2.16
SA7-91 22.4.08	31	R CA	276	4.84	0.40	20.72	89	390	0.0943	0.500	3.343	1.206	0.257	1.098	0.91	1514	19	1491	19	1475	29	2.55
SA8-45 13.5.09	11	S CA	34	11.60	0.98	29.70	112	381	0.0950	0.350	3.899	1.315	0.298	1.268	0.96	1527	13	1613	21	1680	37	-10.03
SA8-45 13.5.09	12	S CA	210	12.52	1.05	32.58	121	418	0.0944	0.350	3.684	1.131	0.283	1.076	0.95	1515	13	1568	18	1607	31	-6.09
SA8-45 13.5.09	13	S CA	91	5.96	0.50	12.11	58	155	0.0940	0.350	4.743	1.100	0.366	1.043	0.95	1508	13	1775	18	2010	36	-33.25
SA8-45 13.5.09	14	S CA	-109	11.07	0.93	29.80	107	382	0.0942	0.350	3.616	1.185	0.279	1.132	0.96	1511	13	1553	19	1584	32	-4.82
SA8-45 13.5.09	15	S CA	-69	11.47	0.96	31.24	111	401	0.0941	0.350	3.577	1.167	0.276	1.113	0.95	1511	13	1544	18	1569	31	-3.88
SA8-45 13.5.09	18	S CA	-196	6.15	0.51	12.18	59	156	0.0936	0.350	4.850	1.755	0.376	1.720	0.98	1500	13	1794	29	2057	60	-37.11
SA8-45 13.5.09	1	S U	65	9.21	0.78	26.39	89	338	0.0950	0.350	3.687	1.358	0.281	1.312	0.97	1529	13	1569	21	1598	37	-4.53
SA8-45 13.5.09	3	S U	200	11.04	0.93	32.28	107	414	0.0951	0.350	3.656	1.420	0.279	1.376	0.97	1530	13	1562	22	1585	39	-3.64
SA8-45 13.5.09	4	S U	185	7.70	0.65	24.28	74	311	0.0951	0.350	3.417	1.391	0.260	1.347	0.97	1531	13	1508	22	1492	36	2.51
SA8-45 13.5.09	5	S U	184	4.81	0.40	19.56	46	251	0.0929	0.350	2.537	2.066	0.198	2.036	0.99	1485	13	1283	30	1165	43	21.51
SA8-45 13.5.09	6	S U	321	11.13	0.94	32.41	107	416	0.0949	0.350	3.643	1.116	0.278	1.060	0.95	1526	13	1559	18	1584	30	-3.80
SA8-45 13.5.09	7	S U	194	10.82	0.91	30.96	104	397	0.0945	0.350	3.691	1.407	0.283	1.363	0.97	1519	13	1569	22	1607	39	-5.82
SA8-45 13.5.09	1	R U	82	5.19	0.45	17.67	120	463	0.0950	0.350	3.548	2.091	0.271	2.062	0.99	1529	13	1538	33	1545	56	-1.04
SA8-45 13.5.09	2	R U	63	5.05	0.43	17.85	117	468	0.0964	0.360	3.423	2.620	0.258	2.595	0.99	1555	14	1510	40	1478	68	4.96
SA8-45 13.5.09	9	R CA	-260	5.37	0.46	16.35	124	429	0.0942	0.406	3.735	1.193	0.288	1.122	0.94	1512	15	1579	19	1630	32	-7.78
SA8-45 13.5.09	11	R CA	-49	6.41	0.55	19.88	149	521	0.0947	0.350	3.779	1.273	0.289	1.224	0.96	1523	13	1588	20	1638	35	-7.59
SA8-45 13.5.09	12	R CA	11	4.80	0.41	16.00	111	419	0.0948	0.350	3.502	1.021	0.268	0.959	0.94	1524	13	1528	16	1530	26	-0.39
SA8-45 13.5.09	13	R CA	-70	4.59	0.39	15.28	106	401	0.0946	0.350	3.498	1.514	0.268	1.473	0.97	1520	13	1527	24	1532	40	-0.83
SA8-45 13.5.09	19	R CA	-5	4.43	0.38	14.51	103	380	0.0945	0.350	3.624	2.614	0.278	2.591	0.99	1517	13	1555	41	1583	72	-4.31
SA8-45 13.5.09	20	R CA	197	3.88	0.33	13.00	90	341	0.0947	0.350	3.580	1.013	0.274	0.950	0.94	1522	13	1545	16	1562	26	-2.64
SA8-45 13.5.09	23	R CA	30	4.19	0.36	13.51	97	354	0.0942	0.350	3.658	1.831	0.282	1.797	0.98	1512	13	1562	29	1600	51	-5.80
SA8-45 13.5.09	24	R CA	96	3.11	0.27	10.68	72	280	0.0942	0.418	3.509	1.585	0.270	1.529	0.96	1512	16	1529	25	1542	42	-2.00
SA8-45 13.5.09	15	R CA	-190	5.98	0.51	19.19	139	503	0.0944	0.350	3.689	1.111	0.283	1.054	0.95	1516	13	1569	18	1608	30	-6.09

Date	Zir	Tm	204 cps	206Pb mV	207Pb mV	238U mV	Pb ppm	U ppm	207Pb/ 206Pb	1σ %	207Pb/ 235U	1σ %	206Pb/ 238U	1σ %	Rho	207Pb/ 206Pb	2σ	207Pb/ 235U	2σ	206Pb/ 238U	2σ	Disc.	
SA8-45	13.5.09	18	R CA	49	2.75	0.24	8.52	64	223	0.0946	0.468	3.938	4.070	0.302	4.043	0.99	1519	18	1622	64	1702	120	-11.99
SA8-69	14.5.09	2	R CA	-45	2.71	0.18	13.45	57	322	0.0745	0.561	1.879	1.749	0.183	1.656	0.95	1056	23	1074	23	1083	33	-2.47
SA8-69	14.5.09	5	R CA	-8	4.36	0.29	22.63	92	541	0.0745	0.369	1.788	1.712	0.174	1.672	0.98	1056	15	1041	22	1034	32	2.02
SA8-69	14.5.09	12	R CA	110	1.23	0.09	6.02	26	144	0.0761	1.162	2.014	2.632	0.192	2.362	0.90	1097	47	1120	35	1132	49	-3.17
SA8-69	14.5.09	13	R CA	-22	2.45	0.17	12.26	52	293	0.0754	0.643	1.907	2.392	0.184	2.304	0.96	1078	26	1084	31	1086	46	-0.80
SA8-69	14.5.09	14	R CA	38	1.20	0.10	5.84	25	140	0.0860	1.775	2.195	2.385	0.185	1.593	0.67	1339	69	1179	33	1094	32	18.25
SA8-69	14.5.09	17	R CA	-111	1.75	0.12	9.24	37	221	0.0751	0.807	1.858	2.689	0.179	2.565	0.95	1072	32	1066	35	1064	50	0.75
SA8-69	14.5.09	19	R CA	-144	3.03	0.21	14.43	64	345	0.0750	0.533	2.027	3.737	0.196	3.699	0.99	1069	21	1125	50	1154	78	-7.93
SA8-69	14.5.09	20	R U	32	6.43	0.44	31.94	135	764	0.0747	0.350	1.861	1.427	0.181	1.383	0.97	1061	14	1067	19	1071	27	-0.90
SA8-69	14.5.09	21	R U	-73	5.62	0.38	30.34	118	726	0.0750	0.456	1.754	4.278	0.170	4.253	0.99	1069	18	1029	54	1010	79	5.55
SA8-69	14.5.09	22	R U	-290	4.72	0.32	23.58	99	564	0.0751	0.446	1.849	2.351	0.179	2.308	0.98	1070	18	1063	31	1060	45	1.02
SA8-69	14.5.09	23	R U	-117	4.13	0.28	20.66	87	494	0.0764	0.949	1.820	1.931	0.173	1.681	0.87	1106	38	1053	25	1027	32	7.09
SA8-69	14.5.09	24	R U	-310	3.60	0.24	18.07	76	432	0.0747	0.467	1.816	2.173	0.176	2.122	0.98	1061	19	1051	28	1047	41	1.34
SA8-69	14.5.09	25r	R U	-175	4.64	0.31	24.20	97	579	0.0760	0.417	1.815	2.956	0.173	2.927	0.99	1095	17	1051	38	1030	55	5.92
SA8-69	14.5.09	25c	R U	-229	2.30	0.16	11.64	48	279	0.0743	0.661	1.794	1.743	0.175	1.613	0.93	1051	27	1043	22	1040	31	1.06
SA7-130	23.4.08	1	R CA	62	2.27	0.18	9.65	50	206	0.0929	0.565	3.363	1.056	0.263	0.893	0.85	1486	21	1496	16	1503	24	-1.14
SA7-130	23.4.08	5	R CA	86	4.28	0.35	18.11	94	387	0.0938	0.500	3.419	1.008	0.264	0.875	0.87	1505	19	1509	16	1512	24	-0.43
SA7-130	23.4.08	7	R CA	180	1.54	0.12	6.55	34	140	0.0927	0.770	3.347	1.176	0.262	0.889	0.76	1483	29	1492	18	1499	24	-1.10
SA7-130	23.4.08	9	R CA	-12	1.94	0.16	8.25	42	176	0.0926	0.643	3.356	1.086	0.263	0.876	0.81	1480	24	1494	17	1504	23	-1.58
SA7-130	23.4.08	11	R CA	110	1.66	0.13	7.09	36	152	0.0927	0.740	3.322	1.151	0.260	0.882	0.77	1481	28	1486	18	1490	23	-0.57
SA7-130	23.4.08	17	R CA	-131	2.65	0.22	11.33	58	242	0.0944	0.500	3.425	1.011	0.263	0.878	0.87	1517	19	1510	16	1505	24	0.79
SA7-130	23.4.08	16	R CA	-340	1.65	0.14	7.05	36	151	0.0949	0.714	3.445	1.126	0.263	0.871	0.77	1525	27	1515	18	1507	23	1.16
SA7-130	23.4.08	14	R CA	-224	3.98	0.33	16.96	87	363	0.0952	0.500	3.458	1.006	0.263	0.873	0.87	1533	19	1518	16	1507	23	1.69
SA7-130	23.4.08	15	R CA	-353	1.78	0.14	7.60	39	162	0.0943	0.705	3.421	1.120	0.263	0.870	0.78	1514	27	1509	17	1506	23	0.59
SA7-130	23.4.08	2	R CA	-121	4.20	0.34	17.86	92	382	0.0944	0.500	3.445	1.006	0.265	0.873	0.87	1517	19	1515	16	1513	23	0.22
SA8-19	11.5.09	39	R U	42	2.8	0.18	8.0	18	89	0.0733	0.57	1.755	0.98	0.1737	0.80	0.817	1021	23	1029	13	1032	15	-1.1
SA8-19	11.5.09	33	R U	42	2.3	0.15	6.6	15	74	0.0734	0.67	1.762	1.16	0.1742	0.95	0.818	1024	27	1032	15	1035	18	-1.1
SA8-19	11.5.09	29	R U	69	7.3	0.51	19.1	46	214	0.0801	0.45	2.121	1.68	0.1922	1.61	0.963	1198	18	1156	23	1133	33	5.4

Date	Zm	Tm	204 cps	206Pb mV	207Pb mV	238U mV	Pb ppm	U ppm	207Pb/ 206Pb	1 σ %	207Pb/ 235U	1 σ %	206Pb/ 238U	1 σ %	Rho	207Pb/ 206Pb	2 σ	207Pb/ 235U	2 σ	206Pb/ 238U	2 σ	Disc.	
																							204
SA8-19	11.5.09	24	R U	-78	1.9	0.14	4.6	12	52	0.0822	0.81	2.364	1.07	0.2085	0.70	0.658	1251	32	1232	15	1221	16	2.4
SA8-19	11.5.09	5	R U	-133	3.4	0.25	7.9	22	88	0.0844	0.45	2.546	1.10	0.2187	1.00	0.911	1302	18	1285	16	1275	23	2.1
SA8-19	11.5.09	2	R U	-118	2.6	0.20	5.7	17	64	0.0853	0.63	2.725	0.94	0.2316	0.69	0.738	1323	25	1335	14	1343	17	-1.5
SA8-19	11.5.09	35	R U	-132	3.0	0.23	6.5	19	72	0.0872	0.67	2.893	1.33	0.2406	1.15	0.866	1365	26	1380	20	1390	29	-1.8
SA8-19	11.5.09	16	R U	-26	2.2	0.18	4.4	14	50	0.0898	0.58	3.102	1.19	0.2506	1.04	0.873	1421	22	1433	18	1441	27	-1.4
SA8-19	11.5.09	13	R U	-200	2.7	0.22	5.4	17	60	0.0911	0.50	3.139	1.09	0.2498	0.97	0.888	1449	19	1442	17	1438	25	0.8
SA8-19	11.5.09	37	R U	7	3.1	0.25	6.3	20	70	0.0914	0.51	3.161	0.94	0.2507	0.79	0.842	1456	19	1448	14	1442	20	0.9
SA8-19	11.5.09	46	R U	-35	2.4	0.20	4.5	16	50	0.0927	0.53	3.327	0.93	0.2602	0.77	0.823	1482	20	1487	14	1491	20	-0.6
SA8-19	11.5.09	21	R U	-178	2.5	0.21	4.7	16	52	0.0928	0.52	3.405	1.12	0.2661	0.99	0.887	1484	20	1506	17	1521	27	-2.5
SA8-19	11.5.09	36	R U	175	4.3	0.35	7.7	27	86	0.0930	0.33	3.522	0.90	0.2745	0.83	0.930	1489	13	1532	14	1564	23	-5.0
SA8-19	11.5.09	28	R U	-237	3.8	0.31	7.2	24	80	0.0932	0.36	3.449	0.83	0.2685	0.75	0.902	1491	14	1516	13	1533	21	-2.8
SA8-19	11.5.09	3	R U	-161	3.1	0.25	5.6	20	62	0.0933	0.44	3.527	1.12	0.2743	1.03	0.919	1494	17	1533	18	1562	29	-4.6
SA8-19	11.5.09	4	R U	5	2.9	0.24	5.4	19	60	0.0933	0.46	3.458	0.99	0.2687	0.88	0.887	1495	17	1518	16	1534	24	-2.6
SA8-19	11.5.09	16	R U	-47	7.1	0.59	13.3	45	149	0.0939	0.25	3.448	1.02	0.2663	0.99	0.969	1506	9	1516	16	1522	27	-1.0
SA8-19	11.5.09	11	R U	-9	6.9	0.58	13.0	44	146	0.0941	0.25	3.522	0.85	0.2715	0.81	0.955	1509	9	1532	13	1548	22	-2.6
SA8-19	11.5.09	15	R U	-4	4.4	0.37	8.0	28	90	0.0942	0.31	3.580	1.11	0.2757	1.06	0.959	1512	12	1545	17	1570	29	-3.9
SA8-32	11.5.09	11	R U	99	10.9	0.89	32.3	71	379	0.0919	0.25	3.163	1.05	0.2498	1.02	0.971	1464	9	1448	16	1437	26	1.9
SA8-32	11.5.09	9	R U	43	13.0	1.07	35.3	85	414	0.0927	0.25	3.381	1.22	0.2644	1.20	0.979	1482	9	1500	19	1512	32	-2.0
SA8-32	11.5.09	13	R U	-32	17.2	1.41	49.7	113	582	0.0928	0.25	3.325	1.15	0.2597	1.12	0.976	1485	9	1487	18	1489	30	-0.3
SA8-32	11.5.09	26	R U	-69	7.6	0.63	15.0	50	175	0.0931	0.25	3.293	1.28	0.2565	1.26	0.981	1490	9	1479	20	1472	33	1.2
SA8-32	11.5.09	7	R U	-113	11.2	0.92	30.8	73	361	0.0931	0.25	3.428	0.92	0.2671	0.89	0.962	1490	9	1511	14	1526	24	-2.4
SA8-32	11.5.09	2	R U	-134	9.0	0.75	23.7	59	277	0.0932	0.25	3.407	1.22	0.2651	1.20	0.979	1492	9	1506	19	1516	32	-1.6
SA8-32	11.5.09	46	R U	35	14.3	1.19	27.2	94	318	0.0932	0.25	3.308	0.98	0.2574	0.95	0.967	1493	9	1483	15	1476	25	1.1
SA8-32	11.5.09	45	R U	186	12.8	1.06	25.0	84	292	0.0935	0.25	3.289	0.94	0.2552	0.90	0.964	1497	9	1478	14	1465	24	2.1
SA8-32	11.5.09	1	R U	275	11.0	0.91	30.2	72	353	0.0936	0.25	3.382	0.86	0.2621	0.82	0.957	1500	9	1500	13	1500	22	0.0
SA8-32	11.5.09	38	R U	-162	10.7	0.89	19.9	71	233	0.0938	0.25	3.384	1.03	0.2615	1.00	0.970	1505	9	1501	16	1498	27	0.5
SA8-23	11.5.09	1	R CA	118	3.6	0.23	14.1	20	122	0.0744	0.45	1.859	1.26	0.1812	1.17	0.933	1052	18	1067	16	1074	23	-2.1
SA8-23	11.5.09	17	R CA	104	5.1	0.34	20.4	30	177	0.0744	0.35	1.877	1.10	0.1829	1.05	0.949	1053	14	1073	15	1083	21	-2.8
SA8-23	11.5.09	15	R CA	29	5.7	0.38	22.7	33	197	0.0745	0.30	1.874	1.33	0.1824	1.30	0.974	1056	12	1072	17	1080	26	-2.2

Date	Zm	Tm	204 cps	206Pb mV	207Pb mV	238U mV	Pb ppm	U ppm	1 σ %		Rho		2 σ		Disc.								
									207Pb/ 206Pb	1 σ %	206Pb/ 238U	207Pb/ 206Pb	1 σ %	206Pb/ 238U		207Pb/ 235U	206Pb/ 238U						
SA8-23	11.5.09	26	R CA	3	13.3	0.87	55.2	77	479	0.0747	0.25	1.827	1.17	0.1775	1.14	0.977	1059	10	1055	15	1053	22	0.6
SA8-23	11.5.09	9	R CA	-33	3.2	0.21	11.9	18	103	0.0747	0.51	2.002	1.11	0.1945	0.99	0.890	1060	20	1116	15	1145	21	-8.1
SA8-23	11.5.09	25	R CA	40	4.2	0.28	17.3	24	151	0.0747	0.39	1.824	1.25	0.1772	1.19	0.949	1060	16	1054	16	1052	23	0.8
SA8-23	11.5.09	8	R CA	88	7.6	0.50	30.4	44	264	0.0747	0.25	1.870	1.08	0.1815	1.05	0.973	1061	10	1071	14	1075	21	-1.3
SA8-23	11.5.09	6	R CA	217	9.2	0.61	36.7	53	319	0.0750	0.25	1.882	1.20	0.1820	1.17	0.978	1069	10	1075	16	1078	23	-0.8
SA8-23	11.5.09	4	R CA	81	4.7	0.31	18.8	27	164	0.0750	0.35	1.881	1.35	0.1818	1.30	0.965	1070	14	1074	18	1077	26	-0.7
SA8-23	11.5.09	7	R CA	197	4.4	0.29	17.6	25	153	0.0751	0.38	1.899	1.19	0.1834	1.12	0.948	1071	15	1081	16	1085	22	-1.3
SA8-23	11.5.09	5	R CA	206	3.3	0.22	12.9	19	112	0.0752	0.48	1.921	1.22	0.1853	1.12	0.919	1074	19	1088	16	1096	22	-2.0
SA8-26	12.5.09	29	R CA	-310	2.3	0.15	11.9	18	124	0.0718	0.71	1.506	1.23	0.1523	1.01	0.819	979	29	933	15	914	17	6.7
SA8-26	12.5.09	34	R CA	221	5.9	0.38	25.8	47	270	0.0729	0.31	1.723	1.25	0.1713	1.21	0.968	1012	13	1017	16	1019	23	-0.7
SA8-26	12.5.09	2	R CA	-176	5.7	0.37	26.8	46	281	0.0737	0.32	1.698	0.97	0.1672	0.91	0.943	1032	13	1008	12	997	17	3.4
SA8-26	12.5.09	32	R CA	193	1.5	0.10	7.0	12	74	0.0740	0.98	1.761	2.38	0.1727	2.17	0.910	1040	40	1031	30	1027	41	1.3
SA8-26	12.5.09	9	R CA	-21	14.4	0.94	68.7	115	718	0.0741	0.25	1.691	1.00	0.1656	0.97	0.969	1043	10	1005	13	988	18	5.3
SA8-26	12.5.09	12	R CA	46	7.8	0.51	35.6	63	373	0.0742	0.25	1.740	1.24	0.1700	1.21	0.979	1048	10	1023	16	1012	23	3.4
SA8-26	12.5.09	21	R CA	146	11.5	0.75	53.2	92	557	0.0747	0.30	1.736	1.05	0.1685	1.00	0.959	1062	12	1022	13	1004	19	5.4
SA8-26	12.5.09	11	R CA	23	8.4	0.60	37.2	67	389	0.0803	0.25	1.900	1.10	0.1715	1.08	0.974	1205	10	1081	15	1020	20	15.3
SA8-26	12.5.09	27	R CA	120	6.1	0.44	22.1	48	231	0.0834	0.31	2.416	1.37	0.2101	1.33	0.974	1278	12	1247	19	1230	30	3.8
SA8-26	12.5.09	10	R CA	-64	8.2	0.61	32.2	66	337	0.0842	0.76	2.292	2.47	0.1975	2.36	0.952	1297	30	1210	34	1162	50	10.4
SA8-26	12.5.09	22	R CA	98	7.2	0.55	25.4	57	265	0.0871	0.33	2.573	1.55	0.2144	1.51	0.977	1362	13	1293	22	1252	34	8.1
SA8-26	12.5.09	43	R CA	-91	9.4	0.73	41.6	75	435	0.0878	0.71	2.421	1.91	0.1753	1.77	0.928	1377	27	1156	26	1041	34	24.4
SA8-26	12.5.09	37	R CA	70	9.7	0.79	32.3	78	338	0.0920	0.25	2.902	1.54	0.2289	1.52	0.987	1466	9	1382	23	1329	36	9.4
SA8-26	12.5.09	5	R CA	278	8.1	0.65	25.0	64	262	0.0920	0.25	3.122	1.09	0.2460	1.06	0.973	1468	9	1438	17	1418	27	3.4
SA8-26	12.5.09	4	R CA	-214	2.6	0.21	8.5	21	89	0.0922	0.50	3.049	1.23	0.2399	1.13	0.915	1471	19	1420	19	1386	28	5.8
SA8-26	12.5.09	40	R CA	-313	17.9	1.46	53.8	143	563	0.0924	0.25	3.170	0.98	0.2489	0.95	0.967	1475	9	1450	15	1433	24	2.8
SA8-26	12.5.09	17	R CA	-277	10.4	0.85	32.0	83	334	0.0929	0.25	3.064	1.25	0.2393	1.23	0.980	1485	9	1424	19	1383	30	6.9
SA8-26	12.5.09	23	R CA	-272	7.6	0.62	25.8	61	270	0.0930	0.64	2.950	1.89	0.2301	1.78	0.941	1487	24	1395	28	1335	43	10.2
SA8-26	12.5.09	20	R CA	38	3.3	0.27	10.0	26	105	0.0934	0.40	3.352	1.13	0.2602	1.06	0.936	1497	15	1493	18	1491	28	0.4
SA8-26	12.5.09	36	R CA	252	2.6	0.21	8.3	21	87	0.0938	0.50	3.032	1.44	0.2345	1.35	0.937	1504	19	1416	22	1358	33	9.7
SA8-26	12.5.09	14	R CA	77	4.3	0.37	14.5	35	151	0.0951	0.34	3.035	0.96	0.2315	0.90	0.937	1530	13	1416	15	1342	22	12.3

Date	Zir	Tm	204 cps	206Pb mV	207Pb mV	238U mV	Pb ppm	U ppm	207Pb/ 1σ %		206Pb/ 1σ %		Rho	207Pb/ 2σ		206Pb/ 2σ		Disc.				
									206Pb	235U	206Pb	238U		206Pb	235U	206Pb	238U					
SA8-26	12.5.09	39	R CA	182	2.9	0.24	9.5	100	0.0971	0.46	3.114	1.36	0.2325	1.28	0.941	1570	17	1436	21	1348	31	14.1
SA8-26	12.5.09	33	R CA	94	7.3	0.63	19.7	207	0.0987	0.25	3.714	1.14	0.2729	1.11	0.976	1600	9	1574	18	1556	31	2.7
SA8-26	12.5.09	25	R CA	159	8.9	0.77	26.9	71	0.0989	0.25	3.537	1.41	0.2594	1.39	0.984	1604	9	1536	22	1487	37	7.3
SA8-26	12.5.09	41	R CA	-126	1.5	0.13	4.2	44	0.0997	0.74	3.764	1.43	0.2737	1.22	0.853	1619	28	1585	23	1560	34	3.7
SA8-26	12.5.09	47	R CA	-247	9.2	0.81	24.4	255	0.0999	0.25	4.052	1.19	0.2942	1.17	0.978	1622	9	1645	19	1663	34	-2.5
SA8-26	12.5.09	38	R CA	261	6.8	0.60	17.8	186	0.0999	0.25	3.954	1.02	0.2870	0.99	0.968	1623	9	1625	16	1627	28	-0.2
SA8-26	12.5.09	35	R CA	257	9.6	0.85	26.2	274	0.1004	0.25	3.931	1.09	0.2841	1.06	0.973	1631	9	1620	18	1612	30	1.1
SA8-26	12.5.09	24	R CA	38	2.8	0.25	7.0	74	0.1006	0.43	4.206	1.32	0.3033	1.25	0.945	1635	16	1675	21	1708	37	-4.4
SA8-26	12.5.09	19	R CA	105	8.9	0.80	24.7	259	0.1013	0.25	3.881	0.95	0.2780	0.91	0.965	1647	9	1610	15	1581	26	4.0
SA8-26	12.5.09	28	R CA	82	4.0	0.36	10.9	32	0.1013	0.32	4.030	1.22	0.2884	1.18	0.965	1649	12	1640	20	1634	34	0.9
SA8-26	12.5.09	7	R CA	260	3.0	0.27	8.2	86	0.1014	0.40	4.044	1.10	0.2894	1.03	0.932	1649	15	1643	18	1638	30	0.7
SA8-26	12.5.09	46	R CA	-282	3.4	0.31	9.0	94	0.1014	0.37	4.188	1.08	0.2996	1.01	0.939	1650	14	1672	18	1689	30	-2.4
SA8-26	12.5.09	6	R CA	-191	2.0	0.18	5.5	58	0.1019	0.59	4.044	1.28	0.2877	1.13	0.886	1660	22	1643	21	1630	32	1.8
SA8-26	12.5.09	8	R CA	171	5.0	0.45	13.3	139	0.1020	0.26	4.046	1.02	0.2878	0.99	0.967	1660	10	1644	16	1631	28	1.8
SA8-26	12.5.09	16	R CA	107	3.5	0.32	9.4	99	0.1025	0.36	4.071	1.16	0.2879	1.10	0.951	1671	13	1648	19	1631	32	2.4
SA8-26	12.5.09	42	R CA	2	23.5	2.13	67.9	711	0.1027	0.25	3.754	1.58	0.2651	1.56	0.987	1673	9	1583	25	1516	42	9.4
SA8-26	12.5.09	45	R CA	-983	14.2	0.73	48.9	89	0.0733	0.25	4.755	4.36	0.4736	4.33	0.983	4023	40	4029	47	4032	25	-0.8
SA8-26	12.5.09	44	R CA	-374	4.9	0.47	5.4	54	0.1041	0.69	3.803	4.46	0.2728	4.28	0.879	1645	26	4593	23	4555	35	5.4
SA8-26	12.5.09	30	R CA	365	4.3	0.39	11.1	146	0.1043	0.31	4.250	4.26	0.3044	4.22	0.968	1647	42	4684	21	4743	37	-4.0
SA8-27	13.5.09	37	R U	-45	9.4	0.47	72.2	87	0.0563	0.26	0.744	1.06	0.0958	1.03	0.969	465	12	565	9	590	12	-26.8
SA8-27	13.5.09	28r	R U	37	11.1	0.56	101.2	103	0.0564	0.25	0.621	1.08	0.0799	1.06	0.973	468	11	490	8	495	10	-5.8
SA8-27	13.5.09	24r	R U	-10	4.8	0.24	33.6	45	0.0567	0.45	0.798	1.28	0.1021	1.20	0.937	479	20	596	11	627	14	-30.9
SA8-27	13.5.09	6	R U	-72	6.9	0.35	61.3	64	0.0569	0.33	0.635	1.35	0.0809	1.31	0.970	488	14	499	11	502	13	-2.9
SA8-27	13.5.09	22	R U	-335	8.5	0.43	78.8	79	0.0572	0.33	0.628	0.91	0.0796	0.85	0.933	500	14	495	7	494	8	1.3
SA8-27	13.5.09	2-29	R CA	-70	4.7	0.28	29.0	44	0.0658	0.49	1.086	2.13	0.1197	2.07	0.973	800	21	746	22	729	29	8.8
SA8-27	13.5.09	24	R U	-293	6.7	0.40	39.9	62	0.0679	0.67	1.128	2.09	0.1204	1.98	0.947	867	28	767	22	733	27	15.4
SA8-27	13.5.09	2-15	R CA	-24	4.3	0.27	21.9	43	0.0687	0.42	1.357	1.09	0.1432	1.00	0.922	891	17	871	13	863	16	3.1
SA8-27	13.5.09	2-4	R U	301	2.5	0.15	11.7	24	0.0700	0.65	1.514	1.11	0.1569	0.90	0.812	929	27	936	14	939	16	-1.2

Date	Zir	Tm	204 cps	206Pb mV	207Pb mV	238U mV	Pb ppm	U ppm	207Pb/1 σ %		206Pb/1 σ %		Rho	207Pb/2 σ		206Pb/2 σ		Disc.					
									206Pb	235U	238U	235U		206Pb	235U	206Pb	238U						
SA8-27	13.5.09	2-8	RCA	41	1.5	0.10	6.7	15	94	0.0701	1.02	1.601	1.34	0.1656	0.87	0.651	931	42	970	17	988	16	-6.0
SA8-27	13.5.09	2-23	RCA	-128	2.3	0.14	10.0	21	132	0.0704	0.70	1.579	1.03	0.1627	0.75	0.733	939	29	962	13	972	14	-3.5
SA8-27	13.5.09	2-11	RCA	44	1.1	0.07	4.9	11	69	0.0704	1.31	1.568	1.71	0.1614	1.09	0.638	941	54	958	21	965	19	-2.5
SA8-27	13.5.09	2-30	RCA	-2	0.8	0.05	4.0	8	53	0.0706	1.70	1.481	1.86	0.1522	0.76	0.408	945	70	923	22	913	13	3.3
SA8-27	13.5.09	8	R U	-181	4.6	0.29	21.5	42	277	0.0706	0.38	1.514	1.06	0.1555	0.99	0.932	947	16	936	13	932	17	1.6
SA8-27	13.5.09	2-27	RCA	-75	2.3	0.14	10.3	21	135	0.0707	0.69	1.588	1.02	0.1629	0.76	0.740	949	28	965	13	973	14	-2.5
SA8-27	13.5.09	2-31	RCA	19	0.9	0.06	4.1	9	54	0.0708	1.50	1.605	1.75	0.1644	0.90	0.516	952	61	972	22	981	16	-3.1
SA8-27	13.5.09	2-16	RCA	126	0.8	0.05	3.7	8	52	0.0709	1.74	1.542	2.09	0.1579	1.15	0.552	954	71	947	25	945	20	0.9
SA8-27	13.5.09	2-26	RCA	216	2.4	0.15	10.2	22	135	0.0710	0.67	1.636	1.04	0.1672	0.80	0.768	956	27	984	13	997	15	-4.2
SA8-27	13.5.09	2-20	RCA	-22	1.0	0.07	4.7	10	62	0.0710	1.36	1.566	1.65	0.1600	0.92	0.558	957	56	957	20	957	16	0.0
SA8-27	13.5.09	26	R U	130	1.7	0.10	7.6	15	98	0.0710	0.90	1.564	1.36	0.1598	1.02	0.752	957	37	956	17	956	18	0.1
SA8-27	13.5.09	2-10	RCA	-21	4.4	0.28	20.0	43	281	0.0710	0.40	1.545	0.96	0.1577	0.87	0.907	958	16	948	12	944	15	1.5
SA8-27	13.5.09	32b	R U	146	2.1	0.13	9.3	19	120	0.0711	0.75	1.591	1.14	0.1623	0.86	0.751	960	31	967	14	969	15	-1.0
SA8-27	13.5.09	2-24	RCA	-153	1.5	0.09	6.6	14	87	0.0716	1.05	1.586	1.27	0.1606	0.72	0.566	975	43	965	16	960	13	1.6
SA8-27	13.5.09	2-25	RCA	244	1.8	0.11	7.6	16	100	0.0718	0.85	1.673	1.08	0.1691	0.67	0.618	979	35	998	14	1007	12	-2.9
SA8-27	13.5.09	2-12	RCA	83	0.7	0.05	3.2	7	45	0.0721	1.81	1.659	2.06	0.1669	0.99	0.479	989	74	993	26	995	18	-0.6
SA8-27	13.5.09	2-6	RCA	118	1.0	0.07	4.9	10	68	0.0723	1.35	1.544	1.69	0.1550	1.02	0.603	993	55	948	21	929	18	6.5
SA8-27	13.5.09	30	R U	6	1.2	0.08	5.5	11	71	0.0725	1.14	1.655	1.55	0.1656	1.05	0.676	999	46	992	19	988	19	1.1
SA8-27	13.5.09	2-32	RCA	-67	2.7	0.18	12.6	25	166	0.0730	0.64	1.598	0.95	0.1587	0.70	0.736	1014	26	969	12	950	12	6.4
SA8-27	13.5.09	2-9	RCA	234	2.1	0.13	8.6	20	121	0.0736	0.73	1.753	1.25	0.1727	1.01	0.811	1031	30	1028	16	1027	19	0.4
SA8-27	13.5.09	2-19	RCA	55	4.4	0.29	18.4	41	242	0.0740	0.38	1.796	0.86	0.1761	0.78	0.899	1041	15	1044	11	1046	15	-0.4
SA8-27	13.5.09	2-22	RCA	-209	4.2	0.28	17.5	39	230	0.0741	0.40	1.812	0.99	0.1774	0.90	0.913	1044	16	1050	13	1053	18	-0.9
SA8-27	13.5.09	2-7	RCA	-7	1.5	0.10	6.5	15	92	0.0743	0.91	1.769	1.42	0.1727	1.09	0.769	1050	37	1034	18	1027	21	2.2
SA8-27	13.5.09	35	R U	-70	7.0	0.47	31.0	65	399	0.0749	0.27	1.714	1.13	0.1660	1.10	0.972	1066	11	1014	14	990	20	7.1
SA8-27	13.5.09	2-3	RCA	162	1.7	0.11	6.3	16	89	0.0749	0.88	1.986	1.39	0.1923	1.07	0.773	1066	35	1111	19	1134	22	-6.3
SA8-27	13.5.09	39	R U	309	3.8	0.27	15.3	36	197	0.0781	0.45	2.002	1.06	0.1860	0.96	0.907	1148	18	1116	14	1100	19	4.2
SA8-27	13.5.09	23	R U	24	5.7	0.39	24.7	53	318	0.0783	1.31	2.187	7.05	0.2026	6.93	0.983	1155	52	1177	94	1189	149	-3.0
SA8-27	13.5.09	4	R U	-314	10.6	0.76	49.8	99	641	0.0797	0.79	1.743	2.40	0.1586	2.27	0.944	1190	31	1025	31	949	40	20.3
SA8-27	13.5.09	2	R U	-174	12.6	1.05	35.6	117	458	0.0935	0.25	3.331	0.82	0.2585	0.78	0.953	1497	9	1488	13	1482	21	1.0

Date	Zrn	Tm	204 cps	206Pb mV	207Pb mV	238U mV	Pb ppm	U ppm	207Pb/ 206Pb	1σ %	207Pb/ 1σ %	235U	1σ %	206Pb/ 238U	Rho	207Pb/ 206Pb	2σ	207Pb/ 235U	2σ	206Pb/ 238U	2σ	Disc.	
																							206Pb
SA8-27	13.5.09	2-28	R CA	7	4.9	0.41	13.3	46	175	0.0937	0.28	3.532	0.87	0.2732	0.82	0.945	1503	11	1534	14	1557	23	-3.6
SA8-27	13.5.09	2-17	R CA	163	3.0	0.25	8.6	30	121	0.0938	0.44	3.368	1.10	0.2605	1.01	0.918	1503	16	1497	17	1492	27	0.7
SA8-27	13.5.09	2-18	R CA	325	4.5	0.38	11.9	44	168	0.0944	0.30	3.612	1.58	0.2775	1.55	0.982	1516	11	1552	25	1579	43	-4.2
SA8-27	13.5.09	28c	R U	198	5.9	0.50	18.1	55	233	0.0951	0.46	3.024	1.83	0.2306	1.77	0.968	1531	17	1414	28	1338	43	12.6
SA8-27	13.5.09	2-14	R CA	261	5.5	0.49	14.0	54	197	0.0994	0.28	3.896	1.26	0.2844	1.23	0.976	1612	10	1613	20	1613	35	-0.1
SA8-27	13.5.09	2-13	R CA	57	3.5	0.33	8.1	34	114	0.1060	0.34	4.583	1.25	0.3136	1.21	0.961	1732	13	1746	21	1758	37	-1.5
SA8-27	13.5.09	41	R U	87	8.4	0.80	20.3	78	261	0.1066	0.25	4.555	1.00	0.3098	0.96	0.968	1742	9	1741	16	1740	29	0.1
SA8-27	13.5.09	2-5	R CA	112	6.4	0.62	15.1	63	213	0.1084	0.25	4.630	0.97	0.3099	0.94	0.966	1772	9	1755	16	1740	28	1.8
SA8-27	13.5.09	25	R U	19	14.1	1.37	35.0	131	450	0.1097	0.28	4.379	1.47	0.2896	1.45	0.982	1794	10	1708	24	1639	42	8.6
SA8-27	13.5.09	46	R U	424	40.8	0.68	52.0	400	669	0.0709	0.26	4.465	4.05	0.4499	4.04	0.969	954	44	946	43	904	47	5.6
F11	12.5.09	1	R U	80	10.08	0.73	36.89	79	377	0.082	0.500	2.370	0.917	0.211	0.769	0.84	1234	20	1234	13	1233	17	0.10
F11	12.5.09	2	R U	235	12.19	0.89	43.88	95	446	0.083	0.661	2.444	1.059	0.212	0.828	0.78	1280	26	1256	15	1242	19	2.98
F11	12.5.09	3	R U	81	11.31	0.81	42.28	88	432	0.081	0.500	2.384	1.025	0.213	0.894	0.87	1230	20	1238	15	1242	20	-0.96
F11	12.5.09	4	R U	-6	10.71	0.77	39.37	83	402	0.082	0.500	2.371	1.059	0.211	0.934	0.88	1235	20	1234	15	1234	21	0.09
F11	12.5.09	5	R U	-30	18.14	1.31	67.65	141	691	0.082	0.500	2.370	1.269	0.210	1.167	0.92	1237	20	1233	18	1231	26	0.51
F11	12.5.09	6	R U	86	5.18	0.37	19.15	40	196	0.081	0.500	2.300	1.451	0.205	1.362	0.94	1232	20	1212	20	1201	30	2.46
F11	12.5.09	7	R U	182	14.34	1.03	52.82	112	540	0.081	0.500	2.327	1.561	0.208	1.478	0.95	1229	20	1220	22	1216	33	1.03
F11	12.5.09	8	R U	33	7.33	0.52	27.74	57	283	0.080	0.500	2.251	1.630	0.203	1.552	0.95	1208	20	1197	23	1191	34	1.39
F11	12.5.09	9	R U	222	9.68	0.72	40.47	184	863	0.082	0.500	2.450	1.213	0.216	1.105	0.91	1254	20	1258	17	1260	25	-0.50
F11	12.5.09	10	R U	255	11.48	0.85	51.64	218	1127	0.082	0.500	2.253	2.280	0.200	2.224	0.98	1243	20	1198	32	1173	48	5.65
F11	12.5.09	11	R U	298	3.27	0.24	13.21	62	288	0.082	0.659	2.594	4.866	0.229	4.821	0.99	1252	26	1299	69	1327	115	-5.98
F11	12.5.09	12	R U	58	4.90	0.36	20.13	93	439	0.081	0.500	2.416	1.713	0.217	1.639	0.96	1215	20	1247	24	1266	38	-4.26
F11	12.5.09	13	R U	235	14.61	1.08	61.12	278	1334	0.082	0.500	2.392	1.317	0.211	1.219	0.93	1248	20	1240	19	1236	27	0.92
F11	12.5.09	14	R U	186	8.37	0.62	35.33	159	771	0.082	0.500	2.339	2.007	0.208	1.944	0.97	1234	20	1224	28	1219	43	1.18
F11	12.5.09	15	R U	239	8.92	0.66	38.59	170	842	0.082	0.500	2.512	3.345	0.222	3.307	0.99	1251	20	1276	47	1290	77	-3.14
F11	12.5.09	16	R U	-126	3.55	0.26	15.24	68	333	0.083	0.563	2.441	1.593	0.212	1.490	0.94	1279	22	1255	23	1241	34	2.98
F11	12.5.09	17	R U	-84	8.11	0.59	35.04	154	765	0.081	0.500	2.351	0.955	0.211	0.814	0.85	1219	20	1228	14	1233	18	-1.18
F11	12.5.09	18	R U	176	4.11	0.30	17.41	78	380	0.080	0.500	2.327	1.544	0.210	1.461	0.95	1209	20	1221	22	1227	33	-1.50

Table 10.4. LA-ICP-MS U-Pb data. Zrn = zircon, Tm = Treatment, R = Raster, S = Spot, CA = chemically abraded, U = untreated, cps = counts pers second, disc = % ($^{206}\text{Pb}/^{238}\text{U}$)/($^{207}\text{Pb}/^{206}\text{Pb}$). Analyses striked through are rejected due to high common lead.

Sample	Zircon	Disc.	Age	1 σ	Tot.Hf	$^{178}\text{Hf}/^{177}\text{Hf}$	1 $\sigma\%$	$^{176}\text{Hf}/^{177}\text{Hf}$	1 $\sigma\%$	$^{175}\text{Yb}/^{177}\text{Hf}$	1 $\sigma\%$	$^{176}\text{Lu}/^{177}\text{Hf}$	1 $\sigma\%$	$^{176}\text{Hf}/^{177}\text{Hf}_{\text{int}}$	$^{176}\text{Hf}/^{177}\text{Hf}_{\text{ap}}$	$\epsilon\text{Hf}_{(\text{int})}$	2 σ	TDM _c
MM2235	5.16	0.69	1484	10	6.52	1.46727	0.0057	0.281955	0.0091	0.048922	15.02	0.001335	26.62	0.281918	0.281955	2.73	1.49	2061
MM2235	5.2	4.6	1484	10	5.66	1.46730	0.0041	0.281948	0.0098	0.045210	13.42	0.001129	26.64	0.281917	0.281948	2.68	1.50	2064
MM2235	5.3	-2.77	1484	10	6.89	1.46649	0.0119	0.281929	0.0110	0.010968	15.14	0.001493	13.80	0.281887	0.281929	1.62	1.41	2131
MM2235	5.5	-0.62	1484	10	6.88	1.46650	0.0108	0.281892	0.0087	0.008727	16.43	0.000346	14.85	0.281882	0.281892	1.45	1.04	2142
MM2235	5.6	-1.45	1484	10	5.24	1.46733	0.0042	0.281989	0.0100	0.033560	12.43	0.000896	26.62	0.281964	0.281989	4.37	1.46	1956
MM2235	5.7	-2.69	1484	10	6.03	1.46733	0.0041	0.281934	0.0086	0.061513	20.40	0.001625	27.04	0.281889	0.281934	1.69	1.51	2127
MM2235	5.9	0.28	1484	10	5.61	1.46726	0.0032	0.281955	0.0089	0.057303	19.69	0.001456	27.00	0.281914	0.281955	2.60	1.50	2068
MM2235	6.1	0.19	1484	10	6.69	1.46662	0.0150	0.281895	0.0124	0.012397	14.60	0.001226	13.32	0.281860	0.281895	0.68	1.51	2191
MM2235	6.7	8.65	1484	10	6.94	1.46672	0.0102	0.281883	0.0090	0.008948	14.94	0.000947	13.76	0.281856	0.281883	0.53	1.14	2200
MM2235	5.11a	-0.18	1484	10	8.50	1.46680	0.0150	0.281922	0.0107	0.010696	15.91	0.001752	14.60	0.281873	0.281922	1.12	1.44	2163
MM2235	5.11b	-0.18	1484	10	5.71	1.46727	0.0043	0.281950	0.0100	0.049167	18.08	0.001261	26.81	0.281915	0.281950	2.62	1.56	2067
MM2235	5.11b rep	-0.18	1484	10	7.93	1.46684	0.0097	0.281962	0.0081	0.008121	14.62	0.001232	13.33	0.281927	0.281962	3.05	1.09	2040
MM2235	5.1a	18.31	1484	10	6.50	1.46647	0.0125	0.281931	0.0107	0.010695	14.75	0.001502	13.43	0.281889	0.281931	1.68	1.38	2127
MM2235	5.1b	18.31	1484	10	6.58	1.46724	0.0055	0.281943	0.0098	0.044069	12.92	0.001199	26.60	0.281910	0.281943	2.43	1.52	2079
MM2235	5.1b rep	18.31	1484	10	7.11	1.46655	0.0097	0.281949	0.0090	0.008947	14.54	0.000995	13.23	0.281921	0.281949	2.83	1.14	2054
MM2235	5.2 rep	4.60	1484	10	6.93	1.46667	0.0125	0.281937	0.0115	0.011528	14.66	0.001086	13.32	0.281906	0.281937	2.31	1.41	2087
MM2235	5.4a	-2.63	1484	10	6.47	1.46682	0.0194	0.281870	0.0121	0.012104	14.55	0.001276	13.24	0.281834	0.281870	-0.25	1.49	2251
MM2235	5.4b	-2.63	1484	10	7.44	1.46637	0.0097	0.281916	0.0097	0.009657	14.59	0.001009	13.29	0.281887	0.281916	1.64	1.21	2130
MM2235	5.6 rep	-1.45	1484	10	7.28	1.46650	0.0144	0.281957	0.0102	0.010164	14.67	0.000897	13.29	0.281932	0.281957	3.21	1.25	2030
MM2235	5.9 rep	0.28	1484	10	7.07	1.46654	0.0108	0.281923	0.0110	0.010969	15.16	0.001136	13.83	0.281891	0.281923	1.77	1.37	2122
MM2235	n=20		1484	10		1.46684		0.000061		0.023683		0.001190		0.281899		2.04		2105
						0.00071		0.000059		0.038863		0.000621		0.000060		2.12		

Sample	Zircon	Disc.	Age	1 σ	Tot.Hf	$^{178}\text{Hf}/^{177}\text{Hf}$	1 $\sigma\%$	$^{176}\text{Hf}/^{177}\text{Hf}$	1 $\sigma\%$	$^{176}\text{Yb}/^{177}\text{Hf}$	1 $\sigma\%$	$^{176}\text{Lu}/^{177}\text{Hf}$	1 $\sigma\%$	$^{176}\text{Hf}/^{177}\text{Hf}_{\text{int}}$	$^{176}\text{Hf}/^{177}\text{Hf}_{\text{ap}}$	$\epsilon\text{Hf}_{(\text{int})}$	2 σ	TDM _c
MM2241	10.8	2.54	1486	4	7.20	1.46730	0.0053	0.281949	0.0087	0.0322150	12.71	0.000822	26.61	0.281926	0.281949	3.07	1.18	2040
MM2241	9.3	-0.98	1486	4	5.89	1.46725	0.0072	0.282051	0.0096	0.0660333	14.01	0.001737	26.70	0.282003	0.282051	5.77	1.51	1867
MM2241	10.3		1486	4	6.02	1.46659	0.0137	0.281959	0.0121	0.0121102	14.55	0.001898	13.23	0.281905		2.33	1.57	2088
MM2241	10.4	-4.29	1486	4	5.78	1.46675	0.0188	0.281910	0.0130	0.012991	14.99	0.001327	13.60	0.281872	0.281910	1.16	1.59	2162
MM2241	10.7	2.31	1486	4	6.05	1.46686	0.0137	0.281911	0.0099	0.009908	14.60	0.001099	13.28	0.281880	0.281911	1.42	1.25	2146
MM2241	10.9	5.43	1486	4	6.65	1.46652	0.0150	0.281911	0.0099	0.009908	14.63	0.001477	13.27	0.281869	0.281911	1.04	1.30	2170
MM2241	9.15	-0.75	1486	4	5.25	1.46725	0.0047	0.281980	0.0091	0.054330	12.92	0.001371	26.60	0.281942	0.281980	3.62	1.37	2005
MM2241	10.2	2.50	1486	4	6.13	1.46727	0.0049	0.281956	0.0105	0.041773	35.71	0.001065	27.84	0.281926	0.281956	3.07	1.44	2040
MM2241	10.6	0.57	1486	4	5.41	1.46725	0.0036	0.281977	0.0096	0.041141	16.32	0.001028	26.70	0.281948	0.281977	3.86	1.32	1990
MM2241	9.1	-0.07	1486	4	5.27	1.46729	0.0037	0.281966	0.0087	0.054414	12.76	0.001327	26.62	0.281929	0.281966	3.17	1.31	2034
MM2241	9.5	6.47	1486	4	6.60	1.46656	0.0188	0.281939	0.0104	0.010427	14.94	0.001627	13.52	0.281893	0.281939	1.89	1.37	2116
MM2241	9.7	6.03	1486	4	5.64	1.46640	0.0125	0.281967	0.0113	0.011245	14.57	0.002503	13.26	0.281896	0.281967	2.01	1.56	2108
MM2241	9.8	-0.37	1486	4	6.01	1.46666	0.0114	0.281930	0.0107	0.010696	15.06	0.001869	13.99	0.281877	0.281930	1.33	1.44	2152
MM2241	n=13		1486	4		1.46692		0.281954		0.028240		0.001473		0.281913		2.59		2071
						0.00071		0.000077		0.041785		0.000908		0.000076		2.70		
MM36631	1	1.84	1521	6	6.22	1.46719	0.0047	0.282081	0.0098	0.027010	13.68	0.000770	26.70	0.282059	0.282081	8.59	1.32	1715
MM36631	3	-1.22	1521	6	5.54	1.46717	0.0044	0.282075	0.0098	0.046085	16.00	0.001246	26.72	0.282039	0.282075	7.89	1.45	1760
MM36631	4	-0.80	1521	6	7.74	1.46714	0.0049	0.282074	0.0108	0.021990	21.23	0.000694	26.69	0.282054	0.282074	8.42	1.40	1726
MM36631	5	-0.69	1521	6	5.48	1.46721	0.0056	0.282101	0.0113	0.025687	14.38	0.000729	26.62	0.282080	0.282101	9.34	1.46	1666
MM36631	8	-1.93	1521	6	5.31	1.46718	0.0048	0.282071	0.0093	0.016074	17.08	0.000485	26.79	0.282057	0.282071	8.52	1.20	1719
MM36631	9	-1.27	1521	6	6.63	1.46719	0.0047	0.282092	0.0093	0.072174	21.83	0.002082	26.68	0.282032	0.282092	7.64	1.63	1776
MM36631	14	2.72	1521	6	5.67	1.46721	0.0053	0.282121	0.0098	0.027609	13.07	0.000805	26.70	0.282098	0.282121	9.97	1.33	1626

Sample	Zircon	Age	1 σ	Tot.Hf	¹⁷⁸ Hf/ ¹⁷⁷ Hf	1 σ	¹⁷⁶ Hf/ ¹⁷⁷ Hf	1 σ	¹⁷⁶ Yb/ ¹⁷⁷ Hf	1 σ	¹⁷⁶ Lu/ ¹⁷⁷ Hf	1 σ	¹⁷⁶ Hf/ ¹⁷⁷ Hf _{int}	¹⁷⁶ Hf/ ¹⁷⁷ Hf _{ap}	ϵ Hf _(int)	2 σ	TDM _c	
MM36631	15	0.98	1521	6	5.46	1.46725	0.0056	0.282091	0.0087	0.022347	13.83	0.000643	26.61	0.282073	0.282091	9.07	1.18	1683
MM36631	n=8		1521	6	1.46719	0.282089	0.000932	0.032372	0.000932	0.000932	0.000932	0.000932	0.282062	0.282062	8.68		1709	
					0.00006	0.000034	0.036585	0.000043	0.001027				0.000043		1.53			
MM36676	3	0.19	1495	7	6.39	1.46726	0.0066	0.282031	0.0105	0.091332	15.00	0.002146	26.65	0.281971	0.282031	4.85	1.77	1934
MM36676	4	-3.57	1495	7	8.92	1.46724	0.0049	0.282042	0.0082	0.075220	26.92	0.002114	26.92	0.281983	0.282042	5.27	1.54	1907
MM36676	5	1.31	1495	7	6.16	1.46726	0.0058	0.282033	0.0100	0.071633	30.52	0.001934	26.87	0.281979	0.282033	5.13	1.67	1916
MM36676	7	0.24	1495	7	5.32	1.46723	0.0068	0.282031	0.0118	0.084676	16.12	0.002076	26.63	0.281973	0.282031	4.92	1.89	1929
MM36676	8	-1.31	1495	7	7.19	1.46727	0.0069	0.281995	0.0105	0.058417	28.48	0.001684	27.07	0.281948	0.281995	4.04	1.66	1986
MM36676	14	-1.77	1495	7	6.72	1.46721	0.0061	0.282030	0.0108	0.062278	13.76	0.001552	26.64	0.281986	0.282030	5.41	1.64	1898
MM36676	n=6		1495	7	1.46725	0.282027	0.000033	0.073926	0.001918	0.281973	0.000028	0.000493	4.94		0.98		1928	
Ro-102b	3	-0.05	1485	8	5.83	1.46725	0.0056	0.281880	0.0063	0.028570	3.04	0.000649	26.60	0.281862	0.281880	0.77	0.98	2186
Ro-102b	4	-2.22	1485	8	7.53	1.46725	0.0037	0.281927	0.0066	0.030398	4.70	0.000683	26.61	0.281908	0.281927	2.41	0.97	2082
Ro-102b	5	0.86	1485	8	7.22	1.46727	0.0036	0.281927	0.0057	0.022482	2.43	0.000597	26.61	0.281911	0.281927	2.49	0.91	2076
Ro-102b	11	2.31	1485	8	6.75	1.46722	0.0027	0.281908	0.0049	0.040215	8.43	0.000985	26.64	0.281881	0.281908	1.43	1.04	2144
Ro-102b	18	0.34	1485	8	7.42	1.46726	0.0028	0.281932	0.0054	0.031853	3.58	0.000680	26.60	0.281913	0.281932	2.59	0.92	2070
Ro-102b	21	2.02	1485	8	7.52	1.46725	0.0034	0.281903	0.0063	0.032840	13.54	0.000672	26.89	0.281885	0.281903	1.57	1.03	2135
Ro-102b	26	-0.63	1485	8	7.67	1.46730	0.0026	0.281832	0.0082	0.023339	6.30	0.000602	26.73	0.281816	0.281832	-0.88	1.14	2291
Ro-102b	27	2.20	1485	8	6.99	1.46727	0.0039	0.281941	0.0057	0.027316	3.04	0.000644	26.60	0.281923	0.281941	2.94	0.98	2048
Ro-102b	30	1.16	1485	8	6.38	1.46728	0.0039	0.281919	0.0054	0.024382	12.86	0.000596	26.75	0.281903	0.281919	2.21	0.88	2094

Sample	Zircon	Disc.	Age	1 σ	Tot.Hf	$^{178}\text{Hf}/^{177}\text{Hf}$	1 $\sigma\%$	$^{176}\text{Hf}/^{177}\text{Hf}$	1 $\sigma\%$	$^{175}\text{Yb}/^{177}\text{Hf}$	1 $\sigma\%$	$^{176}\text{Lu}/^{177}\text{Hf}$	1 $\sigma\%$	$^{176}\text{Hf}/^{177}\text{Hf}_{\text{int}}$	$^{176}\text{Hf}/^{177}\text{Hf}_{\text{ap}}$	$\epsilon\text{Hf}_{(\text{int})}$	2 σ	TDM _c
Ro-102b	n=9		1485	8		1.46726	0.00005	0.281908	0.000067	0.029044	0.000067	0.000679	0.000679	0.281889	0.281889	1.73	2.38	2125
ROG525	10a	2.83	1504	4	7.25	1.46712	0.0239	0.282029	0.0132	0.013189	0.0132	0.001017	0.001017	0.282001	0.282029	6.12	1.46	1860
ROG525	10b	2.83	1504	4	7.52	1.46723	0.0230	0.282017	0.0117	0.011672	0.0117	0.001193	0.001193	0.281983	0.282017	5.51	1.32	1898
ROG525	11	-0.70	1504	4	6.72	1.46574	0.0387	0.282031	0.0166	0.016629	0.0166	0.002521	0.002521	0.281960	0.282031	4.67	1.89	1953
ROG525	13	0.40	1504	4	6.65	1.46720	0.0243	0.282102	0.0135	0.013456	0.0135	0.001294	0.001294	0.282066	0.282102	8.43	1.50	1712
ROG525	16	-0.30	1504	4	6.58	1.46634	0.0353	0.281983	0.0127	0.012665	0.0127	0.000541	0.000541	0.281968	0.281983	4.96	1.39	1934
ROG525	20a	-2.90	1504	4	8.49	1.46731	0.0227	0.282051	0.0117	0.011671	0.0117	0.001711	0.001711	0.282003	0.282051	6.19	1.34	1855
ROG525	20b	-2.90	1504	4	7.95	1.46725	0.0212	0.282029	0.0114	0.011438	0.0114	0.001148	0.001148	0.281997	0.282029	5.98	1.30	1868
ROG525	24	0.90	1504	4	7.72	1.46736	0.0224	0.282075	0.0135	0.013456	0.0135	0.001548	0.001548	0.282031	0.282075	7.21	1.51	1790
ROG525	4	-0.03	1504	4	6.52	1.46586	0.0364	0.282012	0.0149	0.014857	0.0149	0.002834	0.002834	0.281932	0.282012	3.68	1.72	2016
ROG525	8	-3.25	1504	4	7.84	1.46720	0.0224	0.282121	0.0112	0.011209	0.0112	0.003019	0.003019	0.282035	0.282121	7.36	1.36	1780
ROG525	9	1.02	1504	4	6.98	1.46630	0.0347	0.282058	0.0140	0.014006	0.0140	0.001413	0.001413	0.282018	0.282058	6.74	1.57	1819
ROG525	n=11		1504	4		1.46681	0.00124	0.282047	0.000081	0.013113	0.000081	0.001658	0.001658	0.281999	0.281999	6.08	2.70	1862
SA3-04	17	1.68	1509	6	5.70	1.46576	0.0464	0.281846	0.0173	0.017246	0.0173	0.000692	0.000692	0.281827	0.281846	0.06	1.85	2250
SA3-04	19		1509	6	5.62	1.46539	0.0342	0.281863	0.0137	0.013735	0.0137	0.000848	0.000848	0.281839	0.281863	0.51	1.51	2222
SA3-04	20		1509	6	6.11	1.46615	0.0315	0.281918	0.0119	0.011914	0.0119	0.001263	0.001263	0.281882	0.281918	2.04	1.37	2124
SA3-04	3	-0.09	1509	6	6.95	1.46644	0.0320	0.281924	0.0129	0.012927	0.0129	0.000605	0.000605	0.281907	0.281924	2.92	1.42	2068
SA3-04	34		1509	6	7.33	1.46622	0.0342	0.281921	0.0166	0.016634	0.0166	0.001262	0.001262	0.281885	0.281921	2.15	1.83	2118

Sample	Zircon	Disc.	Age	1 σ	Tot.Hf	$^{178}\text{Hf}/^{177}\text{Hf}$	1 $\sigma\%$	$^{176}\text{Hf}/^{177}\text{Hf}$	1 $\sigma\%$	$^{175}\text{Yb}/^{177}\text{Hf}$	1 $\sigma\%$	$^{176}\text{Lu}/^{177}\text{Hf}$	1 $\sigma\%$	$^{176}\text{Hf}/^{177}\text{Hf}_{\text{int}}$	$^{176}\text{Hf}/^{177}\text{Hf}_{\text{ap}}$	$\epsilon\text{Hf}_{(\text{int})}$	2 σ	TDM _c
SA3-04	39		1509	6	7.52	1.46660	0.0295	0.281951	0.0129	0.012926	10.49	0.000718	5.16	0.281931	0.281931	3.76	1.42	2014
SA3-04	46		1509	6	6.36	1.46619	0.0347	0.281905	0.0124	0.012411	10.54	0.001068	5.23	0.281875	0.281875	1.77	1.39	2141
SA3-04	59		1509	6	7.10	1.46669	0.0285	0.281884	0.0108	0.010777	10.99	0.000616	6.21	0.281867	0.281867	1.49	1.21	2160
SA3-04	59		1509	6	8.03	1.46651	0.0305	0.281927	0.0124	0.012410	10.47	0.000739	5.17	0.281906	0.281906	2.89	1.37	2070
SA3-04	60		1509	6	7.83	1.46623	0.0320	0.281899	0.0106	0.010571	10.52	0.000520	5.18	0.281885	0.281885	2.12	1.17	2119
SA3-04	n=10		1509	6		1.46622		0.281904		0.013155		0.000833		0.281880	0.281880	1.97		2129
						0.00079		0.000064		0.004435		0.000543		0.000062	0.000062	2.22		
SA3-60	3	0.67	1518	6	5.41	1.46732	0.0037	0.282049	0.0076	0.068023	13.47	0.002314	26.65	0.281983	0.282049	5.81	1.54	1891
SA3-60	4	-1.67	1518	6	4.30	1.46735	0.0045	0.282083	0.0107	0.065214	12.69	0.002229	26.62	0.282019	0.282083	7.10	1.82	1808
SA3-60	5	-0.35	1518	6	6.53	1.46726	0.0067	0.282047	0.0084	0.045174	15.35	0.001182	26.62	0.282013	0.282047	6.89	1.31	1821
SA3-60	6	0.69	1518	6	6.70	1.46732	0.0045	0.282056	0.0081	0.057095	18.31	0.001471	26.64	0.282014	0.282056	6.92	1.36	1819
SA3-60	6	0.69	1518	6	3.39	1.46736	0.0042	0.282055	0.0067	0.043543	2.46	0.001414	1.40	0.282014	0.282055	6.93	0.84	1819
SA3-60	11	0.03	1518	6	2.17	1.46756	0.0077	0.282017	0.0343	0.062934	9.93	0.001985	2.75	0.281960	0.282017	5.00	3.64	1942
SA3-60	15	0.83	1518	6	2.03	1.46743	0.0041	0.282028	0.0101	0.065413	5.80	0.002064	2.35	0.281969	0.282028	5.31	1.21	1923
SA3-60	18	0.44	1518	6	6.77	1.46729	0.0046	0.282088	0.0079	0.078418	12.46	0.002534	26.65	0.282015	0.282088	6.97	1.62	1816
SA3-60	2	0.50	1518	6	7.46	1.46732	0.0246	0.282098	0.0158	0.015829	17.15	0.001990	16.44	0.282040	0.282098	7.85	2.02	1760
SA3-60	8	2.69	1518	6	6.90	1.46635	0.0393	0.282029	0.0153	0.015347	17.19	0.001886	16.23	0.281974	0.282029	5.51	1.95	1910
SA3-60	n=10		1518	6		1.46726		0.282055		0.051699		0.001907		0.282000	0.282000	6.43		1851
						0.00066		0.000055		0.043327		0.000859		0.000053	0.000053	1.89		
SA7-04	7	16.21	1497	22	9.10	1.46732	0.0030	0.282016	0.0054	0.039815	4.94	0.001240	1.53	0.281981	0.282016	5.26	1.13	1909

Sample	Zircon	Disc.	Age	1 σ	Tot.Hf	$^{178}\text{Hf}/^{177}\text{Hf}$	1 $\sigma\%$	$^{176}\text{Hf}/^{177}\text{Hf}$	1 $\sigma\%$	$^{175}\text{Yb}/^{177}\text{Hf}$	1 $\sigma\%$	$^{176}\text{Lu}/^{177}\text{Hf}$	1 $\sigma\%$	$^{176}\text{Hf}/^{177}\text{Hf}_{\text{int}}$	$^{176}\text{Hf}/^{177}\text{Hf}_{\text{ap}}$	$\epsilon\text{Hf}_{(\text{int})}$	2 σ	TDM _c
SA7-04	1	10.57	1497	22	8.59	1.46702	0.0317	0.281964	0.0163	0.016333	19.55	0.001811	17.67	0.281912	0.281964	2.82	2.07	2065
SA7-04	14	0.42	1497	22	3.68	1.46724	0.0067	0.281950	0.0090	0.041200	6.30	0.001423	26.63	0.281910	0.281950	2.74	1.84	2070
SA7-04	17	17.34	1497	22	7.57	1.46717	0.0036	0.281959	0.0076	0.081137	8.11	0.001580	3.45	0.281914	0.281959	2.89	1.38	2060
SA7-04	19	1.90	1497	22	5.51	1.46730	0.0032	0.281942	0.0056	0.057270	1.68	0.001838	1.38	0.281890	0.281942	2.03	1.15	2115
SA7-04	2		1497	22	6.40	1.46729	0.0203	0.281931	0.0147	0.014657	17.11	0.001635	16.37	0.281884		1.83	1.85	2128
SA7-04	21	9.78	1497	22	8.22	1.46734	0.0028	0.281995	0.0056	0.036351	15.18	0.001003	1.83	0.281967	0.281995	4.75	1.16	1942
SA7-04	23	0.02	1497	22	5.39	1.46732	0.0048	0.281927	0.0076	0.040480	12.60	0.001412	26.61	0.281887	0.281927	1.94	1.70	2121
SA7-04	4		1497	22	6.41	1.46720	0.0184	0.281962	0.0138	0.013808	18.46	0.001372	17.82	0.281923		3.19	1.74	2041
SA7-04	5		1497	22	8.37	1.46677	0.0258	0.281976	0.0158	0.015832	17.47	0.001250	16.98	0.281940		3.81	1.91	2002
SA7-04	6		1497	22	8.32	1.46706	0.0208	0.281969	0.0138	0.013808	17.08	0.001487	16.20	0.281926		3.33	1.73	2033
SA7-04	n=11		1497	22		1.46718		0.281963		0.033699		0.001459		0.281921		3.15		2044
						0.00035		0.000053		0.043485		0.000500		0.000062		2.22		
SA7-86	1a	0.47	1498	2	7.63	1.46733	0.0037	0.282034	0.0074	0.020015	12.41	0.000596	26.60	0.282017	0.282034	6.58	1.05	1825
SA7-86	1b	0.47	1498	2	5.99	1.46727	0.0046	0.281995	0.0061	0.028851	3.27	0.000755	1.94	0.281974	0.281995	5.02	0.79	1925
SA7-86	4	0.45	1498	2	6.87	1.46730	0.0056	0.282006	0.0084	0.028754	13.57	0.000797	26.65	0.281984	0.282006	5.38	1.21	1902
SA7-86	6a	0.46	1498	2	7.03	1.46732	0.0036	0.282010	0.0071	0.015687	18.23	0.000411	26.78	0.281999	0.282010	5.91	0.98	1868
SA7-86	6b	0.46	1498	2	5.97	1.46730	0.0044	0.282033	0.0070	0.023742	10.19	0.000626	5.25	0.282015	0.282033	6.50	0.89	1830
SA7-86	10a	0.88	1498	2	6.93	1.46727	0.0035	0.281983	0.0076	0.008547	13.74	0.000231	26.66	0.281977	0.281983	5.14	0.98	1918
SA7-86	10b	0.88	1498	2	5.72	1.46727	0.0033	0.282001	0.0064	0.011828	3.93	0.000273	1.42	0.281993	0.282001	5.72	0.81	1880
SA7-86	14	0.87	1498	2	6.70	1.46720	0.0040	0.281984	0.0050	0.019446	1.51	0.000413	1.45	0.281972	0.281984	4.98	0.66	1928
SA7-86	15a	0.79	1498	2	7.00	1.46733	0.0038	0.282024	0.0065	0.013096	12.45	0.000378	26.60	0.282014	0.282024	6.44	0.91	1834
SA7-86	15b	0.79	1498	2	6.10	1.46722	0.0038	0.281983	0.0059	0.013688	1.39	0.000380	1.45	0.281972	0.281983	4.98	0.75	1928

Sample	Zircon	Disc.	Age	1 σ	Tot.Hf	$^{178}\text{Hf}/^{177}\text{Hf}$	1 $\sigma\%$	$^{176}\text{Hf}/^{177}\text{Hf}$	1 $\sigma\%$	$^{175}\text{Yb}/^{177}\text{Hf}$	1 $\sigma\%$	$^{176}\text{Lu}/^{177}\text{Hf}$	1 $\sigma\%$	$^{176}\text{Hf}/^{177}\text{Hf}_{\text{int}}$	$^{176}\text{Hf}/^{177}\text{Hf}_{\text{ap}}$	$\epsilon\text{Hf}_{(\text{int})}$	2 σ	TDM _c
SA7-86	17	1.16	1498	2	6.93	1.46723	0.0071	0.282027	0.0088	0.011700	2.13	0.000271	1.37	0.282019	0.282027	6.65	1.04	1821
SA7-86	18	2.30	1498	2	6.36	1.46730	0.0051	0.282033	0.0067	0.021839	3.11	0.000551	1.74	0.282017	0.282033	6.58	0.84	1825
SA7-86	22	4.46	1498	2	8.80	1.46692	0.0163	0.281955	0.0142	0.014221	17.01	0.000377	16.18	0.281944	0.281955	3.97	1.60	1992
SA7-86	23	1.10	1498	2	6.64	1.46516	0.0530	0.282026	0.0171	0.017109	22.12	0.000675	19.97	0.282006	0.282026	6.19	1.96	1850
SA7-86	27	3.21	1498	2	8.88	1.46656	0.0179	0.282000	0.0126	0.012573	17.09	0.000435	16.21	0.281987	0.282000	5.51	1.44	1894
SA7-86	29	2.60	1498	2	8.22	1.46671	0.0179	0.281981	0.0127	0.012727	17.04	0.000490	16.19	0.281967	0.281981	4.78	1.47	1941
SA7-86	31	3.10	1498	2	7.11	1.46682	0.0179	0.282004	0.0129	0.012889	17.17	0.000679	16.25	0.281984	0.282004	5.40	1.51	1901
SA7-86	36b	2.51	1498	2	6.72	1.46685	0.0167	0.282026	0.0140	0.014011	17.02	0.001527	16.18	0.281982	0.282026	5.33	1.76	1905
SA7-86	40	2.21	1498	2	7.98	1.46703	0.0184	0.282000	0.0132	0.013236	17.35	0.000636	16.63	0.281982	0.282000	5.30	1.54	1907
SA7-86	44	1.75	1498	2	8.86	1.46669	0.0224	0.281974	0.0149	0.014882	18.79	0.000716	16.79	0.281953	0.281974	4.30	1.72	1971
SA7-86	7	0.66	1498	2	7.55	1.46715	0.0184	0.282011	0.0131	0.013059	21.42	0.000681	20.69	0.281991	0.282011	5.65	1.56	1885
SA7-86	n=21		1498	2		1.46701		0.282004		0.016281		0.000567		0.281988		5.54		1892
						0.00098		0.000044		0.011059		0.000555		0.000043		1.52		
SA7-91	12	1.00	1503	1	7.15	1.46627	0.0310	0.282084	0.0149	0.014854	10.50	0.002461	6.01	0.282014	0.282084	6.59	1.70	1829
SA7-91	17	0.89	1503	1	5.53	1.46604	0.0410	0.282026	0.0176	0.017545	10.49	0.002312	6.23	0.281961	0.282026	4.68	1.97	1951
SA7-91	20		1503	1	6.19	1.46660	0.0280	0.282067	0.0149	0.014855	10.62	0.002097	5.92	0.282008		6.35	1.68	1844
SA7-91	27		1503	1	6.74	1.46653	0.0310	0.282067	0.0140	0.014006	11.01	0.002602	5.97	0.281993		5.84	1.62	1877
SA7-91	31	1.50	1503	1	7.26	1.46699	0.0224	0.282068	0.0119	0.011911	11.00	0.001845	6.29	0.282016	0.282068	6.64	1.38	1825
SA7-91	32		1503	1	6.75	1.46623	0.0305	0.282051	0.0154	0.015437	10.58	0.002194	7.00	0.281989		5.69	1.77	1887
SA7-91	33		1503	1	6.64	1.46634	0.0336	0.281997	0.0160	0.016030	10.54	0.001588	5.51	0.281952		4.38	1.76	1970
SA7-91	4	0.97	1503	1	6.73	1.46702	0.0263	0.282097	0.0114	0.011437	10.56	0.001895	5.17	0.282044	0.282097	7.62	1.31	1762
SA7-91	5		1503	1	6.78	1.46700	0.0267	0.282085	0.0146	0.014568	10.64	0.002940	6.19	0.282002		6.14	1.71	1857

Sample	Zircon	n	Age	Disc.	1 σ	Tot.Hf	$^{178}\text{Hf}/^{177}\text{Hf}$	1 $\sigma\%$	$^{176}\text{Hf}/^{177}\text{Hf}$	1 $\sigma\%$	$^{176}\text{Yb}/^{177}\text{Hf}$	1 $\sigma\%$	$^{176}\text{Lu}/^{177}\text{Hf}$	1 $\sigma\%$	$^{176}\text{Hf}/^{177}\text{Hf}_{\text{int}}$	$^{176}\text{Hf}/^{177}\text{Hf}_{\text{ap}}$	$\epsilon\text{Hf}_{(\text{int})}$	2 σ	TDM _c
SA7-91	9	1	1503	1.69	1	6.69	1.46713	0.0227	0.282078	0.0137	0.013729	10.56	0.002860	5.28	0.281997	0.282078	5.97	1.59	1868
SA7-91	n=10	1	1503		1		1.46662		0.282062		0.014437		0.002279		0.281998		5.99		1867
							0.00079		0.000060		0.003629		0.000886		0.000053		1.89		
SA7-130	1	3	1511	-0.32	3	6.47	1.46725	0.0046	0.282046	0.0081	0.048610	14.75	0.001286	26.61	0.282010	0.282046	6.60	1.31	1834
SA7-130	1 rep	3	1511	-0.32	3	4.32	1.46747	0.0055	0.282086	0.0107	0.062953	5.70	0.002055	2.05	0.282027	0.282086	7.22	1.27	1794
SA7-130	5	3	1511	0.09	3	6.31	1.46714	0.0055	0.282074	0.0095	0.076596	21.01	0.002165	26.73	0.282012	0.282074	6.70	1.68	1828
SA7-130	5 rep	3	1511	0.09	3	5.82	1.46726	0.0027	0.282062	0.0073	0.070532	4.98	0.002146	2.60	0.282001	0.282062	6.28	0.93	1855
SA7-130	7	3	1511	-0.29	3	5.15	1.46741	0.0050	0.282027	0.0089	0.059622	14.00	0.001949	26.83	0.281972	0.282027	5.25	1.57	1921
SA7-130	7 rep	3	1511	-0.29	3	2.19	1.46729	0.0042	0.282028	0.0094	0.070125	2.02	0.002255	1.44	0.281964	0.282028	4.96	1.13	1939
SA7-130	9	3	1511	-0.57	3	5.73	1.46732	0.0049	0.282029	0.0081	0.083568	15.08	0.001961	26.73	0.281973	0.282029	5.31	1.49	1917
SA7-130	9 rep	3	1511	-0.57	3	6.65	1.46733	0.0058	0.282077	0.0070	0.063855	5.47	0.001630	2.00	0.282030	0.282077	7.34	0.88	1787
SA7-130	11	3	1511	0.02	3	6.21	1.46728	0.0039	0.282030	0.0074	0.077117	20.92	0.001890	27.11	0.281976	0.282030	5.42	1.40	1910
SA7-130	11 rep	3	1511	0.02	3	5.13	1.46733	0.0041	0.282023	0.0076	0.074564	6.04	0.002402	2.13	0.281954	0.282023	4.64	0.96	1960
SA7-130	16	3	1511	0.44	3	5.71	1.46729	0.0049	0.282069	0.0074	0.062910	12.71	0.001516	26.64	0.282026	0.282069	7.18	1.30	1797
SA7-130	16 rep	3	1511	0.44	3	3.46	1.46758	0.0049	0.282055	0.0114	0.076295	4.63	0.002445	1.80	0.281985	0.282055	5.73	1.33	1890
SA7-130	17	3	1511	0.23	3	8.37	1.46713	0.0293	0.282032	0.0179	0.017917	17.94	0.001497	17.08	0.281989	0.282032	5.86	2.16	1882
SA7-130	8	3	1511		3	7.17	1.46636	0.0497	0.282005	0.0214	0.021374	17.30	0.002151	16.29	0.281943		4.24	2.60	1986
SA7-130	n=14	3	1511		3		1.46725		0.282046		0.061860		0.001953		0.281990		5.91		1879
							0.00056		0.000049		0.039967		0.000706		0.000056		2.00		

Sample	Zircon	Disc.	Age	1σ	Tot.Hf	$^{178}\text{Hf}/^{177}\text{Hf}$	$1\sigma\%$	$^{176}\text{Hf}/^{177}\text{Hf}$	$1\sigma\%$	$^{176}\text{Yb}/^{177}\text{Hf}$	$1\sigma\%$	$^{176}\text{Lu}/^{177}\text{Hf}$	$1\sigma\%$	$^{176}\text{Hf}/^{177}\text{Hf}_{\text{int}}$	$^{176}\text{Hf}/^{177}\text{Hf}_{\text{ap}}$	$e\text{Hf}_{(\text{int})}$	2σ	TDM _c
MM26297	8	1.63	1514	11	8.96	1.46726	0.0036	0.282062	0.0080	0.048047	20.20	0.001389	26.67	0.282022	0.282062	7.11	1.43	1796
MM26297	11	-0.45	1507	6	11.13	1.46719	0.0059	0.282101	0.0089	0.060109	17.27	0.001379	26.60	0.282061	0.282101	8.34	1.39	1713
MM26297	14	0.71	1510	12	9.71	1.46723	0.0038	0.282217	0.0113	0.046549	34.16	0.001170	26.91	0.282183	0.282217	12.74	1.72	1441
MM26297	16	-0.54	1515	12	8.14	1.46722	0.0034	0.282087	0.0078	0.089757	21.73	0.001893	26.75	0.282032	0.282087	7.51	1.56	1772
MM26297	20	0.13	1523	8	10.86	1.46734	0.0046	0.282178	0.0077	0.057283	19.29	0.001467	26.72	0.282135	0.282178	11.34	1.34	1539
MM26297	25	-0.31	1503	7	10.22	1.46723	0.0044	0.282160	0.0094	0.051749	24.92	0.001314	26.67	0.282122	0.282160	10.41	1.45	1581
MM2230	5	-1.11	1484	11	7.30	1.46741	0.0052	0.282212	0.0116	0.035494	21.38	0.001186	26.75	0.282179	0.282212	12.00	1.71	1466
MM2230	10	-0.58	1507	12	6.50	1.46728	0.0050	0.282096	0.0098	0.048784	13.06	0.001194	26.60	0.282062	0.282096	8.37	1.56	1711
MM2230	14	-6.36	1473	10	5.44	1.46748	0.0066	0.282169	0.0118	0.031907	29.64	0.000940	26.84	0.282143	0.282169	10.47	1.66	1553
MM2230	20	-2.35	1457	23	5.54	1.46747	0.0066	0.282160	0.0113	0.034903	28.07	0.001278	26.81	0.282125	0.282160	9.45	1.96	1604
MM2230	7	10.69	1020	31	7.36	1.46731	0.0056	0.282199	0.0113	0.031289	12.74	0.000935	26.89	0.282181	0.282199	1.50	1.98	1757
MM2230	8	15.96	1020	31	8.06	1.46752	0.0052	0.282241	0.0087	0.025088	13.53	0.000931	26.65	0.282223	0.282241	2.99	1.72	1663
MM2230	11	6.07	1020	31	8.84	1.46732	0.0039	0.282200	0.0087	0.031902	19.94	0.001010	27.43	0.282181	0.282200	1.49	1.74	1758
MM2230	n=3		1020	31		1.46738		0.282214		0.029426		0.000958		0.282195		1.99		
						0.00024		0.000048		0.007539		0.000089		0.000049		1.73		
MM2247	13.9	0.32	1043	3	7.67	1.46725	0.0043	0.282207	0.0086	0.025593	30.36	0.000700	27.28	0.282194	0.282207	2.46	1.06	1715
MM2247	13.5	-2.38	1043	3	7.62	1.46726	0.0058	0.282222	0.0103	0.020370	15.17	0.000583	26.62	0.282211	0.282222	3.07	1.20	1677
MM2247	14.9	-1.88	1043	3	6.67	1.46729	0.0041	0.282212	0.0086	0.019526	20.92	0.000626	26.92	0.282200	0.282212	2.69	1.04	1701
MM2247	14.15	-0.90	1043	3	6.83	1.46733	0.0045	0.282199	0.0096	0.022827	24.00	0.000632	27.13	0.282187	0.282199	2.22	1.14	1730

Sample	Zircon	Disc.	Age	1 σ	Tot.Hf	$^{178}\text{Hf}/^{177}\text{Hf}$	1 $\sigma\%$	$^{176}\text{Hf}/^{177}\text{Hf}$	1 $\sigma\%$	$^{176}\text{Yb}/^{177}\text{Hf}$	1 $\sigma\%$	$^{176}\text{Lu}/^{177}\text{Hf}$	1 $\sigma\%$	$^{176}\text{Hf}/^{177}\text{Hf}_{\text{int}}$	$^{176}\text{Hf}/^{177}\text{Hf}_{\text{ap}}$	$e\text{Hf}_{\text{int}}$	2 σ	TDM _c
MM2247	13.13	-0.88	1043	3	6.70	1.46729	0.0040	0.282225	0.0086	0.021568	13.72	0.000589	26.65	0.282214	0.282225	3.17	1.03	1670
MM2247	13.18	-3.06	1043	3	5.51	1.46723	0.0045	0.282194	0.0089	0.040441	18.36	0.000996	26.89	0.282175	0.282194	1.79	1.15	1757
MM2247	n=6		1043	3	1.46728			0.282210	0.025054			0.000688		0.282197		2.57		
					0.00007			0.000025	0.015663			0.000314		0.000030		1.05		
MM2277	21	5.09	991	18	11.96	1.46720	0.0047	0.282185	0.0074	0.051693	18.30	0.001446	26.62	0.282158	0.282185	0.00	1.38	1828
MM2277	27	3.62	991	18	10.58	1.46720	0.0039	0.282187	0.0072	0.047326	22.66	0.001264	26.63	0.282163	0.282187	0.19	1.33	1816
MM2277	29	-1.57	991	18	10.35	1.46729	0.0048	0.282180	0.0077	0.030262	30.44	0.000862	26.94	0.282164	0.282180	0.21	1.31	1815
MM2277	n=3		991	18	1.46723			0.282184	0.043094			0.001191		0.282161		0.14		
					0.00010			0.000007	0.022650			0.000598		0.000007		0.23		
MM26226	12	-5.89	993	8	7.21	1.46727	0.0040	0.282168	0.0087	0.038383	17.38	0.001142	26.79	0.282147	0.282168	-0.33	1.25	1850
MM26226	18	-3.75	993	8	6.42	1.46749	0.0053	0.282224	0.0096	0.026329	15.56	0.000841	26.85	0.282209	0.282224	1.86	1.28	1713
MM26226	21	-4.12	993	8	7.85	1.46729	0.0053	0.282178	0.0105	0.037869	19.05	0.000874	26.69	0.282162	0.282178	0.20	1.38	1817
MM26226	23	-0.55	993	8	6.53	1.46749	0.0055	0.282235	0.0179	0.043632	14.46	0.001225	26.72	0.282212	0.282235	1.99	2.18	1705
MM26226	n=4		993	8	1.46739			0.282202	0.036553			0.001021		0.282183		0.93		
					0.00024			0.000066	0.014593			0.000383		0.000066		2.34		
MM26302	13		1022	3	11.60	1.46727	0.0236	0.282168	0.0106	0.010568	10.47	0.000615	5.14	0.282157		0.67	1.15	1810
MM26302	17		1022	3	8.87	1.46736	0.0219	0.282173	0.0114	0.011435	11.20	0.000799	6.73	0.282158		0.72	1.25	1807
MM26302	18	-2.24	1022	3	10.56	1.46730	0.0230	0.282173	0.0119	0.011909	15.95	0.001068	12.97	0.282153	0.282173	0.54	1.35	1819

Sample	Zircon	Disc.	Age	1 σ	Tot.Hf	$^{178}\text{Hf}/^{177}\text{Hf}$	1 $\sigma\%$	$^{176}\text{Hf}/^{177}\text{Hf}$	1 $\sigma\%$	$^{176}\text{Yb}/^{177}\text{Hf}$	1 $\sigma\%$	$^{176}\text{Lu}/^{177}\text{Hf}$	1 $\sigma\%$	$^{176}\text{Hf}/^{177}\text{Hfint}$	$^{176}\text{Hf}/^{177}\text{Hfap}$	$\epsilon\text{Hf}_{(int)}$	2 σ	TDM _c
MM26302	6		1022	3	12.48	1.46691	0.0300	0.282128	0.0112	0.011209	13.87	0.000829	11.17	0.282113		-0.89	1.25	1908
MM26302	25		1022	3	10.20	1.46707	0.0336	0.282155	0.0122	0.012154	11.26	0.001103	7.14	0.282134		-0.12	1.33	1860
MM26302	27		1022	3	8.80	1.46705	0.0258	0.282132	0.0127	0.012661	10.47	0.000553	5.13	0.282122		-0.56	1.35	1887
MM26302	n=6		1022	3		1.46716		0.282155		0.011656		0.000828		0.282139		0.06		
							0.00035	0.000041		0.001485		0.000452		0.000039		1.38		
MM26306	3	-2.09	1046	3	6.07	1.46728	0.0038	0.282179	0.0093	0.023546	12.39	0.000588	26.61	0.282168	0.282179	1.61	1.11	1770
MM26306	6	-9.34	1046	3	5.59	1.46728	0.0038	0.282198	0.0089	0.033346	12.84	0.000805	26.63	0.282183	0.282198	2.13	1.11	1738
MM26306	9	-1.43	1046	3	7.58	1.46726	0.0041	0.282163	0.0084	0.069571	15.38	0.001828	27.00	0.282127	0.282163	0.18	1.25	1860
MM26306	12	-0.87	1046	3	7.06	1.46723	0.0066	0.282138	0.0108	0.035643	13.79	0.000890	26.62	0.282121	0.282138	-0.06	1.31	1874
MM26306	14	-2.78	1046	3	5.64	1.46720	0.0045	0.282134	0.0093	0.022147	14.29	0.000554	26.61	0.282123	0.282134	0.04	1.10	1869
MM26306	15	-5.49	1046	3	5.44	1.46718	0.0049	0.282112	0.0112	0.024052	12.68	0.000601	26.60	0.282101	0.282112	-0.78	1.30	1919
MM26306	17	0.20	1046	3	5.83	1.46722	0.0050	0.282143	0.0087	0.041563	14.53	0.001007	26.67	0.282124	0.282143	0.04	1.13	1868
MM26306	23	1.47	1046	3	10.76	1.46702	0.0236	0.282277	0.0100	0.009999	10.47	0.000851	5.12	0.282261	0.282277	4.90	1.10	1564
MM26306	26	-1.75	1046	3	10.01	1.46701	0.0239	0.282246	0.0108	0.010773	10.51	0.000979	5.24	0.282227	0.282246	3.71	1.18	1639
MM26306	n=9		1046	3		1.46719		0.282177		0.030071		0.000900		0.282159		1.31		
							0.00021	0.000110		0.036407		0.000773		0.000110		3.88		
ROG218	4	1.86	1027	12	9.68	1.46739	0.0048	0.282180	0.0108	0.079585	20.12	0.002208	27.27	0.282137	0.282180	0.08	1.74	1851
ROG218	9		1027	12	10.70	1.46713	0.0033	0.282169	0.0078	0.082118	28.24	0.001915	27.18	0.282132		-0.10	1.39	1863
ROG218	17	8.16	1027	12	9.10	1.46730	0.0051	0.282198	0.0089	0.063283	21.76	0.001806	26.69	0.282163	0.282198	1.00	1.48	1794
ROG218	23	6.43	1027	12	9.15	1.46722	0.0047	0.282179	0.0087	0.055389	17.81	0.001333	27.00	0.282153	0.282179	0.65	1.37	1816

Sample	Zircon	Disc.	Age	1σ	Tot.Hf	$^{178}\text{Hf}/^{177}\text{Hf}$	1σ%	$^{176}\text{Hf}/^{177}\text{Hf}$	1σ%	$^{176}\text{Yb}/^{177}\text{Hf}$	1σ%	$^{176}\text{Lu}/^{177}\text{Hf}$	1σ%	$^{176}\text{Hf}/^{177}\text{Hf}_{\text{int}}$	$^{176}\text{Hf}/^{177}\text{Hf}_{\text{ap}}$	$e\text{Hf}_{\text{int}}$	2σ	TDM _c
ROG218	26	8.16	1027	12	10.10	1.46711	0.0045	0.282157	0.0077	0.037877	16.88	0.000849	26.66	0.282140	0.282157	0.20	1.18	1843
ROG218	n=5		1027	12		1.46723		0.282176		0.063650		0.001622		0.282145		0.37		
						0.00023		0.000030		0.036437		0.001070		0.000025		0.90		
ROG275	9	-0.42	1003	21	11.12	1.46718	0.0044	0.282170	0.0078	0.037231	16.76	0.000934	26.81	0.282152	0.282170	0.07	1.41	1833
ROG275	11	-0.51	1003	21	12.60	1.46726	0.0042	0.282153	0.0075	0.028726	27.26	0.000779	26.71	0.282138	0.282153	-0.42	1.35	1864
ROG275	22	0.27	1003	21	9.08	1.46720	0.0051	0.282189	0.0085	0.042382	18.08	0.000948	26.65	0.282171	0.282189	0.74	1.47	1791
ROG275	24	-3.31	1003	21	8.32	1.46716	0.0036	0.282103	0.0085	0.056118	18.93	0.001226	26.69	0.282079	0.282103	-2.50	1.52	1993
ROG275	27	3.62	1003	21	10.60	1.46716	0.0042	0.282118	0.0082	0.034580	16.77	0.000965	26.75	0.282099	0.282118	-1.79	1.46	1949
ROG275	n=5		1003	21		1.46719		0.282146		0.039808		0.000970		0.282128		-0.78		
						0.00008		0.000071		0.020722		0.000322		0.000075		2.67		
ROG641	14	2.99	924	3	13.42	1.46725	0.0422	0.282266	0.0166	0.016619	10.73	0.002128	6.35	0.282229	0.282266	1.03	1.81	1711
ROG641	16	-1.38	924	3	9.34	1.46767	0.0280	0.282199	0.0137	0.013726	10.64	0.000535	6.00	0.282190	0.282199	-0.36	1.46	1798
ROG641	4		924	3	14.80	1.46702	0.0221	0.282241	0.0104	0.010369	11.17	0.002062	6.21	0.282206		0.19	1.18	1764
ROG641	7	28.02	924	3	13.12	1.46686	0.0369	0.282198	0.0143	0.014282	15.15	0.000908	12.38	0.282183	0.282198	-0.63	1.56	1815
ROG641	n=4		924	3		1.46720		0.282226		0.013749		0.001408		0.282202		0.06		
						0.00070		0.000067		0.005157		0.001616		0.000041		1.46		
ROG80	11.2		1046	3	5.75	1.46732	0.0046	0.282195	0.0096	0.013044	24.75	0.000472	27.55	0.282186		2.26	1.11	1730
ROG80	11.2 rep		1046	3	5.56	1.46721	0.0052	0.282201	0.0084	0.046786	32.36	0.001161	27.40	0.282178		1.99	1.13	1747

Sample	Zircon	Disc.	Age	1 σ	Tot.Hf	¹⁷⁸ Hf/ ¹⁷⁷ Hf	1 σ %	¹⁷⁶ Hf/ ¹⁷⁷ Hf	1 σ %	¹⁷⁶ Yb/ ¹⁷⁷ Hf	1 σ %	¹⁷⁶ Lu/ ¹⁷⁷ Hf	1 σ %	¹⁷⁶ Hf/ ¹⁷⁷ Hfint	¹⁷⁶ Hf/ ¹⁷⁷ Hfap	eHf _(int)	2 σ	TDM _c
ROG80	11.4		1046	3	8.99	1.46723	0.0042	0.282195	0.0087	0.008388	13.31	0.000350	26.64	0.282188		2.34	1.01	1725
ROG80	11.10		1046	3	6.13	1.46727	0.0046	0.282165	0.0093	0.020207	18.55	0.000602	26.87	0.282154		1.10	1.11	1802
ROG80	12.12	2.81	1046	3	6.21	1.46721	0.0057	0.282170	0.0096	0.016284	25.31	0.000488	27.22	0.282161	0.282170	1.36	1.12	1786
ROG80	12.4		1046	3	6.53	1.46725	0.0048	0.282175	0.0091	0.014291	14.18	0.000432	26.66	0.282167		1.58	1.06	1773
ROG80	12.13	0.39	1046	3	5.11	1.46720	0.0049	0.282198	0.0098	0.034406	19.50	0.000890	26.70	0.282181	0.282198	2.07	1.21	1742
ROG80	n=7		1046	3		1.46724		0.282186		0.021915		0.000628		0.282174		1.81		
						0.00009		0.000030		0.027435		0.000585		0.000027		0.95		
SA3-01	2	0.13	1039	7	7.02	1.46725	0.0041	0.282150	0.0076	0.032293	12.93	0.000733	26.61	0.282136	0.282150	0.32	1.05	1845
SA3-01	2		1039	7	5.84	1.46719	0.0036	0.282190	0.0067	0.034987	1.47	0.000729	1.46	0.282176		1.73	0.83	1757
SA3-01	7	0.20	1039	7	7.13	1.46728	0.0042	0.282147	0.0065	0.026132	14.76	0.000595	26.63	0.282136	0.282147	0.31	0.91	1846
SA3-01	7		1039	7	6.38	1.46725	0.0034	0.282180	0.0059	0.025846	8.22	0.000780	3.97	0.282165		1.34	0.76	1782
SA3-01	11	0.55	1039	7	8.53	1.46731	0.0038	0.282191	0.0069	0.035032	12.42	0.000796	26.60	0.282176	0.282191	1.73	0.99	1757
SA3-01	11		1039	7	7.23	1.46725	0.0036	0.282144	0.0051	0.032993	5.01	0.000812	1.68	0.282128	0.282144	0.05	0.68	1863
SA3-01	12	3.04	1039	7	8.94	1.46766	0.0257	0.282151	0.0149	0.014878	18.42	0.000890	16.51	0.282133	0.282151	0.22	1.74	1852
SA3-01	13	0.37	1039	7	7.50	1.46716	0.0179	0.282147	0.0129	0.012888	17.07	0.001157	16.24	0.282124	0.282147	-0.11	1.57	1872
SA3-01	14		1039	7	6.46	1.46731	0.0040	0.282165	0.0070	0.028048	6.19	0.000553	1.68	0.282154		0.97	0.86	1805
SA3-01	15	2.71	1039	7	8.58	1.46713	0.0198	0.282156	0.0136	0.013608	17.53	0.000647	16.42	0.282143	0.282156	0.57	1.59	1830
SA3-01	16	-3.85	1039	7	9.28	1.46711	0.0184	0.282145	0.0134	0.013418	17.02	0.000922	16.21	0.282127	0.282145	-0.01	1.60	1866
SA3-01	18	0.96	1039	7	8.92	1.46730	0.0229	0.282153	0.0142	0.014218	17.07	0.000629	16.18	0.282140	0.282153	0.47	1.65	1836
SA3-01	19	0.26	1039	7	9.42	1.46710	0.0198	0.282142	0.0129	0.012888	17.01	0.000566	16.21	0.282130	0.282142	0.13	1.51	1857
SA3-01	22	-2.00	1039	7	9.59	1.46702	0.0198	0.282179	0.0127	0.012726	17.57	0.000851	16.54	0.282162	0.282179	1.24	1.52	1788
SA3-01	24	0.77	1039	7	7.02	1.46717	0.0040	0.282201	0.0054	0.033954	4.03	0.000670	1.37	0.282188	0.282201	2.16	0.70	1730

Sample	Zircon	Disc.	Age	1σ	Tot.Hf	$^{178}\text{Hf}/^{177}\text{Hf}$	1σ%	$^{176}\text{Hf}/^{177}\text{Hf}$	1σ%	$^{176}\text{Yb}/^{177}\text{Hf}$	1σ%	$^{176}\text{Lu}/^{177}\text{Hf}$	1σ%	$^{176}\text{Hf}/^{177}\text{Hf}_{\text{int}}$	$^{176}\text{Hf}/^{177}\text{Hf}_{\text{ap}}$	$e\text{Hf}_{(\text{int})}$	2σ	TDM _c
SA3-01	29	0.37	1039	7	8.10	1.46721	0.0029	0.282165	0.0056	0.033255	7.03	0.000714	1.37	0.282151	0.282165	0.86	0.73	1812
SA3-01	38	0.49	1039	7	8.78	1.46703	0.0208	0.282129	0.0149	0.014879	17.04	0.000858	16.18	0.282112	0.282129	-0.54	1.74	1899
SA3-01	4	4.07	1039	7	7.49	1.46719	0.0167	0.282180	0.0142	0.014217	17.01	0.000875	16.20	0.282162	0.282180	1.26	1.67	1787
SA3-01	45	-0.03	1039	7	10.23	1.46704	0.0175	0.282165	0.0129	0.012888	18.20	0.000722	17.01	0.282150	0.282165	0.84	1.53	1813
SA3-01	n=19		1039	7	1.46721			0.282162		0.022060		0.000763		0.282147		0.71		
					0.00029			0.000040		0.018886		0.000293		0.000041		1.45		

Table 10.5. LA-ICP-MS in-situ hafnium in zircon data. Disc. = % ($^{206}\text{Pb}/^{238}\text{U}$)/($^{207}\text{Pb}/^{206}\text{Pb}$), Tot. Hf = total hafnium signal in mV, $^{176}\text{Hf}/^{177}\text{Hf}_{\text{int}}$ = time-corrected ratio using the intrusion age, $^{176}\text{Hf}/^{177}\text{Hf}_{\text{ap}}$ = time-corrected ratio using the zircon $^{207}\text{Pb}/^{206}\text{Pb}$ age, Age = $^{207}\text{Pb}/^{206}\text{Pb}$, disc. = % ($^{206}\text{Pb}/^{238}\text{U}$)/($^{207}\text{Pb}/^{206}\text{Pb}$), TDM_c = two stage model age using Lu/Hf = 0.015. Means (non-italics) and 2.s.d. (italics) are shown after each sample.

Table 10.6. Oxygen isotope data (Ionprobe) for Chapter 5.

analyses no.	grain no.	n	$^{18}\text{O}/^{16}\text{O}$ (measured)	1s.e. %	$^{18}\text{O}/^{16}\text{O}$ (corrected)	1s.e. %	$\delta^{18}\text{O}$ [‰] VSMOW
07/08/2008							
91500	15	10	0.0020284	0.0088	0.0020272	0.0088	10.65
91500	15	6	0.0020242	0.0126	0.0020257	0.0126	9.32
91500	15	5	0.0020251	0.0122	0.0020252	0.0122	10.04
MM2241	10.3		0.0020193	0.0200	0.0020250	0.0200	7.23
MM2241	10.3		0.0020173	0.0090	0.0020250	0.0090	6.27
MM2241	10.4		0.0020186	0.0101	0.0020249	0.0101	6.90
MM2241	10.7		0.0020196	0.0095	0.0020249	0.0095	7.45
MM2241	10.8		0.0020185	0.0099	0.0020248	0.0099	6.92
MM2241	10.9		0.0020174	0.0103	0.0020247	0.0103	6.44
MM2241	9.8		0.0020190	0.0148	0.0020247	0.0148	7.22
MM2241	9.7		0.0020213	0.0091	0.0020246	0.0091	8.39
MM2241	9.5		0.0020172	0.0088	0.0020246	0.0088	6.38
MM2241	9.2		0.0020184	0.0168	0.0020248	0.0168	6.87
91500	15	10	0.0020243	0.0096	0.0020239	0.0096	10.28
MM2235	6.1		0.0020219	0.0110	0.0020236	0.0110	9.21
MM2235	5.1		0.0020197	0.0107	0.0020236	0.0107	8.12
MM2235	5.2		0.0020207	0.0105	0.0020235	0.0105	8.68
MM2235	5.3		0.0020207	0.0084	0.0020235	0.0084	8.69
MM2235	5.4		0.0020206	0.0110	0.0020234	0.0110	8.66
MM2235	5.5		0.0020212	0.0130	0.0020234	0.0130	9.00
MM2235	5.6		0.0020186	0.0084	0.0020233	0.0084	7.70
MM2235	6.7		0.0020224	0.0073	0.0020233	0.0073	9.65
MM2235	5.9		0.0020205	0.0153	0.0020232	0.0153	8.71
MM2235	5.11		0.0020191	0.0106	0.0020232	0.0106	8.05
91500	15	10	0.0020232	0.0125	0.0020225	0.0125	10.42
08/08/2008							
91500	15	10	0.0020248	0.0148	0.0020249	0.0148	10.00
91500	15	10	0.0020245	0.0137	0.0020248	0.0137	9.93
KIM	9	10	0.0020137	0.0152	0.0020247	0.0152	4.55
91500	15	10	0.0020246	0.0123	0.0020246	0.0123	10.03
91500	1	10	0.0020253	0.0121	0.0020246	0.0121	10.43
ROG525	24		0.0020168	0.0106	0.0020245	0.0106	6.20
ROG525	13		0.0020174	0.0106	0.0020245	0.0106	6.55
ROG525	4		0.0020160	0.0143	0.0020245	0.0143	5.85
ROG525	16		0.0020169	0.0109	0.0020245	0.0109	6.28
ROG525	20		0.0020164	0.0073	0.0020245	0.0073	6.02
ROG525	20		0.0020173	0.0134	0.0020245	0.0134	6.50
ROG525	9		0.0020179	0.0151	0.0020245	0.0151	6.79
ROG525	8		0.0020176	0.0128	0.0020245	0.0128	6.65
ROG525	10		0.0020174	0.0115	0.0020244	0.0115	6.55
ROG525	11		0.0020163	0.0160	0.0020244	0.0160	6.00
ROG525	10		0.0020173	0.0066	0.0020244	0.0066	6.53
ROG525	13		0.0020164	0.0125	0.0020244	0.0125	6.08
91500	1	10	0.0020244	0.0126	0.0020244	0.0126	10.09
91500	1	5	0.0020243	0.0112	0.0020242	0.0112	10.09
91500	1	5	0.0020235	0.0129	0.0020241	0.0129	9.79
91500	1	10	0.0020239	0.0108	0.0020239	0.0108	10.07
09/08/2008							
91500	15	10	0.0020269	0.0188	0.0020263	0.0188	10.36
KIM	9	10	0.0020147	0.0095	0.0020263	0.0095	4.31
91500	15	5	0.0020268	0.0099	0.0020263	0.0099	10.30
SA7-86	31		0.0020201	0.0125	0.0020263	0.0125	7.00
SA7-86	6		0.0020186	0.0094	0.0020263	0.0094	6.21
SA7-86	7a		0.0020212	0.0146	0.0020263	0.0146	7.53
SA7-86	23		0.0020197	0.0130	0.0020263	0.0130	6.80

analyses no.	grain no.	n	$^{18}\text{O}/^{16}\text{O}$ (measured)	1s.e. %	$^{18}\text{O}/^{16}\text{O}$ (corrected)	1s.e. %	$\delta^{18}\text{O}$ [‰] VSMOW
SA7-86	22		0.0020198	0.0109	0.0020263	0.0109	6.80
SA7-86	27		0.0020194	0.0139	0.0020263	0.0139	6.65
SA7-86	40		0.0020204	0.0126	0.0020263	0.0126	7.13
SA7-86	36a		0.0020191	0.0100	0.0020263	0.0100	6.48
SA7-86	44		0.0020196	0.0130	0.0020263	0.0130	6.75
91500	15	10	0.0020279	0.0244	0.0020263	0.0244	10.85
91500	15	8	0.0020260	0.0089	0.0020263	0.0089	9.90
SA3-60	8		0.0020200	0.0124	0.0020263	0.0124	6.93
SA3-60	2		0.0020192	0.0093	0.0020263	0.0093	6.53
SA7-04	b1		0.0020255	0.0247	0.0020263	0.0247	9.67
SA7-04	b2		0.0020210	0.0155	0.0020263	0.0155	7.42
SA7-04	b4		0.0020192	0.0112	0.0020263	0.0112	6.53
SA7-04	b6		0.0020174	0.0067	0.0020263	0.0067	5.61
SA7-04	b7		0.0020234	0.0160	0.0020263	0.0160	8.59
91500	15	5	0.0020261	0.0092	0.0020263	0.0092	9.95
SA7-86	36b		0.0020206	0.0094	0.0020263	0.0094	7.20
SA7-86	36c		0.0020199	0.0135	0.0020263	0.0135	6.88
SA7-86	11		0.0020192	0.0086	0.0020263	0.0086	6.52
SA7-86	13		0.0020197	0.0095	0.0020263	0.0095	6.75
SA7-86	7b		0.0020192	0.0124	0.0020263	0.0124	6.52
SA7-86	28		0.0020204	0.0112	0.0020263	0.0112	7.11
SA7-86	29		0.0020203	0.0077	0.0020263	0.0077	7.09
91500	15	10	0.0020264	0.0098	0.0020263	0.0098	10.11
10/08/2009							
91500	13	9	0.0020275	0.0137	0.0020270	0.0137	10.29
91500	13	10	0.0020270	0.0136	0.0020272	0.0136	9.94
KIM	9	10	0.0020165	0.0137	0.0020274	0.0137	4.65
91500	13	8	0.0020272	0.0143	0.0020276	0.0143	9.87
SA7-91	4		0.0020186	0.0160	0.0020277	0.0160	5.53
SA7-91	5		0.0020185	0.0152	0.0020277	0.0152	5.48
SA7-91	6		0.0020190	0.0153	0.0020277	0.0153	5.70
SA7-91	14		0.0020194	0.0162	0.0020277	0.0162	5.90
SA7-91	21		0.0020179	0.0147	0.0020278	0.0147	5.18
SA7-91	3		0.0020190	0.0141	0.0020278	0.0141	5.71
SA7-91	9		0.0020174	0.0094	0.0020278	0.0094	4.88
SA7-91	12		0.0020161	0.0178	0.0020278	0.0178	4.24
SA7-91	17		0.0020193	0.0126	0.0020278	0.0126	5.79
SA7-91	30		0.0020196	0.0121	0.0020279	0.0121	5.96
SA7-91	31		0.0020181	0.0144	0.0020279	0.0144	5.18
SA7-91	33		0.0020180	0.0144	0.0020279	0.0144	5.16
SA7-91	32		0.0020189	0.0143	0.0020279	0.0143	5.57
SA7-91	20		0.0020193	0.0082	0.0020279	0.0082	5.77
SA7-91	27		0.0020187	0.0139	0.0020280	0.0139	5.45
91500	13	8	0.0020282	0.0154	0.0020280	0.0154	10.13
SA3-04	46		0.0020238	0.0145	0.0020281	0.0145	7.90
SA3-04	39a		0.0020238	0.0182	0.0020282	0.0182	7.89
SA3-04	39b		0.0020238	0.0116	0.0020282	0.0116	7.90
SA3-04	19		0.0020231	0.0166	0.0020282	0.0166	7.52
SA3-04	20		0.0020224	0.0141	0.0020282	0.0141	7.18
SA3-04	3		0.0020254	0.0145	0.0020282	0.0145	8.65
SA3-04	59		0.0020238	0.0113	0.0020283	0.0113	7.86
SA3-04	17		0.0020240	0.0115	0.0020283	0.0115	7.92
SA3-04	34		0.0020230	0.0149	0.0020283	0.0149	7.42
SA3-04	60		0.0020253	0.0191	0.0020284	0.0191	8.53
SA3-04	51a		0.0020246	0.0173	0.0020284	0.0173	8.21
SA3-04	51b		0.0020249	0.0176	0.0020284	0.0176	8.35
91500	13	10	0.0020286	0.0173	0.0020285	0.0173	10.12

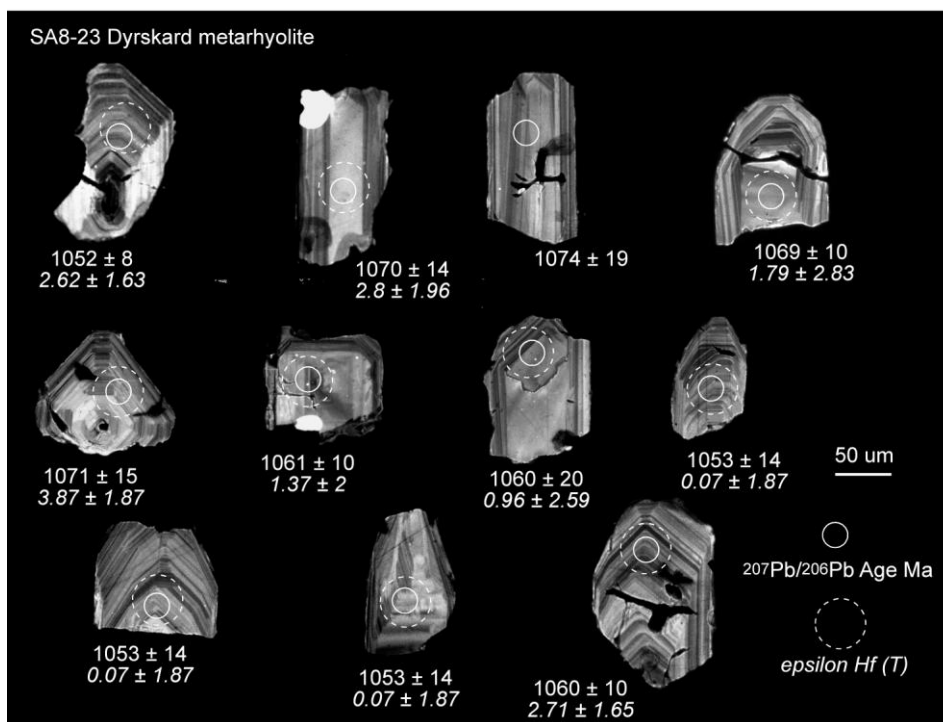
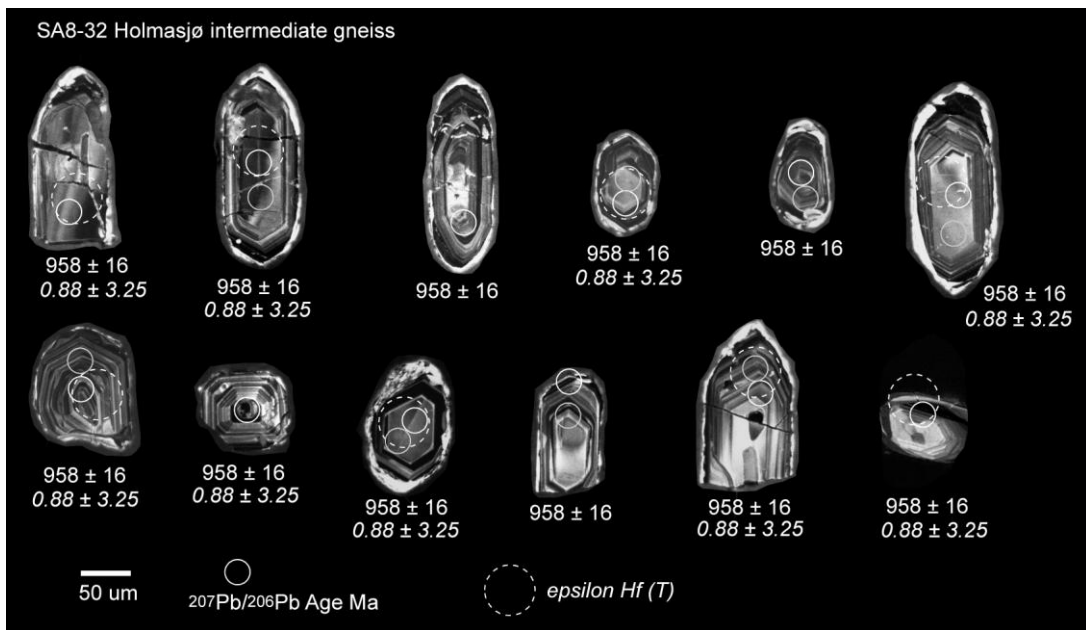
Table 10.7. Oxygen isotope data (Ionprobe) for Chapter 6

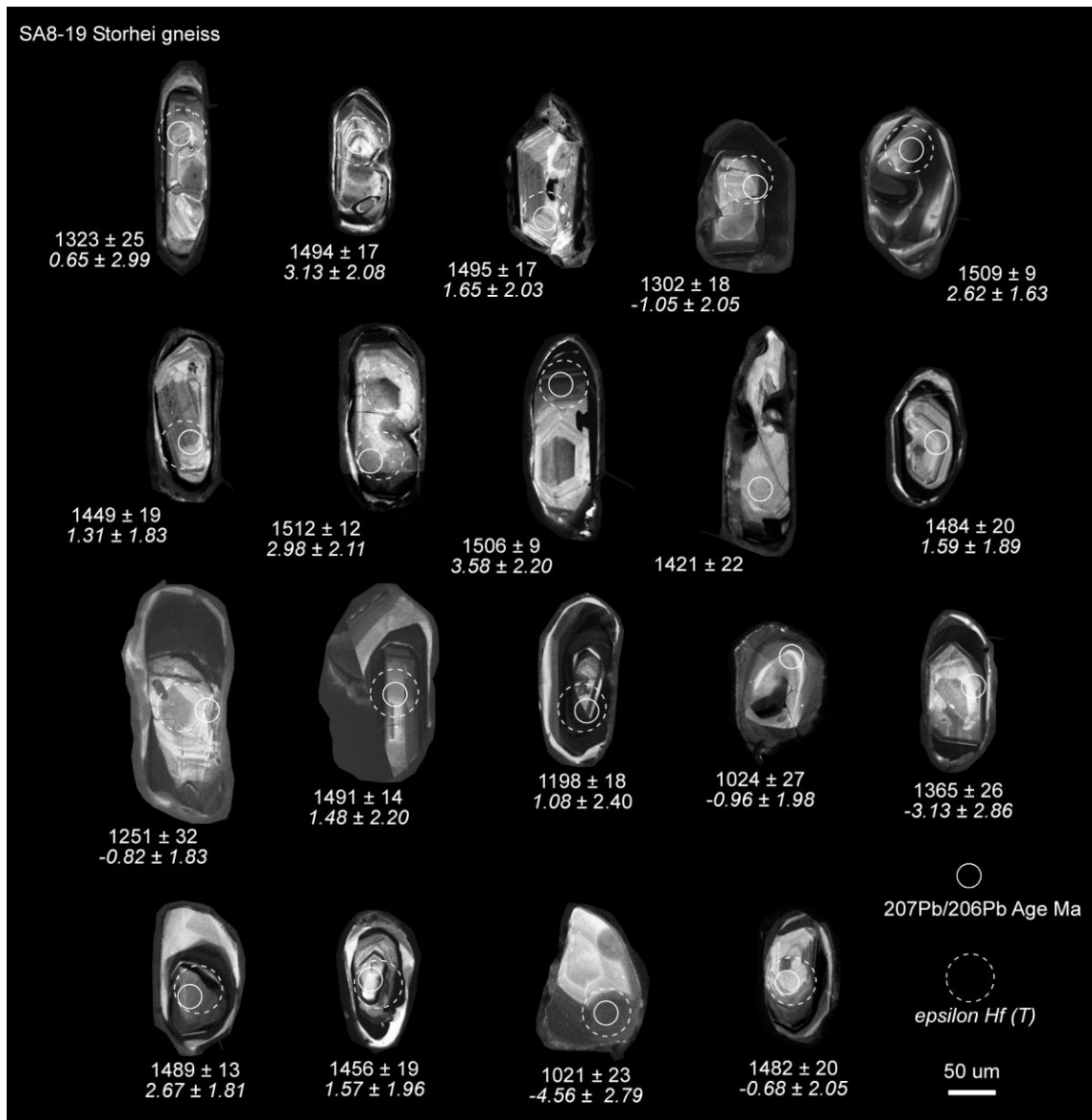
analyses no.	grain no.	n	$^{18}\text{O}/^{16}\text{O}$ (measured)	1s.e. %	$^{18}\text{O}/^{16}\text{O}$ (corrected)	1s.e. %	$\delta^{18}\text{O}$ [‰] VSMOW
07/08/2008							
91500	15	10	0.00202838	0.0088	0.00202722	0.0088	10.65
91500	15	6	0.00202417	0.0126	0.00202567	0.0126	9.32
91500	15	5	0.00202510	0.0122	0.00202516	0.0122	10.04
ROG 80	11.10		0.00201933	0.0200	0.00202501	0.0200	7.23
ROG 80	11.11		0.00201734	0.0090	0.00202496	0.0090	6.27
ROG 80	11.14		0.00201857	0.0101	0.00202492	0.0101	6.90
ROG 80	11.2		0.00201961	0.0095	0.00202487	0.0095	7.45
ROG 80	11.4		0.00201851	0.0099	0.00202482	0.0099	6.92
ROG 80	12.1		0.00201744	0.0103	0.00202472	0.0103	6.44
ROG 80	12.12		0.00201897	0.0148	0.00202467	0.0148	7.22
ROG 80	12.4		0.00202126	0.0091	0.00202463	0.0091	8.39
ROG 80	12.5		0.00201717	0.0088	0.00202458	0.0088	6.38
MM2241	10.3		0.00201836	0.0168	0.00202477	0.0168	6.87
MM2241	10.3		0.00201625	0.0078	0.00202453	0.0078	5.94
MM2241	10.4		0.00201629	0.0098	0.00202448	0.0098	5.98
MM2241	10.7		0.00201488	0.0090	0.00202443	0.0090	5.31
MM2241	10.8		0.00201688	0.0086	0.00202438	0.0086	6.32
MM2241	10.9		0.00201617	0.0144	0.00202433	0.0144	6.00
MM2241	9.8		0.00201693	0.0320	0.00202429	0.0320	6.40
MM2241	9.7		0.00201819	0.0124	0.00202424	0.0124	7.05
MM2241	9.5		0.00201472	0.0083	0.00202419	0.0083	5.34
MM2241	9.2		0.00201376	0.0109	0.00202414	0.0109	4.89
91500	15	10	0.00202429	0.0096	0.00202387	0.0096	10.28
91500	15	10	0.00202322	0.0125	0.00202251	0.0125	10.42
08/08/2008							
91500	15	10	0.00202475	0.0148	0.00202489	0.0148	10.00
91500	15	10	0.00202452	0.0137	0.00202480	0.0137	9.93
KIM	9	10	0.00201367	0.0152	0.00202472	0.0152	4.55
91500	15	10	0.00202457	0.0123	0.00202464	0.0123	10.03
91500	1	10	0.00202528	0.0121	0.00202456	0.0121	10.43
91500	1	10	0.00202441	0.0126	0.00202438	0.0126	10.09
MM26306	26		0.00202797	0.0129	0.00202433	0.0129	11.88
MM26306	23		0.00202776	0.0129	0.00202433	0.0129	11.78
MM26306	3		0.00202696	0.0135	0.00202432	0.0135	11.39
MM26306	21		0.00202725	0.0141	0.00202431	0.0141	11.54
MM26306	7		0.00202783	0.0137	0.00202430	0.0137	11.83
MM26306	17		0.00202760	0.0113	0.00202429	0.0113	11.72
MM26306	12		0.00202637	0.0126	0.00202428	0.0126	11.11
MM26306	13		0.00202729	0.0141	0.00202428	0.0141	11.58
MM26306	15		0.00202697	0.0113	0.00202427	0.0113	11.42
MM26306	18		0.00202832	0.0167	0.00202426	0.0167	12.09
91500	1	5	0.00202427	0.0112	0.00202424	0.0112	10.09
MM26302	26		0.00201781	0.0104	0.00202421	0.0104	6.88
MM26302	27		0.00201963	0.0116	0.00202420	0.0116	7.79
MM26302	25		0.00201804	0.0118	0.00202419	0.0118	7.00
MM26302	17		0.00201601	0.0155	0.00202419	0.0155	5.99
MM26302	13		0.00201564	0.0167	0.00202418	0.0167	5.81
MM26302	10		0.00201705	0.0083	0.00202417	0.0083	6.52
MM26302	11		0.00201754	0.0083	0.00202416	0.0083	6.77
MM26302	5		0.00201727	0.0123	0.00202415	0.0123	6.64
MM26302	6		0.00201493	0.0115	0.00202414	0.0115	5.47
MM26302	4		0.00201801	0.0104	0.00202413	0.0104	7.02
91500	1	5	0.00202354	0.0129	0.00202410	0.0129	9.79

analyses no.	grain no.	n	$^{18}\text{O}/^{16}\text{O}$ (measured)	1s.e. %	$^{18}\text{O}/^{16}\text{O}$ (corrected)	1s.e. %	$\delta^{18}\text{O}$ [‰] VSMOW
MM26302	18		0.00201750	0.0106	0.00202408	0.0106	6.79
MM26302	16		0.00201749	0.0168	0.00202407	0.0168	6.79
ROG 641	14		0.00201773	0.0163	0.00202406	0.0163	6.91
ROG 641	16		0.00201927	0.0112	0.00202406	0.0112	7.68
ROG 641	4		0.00201756	0.0129	0.00202405	0.0129	6.83
ROG 641	7		0.00201759	0.0104	0.00202404	0.0104	6.85
91500	1	10	0.00202392	0.0108	0.00202392	0.0108	10.07
09/08/2008							
91500	15	10	0.00202687	0.0188	0.00202630	0.0188	10.36
KIM	9	10	0.00201474	0.0095	0.00202630	0.0095	4.31
91500	15	5	0.00202677	0.0099	0.00202631	0.0099	10.30
91500	15	10	0.00202787	0.0244	0.00202631	0.0244	10.85
SA3-01	16		0.00201967	0.0184	0.00202631	0.0184	6.76
SA3-01	15		0.00201938	0.0143	0.00202631	0.0143	6.62
SA3-01	10		0.00201709	0.0144	0.00202631	0.0144	5.48
SA3-01	19a		0.00201938	0.0144	0.00202631	0.0144	6.62
SA3-01	18		0.00201797	0.0127	0.00202631	0.0127	5.91
SA3-01	7		0.00201972	0.0087	0.00202631	0.0087	6.78
SA3-01	22		0.00202004	0.0140	0.00202631	0.0140	6.94
SA3-01	24		0.00201923	0.0145	0.00202631	0.0145	6.54
SA3-01	45		0.00201871	0.0138	0.00202631	0.0138	6.28
SA3-01	38		0.00201995	0.0137	0.00202631	0.0137	6.90
SA3-01	33a		0.00201930	0.0129	0.00202631	0.0129	6.57
91500	15	8	0.00202598	0.0089	0.00202631	0.0089	9.90
91500	15	5	0.00202608	0.0092	0.00202632	0.0092	9.95
SA3-01	17		0.00201908	0.0104	0.00202632	0.0104	6.46
SA3-01	13		0.00201894	0.0120	0.00202632	0.0120	6.39
SA3-01	5		0.00201807	0.0098	0.00202632	0.0098	5.96
SA3-01	4		0.00201798	0.0064	0.00202632	0.0064	5.92
SA3-01	12a		0.00201983	0.0124	0.00202632	0.0124	6.84
SA3-01	12b		0.00202002	0.0121	0.00202632	0.0121	6.93
SA3-01	33b		0.00202030	0.0089	0.00202632	0.0089	7.07
SA3-01	33c		0.00201981	0.0090	0.00202632	0.0090	6.82
SA3-01	19b		0.00202046	0.0104	0.00202632	0.0104	7.15
91500	15	10	0.00202640	0.0098	0.00202632	0.0098	10.11
10/08/2009							
91500	13	9	0.0020275	0.0137	0.0020270	0.0137	10.29
91500	13	10	0.0020270	0.0136	0.0020272	0.0136	9.94
KIM	9	10	0.0020165	0.0137	0.0020274	0.0137	4.65
91500	13	8	0.0020272	0.0143	0.0020276	0.0143	9.87
91500	13	8	0.0020282	0.0154	0.0020280	0.0154	10.13
91500	13	10	0.0020286	0.0173	0.0020285	0.0173	10.12

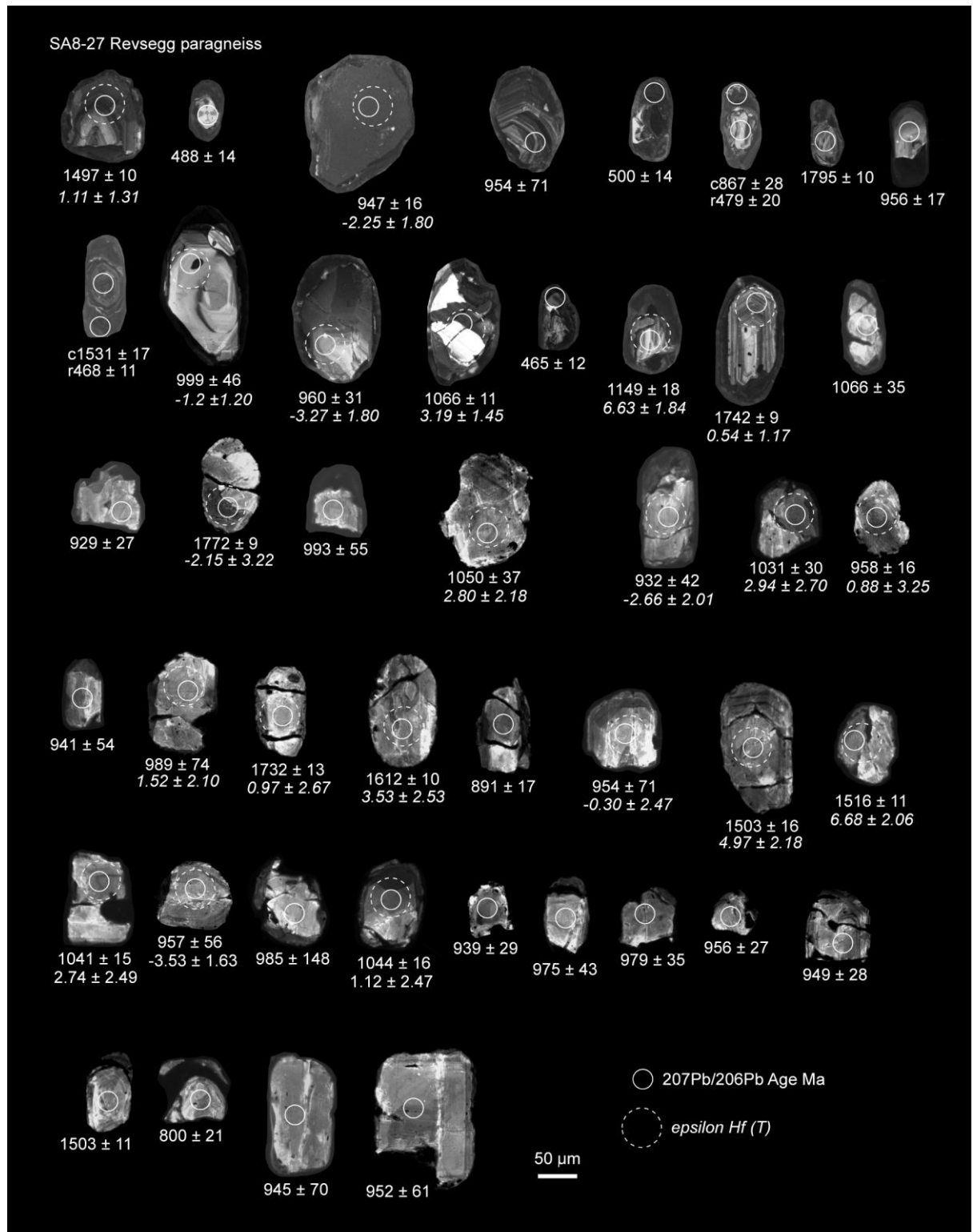
Corrected values are normalised to the daily average (or regressed value if drift is recognised) of the 91500 standard. 91500 and KIM are bracketing standards. $\delta^{18}\text{O}$ is reported relative to the VMSOW.

CL images of zircons analysed in Chapter 8.









Bibliography

- Åhäll, K.-I., Connelly, J., 1998. Intermittent 1.53-1.13 Ga magmatism in western Baltica; age constraints and correlations within a postulated supercontinent. *Precambrian Research* 92, 1-20.
- Åhäll, K.-I., Connelly, J.N., Brewer, T.S., 2000. Episodic rapakivi magmatism due to distal orogenesis?: Correlation of 1.69-1.50 Ga orogenic and inboard, 'anorogenic' events in the Baltic Shield. *Geology* 28, 823-826.
- Åhäll, K.-I., Connelly, J.N., 2008. Long-term convergence along SW Fennoscandia: 330 m.y. of Proterozoic crustal growth. *Precambrian Research* 161, 452-474.
- Åhäll, K.-I., Cornell, D.H., Armstrong, R.A., 1998. Ion probe dating of metasedimentary units across the Skagerrak: new constraints for early Mesoproterozoic growth of the Baltic Shield. *Precambrian Research* 87, 117-134.
- Åhäll, K.-I., Daly, J.S., Schöberg, H., 1990. Geochronological constraints on mid-Proterozoic magmatism in the Østfold-Marstrand belt; implications for crustal evolution in southwest Sweden. In Gower, C.F., Rivers, T., Ryan, B.(eds.) *Mid-Proterozoic Laurentia-Baltica*, Geological Association of Canada Special Paper 38, 97-115.
- Åhäll, K.-I., Larson, S.-Å., 2000. Growth-related 1.85-1.55 Ga magmatism in the Baltic Shield; a review addressing the tectonic characteristics of Svecofennian, TIB 1 -related, and Gothian events. *GFF* 122, 193-206.
- Åhäll, K.-I., Samuelsson, L., Persson, P.-O., 1997. Geochronology and structural setting of the 1.38 Ga Torpa granite; implications for charnockite formation in SW Sweden. *GFF* 119, 37-43.
- Ali, K.A., Stern, R.J., Manton, W.I., Johnson, P.R., Mukherjee, S.K., 2009a. Neoproterozoic diamictite in the Eastern Desert of Egypt and Northern Saudi Arabia: evidence of ~750 Ma glaciation in the Arabian-Nubian Shield? *International Journal of Earth Science* 99, 705-726.
- Ali, K.A., Stern, R.J., Manton, W.I., Kimura, J.-I., Khamees, H.A., 2009b. Geochemistry, Nd isotopes and U-Pb SHRIMP zircon dating of Neoproterozoic volcanic rocks from the Central Eastern Desert of Egypt: New insights into the ~750 Ma crust-forming event. *Precambrian Research* 171, 1-22.
- Alm, E., Kumpulainen, R., Sundblad, C., 1997. Mesoproterozoic sediment-hosted strata-bound copper deposits in the Dal Group, Sweden. In: Charlet, J.-M. (ed.): *Proceedings of the International Cornet Symposium*, Royal Academy of Overseas Sciences, Belgium, 217-243.
- Amelin, Y., Lee, D., Halliday, A.N., Pidgeon, R.T., 1999. Nature of the Earth's earliest crust from hafnium isotopes in single detrital zircons. *Nature* 399, 252-255.
- Andersen, T., 2005. Terrane analysis, regional nomenclature and crustal evolution in the Southwest Scandinavian Domain of the Fennoscandian Shield. *GFF* 127, 159-168.
- Andersen, T., 1997. Radiogenic isotope systematics of the Herefoss granite, South Norway: an indicator of Sveconorwegian (Grenvillian) crustal evolution in the Baltic Shield. *Chemical Geology* 135, 139-158.
- Andersen, T., Andersson, U.B., Graham, S., Åberg, G., Simonsen, S.L., 2009a. Granitic magmatism by melting of juvenile continental crust: New constraints on the source of Palaeoproterozoic granitoids in Fennoscandia from Hf isotopes in zircon. *Journal of the Geological Society* 166, 233-247.
- Andersen, T., Andresen, A., Sylvester, A.G., 2002a. Timing of late- to post-tectonic Sveconorwegian granitic magmatism in South Norway. *NGU Bulletin* 440, 5-18.

- Andersen, T., Andresen, A., Sylvester, A.G., 2001. Nature and distribution of deep crustal reservoirs in the southwestern part of the Baltic Shield: evidence from Nd, Sr and Pb isotope data on late Sveconorwegian granites. *Journal of the Geological Society, London* 158, 253-267.
- Andersen, T., Graham, S., Sylvester, A.G., 2007a. Timing and tectonic significance of Sveconorwegian A-type granitic magmatism in Telemark, southern Norway: New results from laser-ablation ICPMS U-Pb dating of zircon. *NGU Bulletin* 447, 17-31.
- Andersen, T., Graham, S., Sylvester, A.G., 2009b. The geochemistry, Lu-Hf isotope systematics, and petrogenesis of Late Mesoproterozoic A-type granites in southwestern Fennoscandia. *Canadian Mineralogist* 47, 1399-1422.
- Andersen, T., Griffin, W.L., 2004. Lu-Hf and U-Pb isotope systematics of zircons from the Storgangen intrusion, Rogaland Intrusive Complex, SW Norway: implications for the composition and evolution of Precambrian lower crust in the Baltic Shield. *Lithos* 73, 271-288.
- Andersen, T., Griffin, W.L., Jackson, S.E., Knudson, T.-L., Pearson, N.J., 2004a. Mid-Proterozoic magmatic arc evolution at the southwest margin of the Baltic Shield. *Lithos* 73, 289-318.
- Andersen, T., Griffin, W.L., Pearson, N.J., 2002b. Crustal Evolution in the SW part of the Baltic Shield: the Hf Isotope Evidence. *Journal of Petrology* 43, 1725-1747.
- Andersen, T., Griffin, W.L., Sylvester, A.G., 2007b. Sveconorwegian crustal underplating in southwestern Fennoscandia: LAM-ICPMS U-Pb and Lu-Hf isotope evidence from granites and gneisses in Telemark, southern Norway. *Lithos* 93, 273-287.
- Andersen, T., Hagelia, P., Whitehouse, M.J., 1994. Precambrian multi-stage crustal evolution in the Bamble sector of south Norway: Pb isotopic evidence from a Sveconorwegian deep-seated granitic intrusion. *Chemical Geology* 116, 327-343.
- Andersen, T., Laajoki, K., Saeed, A., 2004b. Age, provenance and tectonostratigraphic status of the Mesoproterozoic Blefjell quartzite, Telemark sector, southern Norway. *Precambrian Research* 135, 217-244.
- Anderson, I.C., Frost, C.D., Frost, B.R., 2003. Petrogenesis of the Red Mountain pluton, Laramie anorthosite complex, Wyoming: Implications for the origin of A-type granite. *Precambrian Research* 124, 243-267.
- Anderson, J.L., 1983. Proterozoic anorogenic granite plutonism of North America. *Proterozoic Geology* 161, 133-154.
- Andersson, J., Möller, C., Johansson, L., 2002. Zircon geochronology of migmatite gneisses along the Mylonite Zone (S Sweden): a major Sveconorwegian terrane boundary in the Baltic Shield. *Precambrian Research* 114, 121.
- Andersson, J., Söderlund, U., Cornell, D., Johansson, L., Möller, C., 1999. Sveconorwegian (-Grenvillian) deformation, metamorphism and leucosome formation in SW Sweden, SW Baltic Shield: constraints from a Mesoproterozoic granite intrusion. *Precambrian Research* 98, 151-171.
- , P.-G., Rodhe, A., 1994. Ductile and brittle deformation within the Protogine Zone, southern Sweden: A discussion. *GFF* 116, 115-116.
- Andresen, A., 1974. Petrographic and structural history of the Caledonian rocks north of Haukelisæter, Hardangervidda. *Norges Geologiske Undersøkelse* 314, 1-52.
- Andresen, A., 1978. Lithostratigraphy of the autochthonous/parautochthonous Lower Palaeozoic metasediments on Hardangervidda, south Norway. *Norges Geologiske Undersøkelse* 338, 59-69.
- Andresen, A., Færseth, R., 1982. An evolutionary model for the southwest Norwegian Caledonides. *American Journal of Science* 282, 756-782.

- Andresen, A., Gabrielsen, R.H., 1979. Major element chemistry of metavolcanic rocks and tectonic setting of the Precambrian Dyrskard Group, Hardangervidda, south Norway. *Norsk geologisk tidsskrift* 49, 47-59.
- Andresen, A., Heier, K.S., 1975. A Rb-Sr whole rock isochron date on an igneous rock-body from the Stavanger area, South Norway. *International Journal of Earth Science* 64, 260-265.
- Andresen, A., Heier, K.S., Jorde, K., Naterstad, J., 1974. A preliminary Rb/Sr geochronological study of the Hardangervidda-Ryfylke nappe system in the Røldal area, south Norway. *Norsk geologisk tidsskrift* 54, 35-47.
- Annen, C., Blundy, J.D., Sparks, R.S.J., 2006. The Genesis of Intermediate and Silicic Magmas in Deep Crustal Hot Zones. *Journal of Petrology* 47, 505-539.
- Appleby, S.K., Gillespie, M.R., Graham, C.M., Hinton, R.W., Oliver, G.J.H., Kelly, N.M., 2009. Do S-type granites commonly sample infracrustal sources? New results from an integrated O, U-Pb and Hf isotope study of zircon. *Contributions to Mineralogy and Petrology*, 1-18.
- Appleby, S.K., Graham, C.M., Gillespie, M.R., Hinton, R.W., Oliver, G.J.H., EIMF, 2008. A cryptic record of magma mixing in diorites revealed by high-precision SIMS oxygen isotope analysis of zircons. *Earth and Planetary Science Letters* 269, 105-117.
- Armstrong, R.L., 1968. A model for the evolution of strontium and lead isotopes in a dynamic Earth. *Reviews in Geophysics* 6, 175-199.
- Armstrong, R.L., 1971. Isotopic and chemical constraints on models of magma genesis in volcanic arcs. *Earth & Planetary Science Letters* 12, 137-142.
- Armstrong, R.L., 1981. Radiogenic isotopes: The case for crustal recycling on a near-steady-state non-continental-growth Earth. *Philosophical Transactions of the Royal Society of London* 301, 443-472.
- Arndt, N.T., Goldstein, S.L., 1989. An open boundary between lower continental crust and mantle: its role in crust formation and crustal recycling. *Tectonophysics* 161, 201-212.
- Austin-Hegardt, E., Claesson, L., Cornell, D., Simakov, S.K., 2004. Eclogites in the central part of the Sveconorwegian Eastern Segment of the Baltic Shield: support for a Subduction-Extrusion model. *GFF* 126, 17.
- Austin-Hegardt, E., Cornell, D.H., Hellström, F.A., Lundqvist, I., 2007. Emplacement ages of the mid-Proterozoic Kungsbacka bimodal suite, SW Sweden. *GFF* 129, 227-234.
- Austrheim, H., Corfu, F., 2009. Formation of planar deformation features (PDFs) in zircon during coseismic faulting and an evaluation of potential effects on U-Pb systematics. *Chemical Geology* 261, 24-30.
- Austrheim, H., Corfu, F., Bryhni, I., Andersen, T.B., 2003. The Proterozoic Hustad igneous complex: A low strain enclave with a key to the history of the Western Gneiss Region of Norway. *Precambrian Research* 120, 149-175.
- Bahlburg, H., Vervoort, J.D., Du Frane, S.A., Bock, B., Augustsson, C., Reimann, C., 2009. Timing of crust formation and recycling in accretionary orogens: Insights learned from the western margin of South America. *Earth Science Reviews* 97, 227-253.
- Baitis, H.W., Lindstrom, M.M., 1980. Geology, petrography, and petrology of Pinzon Island, Galapagos Archipelago. *Contributions to Mineralogy and Petrology* 72, 367-386.

- Baker, M.B., Grove, T.L., Price, R., 1994. Primitive basalts and andesites from the Mt. Shasta region, N. California: products of varying melt fraction and water content. *Contributions to Mineralogy and Petrology* 118, 111-129.
- Barbarin, B., 1999. A review of the relationships between granitoid types, their origins and their geodynamic environments. *Lithos* 46, 605-626.
- Barry, T.L., Pearce, J.A., Leat, P.T., Millar, I.L., le Roex, A.P., 2006. Hf isotope evidence for selective mobility of high-field-strength elements in a subduction setting: South Sandwich Islands. *Earth and Planetary Science Letters* 252, 223-244.
- Be'eri-Shlevin, Y., Katzir, Y., Valley, J.W., 2009. Crustal evolution and recycling in a juvenile continent: Oxygen isotope ratio of zircon in the northern Arabian Nubian Shield. *Lithos* 107, 169-184.
- Begg, G., Belousova, E., Griffin, W.L., O'Reilly, S.Y., Natapov, L., 2009. Continental versus crustal growth: Resolving the paradox. *Geochimica et Cosmochimica Acta* 73, Supplement 1, A103.
- Behn, M.D., Kelemen, P.B., 2006. Stability of arc lower crust: Insights from the Talkeetna arc section, south central Alaska, and the seismic structure of modern arcs. *Journal of Geophysical Research B: Solid Earth* 111, 1-20.
- Belousova, E.A., Reid, A.J., Griffin, W.L., O'Reilly, S.Y., 2009. Rejuvenation vs. recycling of Archean crust in the Gawler Craton, South Australia: Evidence from U-Pb and Hf isotopes in detrital zircon. *Lithos* 113, 570-582.
- Berthelsen, A., 1980. Towards a palinspastic tectonic analysis of the Baltic Shield. In Cogné, J. & Slansky, M. (eds.), *Geology of Europe, from Precambrian to the post-Hercynian sedimentary basins* 108, 5-21.
- Betts, P.G., Giles, D., 2006. The 1800-1100 Ma tectonic evolution of Australia. *Precambrian Research* 144, 92-125.
- Betts, P.G., Giles, D., Schaefer, B.F., 2008. Comparing 1800-1600 Ma accretionary and basin processes in Australia and Laurentia: Possible geographic connections in Columbia. *Precambrian Research* 166, 81-92.
- Betts, P.G., Giles, D., Schaefer, B.F., Mark, G., 2007. 1600-1500 Ma hotspot track in eastern Australia: Implications for Mesoproterozoic continental reconstructions. *Terra Nova* 19, 496-501.
- Bindeman, I.N., Eiler, J.M., Yagodinski, G.M., Tatsumi, Y., Stern, C.R., Grove, T.L., Portnyagin, M., Hoernle, K., Danyushevsky, L.V., 2005. Oxygen isotope evidence for slab melting in modern and ancient subduction zones. *Earth and Planetary Science Letters* 235, 480-496.
- Bindeman, I.N., Ponomareva, V.V., Bailey, J.C., Valley, J.W., 2004. Volcanic arc of Kamchatka: A province with high- $\delta^{18}\text{O}$ magma sources and large-scale $^{18}\text{O}/^{16}\text{O}$ depletion of the upper crust. *Geochimica et Cosmochimica Acta* 68, 841-865.
- Bingen, B., Andersson, J., Söderlund, U., Möller, C., 2008a. The Mesoproterozoic in the Nordic countries. *Episodes* 31, 29-34.
- Bingen, B., Austrheim, H., Whitehouse, M., 2001a. Ilmenite as a source for zirconium during high-grade metamorphism? textural evidence from the caledonides of Western Norway and implications for zircon geochronology. *Journal of Petrology* 42, 355-375.
- Bingen, B., Birkeland, A., Nordgulen, Ø., Sigmond, E.M.O., 2001b. Correlation of supracrustal sequences and origin of terranes in the Sveconorwegian orogen of SW Scandinavia: SIMS data on zircon in clastic metasediments. *Precambrian Research* 108, 293-318.

- Bingen, B., Davis, W.J., Hamilton, M.A., Engvik, A.K., Stein, H.J., Skår, Ø., Nordgulen, Ø., 2008b. Geochronology of high-grade metamorphism in the Sveconorwegian belt, S. Norway: U-Pb, Th-Pb and Re-Os data. *Norsk Geologisk Tidsskrift* 88, 13-42.
- Bingen, B., Demaiffe, D., Hertogen, J., Weis, D., Michot, J., 1993. K-rich calc-alkaline augen gneisses of Grenvillian age in southern Norway: mingling of mantle-derived and crustal components. *Journal of Geology* 101, 763-778.
- Bingen, B., Griffin, W.L., Torsvik, T.H., Saeed, A., 2005a. Timing of Late Neoproterozoic glaciation in Baltica constrained by detrital zircon geochronology in the Hedmark Group, south-east Norway. *Terra Nova* 17, 250-258.
- Bingen, B., Mansfeld, J., Sigmund, E.M.O., Stein, H.J., 2002. Baltica-Laurentia link during the Mesoproterozoic: 1.27 Ga development of continental basins in the Sveconorwegian Orogen, southern Norway. *Canadian Journal of Earth Sciences* 39, 1425-1440.
- Bingen, B., Nordgulen, Ø., Sigmund, E.M.O., Tucker, R., Mansfeld, J., Högdahl, K., 2003. Relations between 1.19-1.13 Ga continental magmatism, sedimentation and metamorphism, Sveconorwegian province, S Norway. *Precambrian Research* 124, 215-241.
- Bingen, B., Nordgulen, Ø., Viola, G., 2008c. A four-phase model for the Sveconorwegian orogeny, SW Scandinavia. *Norsk Geologisk Tidsskrift* 88, 43-72.
- Bingen, B., Skår, Ø., Marker, M., Sigmund, E.M.O., Nordgulen, Ø., Ragnhildstveit, J., Mansfeld, J., Tucker, R.D., Liégeois, J.-P., 2005b. Timing of continental building in the Sveconorwegian orogen, SW Scandinavia. *Norsk Geologisk Tidsskrift* 85, 87-105.
- Bingen, B., Solli, A., 2009. Geochronology of magmatism in the Caledonian and Sveconorwegian belts of Baltica: Synopsis for detrital zircon provenance studies. *Norsk Geologisk Tidsskrift* 89, 267-290.
- Bingen, B., Stein, H.J., 2003. Molybdenite Re-Os dating of biotite dehydration melting in the Rogaland high-temperature granulites, S. Norway. *Earth and Planetary Science Letters* 208, 181-195.
- Bingen, B., Stein, H.J., Bogaerts, M., Bolle, O., Mansfeld, J., 2006. Molybdenite Re-Os dating constrains gravitational collapse of the Sveconorwegian orogen, SW Scandinavia. *Lithos* 87, 328-346.
- Bingen, B., Van Breemen, O., 1998. Tectonic regimes and terrane boundaries in the high-grade Sveconorwegian belt of SW Norway, inferred from U-Pb zircon geochronology and geochemical signature of augen gneiss suites. *Journal of the Geological Society, London* 155, 143-154.
- Birkeland, A., Sigmund, E.M.O., Whitehouse, M.J., Vestin, J., 1997. From Archaean to Proterozoic on Hardangervidda, South Norway. *NGU Bulletin* 433, 4-5.
- Bispo-Santos, F., D'Agrella-Filho, M.S., Pacca, I.I.G., Janikian, L., Trindade, R.I.F., Elming, S.-A., Silva, J.A., Barros, M.A.S., Pinho, F.E.C., 2008. Columbia revisited: Paleomagnetic results from the 1790 Ma colider volcanics (SW Amazonian Craton, Brazil). *Precambrian Research* 164, 40-49.
- Bleeker, W., 2003. The late Archean record: A puzzle in ca. 35 pieces. *Lithos* 71, 99-134.
- Bleiner, D., Günther, D., 2001. Theoretical description and experimental observation of aerosol transport processes in laser ablation inductively coupled plasma mass spectrometry. *Journal of Analytical Atomic Spectrometry* 16, 449-456.
- Bogaerts, M., Scaillet, B., Vander Auwera, J., 2006. Phase equilibria of the Lyngdal granodiorite (Norway): Implications for the origin of metaluminous ferroan granitoids. *Journal of Petrology* 47, 2405-2431.

- Bogaerts, M., Scaillet, B., Liegeois, J.-P., Vander Auwera, J., 2003. Petrology and geochemistry of the Lyngdal granodiorite (Southern Norway) and the role of fractional crystallisation in the genesis of Proterozoic ferro-potassic A-type granites. *Precambrian Research* 124, 149-184.
- Bogdanova, S.V., Bingen, B., Gorbatshev, R., Kheraskova, T.N., Kozlov, V.I., Puchkov, V.N., Volozh, Y.A., 2008. The East European Craton (Baltica) before and during the assembly of Rodinia. *Precambrian Research* 160, 23-45.
- Bogdanova, S.V., Page, L.M., Skridlaite, G., Taran, L.N., 2001. Proterozoic tectonothermal history in the western part of the East European Craton: $^{40}\text{Ar}/^{39}\text{Ar}$ geochronological constraints. *Tectonophysics* 339, 39-66.
- Bolle, O., Demaiffe, D., Duchesne, J.-C., 2003a. Petrogenesis of jotunitic and acidic members of an AMC suite (Rogaland anorthosite province, SW Norway): a Sr and Nd isotopic assessment. *Precambrian Research* 124, 185.
- Bolle, O., Diot, H., Trindade, R.I.F., 2003b. Magnetic fabrics in the Holum granite (Vest-Agder, southernmost Norway): implications for the late evolution of the Sveconorwegian (Grenvillian) orogen of SW Scandinavia. *Precambrian Research* 121, 221-249.
- Bonin, B., 2007. A-type granites and related rocks: Evolution of a concept, problems and prospects. *Lithos* 97, 1-29.
- Botcharnikov, R.E., Almeev, R.R., Koepke, J., Holtz, F., 2008. Phase relations and liquid lines of descent in hydrous ferrobalt - Implications for the Skaergaard intrusion and Columbia river flood basalts. *Journal of Petrology* 49, 1687-1727.
- Bouvier, A., Vervoort, J.D., Patchett, P.J., 2008. The Lu-Hf and Sm-Nd isotopic composition of CHUR: Constraints from unequilibrated chondrites and implications for the bulk composition of terrestrial planets. *Earth and Planetary Science Letters* 273, 48-57.
- Bowen, N.L., 1928. *The Evolution of the Igneous Rocks*. Princeton University Press, Princeton, New Jersey.
- Brander, L., Söderlund, U., 2009. Mesoproterozoic (1.47-1.44 Ga) orogenic magmatism in Fennoscandia; Baddeleyite U-Pb dating of a suite of massif-type anorthosite in S. Sweden. *International Journal of Earth Science* 98, 499-516.
- Brenan, J.M., Shaw, H.F., Phinney, D.L., Ryerson, F.J., 1994. Rutile-aqueous fluid partitioning of Nb, Ta, Hf, Zr, U and Th: implications for high field strength element depletions in island-arc basalts. *Earth and Planetary Science Letters* 128, 327-339.
- Brewer, T.S., 1985. *Geochemistry, geochronology and tectonic setting of the Proterozoic Telemark supracrustals, southern Norway*. Unpublished PhD thesis, Nottingham University.
- Brewer, T.S., Åhäll, K.-I., Darbyshire, D.P.F., Menuge, J.F., 2002. Geochemistry of late Mesoproterozoic volcanism in southwestern Scandinavia: implications for Sveconorwegian/Grenvillian plate tectonics models. *Journal of the Geological Society, London* 159, 129-144.
- Brewer, T.S., Åhäll, K.-I., Menuge, J.F., Storey, C.D., Parrish, R.R., 2004. Mesoproterozoic bimodal volcanism in SW Norway, evidence for recurring pr-Sveconorwegian continental margin tectonism. *Precambrian Research* 134, 249-273.
- Brewer, T.S., Daly, J.S., Åhäll, K.-I., 1998. Contrasting magmatic arcs in the Palaeoproterozoic of the south-western Baltic Shield. *Precambrian Research* 92, 297-315.
- Brophy, J.G., 2008. A study of rare earth element (REE)-SiO₂ variations in felsic liquids generated by basalt fractionation and amphibolite melting: A potential test for discriminating between the two different processes. *Contributions to Mineralogy and Petrology* 156, 337-357.

- Brown, M., 1994. The generation, segregation, ascent and emplacement of granite magma: the migmatite-to-crustally-derived granite connection in thickened orogens. *Earth Science Reviews* 36, 83-130.
- Buchan, K.L., Mertanen, S., Park, R.G., Pesonen, L.J., Elming, S.-Å., Abrahamsen, N., Bylund, G., 2000. Comparing the drift of Laurentia and Baltica in the Proterozoic: the importance of key palaeomagnetic poles. *Tectonophysics* 319, 167-198.
- Burton, K.W., Kohn, M.J., Cohen, A.S., O'Nions, K. R., 1995. The relative diffusion of Pb, Nd, Sr and O in garnet. *Earth Planetary. Science Letters* 133 (1-2), 199-211.
- Campbell, I.H., Allen, C.M., 2008. Formation of supercontinents linked to increases in atmospheric oxygen. *Nature Geoscience* 1, 554-558.
- Carmichael, I.S.E., 1964. The petrology of Thingmuli, a Tertiary volcano in eastern Iceland. *Journal of Petrology* 5, 435-460.
- Carmichael, I.S.E., Ghiorso, M.S., 1990. Controls on oxidation-reduction relations in magmas. *Reviews in Mineralogy and Geochemistry* 24, 191-212.
- Carr, S.D., Easton, R.M., Jamieson, R.A., Culshaw, N.G., 2000. Geologic transect across the Grenville orogen of Ontario and New York. *Canadian Journal of Earth Sciences* 37, 193-216.
- Cawood, P.A., Kröner, A., Collins, W.J., Kusky, T.M., Mooney, W.D., Windley, B.F., 2009. Accretionary orogens through Earth history. In: Cawood, P.A. & Kröner, A. (eds.) *Earth Accretionary Systems in Space and Time*, Geological Society of London, Special Publication 318, 1-36.
- Cawood, P.A., Nemchin, A.A., Strachan, R., Prave, T., Krabbendam, M., 2007. Sedimentary basin and detrital zircon record along East Laurentia and Baltica during assembly and breakup of Rodinia. *Journal of the Geological Society* 164, 257-275.
- Cawood, P.A., Nemchin, A.A., Strachan, R.A., Kinny, P.D., Loewy, S., 2004. Laurentian provenance and an intracratonic tectonic setting for the Moine Supergroup, Scotland, constrained by detrital zircons from the Loch Eil and Glen Urquhart successions. *Journal of the Geological Society* 161, 861-874.
- Cawood, P.A., Strachan, R., Cutts, K., Kinny, P.D., Hand, M., Pisarevsky, S., 2010. Neoproterozoic orogeny along the margin of Rodinia: Valhalla orogen, North Atlantic. *Geology* 38, 99-102.
- Chadwick, B., Garde, A.A., 1996. Palaeoproterozoic oblique plate convergence in South Greenland: a reappraisal of the Ketilidian Orogen. In: Brewer, T.S. (Ed.), *Precambrian Crustal Evolution in the North Atlantic Region*. Geological Society of London, Special Publications 112, 179-196.
- Chappell, B.W., White, A.J.R., 1974. Two contrasting granite types. *Pacific Geology* 8, 173-174.
- Christiansen, E.H., McCurry, M., 2008. Contrasting origins of Cenozoic silicic volcanic rocks from the western Cordillera of the United States. *Bulletin of Volcanology* 70, 251-267.
- Christoffel, C.A., Connelly, J.N., Åhäll, K., 1999. Timing and characterisation of recurrent pre-Sveconorwegian metamorphism and deformation in the Varberg-Halmstad region of SW Sweden. *Precambrian Research* 98, 173-195.
- Claesson, S., 1987. Isotopic evidence for the Precambrian provenance and Caledonian metamorphism of high grade paragneisses from the Seve Nappes, Scandinavian Caledonides - I. Conventional U-Pb zircon and Sm-Nd whole rock data. *Contributions to Mineralogy and Petrology* 97, 196-204.
- Clemens, J.D., Holloway, J.R., White, A.J.R., 1986. Origin of an A-type granite: experimental constraints. *American Mineralogist* 71, 317-324.

- Clift, P.D., Draut, A.E., Kelemen, P.B., Blusztajn, J., Greene, A., 2005. Stratigraphic and geochemical evolution of an oceanic arc upper crustal section: The Jurassic Talkeetna Volcanic Formation, south-central Alaska. *Bulletin of the Geological Society of America* 117, 902-925.
- Clift, P.D., Schouten, H., Vannucchi, P., 2009. Arc-continent collisions, sediment recycling and the maintenance of the continental crust. In: Cawood, P.A. & Kröner, A. (eds.) *Earth Accretionary Systems in Space and Time*, Geological Society of London, Special Publication 318, 75-103.
- Collins, W.J., 2002. Hot orogens, tectonic switching, and creation of continental crust. *Geology* 30, 535-538.
- Collins, W.J., Beams, S.D., White, A.J.R., Chappell, B.W., 1982. Nature and origin of A-type granites with particular reference to southeastern Australia. *Contributions to Mineralogy and Petrology* 80, 189-200.
- Condie, K.C., 2002. Continental growth during a 1.9-Ga superplume event. *Journal of Geodynamics* 34, 249-264.
- Condie, K.C., 1998. Episodic continental growth and supercontinents: a mantle avalanche connection? *Earth and Planetary Science Letters* 163, 97-108.
- Condie, K.C., 2005. *Earth as an Evolving Planetary System*. Elsevier, Amsterdam, 1-350.
- Condie, K.C., 2004. Supercontinents and superplume events: distinguishing signals in the geologic record. *Physics of the Earth and Planetary Interiors* 146, 319-332.
- Condie, K.C., Belousova, E., Griffin, W.L., Sircombe, K.N., 2009. Granitoid events in space and time: Constraints from igneous and detrital zircon age spectra. *Gondwana Research* 15, 228-242.
- Connelly, J.N., Åhäll, K., 1996. The Mesoproterozoic cratonization of Baltica - new age constraints from SW Sweden. In: Brewer, T.S. (Ed.), *Precambrian Crustal Evolution in the North Atlantic Region*. Geological Society of London, Special Publications 112, 261-273.
- Connelly, J.N., Berglund, J., Larson, S.Å., 1996. Thermotectonic evolution of the Eastern Segment of southwestern Sweden: tectonic constraints from U-Pb geochronology. In: Brewer, T.S. (Ed.), *Precambrian Crustal Evolution in the North Atlantic Region*. Geological Society of London, Special Publications 112, 297-313.
- Cordani, U.G., Teixeira, W., D'Agrella-Filho, M.S., Trindade, R.I., 2009. The position of the Amazonian Craton in supercontinents. *Gondwana Research* 15, 396-407.
- Corfu, F., 2007. Multistage metamorphic evolution and nature of the amphibolite-granulite facies transition in Lofoten-Vesterålen, Norway, revealed by U-Pb in accessory minerals. *Chemical Geology* 241, 108-128.
- Corfu, F., 2004. U-Pb age, setting and tectonic significance of the anorthosite-mangerite-charnockite-granite suite, Lofoten-Vesterålen, Norway. *Journal of Petrology* 45, 1799-1819.
- Corfu, F., 1980. U-Pb and Rb-Sr systematics in a polyorogenic segment of the Precambrian shield, central southern Norway. *Lithos* 13, 305-323.
- Corfu, F., Andersen, T.B., 2002. U-Pb ages of the Dalsfjord complex, SW Norway, and their bearing on the correlation of allochthonous crystalline segments of the Scandinavian Caledonides. *International Journal of Earth Science* 91, 955-963.
- Corfu, F., Armitage, P.E.B., Kullerud, K., Bergh, S.G., 2003. Preliminary U-Pb geochronology in the West Troms Basement Complex, North Norway: Archaean and Palaeoproterozoic events and younger overprints. *Norges Geologiske Undersøkelse Bulletin* 441, 61-72.

- Corfu, F., Emmett, T., 1992. U-Pb age of the Leirungmyran gabbroic complex, Jotun Nappe, southern Norway. *Norsk Geologisk Tidsskrift* 72, 369-374.
- Corfu, F., Laajoki, K., 2008. An uncommon episode of mafic magmatism at 1347 Ma in the Mesoproterozoic Telemark supracrustals, Sveconorwegian orogen-Implications for stratigraphy and tectonic evolution. *Precambrian Research* 160, 299-307.
- Corfu, F., Roberts, R.J., Torsvik, T.H., Ashwal, L.D., Ramsay, D.M., 2007. Peri-Gondwanan elements in the Caledonian Nappes of Finnmark, Northern Norway: Implications for the paleogeographic framework of the Scandinavian Caledonides. *American Journal of Science* 307, 434-458.
- Cornell, D.H., Austin-Hegardt, E., 2004. When, where and how did the Sveconorwegian Terranes of Sweden meet? *GFF* 126, 20.
- Creaser, R.A., Price, R.C., Wormald, R.J., 1991. A-type granites revisited: assessment of a residual-source model. *Geology* 19, 163-166.
- Crowley, J.L., Schoene, B., Bowring, S.A., 2007. U-Pb dating of zircon in the Bishop Tuff at the millennial scale. *Geology* 35, 1123-1126.
- Dahlgren, S., Heaman, L., Krogh, T., 1990. Geological evolution and U-Pb geochronology of the Proterozoic central Telemark area, Norway. *Geonytt* 17, 38-39.
- Dall'Agnol, R., de Oliveira, D.C., 2007. Oxidized, magnetite-series, rapakivi-type granites of Carajás, Brazil: Implications for classification and petrogenesis of A-type granites. *Lithos* 93, 215-233.
- Dall'Agnol, R., Rämö, O.T., De Magalhães, M.S., Macambira, M.J.B., 1999. Petrology of the anorogenic, oxidised Jamon and Musa granites, Amazonian Craton: Implications for the genesis of Proterozoic A-type granites. *Lithos* 46, 431-462.
- Dalziel, I.W.D., 1991. Pacific margins of Laurentia and East Antarctica-Australia as a conjugate rift pair: evidence and implications for an Eocambrian supercontinent. *Geology* 19, 598-601.
- Davidson, J., 1985. Mechanisms of contamination in Lesser Antilles island arc magmas from radiogenic and oxygen isotope relationships. *Earth and Planetary Science Letters* 72, 163-174.
- de Haas, G.J.L.M., Andersen, T., Vestin, J., 1999. Detrital zircon geochronology: new evidence for an old model for accretion of the SW Baltic Shield. *Journal of Geology* 107, 569-586.
- de Haas, G.J.L.M., Nijland, T.G., Andersen, T., Corfu, F., 2002. New constraints on the timing of deposition and metamorphism in the Bamble sector, south Norway: zircon and titanite U-Pb data from the Nelaug area. *GFF* 124, 73-78.
- Deering, C.D., Gravley, D.M., Vogel, T.A., Cole, J.W., Leonard, G.S., 2010. Origins of cold-wet-oxidizing to hot-dry-reducing rhyolite magma cycles and distribution in the Taupo Volcanic Zone, New Zealand. *Contributions to Mineralogy and Petrology*, 1-21.
- Defant, M.J., Drummond, M.S., 1990. Derivation of some modern arc magmas by melting of young subducted lithosphere. *Nature* 347, 662-665.
- Dickin, A.P., Higgins, M.D., 1992. Sm/Nd evidence for a major 1.5 Ga crust-forming event in the central Grenville Province. *Geology* 20, 137-140.
- Dostal, J., Dupuy, C., Carron, J.P., Le Guen de Kerneizon, M., Maury, R.C., 1983. Partition coefficients of trace elements: Application to volcanic rocks of St. Vincent, West Indies. *Geochimica et Cosmochimica Acta* 47, 525-533.
- Duchesne, J.-C., Liégeois, J.-P., Vander Auwera, J., Longhi, J., 1999. The crustal tongue melting model and the origin of massive anorthosites. *Terra Nova* 11, 100-105.

- Emslie, R.F., 1985. Proterozoic anorthosite massifs. In Tobi, A.C., Touret, J.L.R.(eds.), *The Deep Proterozoic Crust in the North Atlantic Provinces*, NATO Advanced Study Institute Series, 39-60.
- Ernst, R.E., Buchan, K.L., 2002. Maximum size and distribution in time and space of mantle plumes: Evidence from large igneous provinces. *Journal of Geodynamics* 34, 309-342.
- Ernst, R.E., Wingate, M.T.D., Buchan, K.L., Li, Z.X., 2008. Global record of 1600-700 Ma Large Igneous Provinces (LIPs): Implications for the reconstruction of the proposed Nuna (Columbia) and Rodinia supercontinents. *Precambrian Research* 160, 159-178.
- Evans, D.A.D., 2009. The palaeomagnetically viable, long-lived and all-inclusive Rodinia supercontinent reconstruction. In Murphy, J.B., Keppie, J.D. & Hynes, A.J. (Eds.) *Ancient Orogens and Modern Analogues*. Geological Society of London, Special Publication 327, 371-404.
- Ewart, A., Marsh, J.S., Milner, S.C., Duncan, A.R., Kamber, B.S., Armstrong, R.A., 2004. Petrology and geochemistry of early cretaceous bimodal continental flood volcanism of the NW Etendeka, Namibia. part 1: Introduction, mafic lavas and re-evaluation of mantle source components. *Journal of Petrology* 45, 59-105.
- Feig, S.T., Koepke, J., Snow, J.E., 2006. Effect of water on tholeiitic basalt phase equilibria: An experimental study under oxidizing conditions. *Contributions to Mineralogy and Petrology* 152, 611-638.
- Fitton, J.G., Saunders, A.D., Norry, M.J., Hardarson, B.S., Taylor, R.N., 1997. Thermal and chemical structure of the Iceland plume. *Earth and Planetary Science Letters* 153, 197-208.
- Flem, B., Grimstvedt, A., Slagstad, T., Skår, Ø., 2005. Bulkanalyse av Th og U i bergartsprøver med LA-ICP-MS. Metodebeskrivelse. NGU Rapport NGU, 2005-031, ISSN 0800-3416.
- Fossen, H., Hurich, C.A., 2005. The Hardangerfjord Shear Zone in SW Norway and the North Sea: A large-scale low-angle shear zone in the Caledonian crust. *Journal of the Geological Society* 162, 675-687.
- Foster, D.A., Gray, D.R., Spaggiari, C., Kamenov, G., Bierlein, F.P., 2009. Palaeozoic Lachlan orogen, Australia; accretion and construction of continental crust in a marginal ocean setting: Isotopic evidence from Cambrian metavolcanic rocks. In: Cawood, P.A. & Kröner, A. (eds.) *Earth Accretionary Systems in Space and Time*, Geological Society of London, Special Publication 318, 329-349.
- Frost, B.R., Barnes, C.G., Collins, W.J., Arculus, R.J., Ellis, D.J., Frost, C.D., 2001. A Geochemical Classification for Granitic Rocks. *Journal of Petrology* 42, 2033-2048.
- Frost, C.D., Frost, B.R., 1997. Reduced rapakivi-type granites: The tholeiite connection. *Geology* 25, 647-650.
- Frost, C.D., Frost, B.R., Chamberlain, K.R., Edwards, B.R., 1999. Petrogenesis of the 1.43 Ga Sherman batholith, SE Wyoming, USA: A reduced, rapakivi-type anorogenic granite. *Journal of Petrology* 40, 1771-1802.
- Fujimaki, H., Tatsumoto, M., Aoki, K., 1984. Partition coefficients of Hf, Zr, and REE between phenocrysts and groundmasses. *Journal of Geophysical Research* 89, 662-672.
- Fujinawa, A., 1988. Tholeiitic and calc-alkaline magma series at Adatara volcano, northeast Japan: 1. Geochemical constraints on their origin. *Lithos* 22, 135-158.
- Gaál, G., Gorbatshev, R., 1987. An Outline of the Precambrian evolution of the Baltic Shield. *Precambrian Research* 35, 15-52.
- Gabrielsen, R.H., 1980. The Precambrian Dyrskard group of the Hardangervidda-Ryfylke nappe complex, Haukelisæter-Røldal area, southwestern Norway. *Norges Geologiske Undersøkelse* 355, 1-20.

- Gabrielsen, R.H., Naterstad, H., Rahein, A., 1979. A Rb-Sr study of a possible Precambrian thrust zone, Hardangervidda-Ryfylke Nappe complex, southwest Norway. *Norsk Geologisk Tidsskrift* 59, 253-263.
- Gabrielsen, R.H., Solheim, S., 1980. New radiometric data on the Revsegg Formation, Hardangervidda-Ryfylke nappe complex, southwest Norway. *Norges Geologiske Undersøkelse* 355, 21-26.
- Gaetani, G.A., Grove, T.L., 1998. The influence of water on melting of mantle peridotite. *Contributions to Mineralogy and Petrology* 131, 323-346.
- Gaetani, G.A., Grove, T.L., Bryan, W.B., 1993. The influence of water on the petrogenesis of subduction-related igneous rocks. *Nature* 365, 332-334.
- Garde, A.A., Hamilton, M.A., Chadwick, B., Grocott, J., McCaffrey, K.J.W., 2002. The Ketilidian orogen of South Greenland: Geochronology, tectonics, magmatism, and fore-arc accretion during Palaeoproterozoic oblique convergence. *Canadian Journal of Earth Sciences* 39, 765-793.
- Gasparon, M., Hilton, D.R., Varne, R., 1994. Crustal contamination processes traced by helium isotopes: Examples from the Sunda arc, Indonesia. *Earth and Planetary Science Letters* 126, 15-22.
- Gastil, G., 1960. The distribution of mineral dates in time and space. *American Journal of Science* 258, 1-35.
- Gee, D.G., 1975. A tectonic model for the central part of the Scandinavian Caledonides. *American Journal of Science* 275, 468-515.
- Gee, D.G., Fossen, H., Henriksen, N., Higgins, A.K., 2008. From the early Paleozoic platforms of Baltica and Laurentia to the Caledonide Orogen of Scandinavia and Greenland. *Episodes* 31, 44-51.
- Geraldes, M.C., Van Schmus, W.R., Condie, K.C., Bell, S., Teixeira, W., Babinski, M., 2001. Proterozoic geologic evolution of the SW part of the Amazonian Craton in Mato Grosso state, Brazil. *Precambrian Research* 111, 91-128.
- Gerstenberger, H., Haase, G., 1997. A highly effective emitter substance for mass spectrometric Pb isotope ratio determinations. *Chemical Geology* 136, 309-312.
- Gibson, S.A., Thompson, R.N., Dickin, A.P., 2000. Ferropicrites: Geochemical evidence for Fe-rich streaks in upwelling mantle plumes. *Earth and Planetary Science Letters* 174, 355-374.
- Giles, D., Betts, P.G., Lister, G.S., 2004. 1.8-1.5-Ga links between the North and South Australian Cratons and the Early-Middle Proterozoic configuration of Australia. *Tectonophysics* 380, 27-41.
- Gill, J.B., 1981. *Orogenic Andesites and Plate Tectonics*. Springer-Verlag, New York, 1-390.
- Gower, C.F., 1996. The evolution of the Grenville Province in eastern Labrador, Canada. In Brewer, T.S.(ed.) *Precambrian crustal evolution in the North Atlantic Regions*. Geological Society of London, Special Publication 112, 197-218.
- Gower, C.F., 1985. Correlations between the Grenville province and Sveconorwegian orogenic belt - implications for Proterozoic evolution of the southern margins of the Canadian and Baltic Shields. In Tobi, A.C., Touret, J.L.R.(eds.), *The Deep Proterozoic Crust in the North Atlantic Provinces*, NATO Advanced Study Institute Series, 247-257.
- Gower, C.F., Kamo, S.L., Kwok, K., Krogh, T.E., 2008. Proterozoic southward accretion and Grenvillian orogenesis in the interior Grenville Province in eastern Labrador: Evidence from U-Pb geochronological investigations. *Precambrian Research* 165, 61-95.
- Gower, C.F., Ryan, A.B., Rivers, T., 1990. Mid-Proterozoic Laurentia-Baltica: an overview of its geological evolution and a summary of the contributions made by this volume. In Gower, C.F.,

- Rivers, T., Ryan, B.(eds.), Mid-Proterozoic Laurentia-Baltica, Geological Association of Canada, Special Paper 38, 1-20.
- Green, T.H., 1981. Experimental evidence for the role of accessory phases in magma genesis. *Journal of Volcanology and Geothermal Research* 10, 405-422.
- Greene, A.R., Debari, S.M., Kelemen, P.B., Blusztajn, J., Clift, P.D., 2006. A detailed geochemical study of island arc crust: The Talkeetna Arc section, south-central Alaska. *Journal of Petrology* 47, 1051-1093.
- Griffin, W.L., O'Reilly, S.Y., Afonso, J.C., Begg, G.C., 2009. The composition and evolution of lithospheric mantle: a re-evaluation and its tectonic implications. *Journal of Petrology* 50, 1185-1204.
- Griffin, W.L., Pearson, N.J., Belousova, E., Jackson, S.E., van Achterbergh, E., O'Reilly, S.Y., Shee, S.R., 2000. The Hf isotope composition of cratonic mantle: LAM-MC-ICPMS analysis of zircon megacrysts in kimberlites. *Geochimica et Cosmochimica Acta* 64, 133-147.
- Grove, T.L., Elkins-Tanton, L.T., Parman, S.W., Chatterjee, N., Müntener, O., Gaetani, G.A., 2003. Fractional crystallization and mantle-melting controls on calc-alkaline differentiation trends. *Contributions to Mineralogy and Petrology* 145, 515-533.
- Grove, T.L., Baker, M.B., 1984. Phase equilibrium controls on the tholeiitic versus calc-alkaline differentiation trends. *Journal of Geophysical Research* 89, 3253-3274.
- Haapala, I., Rämö, O.T., Frindt, S., 2005. Comparison of proterozoic and phanerozoic rift-related basaltic-granitic magmatism. *Lithos* 80, 1-32.
- Hageskov, B., 1997. Geochemistry and tectonic significance of late Gothian mafic dykes in the Østfold-Marstrand belt of SE Norway and W Sweden. *Precambrian Research* 82, 287-309.
- Hamada, M., Fujii, T., 2008. Experimental constraints on the effects of pressure and H₂O on the fractional crystallization of high-Mg island arc basalt. *Contributions to Mineralogy and Petrology* 155, 767-790.
- Handke, M.J., Tucker, R.D., Robinson, P., 1995. Contrasting U-Pb Ages for the Risberget Augen Gneiss in the Norwegian Caledonides: Getting to the root of the problem. *Geological Society of America Abstracts* 27, A-226.
- Hargrove, U.S., Stern, R.J., Kimura, J.-I., Manton, W.I., Johnson, P.R., 2006. How juvenile is the Arabian–Nubian Shield? Evidence from Nd isotopes and pre-Neoproterozoic inherited zircon in the Bi'r Umq suture zone, Saudi Arabia. *Earth and Planetary Science Letters* 252, 308-326.
- Hawkesworth, C., Cawood, P., Kemp, T., Storey, C., Dhuime, B., 2009. Geochemistry: A matter of preservation. *Science* 323, 49-50.
- Hawkesworth, C.J., Dhuime, B., Pietranik, A.B., Cawood, P.A., Kemp, A.I.S., Storey, C.D., 2010. The generation and evolution of the continental crust. *Journal of the Geological Society* 167, 229-248.
- Hawkesworth, C.J., Kemp, A.I.S., 2006. Using hafnium and oxygen isotopes in zircons to unravel the record of crustal evolution. *Chemical Geology* 226, 144-162.
- Hawkesworth, C.J., O'Nions, R.K., Arculus, R.J., 1979. Nd and Sr isotope geochemistry of island arc volcanics, Grenada, Lesser Antilles. *Earth and Planetary Science Letters* 45, 237-248.
- He, Y., Zhao, G., Sun, M., Han, Y., 2010. Petrogenesis and tectonic setting of volcanic rocks in the Xiaoshan and Waifangshan areas along the southern margin of the North China Craton: Constraints from bulk-rock geochemistry and Sr-Nd isotopic composition. *Lithos* 114, 186-199.

- He, Y., Zhao, G., Sun, M., Wilde, S.A., 2008. Geochemistry, isotope systematics and petrogenesis of the volcanic rocks in the Zhongtiao Mountain: An alternative interpretation for the evolution of the southern margin of the North China Craton. *Lithos* 102, 158-178.
- Hildreth, W., Moorbath, S., 1988. Crustal contributions to arc magmatism in the Andes of Central Chile. *Contributions to Mineralogy and Petrology* 98, 455-489.
- Hill, B.M., Bickford, M.E., 2001. Paleoproterozoic rocks of central Colorado: Accreted arcs or extended older crust? *Geology* 29, 1015-1018.
- Hirata, T., 1997. Soft ablation technique for laser ablation-inductively coupled plasma mass spectrometry. *Journal of Analytical Atomic Spectrometry* 12, 1337-1342.
- Hirata, T., Nesbitt, R.W., 1995. U-Pb isotope geochronology of zircon: evaluation of the laser probe-inductively coupled plasma mass spectrometry technique. *Geochimica et Cosmochimica Acta* 59, 2491-2500.
- Hoffman, P.F., 1997. Tectonic genealogy of North America. In: van der Pluijm, B.A., Marshak, S., (eds.) *Earth structure: An introduction to structural geology and tectonics*, 459-464.
- Hoffman, P.F., 1988. United plates of America, the birth of a craton: Early Proterozoic assembly and growth of Laurentia. *Annual review of Earth and Planetary Sciences* 16, 543-603.
- Hoffman, P.F., 1991. Did the breakout of Laurentia turn Gondwanaland inside-out? *Science* 252, 1409-1412.
- Högdahl, K., Andersson, U.B., Eklund, O., 2004. The Transscandinavian Igneous Belt (TIB) in Sweden: A review of its character and evolution. *Special Paper of the Geological Survey of Finland* 37, 1-125.
- Hooper, P.R., 2000. Chemical discrimination of Columbia River basalt flows. *Geochemistry Geophysics Geosystems* 1 (6).
- Hora, J.M., Singer, B.S., Wörner, G., Beard, B.L., Jicha, B.R., Johnson, C.M., 2009. Shallow and deep crustal control on differentiation of calc-alkaline and tholeiitic magma. *Earth and Planetary Science Letters* 285, 75-86.
- Horn, I., Rudnick, R.L., McDonough, W.F., 2000. Precise elemental and isotope ratio determination by simultaneous solution nebulization and laser ablation-ICP-MS: application to U-Pb geochronology. *Chemical Geology* 164, 281-301.
- Horstwood, M.S.A., Foster, G.L., Parrish, R.R., Noble, S.R., Nowell, G.M., 2003. Common-Pb corrected in situ U-Pb accessory mineral geochronology by LA-MC-ICP-MS. *Journal of Analytical Atomic Spectrometry* 18, 837-846.
- Horstwood, M.S.A., Parrish, R.R., Condon, D.J., Pashley, V., 2006. Laser ablation acquisition protocols and non-matrix matched standardisation of U-Pb data. *Geochimica et Cosmochimica Acta* 70, Supplement 1, A264.
- Hou, G., Santosh, M., Qian, X., Lister, G.S., Li, J., 2008a. Configuration of the Late Paleoproterozoic supercontinent Columbia: Insights from radiating mafic dyke swarms. *Gondwana Research* 14, 395-409.
- Hou, G., Santosh, M., Qian, X., Lister, G.S., Li, J., 2008b. Tectonic constraints on 1.3~1.2 Ga final breakup of Columbia supercontinent from a giant radiating dyke swarm. *Gondwana Research* 14, 561-566.
- Hubbard, F.H., 1975. The Precambrian crystalline complex of SW Sweden. The geology and petrogenetic development of the Varberg Region. *GFF* 97, 223-236.

- Hunter, A.G., 1998. Intracrustal Controls on the Coexistence of Tholeiitic and Calc-alkaline Magma Series at Aso Volcano, SW Japan. *Journal of Petrology* 39, 1255-1284.
- Iizuka, T., Komiya, T., Rino, S., Maruyama, S., Hirata, T., 2010. Detrital zircon evidence for Hf isotopic evolution of granitoid crust and continental growth. *Geochimica et Cosmochimica Acta* 74, 2450-2472.
- Irvine, T.N., Baragar, W.R.A., 1971. A guide to the chemical classification of the common volcanic rocks. *Canadian Journal of Earth Sciences* 8, 523-548.
- Jackson, S.E., Pearson, N.J., Griffin, W.L., Belousova, E.A., 2004. The application of laser ablation-inductively coupled plasma-mass spectrometry to in situ U–Pb zircon geochronology. *Chemical Geology* 211, 47-69.
- James, D.E., 1981. The combined use of oxygen and radiogenic isotopes as indicators of crustal contamination. *Annual Reviews in Earth and Planetary Science* 15, 395-396.
- Johansson, Å., 1990. Age of the Önnestad syenite and some gneissic granites along the southern part of the Protogine Zone, southern Sweden. In Gower, C.F., Rivers, T., Ryan, B.(eds.), *Mid-Proterozoic Laurentia-Baltica*, Geological Association of Canada, Special Paper 38, 131-148.
- Johansson, Å., 2009. Baltica, Amazonia and the SAMBA connection-1000 million years of neighbourhood during the Proterozoic? *Precambrian Research* 175, 221-234.
- Johansson, L., Schöberg, H., Solyom, Z., 1993. The age and regional correlation of the Svecofennian Geitfjell granite, Vestranden, Norway. *Norsk Geologisk Tidsskrift* 73, 133-143.
- Karlstrom, K.E., Åhäll, K.-I., Harlan, S.S., Williams, M.L., McLelland, J., Geissman, J.W., 2001. Long-lived (1.8-1.0 Ga) convergent orogen in southern Laurentia, its extensions to Australia and Baltica, and implications for refining Rodinia. *Precambrian Research* 111, 5-30.
- Karlstrom, K.E., Harlan, S.S., Williams, M.L., McLelland, J., Geissman, J.W., Åhäll, K.-I., 1999. Refining Rodinia: Geologic evidence for the Australia-Western U.S. Connection in the Proterozoic. *GSA Today* 9, 2-7.
- Kawamoto, T., 1996. Experimental constraints on differentiation and H₂O abundance of calc-alkaline magmas. *Earth and Planetary Science Letters* 144, 577-589.
- Kay, S.M., Kay, R.W., 1985. Role of crystal cumulates and the oceanic crust in the formation of the lower crust of the Aleutian arc. *Geology* 13, 461-464.
- Kay, S.M., Kay, R.W., Citron, G.P., 1982. Tectonic controls on tholeiitic and calc-alkaline magmatism in the Aleutian Arc. *Journal of Geophysical Research* 87, 4051-4072.
- Kelemen, P.B., Shimizu, N., Dunn, T., 1993. Relative depletion of niobium in some arc magmas and the continental crust: partitioning of K, Nb, La and Ce during melt/rock reaction in the upper mantle. *Earth and Planetary Science Letters* 120, 111-134.
- Kemp, A.I.S., Hawkesworth, C.J., Collins, W.J., Gray, C.M., Blevin, P.L., 2009. Isotopic evidence for rapid continental growth in an extensional accretionary orogen: The Tasmanides, eastern Australia. *Earth and Planetary Science Letters* 284, 455-466.
- Kemp, A.I.S., Hawkesworth, C.J., Foster, G.L., Paterson, B.A., Woodhead, J.D., Hergt, J.M., Gray, C.M., Whitehouse, M.J., 2007. Magmatic and crustal differentiation history of granitic rocks from Hf-O isotopes in zircon. *Science* 315, 980-983.
- Kemp, A.I.S., Wormald, R.J., Whitehouse, M.J., Price, R.C., 2005. Hf isotopes in zircon reveal contrasting sources and crystallization histories for alkaline to peralkaline granites of Temora, southeastern Australia. *Geology* 33, 797-800.

- Kerr, A., Ryan, B., Gower, C.F., Wardle, R.J., 1996. The Makkovik Province: extension of the Ketilidian Mobile Belt in mainland North America. In: Brewer, T.S.(ed.) Precambrian crustal evolution in the North Atlantic Regions. Geological Society of London, Special Publication 112, 155-177.
- Ketchum, J.W.F., Jackson, S.E., Culshaw, N.G., Barr, S.M., 2001. Depositional and tectonic setting of the Paleoproterozoic Lower Aillik Group, Makkovik Province, Canada: Evolution of a passive margin-foredeep sequence based on petrochemistry and U-Pb (TIMS and LAM-ICP-MS) geochronology. *Precambrian Research* 105, 331-356.
- Kirkland, C.L., Daly, J.S., Whitehouse, M.J., 2008a. Basement-cover relationships of the Kalak Nappe Complex, Arctic Norwegian Caledonides and constraints on Neoproterozoic terrane assembly in the North Atlantic region. *Precambrian Research* 160, 245-276.
- Kirkland, C.L., Daly, J.S., Whitehouse, M.J., 2006. Granitic magmatism of grenvillian and late neoproterozoic age in Finnmark, Arctic Norway - Constraining pre-Scandian deformation in the Kalak Nappe Complex. *Precambrian Research* 145, 24-52.
- Kirkland, C.L., Daly, J.S., Whitehouse, M.J., 2007. Provenance and terrane evolution of the Kalak Nappe Complex, Norwegian Caledonides: Implications for neoproterozoic paleogeography and tectonics. *Journal of Geology* 115, 21-41.
- Kirkland, C.L., Strachan, R.A., Prave, A.R., 2008b. Detrital zircon signature of the Moine Supergroup, Scotland: Contrasts and comparisons with other Neoproterozoic successions within the circum-North Atlantic region. *Precambrian Research* 163, 332-350.
- Knudsen, T.-L., Andersen, T., 1999. Petrology and geochemistry of the Tromøy gneiss complex, South Norway, an alleged example of Proterozoic depleted lower continental crust. *Journal of Petrology* 40, 909-933.
- Knudsen, T.-L., Andersen, T., Whitehouse, M.J., Vestin, J., 1997. Detrital zircon ages from southern Norway - implications for the Proterozoic evolution of the southwestern Baltic Shield. *Contributions to Mineralogy and Petrology* 130, 47-58.
- Korja, A., Lahtinen, R., Nironen, M., 2006. The Svecofennian orogen: a collage of microcontinents and island arcs. In: Gee, D.G. and Stephenson, R.A. (Eds.), *European Lithosphere Dynamics*. Geological Society of London Memoirs 32, 561-578.
- Krogh, T.E., 1973. A low-contamination method for hydrothermal decomposition of zircon and extraction of U and Pb for isotopic age determinations. *Geochimica et Cosmochimica Acta* 37, 485-494.
- Krogh, T.E., 1982. Improved accuracy of U-Pb zircon ages by the creation of more concordant systems using an air abrasion technique. *Geochimica et Cosmochimica Acta* 46, 637-649.
- Kröner, A., Windley, B.F., Badarch, G., Tomurtogoo, O., Hegner, E., Jahn, B.M., Gruschka, S., Khain, E.V., Demoux, A., Wingate, M.T.D., 2007. Accretionary growth and crust formation in the Central Asian Orogenic Belt and comparison with the Arabian-Nubian shield. In: Hatcher, R.D., Carlson, M.P., McBride, J.J., & Martínez Catalán, J.R. (eds.) *4-D Framework of Continental Crust*, Geological Society of America Memoir 200, 181-209.
- Kullerud, K., Skjerlie, K.P., Corfu, F., de la Rosa, J.D., 2006. The 2.40 Ga Ringvassøy mafic dykes, West Troms Basement Complex, Norway: The concluding act of early Palaeoproterozoic continental breakup. *Precambrian Research* 150, 183-200.
- Kuritani, T., Kitagawa, H., Nakamura, E., 2005. Assimilation and fractional crystallization controlled by transport process of crustal melt: Implications from an alkali basalt-dacite suite from Rishiri Volcano, Japan. *Journal of Petrology* 46 (7), 1421-1442.
- Kusky, T., Li, J., Santosh, M., 2007. The Paleoproterozoic North Hebei Orogen: North China craton's collisional suture with the Columbia supercontinent. *Gondwana Research* 12, 4-28.

- Kusky, T.M., Santosh, M., 2009. The Columbia connection in North China. In: Reddy, S.M., Mazumber, R., Evans, D.A.D. & Collins, A.S. (Eds.) Palaeoproterozoic Supercontinents and Global Evolution. Geological Society of London, Special Publication 323, 49-71.
- Laajoki, K., Corfu, F., 2007. Lithostratigraphy of the Mesoproterozoic Vemork formation, central Telemark, Norway. *Bulletin of the Geological Society of Finland* 79, 41-67.
- Laajoki, K., Corfu, F., Andersen, T., 2002. Lithostratigraphy and U-Pb geochronology of the Telemark supracrustals in the Bandak-Sauland area, Telemark, South Norway. *Norsk Geologisk Tidsskrift* 82, 119-138.
- Lackey, J.S., Valley, J.W., Saleeby, J.B., 2005. Supracrustal input to magmas in the deep crust of Sierra Nevada batholith: Evidence from high- $\delta^{18}\text{O}$ zircon. *Earth and Planetary Science Letters* 235, 315-330.
- Ladenberger, A., Gee, D.G., Claesson, S., Majka, J., 2009. Interpreting Himalayan orogeny via the Paleozoic Scandian analogue. *Geochimica et Cosmochimica Acta* 73, Supplement 1, A714.
- Lahtinen, R., Korja, A., Nironen, M., Heikkinen, P., 2009. Palaeoproterozoic accretionary processes in Fennoscandia. In: Cawood, P.A. & Kröner, A. (eds.) *Earth Accretionary Systems in Space and Time*, Geological Society of London, Special Publication 318, 237-256.
- Landenberger, B., Collins, W.J., 1996. Derivation of A-type granites from a dehydrated charnockitic lower crust: Evidence from the Chaelundi Complex, Eastern Australia. *Journal of Petrology* 37, 145-170.
- Larsen, B.T., Olaussen, S., Sundvoll, B., Heeremans, M., 2008. The Permo-carboniferous Oslo rift through six stages and 65 million years. *Episodes* 31, 52-58.
- Larsen, Ø., Skår, Ø., Pedersen, R.-B., 2002. U-Pb zircon and titanite geochronological constraints on the late/post-Caledonian evolution of the Scandinavian Caledonides in north-central Norway. *Norsk Geologisk Tidsskrift* 82, 1-13.
- Larson, S.Å., Berglund, J., Stigh, J., Tullborg, E.-L., 1990. The Protogine Zone, southwest Sweden: a new model - an old issue. In Gower, C.F., Rivers, T., Ryan, B.(eds.), *Mid-Proterozoic Laurentia-Baltica*, Geological Association of Canada, Special Paper 38, 317-333.
- Larson, S.Å., Cornell, D.H., Armstrong, R.A., 1999. Emplacement ages and metamorphic overprinting of granitoids in the Sveconorwegian Province in Varmland, Sweden - an ion probe study. *Norsk Geologisk Tidsskrift* 79, 97-96.
- Leeman, W.P., Vitaliano, C.J., Prinz, M., 1976. Evolved lavas from the Snake River Plain: Craters of the Moon National Monument, Idaho. *Contributions to Mineralogy and Petrology* 56, 35-60.
- Li, Z.-X., Bogdanova, S.V., Collins, A.S., Davidson, A., De Waele, B., Ernst, R.E., Fitzsimons, I.C.W., Fuck, R.A., Gladkochub, D.P., Jacobs, J., Karlstrom, K.E., Lu, S., Natapov, L.M., Pease, V., Pisarevsky, S.A., Thrane, K., Vernikovsky, V., 2008. Assembly, configuration, and break-up history of Rodinia: A synthesis. *Precambrian Research* 160, 179-210.
- Li, Z.-X., Zhong, S., 2009. Supercontinent-superplume coupling, true polar wander and plume mobility: Plate dominance in whole-mantle tectonics. *Physics of the Earth and Planetary Interiors* 176, 143-156.
- Liégeois, J.-P., Stern, R.J., 2010. Sr-Nd isotopes and geochemistry of granite-gneiss complexes from the Meatiq and Hafafit domes, Eastern Desert, Egypt: No evidence for pre-Neoproterozoic crust. *Journal of African Earth Sciences* 57, 31-40.
- Longhi, J., Vander Auwera, J., Fram, M.S., Duchesne, J., 1999. Some Phase Equilibrium Constraints on the Origin of Proterozoic (Massif) Anorthosites and Related Rocks. *Journal of Petrology* 40, 339-362.

- Longhi, J., Fram, M.S., Vander Auwera, J., Montieth, J.N., 1993. Pressure effects, kinetics, and rheology of anorthositic and related magmas. *American Mineralogist* 78, 1016-1030.
- Ludwig, K.R., 2003. User's manual for Isoplot 3.00 A Geochronological Toolkit for Excel. Berkeley Geochronological Center Special Publication 4.
- Lundberg, B., 1973. Granite intrusions in the Dal group, Central Sweden. *GFF* 95, 113-119.
- Lundmark, A.M., Corfu, F., 2008. Late-orogenic Sveconorwegian massif anorthosite in the Jotun Nappe Complex, SW Norway, and causes of repeated AMCG magmatism along the Baltoscandian margin. *Contributions to Mineralogy and Petrology* 155, 147-163.
- Lundmark, A.M., Corfu, F., Spürgin, S., Selbekk, R.S., 2007. Proterozoic evolution and provenance of the high-grade Jotun Nappe Complex, SW Norway: U-Pb geochronology. *Precambrian Research* 159, 133-154.
- Marsh, B.D., 1982. On the mechanics of igneous diapirism, stoping, and zone melting. *American Journal of Science* 282, 808-855.
- Martin, R.F., 2006. A-type granites of crustal origin ultimately result from open-system fenitization-type reactions in an extensional environment. *Lithos* 91, 125-136.
- Maruyama, S., Santosh, M., Zhao, D., 2007. Superplume, supercontinent, and post-perovskite: Mantle dynamics and anti-plate tectonics on the Core-Mantle Boundary. *Gondwana Research* 11, 7-37.
- Mattinson, J.M., 1997. Analysis of zircon by multi-step partial dissolutions: The good, the bad, and the ugly. Geological Association of Canada Annual Meeting, Program with abstracts, Ontario, A98.
- Mattinson, J.M., 2005. Zircon U-Pb chemical abrasion ("CA-TIMS") method: Combined annealing and multi-step partial dissolution analysis for improved precision and accuracy of zircon ages. *Chemical Geology* 220, 47-66.
- McCammon, C., 2005. The paradox of mantle redox. *Science* 308, 807-808.
- McCulloch, M.T., Gamble, J.A., 1991. Geochemical and geodynamical constraints on subduction zone magmatism. *Earth and Planetary Science Letters* 102, 358-374.
- McCurry, M., Hayden, K.P., Morse, L.H., Mertzman, S., 2008. Genesis of post-hotspot, A-type rhyolite of the Eastern Snake River Plain volcanic field by extreme fractional crystallization of olivine tholeiite. *Bulletin of Volcanology* 70, 361-383.
- Menuge, J.F., 1988. The petrogenesis of massif anorthosites: a Nd and Sr isotopic investigation of the Proterozoic of Rogaland/Vest-Agder, SW Norway. *Contributions to Mineralogy and Petrology* 98, 363.
- Menuge, J.F., Brewer, T.S., 1996. Mesoproterozoic anorogenic magmatism in southern Norway. In Brewer, T.S.(ed.), *Precambrian crustal evolution in the North Atlantic Region*. Geological Society of London, Special Publication 112, 275-295.
- Menuge, J.F., Daly, J.S., 1994. The Annagh Gneiss Complex in County Mayo, Ireland. In: Gibbons, W. and Harris, A.L. (Eds.), *A Revised Correlation of Precambrian Rocks in the British Isles*. Geological Society of London Special Report 22, 59-62.
- Miller, C.F., McDowell, S.M., Mapes, R.W., 2003. Hot and cold granites: Implications of zircon saturation temperatures and preservation of inheritance. *Geology* 31, 529-532.
- Miller, R.G., O'Nions, R.K., Hamilton, P.J., Welin, E., 1986. Crustal residence ages of clastic sediments, orogeny and continental evolution. *Chemical Geology* 57, 87-99.

- Mitchell, J.N., Scoates, J.S., Frost, C.D., Kolker, A., 1996. The geochemical evolution of anorthosite residual magmas in the Laramie anorthosite complex, Wyoming. *Journal of Petrology* 37, 637-660.
- Möller, A., O'Brien, P.J., Kennedy, A., Kröner, A., 2002. Polyphase zircon in ultrahigh-temperature granulites (Rogaland, SW Norway): constraints for Pb diffusion in zircon. *Journal of Metamorphic Geology* 20, 727.
- Möller, A., O'Brien, P.J., Kennedy, A., Kröner, A., 2003. Linking growth episodes of zircon and metamorphic textures to zircon chemistry: An example from the ultrahigh-temperature granulites of Rogaland (SW Norway). *Geological Society Special Publication*, 65-81.
- Möller, C., Andersson, J., Lundqvist, I., Hellström, F., 2007. Linking deformation, migmatite formation and zircon U-Pb geochronology in polymetamorphic orthogneisses, Sveconorwegian Province, Sweden. *Journal of Metamorphic Geology* 25, 727-750.
- Moorbath, S., 1978. Timing of continental growth and emergence. *Nature* 273, 75-76.
- Morton, A.C., Taylor, P.N., 1991. Geochemical and isotopic constraints on the nature and age of basement rocks from Rockall Bank, NE Atlantic. *Journal of the Geological Society* 148, 631-634.
- Muir, R.J., Fitches, W.R., Maltman, A.J., 1994. The Rhinns Complex: Proterozoic basement on Islay and Colonsay, Inner Hebrides, Scotland, and on Inishtrahull, NW Ireland. *Transactions of the Royal Society of Edinburgh: Earth Sciences* 85, 77-90.
- Murphy, J.B., Nance, R.D., 2003. Do supercontinents introvert or extrovert?: Sm-Nd isotope evidence. *Geology* 31, 873-876.
- Murphy, J.B., Nance, R.D., Gutiérrez-Alonso, G., Keppie, J.D., 2009. Supercontinent reconstruction from recognition of leading continental edges. *Geology* 37, 595-598.
- Myers, J.D., Krishna Sinha, A., Marsh, B.D., 1984. Assimilation of crustal material by basaltic magma: strontium isotopic and trace element data from the Edgecumbe volcanic field, SE Alaska. *Journal of Petrology* 25, 1-26.
- Naterstad, J., Andresen, A., Jorde, K., 1973. Tectonic succession of the Caledonian Nappe Front in the Haukelisæter-Røldal Area, Southwestern Norway. *NGU Bulletin* 292, 1-20.
- Nekvasil, H., Dondolini, A., Horn, J., Filiberto, J., Long, H., Lindsley, D.H., 2004. The origin and evolution of silica-saturated alkalic suites: An experimental study. *Journal of Petrology* 45, 693-721.
- Nekvasil, H., Dondolini, A., Litvin, V., Rossier, L., Lindsley, D., 2001. Linking tholeiites and alkalic rocks: the role of dissolved water. *GSA Annual Meeting, Abstracts*, 33-0.
- Nowell, G., Parrish, R.R., 2001. Simultaneous acquisition of isotope compositions and parent/daughter ratios by non-isotope dilution solution-mode Plasma Ionisation Multi-collector Mass Spectrometry (PIMMS). *7th International Conference on Plasma Source Mass Spectrometry* 267, 298-310.
- O'Nions, R.K., Evensen, N.M., Hamilton, P.J., 1979. Geochemical modeling of mantle differentiation and crustal growth. *Journal of Geophysical Research* 84, 6091-6101.
- Park, R.G., Åhäll, K., Boland, M.P., 1991. The Sveconorwegian shear-zone network of SW Sweden in relation to mid-Proterozoic plate movements. *Precambrian Research* 49, 245-260.
- Parkinson, I.J., Arculus, R.J., 1999. The redox state of subduction zones: Insights from arc-peridotites. *Chemical Geology* 160, 409-423.

- Patchett, P.J., Tatsumoto, M., 1981. A routine high-precision method for Lu-Hf isotope geochemistry and chronology. *Contributions to Mineralogy and Petrology* 75, 263-267.
- Patiño Douce, A.E., 1997. Generation of metaluminous A-type granites by low-pressure melting of calc-alkaline granitoids. *Geology* 25, 743-746.
- Paulsson, O., Andréasson, P.-G., 2002. Attempted break-up of Rodinia at 850 Ma: Geochronological evidence from the Seve-Kalak Superterrane, Scandinavian Caledonides. *Journal of the Geological Society* 159, 751-761.
- Payne, J.L., Ferris, G., Barovich, K.M., Hand, M., 2010. Pitfalls of classifying ancient magmatic suites with tectonic discrimination diagrams: An example from the Paleoproterozoic Tunkillia Suite, southern Australia. *Precambrian Research* 177, 227-240.
- Payne, J.L., Hand, M., Barovich, K.M., Reid, A., Evans, D.A.D., 2009. Correlations and reconstruction models for the 2500-1500 Ma evolution of the Mawson Continent. In: Reddy, S.M., Mazumber, R., Evans, D.A.D. & Collins, A.S. (Eds.) *Palaeoproterozoic Supercontinents and Global Evolution*. Geological Society of London, Special Publication 323, 319-355.
- Pearce, J.A., 1983. Role of the sub-continental lithosphere in magma genesis at active continental margins. In: Hawesworth, C.J. & Norry, M.J. (eds.) *Continental Basalts and Mantle Xenoliths*, Cheshire, U.K., Shiva Publishing Limited, 230-249.
- Pearce, J.A., 1982. Trace element characteristics of lavas from destructive plate boundaries. In: Thorpe, R.S. (ed.) *Andesites: Orogenic Andesites and Related Rocks*, Chichester, U.K., John Wiley & Sons, 525-548.
- Pearce, J.A., Kempton, P.D., Nowell, G.M., Noble, S.R., 1999. Hf-Nd element and isotope perspective on the nature and provenance of mantle and subduction components in Western Pacific Arc-basin systems. *Journal of Petrology* 40, 1579-1611.
- Peck, W.H., Valley, J.W., Corriveau, L., Davidson, A., McLelland, J., Farber, D.A., 2004. Oxygen-isotope constraints on terrane boundaries and origin of 1.18-1.13 Ga granitoids in the southern Grenville Province. In: Tollo, R.P., Corriveau, L., McLelland, J. and Bartholomew, M.J.I. (Eds.), *Proterozoic Tectonic Evolution of the Grenville Orogen in North America*. Geological Society of America Memoir 197, 163-182.
- Pedersen, S., Andersen, T., Konnerup-Madsen, J., Griffin, W.L., 2009. Recurrent Mesoproterozoic continental magmatism in South-Central Norway. *International Journal of Earth Science* 98, 1151-1171.
- Peng, P., Zhai, M., Ernst, R.E., Guo, J., Liu, F., Hu, B., 2008. A 1.78 Ga large igneous province in the North China craton: The Xiong'er Volcanic Province and the North China dyke swarm. *Lithos* 101, 260-280.
- Persson, P.O., Wahlgren, C.H., Hansen, B.T., 1983. U-Pb ages of Proterozoic metaplutonics in the gneiss complex of southern Varmland, south-western Sweden. *GFF* 105, 1-8.
- Pesonen, L.J., Elming, S.-Å., Mertanen, S., Pisarevsky, S., D'Agrella-Filho, M.S., Meert, J.G., Schmidt, P.W., Abrahamsen, N., Bylund, G., 2003. Palaeomagnetic configuration of continents during the Proterozoic. *Tectonophysics* 375, 289-324.
- Petford, N., Cruden, A.R., McCaffrey, K.J.W., Vigneresse, J.-L., 2000. Granite magma formation, transport and emplacement in the Earth's crust. *Nature* 408, 669-673.
- Philpotts, J.A., Schnetzler, C.C., 1970. Phenocryst-matrix partition coefficients for K, Rb, Sr and Ba, with applications to anorthosite and basalt genesis. *Geochimica et Cosmochimica Acta* 34, 307-322.
- Pietranik, A.B., Hawkesworth, C.J., Storey, C., Kemp, T., 2009. Depleted mantle evolution and how it is recorded in zircon. *Geochimica et Cosmochimica Acta* 73, Supplement 1, A1028.

- Piontek, J.E., Connelly, J.N., Åhäll, K.-I., 1998. 1.3 Ga anorogenic magmatism in Southwest Sweden. *GSA Annual Meeting* 30, A293.
- Plank, T., Langmuir, C.H., 1993. Tracing trace elements from sediment input to volcanic output at subduction zones. *Nature* 362, 739-743.
- Pózer Bue, E., 2008. Age and origin of the Mesoproterozoic basement of the Nesodden Peninsula, SE Norway, A geochronological and isotopic study. Unpublished Masters Thesis. University of Oslo.
- Putirka, K.D., Kuntz, M.A., Unruh, D.M., Vaid, N., 2009. Magma evolution and ascent at the craters of the moon and neighboring volcanic fields, Southern Idaho, USA: Implications for the evolution of polygenetic and monogenetic volcanic fields. *Journal of Petrology* 50, 1639-1665.
- Ragnhildstveit, J., Sigmond, E.M.O., Tucker, R.D., 1994. Early Proterozoic supracrustal rocks west of the Mandal-Ustaoset fault zone, Hardangervidda, South Norway. *Terra Nova Abstract Supplement* 2, 15-16.
- Reagan, M.K., Sims, K.W.W., Erich, J., Thomas, R.B., Cheng, H., Edwards, R.L., Layne, G., Ball, L., 2003. Time-scales of differentiation from mafic parents to rhyolite in North American Continental Arcs. *Journal of Petrology* 44, 1703-1726.
- Rehnström, E.F., 2003. Geochronology and petrology of the Tielma Magmatic Complex, northern Swedish Caledonides - Results and tectonic implications. *Norsk Geologisk Tidsskrift* 83, 243-257.
- Rehnstrom, E.F., Corfu, F., 2004. Palaeoproterozoic U-Pb ages of autochthonous and allochthonous granites from the northern Swedish Caledonides - Regional and palaeogeographic implications. *Precambrian Research* 132, 363-378.
- Rehnström, E.F., Corfu, F., Torsvik, T.H., 2002. Evidence of a late Precambrian (637 Ma) deformational event in the Caledonides of northern Sweden. *Journal of Geology* 110, 591-601.
- Rehnström, E.F., Torsvik, T.H., 2003. Cambrian sediments and Proterozoic granites in the Dividalen-Torneträsk area, northern Scandinavia: Palaeomagnetism and U-Pb geochronology. *GFF* 125, 131-138.
- Rimša, A., Johansson, L., Whitehouse, M.J., 2007. Constraints on incipient charnockite formation from zircon geochronology and rare earth element characteristics. *Contributions to Mineralogy and Petrology* 154, 357-369.
- Roberts, D., 2007. Palaeocurrent data from the Kalak Nappe Complex, northern Norway: A key element in models of terrane affiliation. *Norsk Geologisk Tidsskrift* 87, 319-328.
- Roberts, D., 2003. The Scandinavian Caledonides: Event chronology, palaeogeographic settings and likely modern analogues. *Tectonophysics* 365, 283-299.
- Roberts, D., Gee, D.G., 1985. An introduction to the structure of the Scandinavian Caledonides. In: Gee, D.G. & Sturt, B.A. (eds.) *The Caledonian Orogen - Scandinavia and Related areas*, Chichester, U.K., John Wiley & Sons, 56-68.
- Roberts, D., Nissen, A.L., Walker, N., 1999. U-Pb zircon age and geochemistry of the Blafjellhatten granite, Grong-Olden Culmination, Central Norway. *Norsk Geologisk Tidsskrift* 79, 161-168.
- Rogers, J.J.W., Santosh, M., 2002. Configuration of Columbia, a Mesoproterozoic Supercontinent. *Gondwana Research* 5, 5-22.
- Røhr, T.S., Corfu, F., Austrheim, H., Andersen, T.B., 2004. Sveconorwegian U-Pb zircon and monazite ages of granulite-facies rocks, Hisarøya, Gulen, Western Gneiss Region, Norway. *Norsk Geologisk Tidsskrift* 84, 251-256.

- Rollinson, H.R., 1993. Using geochemical data: evaluation, presentation, interpretation. Longman Geochemistry Series, London , 66-71.
- Romer, R.L., 1996. Contiguous Laurentia and Baltica before the Grenvillian-Sveconorwegian orogeny? *Terra Nova* 8, 173-181.
- Romer, R.L., 2003. Alpha-recoil in U-Pb geochronology: Effective sample size matters. *Contributions to Mineralogy and Petrology* 145, 481-491.
- Romer, R.L., Smeds, S.A., 1996. U-Pb columbite ages of pegmatites from Sveconorwegian terranes in southwestern Sweden. *Precambrian Research* 76, 15-30.
- Root, D.B., Hacker, B.R., Gans, P.B., Ducea, M.N., Eide, E.A., Mosenfelder, J.L., 2005. Discrete ultrahigh-pressure domains in the Western Gneiss Region, Norway: Implications for formation and exhumation. *Journal of Metamorphic Geology* 23, 45-61.
- Root, D.B., Hacker, B.R., Mattinson, J.M., Wooden, J.L., 2004. Zircon geochronology and ca. 400 Ma exhumation of Norwegian ultrahigh-pressure rocks: An ion microprobe and chemical abrasion study. *Earth and Planetary Science Letters* 228, 325-341.
- Rowe, M.C., Kent, A.J.R., Nielsen, R.L., 2009. Subduction influence on oxygen fugacity and trace and volatile elements in basalts across the cascade volcanic arc. *Journal of Petrology* 50, 61-91.
- Rudnick, R.L., Gao, S., 2003. Composition of the continental crust. *Treatise on Geochemistry* 3, 1-64.
- Sakuyama, M., 1981. Petrological study of the Myoko and Kurohime volcanoes, Japan: crystallization sequence and evidence for magma mixing. *Journal of Petrology* 22, 553-583.
- Salters, V.J.M., Stracke, A., 2004. Composition of the depleted mantle. *Geochemistry Geophysics Geosystems* 5.
- Santosh, M., 2010. Assembling North China Craton within the Columbia supercontinent: The role of double-sided subduction. *Precambrian Research* 178, 149-167.
- Saunders, A.D., Norry, M.J., Tarney, J., 1991. Fluid influence on the trace element compositions of subduction zone magmas. *Philosophical Transactions of the Royal Society of London*, A335, 377-392.
- Saunders, A.D., Tarney, J., Weaver, S.D., 1980. Transverse geochemical variations across the Antarctic Peninsula: Implications for the genesis of calc-alkaline magmas. *Earth and Planet Science Letters* 46, 344-360.
- Schärer, U., 1980. U-Pb and Rb-Sr dating of a polymetamorphic nappe terrain: The Caledonian Jotun nappe, southern Norway. *Earth and Planetary Science Letters* 49, 205-218.
- Schärer, U., Wilmar, E., Duchesne, J.-C., 1996. The short duration and anorogenic character of anorthosite magmatism: U-Pb dating of the Rogaland complex, Norway. *Earth and Planetary Science Letters* 139 , 335-350.
- Schellart, W.P., 2008. Subduction zone trench migration: Slab driven or overriding-plate-driven? *Physics of the Earth and Planetary Interiors* 170, 73-88.
- Schellart, W.P., Stegman, D.R., Freeman, J., 2008. Global trench migration velocities and slab migration induced upper mantle volume fluxes: Constraints to find an Earth reference frame based on minimizing viscous dissipation. *Earth Science Reviews* 88, 118-144.
- Scherstén, A., 2002. ¹⁸⁷Re-¹⁸⁷Os evidence for crustal lenses of Svecofennian age within the Mylonite Zone, SW Sweden. *GFF* 124, 35-39.

- Schiellerup, H., Lambert, D.D., Prestvik, T., Robins, B., McBride, J.S., Larsen, R.B., 2000. Re-Os isotopic evidence for a lower crustal origin of massif-type anorthosites. *Nature* 405, 781-784.
- Schmitz, M.D., Schoene, B., 2007. Derivation of isotope ratios, errors, and error correlations for U-Pb geochronology using ^{205}Pb - ^{235}U -(^{233}U)-spiked isotope dilution thermal ionization mass spectrometric data. *Geochemistry Geophysics Geosystems* 8.
- Schnetzer, C.C., Philpotts, J.A., 1970. Partition coefficients of rare-earth elements between igneous matrix material and rock-forming mineral phenocrysts-II. *Geochimica et Cosmochimica Acta* 34, 331-340.
- Schock, H.H., 1979. Distribution of rare-earth and other trace elements in magnetites. *Chemical Geology* 26, 119-133.
- Scholl, D.W., Von Huene, R., 2009. Implications of estimated magmatic additions and recycling losses at the subduction zones of accretionary (non-collisional) and collisional (suturing) orogens. In: Cawood, P.A. & Kröner, A. (eds.) *Earth Accretionary Systems in Space and Time*, Geological Society of London, Special Publication 318, 105-125.
- Scholl, D.W., Von Huene, R., 2007. Crustal recycling at modern subduction zones applied to the past-issues of growth and preservation of continental basement crust, mantle geochemistry, and supercontinent reconstruction. In: Hatcher, R.D., Carlson, M.P., McBride, J.J., & Martínez Catalán, J.R. (eds.) *4-D Framework of Continental Crust*, Geological Society of America Memoir 200, 9-32.
- Schwartz, J.J., John, B.E., Cheadle, M.J., Miranda, E.A., Grimes, C.B., Wooden, J.L., Dick, H.J.B., 2005. Dating the growth of oceanic crust at a slow-spreading ridge. *Science* 310, 654-657.
- Scoates, J.S., Frost, C.D., Mitchell, J.N., Lindsley, D.H., Frost, B.R., 1996. Residual-liquid origin for a monzonitic intrusion in a mid-Proterozoic anorthosite complex: The Sybille intrusion, Laramie anorthosite complex, Wyoming. *Bulletin of the Geological Society of America* 108, 1357-1371.
- Shuto, K., Ishimoto, H., Hirahara, Y., Sato, M., Matsui, K., Fujibayashi, N., Takazawa, E., Yabuki, K., Sekine, M., Kato, M., Rezanov, A.I., 2006. Geochemical secular variation of magma source during Early to Middle Miocene time in the Niigata area, NE Japan: Asthenospheric mantle upwelling during back-arc basin opening. *Lithos* 86, 1-33.
- Sigmond, E.M.O., 1975. Geologisk kart over Norge, berggrunnskart Sauda, 1:250000. Geological Survey of Norway
- Sigmond, E.M.O., 1978. Beskrivelse til det berggrunnsgeologiske kartbladet Sauda 1:250000. NGU Bulletin 341, 1-94.
- Sigmond, E.M.O., 1998. Bedrock geology map, Odda, 1:250,000. Geological Survey of Norway.
- Sigmond, E.M.O., Andresen, A., 1976. A Rb-Sr isochron age on metaandesites from Skorpehei, Suldal, south Norway. *Norsk Geologisk Tidsskrift* 56, 315-319.
- Sigmond, E.M.O., Birkeland, A., Bingen, B., 2000. A possible basement to the Mesoproterozoic quartzites on Hardangervidda, South-central Norway: zircon U-Pb geochronology of a migmatitic gneiss. *NGU Bulletin* 437, 25-32.
- Sigmond, E.M.O., Gjelle, S., Solli, A., 1997. The Rjukan Proterozoic rift basin, its basement and cover, volcanic and sedimentary infill, and associated intrusions. *Norges Geologiske Undersøkelse Bulletin* 433, 6-7.
- Simon, L., Lécuyer, C., 2005. Continental recycling: The oxygen isotope point of view. *Geochemistry Geophysics Geosystems* 6, Q08004.

- Sisson, T.W., Grove, T.L., 1993. Experimental investigations of the role of H₂O in calc-alkaline differentiation and subduction zone magmatism. *Contributions to Mineralogy and Petrology* 113, 143-166.
- Sisson, T.W., Layne, G.D., 1993. H₂O in basalt and basaltic andesite glass inclusions from four subduction-related volcanoes. *Earth and Planetary Science Letters* 117, 619-635.
- Sisson, T.W., Ratajeski, K., Hankins, W.B., Glazner, A.F., 2005. Voluminous granitic magmas from common basaltic sources. *Contributions to Mineralogy and Petrology* 148, 635-661.
- Skår, Ø., 2002. U-Pb geochronology and geochemistry of early Proterozoic rocks of the tectonic basement windows in central Nordland, Caledonides of north-central Norway. *Precambrian Research* 116, 265-283.
- Skår, Ø., Furnes, H., Claesson, S., 1994. Proterozoic orogenic magmatism within the Western Gneiss Region, Sunnfjord, Norway. *Norsk Geologisk Tidsskrift* 74, 114-126.
- Skår, Ø., Pedersen, R.-B., 2003. Relations between granitoid magmatism and migmatization: U - Pb geochronological evidence from the Western Gneiss Complex, Norway. *Journal of the Geological Society* 160, 935-946.
- Slagstad, T., Marker, M., Skår, Ø., 2008. Mesoproterozoic growth, rifting, drifting and continental collision in Rogaland, SW Sveconorwegian Province. Abstract HPP-001, 33rd International Geological Congress, Oslo, 6–14 August.
- Slagstad, T., Culshaw, N.G., Daly, J.S., Jamieson, R.A., 2009. Western Grenville Province holds key to midcontinental Granite-Rhyolite Province enigma. *Terra Nova* 21, 181-187.
- Slagstad, T., Culshaw, N.G., Jamieson, R.A., Ketchum, J.W.F., 2004. Early Mesoproterozoic tectonic history of the southwestern Grenville Province, Ontario: Constraints from geochemistry and geochronology of high-grade gneisses. In: Tollo, R.P., Corriveau, L., McLelland, J. and Bartholomew, M.J.I. (Eds.), *Proterozoic Tectonic Evolution of the Grenville Orogen in North America*. Geological Society of America Memoir 197, 209-241.
- Slagstad, T., Jamieson, R.A., Culshaw, N.G., 2005. Formation, crystallization, and migration of melt in the mid-orogenic crust: Muskoka domain migmatites, Grenville Province, Ontario. *Journal of Petrology* 46, 893-919.
- Sláma, J., Košler, J., Condon, D.J., Crowley, J.L., Gerdes, A., Hanchar, J.M., Horstwood, M.S.A., Morris, G.A., Nasdala, L., Norberg, N., Schaltegger, U., Schoene, B., Tubrett, M.N., Whitehouse, M.J., 2008. Plešovice zircon — A new natural reference material for U–Pb and Hf isotopic microanalysis. *Chemical Geology* 249, 1-35.
- Smith, I.E.M., Worthington, T.J., Stewart, R.B., Price, R.C., Gamble, J.A., 2003. Felsic volcanism in the Kermadec arc, SW Pacific: Crustal recycling in an oceanic setting. *Geological Society Special Publication*, 99-118.
- Snyder, D., Carmichael, I.S.E., Wiebe, R.A., 1993. Experimental study of liquid evolution in an Fe-rich, layered mafic intrusion: constraints of Fe-Ti oxide precipitation on the T-f_{O₂} and T-ρ paths of tholeiitic magmas. *Contributions to Mineralogy and Petrology* 113, 73-86.
- Söderlund, U., Ask, R., 2006. Mesoproterozoic bimodal magmatism along the Protogine Zone, S Sweden: Three magmatic pulses at 1.56, 1.22 and 1.205 Ga, and regional implications. *GFF* 128, 303-310.
- Söderlund, U., Elming, S., Ernst, R.E., Schissel, D., 2006. The Central Scandinavian Dolerite Group - Protracted hotspot activity or back-arc magmatism? Constraints from U-Pb baddeleyite geochronology and Hf isotope data. *Precambrian Research* 150, 136.
- Söderlund, U., Isachsen, C.E., Bylund, G., Heaman, L.M., Patchett, P.J., Vervoort, J.D., Andersson, U.B., 2005. U-Pb Baddelyite ages and Hf, Nd isotope chemistry constraining repeated mafic magmatism

- in the Fennoscandian Shield from 1.6 to 0.9 Ga. *Contributions to Mineralogy and Petrology* 150, 174.
- Söderlund, U., Jarl, L.-G., Persson, P.-O., Stephens, M.B., Wahlgren, C.-H., 1999. Protolith ages and timing of deformation in the eastern, marginal part of the Sveconorwegian orogen, southwestern Sweden. *Precambrian Research* 94, 29-48.
- Soderlund, U., Möller, C., Andersson, J., Johansson, L., Whitehouse, M., 2002. Zircon geochronology in polymetamorphic gneisses in the Sveconorwegian orogen, SW Sweden: ion microprobe evidence for 1.46-1.42 and 0.98-0.96 Ga reworking. *Precambrian Research* 113, 193-225.
- Soderlund, U., Patchett, P.J., Vervoort, J.D., Isachsen, C.E., 2004. The ^{176}Lu decay constant determined by Lu-Hf and U-Pb isotope systematics of Precambrian mafic intrusions. *Earth and Planetary Science Letters* 219, 311-324.
- Solli, A., Naterstad, J., Andresen, A., 1978. Structural succession in a part of the outer Hardangerfjord area, west Norway. *Norges Geologiske Undersøkelse* 343, 39-51.
- Spulber, S.D., Rutherford, M.J., 1983. The origin of rhyolite and plagiogranite in oceanic crust: an experimental study. *Journal of Petrology* 24, 1-25.
- Starmer, I.C., 1996. Accretion, rifting, rotation and collision in the North Atlantic supercontinent, 1770-950 Ma. In Brewer, T.S. (ed.) *Precambrian crustal evolution in the North Atlantic Regions*. Geological Society of London, Special Publication 112, 219-248.
- Stein, H.J., Bingen, B., 2002. 1.05-1.01 Ga Sveconorwegian metamorphism and deformation of the supracrustal sequence at Sæsvatn, South Norway: Re-Os dating of Cu-Mo mineral occurrences. In: Blundell, D., Neubauer, F. and von Quadt, A. (Eds.) *The Timing and Location of Major Ore Deposits in an Evolving Orogen*. Geological Society of London, Special Publication 204, 313-335.
- Stephens, M.B., Gee, D.G., 1985. A tectonic model for the eugeoclinal terranes in the central Scandinavian Caledonides. In: Gee, D.G. & Sturt, B.A. (eds.) *The Caledonian Orogen - Scandinavia and Related areas*, Chichester, U.K., John Wiley & Sons, 953-970.
- Stephens, M.B., Wahlgren, C.-H., Weijermars, R., 1996. Left-lateral transpressive deformation and its tectonic implications, Sveconorwegian orogen, Baltic Shield, southwestern Sweden. *Precambrian Research* 79, 261-279.
- Storey, C.D., Jeffries, T.E., Smith, M., 2006. Common lead-corrected laser ablation ICP-MS U-Pb systematics and geochronology of titanite. *Chemical Geology* 227, 37-52.
- Stout, M.Z., Nicholls, J., Kuntz, M.A., 1994. Petrological and mineralogical variations in 2500-2000 yr B.P. lava flows, Craters on the Moon lava field, Idaho. *Journal of Petrology* 35, 1681-1715.
- Stracke, A., Bizimis, M., Salters, V.J.M., 2003. Recycling oceanic crust: Quantitative constraints. *Geochemistry Geophysics Geosystems* 4 (3).
- Sun, S.S., McDonough, 1989. Chemical and isotopic systematics of oceanic basalts: implications for mantle composition and processes. In: Saunders, A.D. and Norry, M.J. (Eds.), *Magmatism in the Ocean Basins*. Geological Society of London, Special Publication 42, 313-345.
- Tamaki, K., 1995. Opening tectonics of the Japan Sea. In: Taylor, B. (ed.) *Backarc Basins: Tectonics and Magmatism*, Plenum Press, New York, 407-420.
- Tamura, Y., Tatsumi, Y., 2002. Remelting of an andesitic crust as a possible origin for rhyolitic magma in oceanic arcs: An example from the Izu-Bonin arc. *Journal of Petrology* 43, 1029-1047.
- Thirlwall, M.F., Graham, A.M., 1984. Evolution of high-Ca, high-Sr C-series basalts from Grenada, Lesser Antilles: the effects of intra-crustal contamination. *Journal of the Geological Society* 141, 427-445.

- Thompson, R.N., Morrison, M.A., Dickin, A.P., Hendry, G.L., 1983. Continental flood basalts...arachnids rule OK? . In: Hawkesworth, C.J. & Norry, M.J. (eds.) *Continental Basalts and Mantle Xenoliths*, Cheshire, U.K., Shiva Publishing Limited, 158-185.
- Thy, P., Leshner, C.E., Nielsen, T.F.D., Brooks, C.K., 2006. Experimental constraints on the Skaergaard liquid line of descent. *Lithos* 92, 154-180.
- Tobi, A.C., Hermans, G.A.E.M., Maijer, C., Jansen, J.B.H., 1985. Metamorphic zoning in the high-grade Proterozoic of Rogaland - Vest Agder, SW Norway. . In Tobi, A.C., Touret, J.L.R.(eds.), *The Deep Proterozoic Crust in the North Atlantic Provinces*, NATO Advanced Study Institute Series, 477-497.
- Toplis, M.J., Carroll, M.R., 1995. An experimental study of the influence of oxygen fugacity on Fe-Ti oxide stability, phase relations, and mineral-melt equilibria in ferro-basaltic systems. *Journal of Petrology* 36, 1137-1170.
- Torkse, T., 1985. Terrain displacement and Sveconorwegian rotation of the Baltic Shield: a working hypothesis. In Tobi, A.C., Touret, J.L.R.(eds.), *The Deep Proterozoic Crust in the North Atlantic Provinces*, NATO Advanced Study Institute Series, 333-343.
- Tucker, R.D., Krogh, T.E., Råheim, A., 1990. Proterozoic evolution and age - province boundaries in the central part of the Western Gneiss Region, Norway: results of U-Pb dating of accessory minerals from Trondheimsfjord to Geiranger. In: Gower, C.F., Rivers, T. and Ryan, B. (Eds.) *Mid-Proterozoic Laurentia-Baltica*. Geological Association of Canada, Special Paper 38, 149-173.
- Tucker, R.D., Råheim, A., Krogh, T.E., Corfu, F., 1987. Uranium-lead zircon and titanite ages from the northern portion of the Western Gneiss Region, south-central Norway. *Earth and Planetary Science Letters* 81, 203-211.
- Tucker, R.D., Robinson, P., Solli, A., Gee, D.G., Thorsnes, T., Krogh, T.E., Nordgulen, Ø., Bickford, M.E., 2004. Thrusting and extension in the Scandian Hinterland, Norway: New U-Pb ages and tectonostratigraphic evidence. *American Journal of Science* 304, 477-532.
- Valley, J.W., 2003. Oxygen isotopes in zircon. *Reviews in Mineralogy and Geochemistry* 53, 343-385.
- Valley, J.W., Kinny, P.D., Schulze, D.J., Spicuzza, M.J., 1998. Zircon megacrysts from kimberlite: Oxygen isotope variability among mantle melts. *Contributions to Mineralogy and Petrology* 133, 1-11.
- Valley, J.W., Lackey, J.S., Cavosie, A.J., Clechenko, C.C., Spicuzza, M.J., Basei, M.A.S., Bindeman, I.N., Ferreira, V.P., Sial, A.N., King, E.M., Peck, W.H., Sinha, A.K., Wei, C.S., 2005. 4.4 billion years of crustal maturation: Oxygen isotope ratios of magmatic zircon. *Contributions to Mineralogy and Petrology* 150, 561-580.
- Vander Auwera, J., Bogaerts, M., Liégeois, J.-P., Demaiffe, D., Wilmart, E., Bolle, O., Duchesne, J.-C., 2003. Derivation of the 1.0-0.9 Ga ferro-potassic A-type granitoids of southern Norway by extreme derivation from basic magmas. *Precambrian Research* 124, 107-148.
- Vander Auwera, J., Longhi, J., Duchesne, J.-C., 1998. A Liquid Line of Descent of the Jotunite (Hypersthene Monzodiorite) Suite. *Journal of Petrology* 39, 439-468.
- Vander Auwera, J., Bogaerts, M., Bolle, O., Longhi, J., 2008. Genesis of intermediate igneous rocks at the end of the Sveconorwegian (Grenvillian) orogeny (S Norway) and their contribution to intracrustal differentiation. *Contributions to Mineralogy and Petrology* 156, 721-743.
- Vander Auwera, J., Longhi, J., 1994. Experimental study of a jotunite (hypersthene monzodiorite): constraints on the parent magma composition and crystallization conditions (P, T, f_{O_2}) of the Bjerkreim-Sokndal layered intrusion (Norway). *Contributions to Mineralogy and Petrology* 118, 60-78.

- Woodhead, J.D., Hergt, J.M., Davidson, J.P., Eggins, S.M., 2001. Hafnium isotope evidence for 'conservative' element mobility during subduction zone processes. *Earth and Planetary Science Letters* 192, 331-346.
- Workman, R.K., Eiler, J.M., Hart, S.R., Jackson, M.G., 2008. Oxygen isotopes in Samoan lavas: Confirmation of continent recycling. *Geology* 36, 551-554.
- Zariņš, K., Johansson, Å., 2009. U-Pb geochronology of gneisses and granitoids from the Danish island of Bornholm: New evidence for 1.47-1.45 Ga magmatism at the southwestern margin of the East European Craton. *International Journal of Earth Science* 98, 1561-1580.
- Zhang, S.-H., Zhao, Y., Yang, Z.-Y., He, Z.-F., Wu, H., 2009. The 1.35 Ga diabase sills from the northern North China Craton: Implications for breakup of the Columbia (Nuna) supercontinent. *Earth and Planetary Science Letters* 288, 588-600.
- Zhao, G., Cawood, P.A., Wilde, S.A., Sun, M., 2002. Review of global 2.1-1.8 Ga orogens: Implications for a pre-Rodinia supercontinent. *Earth Science Reviews* 59, 125-162.
- Zhao, G., He, Y., Sun, M., 2009. The Xiong'er volcanic belt at the southern margin of the North China Craton: Petrographic and geochemical evidence for its outboard position in the Paleo-Mesoproterozoic Columbia Supercontinent. *Gondwana Research* 16, 170-181.
- Zhao, G., Sun, M., Wilde, S.A., Li, S., 2004. A Paleo-Mesoproterozoic supercontinent: Assembly, growth and breakup. *Earth Science Reviews* 67, 91-123.
- Zhao, G., Sun, M., Wilde, S.A., Li, S., 2003. Assembly, accretion and breakup of the Paleo-mesoproterozoic Columbia supercontinent: Records in the North China Craton. *Gondwana Research* 6, 417-434.
- Zhao, G., Sun, M., Wilde, S.A., Li, S., Zhang, J., 2006. Some key issues in reconstructions of Proterozoic supercontinents. *Journal of Asian Earth Sciences* 28, 3-19.
- Zhao, G., Wilde, S.A., Cawood, P.A., Sun, M., 2001. Archean blocks and their boundaries in the North China Craton: Lithological, geochemical, structural and P-T path constraints and tectonic evolution. *Precambrian Research* 107, 45-73.
- Zhao, X., Zhou, M., Li, J., Wu, F., 2008. Association of Neoproterozoic A- and I-type granites in South China: Implications for generation of A-type granites in a subduction-related environment. *Chemical Geology* 257, 1-15.
- Zhou, X.Q., Bingen, B., Demaiffe, D., Liégeois, J.-P., Hertogen, J., Weis, D., Michot, J., 1995. The 1160 Ma old Hidderskog meta-charnockite: implications of this A-type pluton for the Sveconorwegian belt in Vest Agder (SW Norway). *Lithos* 36, 51-66.